ANNUAL REVIEW

INSTITUTE FOR MOLECULAR SCIENCE

1992

ANNUAL REVIEW

INSTITUTE FOR MOLECULAR SCIENCE

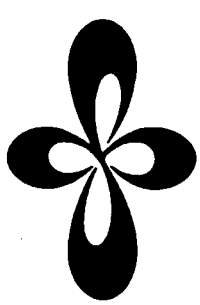

1992

Published by
Institute for Molecular Science
Okazaki National Research Institutes
Myodaiji, Okazaki 444, Japan
Phone 0564-55-7418 (Secretary room)
Telex 4537-475 KOKKEN J
Fax 0564-54-2254

Editorial Committee 1992: Kiyoshi Isobe (Chairman),
Kaoru Iwano, Asuka Fujii,
Hrvoje Petek, Kazushi Kanoda,
Yasushi Morita, Hiroaki Yoshida,
Tamotsu Takahashi, Fuminori Misaizu,
Goro Isoyama, and Kayoko Sugiyama

IMS 1992

Here we present Annual Review for 1992. With more than ten new research groups over the last few years, IMS has been changing the focus of its research projects. I believe that the continuous change is the source of activity and vigor of IMS.

It is my opinion that the mainstream of molecular science research is advancing in two directions. First, based on a long history and high level of research on molecular structure in Japan, the branch of molecular science is shifting from the study of static molecular structure to that of molecular dynamics. This research field is making great progress, with contributions also from rapid progress in theories of reaction dynamics.

Another major research field in molecular science is materials science whose main theme is to give functions to molecules and molecular assemblies. To achieve this goal a close collaboration is needed among the researchers working in such fields as chemical synthesis, structural determination, and solid state chemistry and physics. In fact a very strong collaboration is in progress.

Personnel turnover at this Institute has been very active. This in part is due to mandatory retirement age of 60 for the faculty and staff at IMS. Prof. Katsumi Kimura reached the retirement age and moved to JAIST, Japan Advanced Institute of Science and Technology, Hokuriku. Dr. Keiichiro Nasu, Associate Professor of Theoretical Chemistry II, was promoted and moved to National Laboratory for High Energy Physics in Tsukuba. On the other hand new members have joined the faculty of IMS from various universities in Japan. We have hired Dr. Tatsuhisa Kato as Associate Professor, Laboratory of Molecular Dynamics, Dr. Toshinori Suzuki as Associate Professor, Laboratory of Excited State Dynamics, Dr. Seiichi Miyajima as Associate Professor, Laboratory of Molecular Assemblies Dynamics, and Dr. Tsuneo Urisu as Professor of the newly established laboratory, Laboratory of Reaction Dynamics, Department of Vacuum UV Photoscience.

Further we have invited Prof. Yutaka Fukuda of Department of Chemistry, Ochanomizu University, to the position of Professor of Laboratory of Synthetic Coordination Chemistry for two-year term, and Dr. Kiyoshi Sawada of Department of Chemistry, Niigata University, to the position of Associate Professor of the same laboratory.

To raise the activities at research facilities of IMS it is of utmost importance to introduce a new program. As a part of the program the staff of Equipment Development Center have been developing original equipment which is needed for molecular science research. The project is called "IMS Machine." I am very happy to announce that the new equipment of IMS's original design has been given birth.

Lastly I am very pleased to report that at UVSOR Facility we succeeded in generating free electron laser oscillation at 5416 Å on May 8th, 1992.

November, 1992

H. Inokuchi

Hiroo INOKUCHI
Director-General

CONTENTS

IMS 1992 ..... Hiroo Inokuchi iii

CONTENTS v

ORGANIZATION AND STAFF 1

COUNCIL 9

BUILDING AND CAMPUS 10

RESEARCH ACTIVITIES I
DEPARTMENT OF THEORETICAL STUDIES 12

A. Potential Energy Surfaces and Dynamics of Elementary Chemical Reaction 12

1. Theoretical Study of the Photodissociation Reaction of HgI_2 12
2. Theoretical Study of Photodissociation Reaction of Formic Acid 12
3. Potential Energy Surface and Classical Trajectory Study of HFCO → HF+CO Dissociation Reaction 12
4. Time-dependent Quantum Mechanical Approach to the Photodissociation Dynamics of CH_3I 12
5. Theoretical Study on the Solvent Effects on ICN Photodissociation 13
6. New Ab Initio Potential Surfaces and Three-Dimensional Quantum Dynamics for Transition State Spectroscopy in Ozone Photodissociation 13

B. Theoretical Studies of Structure and Spectroscopy 13

1. Ab Initio MO Study of C_{60} Anion Radical: the Jahn-Teller Distortion and Electronic Structure 13
2. Ab Initio MO Calculation of $(\eta^2\text{-}C_{60})Pt(PH_3)_2$: Electronic Structure and Interaction between C_{60} and Pt 13
3. AM1 Calculations of Intermediates in Ring Stacking Model for Fullerene Formation 13
4. Theoretical Study of Hydration of Light Alkali and Alkali-earth Metal Atoms and Ions 14
5. Theoretical Study of Hydration of Na_2 14
6. A Theoretical Study on Ligand Substitution Reaction of Pt(II) Complex in Water 14
7. Application of the Natural Population Analysis to Transition Metal Complexes. Should the Empty Metal p Orbitals Be Included in the Valence Space? 14
8. Ab Initio MO Study of Neutral and Cationic Boron Clusters 15
9. An Ab Initio and Monte Carlo Study on Strucure and Stability of $H_3^+(H_2)_n$ (n=3−16) 15

C. Theoretical Studies of Reaction Mechanisms and Structure of Organic and Related Compounds 15

1. Ab Initio MO Study on the Periodic Trends in Structures and Energies of Hypervalent Compounds: Four-Coordinated XH_4^- and XF_4^- Anions Containing a Group 15 Central Atom (X=P, As, Sb, Bi) 15
2. Ab Initio MO Study on the Periodic Trends in Structures and Energies of Hypervalent Compounds: Five-Coordinated XH_5 Species Containing a Group 15 Central Atom (X=P, As, Sb, Bi) 15
3. Transition Structures for H_2 Elimination from XH_4 Hypervalent Species (X=S, Se, Te). Ab Initio MO Study 15
4. Theoretical Studies of Heteroatom-Directed Carbometallation. Addition of MeCu, Me_2Cu^- and MeLi to Substituted Acetylenes 16
5. Triplet-Singlet Intersystem Crossing as the Second Step of Cycloaddition of Triplet Penta-1,4-Diene. An Ab Initio MO Study 16

D. Structure and Reactions of Transition Metal Complexes 16

1. Ab Initio MO Study of the Reaction Mechanism: $MCH_2^+ + H_2 \rightarrow M^+ + CH_4$ (M=Co, Rh and Ir) 16
2. Ab Initio MO Study of the Electronic and Geometrical Structures of Silylene Complexes, $MSiH_2^+$ (M=Co, Rh, and Ir) 16
3. Ab Initio MO Study of the Reaction Mechanism: $RhCO^+ + H_2 \rightarrow Rh^+OCH_{2+} \rightarrow Rh^+ + OCH_2$ 17
4. An Ab Initio Theoretical Study on the Structure of $[Os(PR_3)_3\text{ “}H_4\text{”}]$ and $[Os(PR_3)_3\text{“}H_5\text{”}]^+$ Complexes 17
5. Ab Initio MO Study of Triosmium Carbonyl Complexes 17
6. An Ab Initio MO Study of σ-Metathesis Reaction of $Cl_2Zr(C_2H_4)$ with H_2 18
7. A Theoretical Study on Ethylene Polymerization Using Silylene-Bridged Group 4 Metallocene Catalysts 18
8. A Theoretical Study of Hydride Attack on the η^5-Cyclopentadienyltricarbonyliron Cation 18
9. Ab Initio MO Study of the Reaction Mechanism: $RhCl(PH_3)_2CO + CH_4 \rightarrow RhCl(PH_3)_2CO(H)CH_3$ 19
10. An Ab Initio MO Study on Ethylene and Propylene Insertion into the Ti-CH_3 Bond in $CH_3TiCl_2^+$ as a Model of Homogeneous Olefin Polymerization 19
11. An Ab Initio MO and MM Study on Homogeneous Olefin Polymerization with Silylene-Bridged Zirconocene Catalyst and its Regio-and Stereoselectivity 19

E. Theoretical Studies of Chemical Reactions on Solid Surfaces 19

1. An Ab Initio Molecular Orbital Comparison Study of H_2 Chemisorption on MgO and Lithium-doped MgO 20
2. An Ab Initio MO Study on Adsorption at the MgO Surface I. H_2 Chemisorption on the $(MgO)_4$ Cluster 20

F. Structures and Reactions of Manybody Chemical Systems 20
1. Long Time Fluctuation of Liquid Water; 1/f Spectrum of Energy Fluctuation 20
2. Structure and Dynamics of Water Clusters 20
3. Dynamics and Evaporation of Water Clusters 20
4. A New Approach to Investigate the Energy Relaxation of an Excess Electron in Water Clusters 21
5. Proton Transfer in Liquid Water; Solvent Rearrangement Effect, Interaction Energy Component Analyses 21
6. The Argon Cluster Dynamics in the Melting Region 21
7. Reaction Surface by Gradient Extremal 21

G. Theoretical Studies of Chemical Reaction Dynamics 22
1. Effects of Potential Energy Surface Topography and Isotope Substitution in Atom-Diatom Chemical Reactions: The $Cl+H_2$ and $D+H_2$ Systems 22
2. Variational Principles for Reactive Collisions Based on the Generalized Lagrange Multiplier Method 22

H. Theoretical Studies of Atomic Collision Processes 22
1. Coupled Channel Treatment of Transitions between $Na(^2P_{1/2}m_j)$ and $Na(^2P_{3/2}m_{j'})$ in Collision with $Na(^2S_{1/2}m_{j''})$ 22

I. Theoretical Studies of Highly Excited States of Molecules 22
1. Characteristics and Dynamics of Doubly Excited States of Molecules 23

J. Theory of Nonadiabatic Transition 23
1. The Two-State Linear Curve Crossing Problems Revisited. I. Analysis of Stokes Phenomenon and Expressions for Scattering Matrices 23
2. The Two-State Linear Curve Crossing Problems Revisited. II. Analytical Approximations for Stokes Constant and Scattering Matrix: Landau-Zener Case 23
3. Numerical Method for the Two-State Curve Crossing: Nonadiabatic Tunneling Case 23
4. Nonadiabatic tunneling in One-dimensional Finite Periodic Potential System 23

K. Stokes Phenomenon and Asymptotic Solutions of Ordinary Differential Equations 24
1. Stokes Constants for a Certain Class of Second-Order Ordinary Differential Equations 24

L. Theory for High-Tc Superconductors 24
1. Superconductivity, Metal-Insulator Transitions, and Strong Enhancement and Reduction of Isotope Effects in the Anharmonic Peierls-Hubbard Model 24
2. Enhancement, Reduction and Inversion of Isotope Effects due to Anharmonic Phonons, — Migdal-Eliashberg Theory for Superconductivity — 24
3. Stationary Localized Mode in an Anharmonic Molecular Crystal Model 24

M. Nonlinear Excitations in Halogen-Bridged Mixed-Valence Metal Complexes 25
1. Theory for Spectral Shape of Optical Absorption in Halogen-Bridged Mixed-Valent Metal Complexes 25

N. Optical Nonlinearity of Low Dimensional Materials 25
1. Comment on "Essential-states Mechanism of Optical Nonlinearity in π-conjugated Polymers" 25
2. The Spectrum of Third Harmonic Generation of MX Complex 25
3. Electron Interaction and Optical Gap of Conjugated Polymers 25

RESEARCH ACTIVITIES II
DEPARTMENT OF MOLECULAR STRUCTURE 26

A. Laboratory and Astronomical Spectroscopy of Transient Interstellar Molecules 26
1. The Submillimeter—Wave Spectrum of the $ND(^3\Sigma^-)$ Radical 26
2. The Submillimeter—Wave Spectrum of the PH and PD Radicals in the Ground Electronic State, $(^3\Sigma^-)$ 26

B. Laser Investigation of Autoionizing and Predissociating States of Atoms and Small Molecules 27
1. Rotational State Dependence of Decay Dynamics in the Superexcited $7f$ Rydberg State (v=1) of NO 27
2. Studies on the Competition between Rotational Autoionization and Predissociation in Superexcited *np* Rydberg States of NO 27
3. R-Matrix Calculation of Two-electron Excited $^1S^e$ States of Ca Atom up to the 9s Threshold 28

C. Laser Cooling and Trapping of Neutral Atoms 28
1. Visible Observation of Metastable Helium Atoms Confined in an Infrared/Visible Double Resonance Trap 28

D. Molecular Science of Biomolecules and Their Model Compounds 29
1. Resonance Raman Study on the Active Site Structure of a Cooperative Hemerythrin 29
2. Detection of the Fe-CO Stretching Raman Band for Recombination Transient Species of Photodissociated Carbonmonoxy Myoglobin by Using Pump/Probe Time-Resolved Technique 30
3. Observation of the Fe^{IV}=O Stretching Raman Band for a Thiolate-ligated Heme Protain; Compound I of Chloroperoxidase 30
4. Time-Resolved Resonance Raman Study on the Binding of Carbonmonoxide to Recombinant Human Myoglobin and Its Distal Histidine Mutants 30
5. A Novel Idea for Practical UV Resonance Raman Measurement with a Double-monochrometer and Its Application to Protain Structural Studies 30
6. Synthesis and Characterization of the Dinuclear Copper(II) Complexes $[Cu(HB(3,5\text{-}Me_2pz)_3)]_2X(X=O^{2-}, (OH)_2^{2-}, CO_3^{2-}, O_2^{2-})$ 30
7. (μ-Alkoxo)diiron(II,II) Complexes of N,N,N',N'-Tetrakis(2-(6-methylpridyl)methyl)-1, 3-diaminopropane-2-olate and the Reversible Formation of the O_2-Adducts 31
8. Resonance Raman Studies on the Cu_A Site of Cytochrome *c* Oxidase Using a Multichannel Scanning Raman Spectrometer with a CCD Detector 31
9. Resonance Raman Spectra of Photointermediates in Phytochrome Phototransformation: Deprotonation of the Chromophore in the Bleached Intermediate 31
10. Time-Resolved Resonance Raman Identification of Hydroperoxy and Ferryloxo Intermediates in Cytochrome Oxidase Catalysis 32

E. Vibrational Spectroscopy on Short-lived Molecules and Solution Structure 32
1. Time-Resolved Resonance Raman Spectra of Free-base Octaethylprophyrin in the S_1 and T_1 States 32
2. Time-Resolved Resonance Raman Investigation of Photoreduction of Iron-octaethylporphyrin Complexes by Using Quasi-Simultaneous Pump/Probe Measurement Technique 32
3. A Multi-Reflection Raman Measurement Device for the Study of Dilute Aqueous Solutions 33
4. Peculiar Conformational Behavior of the Oxyethylene Chain in Dilute Aqueous Solutions: A Multi-Reflection Raman Spectroscopic Study 33

F. EPR Studies on Molecular Structure of Metallofullerenes 33
1. Isomers and ^{13}C Hyperfine Structures of Metal Encapsulated Fullerenes, $M@C_{82}$ (M=Sc, Y, and La) .. 33
2. Hydrodynamic Rotational Effects on EPR Spectra of $M@C_{82}$ in Solution 33

RESEARCH ACTIVITIES III
DEPARTMENT OF ELECTRONIC STRUCTURE 34

A. Time and Frequency Resolved Studies of Isomerization in Gas and Solution Phases 34
1. Structure and *trans-cis* Isomerization Dynamics of S_1 States of Tetraenes 34
2. Two-photon Spectroscopy of $2^1A_g \leftarrow 1^1A_g$ Transition of Tetraenes 35
3. Structure and Femtosecond Timescale Internal Conversion Nonradiative Decay Dynamics of S_2 States of Tetraenes 35
4. Excited State Relaxation of Crown Ether Styryl Dyes: Photoisomerization 36

B. Ultrafast Intermolecular Electron Transfer in Electron Donating Solvent 36
1. Femtosecond Inter-Molecular Electron Transfer: Dye in Weakly Polar Electron-Donating Solvent 37
2. Ultrafast Chemical Reaction beyond Solvent Control 37
3. Picosecond Kinetics of Light-Induced Electron Transfer from J-Aggregated Cyanine Dyes to AgBr Microcrystals: Effect of Aggregate Size 38
4. Picosecond Fluorescence Lifetime of J-aggregates of Cyanine Dyes Adsorbed on AgBr and SiO_2: Sample Scanning Effect 38

C. Primary Photochemical Events in Biological Systems 39
1. Retinal Proteins (Photoisomerization): Comparative Study of Two Bacterial Rhodopsins, Bacteriorhodopsin and Halorhodopsin 39
2. Photosystem I Reaction Center (Electron Transfer): First Step of Photosynthesis in Higher Plants 39
3. First Step of Photomorphogeneses in Green Plants 40
4. Picosecond Fluorescence Decay of Lens Crystallin Proteins 40
5. Picosecond Fluorescence Decay in Photolyzed Lens Protein α-Crystallin 41

D. Application of Femtosecond Time-Resolved Coherent Anti-Stokes Raman Scattering 41
1. Femtosecond Time-Resolved Coherent Anti-Stokes Raman Scattering from Liquid Alkanenitriles: Dependence of Vibrational Dephasing on Molecular Size and Solvent-Solute Interactions 42
2. Femtosecond Time-Resolved Coherent Anti-Stokes Raman Scattering from Liquid Alkanedinitriles: Intramolecular Coupling between the Two C≡N Stretching Modes 42
3. Dephasing and Beats of Excitonic-Enhanced Transitions of J-Aggregates Measured by Femtosecond Time-Resolved Resonance CARS 43

E. Spectroscopy of the Cs_2 in a very Cold Supersonic Jet by the Multiphoton Ionization 43
1. New Triplet Excited States of Cs_2 Observed by Resonance Enhanced Two Photon Ionization Spectroscopy in a very Cold Supersonic Jet 43
2. Adiabatic Ionization Potentials of Cs_2 and Cs_3 in a Supersonic Jet 44

F. Development of Ultrafast Spectroscopic Methods 44
1. Fluorescence Up-Conversion Measuring System with Sub-100 Femtosecond Pulses 44
2. Feedback-Controlled Mode-Locking of Nd:Glass Laser Using GaAs 45

G. Dynamical Studies of Exciplex Formation in Donor-Acceptor vdW Complexes in Free Jet Expansions 45
1. Exciplex Formation in Naphthalene-Triethylamine vdW Complexes in Free Jet Expansions 46
2. Exciplex Formation in Anthracene-Dimethylaniline vdW Complexes in Free Jet Expansions 46

H. Photochemistry on Well-Defined Surfaces 47
1. Structure of Adsorbed N_2O on a Pt(111) Surface and Photodissociation at 193 nm: Effective Formation of Oxygen Adatoms 47
2. Laser-induced Photochemistry of Nitrous Oxide on a Pt(111) Surface 47
3. The Mechanism of Photodissociation of N_2O Adsorbed on a Pt(111)Surface 47

I. Dynamical Processes in Electronically-and/or Vibrationally Excited Molecules 48
1. Dynamics of Vibrationally Excited van der Waals Complex: SEP-LIF Spectroscopy of the Anisole · Ar Complex 48
2. Observation of Intermolecular Vibrational Modes in the 2,3-dihydrobenzofuran Dimer 48
3. Lambda Doublet Formation in OH by Chemical Reactions 49
4. Photodissociation of Acetaldehyde Studied by the Photofragment Excitation Spectroscopy in a Supersonic Free Jet 49
5. Double-Resonance Multiphoton Ionization Spectroscopy of the $\tilde{B}$ Rydberg State of Ammonia 49
6. Reaction Dynamics of the 193 nm Photolysis of $HBr \cdot H_2O$ Complex 50
7. Construction of a New System for the Measurement of Emission Spectra of van der Waals Complexes 50
8. The Vibrationally Excited HCO Radical Produced by the Photodissociation of Acetaldehyde at 266 nm 51

J. Self-organization in Chemical Reactions 51
1. Wavelength-Dependence of Relative Cross Section of Photo-Induced pH Oscillation in $Fe(CN)_6^{3-}/Fe(CN)_6^{4-}/H_2O_2/H_2SO_4$ System: Irradiation of $Fe(CN)_6^{3-}$ before Mixing 51
2. Cross Section of Light-Induced Inhibition and Induction of Chemical Oscillations 52
3. Hopf Bifurcation of Hexacyanoferrate(II)/Hydrogen Peroxide/Sulfuric Acid System in a CSTR 52
4. Photo-responce of the Autocatalytic Reaction of Acidic $[Ru(bpy)_3]^{2+}$ with BrO_3^- 52
5. Photo-response of the Briggs-Rauscher Reaction 53
6. On a Phenomenological Model for Nonequilibrium Interaction between Thermally Activated Chemical Reactions 53
7. A Simple Phenomenological Model for Nonequilibrium Interaction between Two Reactions in a Lorentz Gas 54
8. Direct Observation of Nonequilibrium Distribution Function in Systems with a Model Thermally Activated Reaction 54
9. On a Long-time-tail of Reactant Concentration for a Unidirectional Chemical Reaction, which Proceeds in a Dense Medium 55

K. External Magnetic Field Effects on Chemical Reactions 55
1. Magnetic Field Effects on the Perturbed Rotational Levels of CN in the Electronically Excited States 55
2. External Magnetic Field Effects on the β Band Emission of NO 56

RESEARCH ACTIVITIES IV
DEPARTMENT OF MOLECULAR ASSEMBLIES 57

A. Solid State Properties of Phthalocyanine Salts 57
1. Ferromagnetic Interaction in Solid (Octabutoxy-Phthalocyaninato)Cobalt 57
2. Structure and Solid State Properties of Conductive Salts of (Phthalocyaninato)Cobalt, $CoPc(AsF_6)_{0.5}$ 57

B. Strucure and Properties of Organic Metals 57
1. Infrared and Transport Properties of K_xC_{60} 57
2. Rigid Band Feature in K_xC_{60} by *in situ* Infrared Reflectance 57
3. Enhanced Isotope Effect in ^{13}C-rich Superconducting M_xC_{60} (M=K, Rb): Support for Vibronic Pairing 58
4. Low Energy Electronic Excitations and Fano Resonance in K Doped C_{60} from Raman Scattering Excited at 1.16 eV 58

5. Evidence for Jahn-Teller Coupling and Fano Resonance of Lower H_g Modes in K_3C_{60} Films from Raman Scattering ····· 58
6. Magnetic Properties of TDAE-C_{60} and TDAE-C_{70}, A Comparative Study ····· 59
7. Air Stability of K_3C_{60} Superconductors: Low Field Microwave Absorption and ESR Study ····· 59
8. Photoelectron Spectra of Higher Fullerene Compound C_{82} and its Potassium Complex ····· 59
9. Fermi Surface Study of Two-Dimensional Organic Metals $(BEDT\text{-}TTF)_2X$ ····· 59
10. Structure of the Charge-Transfer Complex of (DBTTF)(BTDA-TCNQ) ····· 59
11. Crystal Structures of Metallic and Insulating Molecular Complexes between naphthaceno[5,6-*cd*:11,12-*c'd'*]bis[1,2] diselenole and 4,8-bis(dicyanomethylene)-4*H*,8*H*-benzo[1,2-*c*:4,5-*c'*]bis[1,2,5]thiadiazole: (TSeN)(BTDA-TCNQ) and (TSeN)(BTDA-TCNQ)(C_6H_5Cl) ····· 60

C. Construction of Microspectrophotometer ····· 60
1. Improvement of Microspectrophotometer for the use of IR-VIS-UV region ····· 60
2. Microspectrophotometer for the use of Far-Infrared and Infrared region using a Synchrotron Radiation as a Light Source ····· 60

D. Superconducting Characteristics of Organic Materials ····· 60
1. Upper Critical Field and NMR Relaxation Studies of an Organic Superconductor, κ-$(MDT\text{-}TTF)_2AuI_2$ ····· 60
2. Magnetic Penetration Depth of the κ-Phase Family of Organic Superconductors ····· 61

E. Fermi Surface Topology and Magnetotransport of Organic Metals ····· 61
1. De Haas-van Alphen Effect in κ-$(DMET)_2AuBr_2$ ····· 62
2. De Haas-van Alphen Effect and the Fermi Surface in κ-$(BEDT\text{-}TTF)_2I_3$ ····· 62
3. Quantum Oscillation and Transport Property in κ-$(BEDT\text{-}TTF)_2Ag(CN)_2H_2O$ ····· 62
4. Field-Induced Transitions in a Novel Organic System, $(DMETSeF)_2AuI_2$ ····· 62

F. Synthesis and Characterization of Proton-Transfer/Electron-Transfer System ····· 63
1. Study of Proton Dynamics in the NHO Hydrogen Bonds in the Thermochromic Crystals of N-Salicylideneanilines ····· 63
2. Proton Transfer in N-Salicylideneanilines—Effect of Charge-Transfer Interaction ····· 63
3. Crystal Structure and Transport Properties of a Hydrogen-Bonded 1:1 Charge-Transfer Complex Composed of 1,6-Pyrenediamine and 7,7,8,8-Tetracyanoquinodimethane (DAP-TCNQ) ····· 63

G. Ultra-Thin Organic Film Systems Prepared by Molecular Beam Epitaxy (MBE) Technique ····· 63
1. Epitaxial Growth of Lead Phthalocyanine Film on KI Crystal ····· 64
2. Nonlinear Optical Study of Ultrathin Phthalocyanine Films Prepared by the Molecular-Beam Epitaxy Technique ····· 64

H. Novel Molecular System C_{60}: Fullerites and Fullerides ····· 64
1. Electronic Properties of C_{60} and Alkali Metal Doped C_{60} Thin Films or Single Crystals ····· 64
2. Novel Molecular System C_{60}: Fullerites and Fullerides ····· 64
3. Observation of Metallic Conductivity and Sharp Superconducting Transition at 19 K in Potassium-Doped Fulleride, C_{60}, Crystal ····· 64
4. Charge Transport and Superconducting Transitions in C_{60} Single Crystals and Thin Films Doped with Rubidium ····· 64
5. Electronic Structure of Alkali Metal Doped C_{60} Derived from Thermoelectric Power Measurements ··· 64

I. Preparation and Characterization of Copper Oxide High T_c Superconductor Films ····· 65
1. Atomic Layer-by-Layer Deposition of Well-Oriented Crystalline La-Sr-Cu-O Films ····· 65

J. STM/STS Study on Electronic Structures of Some Superconductors ····· 65
1. Construction of Low Temperature STM-STS System ····· 65

K. Photoelectron Spectroscopy of Organic Solids in Vacuum Ultraviolet Region ····· 65
1. Electronic Structure of bis[1,2,5]thiadiazolo-*p*-quinobis (1,3-dithiole) (BTQBT) Studied by Ultraviolet Photoemission Spectroscopy ····· 65
2. Resonant Photoemission Study of an Al-Cu-Fe Icosahedral Phase ····· 66
3. Electronic Structure of Doped C_{60}; Strong Correlation or Lattice Distortion? ····· 67
4. Anomalous Temperature Dependence of Low-Energy-Electron Transmission Spectra of Thin Films of Tetrakis(nonylthio)tetrathiafulvalene (TTC_9-TTF) ····· 67
5. Angle-resolved Photoemission from Langmuir-Blodgett Films of Copper Tetrakis(n-butoxycarbonyl)phthalocyanine with Synchrotron Radiation ····· 67
6. Pseudo-Gap at the Fermi Level in K_3C_{60} Observed by Photoemission and Inverse Photoemission ····· 67
7. Comparative Photoemission Study of Rb_xC_{60}, Rb_xC_{70} and RbC_8: A Pseudo-gap at the Fermi Level in the Fulleride ····· 67
8. Photoelectron Spectra of a Higher Fullerene Compound C_{82} and Its Potassium Complex ····· 67
9. Photoelectron Spectra of C_{76} and K_xC_{76} ····· 68
10. Ultraviolet Photoelecron Spectra of C_{84} and K_xC_{84} ····· 68

11. Molecular Orientation in Thin Films of Bis(1,2,5-thiadiazolo)-*p*-quinobis(1,3-dithiole) on Graphite Studied by Angle-Resolved Photoelectron Spectroscopy ····· 68
12. Electronic States of Oxidized and Reduced Cytochrome c Observed by X-ray Photoelectron Spectroscopy ····· 69

L. Electrical Conduction and its Related Properties of Organic Solids ····· 69
1. Crystal Structures and Molecular Packing of Tetrakis(alkylthio)tetrathiafulvalene (TTC_n-TTF); part I (n=3,4,6) ····· 69
2. Crystal Structures and Molecular Packing of Tetrakis(alkylthio)tetrathiafulvalene (TTC_n-TTF); part II (n=7,9,11) ····· 69
3. Hall-Effect Observation in the New Organic Semiconductor Bis(1,2,5-thiadiazolo)-*p*-quinobis(1,3-dithiole) (BTQBT) ····· 70

M. Physics and Chemistry of Graphite and its Intercalation Compounds ····· 70
1. Two-Dimensional Metallic Hydrogen Lattice in Potassium-Hydrogen-Graphite Ternary Systems ····· 70

N. Organic Metals ····· 70
1. Structural and Physical Properties of a New Organic Superconductor, $(BEDT\text{-}TTF)_4Pd(CN)_4H_2O$ ····· 70
2. Structural and Conducting Properties of (TTF)(DMeT-DCNQI) ····· 71
3. Synthesis of Tetrathiafulvalene Derivatives by the Use of Organoaluminium Reagents ····· 71

O. Structure and Electronic state of DCNQI-Cu Compounds ····· 71
1. XANES and EXAFS Study in $(R_1,R_2\text{-}DCNQI)_2Cu$ ····· 71

P. The Effect of Microscopic Molecular Environments on the Dynamics of Electronically Excited Molecules Generated in Supersonic Free Jets ····· 71
1. S_1-T_2 Level Inversion of 9,10-Dimethylanthracene Caused by the Coordination of One Rare-gas Atom ····· 72
2. Radiative Lifetime and Electronic Relaxation of 9-Cyanoanthracene in Rare-gas Clusters and in Rare-gas Matrices ····· 72
3. Single Vibronic Level Relaxation in Photoreactive 9-*tert*-Butylanthracene ····· 72

RESEARCH ACTIVITIES V
DEPARTMENT OF APPLIED MOLECULAR SCIENCE ····· 74

A. New Multi-Stage Redox Systems ····· 74
1. Synthesis and Properties of Methyl Chalcogeno Derivatives of 1,6-Diselenapyrene (DSPY) ····· 74
2. Crystal Structure of 1,6-Diselenapyrene (DSPY) ····· 74
3. Crystal Strucure of 3,9-Dithiapyrene (3,9-DTPR) ····· 74

B. New Conjugated Electronic Systems ····· 74
1. Crystal Structure of 2-Phenyl-3-hydroxyphenalenone ····· 75
2. Theoretical Studies of CT Ferromagnets and Ferrimagnets: Metallocenium-TCNE Complexes ····· 75

C. New Cooperative Proton-Electron Transfer (PET) Systems ····· 75
1. Three Dimensional Molecular Architecture of Unsymmetrical Proton—Electron Transfer (PET) System Containing Disufide Bond: 4-Hydroxyphenyldisulfide-Benzoquinone Complex (HPDS-BQ) ····· 75
2. Crystal Structure of Hydrogen-Bonded Charge Transfer Complex Containing Water Molecule: [Bis(4-hydroxyphenylthio)-1,5-naphthalene]-Chloranil-H_2O ····· 76
3. Synthesis and Properties of Benzoquinhydrones with Donor and Acceptor Substituents ····· 76
4. The Extended Conjugated Quinhydrones: Biphenoqunhydrones and Stilbenquinhydrones ····· 76
5. Crystal Structure of Nickel Complex with Modified Diaminoglyoxime Ligand ····· 76
6. Synthesis and Physical Properties of Alkylthiobenzoquinhydrone ····· 77

D. Transition Metal Oxide Clusters ····· 77
1. Trishomocubane-Type Methoxide Cluster $[(RhCp^*)_2Mo_3O_9(OMe)_4$ as a Potential Model for Partial Oxidation MeOH on MoO_3 ····· 77
2. New Type Octamolybdate $[(RhCp^*)_2(SCH_3)_3]_4[Mo_8O_{26}]$ and Hexamolybdate $[(RhCp^*)_2(SCH_3)_3]_2$ $[Mo_6O_{19}]$ ····· 78
3. Linear-Type Tetranuclear Rh_2Mo_2 Complex $[(RhCp^*)_2Mo_2O_5(SCH_3)_6$ Obtained from Reaction of Triple Cubane-Type Cluster $[RhCp^*MoO_4]_4$ with CH_3SH ····· 78
4. Double Oxygen Bridge Tetranuclear Rh_2Mo_2 Complex $[(RhCp^*)_2Mo_2O_4(SCH_3)_6$ ····· 79

E. Transition Metal Sulfide Compounds ····· 79
1. Novel Trinuclear μ-Methylene Rhodium Complex with Capping Sulfur Ligand: $[(RhCp^*)_3(\mu_2\text{-}CH_2)(\mu_3\text{-}S)](BF_4)_2$ ····· 79
2. Synthesis, Structure, and Properties of Oxidized Hexamolybdenum Clusters $[(Mo_6X_7Y)X'_6]^2$ (X=X'=Cl, Br; Y=S, Se) ····· 80

F. Organic Synthesis with Lanthanoids ····· 80

1. Studies on the Catalytic Activity of Lanthanoid(III) Salts in the Glycosylation of Methoxyacetyl Glucoside Derivative ····· 80
2. A Novel Catalytic Glycosylation of 1-Hydroxyglucose Derivatives with the Aid of Methoxyacetic Acid and Ytterbium(III) Triflate ····· 81
3. Methoxyacetate as a New Protective Group for the Hydroxy Functionality: Easy Formation and Selective Cleavage Catalyzed by Ytterbium(III) Triflate ····· 81

G. Development of New Organic Reactions Based on the Design of Reaction Intermediates ····· 81
1. Utility of Phosphonium Enolates as Synthetic Intermediates. A Novel Catalytic [3,3] Rearrangement of Allylic Acrylates ····· 81
2. An Easy Access to Erythrose and Threose by a Sequence of Reactions—Cl-Alkoxy Radical Fragmentation and Acid-Catalyzed Transacetalization ····· 82
3. Methoxyacetyl Glycoside as a New Glycosyl Donor for the Zinc(II) Chloride-Promoted Glycosylation ····· 82
4. Heptadecafluorooctanesulfonic Acid-Catalyzed Stereoselective Glycosylation of Acyl Glycosides ····· 82

H. Synthesis and Conformational Study of Multibridged [3_n]Cyclophanes ····· 82
1. Synthesis of [3_4](1,2,3,5)-and (1,2,4,5)Cyclophanes ····· 83
2. Synthesis and Conformational Study of [3_5](1,2,3,4,5) and [3_6](1,2,3,4,5,6)Cyclophanes ····· 83
3. A MNDO-PM3 Study on the Conformation of Multibridged [3_n]Cyclophanes ····· 83
4. A Conformational Study of [3.3]Metacyclophanes through Variable Temperature ^{1}H NMR and Optical Rotation ····· 83
5. A Conformational Study of [3.3](2,6)Pyridinophanes by Dynamic NMR Method ····· 84
6. Synthesis of Novel Cyclophane Host Molecules Constructed with [3.3]Metacyclophane Units ····· 84

I. Transannular π-π Interaction of (4n)π Systems ····· 85
1. Synthesis and Transannular π-π Interaction of [3.3]Cyclophanes Containing 1,6-Methano[10]annulenes ····· 85

J. Structure-Reactivity Relationship in the Gas Phase ····· 85
1. Substituent Effects of Gas Phase Acidities. Intrinsic Resonance Demand of Negative Ions ····· 86
2. Effect of the Twisted Nitro Group on Gas Phase Acidities of Benzoic Acid, Toluene, Aniline, and Phenol ····· 86
3. Electron Affinities of 2,6-Dimethyl-4-substituted Nitrobenzenes. Substituent Effect on the Stability of Radical Anions ····· 86
4. The Acidities of 4-Substituted Benzoic, Bicyclo[2.2.2]oct-l-yl and Bicyclo[2.2.2]oct-2-enyl Caboxylic Acids ····· 86
5. Theoretical Study on Resonance Demand of Carbenium Ions ····· 87

RESEARCH ACTIVITIES VI
DEPARTMENT OF VACUUM UV PHOTOSCIENCE ····· 88

A. Two-Color cm^{-1}—Resolution Threshold Photoelectron Spectroscopy for Studying Molecular Cations ····· 88
1. REMPI Threshold Photoelectron Spectra of the *cis* and *trans* Rotational Isomers of Jet-Cooled *m*-chlorophenol ····· 88
2. Observation of Torsional Motion in the Ground-State Cation of Jet-Cooled Tolane by Two-Color Threshold Photoelectron Spectroscopy ····· 88
3. Cation Vibrational Spectroscopy of *trans* and *gauche n*-Propylbenzene Rotational Isomers. Two-Colar Threshold Photoelectron Study and *Ab Initio* Calculations ····· 88
4. Vibronic Coupling in the Ground Cationic State of Naphthalene: A Laser Threshold Photoelectron Spectroscopic Study ····· 88
5. Absence of Photoelectron Spectroscopic Evidence for 'Proton Tunneling' in the Cation Ground State of Jet-Cooled Tropolone ····· 89
6. Spectroscopic Studies on 'Proton Tunneling' in the Cation Ground State of 9-Hydroxyphenalenone(9-HPO) ····· 89
7. Two-Color (1+1') REMPI Threshold Photoelectron Study of 2-Hydroxypyridine ····· 90
8. Vibrational Spectra of Aniline-Ar$_n$ van der Waals Cations(n=1 and 2) observed by Two-Color "Threshold Photoelectron" [Zero Kinetic Energy (ZEKE)-Photoelectron] Spectroscopy ····· 90
9. Two-Color (2+1') Multiphoton Ionization Threshold Photoelectron Study of the Ar-NO van der Waals Complex: observation of Intermolecular Vibrational Progressions of the Ar-NO$^+$ Cation ····· 91
10. Laser Threshold Photoelectron Spectra of the *cis* and *trans* Rotational Isomers of *p*-Dimethoxybenzene-Ar$_n$(n=0,1,2): Observation of the Intermolecular van der Waals Stretching and Bending Vibrational Modes in the Cation ····· 91
11. A Study of Phenylacetylene(PA) and Styrene(ST), and Their Argon Complexes, PA-Ar and ST-Ar, with Laser Threshold Photoelectron Spectroscopy ····· 91

12. REMPI Spectroscopic Evidence for Pseudo Rotation in 3*s* Rydberg State of Tetrahydrofuran ····· 92
13. Large-Amplitude Torsional Motion in Ground-State Cation of Jet-Cooled Biphenyl and 4-Fluorobiphenyl observed by Two-Color Threshold Photoelectron Spectroscopy ····· 92
14. Butterfly Motion in the Ground-State Cation of Jet-Cooled 1,2,4,5-Tetrafluorobenzene observed by Two-Color Threshold Photoelectron Spectroscopy ····· 93

B. Synchrotron Radiation Researches of Molecules and Molecular Clusters: Photoionization and Photoelectron Spectroscopy ····· 93
1. Energy Partitioning in the Dissociation Reaction $Ar_3^+ \rightarrow Ar_2^+ + Ar$ ····· 93
2. Photoelectron Spectra of Acetone and Acetone Dimer ····· 93
3. Dissociation Dynamics of CH_4^+ $^2A_1$State ····· 94
4. Improvement of the Photoelectron-Photoelectron Coincidence Spectrometer and the Development of a Program for Displaying the High-Resolution Three-Dimensional Spectrum ····· 94

C. Molecular Beam Studies of Gas Phase and Surface Rection Dynamics ····· 95
1. Translational-Surface Vibrational Energy Transfer in the Collisions of Hyperthermal Xe with Hydrogen-Terminated Si(100) Surface ····· 95
2. Construction of a Molecular Beam-Surface Scattering Apparatus with an Electron Bombardment Ionization Mass Spectrometer Detector ····· 95

D. Vacuum UV Photochemistry of Molecules and Clusters ····· 96
1. Photo-induced Processes of Cl_2 ($1^1\Sigma_u^+$) State Studied by VUV/UV-fluorescence Life-time Measurements ····· 96
2. Construction of a High Temperature Gas Cell for Absorption Spectral Measurements in the Vacuum UV Region ····· 97
3. Fluorescence Polarization Measurements of CN(B → X) Formed in the Photodissociative Excitation Process of ClCN ····· 97
4. Vacuum Ultraviolet Absorption Spectra and Photodissociative Excitation of $CHBr_2Cl$ and $CHBrCl_2$ ····· 97

E. Surface Molecular Dynamics Sensitive to the Structure of Reaction Sites ····· 98
1. Anisotropic Velocity Distribution of Desorbing Product in Carbon Monoxide Oxidation on Palladium(110) ····· 98
2. Reaction Diagram of Carbon Monoxide and Oxygen on Palladium(100) and Angular Distribution of Reactive Carbon Dioxide Desorption ····· 98

F. Synchrotron Radiation Stimulated Surface Reactions ····· 98
1. Fundamental Processes and Reaction Dynamics in Synchrotron Radiation Stimulated Semiconductor Processing ····· 98
2. Development of New Techniques for Synchrotron Radiation Stimulated Desorption ····· 99
3. Mechanisms of Synchrotron Radiation-Excited Etching Reactions of Semiconductor Materials ····· 99

G. Study of Ion-Pair Formation in the Vacuum Ultraviolet Region Using Synchrotron Radiation ····· 99
1. Ion-Pair Formation in Acetylene ····· 99
2. Ion-Pair Formation in Ethane ····· 100

H. Positive Ion-Negative Ion Coincidence Spectroscopy Using Synchrotron Radiation ····· 100
1. Positive Ion-Negative Ion Coincidence Spectroscopy —I— Experimental Technique ····· 100
2. Positive Ion-Negative Ion Coincidence Spectroscopy —II— Ion-Pair Formation from O_2 ····· 101

I. Transition-State Spectroscopy by Photodetachment of Solvated Cluster Anions ····· 101
1. Mass Spectrometry of Positive and Negative Cluster Ions Using Beam-Modulated Time-of-Flight Method ····· 102

J. Preparation and Characterization of Semiconductor Thin Films by New Excitation Processes ····· 102
1. Vacuum-ultraviolet-light-induced Defects in Hydrogenated Amorphous Silicon Films ····· 102
2. Optical Transitions in RF Sputtered $CuIn_xGa_{1-x}Se_2$ Thin Films ····· 103
3. Thin Films of $CuInSe_2$ Prepared by RF Sputtering from Various Compositional Powder Targets ····· 103
4. Effect of Ar Laser-illumination upon ZnTe Growth in Atmospheric-pressure MOVPE ····· 103
5. Chemical Etching of Indium Nitride ····· 103
6. Anisotropic and Damageless Etching of Single-crystalline Silicon Using Chlorine Trifluoride Molecular Beam ····· 103
7. Plasmaless Etching of Silicon Using Chlorine Trifluoride ····· 104

K. Photochemistry of Organometallic Complexes Adsorbed on Solid Surfaces ····· 104
1. Spectroscopic Studies on Adsorption States of Iron Pentacarbonyl Adsorbed on Titanium Dioxide ····· 104
2. Mechanism of the Photolysis of Iron Pentacarbonyl Adsorbed on a Pt Surface ····· 104
3. Photochemistry of Nickel Tetracarbonyl Adsorbed on Silica ····· 104
4. IRAS,XPS, and TPD Study on the Adsorption and Decomposition of $Fe(CO)_5$ on Silver Surface ····· 105

5. Photochemistry of $Fe(CO)_5$ Adsorbed on Silver 105
L. Studies on Catalysis for Automobile Exhaust and Energy Resources 105
1. Activity Enhancement of Copper-containing Oxide Catalysts by Addition of Cesium in the Reduction of Nitric Oxide 105
2. Influence of Hydrocarbons and Water on the NO_x Reduction over Copper-containing Oxide Catalysts 105
3. Photochemical Diode of TiO_2 Film Prepared on SnO_2 Film 105

RESEARCH ACTIVITIES VII
COORDINATION CHEMISTRY LABORATORIES 107

A. Developments of Diastereoisomers of Metal Complexes Having Various Combinations of Chiral Elements 107
1. Helically Chiral Trinuclear Complexes with Ferrocene Group 108
2. Carbon-carbon Bond Formation in Helical Nickel(II) Complex 108
3. Crystal and Molecular Structure of Tetra-palladium Cluster with a C,N,S-Tridentate Ligand 108
4. Rotamers of 1-Phenylethylamine Ligands in (R,S)-and (S,S)-trans-Bis(succinimidato)bis(1-phenylethylamine) palladium(II) Complexes 108
5. Rotamers of 1-Phenylethylamine Ligands in trans-Bis(cyclicimidato) bis (1-phenylethylamine)copper(II)Complexes 108

B. Syntheses, Structures and Functions of Chromotropic Complexes 108
1. Synthesis of Fe(II) Complexes with Aminomethylpyridine Derivatives and Their Spin-crossover Phenomena in Solution 108
2. Mixed Ligand Complexes as Anion Sensing Materials 108
3. Synthesis of Dinuclear Complexes Composed by Mono-nuclear Mixed Ligand Complexes 109

C. Thermodynamic and Molecular Approach to the Solute-Solvent Interaction in Solutions 109
1. A Simple Method for the Evaluation of Enthalpy of Proton Dissociation in Water 109
2. Effects of Molecular Conformation on the Packing Density in the Liquid State. 3. Partial Molar Volume Differences of Cis and Trans Conformers at Infinite Dilution 109
3. Partial Molar Volumes of Halogeno Complexes of Platinum and Palladium in Aqueous Solutions and Differences in Volume between Tetra-and Hexa-coordinated Forms 110

D. Structures and Thermodynamics of Ionic and Molecular Ensembles in Solution 110
1. Protonation Equilibria of Nitrilotris(methylenephosphonato)-and Ethylenediaminetetrakis (methylenephosphonato)-Complexes of Scandium, Yttrium, and Lanthanoids 110
2. Structure and NMR Behavior of Cobalt(III)—Polyamine Complexes of Nitrilo-tris(methylenephosphonate) in Aqueous Solution 110
3. Thermodynamic Study of Steric Effect on the Formation of Tetrahedral Pyridine Base Complexes of Cadmium Halides. 110
4. Thermal Properties of Mixed-Ligand Complexes of Transition Metal Chlorides Containing Substituted Pyridines 111
5. Liquid-Liquid Extraction of Alkali and Alkaline-Earth Metals with Non-ionic Surfactant Having a Poly(oxyethylene) Chain (Triton X-100) 111
6. The Solvent Extraction and Dissociation of the Ion Pair of Alkali Metals Complex of Monodisperse Poly (oxyethylene) derivatives with Picrate Ion 111
7. Adsorption of Phosphate on Vaterite 112
8. High Sensitive Spectrophotometer System Coupled with Solvent Extraction/Continuous Phase Separation 112

E. Cyclometallation of Heterocyclic Aromatic Compounds 112
1. Cyclometallation of N,N-Dimethylfuran-2 (and 3)-carboselenoamide with Palladium(II), Rhodium(III), and Ruthenium(II) 112
2. Cyclopalladated N,N-Dimethylthiophene-2-, and -3-carboselenoamide Derivatives 112
3. Cyclorhodation of N,N-Dimethylthiophene-2 (and 3)-carbothio (and seleno) amide 112

F. Structure of Liquids 113
1. Intramolecular and Liquid Structures of Tetramethylurea Studied by Means of X-Ray Diffraction 113

G. Structures of Solvated Metal Ions and Complexes in Solution 113
1. X-Ray Diffraction Studies on the Structure of the Tri-and Tetrathiocyanatomanganate(II) Complexes and Solvated Lithium Ion in *N,N*-Dimethylformamide 113
2. EXAFS and X-Ray Diffraction Studies on the Structure of the Tetrathiocyanatocadmate(II) Complex in Dimethyl Sulfoxide 113
3. Density Functional Calculations on the Geometries and Dissociation Energies of $[M(H_2O)_6]^{2+}$ Ions. M^{2+}=Cr^{2+}, Mn^{2+}, Fe^{2+}, Co^{2+}, Ni^{2+}, Cu^{2+}, and Zn^{2+} 113
4. Structure of Divalent Transition-Metal Complexes at Consecutive Step of Interaction with Halide and Thiocyanate Ions in Solution 114

H. Crystal Structure of Metal Complexes 114
1. X-Ray Structural Studies of $FeCl_2 \cdot 4H_2O$, $CoBr_2 \cdot 4H_2O$, $NiCl_2 \cdot 4H_2O$ and $CuBr_2 \cdot 4H_2O$. *cis*/*trans* Selectivity in Transition Metal(II) Dihalide Tetrahydrate 114
2. Structure of $2RbCl \cdot CuCl_2 \cdot 2H_2O$ 114

I. Molecular Dynamics Simulations of Electrolyte Solutions 114
1. Dissolution and Nucleation Phenomena of Salts in Water. Molecular Dynamic Approaches and Supporting Solution X-Ray Diffraction Measurements 114
2. Molecular Aspects on the Dissolution and Nucleation of Ionic Crystals in Water 115

J. Developments of Novel Multi-functionalized Macrocyclic Compounds and Their Metal Complexes 115
1. A Versatile Macrocyclic [12]aneN_3 for Interconversion of Tetrahedral and Trigonal Bipyramidal Zinc(II) Complexes. Relevance to Four-⇌Five-Coordinate Geometries of Zinc(II) in Carbonic Anhydrase 115
2. The Gold(III)-Cyclam Complexes. X-ray Crystal Structure and Macrocyclic Effect on Reduction of Gold(III) for Development of New Plating 115
3. The First Anionic Sulfonamide-Binding Zinc(II) Complexes with a Macrocyclic Triamine: Chemical Verification of the Sulfonamide Inhibition of Carbonic Anhydrase 116
4. The pH-dependent Coordination Mode of New Bleomycin Synthetic Analogues with Copper(II), Iron(II), and Zinc(II) 116
5. A New Nickel(II) Cyclam Complex Covalently Attached to $Ru(phen)^{2+}$. A New Candidate for the Catalytic Photoreduction of Carbon Dioxide 117
6. A Model for Catalytically Active Zinc(II) Ion in Liver Alcohol Dehydrogenases: A Novel "Hydride Transfer" Reaction Catalyzed by Zn^{II}-Macrocyclic Polyamine Complexes 117
7. Inversion of DNA Helicity Induced by Zinc(II)-Macrocyclic Polyamine Complexes 117

K. Bioinorganic Studies on Metalloporphyrins 118
1. New Mode Complexation of Porphyrin with Nucleobase 118
2. Olefin Oxidation Catalyzed by Electron Deficient Metallo-Porphyrin 118
3. Selective Syntheses of Unsymmetrical Meso-Arylporphyrins 118
4. Iron(III) Porphyrins Substituted with Highly Electron-Withdrawing CF_3 Group: Electronic Absorption MCD, and EPR Spectral Study 118
5. Bis(1-methylimidazole)iron(II) Complex of Porphyrins Substituted with Highly Electron-Withdrawing CF_3 Groups: Electronic Spectra with Split Q-Bands and MCD Spectra with Unusual Features 119
6. Molecular Recognition of Quinones: Two Point Hydrogen-Bonding Strategy for the Construction of Face-to-Face Porphyrin-Quinone Architectures 119

L. Structure and Chemical Properties of Transition Metal Complexes Relevant to Homogeneous Catalysis 119
1. Palladium and Platinum Complexes with π-Allyl and Carbonato Ligands 119
2. Oxidation and Reduction of Polyaniline 119

M. Synthesis of Optically Active Complexes and their Catalytic Properties 120
1. Structure of Two Geometrical Isomers of Dioxo[(*S*)-N-Salicylidene-3-aminopyrrolidine]vanadium(V) 120

N. Chemical Simulation of Biological Nitrogen Cycle and Carbon Dioxide Fixation 120
1. Characterization of Formyl-and Hydroxymethyl Ru(II) Complex as Precursors for Methanol Formation 120
2. Denitrification of NO_2^- on a Copper Site in Water 121
3. Electrochemical Carbon Dioxide Fixation to Thioesters Catalyzed by $[Mo_2Fe_6S_8(SEt)_9]^{3-}$ 121
4. Stabilization of Superoxide Form of an Fe_3S_4 Cluster in Aqueous Media 121
5. Comparative Study on Crystal Structures of $[Ru(bpy)_2(CO)_2](PF_6)_2$, $[Ru(bpy)_2(CO)(C(O)OCH_3)]B(C_6H_5)_4 \cdot CH_3CN$, and $[Ru(bpy)_2(CO)(\eta^1\text{-}CO_2)] \cdot 3H_2O$ (bpy=2,2'-bipyridyl) 122

O. Development of Highly Selective Reactions Using Early Transition Metal Complexes 122
1. Hydrosilation Reactions Catalyzed by Zirconium Complexes 122
2. Novel Head-to-Tail Alkyl-Alkene Coupling via Zirconium Catalyzed Reactions of Alkylmagnesium Derivatives with Monosubstituted Alkenes 123
3. Zirconium Mediated Regioselective Carbon-Carbon Bond Formation Reactions 123
4. Monohalogenation of Zirconacyclopentane Complexes via Alkylalkoxyzirconocene 123
5. Factors Affecting the Unusual Reactivity Order in the β-Hydrogen Abstraction of Dialkylzirconocenes 123

P. Chemistry of Polynuclear Metal Complexes 123

1. Tri-and Tetra-Nuclear Platinum(II) Cluster Complexes Having Novel Triangular Core ····· 124
2. Mixed Chromium(III)-Ruthenium(III) Trinuclear Complex, $[CrRu_2(\mu_3\text{-}O)(\mu\text{-}CH_3COO)_6(pyridine)_3]^+$ ····· 124
3. Multi-Step Redox Behavior of Oxo and Acetato-Bridged Ruthenium and Rhodium Trinuclear Complexes Having Redox-Active Ligand, *N*-Methyl-4,4'-Bipyridinium Ion ····· 124
4. Photosubstitution of Carbonyl Ligand in $[Ru_3(\mu_3\text{-}O)(\mu\text{-}CH_3COO)_6(CO)(L)_2]$ (L=pyridine, 4-cyanopyridine, methanol) in Acetonitrile and Application to the Syntheses of Nitrosyl and Phosphine Complexes ····· 125

Q. Study of Dinuclear and Polynuclear Metal Complexes ····· 125
1. Synthesis and Characterization of a Novel Tetranuclear Iron(II,III,II,III) Mixed Valence Complex: the Reaction Product of Dinuclear Iron(II,II) Complex with Molecular Oxygen ····· 126
2. Syntheses, Characterization, and Redox Behavior of Dinuclear Di(μ-oxo)dimanganese(III,IV) and (IV,IV) Complexes with Coordinated Imidazole Groups ····· 126
3. Mono and Dinuclear Copper(I) Complexes: Syntheses and Reaction with Molecular Oxygen ····· 126
4. Dinuclear Cobalt(II,II) Complexes with an Unsymmetrical Dinucleating Ligand: Syntheses and Reaction with Molecular Oxygen ····· 127
5. Syntheses and Characterization of Novel Linear Tetranuclear Manganese (II,III,III,II) and (II,III,IV,II) Complexes with Di(μ-oxo) Mn_2 core ····· 127
6. Dinuclear Iron(II,II) Complexes with an Unsymmetrical Dinucleating Ligand: Syntheses and Reaction with Molecular Oxygen ····· 127

RESEARCH ACTIVITIES VIII

COMPUTER CENTER ····· 128

A. Theoretical Investigations of Structures and Properties of Molecular Assemblies ····· 128
1. Theoretical Study of Structure and Thermodynamic Properties of Liquid Hydrogen Fluoride ····· 128
2. A Study on GABA and Their Analogues with the Molecular Orbital Method ····· 128

CHEMICAL MATERIALS CENTER

B. Preparation and Propeties of Novel Heterocyclic Compounds ····· 128
1. Structure and Redox Reactions of Tricyclic Pyridinium N-Imines ····· 129
2. Tetracyanoquinodimethines Fused with 1,2,5-Thiadiazole and Pyrazine Units ····· 129
3. 5,8-Bis(1,3-dithiol-2-ylidene)-4,7-dihydro-2,1,3-benzothiadiazoles. Novel Electron Donors Affording Organic Metals ····· 129
4. Tetrathio-Derivatives of *p*-Quinodimethanes Fused with Selenadiazole Units: A Novel type of Electron Donors ····· 129
5. Clathrate Formation and Molecular Recognition by Novel Chalcogen-Cyano Interactions in Tetracyanoquinodimethanes Fused with Thiadiazole and Selenadiazole Rings ····· 130
6. Tetrathienylethylenes, a New Class of Electron Donors—Dications Twisted by 90° Stabilized by Formation of Polymethine Units ····· 130
7. Preparation and Properties of Poly-4-(1,3-dithiol-2-ylidene)-4H-cyclopenta[2,1-b; 3,4-b']dithiophene and Its Derivatives ····· 130
8. Narrow Band Gap Conjugated Polymers Containing Thieno[3,4-c][1,2,5]thiadiazole Units ····· 130

INSTRUMENT CENTER

C. Studies of Solvated Metal Clusters ····· 131
1. Photoionization Study on $Cs(CH_3CN)_n$ Clusters ····· 131
2. Contruction of an Apparatus for Photoelectron Spectroscopy of Mass-Selected Cluster Anions ····· 132
3. Intracluster Reaction in the Formation of Mg^+-Water and Ca^+-Water Clusters ····· 132
4. Photodissociation Spectroscopy of $Mg^+(H_2O)_n$ ····· 132
5. Photoinduced Intracluster Reaction of $Mg^+(H_2O)_n$ Ions ····· 133
6. Photodissociation Spectroscopy of $Ca^+(H_2O)$ ····· 134
7. Formation of Alkali Halide Cluster Ions Solvated with Water ····· 134

D. Physical Properties of Semiconductor Clusters ····· 135
1. Generation of VUV Radiation by High-Order Anti-Stokes Raman Scattering ····· 135
2. Photoionization of Small Silicon Clusters: Ionization Potentials for Si_2 and Si_{40} ····· 135

E. Interatomic Potentials and Inter- and Intra-Multiplet Relaxation of the Excited Group IIB Metal Atoms ····· 136
1. Intersystem Crossing and Intramultiplet Mixing of Excited Zn Atoms by Xe ····· 136

F. Studies of Ultrafine Particles ····· 136
1. Size Dependence of Critical Exponent for ESR Linewidth Observed in Ultrafine MnF_2-IV (metastable phase) Particles ····· 136

G. Formation and Physical Properties of Fullerenes and Metallofullerenes ····· 136

1. Collection Technique under Anaerobic Condition for Fullerenes/or Metallofullerenes Produced by the Gas-Flow Arc Discharge Method 137
2. Anaerobic Sampling and Characterization of Lanthano-Fullerenes: Extraction of LaC_{76} and Other LaC_{2n} 137

LOW-TEMPERATURE CENTER

H. Ferromagnetic Interactions in Molecular Crystals 138
1. α-Nitronyl Nitroxide Cation Radicals 138
2. Ferromagnetic Intermolecular Interaction and Crystal Structure of the *p*-Pyridyl Nitronyl Nitroxide Radical 138
3. Ferromagnetic and Antiferromagnetic Intermolecular Interactions in the Two-Dimensional Triangular Lattice of the *m-N*-Methylpyridinium Nitronyl Nitroxide Cation Radical 138

EQUIPMENT DEVELOPMENT CENTER

I. Activities of Division of "IMS Machines" 138
1. Fast Scan Cyclic Voltammetry with Ultra-Microdisk Electrode 139
2. Ultra-High-Vacuum and Low-Temperature Sample Transfer System for XPS 139

J. Development of Experimental Devices 140
1. Pulse Generator for the Time-of-Flight Mass Spectrometer 140

K. New Materials Research 141
1. Preparation, Separation, and Purification of C_{60}, C_{70}, and Higher Fullerenes 141

L. Studies of Halogen-Bridged Mixed-Valence Systems 141
1. Photo-Generation of Solitons and Polarons in the 1-D Halogen-Bridged Metal Complexes 142
2. Control of CT Instability in 1-D Mixed-Valence Systems 142
3. Electrical Conductivity of the Perovskite-Type Mixed-Valence Compound $Cs_2Au_2I_6$ under High Pressure and Low Temperature 142

M. Studies of H-Bonded CT Complexes 142
1. A New Two-Band System of *d* and π with Interband H Bridges 142
2. X-Ray Photoelectron Spectroscopic Study of H-Bonded CT Complexes 143
3. Infrared Spectroscopy of One-Dimensional Hydrogen-Bonded System 143
4. Intra-and Inter-Molecular Charge Transfer Interactions in H-Bonded DTPP Crystals 144

ULTRAVIOLET SYNCHROTRON ORBITAL RADIATION FACILITY

N. Development of UVSOR Light Source 144
1. Control of the Bunch Length of Electron Beam on the UVSOR Storage Ring 144
2. Free Electron Laser Experiments on the UVSOR Storage Ring 145

O. Development of Beamlines and Equipment for UVSOR 146
1. Test of Holographic SiC Gratings for High-Power Synchrotron Radiation 146

P. Researches by the Use of UVSOR 146
1. X-Ray-Absorption Near-Edge Structure of Solid Rare Gases 146
2. Photo-Stimulated Desorption Study of Ground and Excited State Alkalis from Alkali Halides by using Synchrotron Radiation 147
3. Adsorption of K on the Si(100) and Si(111) Surfaces: Core-Level Photoemission Study 147

RESEARCH FACILITIES 148

Computer Center 148

Chemical Materials Center 148

Instrument Center 148

Low-Temperature Center 148

Equipment Development Center 149

Ultraviolet Synchrotron Orbital Radiation Facility 149

SPECIAL RESEARCH PROJECTS 150

OKAZAKI CONFERENCES 158

JOINT STUDIES PROGRAMS 161
1. Special Projects 161
2. Research Symposia 163
3. Cooperative Research 163
4. Use of Facility 163
5. UVSOR 163

FOREIGN SCHOLARS 165

AWARD 169
LIST OF PUBLICATIONS 170
AUTHOR INDEX-RESEARCH ACTIVITIES AND SPECIAL RESEARCH PROJECTS 185

ORGANIZATION AND STAFF

Organization

The Institute for Molecular Science comprises twenty two research laboratories—each staffed by a professor, an associate professor, two research associates and several technical associates—, two research laboratories with foreign visiting professors, and six research facilities. The laboratories are grouped into six departments and one facility for coordination chemistry:

Department of Theoretical Studies	Theoretical Studies I
	Theoretical Studies II
	Theoretical Studies III[1)]
Department of Molecular Structure	Molecular Structure I
	Molecular Structure II[1)]
	Molecular Dynamics
Department of Electronic Structure	Excited State Chemistry
	Excited State Dynamics
	Electronic Structure[1)]
	Molecular Energy Conversion[2)]
Department of Molecular Assemblies	Solid State Chemistry
	Molecular Assemblies Dynamics
	Molecular Assemblies[1)]
Department of Applied Molecular Science	Applied Molecular Science I
	Applied Molecular Science II[1)]
	Physical Organic Chemistry[3)]
Department of Vacuum UV Photoscience	Photochemistry
	Chemical Dynamics
	Interface Molecular Science[3)]
	Synchrotron Radiation Research[2)]
Coordination Chemistry Laboratories	Synthetic Coordination Chemistry[3)]
	Complex Catalysis
	Functional Coordination Chemistry
	Coordination Bond[1)]
Research facilities are:	Computer Center
	Chemical Materials Center
	Instrument Center
	Low-Temperature Center
	Equipment Development Center
	Ultraviolet Synchrotron Orbital Radiation (UVSOR) Facility

1) Professors and associate professors are adjunct professors from other universities.
2) Research Laboratories with foreign visiting professors.
3) Professors, associate professors, and research associates, along with their positions, are transferred from other universities.

Scientific Staff

Hiroo INOKUCHI	**Professor, Director-General**

Department of Theoretical Studies

Theoretical Studies I

Keiji MOROKUMA	Professor
Iwao OHMINE	Associate Professor
Nobuaki KOGA	Research Associate
Norihiro SHIDA	Research Associate
Yoshiaki AMATATSU	Technical Associate (—March '92)[1]
Shinji SAITO	Technical Associate
Jerzy MOC	JSPS Post-Doctoral Fellow
Djamaladdin G. MUSAEV	JSPS Post-Doctoral Fellow
Jean -F. RIEHL	JSPS Post-Doctoral Fellow (February '92—)
Feliu MASERAS	Research Fellow
Fujiko HASHIMOTO	Research Fellow
Satoru YOSHIDA	Visiting Research Fellow
Tamiki KOMATSUZAKI	Graduate Student
Toshiaki FUJII	Graduate Student
Chizuru MUGURUMA	Graduate Student
Masakatsu ITO	Graduate Student (April '92—)
Masakazu MATSUMOTO	Graduate Student (April '92—)

Theoretical Studies II

Hiroki NAKAMURA	Professor
Keiichiro NASU	Associate Professor
Kaoru IWANO	Research Associate
Masato SUZUKI	Technidal Associate (—March '92)[2]
Shoji TAKADA	Technical Associate
Itsuki BANNO	Technical Associate
Kengo MORIBAYASHI	IMS Fellow (April '92—)
Yasuji INADA	JSPS Post-Doctoral Fellow (April '92—)
Chayugan ZHU	Graduate Student
Kenichiro TSUDA	Graduate Student
Tomiyuki TSUBO	Graduate Student (April '92—)

Theoretical Studies III

Shigeki KATO	Adjunct Professor from Kyoto University (April '92—)
Kouichi YAMASHITA	Adjunct Associate Professor from Institute for Fundamental Chemistry
Kenro HASHIMOTO	Research Associate
Kiyohiko SOMEDA	Research Associate

Department of Molecular Structure

Molecular Structure I

Shuji SAITO	Professor
Norio MORITA	Associate Professor
Shuro TAKANO	Research Associate (November '91—)
Asuka FUJII	Research Associate
Mitsutaka KUMAKURA	Technical Associate
Masahiro GOTO	Graduate Student from Nagoya Univ. (October '91—)

Molecular Structure II

Hiroatsu MATSUURA	Adjunct Professor from Hiroshima Univ.
Tsutomu YABUZAKI	Adjunct Associate Professor from Kyoto Univ. (—March '92)
Kentaro KAWAGUCHI	Adjunct Associate Professor from National Astronomy Observatory (April '92—)
Takashi OGURA	Reseach Associate

Molecular Dynamics

Teizo KITAGAWA	Professor
Tatsuhisa KATO	Associate Professor (March '92–)
Keiji KAMOGAWA	Research Associate
Tsuyoshi EGAWA	Research Associate (–March '92)[3]
Misaki OKUNISHI	Research Associate (–June '92)[4]
Shin-ichiro SATO	Technical Associate
Motoko SOMEDA-ASANO	IMS Fellow (–September '91)[5]
Satoru NAKASHIMA	IMS Fellow (April '92–)
Shoji KAMINAKA	JSPS Post-Doctoral Fellow
Yasuhisa MIZUTANI	Graduate Student (–March '92), JSPS Post-Doctoral Fellow (April '92–)
Satoshi TAKAHASHI	Graduate Student (–March '92), JSPS Post-Doctoral Fellow (April '92–)
Hisashi HAYASHI	Graduate Student (–March '92)[6]
Yoshinao SAKAN	Graduate Student
Shun HIROTA	Graduate Student (April '92–)
Du-Jeon JANG	Visiting Scientist from Seoul National Univ. (December '91–February '92)
Philip. J. JEWSBURY	JSPS Post-Doctoral Fellow (February '92–)

Department of Electronic Structure

Excited State Chemistry

Keitaro YOSHIHARA	Professor
Yoshiyasu MATSUMOTO	Associate Professor
Hrvoje PETEK	Research Associate
Kyoichi SAWABE	Research Associate
Keisuke TOMINAGA	Research Associate (July '92–)
Shigeichi KUMAZAKI	Technical Associate
Hideki KANDORI	IMS Fellow
Ryoji INABA	Graduate Student from the Univ. of Tokyo
Yutaka NAGASAWA	Graduate Student
Valey F. KAMALOV	Visiting Scientist (October '91–May '92)
Irina STRUGANOVA	Visiting Scientist (October '91–May '92)
Abderrazzak DOUHAL	JSPS Post-Doctoral Fellow (–March '92)
Bongsoo KIM	Inoue Science Foundation Fellow (–September '91), JSPS Post-Doctoral Fellow (October '92–)
Andrew J. BELL	JSPS Post-Doctoral Fellow (–October '91)
Arkady YARTSEV	JSPS Post-Doctoral Fellow (October '91–)
Prem B. BISHT	Post-Doctoral Fellow (October '91–)
Young S. CHOI	Visiting Scientist (July '92–August '92)
Keith A. NELSON	Visiting Scientist (July '92–August '92)
Ronald L. CHRISTENSEN	Visiting Scientist (July '92–August '92)
John H. FREDERICK	Visiting Scientist (May '92–July '92)

Excited State Dynamics

Ichiro HANAZAKI	Professor
Nobuyuki NISHI	Professor (–September '91)[7]
Toshinori SUZUKI	Associate Professor (June '92–)
Masao TAKAYANAGI	Research Associate
Teruhiko NISHIYA	Technical Associate
Hong-Lae KIM	Visiting Scientist from Kangweon National University, Korea (June '92–August '92)
Kazuhiro HONDA	Graduate Student
Takumi KOHNO	Graduate Student
Tetsuo SEKIGUCHI	Graduate Student
Tatsuo GEJOH	Graduate Student
Noriaki OKAZAKI	Graduate Student

Electronic Structure

Michiya ITOH	Adjunct Professor from Kanazawa Univ. (–March, '92)
Toru AZUMI	Adjunct Professor from Tohoku Univ. (April, '92–)
Minoru SUMITANI	Adjunct Professor from Shizuoka Institute of Science & Technology
Kaoru SUZUKI	Research Associate
Yoshihito MORI	Research Associate

Molecular Energy Conversion

Raymond A. BORKMAN	Visiting Professor from Georgia Institute of Technology, U.S.A. (September '91–June '92)

Department of Molecular Assemblies

Solid State Chemistry

Kyuya YAKUSHI	Professor
Kazushi KANODA	Associate Professor
Akito UGAWA	Research Associate
Yasuhiro NAKAZAWA	Research Associate (April '92–)
Ken-ichi IMAEDA	Technical Associate
Atsushi KAWAMOTO	IMS Fellow (–March '92), Visiting Research Fellow (April '92–)
Hideo YAMAKADO	Graduate Student (–January '92)[8]
Kentaro IWASAKI	Graduate Student

Molecular Assemblies Dynamics

Yusei MARUYAMA	Professor
Seiichi MIYAJIMA	Associate Professor (August '92–)
Tamotsu INABE	Research Associate (–March '92)[9]
Shinji HASEGAWA	Research Associate
Hajime HOSHI	Technical Associate
Roger WHITEHEAD	JSPS Post-Doctoral Fellow
Toshifumi TERUI	Graduate Student
Hironori OGATA	Graduate Student
Yoshihisa MORI	Graduate Student
Shaoli FANG	Graduate Student
Atsushi SUZUKI	Graduate Student
Chikako NAKANO	Visiting Research Fellow
Naoki NAKAMURA	Visiting Research Fellow from Toyota Motor Co. Ltd. (–March '92)
Keiichi KOHAMA	Visiting Research Fellow from Toyota Motor Co. Ltd. (April '92–)
Zhongfang LIU	Visiting Research Fellow
Shuqin ZHOU	Visiting Research Fellow
Masatsugu SUZUKI	Visiting Research Fellow
Itsuko SUZUKI	Visiting Research Fellow

Molecular Assemblies

Satoshi HIRAYAMA	Adjunct Professor from Kyoto Institute of Technology
Kokichi OSHIMA	Adjunct Associate Professor from Okayama University
Takehiko MORI	Research Associate
Kenji FURUYA	Research Associate (–March '92)[10]

Department of Applied Molecular Science

Applied Molecular Science I

Kazuhiro NAKASUJI	Professor
Kiyoshi ISOBE	Associate Professor
Yoshiki OZAWA	Research Associate (–March '92)[11]
Yasushi MORITA	Research Associate
Makoto TADOKORO	Research Associate (May '92–)
Takanori NISHIOKA	Technical Associate (April '92–)
Kenichi SUGIURA	Graduate Student (–September '92)
Rimo XI	Graduate Student (April '92–)
Tetsuji ITOH	Graduate Student (April '92–)

Kunio HATANAKA	Graduate Student (April '92–)
Shotaro MATSUDA	Graduate Student from Ehime Univ.* (April '91–March '92)
Tian-Wei ZHU	Visiting Professor from Inner Mongolia Normal Univ., China (March '91–August '91)
Bateer WANG	Visiting Professor from Inner Mongolia Normal Univ., China (March '91–August '91)
Kuming ZHAO	Visiting Professor from Inner Mongolia Normal Univ., China (March '91–August '91)
Joon T. PARK	Visiting Professor from Korea Advanced Institute of Science and Technology, Korea (July '92–August '92)

Applied Molecular Science II

Yumihiko YANO	Adjunct Professor from Gunma Univ.
Hiyoshizo KOTSUKI	Adjunct Associate Professor from Kochi Univ.
Hiroki OSHIO	Research Associate (–February '92)[12]
Jiro TOYODA	Research Associate (December '91–), Technical Associate (–November '91)
Takayoshi SUZUKI	Research Associate (July '92–)

Physical Organic Chemistry

Yuho TSUNO	Professor (–September '91)[13]
Junji INANAGA	Associate Professor
Teruo SHINMYOZU	Associate Professor (October '91–)
Masaaki MISHIMA	Research Associate
Takeshi HANAMOTO	Research Associate
Yuji MIKATA	Graduate Student from Kyoto Univ.* (–September '91)
Kenji TAKEHARA	Graduate Student from Kyushu Univ* (–March '92)
Yoshihiro SAEKI	Graduate Student from Kyushu Univ.* (–March '92)
Yasuo YOKOYAMA	Graduate Student from Kyushu Univ.*
Yuichi SUGIMOTO	Graduate Student from Kyushu Univ.*
Shirou KUSUMOTO	Graduate Student from Kyushu Univ.* (October '91–March '92)
Satoshi OSADA	Graduate Student from Kyushu Univ.* (April '92–)

Department of Vacuum UV Photoscience

Photochemistry

Katsumi KIMURA	Professor (–March '92)[14]
Kosuke SHOBATAKE	Associate Professor
Kiyohiko TABAYASHI	Research Associate
Katsuhiko OKUYAMA	Research Associate
Masahiko TAKAHASHI	Technical Associate (–January '92), Research Associate (January '92–March '92)[15]
Haruhiko OHASHI	Graduate Student from Toyohashi Univ. of Technology (–March '92), Visiting Research Fellow (April '92), Technical Associate (May '92–)
Martin COCKETT	JSPS Post-Doctoral Fellow
Hiroyuki OZEKI	Graduate Student (–March '92), JSPS Post-Doctoral Fellow (April '92–)
Hiroshi YOSHIKAWA	Graduate Student
Mitsuhiko KONO	Graduate Student
Koji ITO	Graduate Student from Nagoya Univ. (April '92–)

Chemical Dynamics

Tsuneo URISU	Professor (May '92–)
Koichiro MITSUKE	Associate Professor
Kazuhiko MASE	Research Associate (April '92–)
Hiroaki YOSHIDA	Research Associate (April '92–)
Hideo HATTORI	Technical Associate (April '92–)

Interface Molecular Science

Akira YOSHIDA	Professor
Shinri SATO	Associate Professor

Yuichi OHNO	Research Associate
Seigi MIZUNO	Research Associate
Yuji UKISU	Technical Associate
Makoto IKEJIRI	Graduate Student from Saga Univ. (April '92–)
Toshihiro OGATA	Graduate Student from Saga Univ. (April '92–)
Qi-xin GUO	Graduate Student from Toyohashi Univ. of Technology (October '91–June '92)
Masahiro TOMIDA	Graduate Student from Toyohashi Univ. of Technology (October '91–)
Hisashi OGAWA	Graduate Student from Shinshu Univ. (April '92–)

Synchrotron Radiation Research

Andre D. BANDRAUK	Visiting Professor from Univ. de Sherbrooke, Quebec Canada (December '91–August '92)
Jerzy GORECKI	Visiting Associate Professor from Polish Acad. of Sci., Warsaw, Poland (November '91–October '92)

Coordination Chemistry Laboratories

Hitoshi OHTAKI	Director

Synthetic Coordination Chemistry

Yoshihiko KUSHI	Professor (–March '92)[16]
Yutaka FUKUDA	Professor (April '92–)
Fumio KAWAIZUMI	Associate Professor (–March '92)[17]
Kiyoshi SAWADA	Associate Professor (April '92–)
Tatsuya KAWAMOTO	Research Associate (–March '92)[18]
Matsuo NONOYAMA	Research Associate (–March '92)[19]
Hikaru ICHIDA	Research Associate (April '92–)
Keiichi SATOH	Research Associate (April '92–)
Hiroyuki YOKOYAMA	Graduate Student from Niigata Univ.
Kayoko KASAI	Graduate Student from Ochanomizu Univ.

Complex Catalysis

Hitoshi OHTAKI	Professor
Ei-ichi KIMURA	Adjunct Professor from Hiroshima Univ. (–March '92)
Hisanobu OGOSHI	Adjunct Professor from Kyoto Univ. (April '92–)
Kotaro OSAKADA	Adjunct Associate Professor from Tokyo Institute of Technology (–March '92)
Fumio KAWAIZUMI	Adjunct Associate Professor from Nagoya Univ. (April '92–)
Kiyohiko NAKAJIMA	Research Associate (–March '92)[20]
Kenji WAIZUMI	Technical Associate
Hiroshi SHIMOMURA	Graduate Student from Osaka Univ.
Masahiro TANIO	Graduate Student from Kochi Univ. (October '91–)
Tamas RADNAI	Visiting Associate Professor from Hungarian Academy of Sciences (September '91–August '92)

Functional Coordination Chemistry

Koji TANAKA	Professor
Tamotsu TAKAHASHI	Associate Professor
Hirotaka NAGAO	Research Associate
Noriyuki SUZUKI	Research Associate (October '91–)
Tetsunori MIZUKAWA	Technical Associate (April '92–)
Ryo MIYAMOTO	IMS Fellow (June '92–)
Chirstophe J. ROUSSET	JSPS Post-Doctoral Fellow (September '91–September '92)
Denis Y. KONDAKOV	JSPS Post-Doctoral Fellow (June '92–)
Victor DENISOV	CIBA-GEIGY Exchange Scientist (May '92–)
Nobutoshi KOMEDA	Graduate Student from Osaka Univ.
Hiroaki TANAKA	Graduate Student
Hide KAMBAYASHI	Graduate Student
Koichiro AOYAGI	Graduate Student (April '92–)
Motohiro KAGEYAMA	Graduate Student from Tokyo Univ. (April '92–)
Ryuichiro HARA	Visiting Research Fellow (April '92–)

Daniele CHOUEIRI	Visiting Reseach Fellow from Purdue Univ. U.S.A. (June '92—August '92)
Hideyuki MORI	Visiting Research Fellow (September '91—)
Fidefumi UCHINO	Visiting Research Fellow (April '92—)

Coordination Bond

Tasuku ITOH	Adjunct Professor from Tohoku Univ.
Masatatsu SUZUKI	Adjunct Associate Professor from Kanazawa Univ.

Research Facilities

Computer Center

Keiji MOROKUMA	Director
Kazuo KITAURA	Associate Professor
Umpei NAGASHIMA	Research Associate (—March '92)[21]
Shinkoh NANBU	Research Associate (July '92—)
Kazuhiko HONDA	Technical Associate (—February '92)[22]
Satoshi MINAMINO	Technical Associate (April '92—)

Chemical Materials Center

Kazuhiro NAKASUJI	Director
Yoshiro YAMASHITA	Associate Professor
Shoji TANAKA	Research Associate
Masaaki TOMURA	Technical Associate
Masatoshi KOZAKI	Graduate Student
Katsuhiko ONO	Graduate Student (April '92—)

Instrument Center

Shuji SAITO	Director
Kiyokazu FUKE	Associate Professor
Shunji BANDOW	Research Associate
Fuminori MISAIZU	Research Associate
Keizo TSUKAMOTO	Graduate Student
Masaomi SANEKATA	Graduate Student

Low-Temperature Center

Yusei MARUYAMA	Director
Kunio AWAGA	Research Associate (—March '92)[23]

Equipment Development Center

Teizo KITAGAWA	Director
Tadaoki MITANI	Associate Professor
Hiroshi OKAMOTO	Research Associate (—March '92)[24]
Shuji ASAKA	Research Associate
Hiroshi KITAGAWA	Research Associate
Jeung Sun AHN	Research Associate (April '92—)
Kaoru OKANIWA	Graduate Student (—March '92)[25]
Taro SEKIKAWA	Graduate Student from Univ. of Tokyo (April '92—)

Ultraviolet Synchrotron Orbital Radiation Facility

Kyuya YAKUSHI	Director
Makoto WATANABE	Associate Professor
Goro ISOYAMA	Associate Professor
Masao KAMADA	Associate Professor
Eiji ISHIGURO	Adjunct Associate Professor from Osaka City University (April '91—)
Atsunari HIRAYA	Research Associate
Shin-ichiro TANAKA	Research Associate
Shiro TAKANO	Research Associate (—March '92)[26]
Hiroyuki HAMA	Research Associate
Shigeo OHARA	IMS Fellow (April '92—)
Sayumi HIROSE	Graduate Student

Technical Staff

Akira UCHIDA	Technical Division Head
Keiichi HAYASAKA	Technical Section Chief
Kusuo SAKAI	Technical Section Chief
Fumio NISHIMOTO	Computer Center (Unit Chief)
Fumitsuna TESHIMA	Computer Center
Kunihiko TANAKA	Computer Center
Sachiyo NOMURA	Chemical Materials Center
Takaya YAMANAKA	Instrument Center
Masahiro SAKAI	Instrument Center
Kiyonori KATO	Low-Temperature Center (Unit Chief)
Takashi TAKAYAMA	Low-Temperature Center
Toshio HORIGOME	Equipment Development Center (Unit Chief)
Norio OKADA	Equipment Development Center
Mitsukazu SUZUI	Equipment Development Center
Masaaki NAGATA	Equipment Development Center
Hisashi YOSHIDA	Equipment Development Center
Shinji KATO	Equipment Development Center
Nobuo MIZUTANI	Equipment Development Center
Kouichi UCHIYAMA	Equipment Development Center
Osamu MATSUDO	UVSOR Facility (Unit Chief)
Toshio KINOSHITA	UVSOR Facility
Masami HASUMOTO	UVSOR Facility
Jun-ichiro YAMAZAKI	UVSOR Facility
Eiken NAKAMURA	UVSOR Facility

* Carries out graduate research of IMS on the Cooperative Education Program of IMS with graduate schools.

1) Present Address: Dept. of Education, Akita Univ., Tegatagakuen-cho 1-1, Akita 010
2) Present Address: The Institute of Physical and Chemical Research, Wako, Saitama 351-01
3) Present Address: Dept. of Biochemistry, School of Medicine, Keio Univ., Shinanomachi, Shinjuku-ku, Tokyo 160
4) Present Address: The Research Institute for Scientific Measurements, Tohoku Univ., 2-1-1, Katahira, Aoba-ku, Sendai 980
5) Present Address: Dept. of Chemistry, Tokyo Institute of Technology, O-okayama, Meguro-ku, Tokyo 152
6) Present Address: The Research Institute for Scientific Measurements, Tohoku Univ. Katahira, Aoba-ku, Sendai 980
7) Present Address: Dept. of Chemistry, Faculty of Science, Kyushu Univ., 6-10-1, Hakozaki, Higashi-ku, Fukuoka 812
8) Present Address: College of Arts and Science, Univ. of Tokyo, Komaba, Meguro-ku, Tokyo 153
9) Present Address: Dept. of Chemistry, Faculty of Science, Hokkaido Univ., Kita-ku, Sapporo 060
10) Present Address: Dept. of Chemistry, Faculty of Science, Kyushu Univ., 6-10-1, Hakozaki, Higashi-ku, Fukuoka 812
11) Present Address: Dept. of Materials Science, Faculty of Science, Himeji Institute of Technology, Harima Science Park City, Hyogo 678-12
12) Present Address: Dept. of Chemistry, Faculty of Science, Tohoku Univ., Aramaki, Aoba-ku, Sendai 980
13) Present Address: Dept. of Chemistry, Faculty of Science, Kyushu Univ., 6-10-1, Hakozaki, Higashi-ku, Fukuoka 812
14) Present Address: Dept. of Material Science, Japan Advanced Institute of Science and Technology, Tatsunokuchi, Ishikawa 923-12
15) Present Address: The Research Institute for Scientific Measurements, Tohoku Univ., 2-1-1, Katahira, Aoba-ku, Sendai 980
16) Present Address: College of General Education, Osaka Univ., 1-1 Machikaneyama-cho, Toyonaka 560
17) Present Address: Faculty of Engineering, Nagoya Univ., Furo-cho, Chikusa-ku, Nagoya 464
18) Present Address: College of General Education, Osaka Univ., 1-1 Machikaneyama-cho, Toyonaka 560
19) Present Address: Dept. of Chemistry, Faculty of Science, Nagoya Univ., Furo-cho, Chikusa-ku, Nagoya 464
20) Present Address: Dept. of Chemistry, Aichi Univ. of Education, Hirosawa, Igaya-cho, Kariya 448
21) Present Address: Faculty of Science, Ochanomizu Univ., 2-1- 1 Ohtsuka, Bunkyo-ku, Tokyo 112
22) Present Address: Dept. of Knowledge-Based Engineering, Toyohashi Univ. of Technology, 1-1 Hibarigaoka, Tempaku, Toyohashi 441
23) Present Address: College of Arts and Science, Univ. of Tokyo, Komaba, Meguro-ku, Tokyo 153
24) Present Address: The Research Institute for Scientific Measurements, Tohoku Univ., 2-1-1, Katahira, Aoba-ku, Sendai 980
25) Present Address: Hoechst Japan Corp., 1-3-2, Minamidai, Kawagoe 350
26) Present Address: The Institute of Physical and Chemical Research, Wako, Saitama 351-01

COUNCIL

Hiroo INOKUCHI **Director-General**

Councilors

Chairman	Ikuzo TANAKA	President, National Institute for Academic Degrees
Vice-Chairman	Yutaka TOYOZAWA	Professor, Chuo University
	Hirotsugu AKAIKE	President, The Institute of Statistical Mathematics
	Hideaki CHIHARA	Executive Director, Japan Association for International Chemical Information
	Eiichi FUJITA	Professor Emeritus, Kyoto University
	Kenichi FUKUI	President, Institute for Fundamental Chemistry
	Sachio HAYAKAWA	President, Nagoya University (—February '92)
	Yoshikazu ITO	Chairman of The Board, Toray Industries, Inc.
	Kozo KUCHITSU	Professor, Nagaoka University of Technology
	Yoshio MATSUNAGA	Professor, Kumamoto University
	Akira MIKAZUKI	Professor Emeritus, University of Tokyo
	Kazuo SAITO	Professor, International Christian University
	Hideki SAKURAI	Dean of The Faculty of Science, Tohoku University
	Hirotoshi SANO	President, Tokyo Metropolitan University
	Shinichi SASAKI	President, Toyohashi University of Technology
	Kenji TAMARU	Professor, Science University of Tokyo
	Teijiro YONEZAWA	Professor, Kinki University
	Peter DAY	Director, The Royal Institution of Great Britain
	John C. POLANYI	Professor, University of Toronto

The Council is the advisory board for the Director-General. Two of the councilors are selected among distinguished foreign scientists.

Distinguished Research Consultants

Kenichi FUKUI	President, Institute for Fundamental Chemistry
Saburo NAGAKURA	President, The Graduate University for Advanced Studies
Kenji TAMARU	Professor, Science University of Tokyo
Yasutada UEMURA	Chancellor, Musashi Gakuen

Administration Bureau

Toshio UENO	Director-General, Administration Bureau (—June '92)
Jiro SATO	Director-General, Administration Bureau (July '92—)
Satoshi FUJISAWA	Director, General Affairs Department (—March '92)
Shozo IMAKAWA	Director, General Affairs Department (April '92—)
Yasuyoshi NONAKA	Director, Finance and Facilities Department
Ryoichi ASANO	Head, General Affairs Division
Makoto SUZUKI	Head, Personnel Division
Satoru TAMURA	Head, Research Cooperation and International Affairs Division
Masaaki TSUJITA	Head, Budget Division
Saigyo KAMIYAMA	Head, Accounts Division
Masakazu SASAKI	Head, Construction Division (—March '92)
Hiromu KITAJIMA	Head, Construation Division (April '92—)
Kunikatsu SHOJI	Head, Equipment Division

BUILDINGS AND CAMPUS

The IMS campus covering 62,343 m^2 is located on a low hill in the middle of Okazaki City. The inequality in the surface of the hill and growing trees are preserved as much as possible, and low-storied buildings are adopted for conservation of the environment. The buildings of IMS are separated according to their functions as shown in the map. The Research Office Building and all Research Facilities except for the Computer Center are linked organically to the Main Laboratory Building by corridors. Computer Center, Library and Administration Buildings are situated between IMS and the neighboring National Institute for Basic Biology and National Institute for Physiological Sciences, because the latter two facilities are common to these three institutes.

The loding facility of IMS called Yamate Lodge, located within ten minutes' walk, has sleeping accommodations for 19 guests and two families. Mishima Lodge, located within four minutes' walk east of IMS can accommodate 68 guests and ten families. Scientists who visit IMS as well as the two other institutes can make use of these facilities. Foreign visiting scientists can also live at these lodgings with their families during their stays.

The Institute for Molecular Science

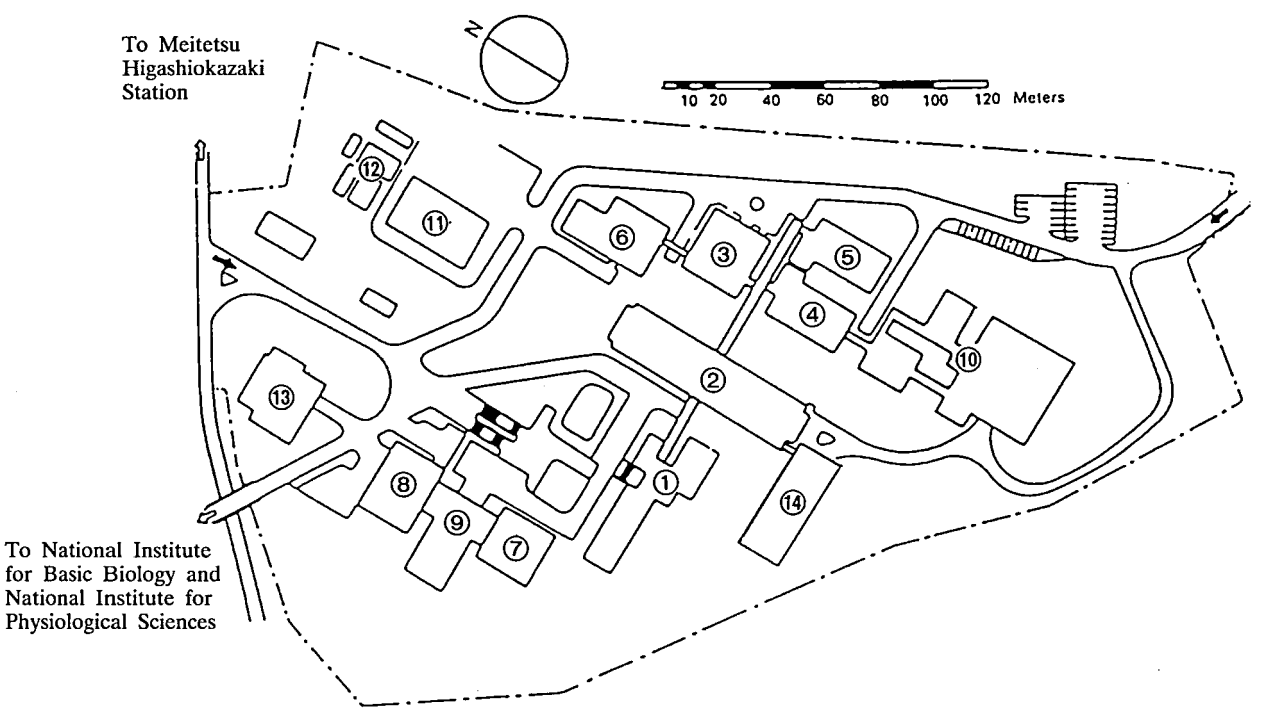

1. Research Office Building
2. Main Laboratory Building
3. Equipment Development Center
4. Instrument Center
5. Chemical Materials Center
6. Low-Temperature Center
7. Computer Center
8. Library
9. Central Administration
10. UVSOR Facility
11. Power Station
12. Waste-Water Disposition Facilities
13. Faculty Club
14. South Laboratory Building

Okazaki (population 300,000) is 260 km southwest of Tokyo, and can be reached by train in about 3 hours from Tokyo via New Tokaido Line (Shinkansen) and Meitetsu Line.
The nearest large city is Nagoya, about 40 km west of Okazaki.

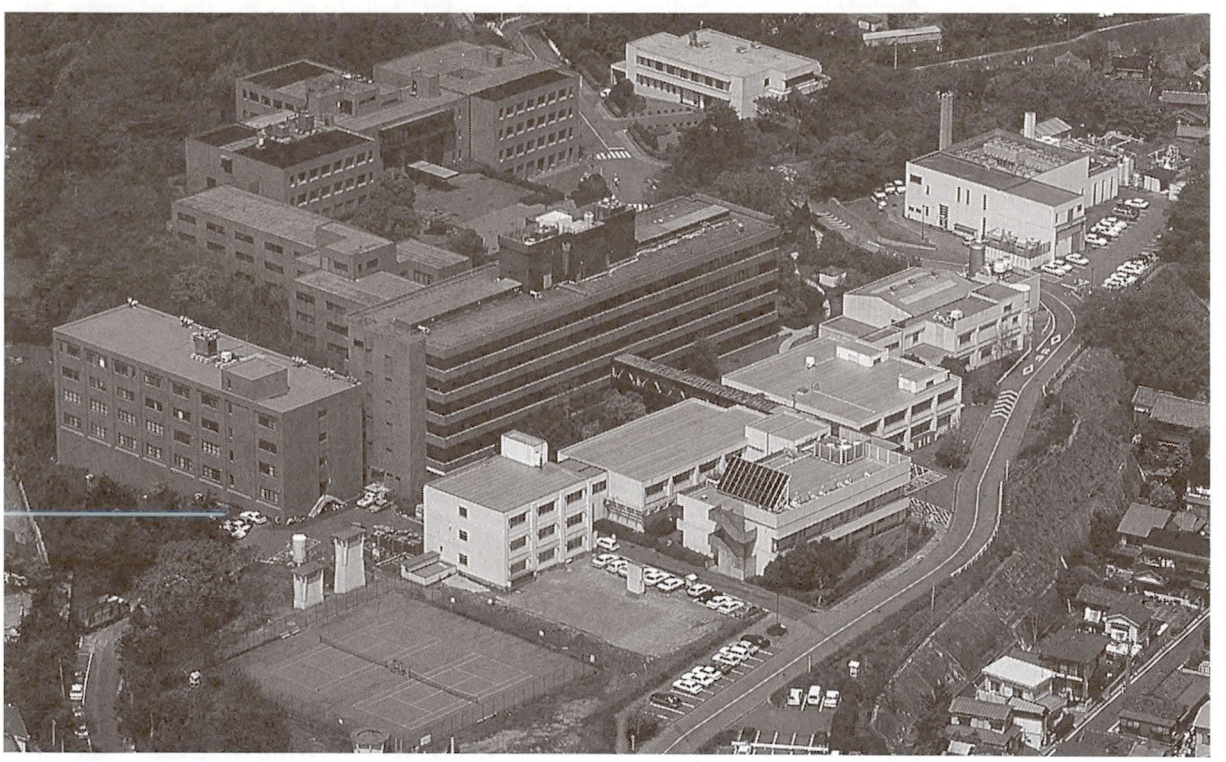

RESEARCH ACTIVITIES I
Department of Theoretical Studies

I—A Potential Energy Surfaces and Dynamics of Elementary Chemical Reactions

Our activity in this field this year has not been as productive as the last several years. Dr. Amatatsu, Technial Associate for the last three years, became Lecturer at Akita University in April 1992. Though we are still collaborating with him and Dr. Yamashita, who moved to Kyoto last year, we were unable to fill the Technical Associate position because of my scheduled departure from IMS in 1993.

I-A-1 Theoretical Study of the Photodissociation Reaction of HgI_2

Kenro HASHIMOTO and Keiji MOROKUMA

The purpose of our research is to analyze the result of femto second transition state spectroscopy on photodissociation of HgI_2 from the view point of electronic states and potential energy srufaces. We have applied the ab initio MO method with the ECP by Christiansen et al. In order to determine the MO's, we employed the average state SCF method in which we take the equal-weight average of all possible electronic configurations obtained by putting 12 electrons into 10 valence MO's (4σ MO's and 3 pairs of π MO's). We performed full valence CI calculations with these MO's and drew the potential energy cuves (PECs) of 36 states for linear dissociation of $HgI_2 \rightarrow HgI+I$. At the present level of calculation, the states whose energies are close to the experimental excitation energy (4.0 eV) at the ground state equilibrium geometry are $1^1\Pi$(3.8 eV), $1^3\Sigma^+$(4.5 eV), $2^1\Pi$(4.4 eV) and $2^3\Pi$(4.1 eV) states. $1^1\Pi$ and $1^3\Sigma^+$ states correlate to the $1^2\Sigma$ state of HgI and the ^2P state of I atom at the dissociation limit, while $2^1\Pi$ and $2^3\Pi$ states do to the $1^2\Pi$ state of HgI and the ^2P state of I atom. The $1^3\Sigma^+$ state crosses with $2^1\Pi$ and $2^3\Pi$ states when one of the HgI bonds lengthens slightly. On the other hand, the states correlating to the B($2^2\Sigma$) state of HgI, become close in energy to those correlating to the C($2^2\Pi$) state when one HgI distance is long (5.0 Å).

I-A-2 Theoretical Study of Photodissociation Reaction of Formic Acid

Toshiaki FUJII *(Grad. Univ. for Adv. Studies and IMS)* **and Keiji MOROKUMA**

The electronic structure and the photodissociation reaction path in the first excited state ($n \rightarrow \pi^*$, S_1) of formic acid were studied by *ab initio* calculation in connection to the photodissociation dynamics experiments.[1),2)]

$$HCOOH \rightarrow HCOOH^*(\tilde{A},A'')$$
$$\rightarrow HCO(\tilde{X},^2A') + OH(X,^2\Pi)$$

The geometries of the equilibrium states, the transition states and the dissociation limit of the S_1 state were determined by the CAS-SCF method. The 6-31G* basis set and 10 electrons/8 orbitals active space were employed. We find two S_1 equilibrium geometries, cis and trans, which are nonplanar with the C=O and the C-OH bond length nearly equal. The two corresponding transition states are late, with a substantial barrier (~20 kcal/mol) relative to the S_1 equilibrium geometries and the H-O-C angle of about 100°. Calculation of the reaction path from the Franck-Condon state through the transition state to the dissociation limit is being carried out.

Reference

1) M. Brouard and J. O'Mahony, *Chem. Phys. Lett.*, **149**, 45 (1988).
2) M. Brouard, J.P. Simons, and J.-X. Wang, *Faraday Discuss. Chem. Soc.*, **91**, 63 (1991).

I-A-3 Potential Energy Surface and Classical Trajectory Study of HFCO → HF+CO Dissociation Reaction

Yoshiaki AMATATSU *(Akita Univ. and IMS)* **and Keiji MOROKUMA**

An analytical potential function has been derived to examine the HFCO dissociation reaction relating to Stimulated Emission Pump experiment. The present approach for the potential energy surface (PES) is different from a conventional one in the following points. (i) We have tried to reproduce the results of ab initio IRC analysis as much as possible,[1)] but not to fit potential energies to analytical functions directly. (ii) The potential energy function is expressed as a linear combination of the force fields for various structures including the reactant, the product and the transition state. Classical trajectory study has been carried out with the analytical potential function. The rate constant for HFCO dissociation reaction has been calculated. Trajectories with a high percentage of the initial HFCO out-of-plane vibrational energy are likely to be nondissociative, which agrees with experimental findings.

Reference

1) K. Kamiya and K. Morokuma, *J. Chem. Phys.*, **94**, 7287 (1991).

I-A-4 Time-Dependent Quantum Mechanical Approach to the Photodissociation Dynamics of CH_3I

Yoshiaki AMATATSU *(Akita Univ. and IMS)*, **Keiji MOROKUMA, Audrey D. HAMMERICH*, and Ronnie KOSLOFF*** *(*The Hebrew Univ., Israel)*

A time-dependent quantum mechanical simulation has been carried out under the assumption of a collinear pseudo-triatomic system. First, by means of the relaxation method (i.e. imaginary-time wave packet propagation), the ground state surface has been improved to reproduce the

experimental vibrational levels within a few percents of error. Second, the $^3Q_0^+$ and $^1Q_1$ surfaces have been modified to reproduce the absorption spectrum. The main changes in both potential energy surfaces were their gradients inside the Franck-Condon region.

I-A-5 Theoretical Study on the Solvent Effects on ICN Photodissociation

Yoshiaki AMATATSU *(Akita Univ. and IMS)* **and Keiji MOROKUMA**

Molecular dynamics simulation, based on Miller-Meyer's method, has been performed to compare the ICN photodissociation reaction dynamics in the solution phase with that in the gas phase. As shown in our previous potential energy surface and classical dynamics studies of ICN photodissociation in gas phase,[1] rotational excitation for the I-channel product takes place after nonadiabatic transition as well as before the transition. The rotational energy for the I-channel product in rare gas is damped with oscillation. The damped oscillation can be rationalized by energy exchange with ICN and rare gas.

Reference

1) Y. Amatatsu, K. Morokuma, and S. Yabushita, IMS Ann. *Rev.*, 14 (1991).

I-A-6 New Ab Initio Potential Surfaces and Three-Dimensional Quantum Dynamics for Transition State Spectroscopy in Ozone Photodissociation

Koichi YAMASHITA, Keiji MOROKUMA, Frederic LE QUERE*, and Claude LEFORESTIER* *(*Université de Paris-Sud)*

[*Chem. Phys. Lett.*, **191**, 515 (1992)]

New ab initio potential energy surfaces (PESs) of the ground and B ($^1B_2$) states of ozone have been calculated with the CASSCF-SECI/DZP method to describe the three-dimensional photodissociation process. The dissociation energy of the ground and the vertical barrier height of the B PES are obtained to be 0.88 and 1.34 eV, respectively, in better agreement with the experimental values than the previous calculaiton. The photodissociation autocorrelation function, calculated on the new B PES, based on exact three-dimensional quantum dynamics, reproduces well the main recurrence feature extracted from the experimental spectra.

I—B Theoretical Studies of Structure and Spectroscopy

We became involved in the fast growing field of C_{60} and fullerene chemistry, by a call of help from experimental groups throughout Japan. We are excited in our study on the model for fullerene formation. Dr. Hashimoto, Research Associate in my group since July 1991, split his time between projects in I—A and I—B, latter being in part supported by a grant to study solvation of alkali and alkali-earth metals.

I-B-1 Ab Initio MO Study of C_{60} Anion Radical: the Jahn-Teller Distortion and Electronic Structure

Nobuaki KOGA and Keiji MOROKUMA

[*Chem. Phys. Lett.*, **196**, 191 (1992)]

The ab initio UHF structure determination of C_{60} anion radical shows that small Jahn-Teller distortions take place to give the D_{5d}, D_{3d}, and D_{2h} symmetric structures. They are almost degenerate and 2 kcal/mol more stable than the I_h symmetric structure. Therefore, the rearrangement among them could take place easily. The nodal properties of SOMO, localized mainly in the vicinity of the equator, make the C_{60} anion ellipsoidal stretched along the principal axis.

I-B-2 Ab Initio MO Calculation of (η^2-C_{60})$Pt(PH_3)_2$: Electronic Structure and Interaction between C_{60} and Pt.

Nobuaki KOGA and Keiji MOROKUMA

[*Chem. Phys. Lett.*, in press]

With an ab initio molecular orbital method, we have calculated the structure of (η^2-C_{60})$Pt(PH_3)_2$, a model of experimentally studied (η^2-C_{60})$Pt(PPh_3)_2$. Compared with $(C_2H_4)Pt(PH_3)_2$, much stronger back-donation from $Pt(PH_3)_2$ to C_{60} takes place; the amount of charge transfer is about 3 times larger and the stabilization energy is about 15 kcal/mol larger. Analysis also shows that the Pt-C σ bonds are formed as a result of back-donation and the interacting PtCC moiety becomes a metallacyclopropane. The electron affinity of the complex is only 0.44 eV smaller than that of C_{60}, suggesting that several metals can simultaneously coordinate with C_{60}.

I-B-3 AM1 Calculations of Intermediates in Ring Stacking Model for Fullerene Formation

Nobuaki KOGA, Fujiko HASHIMOTO, and Keiji MOROKUMA

Recently, Wakabayashi and Achiba have proposed the RIng Stacking Model (RISM) for formation mechanism of fullerenes such as C_{60}. According to this theory, several different paths leading to one fullerene are possible. Therefore, in order to find the most favorable path among them, it is necessary to investigate the structures and stabilities of the intermediates with a theoretical method. We have studied with the semi-empirical AM1 method the structures of the intermediates in the formation mechanisms which start with C_{10} and eventually lead to C_{60} and C_{70}: $C_{10} \rightarrow (+C_{18}) \rightarrow C_{28} \rightarrow (+C_{18}) \rightarrow C_{46} \rightarrow (+C_{12}) \rightarrow C_{58} \rightarrow (+C_2) \rightarrow C_{60}$ and $C_{10} \rightarrow (+C_{18}) \rightarrow C_{28} \rightarrow (+C_{20}) \rightarrow C_{48} \rightarrow (+C_{16}) \rightarrow C_{64} \rightarrow$

$(+3C_2) \rightarrow C_{70}$. The calculations show that these processes are quite exothermic. The first ring stacking step in the C_{60} formation, which gives C_{28}, is slightly endothermic by 5 kcal/mol, whereas the same step in the C_{70} formation is quite endothermic by 98 kcal/mol. On the other hand, the other steps in both formations are exothermic and thus expected to be easy to take place. Therefore, C_{70} formation is less favorable than C_{60} formation because of instability of the C_{28} intermediate. Also, we are studying the C_{30} intermediates which appear in the formation mechanism of higher fullerenes such as C_{78} and C_{84}.

I-B-4 Theoretical Study of Hydration of Light Alkali and Alkali-earth Metal Atoms and Ions

Kenro HASHIMOTO, Shaoren HE, Keiji MOROKUMA, and Suehiro IWATA (*Keio Univ.*)

Hydration of Li, Be, Na and Mg atoms and their ions was investigated systematically by using the ab initio MO method. The molecular structures were optimized by the analytical energy gradient technique for SCF wavefunctions with 3-21G basis set. The most stable structure of $M(H_2O)_n$ ($M=Li^+$, Na^+, Be^{2+} and Mg^{2+} ions) has C_{2v} (n=1), D_{2d} (n=2), D_3 (n=3) and S_4 (n=4) symmetry, irrespective of the metal ions studied. In these structures, oxygen atoms in water moldcules bind directly to the central metal ions. On the other hand, the hydrated structures of the neutral metal atoms depend on the metal up to four-water hydration. The stable structure of the metal atoms with six water molecules however has C_3 symmetry structure for all these metal atoms. In this structure, three water molecules bind to the metal atoms and other three water molecules attach to the water molecules in the first hydration shell with hydrogen bonds. We have found that the hydrogen bonds play an important role in determinig the stable hydration structures. The variation of ionization potential of the hydrated Na atom as a function of the hydration number is good agreement with the experiment. The ionization potentials of hydrated clusters of the other three metals were compared to that of Na though no experimental data is available.

I-B-5 Theoretical Study of Hydration of Na_2

Kenro HASHIMOTO and Keiji MOROKUMA

Ab initio MO calculations were carried out on $Na_2(H_2O)_n$ (n=0–4) as a model of hydration of Na cluster. The molecular structure was optimized by the energy gradient method for the closed-shell SCF wavefunctions. The basis sets used were 3-21G, 6-31G* and the set of TZP for Na and DZP for H_2O. It is found that the water molecules tend to bind to one of the Na atoms. The hydration causes lengthening of the Na-Na distance and the charge polarization in Na_2. The charge polarization is most remarkable when the third water molecule hydrates and the distances between Na and the oxygen atoms become close to those in $[Na(H_2O)_3]^+$. In the case of the four-water hydration, the structure of the cluster becomes just like that of $[Na(H_2O)_4]^+$ bond to Na^-. Thus, it is possible that hydration of Na_2 results in the hydration Na^+ and Na^- ions in the ground electronic state.

I-B-6 A Theoretical Study on Ligand Substitution Reaction of Pt(II) Complex in Water

Chizuru MUGURUMA (*Grad. Univ. for Adv. Studies and IMS*), **Nobuaki KOGA, Kazuo KITAURA, and Keiji MOROKUMA**

The role of solvent in simple chemical reactions has recently been elucidated by molecular simulation such as Monte Carlo and molecular dynamics. However, little such effort has been made for solvent effect on reactions of transition metal complexes. We have set out to carry out molecular dynamics studies on the following ligand exchange reaction in water.

$$[Pt(NH_3)_3Cl]^+ + aq. \rightarrow [Pt(NH_3)_3(H_2O)]^{2+} + Cl^- + aq.$$

We will treat $[Pt(NH_3)_3]^{2+}$, H_2O and Cl^- as rigid fragments. At first we want to determine realistic interaction potential functions from ab initio calculations. To fit the calculation to an analytical form, we use the Kitaura potential represented by a sum of Coulomb interactions among point charges on atoms and orbital interactions in terms of interfragment overlap integrals between bond or lone pair orbitals.

We have already determined good analytical potential functions by using 173 ab initio configurations for $[Pt(NH_3)_3]^{2+}$ and Cl^-, and 505 configurations for $[Pt(NH_3)_3]^{2+}$ and H_2O. Molecular dynamics calculations are in progress.

I-B-7 Application of the Natural Population Analysis to Transition Metal Complexes. Should the Empty Metal p Orbitals Be Included in the Valence Space?

Feliu MASERAS and Keiji MOROKUMA

[*Chem. Phys. Lett.*, **195**, 500 (1992)]

The performance of the Natural Population Analysis (NPA) method of Weinhod and co-workers when applied to transition metal complexes has been studied on the model systems NiH_2 and $[Os(PH_3)_4H(H_2)]^+$. In particular, we were especially concerned with the a priori division made by the procedure between the atomic 'valence' and Rydberg orbitals, two concepts which are rather imprecise in the case of transition metals. In order to assess this question, a small modification was introduced in the original code of the program allowing the performance of NPA population analysis with different 'valence'/Rydberg partitions.

The calculations clearly demonstrate the decisive effect of the initial labeling of the orbitals on the final output of the population analysis. For instance, the analysis of the same wavefunction for the NiH_2 system with different partition schemes yields charges for the Ni atom ranging from +1.10 to +1.74 atomic units. The results are even more dramatic in the case of the $[Os(PH_3)_4H(H_2)]^+$ complex, where the charges on the metal atom change from −0.65 to −1.98 a.u.

I-B-8 Ab Initio MO Study of Neutral and Cationic Boron Clusters

Hiroshi KATO *(Okayama Univ. of Science)*, **Koichi YAMASHITA** *(Institute for Fundamental Chem.)*, **and Keiji MOROKUMA**

[*Chem. Phys. Lett.*, **190**, 361 (1992)]

The geometries, electronic structures and energies of the neutral and cationic boron clusters (B_{2-12} and B^+_{2-12}) have been investigated by the ab initio molecular orbital method. The geometries of boron-cluster cations B^+_{3-12} are essentially the same as those of the neutral clusters, planer (or pseudo-planar) cyclic structures. Clusters of 8–11 atoms characteristically have the most stable structure of a C_{2v} cyclic form with one atom in the middle. The capped pentagon B_6, B_7 and B^+_7 and the trigonal bipyramid B_{12} and B^+_{12} are exceptions.

I-B-9 Ab Initio and Monte Carlo Study on Structure and Stability of $H_3^+(H_2)_n$ (n=3–16)

Umpei NAGASHIMA, Hideki TANAKA *(Kyoto Univ.)*, **and Keiji MOROKUMA**

[*J. Phys. Chem.*, **96**, 4294 (1992)]

The molecular geometries of hydrogen cluster ions, $H_3^+(H_2)_n$ (n=3–16), were investigated by using the classical Monte Carlo and annealing method. The two-body potential functions were obtained by fitting the results of ab initio MP4 (SDTQ) calculations. Molecular structure and stability are mainly determined by an ionic interaction between H_3^+ and H_2. The H_2-H_2 interaction forces H_2 molecules to stay away from each other but seems to have little effect upon the structure and stability of clusters in the vicinity of the equilibrium structure. The n dependency of the binding energy ($-\Delta E_{n-1,n}$) is in good agreement with the experimental trend in $-\Delta H_{n-1,n}$ known for $n \leq 9$. Magic numbers in the stabilization energy have been found at n=3, 6, 9, 12, and 15, where optimized molecular structures are closed shells with 3-hold symmetry and have one to five layers of $(H_2)_3$ solvation shells over the H_3^+ core.

I—C Theoretical Studies of Reaction Mechanisms and Structure of Organic and Related Compounds

Dr. Moc, a JSPS Postdoctoral Fellow from Poland, continues to work on MO studies on hypervalent compounds. He has proceeded from structural problems to transition states of reactions. We also enjoyed and benefitted enormously from our collaboration with Prof. Eiichi Nakamura, an organic chemist from Tokyo Institute of Technology.

I-C-1 Ab Initio MO Study on the Periodic Trends in Structures and Energies of Hypervalent Compounds: Four-coordinated XH_4^- and XF_4^- Anions Containing a Group 15 Central Atom (X=P, As, Sb, Bi)

Jerzy MOC and Keiji MOROKUMA

A systematic ab initio MO study employing effective core potentials on the central atoms has been carried out to predict C_{2v}, C_{4v}, D_{4h} and T_d structures, the corresponding energies and stabilities as well as periodic trends in these molecular properties for the series of hypervalent XH_4^- and XF_4^- anions, where X=P, As, Sb, Bi. The comparative all-electron calculations for the C_{2v} and C_{4v} structures of these species with X=P, As, Sb were also done. The lowest energy forms for both XH_4^- and XF_4^- were those of C_{2v} symmetry. All $XF_4^-(C_{2v})$ were found to be minima on the SCF potential energy surfaces, whereas the inclusion of electron correlation (MP2) changed the nature of $PH_4^-(C_{2v})$ and $AsH_4^-(C_{2v})$ from unstable transition states (TS) to stable minima. D_{4h} forms of XH_4^- and PF_4^- appeared to be TS's for inversion of the C_{4v} forms; on the other hand, $XH_4^-(C_{4v})$ and $XF_4^-(C_{4v})$ were found themselves to be TS's connecting C_{2v} minima. The energy decomposition analysis was used to clarify the periodic trends in both the $E(C_{4v})$-$E(C_{2v})$ energies for XH_4^- and XF_4^- and in the thermodynamic stabilities of these species relative to loss of H^- or F^-.

I-C-2 Ab Initio MO Study on the Periodic Trends in Structures and Energies of Hypervalent Compounds: Five-coordinated XH_5 Species Containing a Group 15 Central Atom (X=P, As, Sb, Bi)

Jerzy MOC and Keiji MOROKUMA

An ab initio MO study employing effective core potentials on the central atoms ha been carried out for the D_{3h} and C_{4v} structures of the hypervalent XH_5 hydrides, where X=P, As, Sb and Bi. The periodic trends in the barriers to Berry pseudorotation of XH_5 and in their thermodynamic stabilities with respect to XH_3+H_2 were explored. In rationalizing the irregular periodic trend revealed in the thermodynamic stabilities of XH_5 relative to XH_3+H_2, the energy decomposition analysis of Morokuma and Kitaura was applied. The parallel all-electron ab initio calculations were also carried out for XH_5 with X=P, As and Sb in order to examine in a systematic way the electron correlation effects (MP2) on their geometries as well as for the sake of comparison with the ab initio ECP predictions.

I-C-3 Transition Structures for H_2 Elimination from XH_4 Hypervalent Species (X=S, Se, Te). Ab Initio MO Study

Jerzy MOC, Andrea E. DORIGO, and Keiji MOROKUMA

Ab initio MO calculations on the fragmentation of XH_4 (X=S, Se, Te) to XH_2 and H_2 show that the preferred transition structure does not have C_{2v} symmetry as suggested previously. Instead, a highly polarized transition structure, which has C_1 symmetry and does not correspond to the least motion pathway, is favored. These results can be

understood in terms of a model in which alternative transition structures are viewed as trigonal bipyramids; here, X is the central atom, and the hydrogen atoms and lone pairs of X are ligands. The factors which determine the ease of decomposition in these simple species should influence the *kinetic* stability of more complex molecular systems of experimental interest.

I-C-4 Theoretical Studies of Heteroatom-Directed Carbometallation. Addition of MeCu, Me_2Cu^- and MeLi to Substitued Acetylenes

Eiichi NAKAMURA*, Yoshimitsu MIYACHI* *(*Tokyo Institute of Technology)*, **Nobuaki KOGA, and Keiji MOROKUMA**

[*J. Am. chem. Soc.*, **114**, 6686 (1992)]

Ab initio theoretical studies of the addition of MeCu, Me_2Cu^-, and MeLi to acetylenes bearing heteroatom-substituents (i.e., OH and SH as well as SiH_3, CH_3, and H) have shown that the calculated and the experimental regioselectivities of carbometallation reactions show excellent correlation, indicating that the activation enthalpy plays a decisive role in the regioselection of heteroatom-directed carbometallatioins. Energy decomposition analysis of the regioisomeric transition states for the MeCu and MeLi additions to the OH- and SH-substituted acetylenes indicate that electrostatic interaction is a dominant contributor to the energy difference between the regioisomeric transition states. On the other hand, the overall interaction energy is dependent on orbital, and electrostatic interactions for the MeCu, and MeLi additions, respectively.

I-C-5 Triplet-Singlet Intersystem Crossing as the Second Step of Cycloaddition of Triplet Penta-1,4-Diene. An Ab Initio MO Study

Masaru OHSAKU *(Yasuda Women's Junior College)*, **Nobuaki KOGA, and Keiji MOROKUMA**

[*J. Chem. Soc., Perkin Trans.*, 2 in press]

To investigate the mechanism of photosensitized cycloaddition reaction of penta-1, 4-diene, we have calculated with an ab initio MO method the lowest point on the crossing seam between the singlet and first excited triplet states, which can be regarded as the transition state for the second step of reaction, the $T_1 \rightarrow S_0$ intersystem crossing and the ring closure on the S_0 surface. The triplet intermediate for cross addition requires only about 1 kcal/mol to reach the lowest crossing point accompanied by 90° internal rotation of the terminal methylene group with relatively small changes in the skeletal structure. On the other hand, the triplet intermediate for parallel closure requires about 10 kcal/mol, accompanied with a drastic change in the molecular skeletal structure. The calculation confirms that this second step is not the rate-determining step of the entire cycloaddition reaction.

I—D Structure and Reactions of Transition Metal Complexes

This year we have had many talented postdoctoral fellows and visiting scientists who wanted to work in this exciting field. The result is very wide activities on various aspects of transition metal chemistry. Dr. Musaev, a JSPS Postdoctoral Fellow from Azerbaijan, continued to concentrate on gas phase reactions of transition meal ions. Dr. Maseras, an EC Fellow from Barcelona, is actively studying the structure of polyhydrides. Dr. Riehl, a JSPS Postdoctoral Fellow from Paris, is involved in study of the structure and reactivity of triosmium carbonyl complexes. Dr. Yoshida, from Tosoh Corp, is working on the mechanism of ethylene polymerization. In addition, Mr. Serra, a graduate student at Barcelona, is visiting us for three months and tackling on nitrogen activation. Of course, behind all these activities is always Dr. Koga, our now veteran Research Associate.

I-D-1 Ab Initio MO Study of the Reaction Mechanism: $MCH_2^+ + H_2 \rightarrow M^+ + CH_4$ (M=Co, Rh and Ir).

Djamaladdin G. MUSAEV, Nobuaki KOGA, and Keiji MOROKUMA

The study of mechanism of gas-phase reactions of both bare transition metal cations and their saturated and unsaturated complexes with H_2 and small alkanes can provide insight into the mechanism of H-H, C-H, and C-C bond activation processes. Therefore, we have been carrying out ab initio MO calculations on the reaction mechanism:

$MCH_2^+ + H_2 \rightarrow M^+ + CH_4$ (1), for M=Cp, Rh and Ir.

We used CASSCF (for geometries) and internally contracted MR-SDCI-CASSCF (for energies) methods.

It was found that the reaction (1) is exothermic by 27.0 and 35.0 kcal/mol for M=Co and Rh, respectively, but is endothermic by 3–5 kcal/mol for M=Ir. It can take place more easily for $RhCH_2^+$ than for $CoCH_2^+$; the barrier height corresponding to the key H-H bond activation step of reaction (1) is 33.5 and 16.3 kcal/mol for M=Co and Rh, respectively. Prior to H-H bond activation the reactants yield a dihydrogen complex, $H_2MCH_2^+$, which is stable by 6.4, 5.6 and 5.1 kcal/mol relative to H_2+MCH_2^+ for M=Co, Rh and Ir, respectively. The complex $HMCH_3^+$ does not exist for M=Co and Rh, but do exist for M=Ir. The ion-molecule complex MCH_4^+ is stable relative to the dissociation limit M^++CH_4 by 27.0, 12.3, and 4.8 kcal/mol for M=Co, Rh and Ir, respectively.

I-D-2 Ab Initio MO Study of the Electronic and Geometrical Structures of Silylene Complexes, $MSiH_2^+$ (M=Co, Rh and Ir).

Djamaladdin G. MUSAEV and Keiji MOROKUMA

We have previously studied electronic and geometrical structures of methylene complexes, MCH_2^+ of M=Co, Rh

and Ir. As an extention, we studied electronic and geometrical structures of silylene complexes, $MSiH_2^+$ of the same metal atoms, in order to compare results with that for MCH_2^+. Geometrical parameters have been optimized at the CASSCF(10/8) level, and the energies were calculated at the internally contracted MR-SDCI-CASSCF(10/8) level. For all $MSiH_2^+$ considered complexes, the ground state is nearly degenerate $^3A_1$ and $^3A_2$ states. Next lower-lying $^3B_1$, $^3B_2$ and $^1A_1$ states are, respectively, 19.6, 5.3, 34.0 for Co, 13.9, 13.3, 13.2 for Rh and 15.1, 15.0, 10.7 kcal/mol for Ir higher than ground state. These results are similar with that for corresponding methylene complexes, except for M=Rh. The character of $M^+{=}CH_2$ and $M^+{=}SiH_2$ double bonds are different: the first of them has mainly covalent character, but the second is of donor-accepter type. The calculated binding energies $M^+{-}SiH_2$ are 61.0, 69.0 and 98.0 kcal/mol for M=Co, Rh and Ir, respectively.

I-D-3 Ab Initio MO Study of the Reaction Mechanism: $RhCO^+ + H_2 \rightarrow Rh^+OCH_2 \rightarrow Rh^+ + OCH_2$.

Djamaladdin G. MUSAEV and Keiji MOROKUMA

By using the second-order pertubation theory (MP2) with seventeen-electron Hay-Wadt ECP and double-zeta basis set for Rh atom and double-zeta+polarization basis sets for H, C and O atoms have been calculated potential energy surfaces (PES) of reactions

$CO + H_2 \rightarrow OCH_2$ (1) and

$RhCO^+ + H_2 \rightarrow Rh^+OCH_2 \rightarrow Rh^+ + OCH_2$ (2)

It was found that reaction (1) and (2) is endothermic by 2.5 and 3.5 kcal/mol, respectively. Neither reaction should take place at moderate temperature because of a large H-H activation barrier height, about 91 and 95 kcal/mol, respectively.

The calculated binding energies $BE\{RhCO^+(^3\Delta) \rightarrow Rh^+(^3F) + CO\}$ and $BE\{Rh^+OCH_2(^3A) \rightarrow Rh^+(^3F) + OCH_2\}$ are about 37.4 and 38.7 kcal/mol, respectively.

I-D-4 An Ab Initio Teoretical Study on the Structure of $[Os(PR_3)_3''H_4'']$ and $[Os(PR_3)_3''H_5'']^+$ Complexes

Feliu MASERAS, Xue-Kui LI *(Jilin Univ. and IMS)*, **Nobuaki KOGA, and Keiji MOROKUMA**

Systematic ab initio calculations have been carried out on the $[Os(PH_3)_3''H_4'']$ and $[Os(PH_3)_3''H_5'']^+$ systems, several isomeric forms being considered in each case. The computational level has consisted of RHF and MP2 geometry optimizations, as well as single-point MP3 and MP4 calculations.

The results for the $[Os(PH_3)_3''H_4'']$ system agree with the experimental neutron-diffraction data in that the absolute minimum is a tetrahydride with a pentagonal bipyramid geometry where the four hydride ligands are in equatorial positions. This result is obtained both at the RHF and MP2 level, although there are meaningful differences between the two methods concerning the nature and relative energy of other local minima.

The inclusion of correlation energy is mandatory in the case of the $[Os(PR_3)_3''H_5'']^+$ system, for which the experimental structure has not been determined yet. The species which seems to be the absolute minimum from the RHF computation, a bis-dihydrogen monohydride $[Os(PH_3)_3H(H_2)_2]^+$ complex, is not even a local minimum at the correlated level. Instead, the predicted absolute minimum is a pentahydride complex $[Os(PH_3)_3H_5]^+$ with a dodecahedral geometry where the hydride ligands occupy the four A (4-neighbor) and one of the four B (5-neighbor) sites.

I-D-5 Ab initio MO Study of Triosmium Carbonyl Complexes

Jean-Frédéric RIEHL, Nobuaki KOGA, and Keiji MOROKUMA

Ab initio methods are employed to investigate the electronic structure and the reactivity of triosmium carbonyl complexes such as $Os_3(CO)_{12}$ (**1**), $Os_3(CO)_{10}(\mu\text{-H})_2$, $Os_3(CO)_{10}(\mu\text{-H})(\mu\text{-Cl})$, $Os_3(CO)_9(\mu\text{-H})_3(\mu_3\text{-CH})$ (**2**) and $Os_3(CO)_9$(Benzene) (**3**). These compounds and their derivatives are involved in many reactions such as the activation of double and triple bonds, the hydrogenation of olefins and carbonyl insertion. The purpose of our study is threefold, to investigate a) the influence of bridging ligands on a metal-metal bond, b) the H exchange processes in $Os_3(CO)_9(\mu\text{-H})_3(\mu_3\text{-CH})$ and c) the rotational barrier of benzene in the "helicopter" complex $Os_3(CO)_9$(Benzene).

The optimized geometry of $Os_3(CO)_{12}$ (**1**) is in good agreement with the experimental data. The calculated Os-Os distance is only 0.042 Å longer that the experimental one (2.919 Å vs. 2.877 Å). This structure is the most stable structure; $Os_3(CO)_{10}(\mu\text{-CO})_2$, a C_{2v} structure which is the most stable for the Fe analog, is higher in energy by 30.1 kcal/mol at the SCF level (16.5 kcal/mol at MP2 level). We estimate that the Os-Os binding energy is around 45 kcal/mol. Secondly, we have shown that if there is no steric constraint, the presence of bridging ligands can significantly shorten the doubly-bridged Os-Os bond, compared to the non-bridged one (2.717 Å vs. 2.844 Å in $Os_3(CO)_{10}(\mu\text{-H})_2$ (**2**) and 2.848 Å vs. 2.884 Å in $Os_3(CO)_{10}(\mu\text{-CO})_2$). In these complexes, the formation of strong Os-L bonds is compensated by the weakening of the Os-Os bond. This is not the case for a singly-bridged bond. Experimentally, in $Os_3(CO)_{10}(\mu\text{-H})_2(\mu\text{-CH}_2)$, the singly-bridged Os-Os bond is longer than both the non-bridged Os-Os bond and the doubly-bridged Os-Os bond (3.053 Å vs. 2.855 Å and 2.824 Å, respectively).

In $Os_3(CO)_9(\mu\text{-H})_3(\mu_3\text{-CH})$, the exchange of H centers can take place through two pathways. The first which conserves a mirror plan involves a direct coordination of a bridging H to the CH fragment and a rotation of CH_2. The second occurs by the insertion of a bridging H in the Os-CH bond. SCF optimizations have shown that the second should be privileged. In $Os_3(CO)_9$(Benzene), we have found a rotational barrier of benzene of 11.0 kcal/mol at the SCF level.

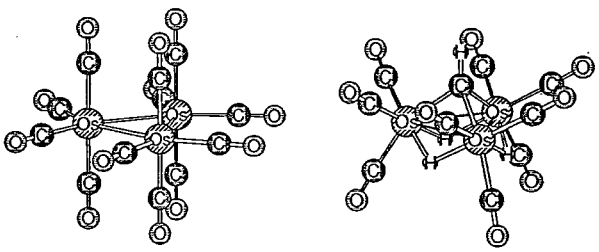

1 2

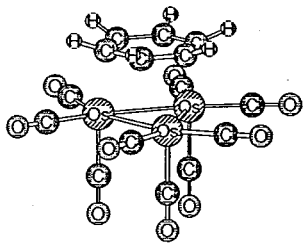

3

I-D-6 An Ab Initio MO Study of σ-Methathesis Reaction of $Cl_2Zr(C_2H_4)$ with H_2

Nobuaki KOGA and Keiji MOROKUMA

X_2Zr(olefin) has been an interesting reactive intermediate in an organotransition metal chemistry. In order to clarify the mechanism of reactions in which X_2Zr(olef) takes part, we studied the reaction mechanism of σ-metathesis: $Cl_2Zr(C_2H_4)+H_2 \rightarrow Cl_2Zr(H)(C_2H_5)$. We determined the structures of the intermediate of η^2-H_2 complex and the transition state as well as the reactant, $Cl_2Zr(C_2H_4)$, and the product, $Cl_2Zr(H)(C_2H_5)$, with the ab initio RHF and RMP2 energy gradient method under the effective core potential approximation. The CC distance in $Cl_2Zr(C_2H_4)$ were calculated to be 1.484 Å and 1.587 Å at the RHF and RMP2 level, respectively, showing that the double bond character in the CC bond is small, because of the strong back-donation from electropositive Zr to π^* orbital of C_2H_4, and thus the reactant has a large zirconacyclopropane character. The binding energy of H_2 in the η^2-H_2 complex is 4 kcal/mol at the RMP2 level. The activation barrier relative to this weak complex is 8 kcal/mol at the RMP2 level. The overall reaction was calculated to be 14 kcal/mol exothermic at the RMP2 level. These computational results show that this σ-metathesis is an easy process. Analysis of MOs at the five-centered transition state shows that vacant d orbitals of Cl_2Zr stabilize the transition state, by accepting electrons from H_2-C_2H_4 fragment. Also, strain in the Zr-C bonds in the zirconacyclopropane reactant increases the exothermicity by 10 kcal/mol, compared with the reaction of $Cl_2Zr(CH_3)_2$ with H_2.

I-D-7 A Theoretical Study on Ethylene Polymerization Using Silylene-Bridged Group 4 Metallocene Catalysts

Tohru YOSHIDA *(Tosoh Corporation and IMS)*, **Nobuaki KOGA, and Keiji MOROKUMA**

Various lines of evidence suggest that cationic group 4 metal alkyl complexes are the catalytically active species in the homogeneous metallocene-based Ziegler-Natta polymerization systems. In this study, we want to elucidate the mechanism of homogeneous polymerization of ethylene with a silylene-bridged group 4 metallocene model catalyst $(H_2SiCp_2M\text{-}R)^+$. We have concentrated on two important reactions in the polymerization: the repetitive insertion of ethylene to the metal-alkyl bond along Cossee's direct insertion

Insertion Reaction

$[M]^+\text{-}R + CH_2CH_2 \rightarrow [M]^+\text{-}R(CH_2CH_2) \rightarrow$ **(TS_1)** $\rightarrow$

(Cation Alkyl) **(π-Complex$_1$)**

$[M]^+\text{-}CH_2CH_2R \rightarrow [M]^+\text{-}CH_2CH_2R$

(γ-Agostic) **(β-Agostic)**

β-Elimination Reaction

$[M]^+\text{-}CH_2CH_2R \rightarrow$ **(TS_2)** $\rightarrow [M]^+\text{-}H(CH_2CHR) \rightarrow$

(β-Agostic) **(π-Complex$_2$)**

$[M]^+\text{-}H + CH_2CHR$

(Metal Hydride)

$[M]^+ = H_2SiCp_2M^+$; M=Ti, Zr, Hf; R=CH_3

mechanism and the β-elimination considered to be a termination or a chain-transfer step. The stationary point structures are optimized at the RHF/3-21G(Ti, Zr, Hf: ECP, H_2SiCp_2: STO- 3G) level. In the direct insertions using Ti, Zr, and Hf cation alkyls, the transition state (TS_1) lies in the midway between the structures of the π-complex$_1$ and the γ-agostic product. On the contrary, the transition state (TS_2) structure in the β-elimination is similar to that of π-complex$_2$, for each metal.

The electron correlation calculation (MP2 level) at the RHF structures in the insertion reactions gives the exothermicity of 43 kcal/mol (Ti), 40.9 kcal/mol (Zr), and 39.2 kcal/mol (Hf), with an activation energy of 1.3 kcal/mol (Ti), 6.0 kcal/mol (Zr), and 7.1 kcal/mol (Hf). These results indicate that the insertion reaction proceeds rapidly and the relative order of the insertion activity is Ti > Zr > Hf.

I-D-8 A Theoretical Study of Hydride Attack on the η^5-Cyclopentadienyltricarbonyliron Cation

David A. BROWN,* Noel J. FITZPATRICK,* Peter J. GROARKE* *(*University College, Dublin)*, **Nobuaki KOGA, and Keiji MOROKUMA**

Various species resulting from hydride attack on $[(\eta^5\text{-}C_5H_5)Fe(CO)_3]^+$ have been studied using ab initio molecular orbital methods. Stationary points were located and characterized for $[(\eta^5\text{-}C_5H_5)Fe(CO)_3]^+$ (I), $[(\eta^5\text{-}C_5H_5)Fe(CO)_3H]$ (II), $[(\eta^5\text{-}C_5H_5)Fe(CO)_2CHO]$ (III) and $[(\eta^4\text{-}C_5H_6)Fe(CO)_3]$ (IV). Second order Moller-Plesset (MP2) optimizations were carried out and showed that inclusion of dynamic electron correlation has a significant effect on the geometries and relative energies of the species considered. The final order of stabilities is (IV) > (II) ≈ (III). The relative stability of the metal-formyl complex (III) correlates with its spectroscopic identification at low temperatures in the reaction of (I) with $NaBH_4$. Although (II) is of comparable stability to (III) it is a weak complex between $[(\eta^5\text{-}C_5H_5)Fe(CO)_2H]$ and CO with the long Fe-CO bond (r(Fe-CO)=4.33Å). Finally, the diene complex, $[(\eta^4\text{-}C_5H_6)Fe(CO)_3]$ (IV) is calculated to be the thermodynamically stable product.

I-D-9 Ab Initio MO Study of the Reaction Mechanism: $RhCl(PH_3)_2CO + CH_4 \rightarrow RhCl(PH_3)_2CO(H)CH_3$

Djamaladdin G. MUSAEV, Nobuaki KOGA, and Keiji MOROKUMA

We have previously studied (N. Koga and K. Morokuma, *J. Phys. Chem.*, **94**, 5454 (1990)) potential energy surface (PES) for methane CH bond activation by coordinatively unsaturated $RhCl(PH_3)_2$ (**I**) complex, and find that reaction $RhCl(PH_3)_2+CH_4 \rightarrow RhCl(PH_3)_2(H)CH_3$ (1) takes place easily. As an extention, we studied PES of reaction

$RhCl(PH_3)_2CO + CH_4 \rightarrow RhCl(PH_3)_2CO(H)CH_3$ (2)

in order to compare it with that of reaction (1) and clarify the effect of the additional CO to methane CH activation process. Geometrical parameters of stationary points of PES of reaction (2) and their energetic parameters have been calculated with the MP2 method by using Hay-Wadt ECP (for Rh, Cl and P) and double-zeta + polarization basis sets. It was found that the most stable structure of $RhCl(PH_3)_2CO$ (**II**) is trans-carbonyl-(**II**), where PH_3-groups are in the trans position. The cis-carbonyl-(**II**) and trans-isocarbonyl-(**II**) isomers lie by 14.0 and 60.0 kcal/mol higher. The calculated height of barrier between trans-carbonyl-(**II**) and trans-isocarbonyl-(**II**) isomers and binding energy (**I**)+CO → trans-carbonyl-(**II**) are 6.1 and 73.0 kcal/mol, respectively. The reaction (2) is endothermic by 20.7 and 8.4 kcal/mol and takes place with 43.1 and 40.5 kcal/mol C-H activation barrier for trans-carbonyl-(**II**) and cis-carbonyl-(**II**) isomers, respectively. Thus, the addition of CO to complex (**I**) makes oxidative addition reaction of CH_4 more difficult.

I-D-10 An Ab Initio MO Study on Ethylene and Propylene Insertion into the Ti-CH_3 Bond in $CH_3TiCl_2^+$ as a Model of Homogeneous Olefin Polymerization

Hiroshi KAWAMURA-KURIBAYASHI *(Sumitomo Chemical Co., Ltd.)*, **Nobuaki KOGA, and Keiji MOROKUMA**

[*J. Am. Chem. Soc.*, **114**, 2359 (1992)]

As a model of olefin polymerization by a homogeneous Ziegler-Natta catalyst, the mechanism of the insertion reaction of ethylene and propylene into $CH_3TiCl_2^+$ has been studied by the ab initio MO method. The structures of the reactant, the intermediate, the transition state, and the product have been optimized with the RHF/3-21G (Ti:MIDI4) method. The transition state is four-centered and is slightly nonplanar to avoid C-H bond eclipsing. In the product strong C^{β}-C^{γ} and C-H agostic interactions take place to donate electrons to Ti vacant d orbitals. The energetics calculated at the unrestricted second-order Moller-Plesset perturbation level with double spin projection (DPUMP2) shows that the reaction proceeds via an ethylene complex with a binding energy of 45 kcal/mol and through the transition state with an activation energy from the ethylene complex of about 4 kcal/mol. In propylene polymerization, the barrier is higher than in ethylene insertion, and the primary insertion is easier than the secondary insertion, both consistent with experiments. The energy decomposition analysis indicates that these chemo- and regioselectivities are controlled by electrostatic and exchange (steric) interactions. The nonplanarity of the transition state makes one of two stereospecific primary insertion pathways substantially more favorable than the other; this tendency of a nonplanar transition state may have significance in determining stereospecificity in olefin polymerizations.

I-D-11 An Ab Initio MO and MM Study on Homogeneous Olefin Polymerization with Silylene-Bridged Zirconocene Catalyst and its Regio- and Stereoselectivity

Hiroshi KAWAMURA-KURIBAYASHI *(Sumitomo Chemical Co., Ltd.)*, **Nobuaki KOGA, and Keiji MOROKUMA**

[*J. Am. Chem. Soc.*, **114**, 8687 (1992)]

The olefin polymerization reaction by silylene-bridged zirconocene catalysts has been investigated theoretically. At first with the ab initio molecular orbital (MO) method the structure and energetics of reactants, π-complex, transition state, and product for insertion of ethylene to $(SiH_2Cp_2)ZrCH_3^+$ have been determined. The nearly C_s-symmetric transition state has a low activation barrier (about 6.0 kcal/mol) from the π-complex. The product shows a strong C^{β}-H agostic interaction. Based on the above transition state structure, molecular mechanics (MM) calculations have been carried out to investigate the effects of alkyl substituents on olefin and methyl and other substituents on the Cp rings as well as those of the alkyl group on Zr, a model polymer chain end. The regioselectivity in propylene polymerization that the primary insertion is preferred to the secondary insertion is reproduced well by the energy difference at the transition state but not by that of the π-complex. As to the stereoselectivity in isotactic polymerization of propylene by $SiH_2(CpMe_n)_2ZrR^+$, the substituents on the Cp rings have been found to determine the conformation of the polymer chain end, and the fixed polymer chain end conformation in turn determines the stereochemistry of olefin insertion at the transition state. The direct steric effect of the Cp methyl groups on the olefin insertion stereochemistry is negligibly small. The same indirect control mechanism is operational also in syndiotactic polymerization of propylene and 4-methyl-1-pentene.

I—E Theoretical Studies of Chemical Reactions on Solid Surfaces

Dr. Anchell, a JSPS Postdoctoral Fellow from USA, found a job at Pacific Northwest Laboratories at Richland, Washington, and left our group in June. A collaboration with him is continuing on the surface chimsorption study.

I-E-1 An *Ab Initio* Molecular Orbital Comparison Study of H_2 Chemisorption on MgO and Lithium-doped MgO

James L. ANCHELL and Keiji MOROKUMA

An *ab initio* study was carried out on the chemisorption of H_2 with the (100) surface of magnesium oxide and lithium doped magnesium oxide. To model the local surface environment we employed cubic and tetragonal clusters composed of eight and twelve atoms, respectively. The lattice constant for the clusters was fixed at the experimentally determined value for bulk MgO, and the geometry of the adsorbate was optimized at the UHF level of theory. Correlation energy was treated at the MP2 level at the UHF optimized geometry. It was found that H_2 undergoes heterolytic dissociation at neighboring Mg_{3c} and O_{3c} sites in MgO with an activation energy of 4.2 kcal/mol and 2.4 kcal/mol at the UHF and MP2 levels, respectively. (The subscript "3c" indicates that the atom is tri-coordinated.) Lithium doped magnesium oxide did not support heterolytic dissociation at neighboring Mg and O sites. Instead H_2 was found to homolytically dissociate without barrier at two O_{3c} sites, and to undergo hydrogen atom abstraction at O_{3c} and O_{4c} sites. At the UHF level it was found that O_{3c} sites abstraction occurs without a barrier, and at O_{4c} sites abstraction occurs with a 15 kcal/mol activation energy.

I-E-2 An Ab Initio MO Study on Adsorption at the MgO Surface I. H_2 Chemisorption on the $(MgO)_4$ Cluster

Kyoichi SAWABE, Nobuaki KOGA, Keiji MOROKUMA, and Yasuhiro IWASAWA *(Univ. of Tokyo)*

[*J. Chem. Phys.*, **97**, 6871 (1992)]

The hydrogen molecule chemisorption on the low coordination or corner site of MgO surface has been studied with the ab initio method, adopting the $(MgO)_4$ cluster as the surface site model. The effect of basis functions and correlation have been examined. Two physisorbed complexes have been found; one is an end-on complex on the oxygen site and the other a side-on complex on the Mg site. These complexes are led to a common transition state (TS) and then to a dissociative chemisorption product. A substantial polarization of charges in the hydrogen molecule takes place at the TS, from where the dissociative chemisorption proceeds ionically. The best estimates of energies of the physisorbed complexes, the TS and the product, relative to the isolated reactants, are −2, +2 and −21 kcal/mol, respectively, for this cubic cluster model. When the effect of Madelung potential is taken into account, the chemisorbed product is further stabilized by 4 kcal/mol.

I—F Structures and Reactions of Manybody Chemical Systems

Electronic structure and dynamical behavior of large systems such as liquids and polymers are investigated theoretically. (a) Collective motions and fluctuations in liquid and cluster (b) Chemical reactions and energy relaxations in liquid and clusters, and (c) Electronic structures and dynamical behaviors of polyenes, are analyzed.

I-F-1 Long Time Fluctuation of Liquid Water; $1/f$ Spectrum of Energy Fluctuation

Masaki SASAI *(Nagoya Univ. and IMS)*, **Iwao OHMINE, and Ramakrishna RAMASWAMY** *(Jawaharlal Nehru Univ. and IMS)*

[*J. Chem. Phys.* **96**, 3045 (1992)]

The power spectra of the potential energy fluctuation of liquid water and argon and clusters are examined. It was found that liquid water and cluster water both yield so called $1/f$ frequency dependence (f is frequency). This indicates that there exists an extended multiplicity of hydrogen bond network relaxations in liquid water. A simple model of cellular dynamics is proposed to explain this frequency dependence. These water spectra are sharp contrast to spectra of simple liquids (for example, liquid argon), which exhibit a near white spectrum. On the other hand, the cluster dynamics of argon also involves energy fluctuations of a $1/f$ type, resulting from various relaxation processes at core and surface.

I-F-2 Structure and Dynamics of Small Water Clusters

David WALES *(Cambridge Univ. and IMS)* **and Iwao OHMINE**

Structure and dynamics of small clusters of 8 and 20 water molecules are investigated. We have performed several nano-second trajectory calculations and determined several thousands inherent structures along trajectories by using the conjugated gradient method. The reaction coordinates connecting these inherent structures and theormodynamical quantities were calculated to investigate the melting mechanism of these clusters.

I-F-3 Dynamics and Evaporation of Water Clusters

Shinji SAITO and Iwao OHMINE

We have been investigating the dynamics of water clusters, especially $(H_2O)108$, at several temperatures. Lindemann's criterion is a good measure of melting in the water clusters, as it works well in the rare gase clusters. The melting point is very high and the surface melting is "observed" below the melting point. The evaporation takes place at the higher energy (or temperature). The minimum energy paths for the evaporation from the cluster surface show that the potential energy change is sharp and the interaction range is short. The evaporation rate by the RRKM theory can reproduce that by the MD simulation. The dielectric and molecular orientational relaxations have been studied. The molecular orientational relaxation at any temperature is able to be represented by a single exponential and close to

that of the liquid water. In clusters the dielectric relaxation time, tD, is faster the molecular orientational relaxation time, ts, on the other hand, tD is slower than ts in the liquid water.

I-F-4 A New Approach to Investigate the Energy Relaxation of an Excess Elextron in Water Clusters

Shinji SAITO and Iwao OHMINE

Dynamical behavior of an excess electron in an attachment to a water cluster has been investigated. Recent experiments suggest that sequential non-adiabatic transitions occur during the relaxation of an electron in the liquid water. Accurate wavefunctions have to be needed to study these non-addiabatic transitions. In previous studies by other authers, the so called r-space grid method has been used because of its simplicity. However, this grid method is not variationally bounded and yields very slow convergece against the number of the grid points employed. It is shown that the accuracy of the energy calculated depends on the r-space positions of the grid points. To overcome these drawbacks of the grid method, we have developed an approach in the momentum space representation. The results of some simple 1-dimensional model and an excess electron in water clusters show that our method is variational and faster convergence. Furthermore, it is found that the grid-dependence of energy in our method is smaller than that in the gird method.

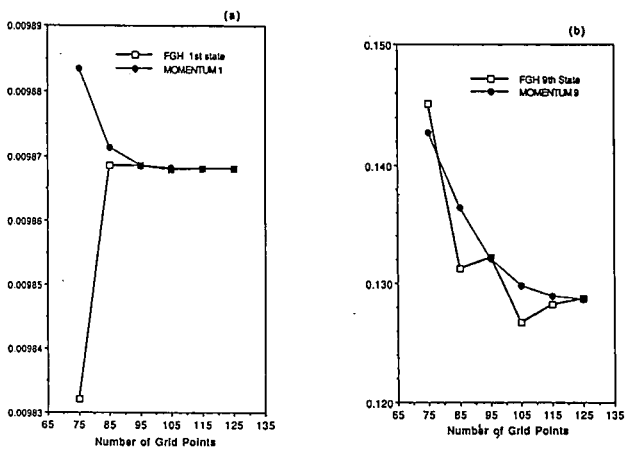

Figure 1. Energy of the ground (a) and the 9-th (b) vibrational state of H2 Morse potential (in Hartree).

I-F-5 Proton Transfer in Liquid Water; Solvent Rearrangement Effect, Interaction Energy Component Analyses

T. KOMATSUZAKI *(Grad. Univ. for Adv. Studies and IMS)* **and I. OHMINE**

In order to analyze the dynamical behavior of proton transfer in liquid water, we have investigated the potential energy surface for one and simultaneous two proton transfer in hydrated proton cluster by using ab initio calculation. We have found that up to three body electronic effect in reaction regio are essential to describe the potential surface. This means at least 14 water and 18 water molecules must be explicitly included to describe these reaction of one and two proton transfer, respectively.

To clarify many body electronic interaction effect of hydrated proton cluster systems and the proton transfer surface, we analyzed the electronic decomposed energy of hydrated proton clusters by new decomposition scheme. It is found that three body effects strongly depend on their configuration and mainly determined by (non-classical) charge transfer, and four body effect is always negligible. From this fact, we employed two models, 12water+(H5O2+) (single PT), 15water+(H7O3+) (double PT); Solvent rearrangement including second solvated shell is essential for kinetics and energetics of these reactions. It is shown that single and cooperative proton transfer can be occurred by almost barrier-less (a few kcal/mol) when large local melting of solvent waters is adiabatically induced. Thermal fluctuations of second shell's waters can also influence largely the proton transfer energy surface.

In order to perform the large scale molecular dynamics calculation we are developing the new potential function that describes properly many body effects of charge transfer by using the scheme of the 'atoms in molecule' in density functional theory.

I-F-6 The Agon Cluster Dynamics in the Melting Region

Norihiro SHIDA and Iwao OHMINE

We have been exploring the mechanism of the melting in argon clusters, continuously from the 1990's research project. We have proposed a new characterization to symbolize the global shapes of potential energy surfaces by using high energy stationary points where the Hessian matrices have more than two negative eigenvalues. The melting of the Ar_7 cluster has been examined by this new characterization. We have also calculated the Lyapnov exponents and the Kolmogorov (metric) entropies for that system to see the extent of the phase space by melting. Based on these studies, we have focused our attention on the configuration entropies to analyze the small cluster melting. The molecular dynamics simulation with the adiabatic switching of the total Hamiltonian was employed to obtain the configuration entropies. We have refined this method and applied it to the Ar_7 cluster. The analysis of these configuration entropies in the melting region is now in progress.

I-F-7 Reaction Surface by Gradient Extremal

Norihiro SHIDA

Decoupling from many degrees of freedom to a few is an important issue in various physical and chemical problems. In this research project, I have proposed a new criterion to define multidimensional subspaces from potential energy surfaces. The idea is an extension of the gradient extremals to multidimensional surfaces. I have developed the algorithm to obtain such subspaces which is applicable in *ab initio* level of calculations. I have used this algorithm and have calculated the two dimensional potential energy surface of the (NH_2-H-NH_2)-system. The dynamics calculations using these subspaces, including the construction of the Reaction Surface Hamiltonian, are now in progress.

I—G Theoretical Studies of Chemical Reaction Dynamics

Clarification of the Reaction Mechanisms and Development of Illuminating Good Approximate Theories are our Ultimate Purposes of the Theoretical Reaction Dynamics Studies.

I-G-1 Effects of Potential Energy Surface Topography and Isotope Substitution in Atom-Diatom Chemical Reactions: The Cl+H_2 and D+H_2 Systems

Shoji TAKADA, Ken-ichiro TSUDA, Akihiko OHSAKI *(Miyazaki Univ.)*, **and Hiroki NAKAMURA**

[*Adv. Mol. Vibr. and Coll. Dynamics: Quantum Reactive Scattering, vol.IIA, edited by J.M. Bowman, (JAI, Greenwich)*, in press]

We report (1) the effects of potential energy surface (PES) topography on the reaction dynamics of D+H_2 → DH+H and Cl+XH →HCl+X, XCl+H (X=H, D), and (2) the kinetic isotope effects (KIE) in the latter reactions, on the basis of the exact 3D quantum mechanical calculations for J=0, where J is the total angular momentum quantum number. For the first subject, we employ the two PES's for each system. In the case of D+H_2, a large difference in the reaction probabilities is found for the two similar PES's with a small difference in the proper reaction zone. On the other hand, in the Cl+H_2 reactions, essentially the same probabilities are obtained for the two quite different PES's, which differ significantly in the H-Cl-H configuration improper for the relevant reaction. As for the KIE study, integral cross sections and thermal rate constants are calculated and compared for the three reactions, Cl+H_2, Cl+HD, and Cl+DH. We show, at first, that the quasiclassical trajectory results deviate from the present quantum mechanical ones not only at very low but also at quite high energies. The following three isotope effects are analyzed: (1) difference in zero-point energies, (2) quantum mechanical tunneling, and (3) initial rotational excitation. The constant centrifugal potential approximation (CCPA) based on the accurate results for J=0 is again proved to work well and applied extensively to investigate the KIE.

I-G-2 Variational Principles for Reactive Collisions Based on the Generalized Lagrange Multiplier Method

Michael BAER *(Soreq Nucl. Res. Cent., Israel and IMS)*, **and Hiroki NAKAMURA**

[*J. Chem. Phys.*, **96**, 6565 (1992)]

In this study is discussed a general approach to derive variational principles for physical magnitudes $Q(\phi)$ which are dependent on functions ϕ known to be solutions of physical equations [see Gerjuoy *et al.*, Rev. Mod. Phys. **55**, 725 (1983)]. The approach is based on Lagrange multipliers which are incorporated into the expression for calculating Q by demanding that the funcitons ϕ fulfill their equations. This approach is first applied to derive a general variational principle for the T-matrix elements based on the Lippmann-Schwinger equation. As special cases we obtained the bilinear forms of the Schwinger and the Newton variational principles. Next this approach is employed to derive a new Kohn-type variational principle for the S-matrix elements for reactive collisions based on the Schrödinger equation which contains complex potentials. Finally, this approach is further utilized to derive a novel variational principle for the flux function.

I—H Theoretical Studies of Atomic Collison Processes

Transitions between Zeeman states in collision have been studied in connection with experiments.

I-H-1 Coupled Channel Treatment of Transitions between Na($^2P_{1/2}$,m_j) and Na($^2P_{3/2}$,m_j) in Collision with Na($^2P_{3/2}$,m_j)

Misako KIMURA, Hajime KATO *(Kobe Univ.)*, **Kiyohiko SOMEDA, and Hiroki NAKAMURA**

[*J. Chem. Phys.*, **97**, 256 (1992)]

Transitions between the Zeeman substates of Na($3p\ ^2P_{1/2}$) and Na($3p\ ^2P_{3/2}$) in collision with Na($3s\ ^2S_{1/2}$) in thermal energy region are investigated by the close-coupling method. Rotational and spin-orbit couplings are taken into consideration, and potential energy functions generated by a quantum chemical calculation are employed. The cross sections strongly depend on the magnetic quantum numbers of the initial and final states. This dependence qualitatively coincides with an experimental observation in the presence of a weak magnetic field, although the magnetic field is not considered in the present calculation. Total cross section of the transition Na($^2P_{3/2}$) → Na($^2P_{1/2}$) is calculated to be 2.7×10^2 Å^2 in good agreement with experiment. The following two mechanisms are found to dominantly contribute to the total cross section: (1) Transitions among the molecular states of Na_2, $^3\Pi_{2u} \leftrightarrow {}^3\Pi_{1u}$ and $^3\Pi_{1u} \leftrightarrow {}^3\Pi_{0u}$, induced by the spin-rotation coupling, and (2) the transition, $^1\Sigma^+_{0g} \leftrightarrow {}^1\Sigma_{1g}$ induced by the Coriolis coupling.

I—I Theoretical Studies of Highly Excited States of Molecules

Highly excited states show various intriguing properties and participate in a variety of dynamic processes. We believe that they will open a new challenging world of science. The ultimate purpose of our studies is to find new collective motions in

these states and understand their participating dynamics.

I-I-1 Characteristics and Dynamics of Doubly Excited States of Molecules

Sungyul Lee *(Kyung Hee Univ. and IMS)*, **Masahiro IWAI, and Hiroki NAKAMURA**

[*Molecules in Laser Fields, edited by A.D. Bandrauk, (M. Dekker)*, in press]

This review article is organized as follows: a variety of studies on the atomic doubly excited states are briefly summarized in Section II. In section III the quantitative information on the potential energies $E_r(R)$ and the autoionization widths $\Gamma(R)$ are presented for the doubly excited states of H_2. Electron correlation and autoionization mechanisms in these molecular doubly excited states are analyzed in Section IV in comparison with these of the corresponding atomic states. Section V briefly reviews the dynamic processes involving superexcited states studied so far. The basic and powerful theoretical tool, i.e., the multichannel quantum defect theory (MQDT) is also outlined there.

I—J Theory of Nonadiabatic Transition

Nonadiabatic transition is one of the very basic mechanisms of state (phase) change in various fields of physics and chemistry. We are interested in developing good analytical formulae for various cases of nonadiabatic transitions and also in nonadiabatic tunneling in one-dimensional periodic system.

Recently, we have succeeded in deriving quantum mechanically exact analytical expresions of reduced scattering matrix for the linear curve crossing problems. We have also derived new compact approximate analytical expressions. These are practically quite useful.

Analysis has also been made to interesting phenomena of complete reflection and transmission in one-dimensional periodic nonadiabatic tunneling system.

I-J-1 The Two-State Linear Curve Crossing Problems Revisited. I. Analysis of Stokes Phenomenon and Expressions for Scattering Matrices

Chaoyuan ZHU, Hiroki NAKAMURA, Nazzareno RE, and Vincenzo AQUILANTI (*Univ. of Perugia, Italy*)

[*J. Chem. Phys.*, **97**, 1892 (1992)]

The classic problems of the two-state linear curve crossing both for the same and the opposite sign of slopes of the linear diabatic potentials are analyzed in a unified way by exactly dealing with the Stokes phenomenon for the four transition pints of the associated second-order differential equations. First, distributions of the transition points and the Stokes lines are fully clarified for the whole range of the two parameters which effectively represent the coupling strength and the collision energy. Secondly, the so-called reduced scattering matrices are found to be expressed in terms of only one (complex) Stokes constant. This is made possible by finding the relations among the six Stokes constants. Finally, this one Stokes constant is given exactly and analytically by a convergent infinite series.

I-J-2 The Two-State Linear Curve Crossing Problems Revisited. II. Analytical Approximations for Stokes Constant and Scattering Matrix: Landau-Zener Case

Chaoyuan ZHU and Hiroki NAKAMURA

[*J. Chem. Phys.*, in press]

Based on the exact solution of the linear curve crossing problems reported in the previous paper of this series, approximate analytical solution is discussed here for the same sign of slopes of the diabatic potentials (Landau-Zener case). A new general method is proposed for connecting wave functions along Stokes lines in the complex plane. Two new compact analytical formulae for reduced scattering matrix are derived and compared with others. The whole range of the two parameters which effectively represent the coupling strength and the collision energy is divided into five regions, in each one of which the best recommended formulae are proposed. The new formulae proposed here are simple and explicit functions of the two parameters, and thus useful for practical application. Especially, a simple and compact formula which works better than the conventional Landau-Zener formula is obtained for nonadiabatic transition probability for one passage of crossing point. Furthermore, in a region near the crossing point at intermediate coupling strength where no analytical approximation works well, certain fitting formulae are provided for the Stokes constant.

I-J-3 Numerical Method for the Two-State Linear Curve Crossing: Nonadiabatic Tunneling Case

Chaoyuan ZHU and Hiroki NAKAMURA

[*Comp. Phys. Commun.*, in press]

A new reliable numerical method is proposed for solving the two-state coupled equations with the two linear potentials which intersect with opposite sign of slopes. The original coupled equations which suffer from a very rapid oscillation are transformed into a new form which gives ordinary sine and cosine solutions asymptotically. The amplitude and phase of the scattering matrix can be stably and accurately calculated.

I-J-4 Nonadiabatic Tunneling in One-dimensional Finite Periodic Potential System

Hiroki NAKAMURA

[*J. Chem. Phys.*, **97**, 256 (1992)]

Nonadiabatic tunneling in an ideal one-dimensional finite periodic potential system is studied. Resonant transmission, complete reflection which does not exist in the case of ordinary adiabatic tunneling, and acceleration of transmission are analyzed. Some peculiar features resulting from the complete reflection are found and discussed. A system with an impurity is also investigated with an emphasis on the role of complete reflection. The analyses are illustrated by numerical examples.

I—K Stokes Phenomenon and Asymptotic Solutions of Ordinary Differential Equations

Recently, we have succeeded in deriving exact analytical expressions of Stokes constants for four new classes of second order ordinary differential equations. This would enable us, in principle, to define and construct new special functions.

I-K-1 Stokes Constants for a Certain Class of Second-Order Ordinary Differential Equations

Chaoyuan ZHU and Hiroki NAKAMURA

[*J. Math. Phys.*, **33**, 2697 (1992)]

By generalizing the coupled wave integral equations method devised by Hinton, the Stokes phenomena of the standard second-order ordinary differential equations with the following coefficient functions $q(z)$ are analyzed: (i) $q(z)=a_{2N}z^{2N}+\Sigma_{j=-\infty}^{N-1}a_jz^j$; (ii) $q(z)=a_{2N-1}z^{2N-1}+\Sigma_{j=-\infty}^{N-2}a_jz^j$; (iii) $q(z)=\Sigma_{j=0}^{4}a_jz^j$, with $a_3=0$; and (iv) $q(z)=\Sigma_{j=0}^{3}a_jz^j$, with $a_2=0$. First the relations are derived among the Stokes constants, which enable the expression of all Stokes constants in terms of only one. Furthermore, this one Stokes constant is shown to be expressed in the analytical form of a convergent infinite series as a function of the coefficients of $q(z)$. This was done for all four cases listed above.

I—L Theory for High-Tc Superconductors

To clarify the origin of superconductivities of Cu-O type ceramics, alkali doped C_{60} crystals, and organic charge transfer salts, we theoretically study their microscopic electronic structures and the nature of electron-phonon couplings in these materials. We are especially interested to clarify the effect of nonlinearity of lattice vibrations on these superconductivities.

I-L-1 Superconductivity, Metal-Insulator Transitions, and Strong Enhancement and Reduction of Isotope Effects in the Anharmonic Peierls-Hubbard Model

Keiichiro NASU

A quasi-two-dimensional Peierls-Hubbard model with the typical two types of anharmonic phonons has been studied, so as to clarify both enhancement and reduction of isotope shifts of superconducting (sp) transition temperature T_c, as well as the competition between the metallic state and the charge-density-wave (CDW) or spin-density-wave (SDW) state. The first type is a sextic anharmonicity like a hard-core repulsion, and the second type is a small negative quartic anharmonicity in addition to the sextic one, just like a mixture of a hard core and a soft one. This theory is based on the mean-field approximation for electrons and a variational method for phonons. In the first type, the Peierls distortion is excessively suppressed, and the sp state becomes more stable than the CDW, even when electron-phonon (e-ph) coupling is very strong. Thus T_c of this case is enhanced, but has no isotope effect. In the second type, in contrast, the sp state is suppressed by the CDW when e-ph coupling is strong. The T_c of this case is reduced, but shows strongly enhanced isotope shift. In both cases, the SDW is always suppressed.

I-L-2 Enhancement, Reduction and Inversion of Isotope Effects due to Anharmonic Phonons, — Migdal-Eliashberg Theory for Superconductivity —

Yasuzi INADA and Keiichiro NASU

Superconducting transition temperatures of many-electron system coupled strongly with anharmonic phonons have been studied, to clarify how drastically anharmonicity changes the isotope effect from the harmonic case. The diagonal self-energy of electron as well as the off-diagonal one was determined within Migdal's approximation. Typical two types of anharmonicities were studied. The first is a sextic anharmonicity like a hard-core repulsion. Isotope shifts become almost zero in this case. When this repulsion is more strong, the shifts are reversed. The second is a small negative quartic anharmonicity in addition to the sextic one, just like a mixture of a hard-core and a soft one. In this case, on the contrary, the shifts are greatly enhanced. Discussion is also given in relation to the observed anomalous isotope effects of newly discovered high-temperature superconductors.

I-L-3 Stationary Localized Mode in an Anharmonic Molecular Crystal Model

B.S. LEE *(Malaysia Science Univ.)* **and Keiichiro NASU**

Stationary and spatially periodic localized modes are found in one-demension for an anharmonic molecular crystal model within the rotating wave approximation. One class of odd modes solves the recurrence relations for the shape function asymptotically exactly in the limit of large anharmonicity. Other classes of odd and even modes which solve the recurrence relations exactly are also found.

I—M Nonlinear Excitations in Halogen-Bridged Mixed-Valence Metal Complexes

To clarify the nonlinear nature of various optical excitations in a one-dimensional charge density wave state, we study singlet excition and its spectral manifestation in the light absorption.

I-M-1 Theory for Spectral Shape of Optical Absorption in Halogen-Bridged Mixed-Valent Metal Complexes

Kaoru IWANO and Keiichiro NASU

Spectral shapes of optical absorptions in the charge density wave states of halogen-bridged mixed-valent metal complexes are theoretically determined for the first time, using a one-dimensional extended Peierls-Hubbard model. Two important effects beyond the mean field theory are taken into account; the electron-hole (e-h) correlation on the metal atoms, and the classical fluctuation of the halogen sub-lattice coordinates. It is shown that the exciton strongly affects the spectral shape of the charge transfer (CT) band. When the e-h binding is weak, the CT band is the mixture of the exciton absorption and the interband ones. When it is strong, on the other hand, the exciton dominates over all the CT band and, consequently, its higher energy side becomes very close to a Lorentzian. From the comparison with experimental data, it is concluded that platinum complexes correspond to strong binding cases. The intragap absorptions associated with nonlinear excitations such as solitons and polarons are also studied in a strong binding regime.

I—N Optical Nonlinearity of Low Dimensional Materials

To clarify the higher order optical processes of low dimensional materials, we study the nature of optical excited states and higher order optical susceptibilities of polyacetylene and metal complexes.

I-N-1 Comment on "Essential-states Mechanism of Optical Nonlinearity in π-conjugated Polymers"

X. SUN, Z. SHUAI, C. WU *(Fudan Univ.)*, **and Keiichiro NASU**

The new concept of "essential states" is instructive to understand the resonant structure of the THG spectrum of the polymers. It is convincing that the essential two-photon state mA associated with 1B is bounded by 1B and 2B and approaches 1B in $N \to \infty$. But, from the above feature, one can't infer that the peak of the two-photon resonance of the trans-polyacetylene is exactly at $E_g/2$, where E_g is the optical gap. The reason why this inference is not true is analyzed in this comment, and a rigorous result of the Peierls-Huckel model unambiguously shows that the peak of the two-photon resonance is near 0.6 E_g rather than $E_g/2$. It is needed to consider the excitation-depended damping, which shifts the peak from 0.6 E_g to $E_g/2$.

I-N-2 The Spectrum of Third Harmonic Generation of MX Complex

Li LIE-MING, X. SUN *(Fudan Univ.)*, **and K. NASU**

The theory of third harmonic generation $\chi^{(3)}(\omega)$ of MX complex is presented on the basis of CDW model. The recent observation on the peak structure of $\chi^{(3)}(\omega)$ for [Pt,Cl] complex can be well interpreted by this theory, which not only shows that the observed peak around 1.7 eV is produced by the two-photon resonance between the bottom edge of valence band and the top edge of conduction band, but also predicts there exist two more peaks outside the observation region.

I-N-3 Electron Interaction and Optical Gap of Conjugated Polymers

X. SUN, Z. SHUAI *(Fudan Univ.)*, **K. NASU, D. LIN** *(New York State Univ.)*, **and T. GEORGE** *(Washington Univ.)*

The controversy regarding whether the optical gap of a polymer is increased or decreased by electron-electron interactions can be clarified by studying the effect of screened Coulomb interactions on the correlation function of the excited states. Since the competition between the diagonal and the off-dimensional parts of the electron interaction depends on the screening, the screening becomes the decisive factor to determine the dependence of the optical gap on the electron interaction. Our theory shows that the electron interaction with weak or normal screening increases the optical gap. However, if the screening is very strong, the optical gap can be reduced by the electron interaction.

RESEARCH ACTIVITIES II
Department of Molecular Structure

II—A Laboratory and Astronomical Spectroscopy of Transient Interstellar Molecules

Vast, cold, and low-density space environment is a unique laboratory, whose physical and chemical conditions are rarely attained in the laboratory on Earth. The unique space laboratory is favorable to the existence of transient molecules such as molecular ions, free radicals, and unstable molecules, most of which are very exotic and non-terrestrial. These exotic transient molecules are generally difficult and challenging problems for laboratory spectroscopy. Laboratory spectroscopy may be enriched by astronomical studies on non-terrestrial transient species which represent new development in high-resolution molecular spectroscopy. On the other hand, detailed knowledge about new transient molecules obtained by laboratory spectroscopy is essential to a deeper understanding of physical and chemical processes in space. We develop a high-sensitivity submillimeter-wave and far-infrared spectrometers suitable for high-resolution spectroscopy of transient molecules of astronomical interest. We expect that our laboratory spectroscopy may accelerate the mutually beneficial aspect between laboratory spectroscopy and astrochemistry and astrophysics.

II-A-1 The Submillimeter-Wave Spectrum of the ND($^3\Sigma^-$) Radical

Shuji SAITO and Masahiro GOTO

The NH radical is generated in space by electron recombination reactions of NH_2^+ or NH_3^+, which are two main sequential ions of interstellar nitrogen chemistry from N^+ to the final product NH_3.[1] The nitrogen chemistry in space may be examined by monitoring the spectral lines of the NH radical. However, the NH radical has its lowest transition at 974 GHz where radio telescopes are not available at present. We have recently detected the lowest rotational transition of its deuterated species, ND($^3\Sigma^-$), around 500 GHz. We rearranged the microwave spectrometer of IMS.[2] A 2 m glow-discharge free-space cell was newly installed and the vacuum line was renewed. Submillimeter-wave radiation was obtained by a combination of frequency multipliers and klystrons. The ND radical was generated by a dc glow-discharge (300 mA) in ND_3 (30 mTorr) at −100 °C. We observed 40 fine and hyperfine components for the lowest rotational transition, N=1-0, of ND in the region of 492 to 546 GHz. Thirty lines free from disturbances and having good line shapes were analyzed by the least squares method to yield molecular constants listed in Table1. The standard deviation of the fit was 28 kHz. The molecular constants determined in the present study agree well with those obtained by FIRLMR spectroscopy.[3]

Table 1. Molecular Constants of the ND($^3\Sigma^-$) Radical[a]

Constant	MW	FIRLMR[b]
B_o	263265.1029(123)	263262.7(45)
D_o	14.489(fixed)	
λ_o	27545.255(27)	27533(36)
γ_o	−883.355(21)	−881(18)
b_F(N)	18.922(133)	20.2(30)
C(N)	−67.550(91)	−74.7(180)
eQq(N)	−1.128(90)	
C_l(N)	−0.213(40)	
b_F(D)	−10.0728(198)	−10.2(30)
C(D)	14.137(132)	15.3(18)
eQq(D)	0.067(114)	

[a] MHz(3σ). [b] Ref. 3)

References

1) E. Herbst, D.J. DeFrees, and A.D. McLean, *Astrophys. J.*, **321**, 898 (1987).
2) Y. Endo, S. Saito, and E. Hirota, *J. Chem. Phys.*, **75**, 4379 (1981).
3) A.D. Wayne and H.E. Radford, *Mol. Phys.*, **32**, 1407 (1976).

II-A-2 The Submillimeter-Wave Spectrum of the PH and PD Radicals in the Ground Electronic State, ($^3\Sigma^-$)

Masahiro GOTO and Shuji SAITO

The PH radical is one of the free radicals of fundamental importance in molecular spectroscopy as well as interstellar phosphorus chemistry. It has been studied with traditional optical spectroscopy and also various kinds of modern laser spectroscopy. However, PH has not been studied by microwave spectroscopy because it has a large rotational constant. We have recently detected its lowest rotational transition around 500 GHz as well as the transitions of its deuterated species. The PH or PD radical was produced in the 2 m free space cell held at −100°C by the reaction of dc glow discharge products of H_2 or D_2 with powdered red phosphorus placed at the bottom of the cell. The optimum signals were obtained at the pressure of 25 mTorr with the dc current of 300 mA. The spectral lines of PH or PD was strong enough to observe most of fine and hyperfine components: 20 lines for the N=1-0 transition of PH at 423 to 553 GHz, and 50 lines for N=1-0 and 2-1 of PD at 181 to 523 GHz. The observed spectral lines were analyzed by using a Hamiltonian for the triplet sigma state with two nuclear spins. All the observed PH lines and 43 lines of PD were subjected to the least squares fitting. The molecular constants determined are listed in Table 1. The standard deviations of the fits were 17 kHz for PH and 40 kHz for

PD. The molecular constants determined in the present study agree well with those obtained with FIRLMR[1] and IRFT[2] spectroscopy.

References

1) N. Ohashi, K. Kawaguchi, and E. Hirota, *J. Mol. Spectrosc.*, **103**. 337 (1984).
2) R.S. Ram and P.F. Bernath, *J. Mol. Spectrosc.*, **122**, 275 (1987).

Table 1. Molecular Constants of the PH and PD Radicals[a]

Constants	PH	PD
B_o	252200.8278(70)	130795.9858(163)
D_o	13.301[b]	3.548(28)
λ_o	66255.7014(180)	66207.174(29)
γ_o	−2305.5846(115)	−1196.489(25)
γ_D	0.392(21)	0.1083(66)
b_F(P)	128.1190(174)	128.953(28)
c(P)	−476.843(78)	−476.907(94)
C_l(P)	0.614(27)	0.320(28)
b_F(H or D)	−46.5451(193)	−7.072(23)
c(H or D)	19.407(135)	3.007(77)
C_l(H or D)	−0.036(28)	−0.006(21)
eQq(D)		0.095(58)

[a]MHz(σ). [b] Ref. 1)

II—B Laser Investigation of Autoionizing and Predissociating States of Atoms and Small Molecules

Highly excited electronic states of molecules and atoms play important roles in inelastic collision processes including chemical reactions. In those states of molecules, many dissociation and ionization channels are generally open and strongly compete with each other, so that the predominating decay channel tends to differ from state to state. In those states, therefore, 'state-resolved' measurements of decay dynamics are particularly important for studying their complicated dynamical behaviors. In atoms, on the other hand, doubly excited states are of particular interest because they do not only play an important role in photoionization processes but they also intrinsically involve strong electron correlation effects, which may lead to cooperative electronic motions. In this study, with the above interest, highly excited states of molecules and atoms are spectroscopically investigated through laser multiphoton and/or multistep excitation methods together with theoretical analyses.

II-B-1 Rotational State Dependence of Decay Dynamics in the Superexcited 7*f* Rydberg State (v=1) of NO

Asuka FUJII and Norio MORITA

[*J. Chem. Phys.* **97**, 327 (1992)]

The decay dynamics of the 7*f* Rydberg state (v=1) of NO has been investigated with laser multiphoton excitation methods; not only NO^+ ions generated by autoionization but also fragment nitrogen atoms produced by predissociation have been directly probed. The fragment atoms have been found to populate both the $2p^3\ ^2D_J$ and $2p^3\ ^4S_{3/2}$ states. Population yield in the ^4S state shows strong dependence on each 7*f* rotational level of NO and this dependence is remarkably correlated with autoionization yield, while no such significant dependence exists for the ^2D state. From the fact that only odd $\mathscr{L}$ levels generate the ^4S state, dissociative states causing this predissociation process have been identified as Σ^+ states. Through detailed analysis, it has been shown that the predissociation rate of this channel is much larger than the autoionization rate, and that the N(^{2}D)-generating predissociation is also mainly caused by dissociative Σ^+ states. Moreover, it has been found that a major part of the total decay rate of each rotational level is strongly correlated with magnitude of its $f\sigma$ character, as shown in Figure 1. From these facts, it has been concluded that the decay process in the 7*f* state is mainly governed by predissociation due to *direct* coupling with dissociative Σ^+ valence states, which have been identified as $A'^2\Sigma^+$ and $I^2\Sigma^+$ for the N(^{4}S)- and N(^{2}D)-generating predissociation channels, respectively.

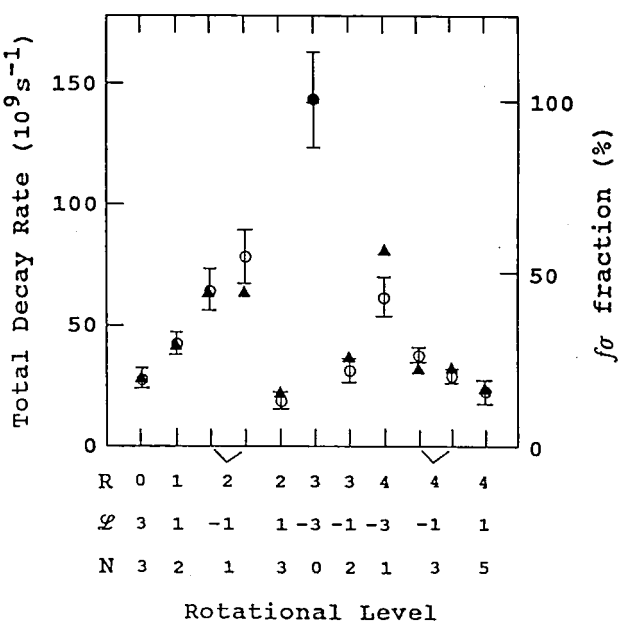

Figure 1. Rotational state dependence of total decay rates (O) and fractions of the $f\sigma$ character (▲) in the 7*f* state (v=1). Total decay rates are taken from Biernacki *et al.* [*J. Chem. Phys.*, **89**, 2599 (1988)]. For each of the R=2, $\mathscr{L}$=−1, N=1 and R=4, $\mathscr{L}$=−1, N=3 levels, two total decay rates obtained from linewidths of different rotational branches are plotted.

II-B-2 Studies on the Competition between Rotational Autoionization and Predissociation in Superexcited *np* Rydberg States of NO

Asuka FUJII and Norio MORITA

Competition between rotational autoionization and pre-

dissociation in high *np* Rydberg states ($n \geq 23$, $v=0$, $N^+=12$, where N^+ is angular momentum of the ion core) of NO has been studied with laser multiphoton excitation methods. A two-color double resonance excitation technique has been used for state-selected excitation of the high Rydberg states. Fragment nitrogen atom ($2p^3\ ^2D_{5/2}$) production competing with rotational autoionization has been directly probed by resonance enhanced multiphoton ionization. Absorption intensities of the high Rydberg states have also been measured by the two-color fluorescence dip method. Figure 1 shows the relative absorption intensity and N(^{2}D)-yield of the *np* Rydberg series. Rotational autoionization channels ejecting ϵd and ϵp electrons open at $n=28$ and $n=33$, respectively (arrows in Figure 1 indicate these thresholds). However, as shown in Figure 1, intensity distributions of the absorption and N(^{2}D)-yield are almost equivalent to each other. This means that the predissociation efficiency is constant across the threshold of rotational autoionization. Therefore, it is concluded that predissociation governs the decay dynamics of these high *np* Rydberg states.

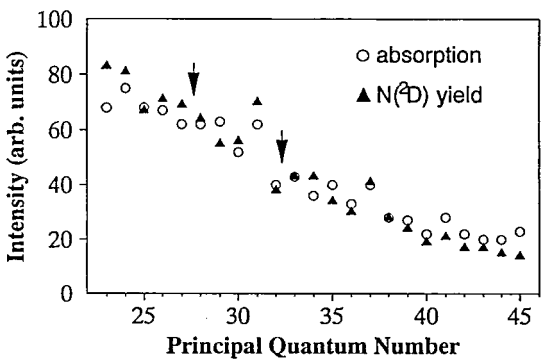

Figure 1. Relative intensity distributions of the absorption and N(^{2}D)-yield in the *np* Rydberg series ($23 \leq n \leq 45$, $v=0$, $N^+=12$) of NO. Arrows indicate the thresholds of rotational autoionization.

II-B-3 R-Matrix Calculation of Two-electron Excited $^1S^e$ States of Ca Atom up to the 9s Threshold

Norio MORITA

By an eigenchannel R-matrix calculation of the final state multichannel quantum-defect parameters in *LS* coupling, the photoexcitation spectrum of doubly excited $^1S^e$ states of atomic calcium from the 6s ionization threshold up to just below the 9s threshold has been obtained with the initial state fixed to the 4s4p state. The maximum number of channels included in the calculation is 36 and the maximum boundary radius is 130 a.u. (The maximum number of two-electron bases is 1798.) The photoionization cross section has been calculated by using both the dipole-length form and dipole-velocity form. The difference in magnitude between the two results is 15—20% throughout the calculated energy region, and very good similarity is seen between their resonance structures. This suggests good accuracy of the calculation. Moreover, we have also carried out a calculation following our experimental excitation scheme, in which the atom is excited from single-electron Rydberg states. The calculated spectra have been compared with the experimental spectra of the 7s*n*s, 8s*n*s and 9s*n*s doubly excited Rydberg series, and both results are in good agreement with each other in peak position as well as in autoionization width. As a result, the tentative assignment experimentally determined for each observed peak has been well confirmed. In particular, the good agreement is also seen in the spectra experimentally assigned to the 9s10s and 9s9s states, which are (nearly) Wannier-ridge-type states. Since this type of states are well known to be extremely difficult to observe, the experimental assignment has not been very credible. This agreement, however, may indicate that the experimentally observed resonance peaks are really due to this type of states, though further investigation is required for its confirmation.

II—C Laser Cooling and Trapping of Neutral Atoms

When an atom absorbs or emits light, it is accelerated or decelerated since light has momentum. In addition, a strong radiation field can modify the internal energy of an atom, so that an atom in an inhomogeneous radiation field receives a force from the field. Using these mechanisms, the translational motion of a neutral atom cannot only be controlled but also cooled to an extremely low temperature by laser radiation. As the translational temperature goes down to a nanokelvin region, the atomic de Broglie wavelength becomes a macroscopic size. At this temperature, a macroscopic quantum-mechanical collective motion of an atomic assembly can be expected to occur in a very thin gas. On the other hand, the long de Broglie wavelength enables us to realize an atomic interferometer, which is analogous to a neutron interferometer and very sensitive to the change of velocity and acceleration. Moreover, the above mechanisms also allow us to trap an atom in a laser beam, so that we can control atomic spatial position as well. Taking a main interest in these matters, we have been studying the laser cooling and trapping of neutral atoms.

II-C-1 Visible Observation of Metastable Helium Atoms Confined in an Infrared/Visible Double Resonance Trap

Mitsutaka KUMAKURA and Norio MORITA

[*Jpn. J. Appl. Phys.*, **31**, L276 (1992)]

We have demonstrated magnetooptical trapping of metastable He atoms by using an infrared laser resonant with the $2s^3S_1 \rightarrow 2p^3P_2$ transition (λ=1083 nm). The trap consists of a quadrupole magnetic field and four infrared laser beams which are aligned to form a tetrahedral configuration. The laser beams are circularly polarized, and each polarization direction is identical with respect to the magnetic field direction. To probe the trapping, a pair of counterpropagating visible laser beams resonant with the $2p^3P_2 \rightarrow 3d^3D_3$ transition (λ=588 nm) is added to the trap center. Detecting the visible resonance fluorescence, only

10^4 atoms confined in a trap with a diameter of 1 mm have been sensitively observed even with the naked eye. The lifetime of the trap has been estimated to be about 19 ms at a background pressure of 5×10^{-7} Torr. Figures 1(a) and 1(b) show the dependence of the fluorescence intensity on detunings of the visible and infrared lasers at higher (20 mW) and lower (0.7 mW) limits of the visible laser power, respectively, where the infrared power is fixed at 17 mW. In Figure 1(a), the fluorescence is observed over a broader infrared detuning range than in Figure 1(b). This suggests that under the former condition the visible laser operates as a trapping laser and considerably extends the capture range of infrared laser detuning.

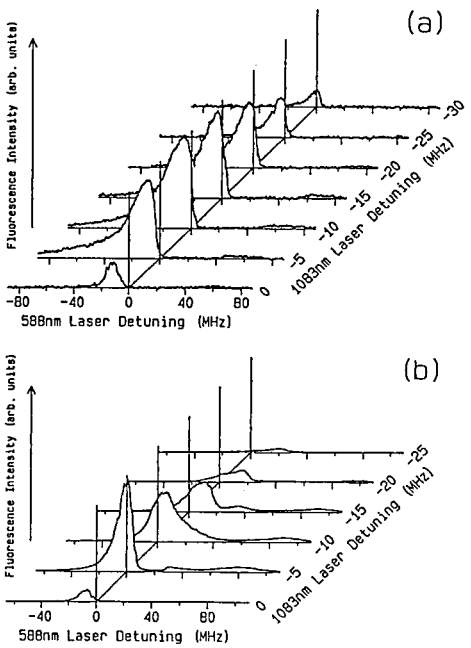

Figure 1. Dependence of the fluorescence intensity on infrared and visible laser detunings at a visible laser power of (a) 20 mW and (b) 0.7 mW. The infrared laser power is fixed at 17 mW.

II—D Molecular Science of Biomolecules and Their Model Compounds

Elucidation of the structure-function relationship of proteins is a current subject of this group. The primary technique used for this project is the stationary and time-resolved resonance Raman and absorption spectroscopies. The main themes that we want to explore are 1) mechanism of oxygen activation by enzymes, 2) electron- and proton-transfers through proteins and their coupling in the energy transducing membrane, 3) the primary process of photoreceptor proteins, 4) dynamical features of higher order protein structures. In category (1), we have treated reaction intermediates of cytochrome *c* oxidase, cytochrome P-450, chloroperoxidase, and horseradish peroxidase by using the mixed-flow transient Raman apparatus and Raman/absorption simultaneous measurement system. We also examined model compounds such as Fe^{IV}=0 porphyrin and its π cation radical. For (2), we have investigated bacteriorhodopsin and cytochrome *c* oxidase, while for (3) we have found the structural difference between P_r and P_{fr} forms of phytochrome and their model compounds. For (4), we observed the UV (200—240 nm)-excited time-resolved resonance Raman spectra of hemoglobin-CO in the time resolution of 10 ns, discussing a mechanism of its quaternary structure change. In order to make the UV Raman experiment more practical, we developed a novel technique based on the combined use of the first/second order dispersions of two gratings in an ordinary double-monochromator and applied it successfully to 244 nm-excited RR spectra of lysozyme. Furthermore, the pump/probe time-resolved Raman system using two 10-ns visible lasers was set up and applied to pursue recombination dynamics of photodissociated CO of myoglobin, hemoglobin and their mutants. These experiments enabled us to explore dynamical features of protein structures.

II-D-1 Resonance Raman Study on the Active Site Structure of a Cooperative Hemerythrin

Shoji KAMINAKA, Hideo TAKIZAWA *(Tokyo Science College)*, **Takashi HANDA** *(Tokyo Science College)*, **Hiroshi KIHARA** *(Jichi Medical College)*, **and Teizo KITAGAWA**

[*Biochemistry*, **31**, 6997—7002 (1992)]

Resonance Raman Spectra were observed for the oxy and azidomet forms of a cooperative hemerythrin (Hr) isolated from *Lingula unguis* and a noncooperative Hr from *Siphonosoma cumanense*. The O-O stretching frequency of the oxy-derivative of the *L. unguis* Hr was lower in the high affinity form generated at pH 7.6 than in the low affinity form generated at pH 6.2, while that of the *S. cumanense* Hr did not change at those two pH values. The Fe-O-Fe symmetric stretching mode of *L. unguis* azidomet Hr exhibited a frequency shift between pH 7.6 and 6.2, while that of *S. cumanense* was not shifted. However, the corresponding band of the oxy form did not show a pH dependent frequency change. Therefore, it is noted that the azidomet form is not a suitable model for studying a mechanism of cooperativity, contrary to the structural similarity between the oxy and azidomet forms. The Fe-O_2 as well as Fe-N_3 stretching frequencies were found to have no relation with the oxygen affinity. Upon exchange of solvent from H_2O to D_2O, the O-O and Fe-O_2 stretching modes of *L. unguis* Hr were shifted to higher and lower frequencies, respectively, and their magnitudes were the same for the high- and low-affinity forms. The same frequency shifts were observed for *S. cumanense* Hr. These observations suggested that the binding of oxygen to an arbitrary subunit

is communicated to another subunit through hydrogen bonding between bound oxygen and a surrounding amino acid residue, and that this hydrogen bond stabilizes more the oxy structure of the high affinity form than that of the low affinity form.

II-D-2 Detection of the Fe-CO Stretching Raman Band for Recombination Transient Species of Photodissociated Carbonmonoxy Myoglobin by Using Pump/Probe Time-Resolved Technique

Yoshinao SAKAN, Takashi OGURA, and Teizo KITAGAWA

[*Chem. Phys. Lett.*, **196**, 150–154 (1992)]

The Fe-CO stretching ($\nu_{Fe\text{-}CO}$) Raman band was observed for recombined transient species of photodissociated carbonmonoxy myoglobin (MbCO) at room temperature by using the pump/probe time-resolved technique. The recovery of the equilibrium $\nu_{Fe\text{-}CO}$ band was significantly faster for the acidic form with $\nu_{Fe\text{-}CO}$ at 492 cm^{-1} than the neutral form with $\nu_{Fe\text{-}CO}$ at 511 cm^{-1} when they were coexistent in the solution near pK_a of distal histidine. This is consistent with the proposed assignments of the 511 and 492 cm^{-1} bands to the 'closed' and 'open' forms of the protein structure, respectively. However, the transient species present in neutral solution 500 $\mu s - 1$ ms after photolysis gave a broad $\nu_{Fe\text{-}CO}$ band around 511 cm^{-1}, but no band around ~490 cm^{-1}, suggesting that the CO binding at neutral pH does not go by way of so-called 'open' form.

II-D-3 Observation of the Fe^{IV}=O Stretching Raman Band for a Thiolate-ligated Heme Protein; Compound I of Chloroperoxidase

Tsuyoshi EGAWA, Hideho MIKI *(Keio University)*, **Takashi OGURA, Ryu MAKINO** *(Keio University)*, **Yuzuru ISHIMURA** *(Keio University)*, **and Teizo KITAGAWA**

[*FEBS Lett.*, **305**, 206–208 (1992)]

The Fe^{IV}=O stretching vibration has never been identified for a cysteine-coordinated heme enzyme. In this study resonance Raman and visible absorption spectra were observed simultaneously for transient species in the catalytic reaction of chloroperoxidase with hydrogen peroxide by using our original apparatus for the mixed-flow and Raman/absorption simultaneous measurements. For the first intermediate, the Fe^{IV}=O stretching Raman band was observed at 790 cm^{-1}, which shifted to 756 cm^{-1} with the ^{18}O derivative, but the ν_4 band was too weak to be identified. This suggested the formation of oxoferryl porphyrin π cation radical. The second intermediate gave an intense ν_4 band at 1372 cm^{-1} but no oxygen-isotope sensitive Raman band, suggesting oxygen exchange with bulk water.

II-D-4 Time-Resolved Resonance Raman Study on the Binding of Carbonmonoxide to Recombinant Human Myoglobin and Its Distal Histidine Mutants

Yoshinao SAKAN, Takashi OGURA, Teizo KITAGAWA, Frank A. FRAUNFELTER *(Case Western Reserve Univ.)*, **Rafael MATTERA** *(Case Western Reserve Univ.)*, **Masao IKEDA-SAITO** *(Case Western Reserve Univ.)*

Time-resolved resonance Raman (RR) spectra of the recombined species of photodissociated CO with recombinant human myoglobin (Mb) and several E7 mutants, in which distal His was replaced by Gly (H64G), Gln (H64Q), Ala (H64A), Ile (H64I), Val (H64V), and Leu (H64L) through site-directed mutagenesis, were observed in the time range −20 ns and 1 ms following photolysis. The Fe-CO stretching ($\nu_{Fe\text{-}CO}$) RR band was observed successfully with pulse excitation when the laser power was greatly reduced. H64H, H64G, and H64Q gave the $\nu_{Fe\text{-}CO}$ band at 505–510 cm^{-1} in their stationary state. In their recovery process 1–100 μs after photodissociation, a broad transient band was observed at slightly lower frequencies than in their equilibrium structures for H64G and H64Q, but a transient $\nu_{Fe\text{-}CO}$ band corresponding to the so-called 'open' form was not identified for any of the three species. A second group, H64A, H64I, H64V, and H64L gave the main $\nu_{Fe\text{-}CO}$ band at 490–495 cm^{-1} with a shoulder around 510 cm^{-1} in the stationary state, and exhibited a much faster recovery than the first. These latter four species gave a broad transient band around 492–500 cm^{-1} in the time range of 100–1000 ns, while the ~510 cm^{-1} band appeared much later, and the relative intensity of the two bands remained unchanged after 500 μs. For all MbCO examined here, the recovery, determined from the area intensity of the $\nu_{Fe\text{-}CO}$ band, exhibited two phases irrespective of the presence of one or two $\nu_{Fe\text{-}CO}$ bands. It is inferred that the ~510 cm^{-1} ('closed') form of MbCO is not generated via the ~490 cm^{-1} ('open') form and that these two species pass different transient states which have appreciable structural disorder.

II-D-5 A Novel Idea for Practical UV Resonance Raman Measurement with a Double-monochromator and Its Application to Protein Structural Studies

Shoji KAMINAKA and Teizo KITAGAWA

A practical system for UV resonance Raman (RR) measurements based on the combined use of the first/second order dispersions of two gratings in a ordinary double-monochromator is proposed. This system rejects visible stray light completely and gives four times larger throughput than the combination of the normal second order dispersion of two gratings and a visible-cut filter. A newly designed f/1.1 Cassegrainian mirror optics and an exquisite spinning cell using ESR sample tube are combined with this spectrometer and applied to measurements of UV RR spectra of hen egg white lysozyme. The continuous wave 244 nm-excited spectra of lysozyme yielded Raman bands of tryptophan (Trp) and deprotonated tyrosine (Tyr^-) residues in 10 min with high signal-to-noise ratios and there was no sample degradation. It is demonstrated that the intensity of the Tyr^- ν_{8a} band in the 244 nm excited spectrum can be used to quantify the number of deprotonated Tyr residues in a stepwise ionization of a protein.

II-D-6 Synthesis and Characterization of the Dinuclear Copper(II) Complexes [Cu(HB(3,5-

$Me_2pz)_3)]_2X$ ($X=O^{2-}$, $(OH)_2^{2-}$, CO_3^{2-}, O_2^{2-})

Nobumasa KITAJIMA *(Tokyo Institute of Tech.)*, **Takayuki KODA** *(Tokyo Institute of Tech.)*, **Shinji HASHIMOTO, Teizo KITAGAWA, and Yoshihiko MOROOKA** *(Tokyo Institute of Tech.)*

[*J. Am. Chem. Soc.*, **113**, 5664–5671 (1991)]

The synthesis and characterization of a series of dinuclear copper(II) complexes ligated by $HB(3,5\text{-}Me_2pz)_3$-(hydrotris(3,5-dimethyl-1-pyrazolyl)borate) are presented. Displacement of the carbonyl group in a mononuclear copper(I) complex Cu(CO) ($HB(3,5\text{-}Me_2pz)_3$) (**1**) with PPh_3 affords Cu(PPh_3) ($HB(3,5\text{-}Me_2pz)_3$) (**2**), quantitatively. The reaction of **2** with an excess amount of PhIO results in the formation of a novel μ-oxo dinuclear copper(II) complex $[Cu(HB(3,5\text{-}Me_2pz)_3)]_2O$ (**3**). Complex **3** is readily converted to a bis(μ-hydroxo) dinuclear complex $[Cu(HB(3,5\text{-}Me_2pz)_3)]_2(OH)_2$ (**4**) in the presence of a trace amount of water. CO_2 reacts with **3** to give an adduct $[Cu(HB(3,5\text{-}Me_2pz)_3)]_2(CO_3)$ (**5**). Treatment of **3** with H_2O_2 yields the μ-peroxo dinuclear copper(II) complex $[Cu(HB(3,5\text{-}Me_2pz)_3)]_2(O_2)$ (**6**), which shows many similarities to oxyhemocyanin in its physicochemical properties: diamagnetic; UV-vis 338 nm (ϵ 20800), 530 nm (ϵ 840); ν(O-O) 731 cm^{-1}. The resonance Raman spectroscopic study with mixed labeled hydrogen peroxide establishes that the coordination mode of the peroxide ion in **6** is symmetric as in oxyhemocyanin. Crystallography was performed on **2**, **4** · $2C_6H_6$, and **5**. Compound **2** crystallizes in the monoclinic space group C2/c with a=26.951 (4) Å, b=18.003 (2) Å, c=18.363 (3) Å, β=124.53 (1)°, V=7340 (1) Å^3, and Z=8. The refinement converged with a final R (R_w) value of 8.72% (8.53%) for 4213 reflections with $F_o \geq 3\sigma(F_o)$. Compound **4** · $2C_6H_6$ crystallizes in the triclinic space group $P\bar{1}$ with a=11.051 (3) Å, b=11.296 (3) Å, c=10.121 (2) Å, α=103.03 (2)°, β=103.51 (2)°, γ=105.45 (2)°, V=1127.0 (5) Å^3, Z=1, and final R (R_w) value of 10.83% (11.00%) for 3243 reflections with $F_o \geq 6\sigma(F_o)$. Compound **5** crystallizes in the monoclinic space group $P2_1$ with a=8.068 (1) Å, b=31.008 (5) Å, c=8.064 (1) Å, β=113.59 (1)°, V=1849.7 (5) Å^3, Z=2, and a final R (R_w) value of 5.88% (5.18%) for 2735 reflections with $F_o \geq 3\sigma(F_o)$.

II-D-7 (μ-Alkoxo)diiron(II,II) Complexes of N,N,N′,N′-Tetrakis(2-(6-methylpyridyl)methyl)-1,3-diaminopropane-2-olate and the Reversible Formation of the O_2-Adducts

Yoshihito HAYASHI *(Kanazawa Univ.)*, **Masatatsu SUZUKI** *(Kanazawa Univ.)*, **Akira UEHARA** *(Kanazawa Univ.)*, **Yasuhisa MIZUTANI, and Teizo KITAGAWA**

[*Chem. Lett.*, 91–94 (1992)]

(μ-Alkoxo)(μ-carboxylato)diiron(II,II) complexes with hindered dinucleating ligand were synthesized and the structure of μ-benzoato derivative was determined by X-ray analysis. The complexes showed reversible oxygenation in acetonitrile and dichloromethane. Resonance Raman spectra of these species demonstrated a possibility of unsymmetrical μ-η^1-$\eta^{1'}$ binding of the oxygen toward the diiron centers.

II-D-8 Resonance Raman Studies on the Cu_A Site of Cytochrome *c* Oxidase Using a Multichannel Scanning Raman Spectrometer with a CCD Detector

Satoshi TAKAHASHI, Takashi OGURA, Kyoko SHINZAWA-ITOH *(Himeji Inst. of Tech.)*, **Shinya YOSHIKAWA** *(Himeji Inst. of Tech.)*, **and Teizo KITAGAWA**

A new Raman measurement system with a CCD detector was constructed and applied successfully to observe far-red excited Raman spectra of bovine cytochrome *c* oxidase. In resonance with the 830 nm absorption band, Raman bands were observed at around 330 cm^{-1} and assigned to the Cu_A-S(Cys) and Cu_A-N(His) stretching vibrations. The frequency and intensity of these bands were influenced by neither the redox and ligation changes in cytochrome a_3-Cu_B center nor the binding of cytochrome *c*, indicating the highly independent nature of the Cu_A center. In the higher frequency region of the far-red excited Raman spectra, some protein modes and pre-resonant heme modes were observed. The amide I and III frequencies indicated predominance of α-helix in the enzyme, and the amido hydrogens were scarecely exchanged with deuterons in D_2O, while some Trp side chain bands clearly displayed the deuteration shift.

II-D-9 Resonance Raman Spectra of the Photointermediates in Phytochrome Phototransformation: Deprotonation of the Chromophore in the Bleached Intermediate

Yasuhisa MIZUTANI, Satoru TOKUTOMI *(National Ins. for Basic Biology)*, **and Teizo KITAGAWA**

Resonance Raman (RR) scattering from a large pea phytochrome was observed at cryogenic as well as ambient temperatures. When the probe wavelength was 364 nm in the two color excitation experiments at ambient temperature, a strong RR band was observed at 1625 cm^{-1} under the far-red light illumination, whereas another RR band at 1599 cm^{-1} was intensified under red light illumination. By comparison of these spectra with those observed at low temperatures and those of stable bleached form (P_{b1}), the 1625 and 1599 cm^{-1} RR bands were reasonably assigned to the red light absorbing form (P_r) and the bleached intermediate (I_{b1}), respectively. The 1625 cm^{-1} RR band of P_r exhibited a frequency shift between the H_2O and D_2O solutions. The RR spectrum of the far-red light absorbing form (P_{fr}) was observed by the 407 nm excitation under the red light irradiation. The prominent RR bands of P_{b1}, I_{b1} and P_{fr} in the C=C stretching region did not exhibit a deuteration shift. This indicates distinct differences in protonation states between P_r and other three species. The similarity of RR frequencies and relative intensities of I_{b1} and P_{fr} and, moreover, their deuteration shifts imply that their chromophore configurations closely resemble each other. The remarkable difference of RR spectral pattern in the C=C stretching region between P_r and other three species suggests that the configurational changes of the chromophore, such as the E-Z photoisomerization, are involved in the primary process of the phototransformation, and that deprotonation of the chromophore follows it in the subsequent process yielding I_{b1}.

II-D-10 Time-Resolved Resonance Raman Identification of Hydroperoxy and Ferryloxo Intermediates in Cytochrome Oxidase Catalysis

Takashi OGURA, Satoshi TAKAHASHI, E. APPELMAN *(Argonne Natl. Lab.)*, **K. SHINZAWA-ITOH** *(Himeji Inst. Tech.)*, **S. YOSHIKAWA** *(Himeji Inst. Tech.)*, **Shun HIROTA, and Teizo KITAGAWA**

The reaction of fully-reduced cytochrome oxidase with molecular oxygen has been investigated by time-resolved resonance Raman spectroscopy at 5°C and 30°C in H_2O and D_2O. Two oxygen isotope sensitive bands were observed at 785 and 804 cm^{-1} for the H_2O solution at 5°C with Δt_d=1.1 ms by using a monochromator with higher resolution than before, and they were downshifted to 751 and 764 cm^{-1} upon $^{18}O_2$ substitution, respectively. In D_2O the 804/764 cm^{-1} pair remained unshifted while the 785/751 cm^{-1} pair upshifted to 796/766 cm^{-1}. On the other hand, the 785/751 cm^{-1} pair lost its intensity at 30°C where only the 804/764 cm^{-1} pair was clearly observed, and showed again no frequency shift in D_2O. The results using $^{16}O^{18}O$ as a substrate at 5°C was incompatible with the assignment that the bands at 785 and 804 cm^{-1} arose from the O-O stretching vibration, since the corresponding band did not appear at an intermediate frequency.

From these observations, it was concluded that the bands at 785 and 804 cm^{-1} were associated with the FeO stretching vibrations of the Fe^{III}-O-O-H and the Fe^{IV}=O intermediates, respectively. The FeO and O-O bonds of the Fe^{III}-O-O-H intermediate were deduced to be fairly strong and weak, respectively, thus being ready to become the next Fe^{IV}=O intermediate. The oxygen atom bound to the heme iron of the Fe^{IV}=O intermediate was not hydrogen-bonded on the contrary to the peroxidase case, suggesting a stabilization of this relatively unstable intermediate in cytochrome oxidase.

II—E Vibrational Spectroscopy on Short-lived Molecules and Solution Structure

Raman spectroscopy reveals the vibrational spectrum of molecule which is sensitive to geometrical as well as electronic structures. When the wavelength of the probe beam is tuned within the absorption band of the molecule in question, resonance enhancement of Raman intensity makes it possible to detect Raman scattering from an excited molecule or a reaction intermediate even if its time is short and thus its population are considerably small. We take this advantage of resonance effect to explore the structures of metallo- and free-base porphyrins in the excited singlet and triplet states. We also investigated intermediates of photoreduction of iron-porphyrins. On the other hand, the array detector combined with an optical fiber enabled us to construct a double beam Raman spectrometer and thus to observe a precise difference spectrum. Accordingly, we have applied it to evaluate relative magnitudes of intermolecular interactions and to explore the concentration-dependent cluster structures in a binary mixture of liquid samples.

II-E-1 Time-Resolved Resonance Raman Spectra of Free-base Octaethylporphyrin in the S_1 and T_1 States

Shin-ichiro SATO, Motoko ASANO-SOMEDA, and Teizo KITAGAWA

[*Chem. Phys. Lett.*, **189**, 443—447 (1992)]

Pump/probe time-resolved resonance Raman experiments were carried out for free-base octaethylporphyrin in benzene at room temperature by using two Nd:YAG lasers, and the vibrational spectra of its lowest excited singlet and triplet states were observed. The spectrum of the S_1 state of $OEPH_2$ pumped by the 532 nm pulse closely resembled that obtained by pumping it to the S_2 state, confirming the fast relaxation from S_2 to S_1. The ν_4 band was shifted down by 23 cm^{-1} in S_1 compared to the S_0 state, but its location in the T_1 state could not be determined. The highest-frequency skeletal stretching mode was also shifted down by 15 cm^{-1} upon excitation to S_1, but it shifted up by 5 cm^{-1} upon intersystem crossing to the T_1 state.

II-E-2 Time-Resolved Resonance Raman Investigation of Photoreduction of Iron-octaethylporphyrin Complexes by Using Quasi-Simultaneous Pump/Probe Measurement Technique

Shin-ichiro SATO, Keiji KAMOGAWA, Katsuhiro AOYAGI *(Fukushima National College of Tech.)*, **and Teizo KITAGAWA**

[*J. Phys. Chem.*, **26**, 10676—10681 (1992)]

A new technique for general pump/probe resonance Raman measurements was developed and applied successfully to identify a transient species involved in photoreduction of a ferric porphyrin complex. This technique emphasizes quasi-simultaneous measurements of the pump/probe, pump-only, probe-only and dark spectra. It is demonstrated that the present method brings about not only a higher signal-to-noise ratio but also provides correct spectra of intermediates even if slight photodecomposition by pump light illumination is involved. With this device the time-resolved resonance Raman spectra were observed for a 2-methylimidazole and methanol complex of octaethylporphyrinatoiron(III) [Fe^{III}(OEP)(2MeIm)(MeOH)] and its meso-deuterated- and $^{15}N_4$-isotopomers for the time range between 0 ns and 1 μs following photolysis. The transient spectra were probed by the 416 nm pulse (width=7 ns) after photoreduction was initiated by a pump pulse at 355 nm. The transient spectrum for the delay time (Δt_d) of 20 ns contained the contribution from tetra-coordinate ferrous intermediate-spin species basides that from the penta-coordinate ferrous high-spin species. The latter dominated the spectrum for Δt_d=1 μs but was discernible even at Δt_d=0 ns. Dependences of the transient spectra on the concentrations of

2MeIm and MeOH were examined for Δt_d=100 ns, suggesting that the photoreduction proceeds in two pathways. Plausible mechanism of photoreduction is discussed on the basis of the observed spectra.

II-E-3 A Multi-reflection Raman Measurement Device for the Study of Dilute Aqueous Solutions

Keiji KAMOGAWA, Motomu TAKAMURA *(Hiroshima Univ.)*, **Hiroatsu MATSUURA** *(Hiroshima Univ.)*, **and Teizo KITAGAWA**

A device for multi-reflection Raman measurements was constructed with two rectangular prisms. This device demonstrated 7 to 10 times enhancement of Raman signals, compared with the single-path measurement for a transparent solution sample and is readily applicable to dilute aqueous solutions with low refractive index. With this device the C-H stretching Raman bands of benzene in water were observed with sufficiently high S/N ratio.

II-E-4 Peculiar Conformational Behavior of the Oxyethylene Chain in Dilute Aqueous Solutions: A Multi-reflection Raman Spectroscopic Study

Motomu TAKAMURA *(Hiroshima Univ.)*, **Keiji KAMOGAWA, Hiroatsu MATSUURA** *(Hiroshima Univ. and IMS)*, **and Teizo KITAGAWA**

A multi-reflection Raman cell system was applied to a conformational analysis of the oxyethylene chain in dilute aqueous solutions. The Raman spectra of CH_3-$(OCH_2CH_2)_4OCH_3$ in water thus observed were analyzed on the basis of normal coordinate treatment. The intensities of the bands at 805 and 852 cm^{-1} associated, respectively, with the trans and gauche conformations of the O-CH_2-CH_2-O group were examined as a function of the solution concentration. A plot of the intensity ratio I_{805}/I_{852} decreased on water addition and gave a minimum at a mole fraction of 0.04. This observation indicates that the population of the trans state is the least around this composition. It is suggested that this peculiar conformational behavior of the oxyethylene chain in water is associated with possible compensating effects involved in this binary system. The present experimental finding is important for elucidating the structural aspect of nonionic surfactants containing the oxyethylene chain as a hydrophilic moiety.

II—F EPR Studies on Molecular Structure of Metallofullerenes

Since the success of laboratory synthesis of C_{60} and other carbon clusters "fullerenes", many papers on the clusters and their chemical derivatives have been reported within a few years. As for the metal encapsulated fullerene, M@C_{82} (M=Sc, Y, and La) has been reported to be the only metallofullerene which is macroscopically prepared. The peculiarity of C_{82} in the formation process of metallofullerene might suggest us the point for the investigation on the formation mechanism of fullerenes. From this point of view the studies on the molecular structure of these endohedral complexes must be unambiguously important. We have reported the structural information on M@C_{82} by using an EPR spectroscopy.

II-F-1 Isomers and ^{13}C Hyperfine Structures of Metal Encapsulated Fullerenes, M@C_{82} (M=Sc, Y, and La)

Shinzo SUZUKI *(Tokyo Metropol. Univ.)*, **Satoshi KAWATA** *(Tokyo Metropol. Univ.)*, **Haruo SHIROMARU** *(Tokyo Metropol. Univ.)*, **Kotaro YAMAUCHI** *(Tokyo Metropol. Univ.)*, **Koichi KIKUCHI** *(Tokyo Metropol. Univ.)*, **Yohji ACHIBA** *(Tokyo Metropol. Univ.)*, **and Tatsuhisa KATO**

[*J. Phys. Chem.*, **96**, 7159 (1992)]

The formation of two isomers of C_{82} with a metal inside, M@C_{82} (M=Sc, Y, and La) was first identified by EPR spectroscopy. The production ratio of two isomers found for M@C_{82} suggests that the cage structure of the isomers of M@C_{82} is closely associated with those of the empty C_{82}. However, contrary to the existence of four or more distinct isomers of empty C_{82}, the observation of only two metallofullerene isomers strongly suggests that a metal is selectively encapsulated in the C_{82} cages with particular structures. An endohedral form of metal-containing C_{82} fullerene was established by observation of well-resolved ESR spectra of hyperfine coupling to ^{13}C in natural abundance on the carbon cages.

II-F-2 Hydrodynamic Rotational Effects on EPR Spectra of M@C_{82} in Solution

Shinzo SUZUKI *(Tokyo Metropol. Univ.)*, **Koichi KIKUCHI** *(Tokyo Metropol. Univ.)*, **Yohji ACHIBA** *(Tokyo Metropol. Univ.)*, **and Tatsuhisa KATO**

The line width of the hyperfine components of the EPR spectra of M@C_{82} (M=Sc, Y, and La) in CS_2 and toluene solutions have been measured as a function of temperature. The line-broadening mechanism not only of the insufficient rotational averaging of the g- and hyperfine tensors but also of the spin-rotation interaction has been seen. The values of anisotropy estimated was small, so the line width of EPR spectra in the solution at the ambient temperature was very sharp. But the slow hydrodynamic rotation, which was due to the extraordinarily large molecular size of M@C_{82}, reflected on the specific temperature dependence of the line broadening phenomena.

RESEARCH ACTIVITIES III
Department of Electronic Structure
III—A Time and Frequency Resolved Studies of Isomerization in Gas and Solution Phases

The study of *cis-trans* isomerization in linear polyenes is important for the understanding of photobiological processes, including energy transfer in photosynthesis, *cis-trans* photoisomerization in visual systems and photosynthetic bacteria, and the photochemistry of vitamin D. The complexity of the naturally occurring polyenes inhibits both computational and experimental investigations into these molecules. We have, therefore, studied less complicated model systems, which contain similar chromophores and have analogous photochemical behavior, such as trienes and tetraenes. The fluorescence excitation and emission spectra, and emission lifetimes of S_1 and S_2 states of *trans,trans*-octatetraene, *all-trans*-nonatetraene, and *all-trans*-decatetraene measured in molecular beams provide unprecedented detail of information on the structure and dynamics of polyenes. The ability to selectively excite a molecule to a specific quantum state with a well defined energy, is exploited to study isomerization dynamics of individual vibrational states. An energy activated nonradiative processes with a barrier of <200 cm^{-1} for trienes and ~ 2100 cm^{-1} for tetraenes is observed. We tentatively attribute this nonradiative channel to *cis-trans* isomerization. Also, a new type of organic molecule, crown ether-styryl dyes, have been studied in solution. The main nonradiative channel of the S_1 state is determined to be *trans-cis* isomerization.

III-A-1 Structure and *trans-cis* Isomerization Dynamics of S_1 States of Tetraenes

H. PETEK, R. CHRISTENSEN *(Bowdoin College)*, **Y.S. CHOI** *(Inha University)*, **A.J. BELL, and K. YOSHIHARA**

The fluorescence excitation spectra and emission lifetimes of the symmetry forbidden $2^1A_g \leftarrow 1^1A_g$ transition ($S_1 \leftarrow S_0$) of *trans,trans*-octatetraene, *all-trans*-nonatetraene, and *all-trans*-decatetraene have been measured in free jet expansions (Figure 1). The spectra show evidence of strong coupling of the S_1 state with both S_2 and S_0, which is key to understanding the nonradiative decay mechanisms of both S_1 and S_2 states. Vibronic origins of b_u symmetry appear in the spectrum with intensities that are proportional to the mode specific Herzberg-Teller coupling between the S_1 and S_2 states. The strongest coupling occurs for the vibronic origins of the spectra, which are due to the lowest frequency in-plane bending. The coupling between S_1 and S_0 states gives rise to annomalously high C-C (1225–1229 cm^{-1}) and C=C (1793–1798 cm^{-1}) stretching frequencies. The high frequencies and large displacements make these good accepting modes for internal conversion from the S_1 state. In addition, the appearance in the spectra of many more vibrations than can be attributed to the expected a_g and b_u modes for C_{2h} symmetry may be due to non-planar equilibrium geometries in the S_1 states.

The fluorescence decay rates at low excess energies show a pronounced mode dependence, which is attributed to both state specific radiative and nonradiative decay. For octatetraene vironic states with <1000 cm^{-1} above the origin the lifetimes range between 380 and 170 ns. Certain vibrations such as CC torsions may be more strongly coupled to nonradiative decay channels such as *trans-cis* isomerization. At ~ 2100 cm^{-1} excess energy all three tetraenes show an increase in nonradiative decay rate, which is attributed to opening up of the *trans-cis* isomerization channel.

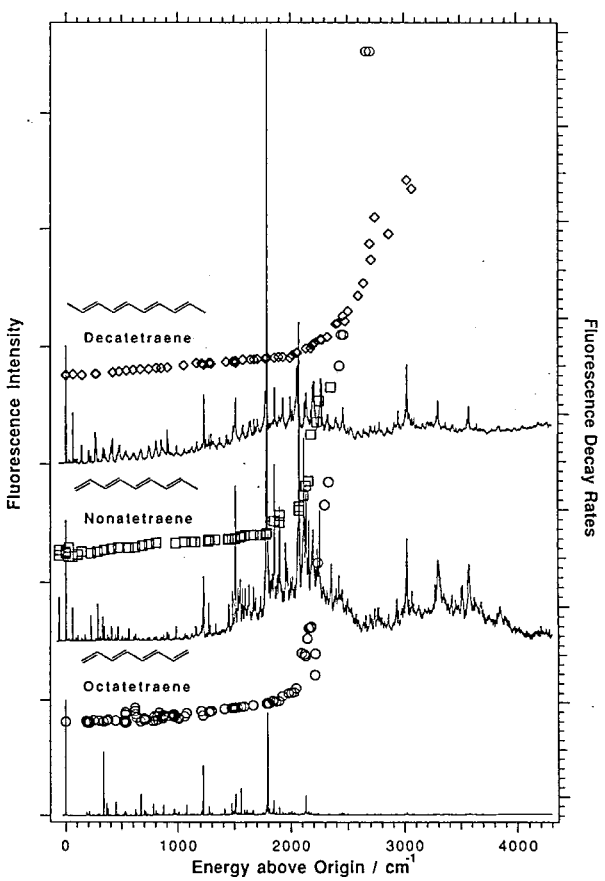

Figure 1. Fluorescence excitation spectra and fluorescence decay rates of the $2^1A_g \leftrightarrow 1^1A_g$ transition ($S_1 \leftrightarrow S_0$) of *trans,trans*-octatetraene, *all-trans*-nonatetraene, and *all-trans*-decatetraene (bottom-to-top). The lowest frequency in-plane bending mode is taken as the origin for each spectrum. Circles, squares, and diamonds represent the fluorescence decay rates. The rates increase from $\sim 2.9\times10^6$ s^{-1} at the origins (each division corresponds to 5.0×10^6 s^{-1}).

III-A-2 Two-photon Spectroscopy of $2^1A_g \leftarrow 1^1A_g$ Transition of Tetraenes

H. PETEK, R. CHRISTENSEN *(Bowdoin College)*, **Y.S. CHOI** *(Inha University)*, **and K. YOSHIHARA**

The structure and vibronic coupling in linear polyenes is studied by one- and two-photon fluorescence excitation spectroscopy of the $2^1A_g \leftarrow 1^1A_g$ ($S_1 \leftarrow S_0$) transition of *all-trans*-octatetraene, nonatetraene, and decatetraene in He free jet expansions (Figure 1). The one-photon $S_1 \leftarrow S_0$ transition of linear polyenes with inversion symmetry is forbidden by symmetry, therefore the spectra consist of only fundamentals and combination bands with b_u symmetry, which derive their transition moments by vibronic coupling with the 1^1B_u (S_2) state. By contrast, the two-photon transitions are symmetry allowed, so only a_g bands appear in the spectra. Therefore in two-photon excitation of *all-trans*-octatetraene and decatetraene the origins are the vibrationless states (0-0 transitions), and in one-photon excitation the origins are the lowest in-plane bending mode with b_u symmetry (1-0 transitions). Since *all-trans*-nonatetraene lacks the inversion symmetry both the electronic origin and the in-plane bending modes can appear in the one- and two-photon spectra. However, the vibronic coupling mechanism dominates the one-photon spectrum. This shows that asymmetric substitution of *all-trans* polyenes is sufficient to destroy the inversion symmetry, but the vibronic coupling is still the major contribution to the transition moment. From the one and two-photon spectra it is possible to determine the electronic origins and the frequencies of the b_u modes. As can be seen in Figure 1, a blue shift of the electronic origin by ~2 and 14 cm^{-1} occurs for each terminal methyl substitution. The fluorescence lifetimes also provide information on vibronic coupling. The lifetimes of one-photon origins are ~340 ns, and for two-photon origins 450, 340, and 490 ns for octatetraene, nonatetraene, and decatetraene. The lifetimes of a_g modes is longer than for the b_u modes since one derives the transition moment from S_0-S_2 coupling and the other from the S_1-S_2 coupling.

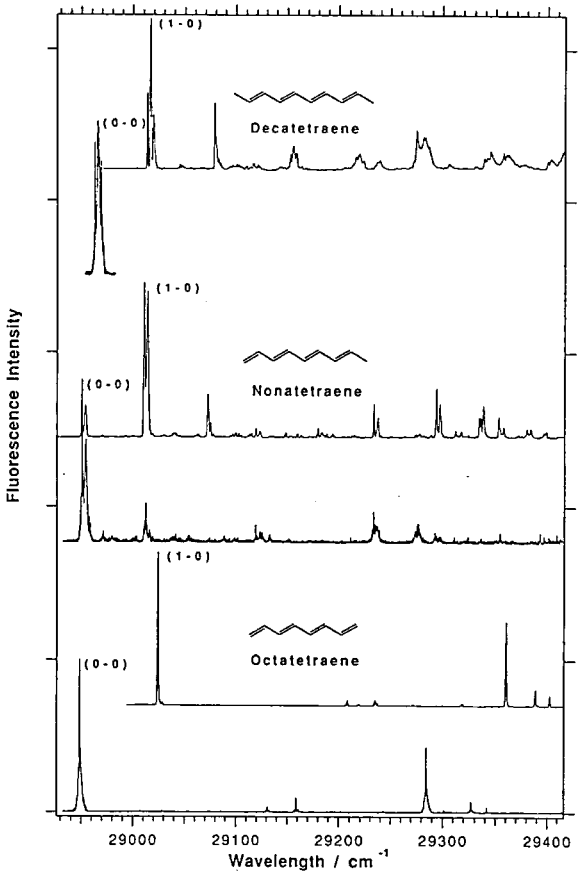

Figure 1. The one- (top) and two-photon (bottom) fluorescence excitation spectra of the $2^1A_g \leftarrow 1^1A_g$ ($S_1 \leftarrow S_0$) transition of *all-trans*-octatetraene, nonatetraene, and decatetraene in He free jet expansions. Relative intensities are normalized to give equal intensities to the vibronic origins and electronic origins in one- and two-photon spectra, respectively.

III-A-3 Structure and Femtosecond Timescale Internal Conversion Nonradiative Decay Dynamics of S_2 States of Tetraenes

H. PETEK, R. CHRISTENSEN *(Bowdoin College)*, **A.J. Bell, and K. YOSHIHARA**

Excitation of tetraenes and pentaenes to the 1^1B_u (S_2) states under isolated conditions gives rise to both $S_2 \rightarrow S_0$ and $S_1 \rightarrow S_0$ emissions.[1] The $S_2 \leftarrow S_0$ fluorescence excitation spectra of *all-trans*-isomers of decatetraene, nonatetraene, and octatetraene were measured in free jet expansions (Figure 1). Since this transitions are due to $\pi^* \leftarrow \pi$ excitation, the spectra are dominated by CC stretching vibrations, reflecting changes in the CC bond lengths. The individual lineshapes can be described by Lorentzian profiles, which are broadened beyond the experimental resolution of ~1 cm^{-1}. This broadening is attributed to $S_2 \rightarrow S_1$ internal conversion on femtosecond timescale. Assuming that statistical coupling limit applies to S_2 states of tetraenes, the Lorentzian linewidths correspond to exponential nonradiative decay rates given by $\tau^{-1}=2\pi c\Gamma$, where τ is the lifetime, c is the speed of light and Γ is the linewidth. The lifetimes range from ~400 fs at the octatetraene origin to ~100 fs for the C=C stretches of nonatetraene and decatetraene. The nonradiative decay rates are about 2 times faster for nonatetraene and decatetraene than for octatetraene. Also, the

rates increase by about a factor of 2 from the origins to CC stretches. The small or no dependence of the decay rates on the methyl substitution implies that the decay rates are not determined by the density of S_1 vibrational states which greatly increase by addition of each methyl group to the tetraene chromophore. Rather, the decay rates may be determined by the location of the conical intersection, which is predicted to occur between the S_1 and S_2 states.

Reference

1) W.G. Bouwman, A.C. Jones, D. Phillips, P. Thibodeau, C. Friel, and R.L. Christensen, *J. Chem. Phys.* **94**, 7429 (1990); H. Petek, A.J. Bell, K. Yoshihara, and R.L. Christensen, *J. Chem. Phys.* **95**, 4739 (1991).

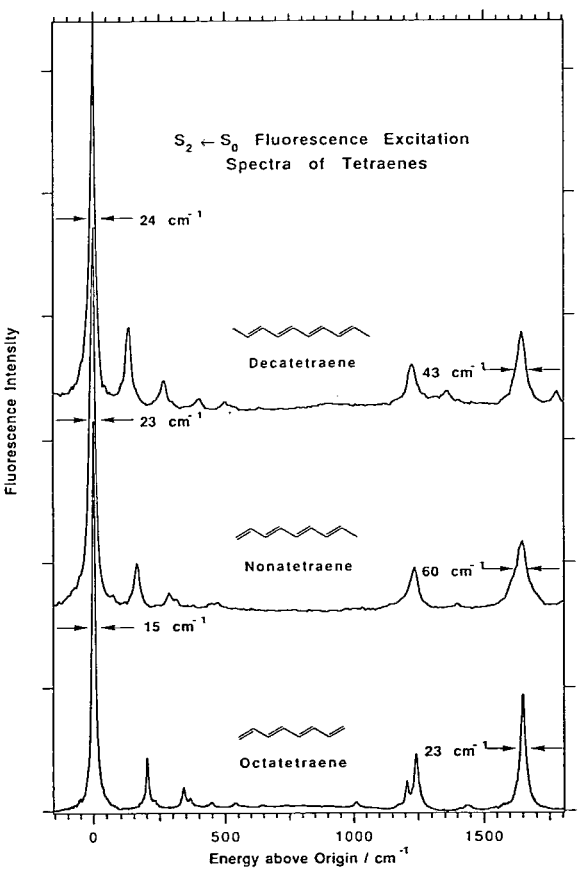

Figure 1. The $S_2 \leftarrow S_0$ fluorescence excitation spectra of *all-trans*-isomers of decatetraene, nonatetraene, and octatetraene in free jet expansions.

III-A-4 Excited State Relaxation of Crown Ether Styryl Dyes: Photoisomerization

Mikhail V. ALFIMOV *(Inst. Chem. Phys., Russian Acad. Sci.)*, **Valey F. KAMALOV, Irina A. STRUGANOVA, and Keitaro YOSHIHARA**

[*Chem. Phys. Lett.* **195**, 262 (1992)]

Photophysical processes are studied in a new class of dyes containing a chromophoric part and a crown ether part (crown ether-styryl dyes, Figure 1). Photoisomerization is proposed to be the main channel of nonradiative decay of the singlet excited electronic state. The temperature dependence of fluorescence decay was measured and the lifetime of the trans-isomer in excited electronic state was found to decrease with temperature in ethanol solutions. Isomerization around the C=C bond is discussed, and the activation barrier is estimated as 2.3 and 1.5 kcal/mol for the two crown ether styryl dyes studied.

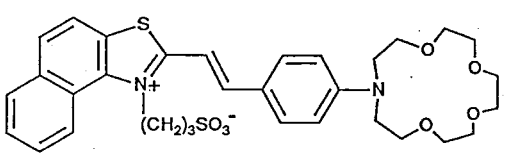

1

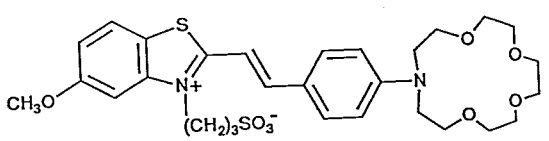

2

Figure 1. Structural formula of crown ether styryl dyes.

III—B Ultrafast Intermolecular Electron Transfer in Electron Donating Solvent

Photo-induced intermolecular electron transfer in non-reactive solvent is usually limited by the translational diffusion rate, which determines the probability of encounter. To study the dynamics of fast electron transfer reaction, it is preferable to perform the experiment in a system, in which electron donor and acceptor are in direct contact, so that the diffusion process may be neglected. One example of such type of system is realized when the solvent itself acts as a donor or an acceptor. We have recently reported ultrasfast fluorescence quenching of exited dye molecule (nile blue A porchlorate) in neat weakly polar electron-donating solvents: aniline and N,N-dimethylaniline, and the dynamics of absorption of reaction products. The rates of electron transfer are in the sub-picosecond range in aniline and a few hundred of femtoseconds in dimethylaniline.

To understand the role of solvent dynamics and intramolecular motion in electron transfer, it is important to study the time dependence of the reaction in detail. Accurate measurements of fluorescence decays were made in two xanthene dyes, nile blue A perchlorate and oxazine 1 perchlorate, both in aniline and N,N-dimethylaniline at several emission wavelengths,

and under the excitation with ~1500 cm^{-1} excess energy and close to the 0-0 transition (**III-B-1**). The effects of the solvent and intermolecular motions were studied with the aid of the shapes of fluorescence decay curves (**III-B-2**).

III-B-1 Femtosecond Inter-Molecular Electron Transfer: Dye in Weakly Polar Electron-Donating Solvent

Keitaro YOSHIHARA, Arkady YARTSEV, Yutaka NAGASAWA, Hideki KANDORI, Abderrazzak DOUHAL, and Klaus KEMNITZ *(Gov. Ind. Res. Inst., Osaka)*

[*Ultrafast Phenomena VIII, Springer Verlag,* in press]

Electron transfer (ET) in solutions of xanthene dyes, nile blue (NB) and oxazine 1 (OX1) in aniline (AN) and N,N-dimethylaniline (DMA) was measured as fluorescence decay of excited dyes by the up-conversion technique with sub-hundred femtosecond time resolution. Clearly nonexponential fluorescence decays (Figure 1a) were measured for OX1 and NB (data not shown) in AN upon the excitation with ~1500 cm^{-1} excess energy (at ~605 nm). To understand the role of vibrational relaxation and solvent Stokes shift in the fluorescence quenching, emission decay curves were measured in a wide spectral range (670–830 nm). The same time behaviour of fluorescence in the all emission spectra is observed indicating that both vibrational relaxation is faster than electron transfer in AN (0.3–5 ps). To eliminate the effects of vibrational relaxation complitely, excitation at 675 nm was used. The same nonexponential fluorescence decays were measured for OX1 in AN. ET kinetics in a case of both OX1 and NB in DMA are well fitted by single exponentials (Figure 1b) with time constants of 280 and 160 fs (data not shown), respectively. It seems that ET in this case occurs about ten times faster than solvent reorientation processes. The exponential character of fluorescence quenching indicates also that vibration relaxation in excited molecules is faster than 100 fs.

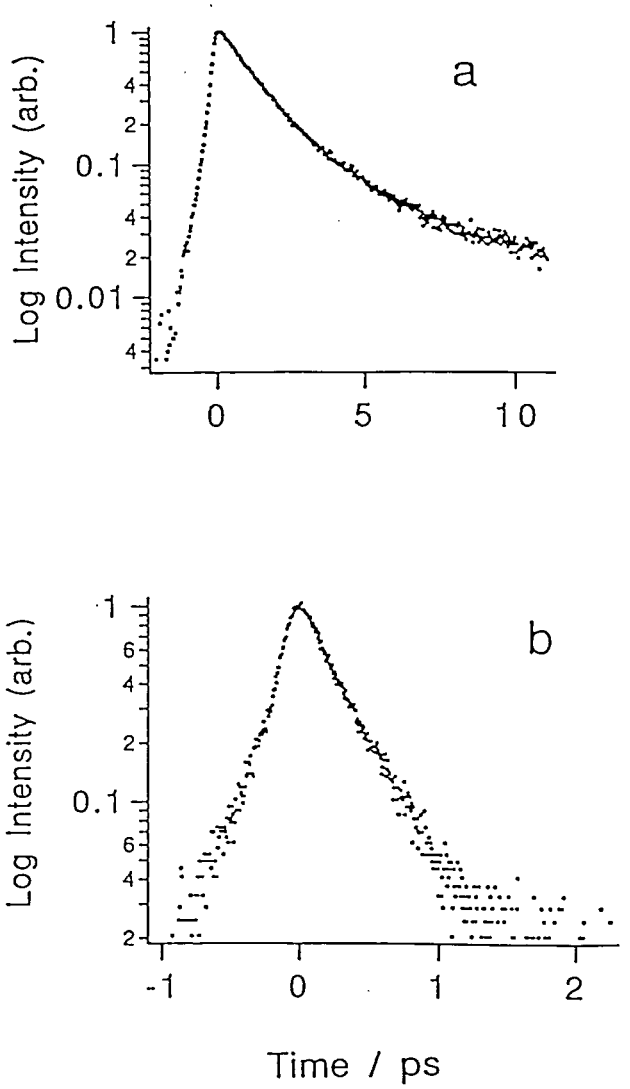

Figure 1. Fluorescence quenching decays of OX1 upon the excitation at 605 nm: **a** - in AN (nonexponential), **b** - in DMA (single exponential).

III-B-2 Ultrafast Chemical Reaction beyond Solvent Control

Keitaro YOSHIHARA, Arkady YARTSEV, and Yutaka NAGASAWA

Chemical reactions in solution are strongly influenced by the nature of solvent and its dynamics. For ultrafast reactions with the rates comparable to solvent fluctuation rate, the motion and structure of solvent can determine the rates of chemical reaciton, which becomes "solvent-controlled". When reaction is faster than solvent relaxation times, a new type of reaction mechanism, induced by intramolecular vibrations may become significant. On a basis of analyses of fluorescence measurements with sub-hundred femtosecond time-resolution (III-B-1), we report the first evidence of an intermolecular electron-transfer reaction beyond solvent control or independent from solvent dynamics, and reaction close to the limit of dynamic solvent control. The former gives a single-exponential time dependence with a rate

constant of 10^{13} s^{-1}, while the latter clear non-exponential dependence.

III-B-3 Picosecond Kinetics of Light-Induced Electron Transfer from J-Aggregated Cyanine Dyes to AgBr Microcrystals: Effect of Aggregate Size

Tadaaki TANI *(Fuji Photo Film Co.)*, **Takeshi SUZUMOTO** *(Fuji Photo Film Co.)*, **Klaus KEMNITZ** *(Gov. Ind. Res. Inst. Osaka)*, **and Keitaro YOSHIHARA**

[*J. Chem. Phys.* **96**, 2778 (1992)]

The light-induced electron transfer from 5,5'-dichloro-9-ethylthiacarbocyanine (dye 1) and related dyes to octahedral silver bromide microcrystals was studied in a photographic emulsion. The energy gap dependence of the quantum yield of electron transfer [$\phi=k_s/(k_s+k_L)$, where k_s and k_L are the rate constants of the electron transfer and competing deactivation channels, respectively] obeyed the Marcus theory with a very small total rearrangement energy of 0.05 eV. The aggregate size of dye 1 on the microcrystals was increased by increasing the agitation temperature of the emulsion. The effect of the aggregate size on the kinetics of electron transfer was studied by means of a time-correlated single-photon-counting system. The film samples were scanned at several centimeters per second to avoid photoinduced damage. For a J-aggregate consisting of ~6 molecules, ϕ_r, k_s, and k_L were 0.44, $1.69\times10^{10}s^{-1}$, and $2.17\times10^{10}s^{-1}$, respectively, and for a larger J-aggregate of ~14 molecules, we obtained 0.20, $1.03\times10^{10}s^{-1}$, and $4.23\times10^{10}s^{-1}$, respectively. It is thought that the proportionality of the radiative rate constant of the J-aggregate to its size, as given by exciton theory, made a substantial contribution to the increase in k_L and to the decrease in ϕ_r with aggregate size (Figure 1). The decrease in k_s with aggregate size is consistent with the mechanism of exciton-trapping supersensitization.

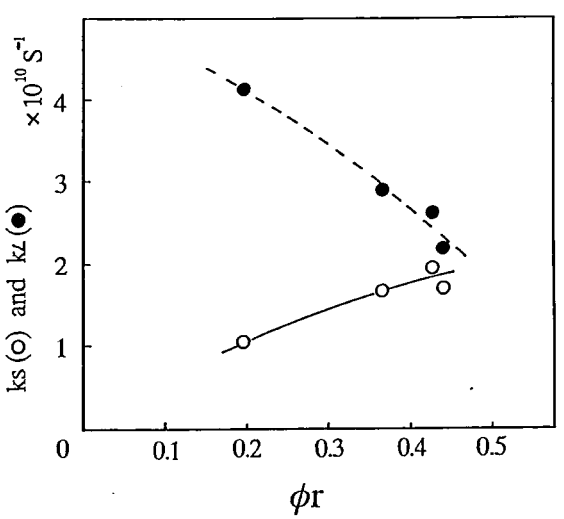

Figure 1. Change of k_s and k_L with change in ϕ_r of J-aggregates of dye 1 formed on octahedral AgBr microcrystals in emulsions, which were agitated for 20 min at 40, 50, 60, and 70°C, aggregate size being increased upon raising temperature. The added amount of each dye was 0.16 mmol/mol of AgBr.

III-B-4 Picosecond Fluorescence Lifetime of J-aggregates of Cyanine Dyes Adsorbed on AgBr and SiO_2: Sample Scanning Effect

Takeshi SUZUMOTO, *(Fuji Photo Film Co.)*, **Klaus KEMNITZ** *(Gov. Ind. Res. Inst., Osaka)*, **Keitaro YOSHIHARA, and Tadaaki TANI** *(Fuji Photo Film Co.)*

A sample composed of J-aggregats of cyanine dyes adsorbed on AgBr and SiO_2 suspended in a dried gelatin layer was scanned by exciting laser pulses for the measurement of the fluorescence lifetimes (τ_F). The value of τ_F of a scanned sample was found to be significantly longer than that of the corresponding static sample (Figure 1). This result indicates that the latter was influenced by some photochemical damage caused by many weak laser pulses incident upon a fixed position on the sample.

The quantum yield of electron transfer from 1,1'-diethyl-2,2'-quinocyanine (PIC) in the lowest excited singlet state to the conduction band of AgBr was small and could be improved by hole-trapping super-sensitization. Electron transfer from a supersensitizer (SS) to PIC in the excited state enhanced a further electron transfer from PIC to AgBr. A set of τ_F obtained by scanning the samples with PIC and SS was in favor of the mechanism of hole-trapping supersensitization, whereas that by static samples was not, especially in the case with small amount of SS. The obtained results indicate that the correct value of τ_F could be obtained by the measurement with each sample scanned by excitation laser pulses.

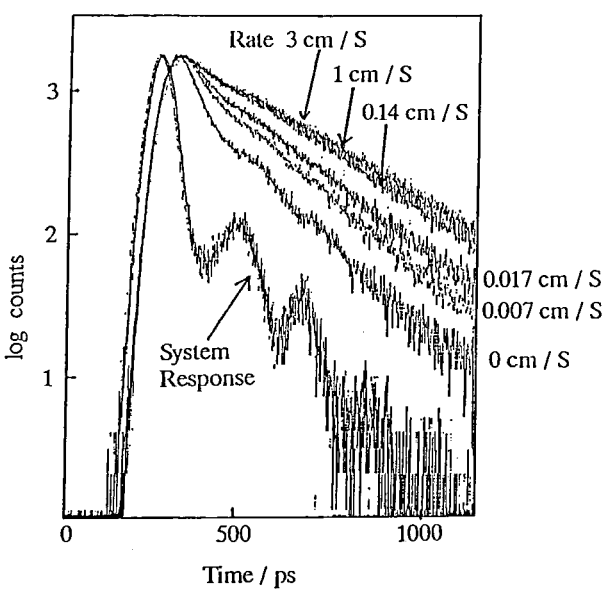

Figure 1. Fluorescence decay curves of 5,5'-dichloro-3,3'-disulfopropyl-9-ethylthiacarbocyanine adsorbed on silica gel (SiO_2), 1.28ps/channel. The scanning rates of the samples were 0, 0.007, 0.017, 0.14, 1 and 3 cm/sec.

III—C Primary Photochemical Events in Biological Systems

Photoreceptive pigments in biological systems utilize light for generating either signal or energy. The typical systems are vision, photosynthesis and photomorphogenesis. In these systems, primary reaction takes place rapidly from their excited state, so that it can overcome the other relaxation processes back to the original state. Thus highly efficient biological systems are realized. We present subpicosecond transient absorption of bacterial rhodopsins, photosynthetic reaction center and phytochrome, to elucidate their primary events. We also studied protein fluorescence from lens crystallins in order to clarify the mechanism of photochemical processes. We observed photochemical modification of lens proteins which may be a contributing factor in human cataracts.

III-C-1 Retinal Proteins (Photoisomerization): Comparative Study of Two Bacterial Rhodopsins, Bacteriorhodopsin and Halorhodopsin

Hideki KANDORI, Keitaro YOSHIHARA, Hiroaki TOMIOKA *(RIKEN)*, **Hiroyuki SASABE** *(RIKEN)*, **and Yoshinori SHICHIDA** *(Kyoto University)*

Subpicosecond time-resolved spectroscopy is applied to investigate the primary photochemical events of bacteriorhodopsin (bR), and they are compared with those of halorhodopsin (hR) investigated under the same experimental conditions [Kandori et al. (1991) *Chem. Phys. Lett.* **187**, 579; Kandori et al. (1992) *J. Phys. Chem.*, in press]. The difference absorption spectrum between bR and its excited state (Figure 1) displays a flat feature in 460—510 nm region, indicating that the spectrum of the excited state of bR has not a single peak but a structured shape as well as that of hR. The spectral feature of stimulated emission from the excited state of bR is also similar to that of hR, whose emission maximum lies at 715 nm. The lifetime of the excited state of bR is estimated to be 0.5 ps which is in good agreement with those reported previously, and about five times shorter than that of hR (2.3 ps). Under the same excitation conditions, bR displays a twice greater absorbance change than hR due to K-intermediate formation, suggesting that the quantum yield of cis-trans isomerization in bR is about twice greater than that in hR. These spectroscopic similarities and differences between bR and hR are discussed in relation to the structural information in bR that Asp_{85} is proposed to be a key residue for the highly efficient cis-trans isomerization.

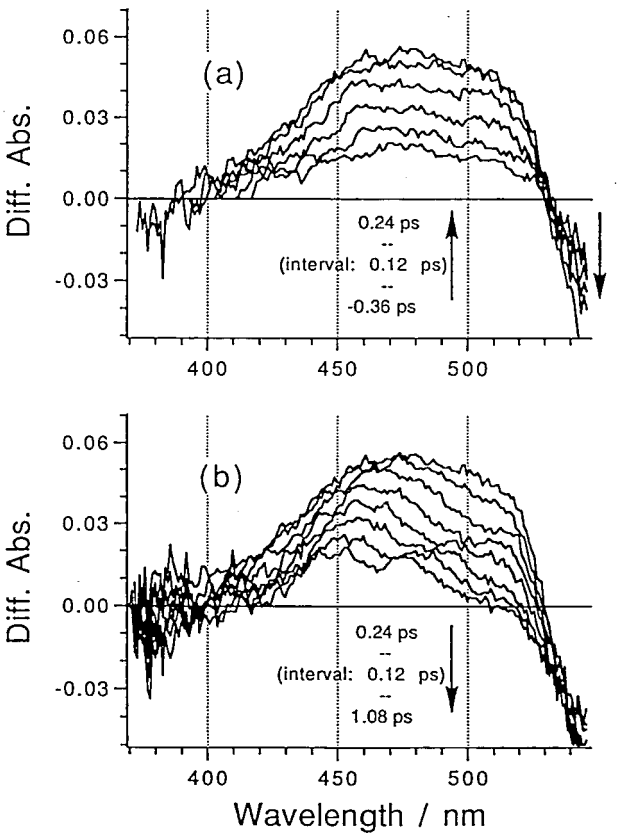

Figure 1. The difference absorption spectra of bR before and after excitation with a 600 nm, 0.5 ps, 30 μJ pulse. (a) The difference spectra at −0.36 to 0.24 ps with 0.12 ps intervals (from bottom to top). The difference absorbance in 430—520 nm increases without changing spectral shapes as time proceeds. These spectra intersect the baseline at same wavelength, 532±1 nm forming an isosbestic point. (b) The difference spectra at 0.24 to 1.08 ps with 0.12 ps intervals (from top to bottom). The difference absorbance in 430—520 nm decreases accompanied by the change of the spectral shape as time proceeds. The intersection point shifts from 532 nm to shorter wavelength side. No isosbestic point among spectra is observed in these wavelengths region.

III-C-2 Photosystem I Reaction Center (Electron Transfer): First Step of Photosynthesis in Higher Plants

Hideki KANDORI, Keitaro YOSHIHARA, and Isamu IKEGAMI *(Teikyo University)*

Transient absorption spectroscopy was applied to spinach PS-I particles having a chl-a/P700 ratio of about 10, in order to study primary photochemical events in PS-I reaction center. Comparative spectral and kinetic investigation between the oxidized and reduced PS-I reaction centers, after weak excitation (8.5% molecules are excited) with a

600 nm, 0.8 ps pulse, enabled us to elucidate the detailed primary processes in PS-I reaction center. Both oxidized and reduced PS-I particles show similar transient absorption spectral features in early picosecond regime, instantaneous depletion of the absorption accompanying excited-state absorption and stimulated emission, and the recovery of the depletion due to energy transfer with time constants of 13—14 ps (Figure 1). By comparing spectral and kinetic data of oxidized and reduced PS-I particles, reduction rate of primary electron acceptor (A_0) is determined to be (14 ps)$^{-1}$. Based upon the present experimental results, two alternative models regarding primary reaction scheme of PS-I particles are presented; (i) primary electron transfer rate is limited by energy transfer rate (14 ps)$^{-1}$, and the former is estimated to be ($<$3 ps)$^{-1}$. (ii) primary electron transfer rate is (14 ps)$^{-1}$, while the energy transfer with (14 ps)$^{-1}$ is not connected to any charge transfer process. Although both possibilities are still open, the first possibility is more likely, i.e., electron transfer in PS-I particles in higher plants is as fast as those obtained for purple bacteria.

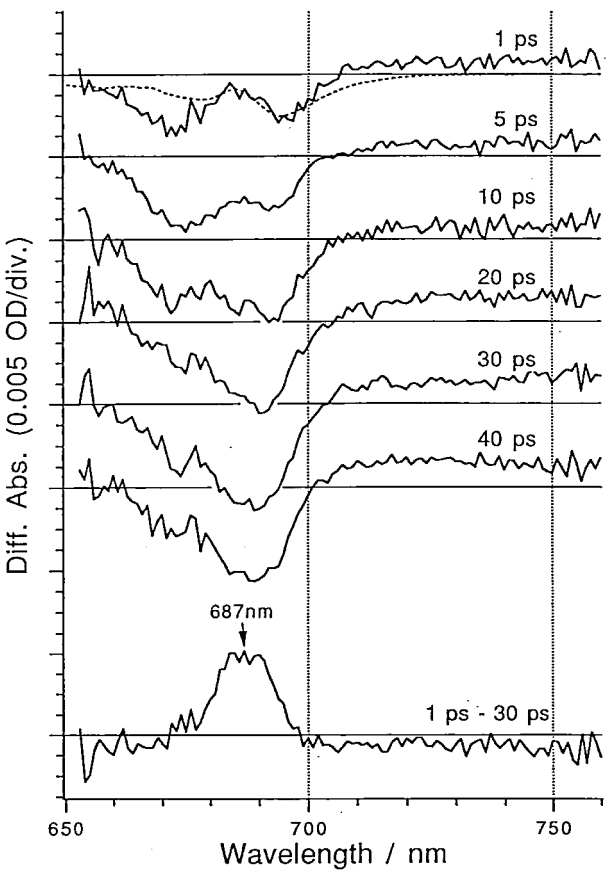

Figure 1. Reduced-minus-oxidized difference absorption spectra. Steady reduced-minus-oxidized difference absorption spectum is superimposed to that at 1 ps (broken line), after being multiplied −0.085 (8.5% photon absorption under the present condition). At the bottom, the difference spectrum between 1 ps and 30 ps of reduced-minus-oxidized spectrum is also shown, which corresponds to the spectral feature depleting (positive side) and appearing (negative side) during 1 ps and 30 ps.

III-C-3 First Step of Photomorphogeneses in Green Plants

Hideki KANDORI, Keitaro YOSHIHARA, and Satoru TOKUTOMI *(National Institute for Basic Biology)*

Primary reaction rate of phytochrome, the chromoprotein which trigers photomorphogenetic processes in plants, is determined by picosecond transient absorption spectroscopy (Figure 1). Excitation of the red-absorbing (Pr) form of pea large phytochrome induces rapid depletion of the original absorption, followed by recovery of the absorption and appearance of the primary photoproduct at about 695 nm. Both time constants are 24 ps, indicating that the product is formed at the expense of the excited state of Pr-form. The primary reaction of phytochrome to express its function has been considered most likely to be Z-E photoisomerization of the tetrapyrrole chromophore, whereas the rate is two-order of magnitude slower than photoisomerization of rhodopsins.

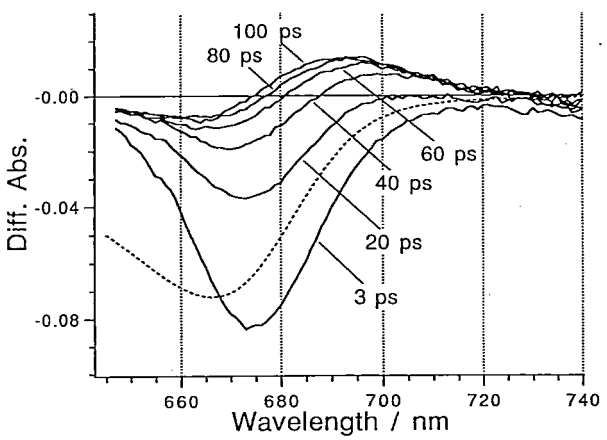

Figure 1. Transient absorption spectra of Pr-form of phytochrome on excitation with a subpicosecond pulse (wavelength; 600 nm, pulse width; 0.8 ps, energy; 16 μJ/1.6 mmϕ). An original absorption spectrum is also shown (broken line) after being multiplied by −0.12 (percentage of excitation). The spectrum at 100 ps is ascribed to the difference between the primary product and the original phytochrome.

III-C-4 Picosecond Fluorescence Decay of Lens Crystallin Proteins

Raymond F. BORKMAN, Abderrazzak DOUHAL, and Keitaro YOSHIHARA

The fluorescence decay of tryptophan residues in the bovine lens crystallins α, β_H, β_L, and γ-II have been measured in aqueous buffer solutions with an instrument having 80 picosecond time resolution. Results were obtained for the three crystallin fractions α, β_H, and β_L as a function of emission wavelength and for the pure protein γ-II crystallin as a function of wavelength, temperature, dissolved oxygen, and denaturing solvent. The crystallins all displayed complex fluorescence decays which could be fit reasonably well with a biexponential model with a long component (few ns) and a short component (few hundred ps). The decay parameters for each crystallin fraction differed significantly from each other. For example, in buffer solution with 360 nm detection: α-crystallin, τ_1=3.5 ns, τ_2=500 ps;

β_H- crystallin, τ_1=2.8 ns, τ_2=420 ps; β_L-crystallin, τ_1=3.3 ns, τ_2=460 ps; and γ-II crystallin, τ_1=1.8 ns, τ_2=300 ps some examples being shown in Figure 1. The fluorescence quantum yield of γ-II crystallin was also measured. This, combined with quantum yield and lifetime data for the reference N-acetyltryptophan amide (NATA), indicated that all four of the Trp residues in γ-II emit and that there is no significant static quenching of any residue.

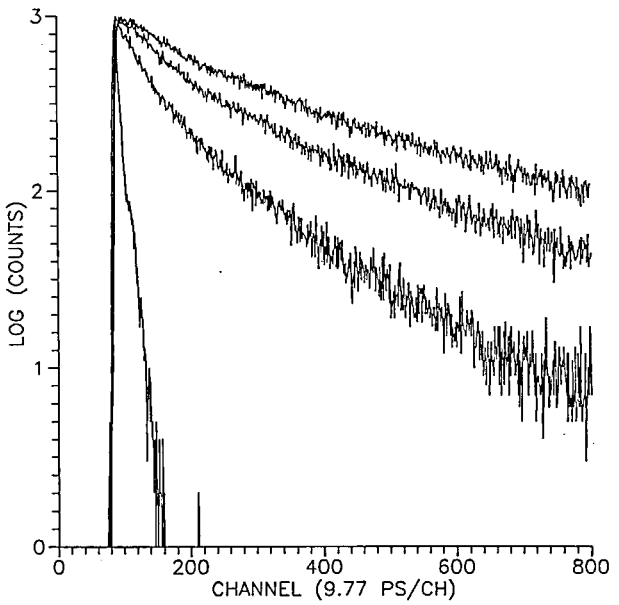

Figure 1. Typical fluorescence decay curves detected at 360 nm for (Top to bottom): Bovine α-crystallin, β_H-crystallin, and γ-II crystallin in Aqueous Buffer Solution pH 7.4 at 23°C. The instrument response function is also shown. Excitation is at 295 nm in all cases.

III-C-5 Picosecond Fluorscence Decay in Photolyzed Lens Protein α-Crystallin

Raymond BORKMAN, Abderrazzak DOUHAL, and Keitaro YOSHIHARA

Photolysis of calf lens protein fraction α-crystallin in aqueous solutions has been monitored by observing changes in fluorescence decay following UV Irradiation at 308 nm. The fluorescence decay was biexponential in dark control solutions and in photolyzed solutions. The best-fit lifetime components in pH 7.4 phosphate buffer solution at 23°C were 3.5 and 0.5 ns, before irradiation, and 2.7 and 0.5 ns after irradiation. As the UV dose increased, the relative weighting coefficient of the 2.7 ns decay component decreased and that of the 0.5 ns component increased resulting in an overall lifetime shortening as shown in Figure 1. Similar results were obtained in 5 *M* guanidine hydrochloride solutions where lifetime components of 2.7 and 0.5 ns were observed. These observations were in contrast to the behavior of tryptophan monomer solutions which did not show any change in fluorescence decay kinetics upon UV photolysis but only a reduced fluorescence intensity. Steady state fluorescence spectra and fluorescence quantum yields were also measured at 23°C for bovine α-crystallin and gave Φ_F=0.11±0.01 in pH 7.4 buffer, and Φ_F=0.10±0.01 in 5 *M* guanidine hydrochloride solutions. The combined steady state and fluorescence decay data were consistent with assignment of the long-lived fluoreoscence decay component in α-crystallin to emission from Trp-9 which was relatively rapidly photolyzed. The short-lived decay component was assigned to Trp-60 which appeared to photolyze much more slowly.

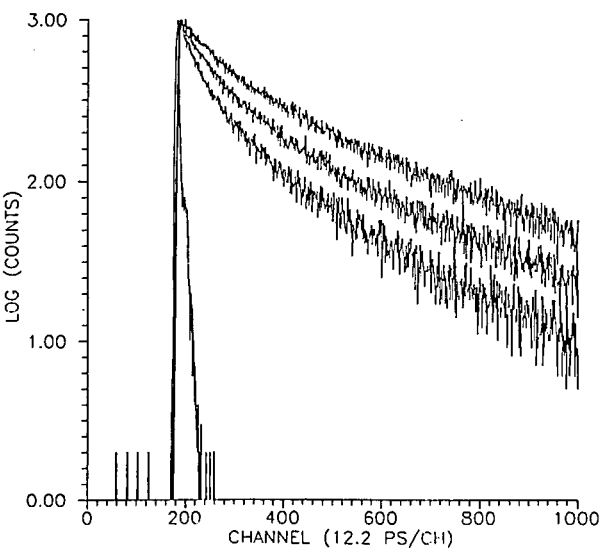

Figure 1. Fluorescence decay data at an emission wavelength of 360 nm for bovine alpha crystallin in pH 7.4 buffer solution at 23°C excited at 295 nm. The three curves (top to bottom) represent 0, 2, and 8 minutes of UV irradiation at 308 nm. The instrument response function is also shown.

III—D Application of Femtosecond Time-Resolved Coherent Anti-Stokes Raman Scattering

Vibrational phase relaxation (dephasing) is a fundamental physical process of molecular dynamics and has recently attracted considerable attention. Both experimental and theoretical studies have been performed to understand microscopic processes of vibrational dephasing. Developments in ultrafast spectroscopy enable us to obtain direct time-domain information on molecular vibrational dynamics. We have constructed a femtosecond time-resolved coherent anti-Stokes Raman scattering (CARS) measuring system, with an overall time resolution of less than 100 fs. This system has been used to study vibrational dephasing of molecules in liquids and solutions. Here we report femtosecond time-resolved CARS for C≡N stretching vibration of various alkanenitriles ($C_nH_{2n+1}CN$ or mononitriles) and α,ω-alkaneditriles ($NCC_mH_{2m}CN$ or dinitriles). From the results obtained for these two series of nitriles, we discuss intramolecular and intermolecular contributions to vibrational dephasing. J-aggregates of dyes are of great interest because of their high non-linear optical properties. In order to investigate electronic and vibrational properties, the first experimental study of resonance coherent CARS has been observed at room temperature.

III-D-1 Femtosecond Time-Resolved Coherent Anti-Stokes Raman Scattering from Liquid Alkanenitriles: Dependence of Vibrational Dephasing on Molecular Size and Solvent-Solute Interactions

Ryoji INABA *(Univ. of Tokyo and IMS)*, **Hiromi OKAMOTO** *(Univ. of Tokyo)*, **Keitaro YOSHIHARA**, and **Mitsuo TASUMI** *(Univ. of Tokyo)*

Femtosecond time-resolved coherent anti-Stokes Raman scattering has been observed for the C≡N stretching at about 2250 cm^{-1} of alkanenitriles ($C_nH_{2n+1}CN$, n=1 ~ 17), some examples being shown in Figure 1. From the plot of vibrational dephasing rates ($1/T_2$) of the C≡N stretching against density of vibrational states, we find that (1)The vibrational dephasing rate is nearly proportional to the logarithm of the density of vibrational states at the energy level of C≡N stretching vibration, and (2)The dephasing of C≡N stretching mode is accelerated in the mixtures with methanol (1:1 in mole ratio) in comparison with that in the neat liquids. The magnitude of acceleration is almost independent of molecular size (~30% decrease in dephasing time).

The former experimental result suggests the domination of the intramolecular process in the dephasing of C≡N stretching while the latter implies that intermolecular interaction plays an important role. These two apparently contradictory results may be consistently combined by assuming that intramolecular and intermolecular dephasing processes cannot be clearly separated.

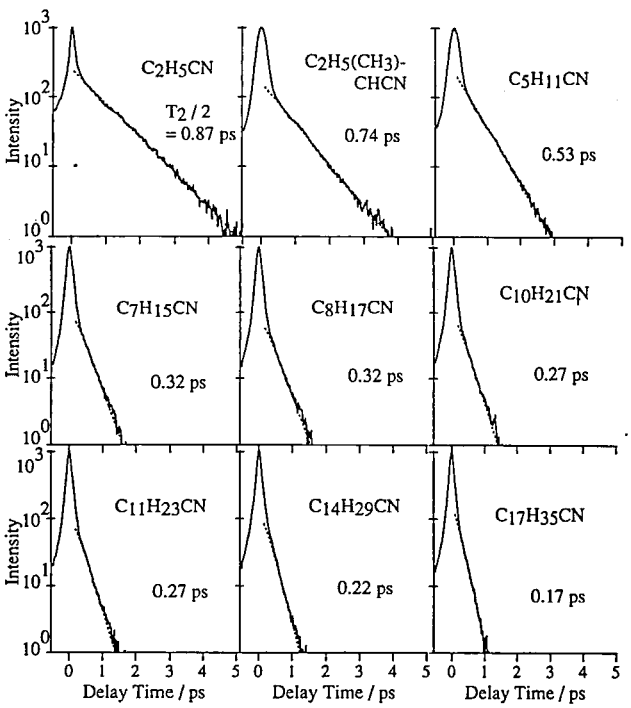

Figure 1. Time-resolved CARS intensities for the C≡N stretching of mononitriles. The strong peaks at zero delay time are due to the nonresonant background. The broken lines are the results of the least-squares fits of the single-exponential decay functions to the observed profiles.

III-D-2 Femtosecond Time-Resolved Coherent Anti-Stokes Raman Scattering from Liquid Alkanedinitriles: Intramolecular Coupling between the Two C≡N Stretching Modes

Ryoji INABA *(Univ. of Tokyo and IMS)*, **Hiromi OKAMOTO** *(Univ. of Tokyo)*, **Keitaro YOSHIHARA**, and **Mitsuo TASUMI** *(Univ. of Tokyo)*

[*J. Phys. Chem.*, in press]

Femtosecond time-resolved coherent anti-Stokes Raman scattering has been observed for the C≡N stretching at about 2250 cm^{-1} of alkanedinitriles ($NCC_nH_{2n}CN$, n=1 ~ 6). In Figure 1, the dephasing time constants of dinitriles and those of mononitriles are plotted against the density of vibrational states at the C≡N stretching frequency of the respective molecule. The vibrational dephasing of small dinitriles like $NCCH_2CN$ is significantly faster than that of the corresponding mononitriles. As the dinitrile becomes larger, the dephasing rate approaches that of the corresponding mononitrile.

The results observed for dinitriles may be explained in terms of the strength of coupling between the Raman active C≡N stretching and background dark states. In dinitriles, the symmetric (strongly Raman active) and antisymmetric (weakly Raman active or forbidden) C≡N stretching modes have nearly the same fundamental frequencies. Therefore, the inter-state coupling between the vibrationally excited states of the symmetric and antisymmetric C≡N stretching modes would be large because of the resonance effect, if the two CN groups are geometrically close. If the distance between the two CN groups is large, the coupling would be weak, so that the dephasing time constants approach those of the corresponding mononitriles.

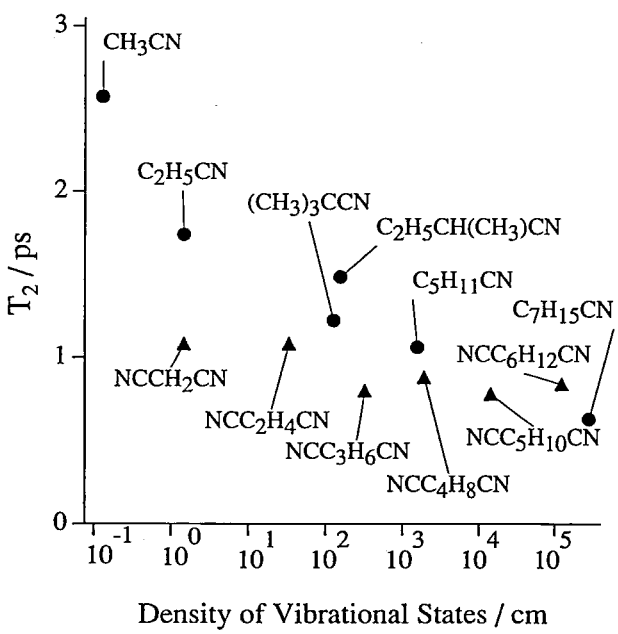

Figure 1. Plot of the vibrational dephasing time constant (T_2) of the C≡N stretching vibration against the calculated density of vibrational states at the C≡N stretching frequency. (●) mononitirles; (▲) dinitriles.

III-D-3 Dephasing and Beats of Excitonic-Enhanced Transitions of J-Aggregates Measured by Femtosecond Time-Resolved Resonance CARS

Valey F. KAMALOV, Ryoji INABA *(Univ. of Tokyo and IMS)*, **and Keitaro YOSHIHARA**

[*Ultrafast Phenomena VIII, Springer*, in press]

J-aggregates of carbocyanine dyes in solutions were studied by femtosecond resonance CARS. The CARS signal intensity plotted against Δt at the fixed frequency difference 2245 cm^{-1} is shown in Figure 1. It is determined by electronic susceptibility of J-aggregate at this frequency difference, no Raman contributions is expected at this frequency. CARS signal at this $\Delta\omega$ coincides practically with the response function of spectrometer, showing that dephasing time of excitonic transition of J-aggregate is shorter than 100 fs. CARS intensity at frequency difference 1000 cm^{-1} presented in Figure 1 shows a fast response at short Δt followed by a longer monoexponential decay with τ=0.43 ps. Two components in CARS decay profile can be assigned to excitonic and Raman susceptibilities, respectively. CARS decay measured at frequency difference 1300 cm^{-1} is shown in Figure 1 (right). Here CARS signal decay accompanying peaks with period of about 180 fs. This 180 fs period corresponds to high frequency, about 5.5 THz (185 cm^{-1}), beats. These beats are due to coherent excitation of two different vibrational modes of J-aggregate by board spectrum of femtosecond pulse (85 fs duration corresponds 400 cm^{-1}).

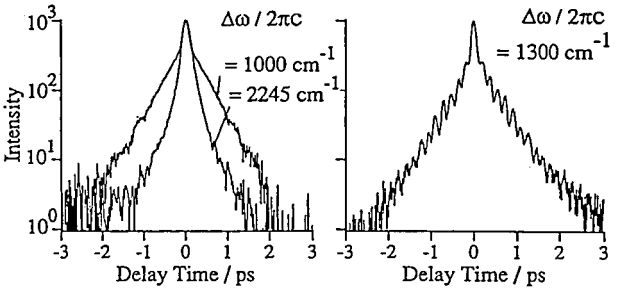

Figure 1. Time-resolved CARS signal of J-aggregate at $\Delta\omega/2\pi c$=2245 cm^{-1} (determined by excitonic transition), 1000 cm^{-1} (excitonic and single Raman mode), 1300 cm^{-1} (excitonic and two Raman modes).

III—E Spectroscopy of the Cs_2 in a very Cold Supersonic Jet by the Multiphoton Ionization

Alkali metal dimers are very suitable for studying perturbations and the photodissociation dynamics of the excited states. They have many electronic states which absorb from near IR to UV region and some of the excited states predissociate to produce excited atoms. Among the alkali dimers Cs_2 has the greatest number of states in the visible region and has been extensively studied. The major difficulty in the spectroscopic study of Cs_2 has been the complexity of the spectrum. Since Cs_2 is a heavy molecule with a low vibrational frequency and a small rotational constant, high vibrational and rotational states are significantly populated even in the cw supersonic jet. Only by applying very high resolution spectroscopic methods could the spectral lines be assigned unambiguously and useful molecular parameters determined.

We have developed a new high temperature pulsed nozzle to generate small alkali metal clusters at very low internal temperatures. Combining this nozzle with the multiphoton ionization method, we greatly simplified the absorption spectrum of Cs_2 and observed many new electronic states of Cs_2 which were hidden under the complex spectral atlas caused by the strong perturbations and the hot bands.

III-E-1 New Triplet Excited States of Cs_2 Observed by Resonance Enhanced Two Photon Ionization Spectroscopy in a very Cold Supersonic Jet

Bongsoo KIM and Keitaro YOSHIHARA

[Submitted to *J. Chem. Phys.*]

Cs_2 was generated by expanding Cs vapors with Ar or Kr gas through a modified automobile fuel injection valve. By cooling the solenoid part with water, the nozzle could be heated up to 600°C. Cs_2 absorption spectrum was obtained by detecting Cs_2^+ ions generated by resonance enhanced two photon ionization. We could detect the Cs_2 ion signals using a time-of-flight mass spectrometer which has a 70 cm flight tube and a dual microchannel plate. In Figure 1 the RE2PI spectrum of Cs_2 near 647 nm is presented. Two different vibrational progressions are observed in this spectrum. These are new bound electronic states of Cs_2 which have not been reported previously. No hot band is observed at present. When the backing pressure is reduced to 100 Torr, hot bands could be seen. The vibrational spacings of the hot bands show that the initial state is Cs_2 X $^1\Sigma_u^+$ state. From the analysis of the spectrum these bands are assigned to i) $0_u^+ - X\ ^1\Sigma_g^+(0_g^+)$ transition for the first progression and ii) $1_u - X\ ^1\Sigma_g^+(0_g^+)$ transition for the second progression. The dissociation energies of the 0_u^+ and 1_u states were estimated from the electronic term values and the dissociation energy of X $^1\Sigma_g^+$ state.

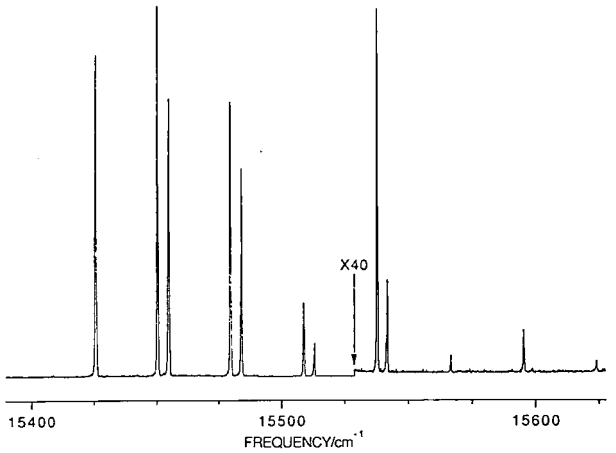

Figure 1. Resonance enhanced two photon ionization spectum of Cs_2 showing new singlet-triplet transitions. The right portion is magnified 40 times. Cs vapor was expanded with 1000 Torr of Ar. The rotational temperature is ~1 K and the vibrational temperature is less than 5 K.

III-E-2 Adiabatic Ionization Potentials of Cs_2 and Cs_3 in a Supersonic Jet

Bongsoo KIM and Keitaro YOSHIHARA

[Submited to *Chem. Phys. Lett.*]

The adiabatic ionization potentials of Cs_2 and Cs_3 have been measured in a pulsed supersonic jet by using the one-photon ionization and the time-of-flight mass spectrometry. Cs_2 and Cs_3 are produced by expanding Cs vapor with Ar gas through a high temperature pulsed nozzle. Accurate ionization energies of the Cs_2 and Cs_3 are determined to be $29208 \pm 1 cm^{-1}$ and 24500 ± 50 cm^{-1}, respectively. High-lying Rydberg states are detected by one-photon ionization and the vibrational frequencies are determined. From the ionization potential of Cs_2 we deduced the dissociation energy of the Cs_2^+, which shows good agreement with the theoretical prediction. Figure 1 shows the Cs_2^+ spectrum which shows the ionization threshold and autoionizing Rydberg states.

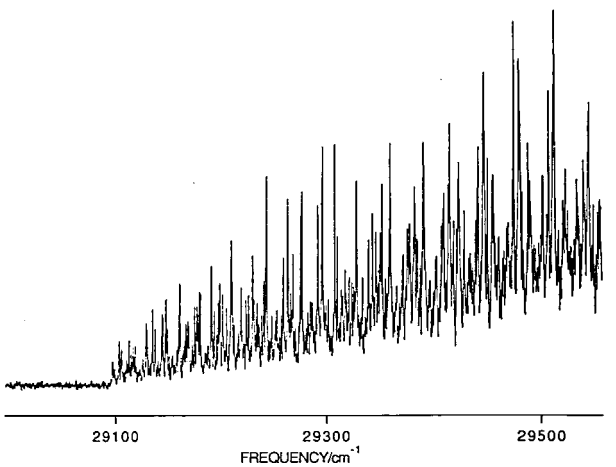

Figure 1. One-photon ionization spectrum of Cs_2. The sharp peaks are due to the autoionization of the Rydberg states.

III—F Development of Ultrafast Spectroscopic Methods

It is generally recognized that many elementary processes in chemical reactions and excited state dynamics fall into picosecond to femtosecond timescale. Development of ultrafast spectroscopic techniques enables us to observe these phenomena in real time. We have been developing suitable ultrafast measuring systems for research subjects described in section III. By developing fluorescence up-conversion measuring system with sub-100 femtosecond pulses (III-F-1), we have been able to study an ultrafast electron transfer reaction beyond solvent-controlled reaction. To obtain a stable, high-power, picosecond pulses for the purpose of exciting optical parametric oscillator, we have constructed a feedback-controlled mode-locked Nd:Glass laser (III-F-2).

III-F-1 Fluorescence Up-Conversion Measuring System with Sub-100 Femtosecond Pulses

Arkady YARTSEV, Yutaka NAGASAWA, and Keitaro YOSHIHARA

Fluorescence up-conversion system was made to achieve sub-hundred femtosecond resolution. Experimental setup (Figure 1) consists of an oscillator of sub-hundred femtosecond pulses, group velocity dispersion precompensator, and optical system for the measurements of fluorescence up-conversion signal. Femtosecond dye laser was improved by removing of the cavity dumper assembly of previous system, using a proper combinations of dyes, installation of special filters, and by fine alignment of the laser. With the 10^{-3} M rhodamine 6G gain jet and 1.5×10^{-5} M DQTCI/ 10^{-5} M DODCI mixed saturable absorber jet, 50—70 fs pulses were generated in a wide spectral region of 583—615 nm with an output power ~100 mW. By using 2×10^{-3} M sulforodamine 101 as a gain media and 5×10^{-4} M DQTCI as a saturable absorber, pulses as short as 36 fs (Figure 1, inset) were generated. Since such short pulses are subject to the group velocity dispersion broadening to a significant extent, a two pass two-prism precompensation system was built. By compensating the dispersion in both branches of Michelson-type interferometer for the up-conversion measurements, time resolution of 80 fs around 600 nm and 60 fs at 675 mm was achieved.

Reference

1) T. Kobayashi, Y. Takagi, H. Kandori, K. Kemnitz, and K. Yoshihara; *Chem. Phys. Lett.* **180**, 416 (1991).

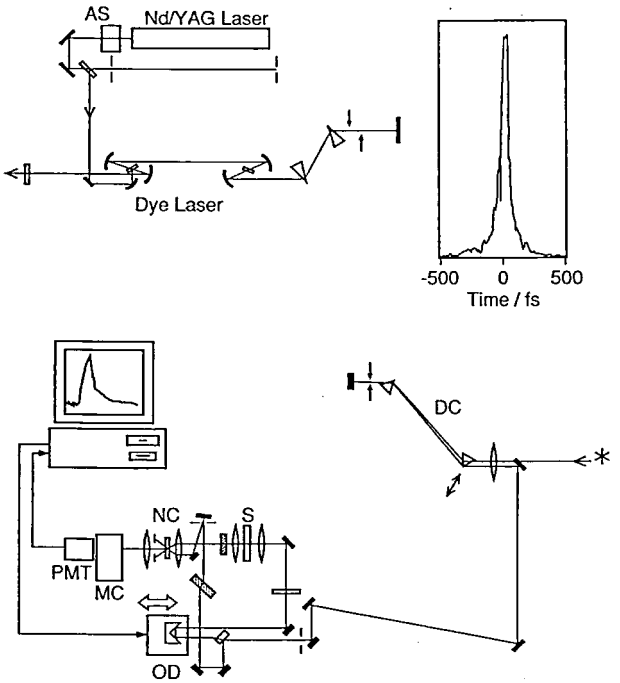

Figure 1. Sub-hundred femtosecond fluorescence up-conversion experimental setup. AS—amplitude stabilizer, DC—dispersion compresensator, S—sample, NC—nonlinear crystal, MC—monochromator, PMT—photomultiplier, OD—optical delay line. Inset—autocorrelation trace, corresponding to ~35 fs pulse width (FWHM).

III-F-2 Feedback-Controlled Mode-Locking of Nd:Glass Laser Using GaAs

Shigeichi KUMAZAKI, Vaclav KUBECEK, Yoshihiro TAKAGI, Giancarlo C. REALI *(Pavia Univ.)*, **and Keitaro YOSHIHARA**

[*Jpn. J. Appl. Phys.* **31**, 413 (1992)]

The passive negative feedback-controlled mode-locking operation of a Nd:glass laser using a GaAs wafer as an intracavity limiter is reported. A long pulse train as long as 700 ns and with a pulse duration of less than 3 ps was generated. The single-pulse energy was 60 μJ, which is 6 times higher than those of Nd:YAP($YAlO_3$) and Nd:YAG lasers.

Detailed pulse-shortening dynamics along the whole train were studied, and single pulse durations (assuming a $sech^2$ single-pulse shape) at different times from the beginning of the train were measured at the optimum saturable dye concentration. The results using different saturable absorbers are shown in Figure 1. The single pulse duration reached a constant value of 8 ps for NDL-112 (Nippon Kankoh-Shikiso) and 5 ps for NDL-102 (Nippon Kankoh-Shikiso). The pulse duration in case of Eastman Kodak dye no.9860 decreased monotonically along the whole train without reaching a steady value, as is achieved in Nd-doped crystalline active media.[1] Only dye no.9860 showed a possibility of obtaining subpicosecond pulses in our experiment.[2]

References

1) V. Kubecek, S. Kumazaki, Y. Takagi, G.C. Reali, and K. Yoshihara: *Jpn. J. Appl. Phys.* **30** 1889 (1991).
2) P. Heinz and A. Laubereau, *J. Opt. Soc. Am.* **B8**, 1574 (1989).

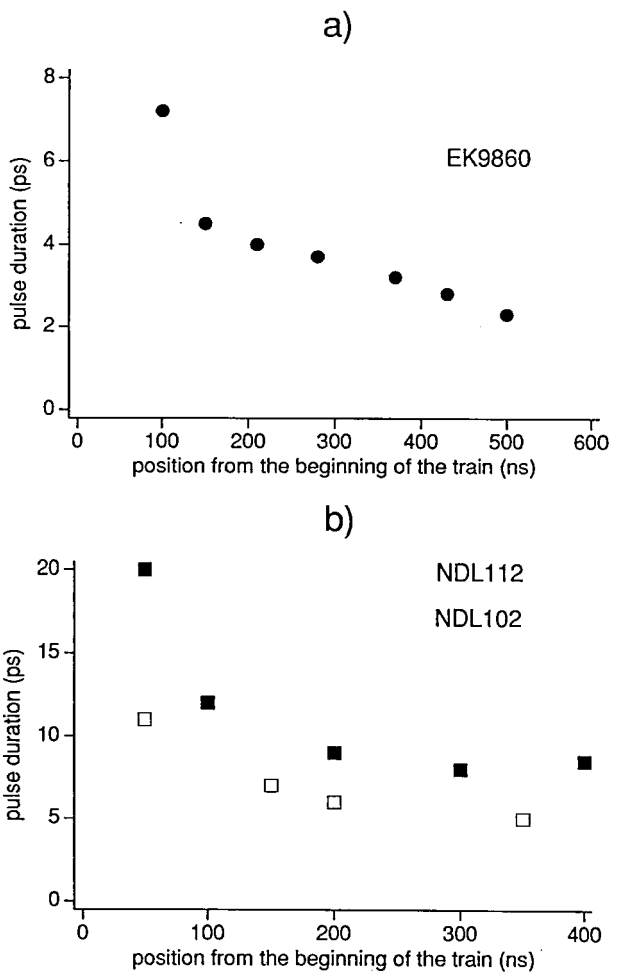

Figure 1. The dependence of pulse duration on the position in the train. (a) dye no.9860/GaAs 400 μm, single-pass small-signal transmission of dye solution 66%, (b) NDL-112 and NDL-102/GaAs 280 μm, dye transmission 80%.

III—G Dynamical Studies of Exciplex Formation in Donor-Acceptor vdW Complexes in Free Jet Expansions

The formation of the CT state (exciplex) by excitation of locally excited (LE) state in a vdW complex of an electron donor and acceptor formed under free jet expansion is a powerful way to study exciplex dynamics. The exciplex state can be monitored with the help of the fluorescence excitation (FE) spectra. Signature of the exciplex formation is the typical broad fluorescence, generally red shifted from the LE emission. The line widths of the FE spectra can reveal the rate of formation of the CT state. The rate, as deduced from the observed widths in the excitation spectra and fluorescence time profiles ranges from ns to several tens of fs. The role of the intramolecular low frequency modes is important in such systems, as some of

these modes are along the reaction coordinate for exciplex formation. Two systems have been chosen for the study of the exciplex dynamics, viz. naphthalene-triethylamine (TEA) and anthracene-dimethylaniline (DMA).

III-G-1 Exciplex Formation in Naphthalene-Triethylamine vdW Complexes in Free Jet Expansions

Prem B. BISHT, Hrvoje PETEK, and Keitaro YOSHIHARA

The vdW complexes of naphthalene-TEA, studied in molecular beam have been found to undergo exciplex formation. In the fluorescence excitation (FE) spectra of the bare naphthalene (Figure 1) a weak S_1 ($^1B_{3u}\leftarrow{}^1A_g$) origin is observed at 32020 cm^{-1} (312.13 nm) followed by an intense transition at 435 cm^{-1}. On addition of TEA to the He:naphthalene expansion, new peaks due to naphthalene: TEA vdW complex appear towards lower energy (~30 cm^{-1}) of each isolated molecule band. The intensity of these new bands increases relative those of LE upon monitoring the fluorescence longer than 380 nm as compared with monitoring between 320–340 nm. In addition, several new peaks appear towards blue of each aforementioned band. These low frequency modes, as expected, are due to intramolecular vibrations of the vdW complex. The widths of the bands due to vdW complexes are limited by the rotational envelopes of 0.7 ~ 0.8 cm^{-1}.

Single vibronic level pumping (SVL) pumping of the corresponding origin band of the vdW complex results in a sharp resonance fluorescence. However, upon pumping with the +432 cm^{-1}, in addition, the spectrum shows broad red shifted fluorescence, which is typical of exciplexes in free jets and in condensed phase. The intensity of the exciplex emission band at ~393 nm increases relative to the UV LE state emission with excitation energy, indicating the energy dependence of the CT state formation. The upper limit of the rate of the formation of the CT state as obtained from the band widths is ~7 ps. The lifetimes of the CT state is about 40 ns, as compared with ~300 ns for the bare molecule.

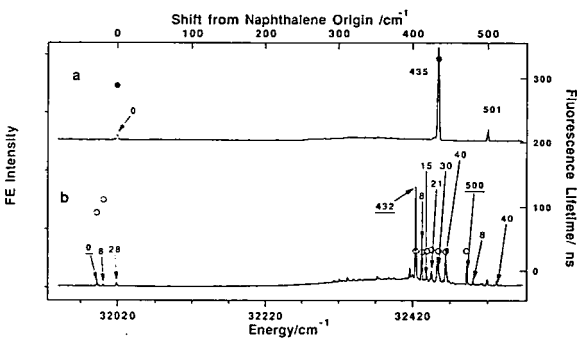

Figure 1. Fluorescence excitation spectrum in origin and +435 cm^{-1} region of naphthalene (a), naphthalene-TEA vdW complex on monitoring fluorescence longer than 380 nm (b), right axis indicates the lifetime of naphthalene (●) and vdW complex obtained by monitoring emission longer than 380 nm (O); experimental conditions: temperature of naphthalene and TEA reservoirs are 28°C and −15°C, respectively, and He stagnation pressure is 1.5 atm.

III-G-2 Exciplex Formation in Anthracene-Dimethylaniline vdW Complexes in Free Jet Expansions

Prem B. BISHT, Hrvoje PETEK, and Keitaro YOSHIHARA

The FE spectrum of anthracene-DMA system shows an overlap of absorption spectra of two isomers.[1] Isomer I has sharp bands and it undergoes exciplex formation with a small barrier (<385 cm^{-1}). By contrast, isomer II has broad line shapes in FE spectra, which correspond to exciplex formation with a 60 fs rate. We are investigating this system as a possible target for a time resolved study of exciplex formation in vdW complexes. Figure 1 shows the FE spectrum in molecular beam taken 300 ns after excitation when only exciplex emits. The broad bands (isomer II) correspond to the main frequencies of the bare molecule, red shifted by ~390 cm^{-1}. The sharp features are due to isomer I, with very first intense transition appearing at 27554 cm^{-1}. The origin of isomer I is 385 cm^{-1} to the lower frequency but it does not appear in Figure 1, as it does not form the exciplex. In addition, a few more intramolecular vibrations of the isomer I appear at 20, 21, 51, and 117 cm^{-1}. The line widths of these bands are of the order of 1 cm^{-1} indicating the rate of the CT state formation slower than several picosecond. The exciplex fluorescence maximum has a peak at 460 nm as compared to that due to 450 nm for isomer II, suggesting two distinct structures. The yield of the exciplex increases with increasing energy suggesting the presence of a barrier between the LE and CT states. The lifetimes obtained on monitoring UV (380 nm) and exciplex (450 nm) fluorescence are drastically different and correspond to the LE (~20 ns) and CT (300 ns) states, respectively.

Reference

1) F. Piuzzi and A. Tramer, *Chem. Phys. Lett.* **166**, 503 (1990).

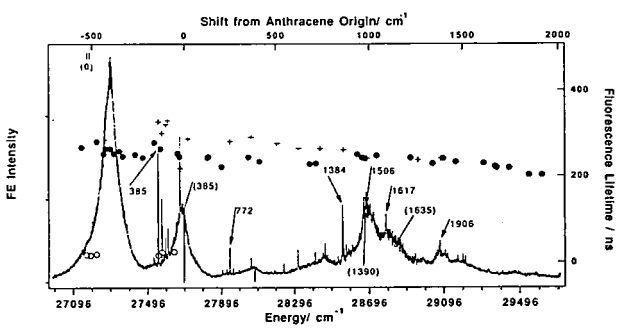

Figure 1. Fluorescene excitation spectrum of isomer I and II taken 300 ns after the excitation pulse. Frequencies indicated in parenthesis are for isomer II (experimental conditions: temperatures of anthracene and DMA are 110°C, and 28°C, respectively; He backing pressure=800 Torr). The right ordinate indicats the lifetimes; isomer II (●) and isomer I on monitoring 450 nm (+) and 380 nm (O). The sharp dips at 27696 cm^{-1} and 28000 cm^{-1} appear due to interference from the intense transitions of the isolated molecule.

III—H Photochemistry on Well-Defined Surfaces

Recently, it has been found that upon the irradiation of light from visible to ultraviolet, a number of adsorbed molecules on metal surfaces reveal variety of photochemical processes, including photodesorption, rearrangement of adsorbed states, photodissociation, and photo-initiated reactions with coadsorbates. Since photo-initiated reactions can be induced without any thermal activation of reactants, various combinations of coadsorbates can be prepared at sufficiently low surface temperatures. Thus, this provides a method for studying a new class of surface reactions which may not be induced thermally. In the last year, we constructed an ultrahigh vacuum chamber to explore photophysics and photochemistry of adsorbates on well-defined solid surfaces. In this year we have focused on a specific system, i.e., nitrous oxide adsorbed on a Pt(111) surface.

III-H-1 Structure of Adsorbed N_2O on a Pt(111) Surface and Photodissociation at 193 nm: Effective Formation of Oxygen Adatoms

Kyoichi SAWABE and Yoshiyasu MATSUMOTO

[*Chem. Phys. Lett.* **194**, 45 (1992)]

Structure of adsorbed N_2O on a Pt(111) surface and photochemistry at 193 nm have been studied by low energy electron diffraction and temprature-programmed desorption. N_2O adsorbs on the Pt(111) surface molecularly at 82 K and is not dissociated thermally. The observed LEED pattern indicates that one monolayer of N_2O has a (3×3) structure with a fractional coverage of 4/9 ML referenced to the Pt substrate. Adsorbed N_2O molecules are dissociated with 193 nm photons and produce oxygen adatoms on the surface. The cross sections of total depletion and photodissociation of N_2O are determined to be $(1.4 \pm 0.2) \times 10^{-18}$ cm^2, and $(7 \pm 1) \times 10^{-19}$ cm^2, respectively. Furthermore, atomic oxygen coverages of up to 0.75 ML are generated with photolysis of adsorbed N_2O at 193 nm.

III-H-2 Laser-induced Photochemistry of Nitrous Oxide on a Pt(111) Surface

Kyoichi SAWABE and Yoshiyasu MATSUMOTO

[Submitted to *Surf. Sci.*]

Photochemistry of N_2O molecularly adsorbed on a clean and oxygen-covered Pt(111) surfaces has been studied by using pulsed excimer laser light with 6.4 eV (193 nm) photon energy. From thermal desorption spectra (TDS) before and after photon irradiation, it is found that adsorbed N_2O molecules are dissociated with 193 nm photons to produce oxygen adatoms. The cross sections for total depletion and photodissociation of N_2O adsorbed on O-covered Pt(111) are not much different from those on clean Pt(111). As shown in Figure 1, the TDS spectra of NO has weak peaks at ~380 and ~530 K only after irradiation by 193 nm photons. Thus, these extra peaks clearly indicates that NO molecules are formed via reactions between photofragments and adsorbed N_2O.

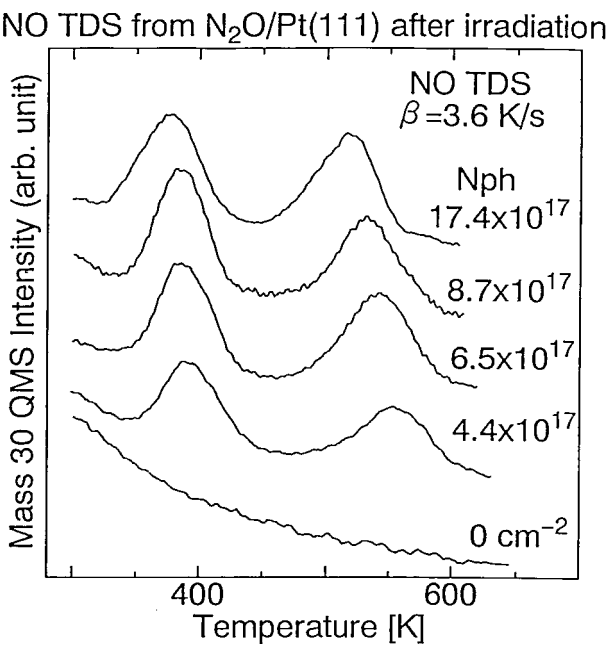

Figure 1. Thermal desorption spectra of NO (30 amu) obtained after various numbers of 193 nm photons on the Pt(111) surface with one monolayer of N_2O (θ=0.44 ML). The numbers of photons directed on the surface are given in the figure.

III-H-3 The Mechanism of Photodissociation of N_2O Adsorbed on a Pt(111) Surface

Kyoichi SAWABE and Yoshiyasu MATSUMOTO

The mechanisms of photochemical processes of adsorbed molecules on metal surfaces are complicated owing to the involvement of substrate excitation. Two mechanisms have been mainly proposed for the primary excitation step: (1) Direct electronic excitation of adsorbate-substrate complex and (2) electron attachment initiated by substrate excitation. While the direct excitation mechanism has been suggested for several systems, the surface mediated mechanism has been proposed in the most of systems studied. In order to clarify the mechanism of photodissociation of N_2O on a Pt(111) surface, we measured the dependence of photodissociation yield on photon polarization and incident angle. As shown in Figure 1, the dependence is in good agreement with that of the bulk absorption predicted from classical electrodynamics. This strongly indicates that the substrate excitation is mostly responsible for the primary step of the photochemistry of N_2O on Pt(111).

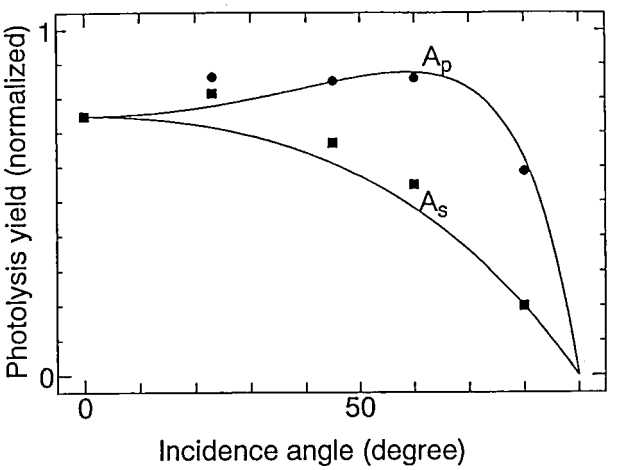

Figure 1. Photodissociation yields of N_2O adsorbed on a Pt(111) surface plotted as a function of incident angle with respect to the surface normal for p-(●) and s-(■) polarized light of 193 nm. One monolayer of N_2O was prepared and number of photons irradiated was kept constant at 4.6×10^{17} cm^2. The solid curves are calculated results for the absorbance of light by the substrate.

III—I Dynamical Processes in Electronically-and/or Vibrationally Excited Molecules

Fundamental molecular aspects of chemical reactions and energy transfer processes in the electronically or vibrationally excited states have been studied. Particular interest has been directed to the dynamics of vibrationally-excited weakly-coupled complexes such as van der Waals and hydrogen-bonded complexes, and the "disproportionation" reaction caused by UV irradiation of the complexes. Dynamics of highly-excited vibrational states (local modes) and chemical reaction induced by their excitation have also been subjects of research.

III-I-1 Dynamics of Vibrationally Excited van der Waals Complex: SEP-LIF Spectroscopy of the Anisole · Ar Complex

Masao TAKAYANAGI and Ichiro HANAZAKI

[Submitted to *J. Chem. Phys.*]

The SEP-LIF (stimulated emission pumping-laser induced fluorescence) technique was applied to investigate the dynamics of vibrationally excited states of van der Waals complexes, anisole-d_0 · Ar and anisole-d_3 · Ar, produced in the supersonic expansion. In the SEP-LIF scheme, the complex excited to a specific vibrational state by SEP is detected by measuring the LIF excitation spectrum with an appropriate delay to probe the vibrational relaxation or predissociation. Five vibrational states, $18b_1$, $6a_1$, 12_1, $6a_118b_1$ (combination band) and 1_1, of the complexes were investigated. Main results obtained in this study are: (1) The SEP excitation of one of 1_1, $6a_118b_1$ and 12_1 gives anisole hot bands in the LIF spectrum due to the anisole monomer produced by vibrational predissociation. (2) Excitation of $18b_1$, whose energy is below the dissociation threshold, does not lead to vibrational relaxation of the complexes. (3) Excitation of $6a_1$ causes the predissociation into vibrationally cold monomers. (4) The predissociation is completed within 300 ns, the shortest available delay time between the SEP and LIF pulses.

III-I-2 Observation of Intermolecular Vibrational Modes in the 2,3-dihydrobenzofuran Dimer

Masao TAKAYANAGI and Ichiro HANAZAKI

[Submitted to *Chem. Phys. Lett.*]

A long progression due to the intermolecular vibrations of the 2,3-dihydrobenzofuran dimer is observed in the LIF-excitation and fluorescence-dip spectra (Figure 1). The origin band of the dimer is red-shifted about 480 cm^{-1} from that of the monomer. The geometry of the dimer and its change upon the electronic excitation are discussed on the basis of the long progression and the large red shift.

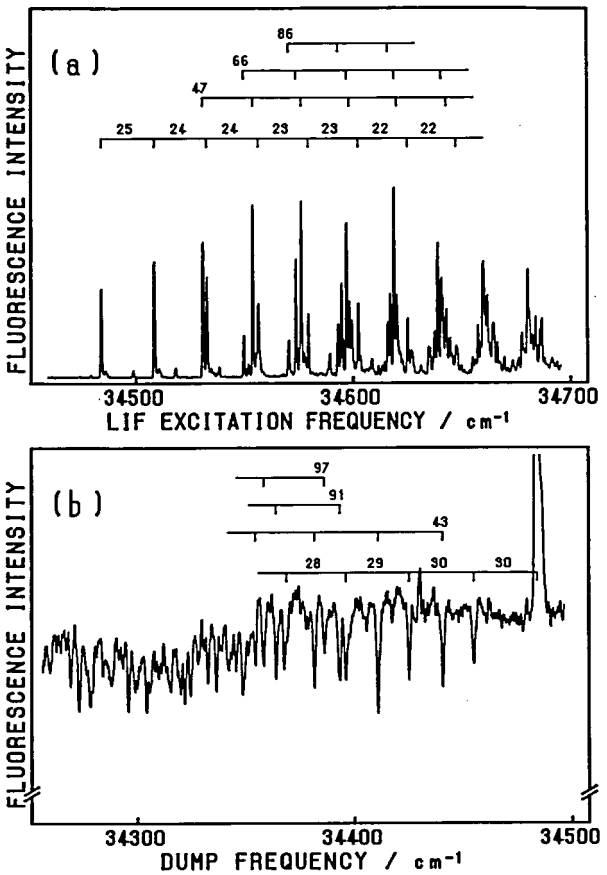

Figure 1. (a) LIF excitation and (b) fluorescence dip spectra of 2,3-dihydrobenzofuran dimer in a molecular beam. The band at 34480 cm^{-1} in each spectrum is the 0–0 band of the dimer. The progressions due to the intermolecular vibrations in the excited and ground electronic states, respectively, are observed.

III-I-3 Lambda Doublet Formation in OH by Chemical Reactions

Ichiro HANAZAKI

The formation of the lambda-doublet levels in the OH ($^2\Pi$) radical produced in the chemical reaction of the type, H+OX→OH+X, has been examined on the basis of a classical model. In contrast to the previous treatment, a detailed examination of the hybridization in the collision complex leads us to conclude that the ratio of population in the lambda-doublet components, A′ and A″ is unity without dynamical preference (see Figure 1). The results are discussed in relation to the existing experimental data. Some examples of the dynamical preference leading to the deviation from the 1:1 ratio are discussed.

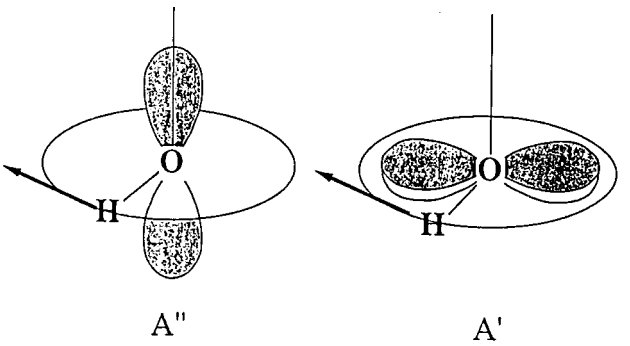

Figure 1. Schematical representation of the A′ and A″ states of Λ-doublet.

III-I-4 Photodissociation of Acetaldehyde Studied by the Photofragment Excitation Spectroscopy in a Supersonic Free Jet

Takumi KONO, Masao TAKAYANAGI, Teruhiko NISHIYA, and Ichiro HANAZAKI

[*Chem. Phys. Lett.*, submitted]

The photofragment excitation spectrum was obtained for the photochemical reaction, $CH_3CHO^* \rightarrow CH_3+HCO$, in a supersonic free jet, by monitoring the $\tilde{B} \leftarrow \tilde{X}$ transition of the HCO radical. The collision-free measurements fix the threshold for the dissociation at 320.5 nm, corresponding to the barrier height of 51.9 $kJmol^{-1}$ on the T_1 surface of acetaldehyde. The decrease of the fluorescence quantum yield of acetaldehyde between 320.5 nm and 317.5 nm was found to be accompanied by the increase of the HCO yield, which was ascribed to the energy-dependent dissociation rate above the barrier.

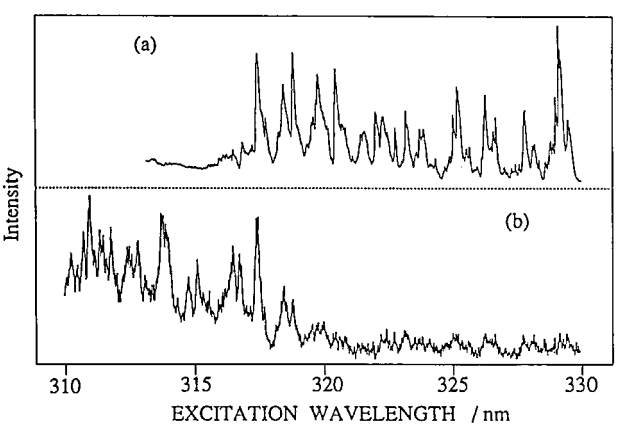

Figure 1. Fluorescence excitation spectrum of acetaldehyde (a) and PHOFEX spectrum of acetaldehyde obtained by monitoring $^QP_0$ (5) of the $\tilde{B}$ (00,2) $\leftarrow \tilde{X}$ (0,0,0) transition of HCO (b).

III-I-5 Double-Resonance Multiphoton Ionization Spectroscopy of the $\tilde{B}$ Rydberg State of Ammonia

Teruhiko NISHIYA, Masao TAKAYANAGI, and Ichiro HANAZAKI

A long progression of the out-of-plane bending (ν_2) vibration appears in the VUV electronic absorption spectrum of ammonia as a consequence of the Franck-Condon (FC) principle. However, there is not much information about

the excited-state stretching vibrations. Therefore, we recorded double-resonance multiphoton ionization (MPI) spectra of the $\tilde{B}$ Rydberg state of ammonia from the symmetric stretching (ν_1) vibrational level of the ground electronic ($\tilde{X}$) state ($\tilde{X}(1,0,0,0)$ level).

Figure 1 shows the spectra (a) with the stimulated Raman pumping (the Q branch) and (b) with the IR excitation (the antisymmetric (*a*) inversion component of the P(2) branch). Excitation of the symmetric (*s*) inversion component does not give a spectrum. Comparing both spectra, we found that Figure 1(a) is comprised of the spectra via J=0,1,2. Vibronic symmetry of the a inversion component of the $\tilde{X}(1,0,0,0)$ state is A_2'' in D_{3h}, and $\tilde{X}-\tilde{B}$ two-photon transition is carried by the $T_1^2(E'')$ component. Then, only a state of E′ vibronic symmetry can be prepared by two-photon excitation from a state of A_2'' symmetry. Rotational selection rules in Figure 1(b) ($|\Delta J|\leq 2$, $|\Delta K|=1$) support the T_1^2 component, and its term value corresponds to that of the $\tilde{B}(0,3,0,0)$ state of E′ symmetry. Symmetry and FC considerations suggest that the $\tilde{B}(1,0,0,0)$ state of E″ symmetry should be observed from the *s* inversion component of the $\tilde{X}(1,0,0,0)$ state, however we conclude that the $\tilde{B}(1,0,0,0)$ state does not have sufficient stability to show double-resonance MPI spectra presumably because of rapid predissociation.

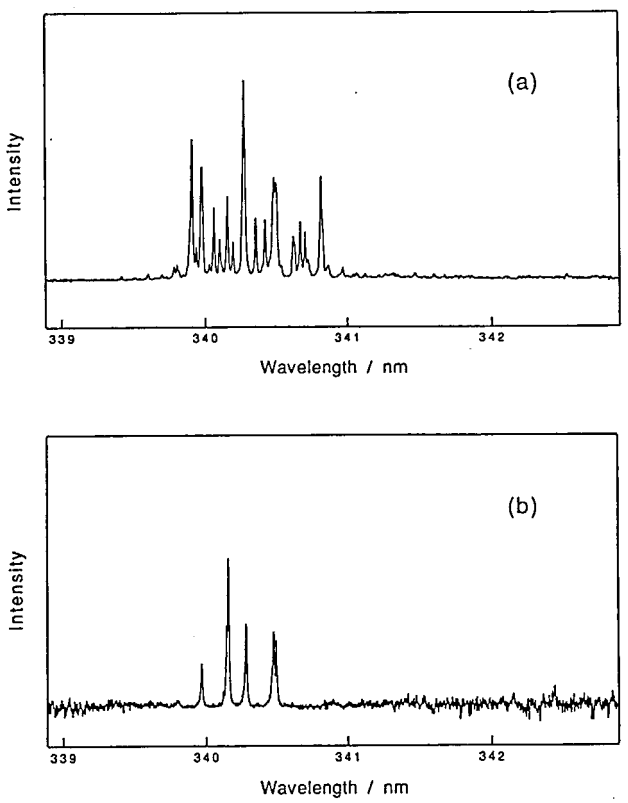

Figure 1. Double-resonance MPI spectra of the $\tilde{B}$ Rydberg state of ammonia from the $\tilde{X}(1,0,0,0)$ state prepared (a) with the stimulated Raman pumping (the Q branch) and (b) with the IR excitation (the *a* inversion component of the P(2) branch).

III-I-6 Reaction Dynamics of the 193 nm Photolysis of HBr · H_2O Complex

Kazuhiro HONDA, Masao TAKAYANAGI, Teruhiko NISHIYA, and Ichiro HANAZAKI

Photochemical reaction of weakly-bound complex HBr · H_2O has been studied in a supersonic free jet. Figure 1 shows the LIF spectrum of the (0,0) band of OH obtained when the complex is irradiated at 193 nm. The LIF signal is weak in comparison with that in the H+N_2O bimolecular reaction under the same condition.[1)]

The structure of HBr · H_2O complex has been predicted by an *ab initio* calculation[2)]; namely, the H atom in HBr is bonded to the oxygen atom in H_2O. The reaction cross section for this conformation may be low in view of the favorable direct abstraction mechanism in the case of the bimolecular reaction.[3)] The cross section in this case would arise from the coupling of the Br-H-O stretching vibrations and other vibrational modes such as the bending motions.

Reference

1) H. Ohoyama, M. Takayanagi, T. Nishiya, and I. Hanazaki, *Chem. Phys. Lett.* **162**, 1 (1989).
2) Y. Hannachi, B. Silvi, J.P. Perchard, and Y. Bouteiller, *Chem. Phys.* **154**, 23 (1991).
3) K. Honda, M. Takayanagi, T. Nishiya, H. Ohoyama, and I. Hanazaki, *Chem. Phys. Lett.* **180**, 4 (1991).

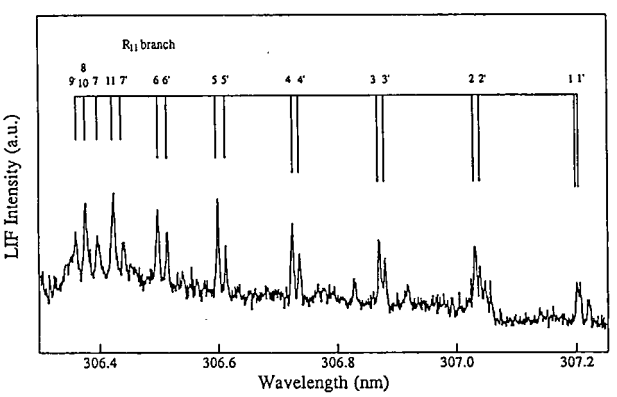

Figure 1. OH $A^2\Sigma^+$ ($V'=0$) LIF excitation spectrum for the reaction HBr · H_2O+hν(193 nm)→OH+H_2+Br. Stagnation pressure is 2.0 atm. Pump-probe delay time is 200 ns. HBr:H_2O:He=2.6:0.9:96.5.

III-I-7 Construction of a New System for the Measurement of Emission Spectra of van der Waals Complexes

Tatsuo GEJO, Masao TAKAYANAGI, Teruhiko NISHIYA, and Ichiro HANAZAKI

We have recently constructed a vacuum chamber and a detection system for the measurements of emission and Raman spectra in a molecular beam. This system is characterized by 1) the simultaneous measurements of emission spectra and mass spectra and 2) the high sensitivity for detection of emission with a large solid angle. We are planning to use this system for the measurement of emission spectra of van der Waals complexes.

III-I-8 The Vibrationally Excited HCO Radical Produced by the Photodissociation of Acetaldehyde at 266 nm

Tatsuo GEJO, Masao TAKAYANAGI, Teruhiko NISHIYA, Takumi KONO, and Ichiro HANAZAKI

Although it is known that the HCO radical is generated by the photolysis of acetaldehyde with a UV laser, the vibrationally excited HCO radical in its electronic ground state has not been detected. During the course of the investigation of photodissociation by monitoring emission spectra, we found that the excitation of acetaldehyde with the Nd:YAG laser fourth harmonic at 266 nm gave an intense emission.

Figure 1 shows the dispersed fluorescence spectrum obtained when we photolyze acetaldehyde at 266 nm. It is assigned to the fluorescence from the B(0,0,0) level of HCO radical to its ground state. The 266 nm radiation can photolize acetaldehyde to create HCO in the X(0,0,2) level and also excite it as X(0,0,2)→B(0,0,1) to induce the observed emission. This is the first evidence for the production of vibrationally excited HCO radicals by the photodissociation of acetaldehyde.

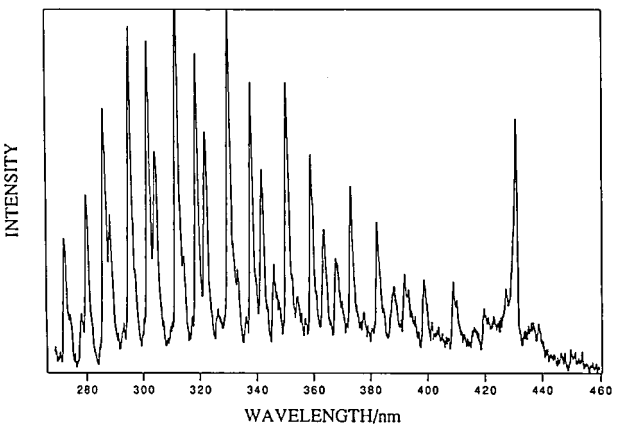

Figure 1. Dispersed fluorescence spectrum obtained when acetaldehyde is photolyzed at 266 nm.

III—J Self-organization in Chemical Reactions

The self-organizing process in chemical systems is known to occur as a result of nonlinear chemical processes. It exhibits the temporal chemical oscillation and the spatial pattern formation. We are particularly interested in the response of chemical oscillators to photo-irradiation. The mechanism of the photo-induction and photo-inhibition of chemically oscillating systems and the structure of related bifurcation phenomena are main subjects of research.

III-J-1 Wavelength-Dependence of Relative Cross Section of Photo-induced pH Oscillation in $Fe(CN)_6^{3-}/Fe(CN)_6^{4-}/H_2O_2/H_2SO_4$ System: Iradiation of $Fe(CN)_6^{3-}$ before Mixing

Yoshihito MORI and Ichiro HANAZAKI

[*J. Phys. Chem.*, in press]

The pH oscillation is induced when the reaction mixture of $Fe(CN)_6^{4-}/H_2O_2/H_2SO_4$ system is irradiated. The wavelength-dependence of the relative cross section suggests that one of the primary absorbers is $Fe(CN)_6^{3-}$.[1] To confirm this, we have examined irradiation of the $Fe(CN)_6^{3-}$ solution in a pre-reactor before mixing in the $Fe(CN)_6^{3-}/Fe(CN)_6^{4-}/H_2O_2/H_2SO_4$ system. The irradiation induces the pH oscillation of the reaction mixture and we have obtained the wavelength-dependence of the relative cross section shown in Figure 1. Peaks at 420 nm and 300 nm of the spectrum of the relative cross section coincide well with those of the absorption spectrum of the $Fe(CN)_6^{3-}$ solution in the prerector. This confirms that one of the primary absorbers is $Fe(CN)_6^{3-}$. The other primary absorber is $Fe(CN)_6^{4-}$ and the primary photochemical process is thought to be the photoaquation yielding $Fe(CN)_5(H_2O)^{3-}$. Photoaquation of $Fe(CN)_6^{3-}$ produces $Fe(CN)_5(H_2O)^{2-}$ which reacts with $Fe(CN)X_6^{4-}$ to yield $Fe(CN)_5(H_2O)^{3-}$.

Irradiation of $Fe(CN)_6^{4-}$ and $Fe(CN)_6^{3-}$ seems to bring about the same effect on the induction of chemical oscillation.

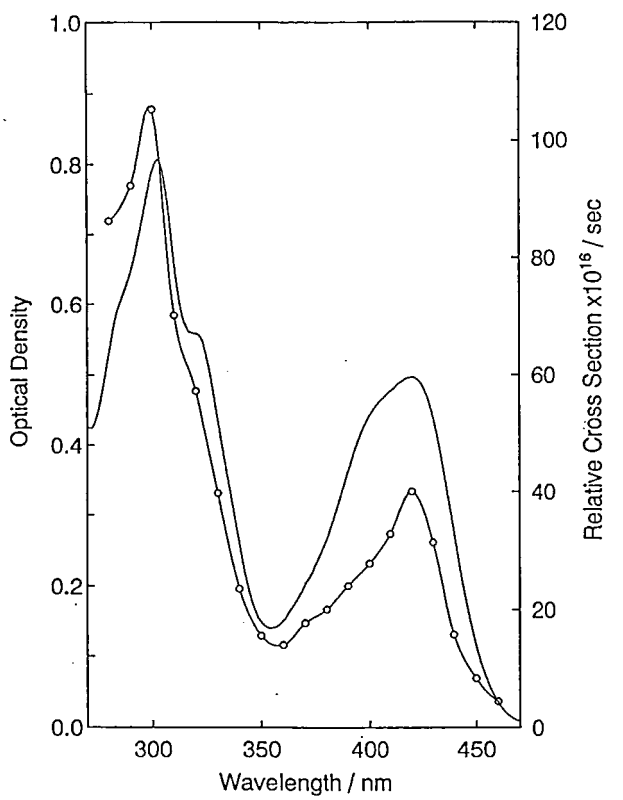

Figure 1. Wavelength-dependence of relative cross section. $[Fe(CN)_6^{3-}]_0$=0.25 mM, $[Fe(CN)_6^{4-}]_0$=3.30mM, $[H_2O_2]_0$=50.0 mM, $[H_2SO_4]_0$=0.900 mM, residence time in main reactor=414 s and T=25.0×0.1°C.

References

1) Mori et al., *Chem. Lett.* 669 (1991).

III-J-2 Cross Section of Light-Induced Inhibition and Induction of Chemical Oscillations

Ichiro HANAZAKI

[*J. Phys. Chem.* **96**, 5652 (1992)]

Cross section is defined for light-induced inhibition and induction of chemical oscillations (see Figure 1). The definition is based on the cross section of photochemical production of the key molecule which controls chemical oscillations, and is shown to be useful in describing photo-sensitivity quantitatively. The cross section can be determined experimentally by measuring the critical light power to stop or start the oscillation. A unified treatment is given for the irradiation of CSTR as well as for the pre-irradiation experiment, in which one of the chemical species is selectively irradiated in a pre-reactor in the flow experiment. A relation is given by which these two kinds of experiment can be correlated. The general procedure developed here is shown to be useful in analyzing the wavelength-dependent irradiation experiments to identify the primary photochemical step, and also in designing an appropriate flow reactor. Examples of its application to typical chemical oscillators are discussed.

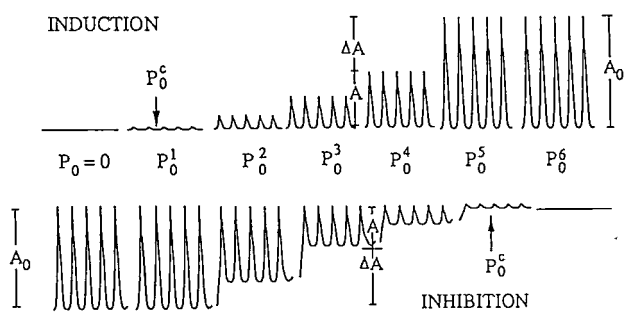

Figure 1. Photo-irradiation effects for the induction and inhibition of chemical oscillation. Light power is indicated by P_0^k where P_0 increases with increasing k. The critical power P_0^c is indicated by an arrow for both cases. Definitions of amplitudes A_0 and A, and $\Delta A \equiv A_0 - A$ are also shown.

III-J-3 Hopf Bifurcation of Hexacyanoferrate(II)/ Hydrogen Peroxide/Sulfuric Acid System in a CSTR

Yoshihito MORI and Ichiro HANAZAKI

The hexacyanoferrate(II)/hydrogen peroxide/sulfuric acid system shows a pH oscillation or a steady state in a continuous flow-stirred tank reactor (CSTR) under appropriate conditions. We have determined the bifurcation diagram to analyze the bifucation from the steady state to the oscillatory state. Figure 1 shows the bifurcation diagram where the flow rate (FR) of the reactants into the CSTR is the control parameter and the pH value of the reaction mixture is the observable parameter. The system bifurcates at FR=1.03 ml · min^{-1} from the steady state at lower pH's to the oscillatory state when the flow rate is decreased. When the flow rate is decreased more, the system bifurcates again at FR=0.81 ml · min^{-1} from the oscillatory state to the other steady state at higher pH's. The former bifurcation is classified as the subcritical Hopf bifurcation and the latter as the supercritical Hopf bifurcation. Although both subcritical and supercritical Hopf bifurcations have been observed in several chemical oscillators, practically it is very difficult to change the control parameter in a wide range to observe both bifurcations in the same system. In the present system, both bifurcations can be observed in a relatively narrow range of the control parameter. This may be because the inflow of sulfuric acid itself acts as a negative feedback process.

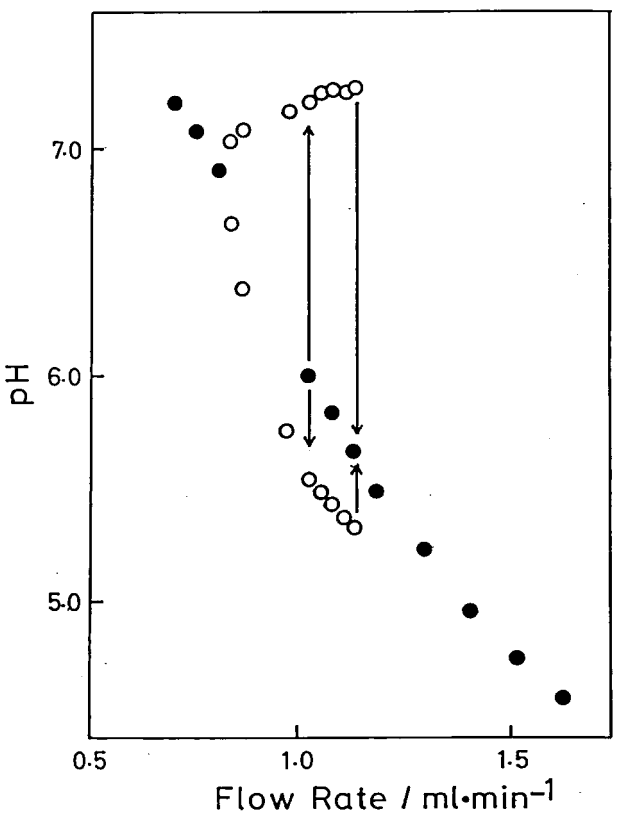

Figure 1. Bifurcation diagram. Closed circles: steady state; open circles: oscillatory state. $[Fe(CN)]_6^{4-}]_0$=3.30 mM, $[H_2O_2]_0$=50.0 mM, $[H_2SO_4]_0$=0.900 mM, T=25.0±0.1°C and the volume of the reactor is 11 ml.

III-J-4 Photo-responce of the Autocatalytic Reaction of Acidic $[Ru(bpy)_3]^{2+}$ with BrO_3^-

Tetsuo SEKIGUCHI, Prem Kumar SRIVASTAVA, Yoshihito MORI, and Ichiro HANAZAKI

It is known that the ruthenium-catalysed B-Z oscillator can be inhibited by photo-irradiation. We have postulated that the primary process of inhibition is due to the absorption of photon by the reduced form of ruthenium complexes. In order to obtain a further information on the mechanism, we have investigated the photo-responce of the oxidation of $[Ru(bpy)_3]^{2+}$ by acidic bromate without substrate in a batch system, by varying the initial concentrations of the hydrogen ion, the bromate ion and the ruthenium complex. We measured the time-evolution of the absorbance of $[Ru(bpy)_3]^{3+}$ and determined the maximum rate of oxidation and the induction period. Figure 1 shows the maximum rate as a function of the proton concentration, which indicates a second order dependence of the rate on $[H^+]$. The light irradiation increases the maximum rate and reduces the induction period, while the slope does not

change appreciably. We are also trying to study this reaction under the CSTR conditon.

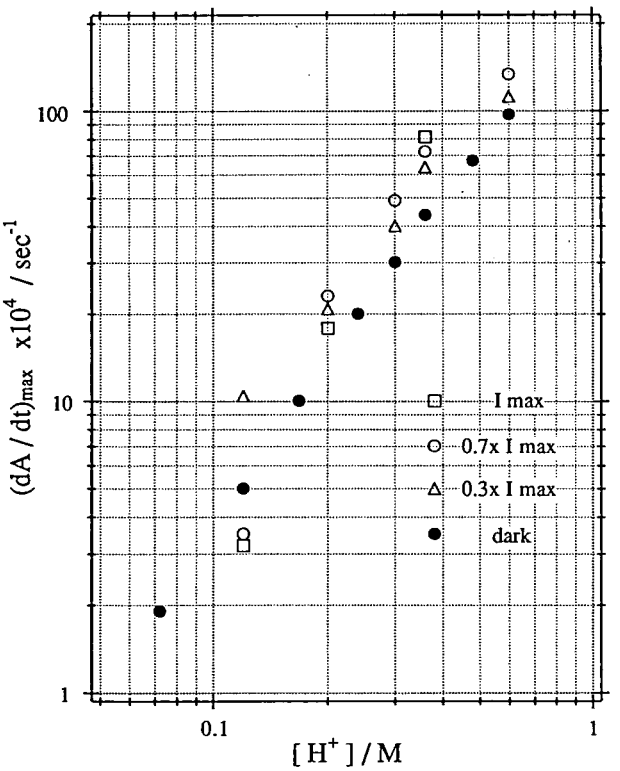

Figure 1. Maximum rate of production of $[Ru(bpy)_3]^{3+}$ versus hydrogen ion concentration with and without irradiation. A is the absorbance of $[Ru(bpy)_3]^{3+}$ at 675.2 nm. Initial concentrations: $[BrO_3^-]_0$=16.5 mM, $[Ru(bpy)_3^{2+}]_0$=0.25 mM at 2.5°C.

III-J-5 Photo-response of the Briggs-Rauscher Reaction

Noriaki OKAZAKI, Yoshihito MORI, and Ichiro HANAZAKI

The Briggs-Rauscher (BR) reaction is one of the most well-known photo-sensitive chemical oscillation reactions. The photo-sensitivity makes the study of this system advantageous because light intensity can be chosen as a control parameter, which enables us to reexamine the phase diagram under dark condition from wider perspective point of view. It has been reported by now that the continuous light irradiation makes the system bifurcate from oscillatory state into steady state (photo-inhibition), and that periodic irradiation brings about synchronization oscillation.[1] However, no experimental verification has been made as to the primary photochemical process responsible for these effects.

In order to identify the primary light absorber, we measured the cross section of photo-inhibition as a function of wavelength (action spectrum) under CSTR configuration, which was shown to provide a general and unified treatment for investigating the light absorption process.[2–4] Results together with the experimental condition are given in Figure 1. The action spectrum and the absorbance spectrum of iodine exhibit quite similar tendency, both possessing the broad band at around 460 nm. This strongly indicates that the primary light absorber in this system is identified as iodine. Characterizatioan of various oscillatory/steady states appeared as light intensity is changed is currently under way.

References

1) E. Dulos and P. De Kepper, *Biophys. Chem.* **18**, 211 (1983).
2) Y. Mori, P.K. Srivastava, and I. Hanazaki, *Chem. Lett.* 669 (1991).
3) P.K. Srivastava, Y. Mori, and I. Hanazaki, *Chem. Phys. Lett.* **190**, 279 (1992).
4) I. Hanazaki, *J. Phys. Chem.* **96**, 5652 (1992).

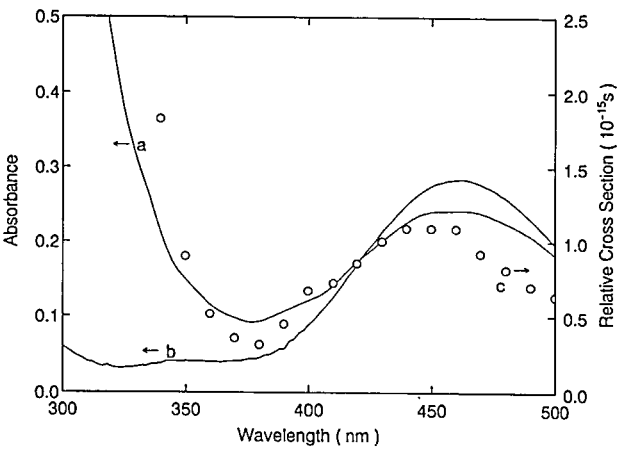

Figure 1. Wavelength dependence in the Briggs-Rauscher reaction. (a) Absorption spectrum of the reaction solution in the steady state induced by the photo-irradiation. (b) Absorption spectrum of the 0.4mM I_2 aqueous solution. (c) The relative cross section of photo-inhibition. The experimental condition is as follows: $[Mn^{2+}]_0$=50mM, $[IO_3^-]_0$=50mM, $[H_2O_2]_0$=0.2M, $[CH_2(COOH)_2]_0$=5mM, $[H_2SO_4]_0$=20mM, residence time=2.6 min, temperature=24.5 ± 0.1°C. The oscillation was followed by monitoring redox potential using a Pt-electrode.

III-J-6 On a Phenomenological Model for Nonequilibrium Interaction between Thermally Activated Chemical Reactions

Jerzy GORECKI

[Submitted to *J. Chem. Phys.*]

It has been recently shown[1] that in the case of coupled thermally activated reactions, which use the same reactant, the nonequilibrium effects are more significant than those where the reactions are treated separately. A fast reaction with a low activation energy may create a nonequilibrium state of reactant, for which rates of those reactions with high activation energies are significantly decreased. Thus it is difficult to predict the behaviour of a system with coupled reactions if the processes are treated independently. In this study a phenomenological approach based on a Maxwellian approximation for the state of reactant is applied to describe the nonequilibrium effects in systems with thermally activated competing reactions:

$$A + A \rightarrow B_j + B_j,\ j=1,\ldots,J$$

The calculations based on phenmenology are compared with molecular dynamics simulations of a model system and a good agreement between the two methods is observed (compare Figure 1). Moreover, for slow reactions, simple formulae to estimate the strength of the nonequilibrium effect have been derived.

Reference

1) J. Gorecki and A.L. Kawczynski, *J. Chem. Phys.* **96**, 4646 (1992).

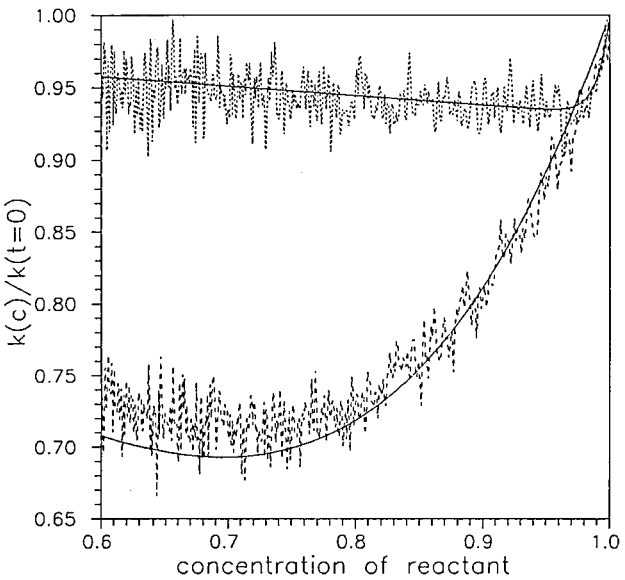

Figure 1. The nonequilibrium rate constant scaled to its equilibrium value as a function of concentraiton of reactant for the system with activation energy E_1=4 k_BT and steric factor δ_1=0.4. The solid line shows the solution of phenomenological equations; the dashed lines present the results of molecular dynamics simulations. The upper pair of curves show the behavior in the system in which no other reaction proceeds, whereas the lower pair of curves describe the situation in which the reaction competes with another characterized by E_2=1 k_BT and δ_2=0.4.

III-J-7 A Simple Phenomenological Model for Nonequilibrium Interaction between Two Reactions in a Lorentz Gas

Jerzy GORECKI and Ichiro HANAZAKI

[*Chem. Phys.*, in preparation]

This work contains a comment on a recently published paper[1] concerned with the nonequilibrium effects created by thermally activated reactions in a Lorenz gas. We have considered a system with two coupled reactions:

$A + B \rightarrow P + Q$

$A + C \rightarrow R + S$

in which the reagents B and C are much heavier than A. Phenomenological equations for temperatures and concentrations of all reactants are derived. Their usefulness is tested by a comparison with molecular dynamics simulations of a model system. In the case studied, the state of reactant A is mainly affected by nonequilibrium effects. A good agreement between the average energy observed in simulations and the nonequilibrium "temperature" of A calculated from phenomenology is obtained. For the case of very slow reactions analytical expressions for the derivatives of nonequilibrium temperatures with respect to the strength of the rate constant are derived. These formulae generalize the results obtained using theory based on the Boltzmann equation.[1]

Reference

1) A.S. Cukrowski, A.L. Kawczynski, J. Popielawski, W. Stiller, and R. Schmidt, *Chem. Phys.* **159**, 39 (1992).

III-J-8 Direct Observation of Nonequilibrium Distribution Function in Systems with a Model Thermally Activated Reaction

Jerzy GORECKI

Any chemical reaction is a local process in which the neighboring molecules are involved. Then diffusion separates the reaction products. If a reaction is very fast, then diffusion is too slow to restore the equilibrium distribution of reagents and transient nonequilibrium spatial correlations should be present at distances comparable to the size of reacting molecules. The molecular dynamics simulations of a model system with reaction:

$A + A \rightarrow B + B$

have been performed and the partial radial distribution functions: g_{AA}, g_{AB} and g_{BB} describing the local spatial correlations between the reagents: A and A, A and B and B and B, respectively, are calculated at a few different concentrations of product (concentration of product measures the progress of reaction and thus it plays the role of time). The simulations have been performed for a few systems characterized by different packing fractions and different activation energies. To observe the nonequilibrium correlations directly it is convenient to scale $g_{IJ}(r)(I,J=A,B)$ by the equilibrium radial distribution function corresponding to a given packing fraction g_{00}. It has been noticed that g_{AA}/g_{00} strongly depends on the packing fraction if a reaction is very fast and a system dense. The nonequilibrium spatial correlations between reactants are enhanced in time, which may indicate that clusters containing molecules of reactant are formed as the reaction progresses (see Figure 1.)

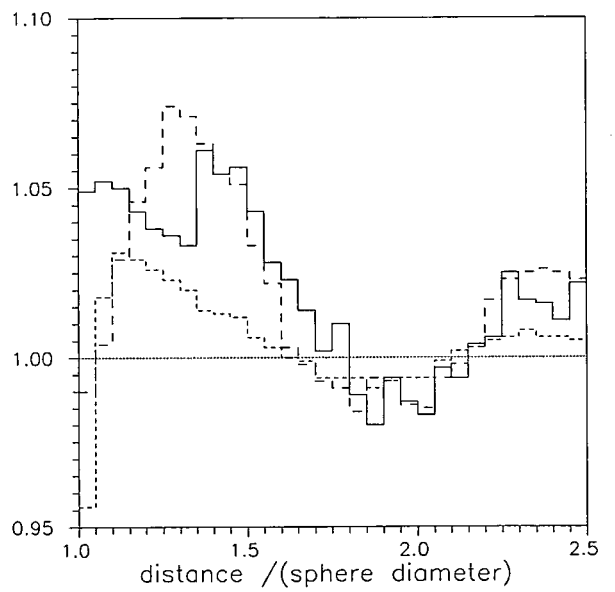

Figure 1. The time dependence of $g_{AA}(r)/g_{00}(r)$ for a reaction with activation energy equal to 1 k_BT; the short dashed, the long dashed and the solid lines correspond to concentrations of B=0.1, 0.3 and 0.5 respectively.

III-J-9 On a Long-time-tail of Reactant Concentration for a Unidirectional Chemical Reaction, Which Proceeds in a Dense Medium

Jerzy GORECKI and Ichiro HANAZAKI

Let us consider a unidirectional reaction:

$$A + B \rightarrow C + D \qquad (1)$$

If the concentrations of reactants A and B are high then its kinetics is controlled by their average densities. However if these concentrations are very low then the molecules of reactants are separated by the products and the kinetics is controlled by diffusion.

To study the transition from the density controlled regime of reaction to the one in which a reaction is controlled by diffusion we performed molecular dynamics simulations for a reaction:

$$A + A \rightarrow B + B \qquad (2)$$

The qualitative behavior of a system with reaction (2) is the same as for reaction (1), but choosing (2) we can avoid inhomogeneities in the initial state which may have an important influence on simulations. For reaction (2) in density controlled regime the time evolution of [A] is given by equation: $d[A]/dt=-k[A]^*[A]$, which leads to the relationship: $\ln([A]^{-1}(t)-[A]^{-1}(t=0))=\ln(k)+\ln(t)$. A typical result of simulations for the long time behavior of [A] is shown in Figure 1. As it may be expected, the moment of transition between regimes strongly depends on the system density.

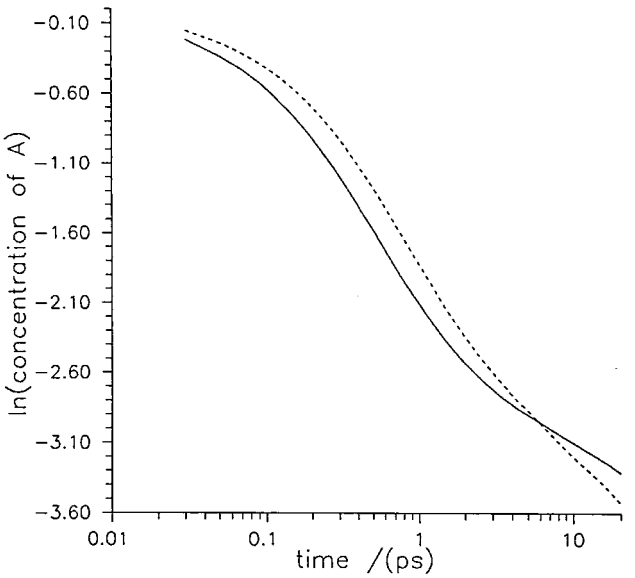

Figure 1. The concentration of A as a function of time obtained from molecular dynamics simulations of a model reaction between hard spheres; the activation energy is $1k_BT$, the solid line shows the results for packing fraction η=0.508, the dashed one correspond to η=0.452.

III—K External Magnetic Field Effects on Chemical Reactions

III-K-1 Magnetic Field Effects on the Perturbed Rotational Levels of CN in the Electronically Exited States

Kaoru SUZUKI and Saburo NAGAKURA *(Grad. Univ. for Adv. Studies)*

Intensity anomalies appearing in the CN violet emission band are known to be due to the perturbation between the $B^2\Sigma^+$ and $A^2\Pi_i$ states and have been studied extensively. Among those studies, the Zeeman effect on the perturbed lines has been studied by Radford and Broida in 1962 as a typical example. Their study was limited, however, to the perturbations at low rotational levels due to the method of formation of the CN radicals in the electronically excited states. In the present study, the external magnetic field effect on the perturbed rotational levels of high J (or N) were examined. Two lasers were used. High rotational levels of CN in the X state were produced by the photolysis of BrCN with an ArF laser (LPX 110i). An excimer laser pumped dye laser (FL2002) was then used to excite $CN(^2\Sigma^+)$ to the B state. A perturbation was observed in the (0,0) band at N′=58. When the external magnetic field was applied, the broadening of the line shape of the perturbed lines was observable due to the Zeeman sublevels of the perturbing $A^2\Pi_i$ state as shown in Figure 1. The fluorescence lifetimes were measured at the peaks of the perturbed rotational lines at a pressure of 6 mTorr. When the external magnetic field of 8.3 kG was applied, the lifetime at the M(main) line lengthened by 5% due to the mixing of the A state which has the longer lifetime than that of the B state.

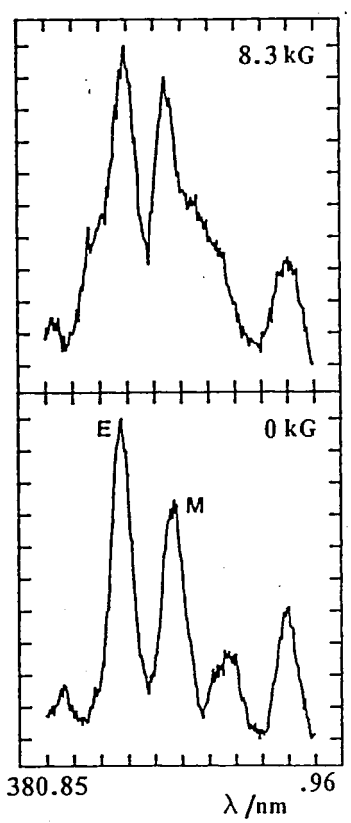

Figure 1. LIF spectra of the CN $B^2\Sigma^+$–$X^2\Sigma^+$ transition around v′=0, N′=58 with and without the external magnetic field.

III-K-2 External Magnetic Field Effects on the β Band Emission of NO

Minoru SUMITANI *(Shizuoka Inst. of Sci. and Tech. and IMS)*, **Kaoru SUZUKI, and Saburo NAGAKURA** *(Grad. Univ. for Adv. Studies)*

Continued efforts have been made on the investigation on the mechanism of the large external magnetic field effect (~85% quenching) of the β band ($B^2\Pi \rightarrow X^2\Pi$) of NO produced in the $N(^4S)+O(^3P)$ chemical reaction. Magnetic field effects were also observed for the β band of NO produced in the reactions of $NO+N_2(A^3\Sigma_u^+, B^3\Pi_g)$ and N_2O+Ar^* to the similar extent. Therefore, magnetic field was thought to be operative in the decay process of NO in the B state. We have, however, contradictory experimental results that no magnetic field effects were observed for the emission from the $B^2\Pi$ state of NO, when it is directly excited to the v=0, 1, 2, and 7 levels with a dye laser. In search for possible other origins of the magnetic field effects, external gas effects were studied. However, SF_6 (electron scavenger) and discharge atmosphere (N, O, N_2, NO, etc) did not affect the magnetic field effects. More detailed investigations are necessary to elucidate the magnetic field effect on the β band of NO.

RESEARCH ACTIVITIES IV
Department of Molecular Assemblies

IV—A Solid State Properties of Phthalocyanine Salts

Some phthalocyanine molecules contain unpaired d-electrons in the conjugated π-electron system. Owing to this special nature, the itinerant π-electrons and localized magnetic moment due to the d-electrons coexist in solid phthalocyanine salts. The exchange interaction of itinerant π-electrons with localized magnetic moments is a new aspect in the field of organic metals. For the basic understanding of these materials and to search for a new phenomenon, where a magnetic interaction takes an important role, we prepare and characterize solid phthalocyanine salts and related compounds.

IV-A-1 Ferromagnetic Interaction in Solid (Octabutoxy-Phthalocyaninato) Cobalt

Hideo YAMAKADO, Kyuya YAKUSHI, Kunio AWAGA, Yusei MARUYAMA, Tadahiro NAKAO*, and Kuninobu KASUGA* *(*Shimane Univ.)*

[*Mol. Cryst. Liq. Cryst.*, in press]

We found a weak ferromagnetic interaction in solid (octabutoxyphthalocyaninato) cobalt $CoPc(OBu)_8$ at low temperature. It is conceivable that a dimer of $CoPc(OBu)_8$ having a triplet ground state is involved in the magnetic property of this material. The structural comparison with paramagnetic CoPc is necessary to understand this new finding.

IV-A-2 Structure and Solid State Properties of Conductive Salts of (Phthalocyaninato) Cobalt, $CoPc(AsF_6)_{0.5}$

Kyuya YAKUSHI, Hideo YAMAKADO, Takashi IDA, Akito UGAWA, Kunio AWAGA, Yusei MARUYAMA, Kenichi IMAEDA, and Hiroo INOKUCHI

[*Synthetic Metals*, to be published]

A conducting crystal of (phthalocyaninato) cobalt hexafluoroarsenate $CoPc(AsF_6)_{0.5}$ is prepared by an electrochemical method. Temperature-dependent electrical conductivity of dc and 9.4 GHz shows that $CoPc(AsF_6)_{0.5}$ is a narrow-gap semiconductor with activation energies of 327 K for dc and 138 K for 9.4 GHz. Thermoelectric power is +40 μV/K—+50 μV/K in the range 100—300 K. The sign of the thermoelectric power is consistent with our earlier spectroscopic result that Pc ring is mainly oxidized contrary to the analogous material CoPcI. Optical spectrum along the *c* axis exhibits strong and weak peaks at 0.29 eV and 1.2 eV. Magnetic susceptibility is composed of a Curie-Weiss part with C=0.056 emu mol^{-1} and a nearly temperature-independent part with the magnitude of 5×10^{-4} emu/mol. All these data indicates the localization of holes ($U>4t$) like in $(TMTTF)_2X$ and $Ag(DMe\text{-}DCNQI)_2$. This localization seems to be related to the exchange interaction between the unpaired *d*-electron on Co and the π-electron on macrocyclic ligand.

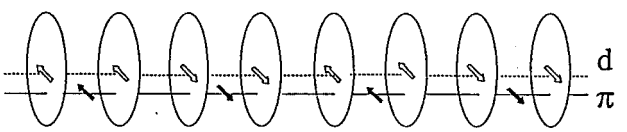

$$J_{d\pi} = \iint \varphi_d(r_1)^* \varphi_\pi(r_2)^* \frac{e^2}{r_{12}} \varphi_d(r_2)\varphi_\pi(r_1) dr_1 dr_2$$

Figure 1. The SDW model induced by the exchange interaction $J_{d\pi}$ between d-electrons and π-holes.

IV—B Structure and Properties of Organic Metals

The study of organic metals rapidly developed when the dimensionality of an intermolecular charge-transfer interaction is expanded. This expansion of dimensionality has been brought about by the discovery of new molecules such as BEDT-TTF or C_{60}. In this project we treat one-, two-, and three-dimensional organic metals and superconductors to know what is most important for stabilizing a metallic state and for designing new superconducting materials.

IV-B-1 Infrared and Transport Properties of K_xC_{60}

Akito UGAWA, Kyuya YAKUSHI, Koichi KIKUCHI*, Shinzo SUZUKI*, K. SATO*, Yoji ACHIBA*, and Isao IKEMOTO* *(*Tokyo Metropolitan Univ.)*

[*Synthetic Metals*, to be published]

Infrared reflectance spectra and electrical resistivity of K_xC_{60} have been measured on bulk. The spectrum of K_3C_{60} demonstrates a metallic dispersion analyzed by the Drued model with ω_p=1.2 eV and γ=0.62 eV, the plasma frequency being coincident with the theoretical calculation by Erwin and Picket. The reflectance results support the rigid band picture of $K_XC_{60}(0<x<3)$ in contrast to the non-rigid band feature of the reported photoemission spectra.

IV-B-2 Rigid Band Feature in K_xC_{60} by *in situ* Infrared Reflectance

Akito UGAWA, Kyuya YAKUSHI, Koichi KIKUCHI*, Shinzo SUZUKI*, Kazuya SAITO*, Isao IKEMOTO*, and Yoji ACHIBA* *(*Tokyo Metropolitan Univ.)*

Infared reflectance spectra of K_xC_{60} have been measured on bulk crystals over a K-doping process. The spectrum of K_3C_{60} demonstrates a metallic dispersion analyzed by the

Drude model with ω_p=1.2 eV and γ=0.62 eV, the plasma frequency being coincident with the theoretical calculation by Erwin and Pickett. The reflectance results support a rigid band picture of K_xC_{60} ($0<x<3$) in contrast to the non-rigid band feature reported on the photoemission spectra. An infrared-active T_{1u} mode of 1429 cm^{-1} in C_{60} is found to decrease in proportion to the degree of charge-transfer x with $\Delta\omega/\Delta\chi$=−20 cm^{-1}.

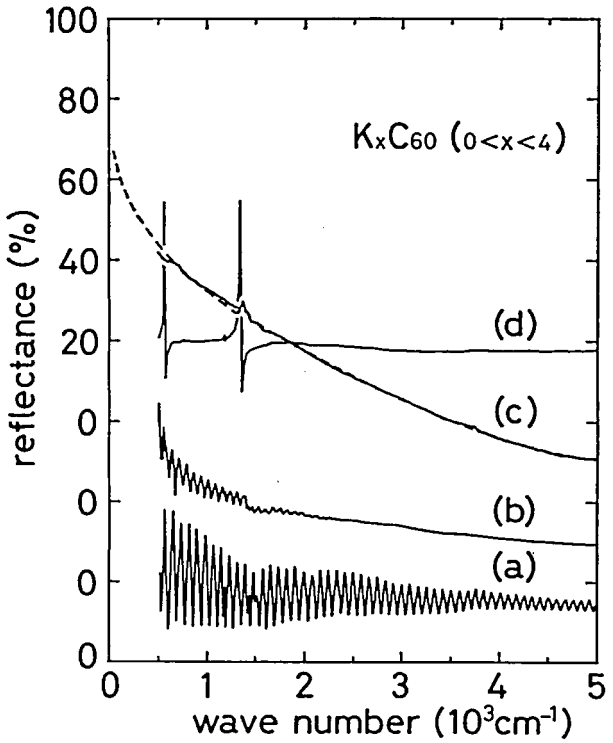

Figure 2. Changes of reflectance spectrum of K_XC_{60} through the K-doping process. The dotted line on the spectrum (c) shows a Drude fit.

IV-B-3 Enhanced Isotope Effect in ^{13}C-rich Superconducing M_xC_{60} (M=K, Rb): Support for Vibronic Pairing

Anvar. A. ZAKHIDOV, Kenichi IMAEDA, David. M. PETTY, Kyuya YAKUSHI, Hiroo INOKUCHI, Koichi KIKUCHI*, Isao IKEMOTO*, Shinzo SUZUKI*, and Yoji ACHIBA* *(*Tokyo Metropolitan Univ.)*

[*Phys. Lett. A*, **164**, 355 (1992)]

By means of non-resonant microwave absorption in low magnetic fields it is found that the superconducing T_c significantly decreases in 60% ^{13}C isotope substituted K_3C_{60} and Rb_3C_{60}. The exponent α of the isotope effect, $T_c \sim 1/m^{\alpha}$, is estimated roughly to be α=1.2–2.25, much higher than predicted by the BCS theory. The intrinsic disorder is observed both in the wide-mass spectrum and the dramatically changed IR spectrum reflecting the inhomogeneous distribution of ^{13}C isotopes in $^{13}C_{60-n}{}^{12}C_n$ molecules. The large positive α supports the intramolecular vibronic pairing and the decrease of the electron-vibron coupling λ due to the disturbed symmetry of H_g modes in mixed $^{13}C_{60-n}{}^{12}C_{60}$ molecules is proposed to contriute to the enhanced α, in addition to the conventional isotope frequency shift.

IV-B-4 Low Energy Electronic Excitations and Fano Resonance in K Dopted C_{60} from Raman Scattering Excited at 1.16 eV

R. DANIELI*, V.N. DENISOV*, G. RUANI*, Roberto ZAMBONI*, Carlo TALIANI*, Anvar. A. ZAKHIDOV, Akito UGAWA, Kenichi IMAEDA, Kyuya YAKUSHI, Hiroo INOKUCHI, Koichi KIKUCHI, Isao IKEMOTO**, Shinzo SUZUKI**, and Yoji ACHIBA**** *(*Inst. of Mol. Spectrosc., **Tokyo Metropolitan Univ.)*

[*Solid State Commun.*, **81**, 257 (1992)]

We present a Raman scattering study of pristine and K dopted C_{60} at various doping levels by exciting in the near-IR at 1.16 eV. The normal metallic state of K_3C_{60} is characterized by a broad scattering background and by the resonance of low energy phonons in the range of 250–500 cm^{-1}. We assign the broad background to an electronic Raman scattering due to low energy electronic excitations. This spectral feature is indicative of an anomalous normal state behaviour and is similar to the case of high temperature ceramic superconductors. In the overdoped K_6C_{60} the squashing mode at 278 cm^{-1} shows a Fano resonance with the electronic scattering associated with localized electronic excitations which are characteristic of isolated regions of K_3C_{60} into the matrix of K_6C_{60} as a result of inhomogeneous doping. The Fano resonance indicates a specific electron-phonon of this Jahn-Teller mode with low energy excitations and suggests that the symmetry of this electronic excitation is h_g (*i.e.* the same of the coupled phonon mode). We discuss the nature of the anomalous electronic Raman scattering in terms of scattering from low energy excitations involving a low lying singlet band resulting from electron correlation and/or dynamical J-T distortion caused by the squashing mode.

IV-B-5 Evidence for Jahn-Teller Coupling and Fano Resonance of Lower H_g Modes in K_3C_{60} and Rb_3C_{60} Films from Raman Scattering

V.N. DENISOV*, Anvar A. ZAKHIDOV*, R. DANIELI*, G. RUANI*, Roberto ZAMBONI*, Carlo TALIANI*, Kenichi IMAEDA, Kyuya YAKUSHI, Hiroo INOKUCHI, and Yoji ACHIBA** *(*Institute of Mol. Spectrosc., **Tokyo Metropolitan Univ.)*

[*J. Modern Phys.*, to be published]

The Raman scattering study of superconducting thin films of A_3C_{60} (A=K, Rb) carried out upon laser excitations at 1.16 and 2.41 eV have revealed the significant broadening and Fano-lineshapes of several low energy Hg intramolecular modes with relative intensities and widths depending on excitation energies. The most interesting feature of the 1.16 eV excited spectrum is the wide asymmetric band at 400cm^{-1} which can be assigned by Fano-shape fitting to enormously broadened $H_g(2)$ mode red shifted compared to its bare frequency of 408 cm^{-1}. The narrowing of all lower Hg modes in insulating A_6 C_{60} phase indicates strong electron-phonon coupling of this Jahn-Teller modes in x=3 phase and suggests that this low energy vibrations are contributing to superconducting pairing. However the possibility to interpret the wide band at 400 cm^{-1} as the

maximum of electronic background can not be ruled out yet and is supported by our preliminary observations of its disappearance at low temperature below T_c.

IV-B-6 Magnetic Properties of TDAE-C_{60} and TDAE-C_{70}. A Comparative Study

Kazuyoshi TANAKA*, Anvar A. ZAKHIDOV*, K. YOSHIZAWA*, K. OKAHARA*, Tokio YAMABE*, Kyuya YAKUSHI, Koichi KIKUCHI, Shinzo SUZUKI**, Isao IKEMOTO**, and Yoji ACHIBA****
*(*Kyoto Univ., **Tokyo Metropolitan Univ.)*

[*Phys. Lett. A*, **164**, 221 (1992)]

Magnetic properties of C_{60} and C_{70} complexes with tetrakis(dimethyamino)ethylene (TDAE) have been studied by Faraday-balance magnetization and ESR measurements. It has been confirmed that TDAE-C_{60} possesses about one radical spin per molecule and shows a ferromagnetic-type transition at T_c=16.7−17.6 K. The appearance of a new broad and intense ESR signal below Tc suggests that the radical spins in the magnetically ordered state localize on each C_{60} molecule and are ferromagnetically correlated. On the contrary, TDAE-C_{70} demonstrates the usual Curie-type narrow ESR peak at all temperatures suggesting the absence of a ferromagnetic transition at least down to 4.5 K.

IV-B-7 Air Stability of K_3C_{60} Superconductors: Low Field Microwave Absorption and ESR Study

Anvar A. ZAKHIDOV*, Ilias I. KHAIRULLIN*, Pulat K. KHABIBULLAEV*, V. Yu. SOKOLOV*, Kenichi IMAEDA, Kyuya YAKUSHI, H. INOKUCHI, and Yoji, ACHIBA** *(*Dept. Thermophys. Uz Acad. of Sci., **Tokyo Metropolitan Univ.)*

[*Synthetic Metals*, to be published]

Using nonresonant microwave absorption in low magnetic field (so called LFS) combined with conventional ESR it is shown that degradation of superconducting (SC) state of K_xC_{60} upon exposure to air is surprisingly slow (*e.g.* compared to *n*-type doped conducting polymers) and partially reversible process. The annealing at 100−130°C in high vacuum of air exposed sample restores both LFS and ESR typical for SC state, suggesting the formation of some unstable (K_xC_{60}-O_2) complex at first stages of oxidation. At longer exposure times superconducting LFS can not be recovered meaning irreversible chemical bonding of O to C_{60}.

IV-B-8 Photoelectron Spectra of Higher Fullerence Compound C_{82} and its Potassium Complex

Shojun HINO*, K. MATSUMOTO*, Shinji HASEGAWA, Kentaro IWASAKI, Kyuya YAKUSHI, T. MORIKAWA, Takashi TAKAHASHI**, Kazuhiko SEKI***, Koichi KIKUCHI****, Shinzo SUZUKI****, Isao IKEMOTO****, and Yoji ACHIBA****** *(*Chiba Univ., **Tohoku Univ., ***Nagoya Univ., ****Tokyo Metropolitan Univ.)*

[*Synthetic Metals*, to be published]

Photoelectron spectra of C_{82}, which has been reported to contain metal atoms inside, are measured with a synchrotron radiation light source. The spectra resemble those of C_{84}. The spectra begin at 1.15 eV below the Fermi level (E_f). The first band consists of two peaks located at 2.2 eV and 3.3 eV accompanied by a slight shoulder structure at the lower binding energy side. This shoulder is not observed in C_{84}. The intensity of the two peaks of the first band oscillates with the incident photon energy change, as are observed in C_{60}, C_{70} and C_{84}. The second band locates between 4 and 6.2 eV with a peak at 5.3 eV and shoulder at the lower binding energy side. The third band locates between 6.2 and 9 eV and consists of a peak at 7.8 eV and a distinct shoulder at 6.5 eV. Potassium dosing brings a new band between the E_f and the first band and its intensity grows as the potassium dosage increases. The spectral onset approaches toward the E_f in accordance with increase of potassium dosage but it does not cross the E_f, which indicates a semiconductive nature of K_xC_{82}.

IV-B-9 Fermi Surface Study of Two-Dimensional Organic Metals (BEDT-TTF)$_2X$

Madoka TOKUMOTO*, Nobumori KINOSHITA*, Hiroyuki ANZAI*, A.G. SWANSON, J.S. BROOKS**, S.T. HANNAHS***, C.C. AGOSTA***, Masafumi TAMURA****, Hiroyuki TAJIMA****, Haruo KURODA****, Akito UGAWA, and Kyuya YAKUSHI**
*(*ETL, **Boston Univ., ***MIT, ****Univ. of Tokyo)*

[*Synth. Met.*, **41−43**, 2459 (1991)]

Observation of Shubnikov-de Haas (SdH) and de Haas-van Alphen (dHvA) oscillations in organic metals (BEDT-TTF)$_2X$, with X=$KHg(SCN)_3$, θ-I_3, and β"-$AuBr_2$ are reported. In $KHg(SCN)_4$ salt, in addition to the SdH osocillations with fundamental frequency of 670 T corresponding to about 16% of the first Brillouin zone (FBZ), we observed splitting of each SdH peak that we ascribed to "spin-splitting". We have also found that the ground state of this salts is not a simple metal but has some magnetic character. In θ-I_3 salt we have succeeded in an observation of dHvA oscillations for the first time. We observed a "saw-tooth" dHvA oscillation characteristic to a highly two-dimensional and extraordinary clean electronic system. In addition to the fundamental frequency of 4170 T corresponding to 50.4% of the FBZ and its higher harmonics, we observed an oscillation with lower frequency of 730 T corresponding to about 8.8% of the FBZ. A new Fermi surface topology for θ-I_3 salt is proposed based on the analysis of the dHvA effect. In β"-$AuBr_2$, we observed complex dHvA oscillations, which can be explained in terms of the mixing of two fundamental frequencies of 47 and 268 T, suggesting the presence of very small pockets corresponding to 0.6 and 2.9% of the FBZ.

IV-B-10 Structure of the Charge-Transfer Complex of (DBTTF)(BTDA-TCNQ)

Kentaro IWASAKI, Takashi IDA, Atsushi KAWAMOTO, Akito UGAWA, Yoshiro YAMASHITA, Kyuya YAKUSHI, and Takanori SUZUKI* *(*Tohoku Univ.)*

[*Acta Crystallogr., Sect. B*, in press]

Dibenzotetrathiafulvalene bis(1,2,5-thiadiazolo)tetracyanoquinodimethane, $C_{26}H_8N_8S_6$, M_r=624.8, orthorhombic, P*nmn*, *a*=12.940(3), *b*=13.551(3), *c*=7.440(2) Å, *V*=1304.6(5) Å^3, and *Z*=2, D_m=1.60 gcm^{-3}, D_x=1.59 gcm^{-3}, λ(MoKα)=0.71073 Å, μ=4.96 cm^{-1}, *F*(000)=632, T=293 K. *R*=0.067 (*wR*=0.062) for 1028 reflections. The components of the complex, DBTTF (donor) and BTDA-TCNQ (acceptor), form a mixed-stack column along the c-axis. There are no intermolecular contacts shorter than the sum of van der Waars radii within the molecular stack and between the stacks.

IV-B-11 Crystal Structures of Metallic and Insulating Molecular Complexes between naphthaceno[5,6-*cd*:11,12-*c'd'*]bis[1,2]diselenole and 4,8-bis(dicyanomethylene)-4*H*,8*H*-benzo[1,2-*c*:4,5-*c'*]bis[1,2,5]thiadiazole: (TSeN)(BTDA-TCMQ) and (TSeN)(BTDA-TCMQ)(C_6H_5Cl)

Kentaro IWASAKI, Akito UGAWA, Atsushi KAWAMOTO, Yoshiro YAMASHITA, Kyuya YAKUSHI, Takanori SUZUKI*, and Tsutomu MIYASHI* *(*Tohoku Univ.)*

[*Bull Chem. Soc. Jpn.*, to be published]

The charge-transfer complex between naphthaceno[5,6-*cd*:11,12-*c'd'*]bis[1,2]diselenole (TSeN) and 4,8-bis(dicyanomethylene)-4*H*,8*H*-benzo[1,2-*c*:4,5-*c'*]bis[1,2,5]thiadiazole (BTDA-TCNQ) is found to show at least three different types of crystal modifications: insulating Type-I has a (1:1:1) ratio containing solvent molecules (chlorobenzene), metallic Type-II has a (1:1) stoichiometry, and semiconductive Type-III is conjectured to have a (1:2) or (2:1) stoichiometry. The crystal structures of Type-I and Type-II are determined by a single crystal X-ray diffraction method. Type-I is composed of mixed-stack molecular columns and Type-II is segregated-stack molecular columns. In both types the neighboring columns are linked along short molecular axes by two Se...N contacts shorter than the corresponding van der Waals contact. In Type-II crystal, there are other short distances between TSeN and BTDA-TCNQ in the direction of long molecular axes. From the C=C bond length in the C=C(CN)$_2$ group of BTDA-TCNQ, the degrees of charge transfer of these molecular complexes are estimated as 0.2 ± 0.3 in Type-I and 0.9 ± 0.2 in Type-II.

IV—C Construction of Microspectrophotometer

We are constructing microspectrophotometric systems to measure the optical reflectivity of a small single crystal in a wide spectral range from ultraviolet region to far-infrared region.

IV-C-1 Improvement of Microspectrophotometer for the Use of IR-VIS-UV Region

Atsushi KAWAMOTO, Hideshi ISHII*, Kentaro IWASAKI, and Kyuya YAKUSHI *(*Univ. of Tokyo)*

To perform the temperature-deppendent spectroscopic experiment, we have installed a hellium-flow type cryostat CF1104 of Oxford Instrument to the microspectrophotometer for the use of 2150 cm^{-1} to 35000 cm^{-1}. The cryostat is fixed on a digital stages driven by pulse motors along the x, y, and z directions. To obtain the absolute value of the reflectivity, the stage moves between the sample and reference mirror within the precision of 1 μm. The program to move the stages was newly written and added to the original program for the measurement of reflectivity. The temperature of the sample reached about 10 K.

IV-C-2 Microspectrophotometer for the Use of Far-Infrared and Infrared Region Using a Synchrotron Radiation as a Light Source

Akito UGAWA, Kyuya YAKUSHI, Hiroshi OKAMOTO, Tadaoki MITANI, Makoto WATANABE, Kusuo SAKAI, Koichi SUZUI, and Shinji KATO

We have prepared Fourier Interferometer for the use from Near-IR to Far-IR region and the shroud to purge H_2O and CO_2 in the atmosphere of the microscope. The optical system to introduce the SR light to FTIR is also completed. The machine is still under construction.

IV—D Superconducting Characteristics of Organic Materials

The superconductivity in organic materials has several unusual properties such as anisotropic electron-pairing and anomalous vortex dynamics in a magnetic field. One way toward understanding of these characteristics is characterization of the superconductivity and inquiry into possible correlation with the anomalies. In this study, superconductivity of a series of κ-phase layered organic superconductors has been examined by measurements of upper critical field and magnetic penetration depth.

IV-D-1 Upper Critical Field and NMR Relaxation Studies of an Organic Superconductor, κ-(MDT-TTF)$_2$AuI$_2$

Kazushi KANODA, Kiyonori KATO, Yoshiaki KOBAYASHI*, Minako KATO*, Toshihiro TAKAHASHI*, Kokichi OSHIMA#, B. HILTI+, and J. ZAMBOUNIS+ *(*Gakushuin Univ., #Okayama Univ., +Ciba-Geigy)*

The superconductivity of κ-(MDT-TTF)$_2$AuI$_2$ has been studied by measurements of H_{c2} and the proton nuclear spin-lattice relaxation rate. The resistive transitions under magnetic fields remain sharp as in a zero field: broadening of the transition, which was encountered in the 10-K superconductors, is not observed. Angular dependence of H_{c2} at 1.5 K well below T_c (4.14 K for our sample) is fitted to the anisotropic Ginzburg-Landau theory of three-dimensional nature with the anisotropic mass ratio of 42. As is shown in Figure 1, the temperature dependences of H_{c2} in both directions of the field are also consistent with the anisotropic Ginzburg-Landau theory: anomalous upturn observed in the perpendicular H_{c2} of the 10-K superconductors is absent in this system. The parallel and perpendicular coherence lengths are estimated at 160 and 20 A. All these results indicate that the supperconductive characateristics such as dimensionality and possibly vortex dynamics and/or critical fluctuations are different between the present system and other κ phase compounds with T_c greater than 10 K. The NMR relaxation rate follows a Korringa relation in a wide temperature range. At a field of 1 tesla, there observed no superconductive behavior of the relaxation rate below T_c.

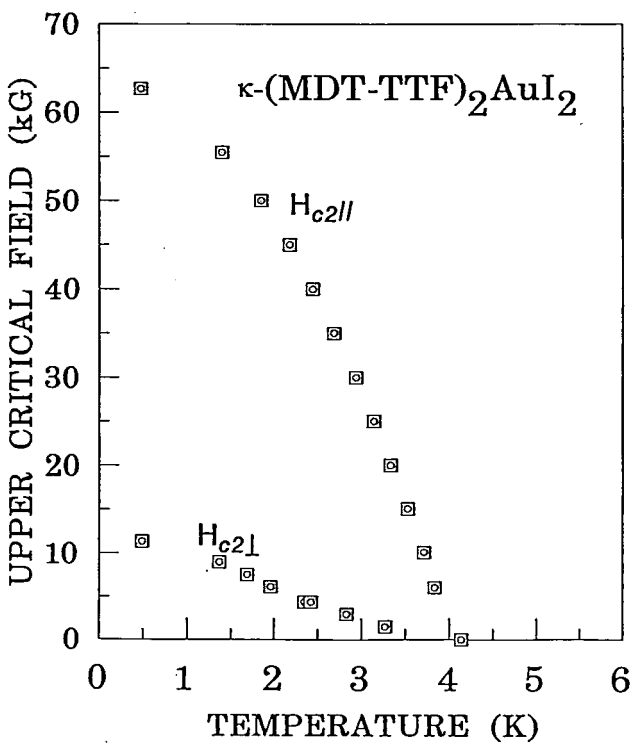

Figure 1. Temperature dependence of upper critical fields at the field parallel and perpendicular to the conducting layer.

IV-D-2 Magnetic Penetration Depth of The κ-Phase Family of Organic Superconductors

Kazushi KANODA, Yuichi TSUBOKURA*, Kumi IKEDA*, Toshihiro TAKAHASHI*, Nozomu MATSUKAWA, Gunzi SAITO**, Hatsumi MORI+, Takehiko MORI, B. HILTI++, and J.S. ZAMBOUNIS++** *(*Gakushuin Univ., **Kyoto Univ., +ISTEC, ++Ciba-Geigy AG)*

In recent years, several organic superconductors with relatively high T_c have been synthesized and most of them belong to the κ-phase of the donor packing. The magnetic penetration depth, λ, of a series of κ-phase organic superconductors has been investigated by complex susceptibility measurements. It has been found that the so-called 10-K superconductors, κ-(BEDT-TTF)$_2$Cu(NCS)$_2$ and κ-(BEDT-TTF)$_2$Cu[N(CN)$_2$]Br, have similar characteristics: power-law temperature-dependence at low temperatures and macroscopic parallel penetration depth (200 μm). κ-(BEDT-TTF)$_2$Ag(CN)$_2$H$_2$O with T_c of 5 K has a smaller value of λ (80 μm). κ-(MDT-TTF)$_2$AuI$_2$ with T_c of 4.3 K has a further smaller depth (less than 20 μm). These results indicate that the interlayer superconducting coupling is strongly dependent on the compound even among the κ-phase family; superconductive dimensionality is the highest in κ-(MDT-TTF)$_2$AuI$_2$ but trends two-dimentional in κ-(BEDT-TTF)$_2$CuX [X=(NCS)$_2$and [N(CN)$_2$]Br].

IV—E Fermi Surface Topology and Magnetotransport of Organic Metals

The Fermi surface topology of several quasi-two-dimensional organic metals has been examined by the high-field magnetization and magnetoresistance measurements. The observation of quantum oscillation has led to determination of profile of the Fermi surface topology. The magnetotransport study of quasi-one-dimensional (DMETSeF)$_2$AuI$_2$ implies some phase transition at higher fields.

IV-E-1 De Haas-van Alphen Effect in κ-$(DMET)_2AuBr_2$

Kazushi KANODA, Kiyonori KATO, Kokichi OSHIMA*, Toshihiro TAKAHASHI, Koichi KICUCHI+, Kazuya SAITO+, and Isao IKEMOTO+**
*(*Okayama Univ., **Gakushuin Univ., +Tokyo Metropolitan Univ.)*

In order to study the Fermi-surface topology of the organic conductor, κ-$(DMET)_2AuBr_2$, we have performed the high-field magnetization measurements up to 12 tesla and down to 0.5 K. The de Haas-van Alphen effect has been clearly observed, as is shown in Figure 1. This is the first report on the quantum oscillation for a κ-phase compound other than the BEDT-TTF salts. The oscillation has two components of frequency, similar to κ-$(BEDT\text{-}TTF)_2I_3$ recently studied by Oshima et al. The faster one corresponds roughly to the cross-sectional area of the 1st Brillouin zone and the other to 20% of that. Such a cross-sectional profile of the Fermi surface is essentially the same as in the κ-phase of BEDT-TTF compounds. However, the simultaneous oscillation even at low field in this system is different from the result for κ-$(BEDT\text{-}TTF)_2Cu(NCS)_2$, where the faster oscillation is reported to occur only at higher field as a magnetic breakdown effect. The present result implies that κ-$(DMET)_2AuBr_2$ has no gap against the crossing of the Fermi surface at the boundary of the 1st Brillouin zone unlikely κ-$(BEDT\text{-}TTF)_2Cu(NCS)_2$. This is consistent with the crystal symmetry.

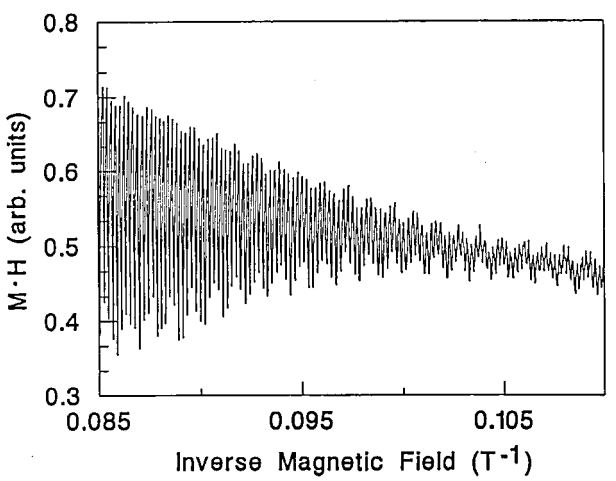

Figure 1. Magnetization as a function of inverse field.

IV-E-2 De Haas-van Alphen Effect and the Fermi Surface in κ-$(BEDT\text{-}TTF)_2I_3$

Kokichi OSHIMA*, Hitoshi YAMAZAKI, Kiyonori KATO, Yusei MARUYAMA, Reizo KATO***, Akiko KOBAYASHI***, and Hayao KOBAYASHI******
*(*Okayama Univ. and IMS, **Okayama Univ., ***The Univ. of Tokyo, ****Toho Univ.)*

[*Synth. Met.*, to be published]

The de Haas-van Alphen effect and the Fermi surface have been studied in the κ-type organic superconductor $(BEDT\text{-}TTF)_2I_3$. The originally proposed Fermi surface using the tight-binding band calculation is different from the ones reported afterwards for the other κ-type salts. The Fermi surface has a simple 2-dimensional cylindrical shape and no band gap exists at the zone boundary due to the crystal symmetry. The absence of band gap at the boundary is known as the band sticking effect. We confirmed the band sticking effect experimentally using the magnetization measurement. The observed quantum oscillation frequency corresponds to the 100% area of the first Brillouin zone. The Fourier analysis has revealed another frequency corresponding to the 20% area of the first zone other than the fundamental one. This frequency corresponds to the ones reported for the other κ-type salts $(BEDT\text{-}TTF)_2Ag(CN)_2H_2O$ and $(BEDT\text{-}TTF)_2Cu(NCS)_2$. The effective mass of the fundamental frequency and the Dingle temperature are 2.7 m_0 and 0.9 K respectively. The many body renormalization effect has been discussed considering mass enhancement and strong coupling model for the superconductor.

IV-E-3 Quantum Oscillation and Transport Property in κ-$(BEDT\text{-}TTF)_2Ag(CN)_2H_2O$

Kokichi OSHIMA*, Takashi DOI, Youko TOKUOKA**, Hitoshi YAMAZAKI**, Kiyonori KATO, Yusei MARUYAMA, Hatsumi MORI***, and Shoji TANAKA*****
*(*Okayama Univ. and IMS, **Okayama Univ., ***ISTEC)*

[*Synth. Met.*, to be published]

The quantum oscillation (de Haas-van Alphen effect and Shubnikov-de Haas effect) has been studied in the κ-type organic superconductor $(BEDT\text{-}TTF)_2Ag(CN)_2H_2O$. The temperature dependence of resistivity is reexamined. The temperature dependence so far reported in κ-$(BEDT\text{-}TTF)_2Ag(CN)_2H_2O$ is monotonic. We found two kinds of conducting behaviors with and without anomaly in resistivity near 100 K. It seems that the T_c is higher for the anomalous one (T_c=6 K). The X-ray structural analysis does not show any marked difference between the two kinds of samples. The origin of the difference in the transport behavior seems to originate in the anion layer. The effect of the inter-plane coupling and the transport anomaly seem to be related.

IV-E-4 Field-Induced Transitions in a Novel Organic System, $(DMETSeF)_2AuI_2$

Kokichi OSHIMA*, Koyonori KATO, Yusei MARUYAMA, Reizo KATO, Akiko KOBAYASHI**, and Hayao KOBAYASHI*****
*(*Okayama Univ. and IMS, **The Univ. of Tokyo, ***Toho Univ.)*

[*Synth. Met.*, to be published]

We have measured magnetoresistance and Hall resistance of a novel organic conductor, $(DMETSeF)_2AuI_2$. DMETSeF (dimethylethylenedithiotetraselenafulvalene) is a newly synthesized donor molecule. The temperature dependence of $(DMETSeF)_2AuI_2$ salt depends on the batch of the sample preparation. Some crystals are metallic down to 0.5 K, and the others are metallic down to 40 K, but the resistivity increases with the log(T) temperature

dependence from 15 K down to 0.5 K. In this material, we found a series of cascade transitions due to the magnetic field similar to the well-known FISDW (Field Induced Spin Density Wave) states in $(TMTSF)_2X$ family. The large magnetoresistance and the period of the step-like transitions cannot be understood as the Shubnikov-de Haas oscillation. The band calculation indicates 1D like Fermi surface and very similar to those of TMTSF family, therefore FISDW can be one of the candidates to understand the state. But the experimental result is somewhat different from those of TMTSF family. This result is the first field induced state in organic systems other than TMTSF family.

IV—F Synthesis and Characterization of Proton-Transfer/ Electron-Transfer System

Hydrogen-Bonded systems, in which the proton transfer is coupled with the π-electron configurational change, are the subject of this study. If the interaction between the molecules is sufficiently strong in the crystalline state, the proton motion is expected to modulate the electronic properties of the crystal. In order to examine such a possibility, a number of compounds which have a common framework of salicylideneaniline have been synthesized as the intramolecular proton transfer system. In order to extend the system to the intermolecular cases, charge transfer complexes of aromatic amines have also been prepared and subjected to structural, electrical, magnetic, and optical studies.

IV-F-1 Study of Proton Dynamics in the NHO Hydrogen Bonds in the Thermochromic Crystals of *N*-Salicylideneanilines

Sadamu TAKEDA *(Osaka Univ.)*, **Hideaki CHIHARA** *(Osaka Univ.)*, **Tamotsu INABE, Tadaoki MITANI, and Yusei MARUYAMA**

[*Chem. Phys. Lett.*, **189**, 13 (1992)]

The precise investigation of the spin-lattice relaxation rate of the proton of the remarkably thermochromic crystal of *N,N'*-bis(salicylidene)-*p*-phenylenediamine provides unique information of proton dynamics in the NHO hydrogen bonds, which is consistent with the temperature dependence of the visible absorption spectra of this crystal and which reveals the presence of interaction between two NHO hydrogen bonds in the molecule through rearrangement of the configuration of π-electrons. This result indicates that the thermochromism of this material is a prototype of "proton-electron cooperation". The transfer rate of proton in the NHO hydrogen bond is strongly affected by a chemical modification, e.g. the fast tunneling.

IV-F-2 Proton Transfer in N-Salicylideneanilines—Effect of Charge-Transfer Interaction

Tamotsu INABE, Kaoru OKANIWA, Hiroshi OKAMOTO, Tadaoki MITANI, Yusei MARUYAMA, and Sadamu TAKEDA *(Osaka Univ.)*

[*Mol. Cryst. Liq. Cryst.*, **216**, 229 (1992)]

The structural and optical studies on the proton transfer in various charge transfer complexes of *N*-salicylideneaniline derivatives are presented. The OH · · · N hydrogen-bond structure has been found to be variable by adjustment of the intermolecular interaction.

IV-F-3 Crystal Structure and Transport Properties of a Hydrogen-Bonded 1:1 Charge-Transfer Complex Composed of 1,6-Pyrenediamine and 7,7,8,8-Tetracyanoquinodimethane (DAP-TCNQ)

Tamotsu INABE, Kaoru OKANIWA, Hironori OGATA, Hiroshi OKAMOTO, Tadaoki MITANI, and Yusei MARUYAMA

[Submitted to *Acta Chim. Hungarica—Models in Chemistry*]

Single crystals of a hydrogen-bonded 1:1 charge-transfer complex, DAP-TCNQ, have been prepared by co-sublimation of the components. The electrical resistivity of the crystal is low, but the temperature dependence is semiconducting with anomalously high activation energy over a wide temperature range. The crystal is composed of two kinds of one-dimensional columns, one of donors and the other of acceptors, with uniform intermolecular separations in each column. No indication of lattice deformation such as dimerization has been detected down to 118 K by the X-ray diffraction technique. The structural study also indicates that the donors and acceptors are interaction two-dimensionally through hydrogen bonds formed between the amino groups of DAP and the cyano groups of TCNQ.

IV—G Ultra-Thin Organic Film Systems Prepared by Molecular Beam Epitaxy (MBE) Technique

As a strategy for the development of new types of organic materials, we have undertaken the fabrication of ultra-thin organic multi-layer systems with the use of an "MBE" technique. We are expecting new types of charge transfer compounds and/or intercalation compounds (hybrid compounds), and also the realization of novel 2-dimensional materials in such systems. We have prepared ultra-thin well-oriented phthalocyanine films on alkali halide single crystal substrates. On the basis of this epitaxial single crystalline film, we are now trying to grow a superlattice of phthalocyanines. Nonlinear optical study of the epitaxial films is in progress.

IV-G-1 Epitaxial Growth of Lead Phthalocyanine Film on KI Crystal

Hajime HOSHI, Shaoli FANG, and Yusei MARUYAMA

[Submitted to *J. Appl. Phys.*]

The molecular-beam epitaxy technique was applied to grow an epitaxial film of lead phthalocyanine (PbPc). The found epitaxy, KI(100)(5×10/7)R45°-PbPc, was a new type with the incommensurate factor 10/7. A new mechanism of the epitaxy, charge transfer interaction between PbPc columns and iodide anion rows, is introduced.

IV-G-2 Nonlinear Optical Study of Ultrathin Phthalocyanine Films Prepared by the Molecular-Beam Epitaxy Technique

Hajime HOSHI, Shaoli FANG, Keiichi KOHAMA *(Toyota Motor Corp. and IMS)*, **and Yusei MARUYAMA**

Nonlinear optical properties of ultrathin phthalocyanine films are studied by second and third harmonic generations. Observed dependence of the harmonic intensities on the polarization of light and two rotational angles of the film is discussed based on the symmetry of the film structure.

IV—H Novel Molecular System C_{60}: Fullerites and Fullerides

After the discovery of superconductivity in potassium doped C_{60} films, much attention has been attracted to the versatility of solid state C_{60} (Fullerite). In this research project, the micro-structural and optical properties of fullerite films prepared by the MBE technique, and the electrical properties of the doped films and single crystals are studied.

IV-H-1 Electronic Properties of C_{60} and Alkali Metal Doped C_{60} Thin Films or Single Crystals

Yusei MARUYAMA, Tamotsu INABE, Hironori OGATA, Hajime HOSHI, Naoki NAKAMURA *(Toyota Motor Corp. and IMS)*, **Yoshihisa MORI, Yohji ACHIBA** *(Tokyo Metropol. Univ.)*, **Shinzo SUZUKI** *(Tokyo Metropol. Univ.)*, **Koichi KIKUCHI** *(Tokyo Metropol. Univ.)*, **and Isao IKEMOTO** *(Tokyo Metropol. Univ.)*

[*Pysica C*, **185—189**, 413 (1991)]

Molecular beam epitaxy technique has been applied to prepare ultra-thin films of C_{60} (fullerite) and some optical properties, absorption spectra and nonlinear optical activities, has been studied. Morphological studies on the sub-mono-molecular layers have been carried out with TEM and STM technique. Electrical conductivities of alkali meal dopted C_{60} (fulleride) have been measured for single crystals as well as thin films including the detection of their superconductivity.

IV-H-2 Novel Molecular System C_{60}: Fullerites and Fullerides

Yusei MARUYAMA, Tamotsu INABE, Hironori OGATA, Hajime HOSHI, Naoki NAKAMURA *(Toyota Motor Corp. and IMS)*, **Yoshihisa MORI, Yohji ACHIBA** *(Tokyo Metropol. Univ.)*, **Shinzo SUZUKI** *(Tokyo Metropol. Univ.)*, **Koichi KIKUCHI** *(Tokyo Metropol. Univ.)*, **and Isao IKEMOTO** *(Tokyo Metropol. Univ.)*

[*Mol. Cryst. Liq. Cryst.*, **218**, 297 (1992)]

Absorption spectra and TEM and STM images are observed on C_{60} thin films prepared by MBE technique. Superconductivity behaviors of alkali metal-dopted single crystals and thin films are also reported.

IV-H-3 Observation of Metallic Conductivity and Sharp Superconducting Transition at 19 K in Potassium-Doped Fulleride, C_{60}, Crystal

Yusei MARUYAMA, Tamotsu INABE, Hironori OGATA, Yohji ACHIBA *(Tokyo Metropol. Univ.)*, **Shinzo SUZUKI** *(Tokyo Metropol. Univ.)*, **Koichi KIKUCHI** *(Tokyo Metropol. Univ.)*, **and Isao IKEMOTO** *(Tokyo Metropol. Univ.)*

[*Chem. Let.*, 1991, 1849]

The first observation of a "metallic" conductivity behavior by resistivity measurements is reported for a potassium-doped C_{60} single crystal. The superconducting transition takes place very sharply with about one degree temperature width, that is, the onset of T_c is 20 K and the resistivity becomes null at 19 K. The details of the doping process are described.

IV-H-4 Charge Transport and Superconducting Transitions in C_{60} Single Crystals and Thin Films Doped with Rubidium

Hironori OGATA, Tamotsu INABE, Hajime HOSHI, Yusei MARUYAMA, Yohji ACHIBA *(Tokyo Metropol. Univ.)*, **Shinzo SUZUKI** *(Tokyo Metropol. Univ.)*, **Koichi KIKUCHI** *(Tokyo Metropol. Univ.)*, **and Isao IKEMOTO** *(Tokyo Metropol. Univ.)*

[*Jpn. J. Appl. Phys.*, **31**, L166 (1992)]

Superconductivity is confirmed in rubidium-doped C_{60} samples prepared from single crystals and thin films, by electrical resistivity measurements. Superconducting transition temperatures (T_c) are observed at T_c(onset)=30 K, T_c(offset)=26 K, and T_c(onset)=22 K, T_c(offset)=2.5 K, respectively. The details of the doping conditions are described.

IV-H-5 Electronic Structure of Alkali Metal Doped C_{60} Drived from Thermoelectric Power Measurements

Tamotsu INABE, Hironori OGATA, Yusei MARUYAMA, Yohji ACHIBA *(Tokyo Metropol. Univ.)*,

Shinzo SUZUKI *(Tokyo Metropol. Univ.)*, **Koichi KIKUCHI** *(Tokyo Metropol. Univ.)*, **and Isao IKEMOTO** *(Tokyo Metropol. Univ.)*

[submitted to *Phys. Rev. Lett.*]

Thermoelectric power of K- and Rb-dopted C_{60} superconductors prepared from single crystals grown from a CS_2 solution is reported. Nearly linear temperature dependences of thermoelectric power with negative sign are observed above the superconducting transition temperatures for both materials. From the slope of the linear correlation, the ratio of the density of states at the Fermi energy, $N^{Rb}(E_F)/N^{K}(E_F)$, is estimated to be 1.5 ~ 1.8.

IV—I Preparation and Characterization of Copper Oxide High T_c Superconductor Films

After the discovery of novel high T_c superconductors, a lot of works including the film preparation have been carried out. We have carried out to fabricate thin films of such superconductors by a sputtering method and an electron-beam evaporation technique with the purpose of searching for new composition, structures, and elements in high T_c superconductors.

IV-I-1 Atomic Layer-by-Layer Deposition of Well-Oriented Crystalline La-Sr-Cu-O Films

Toshifumi TERUI, R.J. FLEMING *(Monash Univ. and IMS)*, **and Yusei MARUYAMA**

[Submitted to *Bull. Chem. Soc. Jpn.*]

Well-Orineted Crystalline La-Sr-Cu-O films has been prepared as-deposited state by an atomic layer-by-layer deposition technique in a high vacuum evaporation system with multi electron-beam-gun sources. The film quality is crucially dependent on the substrate temperature, oxidation gas, and source material, i.e., metal itself or its oxide. It is found that the layer-by-layer successive deposition is superior to the sumiltaneous deposition of the three elements.

IV—J STM/STS Study on Electronic Structures of Some Superconductors

Scanning tunneling microscopy (STM) and spectroscopy (STS) are very useful and direct methods to study the electronic structures of electrical conductors. We are focusing to investigate site-selective superconducting gap structures of orgnaic or copper oxide superconductors. The system for room temperature STM/STS has been set up, and a low temperature system is now under construction.

IV-J-1 Construction of Low Temperature STM-STS System

Yoshihisa MORI and Yusei MARUYAMA

In order to study electronic structure at low temperatures of, for example, superconductors, an STM/STS system which is available at low temperature, 4.2 K, may be very useful. We have been constructing a microscope part of such system, and have succeeded in getting images and STS operation under liquid nitrogen temperature. We are now trying to measure superconducting gaps of high Tc copper oxides and to extend the lower limit of temperature to 4.2 K.

IV—K Photoelectron Spectroscopy of Organic Solids in Vacuum Ultraviolet Region

The work of ultraviolet photoelectron spectroscopy (UPS) with synchrotron radiation lightsource (UVSOR)-UVSOR-UPS-of organic solids, fullerene series has been proceeded to find their quantitative electronic structures. The angle-resolved photoemission work has been applied to the oriented organic films.

IV-K-1 Electronic Structure of bis[1,2,5]thiadiazolo-*p*-quinobis(1,3-dithiole) (BTQBT) Studied by Ultraviolet Photoemission Spectroscopy

Hitoshi FUJIMOTO *(Kumamoto Univ.)*, **Kohji KAMIYA** *(Nagoya Univ. and IMS)*, **Shoji TANAKA, Takehiko MORI, Yoshiro YAMASHITA, Hiroo INOKUCHI, and Kazuhiko SEKI** *(Nagoya Univ.)*

[*Chem. Phys.*, **165**, (1992) in press]

Ultraviolet photoemission spectroscopy (UPS) has been used to investigate the electronic structure of the unusually high conductive organic compound, bis[1,2,5]thiadiazolo-*p*-quinobis(1,3-dithiole) (BTQBT). The observed spectral features were analyzed with the aid of the semiempirical MNDO-SCF-MO (modified neglect of diatomic overlap self-consistent-field molecular orbital) method. BTQBT shows a low photoionization threshold of 4.57 eV in the solid state as compared with the gas phase value of 6.4 eV

which is evaluated from the oxidation potential. This lowering from the gas phase can be explained with respect to the strong intermolecular interactions as shown in Figure 1: if we take the calculated band width of 0.7 eV, the polarization energy and the other solid state effects of about 1.5 eV contribute to this lowering. The work function of BTQBT was found to be 4.3 eV. From this value and the ionization threshold energy, the energy difference between the Fermi level and the top of the valence band is determined to be 0.3 eV. This small value, in agreement with the observed activation energy in electric conduction, should be at least part of the origin of the high conductivity in BTQBT.

These observations show that the strong intermolecular interaction in the solid state of BTQBT, suggested from the crystal structure of this compound, is essential for the high conductivity of this compound.

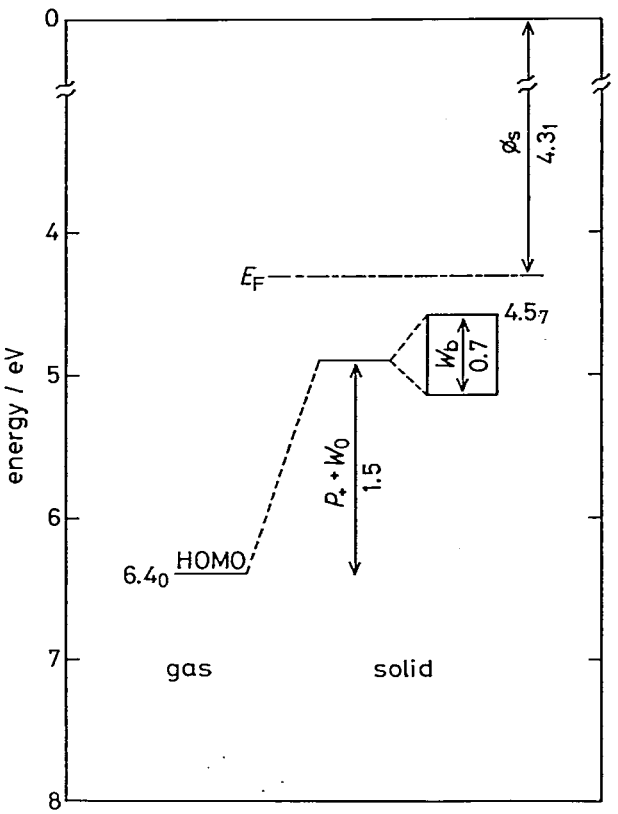

Figure 1. Electronic structures in the top region of the valence band of BTQBT.

IV-K-2 Resonant Photoemission Study of an Al-Cu-Fe Icosahedral Phase

Masahiro MORI[a], Koji KAMIYA, Susumu MATSUO[a], Tsutomu ISHIMASA[a], Hiroshi NAKANO[a], Hitoshi FUJIMOTO[b], and Hiroo INOKUCHI *([a]Nagoya Univ., [b]Kumamoto Univ.)*

[*J. Phys.: Condens. Matter*, 4, L157 (1992)]

The discovery of an icosahedral phase (i-phase) has made a great surprise with forbidden symmetry and sharp diffraction spots. Two remarkable magnetic properties have been found on the stable Al-Cu-Fe i-phase. One is that the magnetic susceptibility is proportional to T^2. The T-dependence suggests existene of a sharp dip in DOS at E_F caused by the energy gap of the Brillouin zone. The other is that the Fe atoms have no magnetic moments. Recently, the dip-like anomaly in DOS near E_F was confirmed with our previous UPS experiment. The purpose is to observe the resonant UPS to discuss about the Friedel's suggestion on the role of the Fe 3d states on the i-phase stability.

UPS studies were performed at room temperature on BL-8B2 of UVSOR. The clean surface was obtained by filing in $3-7\times10^{-8}$ Pa, and the sample was transferred to the UPS chamber in $0.5-3\times10^{-8}$ Pa. As the CIS intensity depends on the photon energy severely, we can not discuss the detailed feature. The fitted spectrum was estimated from the non-resonant spectrum. The spectra in Figure show the relative CIS curves.

Photoemission spectra of the valence band in the i-phase are studied at excitation photon energies near the Fe threshold. The constant-initial-state spectra at the binding energy region between 0–2 eV show a resonant characteristic. The spectrum has an asymmetric shape, in which the weak peak is on the lower photon energy side and the strong dip is on the higher. It's resonant energy seems to be slightly smaller than the 3p-3d core excitation energy of an Fe natural form. The Fe 3d bands are located in the region ranging from E_F to 2–2.5 eV below it with the maximum contribution at around 0.7 eV in the binding energy. The smaller binding energy of Fe 3d bands suggests that Fe atoms have small amounts of extra electrons transferred from the other elements. The smaller binding energy, exactly Fe 3d-states sitting just below E_F, is consistent with the Friedel's suggestion that the stability of the icosahedral phase is enhanced by a crossing effect of 3d-state with nearly-free-electron-like state below E_F which enhances the energy gap of the Brillouin zone.

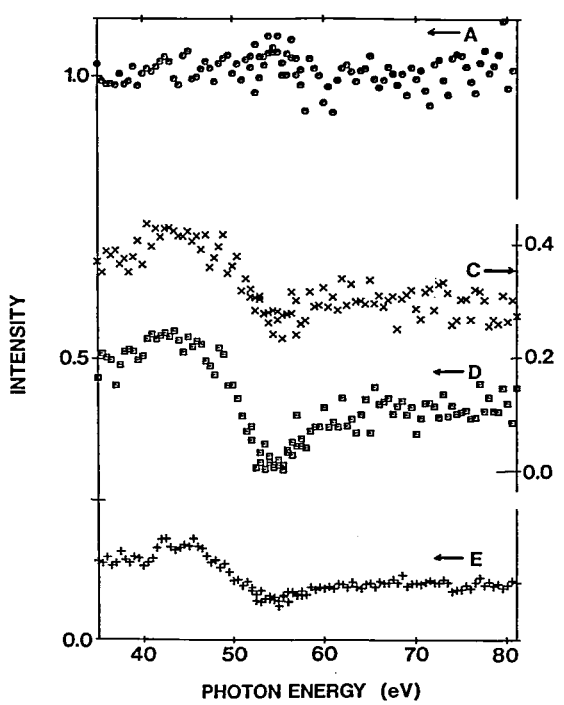

Figure 1. Relative CIS spectra for several binding energies. They represent the CIS spectra divided by the fitted spectrum. A, C, D and E corresponds to the spectrum at the binding energies 5 eV, 2 eV, 1 eV and 0.1 eV, respectively.

IV-K-3 Electronic Structure of Doped C_{60}; Strong Correlation or Lattice Distortion?

Takashi TAKAHASHI[a], Takashi MORIKAWA[a], Hiroshi KATAYAMA-YOSHIDA[a], Shinji HASEGAWA, Hiroo INOKUCHI, Kazuhiko SEKI[b], Shojun HINO[c], Koichi KIKUCHI[d], Shinzo SUZUKI[d], Isao IKEMOTO[d], and Yohji ACHIBA[d] *([a]Touhoku Univ., [b]Nagoya Univ., [c]Chiba Univ., [d]Tokyo Metro. Univ.)*

[*Proceeding of International Conference on Strong Correlated Electron Systems* (Sep.7—11, 1992, Sendai)]

It was found by photoemission and inverse photoemission that an energy gap with a finite density of states at the bottom (a pseudo-gap) opens at the Fermi level for alkali-doped solid C_{60} at the composition of A_3C_{60} (A; alkali metal). Strong electron correlation and lattice distortion (Jahn-Teller effect) were discussed as possible origins for the pseudo-gap.

IV-K-4 Anomalous Temperature Dependence of Low-Energy-Electron Transmission Spectra of Thin Films of Tetrakis(nonylthio)tetrathiafulvalene (TTC_9-TTF)

N. UENO*, H. KUROSU*, K. SEKI *(Nagoya Univ.)*, **G. SAITO** *(Kyoto Univ.)*, **K. SUGITA*, and H. INOKUCHI** *(*Chiba Univ.)*

[*Mol. Cryst. Liq. Cryst.*, **218**, 171 (1992)]

Temperature dependence of low-energy-electron transmission spectra was measured for thin films of a molecular fastner, tetrakis(nonylthio)tetrathiafulvalene. Ten spectral features, which can be ascribed to the structure of the conduction bands, were observed in the energy region of incident electron of 0—15 eV. They showed a large temperature dependence of the energy position as well as of the sharpness and the intensity. The energy positions shifted 0.6 eV to high-energy side by cooling from room temperature to −124°C. Such a large energy shift was not observed for other thin films consisting of long-alkyl molecules, and is considerd as a result of the molecular fastner effects.

IV-K-5 Angle-resolved Photoemission from Langmuir-Blodgett Films of Copper Tetrakis(n-butoxycarbonyl)phthalocyanine with Synchrotron Radiation

Nobuo UENO[a], Koji KAMIYA, Kimiya OGAWA[b], Hisatomo YONEHARA[b], Masahiro TAKAHASHI[c], Hiroo NAKAHARA[c], Kazuhiko SEKI[d], Kazuyuki SUGITA[a], Kiyoshige FUKUDA[c], and Hiroo INOKUCHI *([a]Chiba Univ., [b]Kawamura ICR, [c]Saitama Univ., [d]Nagoya Univ.)*

[*Thin Solid Films*, **210/211**, 678 (1992)]

Angle-resolved ultraviolet photoemission experiments were performed for Langmuir-Blodgett films of copper tetrakis(n-butoxycarbonyl)phthalocyanine[$(BuOCO)_4CuPc$] with synchrotron radiation. A pronounced angular dependence of the photoelectron spectra which can be ascribed to the molecular orientation was observed. The results indicate that the in-plane orientation of CuPc rings is realized in a few surface layers depending on the dipping direction.

IV-K-6 Pseudo-Gap at the Fermi Level in K_3C_{60} Observed by Photoemission and Inverse Photoemission

Takashi TAKAHASHI[a], Satoru SUZUKI[a], Takashi MORIKAWA[a], Hiroshi KATAYAMA-YOSHIDA[a], Shinji HASEGAWA, Hiroo INOKUCHI, Kazuhiko SEKI[b], Koichi KIKUCHI[c], Shinzo SUZUKI[c], Isao IKEMOTO[c], Yohji ACHIBA[c] *([a]Touhoku Univ., [b]Nagoya Univ., [c]Tokyo Metro. Univ.)*

[*Phys. Rev. Lett.*, **68**, 1232 (1992)]

A comparative photoemission and inverse photoemission spectroscopy has been performed on C_{60} and K_3C_{60} to study the change of the electronic structure upon the alkali-doping and its relation to the occurrence of the superconductivity. The experimental results show that the alkali-doping does not lead to a rigid filling of the LUMO band by the doped electrons but causes a transfer of the electronic states from the LUMO band to an additional band produced in the band gap. The comparison of the photoemission and inverse photoemission spectra indicates that a pseudo-gap of about 0.5 eV opens at the Fermi level in K_3C_{60}. Some possible origins for the pseudo-gap and its relation to the superconductivity were discussed.

IV-K-7 Comparative Photoemission Study of Rb_xC_{60}, Rb_xC_{70} and RbC_8: A Pseudo-gap at the Fermi Level in the Fulleride

Takashi TAKAHASHI[a], Takashi MORIKAWA[a], Shinji HASEGAWA, Koji KAMIYA[b], Hitoshi FUJIMOTO[c], Shojun HINO[d], Kazuhiko SEKI[b], Hiroshi KATAYAMA-YOSHIDA[a], Hiroo INOKUCHI, Koichi KIKUCHI[e], Shinzo SUZUKI[e], Isao IKEMOTO[e], and Yohji ACHIBA[e] *([a]Touhoku Univ., [b]Nagoya Univ., [c]Kumamoto Univ., [d]Chiba Univ., [e]Tokyo Metro. Univ.)*

[*Phisica C*, **190**, 205 (1992)]

A comparative photoemission study on Rb_xC_{60}, Rb_xC_{70}, and RbC_8 (graphite intercalation compound) is reported. It was found that the Fermi level of Rb_3C_{60} is located at the bottom of a valley of the density of states, while that of RbC_8 is at a maximum point of the occupied states. This experimental result is explained in terms of the existence of a pseudo-gap at the Fermi level in the fulleride. This indicates that a rigid-band picture is not a good starting point for understanding the change of the electronic structure upon the alkali-doping. It was also found that the density of states at the Fermi level is much smaller in Rb_xC_{70} than in Rb_xC_{60}. This accounts for the less conductive nature and the absence of the superconductivity in Rb_xC_{70}.

IV-K-8 Photoelectron Spectra of a Higher Fullerene Compound C_{82} and Its Potassium Complex

Shojun HINO[a], Kazuo MATSUMOTO[a], Shinji HASEGAWA, Kentaro IWASAKI, Kyuya YAKUSHI, Takashi MORIKAWA[b], Takashi TAKAHASHI[b], Kazuhiko SEKI[c], Koichi KIKUCHI[d], Shinzo SUZUKI[d], Isao

IKEMOTO[d], and Yohji ACHIBA[d] *([a]Chiba Univ., [b]Touhoku Univ., [c]Nagoya Univ., [d]Tokyo Metro. Univ.)*

[*Synth. Metals*, in press]

Photoelectron spectra of C_{82}, which has been reported to contain metal atoms inside, are measured with a synchrotron radiation light source. The spectra resemble those of C_{84}. The spectra begin at 1.1_5 eV below the Fermi level (E_f). The first band consists of two peaks located at 2.2 eV and 3.3 eV accompanied by a slight shoulder structure at the lower binding energy side. This shoulder is not observed in C_{84}. The intensity of the two peaks of the first band oscillates with the incident photon energy change, as are observed in C_{60}, C_{70} and C_{84}. The second band locates between 4 and 6.2 eV with a peak at 5.3 eV and a shoulder at the lower binding energy side. The third band locates between 6.2 and 9 eV and consists of a peak at 7.8 eV and a distinct shoulder at 6.5 eV. Potassium dosing brings a new band between the E_f and the first band and its intensity grows as the potassium dosage increases. The spectral onset approaches toward the E_f in accordance with increase of potassium dosage but it does not cross the E_f, which indicates a semiconductive nature of K_xC_{82}.

IV-K-9 Photoelectron Spectra of C_{76} and K_xC_{76}

Shojun HINO[a], Kazuo MATSUMOTO[a], Shinji HASEGAWA, Hiroo INOKUCHI, Takashi MORIKAWA[b], Takashi TAKAHASHI[b], Kazuhiko SEKI[c], Koichi KIKUCHI[d], Shinzo SUZUKI[d], Isao IKEMOTO[d], and Yohji ACHIBA[d] *([a]Chiba Univ., [b]Touhoku Univ., [c]Nagoya Univ., [d]Tokyo Metro. Univ.)*

[*Chem. Phys. Lett.*, in press]

Ultraviolet photoelectron spectra (UPS) of C_{76}, one of the fullerene family compounds, have been measured with a synchrotron radiation light source. The photoemission spectral onset is 1.3 eV below the Fermi level, which is equal to that of C_{84} but smaller by 0.5 eV than that of C_{60} or C_{70}. The relative intensity of the photoemission spectral shape is independent upon the incident photon energy change. Photoemission spectral change of C_{76} during potassium dosing is also measured. A new band becomes distinct between the Fermi level and the HOMO (highest occupied molecular orbital) band, when potassium content (x in K_xC_{76}) is equal to or greater than 1.1. The new band edge moves toward the Fermi level upon the increase of potassium dosage, and it approaches the vincinity of the Fermi level. This indicates that potassium dosed C_{76} could be either metallic or narrow gap semiconductive.

IV-K-10 Ultraviolet Photoelectron Spectra of C_{84} and K_xC_{84}

Shojun HINO[a], Kazuo MATSUMOTO[a], Shinji HASEGAWA, Koji KAMIYA, Hiroo INOKUCHI, Takashi MORIKAWA[b], Takashi TAKAHASHI[b], Kazuhiko SEKI[c], Koichi KIKUCHI[d], Shinzo SUZUKI[d], Isao IKEMOTO[d], and Yohji ACHIBA[d] *([a]Chiba Univ., [b]Touhoku Univ., [c]Nagoya Univ., [d]Tokyo Metro. Univ.)*

[*Chem. Phys. Lett.*, **190**, 169 (1992)]

Ultraviolet photoelectron spectra (UPS) of C_{84}, one of the fullerene family compounds, and potassium dosed C_{84} have been measured with a synchrotron radiation light. The spectra of C_{84} are compared with those of C_{60} and C_{70}. The photoemission spectral onset of C_{84} is 1.3 eV below the Fermi level, which is smaller by 0.5 eV than that of C_{60} or C_{70}. This indicates its small band gap, which has been expected from their absorption spectra. Upon potassium dosing a new band becomes distinct between the Fermi level and the HOMO (highest occupied molecular orbital) band. The new band edge does not cross the Fermi level, which indicates that potassium dosed C_{84} is not metallic but semiconductive.

IV-K-11 Molecular Orientation in Thin Films of Bis(1,2,5-thiadiazolo)-*p*-quinobis(1,3-dithiole) on Graphite Studied by Angle-Resolved Photoelectron Spectroscopy

Shinji HASEGAWA, Shoji TANAKA, Yoshiro YAMASHITA, Hiroo INOKUCHI, Hitoshi FUJIMOTO *(Kumamoto Univ.)*, **Koji KAMIYA, Kazuhiko SEKI** *(Nagoya Univ.)*, **and Nobuo UENO** *(Chiba Univ.)*

[*Phys. Rev. Lett.*, submitted]

Angle-resolved ultraviolet photoelectron spectra using synchrotron radiation were measured for oriented thin films of bis(1,2,5-thiadiazolo)-p-quinobis(1,3-dithiole) (BTQBT) evaporated on cleaved graphite (HOPG) surface. The take-off angle dependences of photoelectrons from the highest and next highest occupied orbitals (HOMO and $HOMO^{-1}$) were quantitatively analyzed using the independent-atomic-center(IAC) approximation and MNDO molecular orbital calculations, shown in Figure 1. It was first noted that IAC approximation is satisfactorily applicable to the quantitative analysis of the angular distribution of photoelectrons for a fairly large and complex orgnaic molecule as BTQBT. These results revealed that the BTQBT molecules oriented with molecular planes inclining at $\simeq 5°$ to the graphite surface.

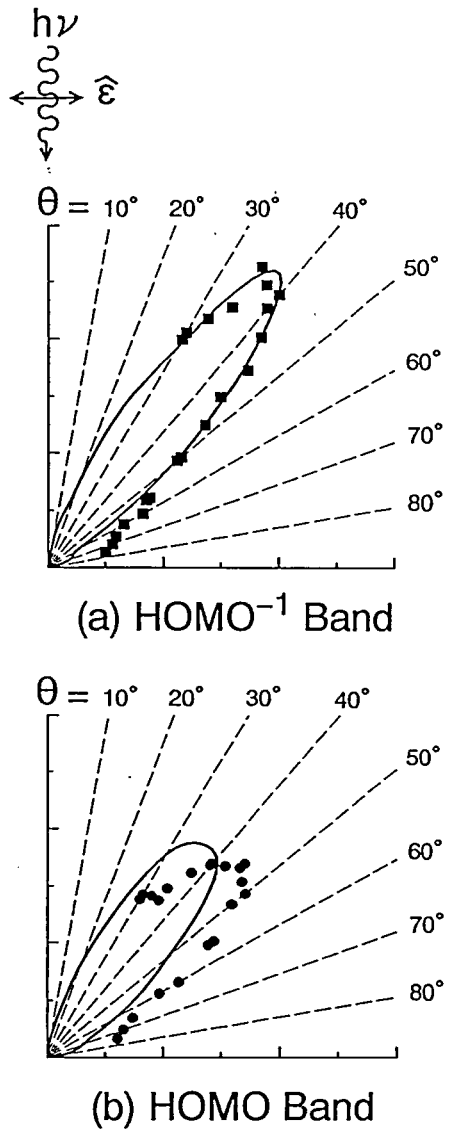

Figure 1. The take-off angle θ dependences of photoelectron intensities for the (a)HOMO^{-1} and (b)HOMO bands at α=0° and hν=40 eV, where both figures (a) and (b) are plotted in the common intensity scale. Full lines are the calculated angular distributions using the inclination angle β=5°. The experimental results are shown by closed squares and circles.

IV-K-12 Electronic States of Oxidized and Reduced Cytochrome c Observed by X-ray Photoelectron Spectroscopy

Kenji ICHIMURA *(Kumamoto Univ.)*, **Yusuke NAKAHARA** *(Tech. College of Miyakonojo)*, **Keisaku KIMURA** *(Himeji Inst. of Tech.)*, **and Hiroo INOKUCHI**

[*J. Mater. Chem.*, in press]

To understand the mechanism of electrical conductivities of cytochromes in terms of the electric and valence states, X-ray photoelectron spectra of oxidized and reduced cytochrome *c* were measured in the Fe 2p, S 2p, O 1s, N 1s, and C 1s regions. The difference between the spectra of both forms shows that changes occur in the electronic states at the sites of porphyrin ring and sulfur-containing amino acids (methionine and cysteine residues). The higher conductivity of ferrocytochrome *c* (reduced form) than ferricytochrome *c* (oxidized form) is attributed to the charge multiplicity of sulfur atoms in addition to the π-electron system.

IV—L Electrical Conduction and its Related Properties of Organic Solids

The electronic properties and crystal structures of single component organic semiconductors have been observed.

IV-L-1 Crystal Structures and Molecular Packing of Tetrakis(alkylthio)tetrathiafulvalene (TTC_n-TTF); part I (n=3,4,6)

Chikako NAKANO,[a] Takehiko MORI, Kenichi IMAEDA, Noritake YASUOKA,[b] Yusei MARUYAMA, Hiroo INOKUCHI, Naoko IWASAWA,[c] and Gunzi SAITO[d] *([a]Toyota Physical and Chemical Research Inst. and IMS, [b]Himeji Inst. of Tech., [c]ISSP, [d]Kyoto Univ.)*

[*Bull. Chem. Soc. Jpn.*, **65**, 1878 (1992)]

The crystal structures of tetrakis(alkylthio)tetrathiafulvalene TTC_n-TTF(n=3,4,6) were determined by X-ray analysis. The structures of TTC_n-TTF drastically changed between n=3 and 4. The TTC_3-TTF molecule has a boat-like shape, like that of TTC_1-TTF and TTC_2-TTF. On the other hand, the TTC_4-TTF and TTC_6-TTF molecules have chair-like shapes, like that of TTC_5-TTF, and columnar structure with intermolecular effective overlaps between the central π-systems. These results can explain the drastic change in the electrical properties between n=3 and 4.

IV-L-2 Crystal Structures and Molecular Packing of Tetrakis(alkylthio)tetrathiafulvalene (TTC_n-TTF); part II (n=7,9,11)

Chikako NAKANO,[a] Takehiko MORI, Kenichi IMAEDA, Noritake YASUOKA,[b] Yusei MARUYAMA, Hiroo INOKUCHI, Naoko IWASAWA,[c] and Gunzi SAITO[d] *([a]Toyota Physical and Chemical Research Inst. and IMS, [b]Himeji Inst. of Tech., [c]ISSP, [d]Kyoto Univ.)*

[*Bull. Chem. Soc. Jpn.*, **65**, 2086 (1992)]

The crystal structures of tetrakis(alkylthio)tetrathiafulvalene (TTC_n-TTF) with long alkyl chains ($7 \leqq n \leqq 11$) can be divided into two different groups (Form I and Form II) according to the difference in the arrangement of the alkyl chains. Although the crystals of TTC_7-TTF exhibit two phases (triclinic and monoclinic), the stacking manner of these phases is nearly the same, Form II. TTC_9-TTF crystallizes in two different forms: Form I (the triclinic phase) and Form II (the monoclinic phase). The TTC_{11}-TTF crystal only adopts the Form I structure. Although the molecules in both forms have chair-like shapes and columnar structures, the alkyl chains in the Form I crystals are arranged parallel to each other, resulting in more strongly fastened packing than in the case of the Form II crystals. These results are associated with changes in the electrical resistivities and activation energies of TTC_n-TTF over the range of large n.

IV-L-3 Hall-Effect Observation in the New Organic Semiconductor Bis(1,2,5-thiadiazolo)-*p*-quinobis(1,3-dithiole) (BTQBT)

Kenichi IMAEDA, Yoshiro YAMASHITA, Yongfang LI, Takehiko MORI, Hiroo INOKUCHI, and Mizuka SANO *(ICU)*

[*J. Mater. Chem.*, **2**, 115 (1992)]

Single crystals of bis(1,2,5-thiadiazolo)-*p*-quinobis(1,3-dithiole) (BTQBT) were grown either by recrystallization from a nitrobenzene solution or by sublimation in nitrogen atmosphere. The electrical resistivities were 1.2×10^3 Ωcm and 2.7×10^5 Ωcm at room temperature for a crystal grown by recrystallization and that obtained by sublimation, respectively. These values are remarkably low for a single-component organic crystal. In addition, the BTQBT crystals have a small anisotropy in resistivity ($\rho_\perp/\rho_\parallel=2$), which is ascribed to strong intermolecular interactions inherent in the crystal structure. They show a Hall effect, which is an unusual observation in organic semiconductors. The sign of carriers was determined to be positive and the Hall mobility was found to be ca. 4 $cm^2s^{-1}V^{-1}$ at room temperature.

IV—M Physics and Chemistry of Graphite and its Intercalation Compounds

The electronic properties and the structures of alkali metal-hydrogen-graphite intercalation compounds have been investigated.

IV-M-1 Two-Dimensional Metallic Hydrogen Lattice in Potassium-Hydrogen-Graphite Ternary Systems

Toshiaki ENOKI*, Keisuke NAKAZAWA*, Kazuya SUZUKI*, Seiichi MIYAJIMA, Takehiko CHIBA *(Nihon Univ.)*, **Yasuhiro IYE** *(ISSP)*, **Hiromichi YAMAMOTO, and Hiroo INOKUCHI** *(*Tokyo Inst. Tech.)*

[*J. Less-Common Metals*, **172—174**, 20 (1991)]

Alkali metal graphite intercalation compounds absorb hydrogen to form alkali metal hydride graphite intercalation compounds. We investigate the electronic properties and the structures of potassium hydride graphite intercalation compounds by means of proton nuclear magnetic resonance, Hall effect, and UV photoelectron spectroscopy. Among the alkali metal hydride intercalation compounds, potassium hydride intercalation compounds, the structure of which consists of ionic K^+ H K^+ sandwich triple atomic layers between graphite sheets, were found to have novel two-dimensional metallic sheets in the intercalate space.

IV—N Organic Metals

In an attempt to develop new organic superconductors and to explore the related phenomena, new organic conductors have been prepared and the physical properties have been investigated. Particularly, this year we found a new organic superconductor, $(BEDT\text{-}TTF)_4Pd(CN)_4H_2O$. This conductor is, together with its Pt analogue, the first organic superconductor with a divalent anion. Another example is a metallic conductor, (TTF)(DMeT-DCNQI), where DMeT-DCNQI is a newly-prepared sulfur-containing acceptor. We also explored a new synthetic route to tetrathiafulvalene derivatives by using organoaluminium reagents.

IV-N-1 Structural and Physical Properties of a New Organic Superconductor, $(BEDT\text{-}TTF)_4Pd(CN)_4H_2O$

Takehiko MORI, Kiyonori KATO, Yusei MARUYAMA, Hiroo INOKUCHI, Hatsumi MORI*, Izumi HIRABAYASHI*, and Shoji TANAKA* *(*ISTEC)*

[*Solid State Commun.*, **82**, 177 (1992)]

Two newly prepared organic conductors, $(BEDT\text{-}TTF)_4Pd(CN)_4H_2O$ and $(BEDT\text{-}TTF)_4Pd(CN)_4$ have quite similar structures, but the angles between the conducting donor sheets and the donor planes are different. The former salt shows a small increase of the resistivity below 70

K, but the results of the thermoelectric power and ESR indicate that there is no energy gap even at low temperatures. This salt becomes superconducting at 1.2 K (midpoint of the resistance drop) under 7 kbar (Figure 1).

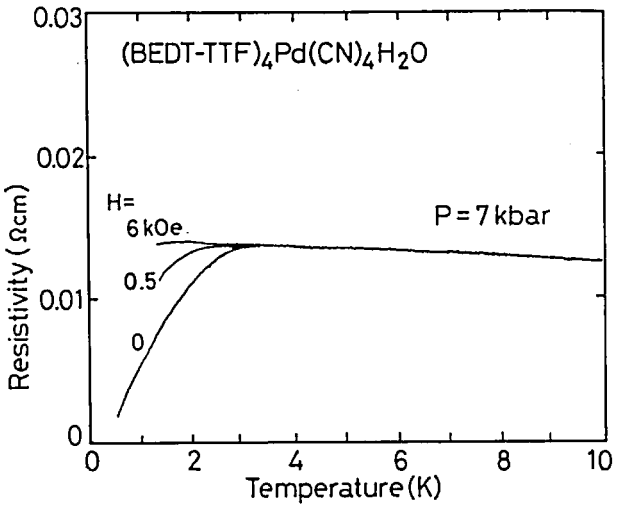

Figure 1. Electrical resistivity of $(BEDT\text{-}TTF)_4Pd(CN)_4$ under pressure.

IV-N-2 Structural and Conducting Properties of (TTF)(DMeT-DCNQI)

Takehiko MORI and Hiroo INOKUCHI

[*Bull. Chem. Soc. Jpn.*, **65**, 1460 (1992)]

The title charge transfer complex, where TTF is tetrathiafulvalene, and DMeT-DCNQI is 2,5-dimethylthio-*N,N'*- dicyanoquinonediimine, crystallizes in triclinic space group P 1, a=15.447(3), b=15.774(3), c=3.834(2) Å, α=96.96(3), β=97.14(3), γ=82.24(2)°, V=913(5) Å^3 and Z=2. The donor and acceptor molecules form segregated columns. This complex shows high electrical conductivity, 400 Scm^{-1} at room temperature, and undergoes a metal-semiconductor transition at round 130 K.

IV-N-3 Synthesis of Tetrathiafulvalene Derivatives by the Use of Organoaluminium Reagents

Takehiko MORI and Hiroo INOKUCHI

[*Chem. Lett.*, **1992**, 1873]

Bis(dimethylaluminium) salts of ethanedithiol, 1,2-benzenedithiol, and ethylenedithiol react with 1,3-dithiolane-2-carboxylate esters to give dihydro- and tetrahydro- tetrathiafulvalenes as well as tetrathiafulvalene derivatives.

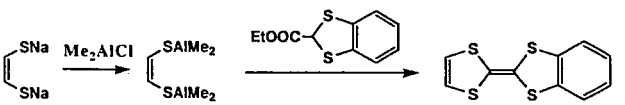

IV—O Structure and Electronic State of DCNQI-Cu Compounds

The family of metal complexes of dicyanoquinonediimine (DCNQI) derivatives, $(2,5\text{-}R_1,R_2\text{-}DCNQI)_2M$ [R_1,R_2=CH_3, CH_3O, Br, Cl; M=Cu, Ag, Li, Na, K] is a novel type of organic conductors. For the Cu compounds, there is an increasing number of evidences showing that the 3d orbitals of Cu ions are mixed with conducting pπ orbitals of organic molecules. In this study, we have examined the valence state of Cu ions and structure of DCNQI-Cu compounds.

IV-O-1 XANES and EXAFS Study in $(R_1,R_2\text{-}DCNQI)_2Cu$

Kokichi OSHIMA*, Takashi DOI, Hiroshi MARUYAMA**, Hironobu MAEDA**, Hitoshi YAMAZAKI**, Reizo KATO***, Akiko KOBAYASHI*** and Toshio NAITO****, and Hayao KOBAYASHI******
*(*Okayama Univ. and IMS, **Okayama Univ., ***The Univ. of Tokyo, ****Toho Univ.)*

[Jpn.J. Appl. Phys. to be published]

XANES and EXAFS measurements at Cu K-edge are reported for $(R_1,R_2\text{-}DCNQI)_2Cu$. The valence state of Cu proposed in this compound has been confirmed by the XANES study. The systematic XANES and EXAFS studies have revealed the differences in the spectra between two groups in this compound (Group I is metallic down to low temperatures, and Group II shows a metal-insulator transistion). The local structural change during the metal-insulator transition in the Group II compound has been confirmed using EXAFS analysis. The clear difference in XANES spectra between two groups has been attributed to the difference in the valence states.

IV—P The Effect of Microscopic Molecular Environments on the Dynamics of Electronically Excited Molecules Generated in Supersonic Free Jets

An ensemble of atoms or molecules coordinated to an electronically excited molecule provide microscopic molecular environments which significantly influence electronic relaxation processes of the uncoordinated excited molecule. Our concern is to clarify the role of the microscopic environments and, if possible, to quantify it for various dynamic processes from electronically excited states. Three recent achievements in this line are presented below, viz, i) modification of intersystem

crossing process by the coordination of rare-gas atoms, ii) effect of a cluster size on the natural radiative lifetime and iii) competition of the intramolecular photoisomerization reaction with the photodissociation of coordinated rare-gas atoms.

IV-P-1 S_1-T_2 Level Inversion of 9,10-Dimethylanthracene Caused by the Coordination of One Rare-gas Atom

Fujio TANAKA *(University of Osaka Prefecture)*, **Satoshi HIRAYAMA,** *(Kyoto Institute of Technology, IMS)*, **and Kosuke SHOBATAKE**

[*Chem. Phys. Lett.*, **195**, 243 (1992)]

Fluorescence lifetimes were measured for isolated 9,10-dimethylanthracene and its van der Waals complexes with rare-gas atoms in supersonic free jets. On the basis of the microscopic solvation effect on intersystem crossing, it is demonstrated that the energy of the S_1 electronic origin is located above that of the T_2 electronic origin for the isolated molecule and that the relative position of these states is inverted upon coordination with one atom of Ar, Kr or Xe. A similar phenomenon is suggested for the complexation of 9,10-dibromoanthracene with a Xe atom.

IV-P-2 Radiative Lifetime and Electronic Relaxation of 9-Cyanoanthracene in Rare-gas Clusters and in Rare-gas Matrices

Mitsuhiko KONO, Yoshiharu KUBO, Satoshi HIRAYAMA *(Kyoto Institute of Technology, IMS)*, **and Kosuke SHOBATAKE**

[*Chem. Phys. Lett.*, in press]

Laser induced fluorescence (LIF) excitation spectra and fluorescence lifetimes were measured for rare-gas (Ar, Kr and Xe) clusters of 9-cyanoanthracene (9CNA) generated in supersonic free jets and for 9CNA isolated in rare-gas matrices at 15 K. Some of the results for the Ar clusters are presented in Figure 1. The natural radiative lifetime, τ_r, of the 9CNA clusters was not influenced greatly by complexation with rare-gas atoms of any kind. The values obtained for the most highly coordinated clusters were 26.5 ± 0.3 ns, 28.2 ± 0.6 ns and 28.4 ± 0.3 ns for Ar, Kr and Xe, respectively. These values are approximately equal to the value for τ_r at the electronic band origin of the bare 9CNA molecule, but are almost two times larger than the radiative lifetimes of 9CNA found in the rare-gas matrices at 15 K, in which the radiative lifetimes measured are correlated satisfactorily through the square of the refractive index. Nevertheless, the relaxation process from higher vibronic levels as well as the spectral band positions of these clusters is simlar to those found in the rare-gas matrices.

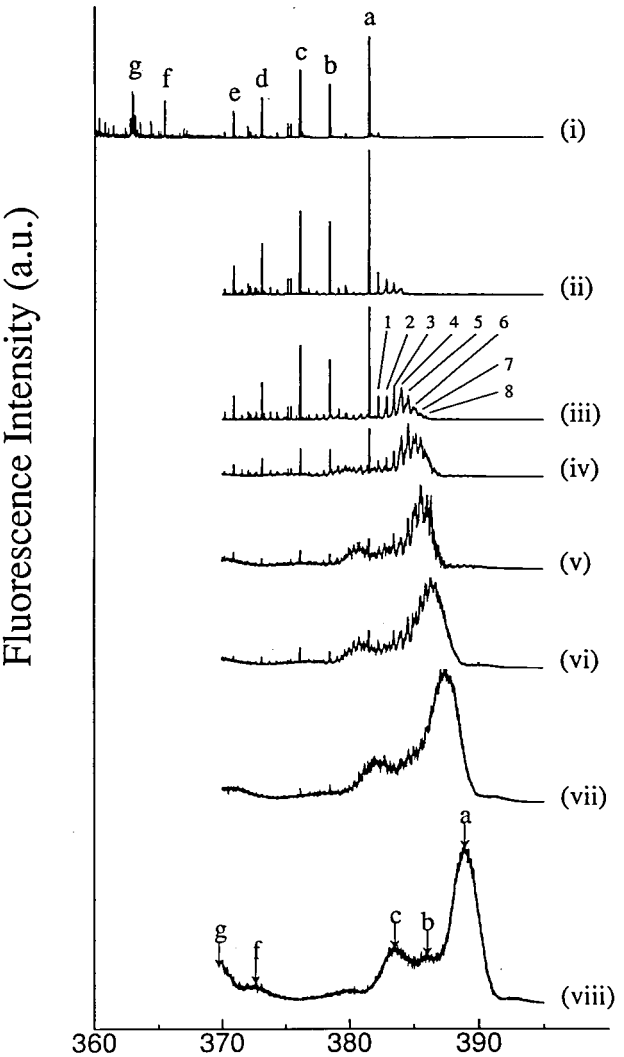

Figure 1. LIF excitation spectra of the Ar clusters of 9CNA. The fluorescence emission was monitored at 414 nm (band pass 7 nm). The top (i) and bottom (viii) spectra are those recorded for the bare 9CNA molecule and the most highly coordinated cluster ($m > 20$), respectively.

IV-P-3 Single Vibronic Level Relaxation in Photoreactive 9-*tert*-Butylanthracene

Satoshi HIRAYAMA, Mitsuhiko KONO, Yoshiharu KUBO *(Kyoto Institute of Technology, IMS)*, **Fujio TANAKA** *(University of Osaka Prefecture)*, **and Kosuke SHOBATAKE**

[*J. Phys. Chem.*, to be published]

The laser-induced fluorescence (LIF) excitation spectrum of photoreactive 9-*tert*-butylanthracene (9TBA) in supersonic free jets shows a rich band structure in the range 25500–26300 cm^{-1} and was found to be characterized by three distinct features, namely, a low intensity of the electronic band origin, a progression of a low frequency torsional vibration mode (≈ 77 cm^{-1}) of the *tert*-butyl group and an absence of fluorescence when excited above 26300 cm^{-1} (an excess energy of 790 cm^{-1}). The fluorescence

lifetime measured for the electronic origin at 25511cm^{-1} is 34.9 ns and remains approximately constant over a few torsional vibration bands. The fluorescence lifetimes decrease significantly above an excess energy of 482 cm^{-1}. The electronic origins of the 1:1 van der Waals complexes of 9TBA with Ar and Xe were observed at 25467 cm^{-1} and 25436 cm^{-1}, respectively, but the LIF excitation spectra are dominated by two broad bands arising from complex formation. In the spectra of both complexes, one of these two broad bands is superposed on the highly structured bands associated with the bare molecule, and the other broad band appears in the range 26700–27400 cm^{-1} where there is no measurable fluoreoscence intensity from the bare molecule. The appearance of this second broad band is ascribed to the photofragmentation of the van der Waals complexes. Excitation in this broad band resulted in fluorescence decay curves which are non-exponential and whose longest-lived component has a fluorescence lifetime comparable with that measured for the bare molecule at the electronic origin. 9-*tert*-Butyl-10-cyanoanthracene was found to be non-fluorescent in supersonic free jets, despite the large increase in the fluorescence quantum yield in the condensed phase in going from room temperature to 77 K. 9-*tert*-Butylanthracene was found to be fluorescent in supersonic jets, in the gas phase and in the condensed phase, indicating that the *tert*-butyl group located at the β-position in the anthracene ring does not quench fluorescence in this molecule. Other examples of anthracene derivatives which do not fluoresce in supersonic free jets are also reported.

RESEARCH ACTIVITIES V
Department of Applied Molecular Science

V—A New Multi-Stage Redox Systems

Interdisciplinary cooperation between synthetic chemistry, physical chemistry, and solid state physics has opened a new field of science which can explore molecular materials having interesting electrical, magnetic, and optical properties in the solid state. In general, molecular level correlation of physical properties between molecules and the solid state is essential to construct new molecular materials. Such a consideration into highly electrically conducting behaviors reveals the importance of conjugated electronic systems having multi-stage redox nature, which can transfer electron smoothly by multi-stage manners. We have designed and synthesized two classes of new multi-stage redox systems, such as peri-condensed Weitz type donors and amphoteric multi-stage redox systems. The peri-condensed Weitz type redox systems are designed by replacing two of the sp^2 carbon atoms in a polycyclic arene by two sulfur atoms. Such heterocycles have produced new organic molecular metals which contain non-TTF and non-TCNQ type components. The amphoteric multi-stage redox systems are designed so as to decrease the difference between the oxidation and the reduction potentials of a molecule. We have already reported the synthesis and properties of conjugated hydrocarbons with the highest amphotericity. Design and synthesis of new types of multi-stage redox systems, and investigations of their physical and solid state properties are actively continued.

V-A-1 Synthesis and Properties of Methyl Chalcogeno Derivatives of 1,6-Diselenapyrene (DSPY)

Yasushi MORITA, Takeshi OHMAE, Jiro TOYODA, Shotaro MASTUDA,[a] Fumio TODA,[a] and Kazuhiro NAKASUJI *([a]Ehime Univ.)*

We modified 1,6-diselenapyrene (DSPY) by introducing methyl chalcogeno groups on the 2 and 7-position. Treatment of DSPY with a large excess of lithium diisopropylamide (LDA) and dimethyldisulfide in THF gave 2,7-bis(methylthio)-1,6-diselenapyrene (MTDSPY) as yellowish orange plates (71% yield). Treatment of DSPY with a large excess of LDA, selenium powder, and iodomethane gave the methylseleno derivatives, 2,7-bis(methylseleno)-1,6-diselenapyrene (MSDSPY) as yellowish brown plates (63% yield). The first oxidation potentials of these donors are 0.41 and 0.44 V, respectively. The CT complexes with TCNQ were obtained. The CT transition energies are as follows: DSPY-TCNQ; 0.37, MTDSPY-TCNQ; 0.72, MSDSPY-TCNQ; 0.75 eV. Among them, DSPY-TCNQ showed the low energy transition, which indicates that this is not usual mixed stacking type complex and has possibility to have the highly electrical conductivity.

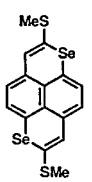

MTDSPY

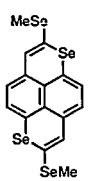

MSDSPY

V-A-2 Crystal Structure of 1,6-Diselenapyrene (DSPY)

Jiro TOYODA, T. OHMAE, and Kazuhiro NAKASUJI

The crystal structure analysis of 1,6-diselenapyrene (DSPY) were performed. The nearly planar molecule of DSPY stacks along the *b* axis. There is an intermolecular Se...Se contact (3.613 Å) shorter than the van der Waals sum. Crystal data for DSPY: $C_{14}H_{18}Se_2$, M=520.11, monoclinic, space group $P2_1/n$, a=12.964, b=4.106, c=10.216 Å, β=94.55°, V=542.1 Å^3, Z=2, Final R=0.0739.

V-A-3 Crystal Structure of 3,9-Dithiapyrene (3,9-DTPR)

Jiro TOYODA and Kazuhiro NAKASUJI

From our interest in exploring high-electrical organic conductors, we have designed and synthesized new sulfur-heterocycles, one of the isomers of DTPY and three of the isomers of DTPR. The crystal structure analysis of 3,9-dithiaperylene (3,9-DTPR) shows that the centrosymmetric and nearly planar molecules stack along the *b* axis to form the columnar structure. The interplanar distance is 3.53 Å. The intermolecular S···S distance is near the sum of van der Waals radii. This contact leads to the molecular arrangement of linear ribbons along the *c* axis. Crystal data for 3,9-DTPR: $C_{18}H_{10}S_2$, M=290.40, monoclinic, space group $P2_1/n$, Crystal dimensions 0.50×0.05×0.01 mm^3, a=15.31(1), b=3.936(2), c=10.885(6) Å, β=109.68(5)°, V=617.6(7) Å, Z=2, Final R=0.086 and R_w=0.080.

V—B New Conjugated Electronic Systems

Design and synthesis of new conjugated electronic systems have been performed as general interests to explore new molecular materials which might have interesting chemical reactivities and physical properties. In this research project, new electronic systems having not only closed shell electronic systems but also open shell electronic systems are searched for. Chemical modifications for known electronic systems are also important. An example is as follows. The stable conjugated neutral radicals have been attracted much attention to explore new materials having potentially interesting solid state properties, for example, single component conductors and magnetically interesting materials. We have utilized odd alternant hydrocarbon,

phenalenyl, as the basic skeleton for neutral radicals, and modified the phenalenyl skeleton by introducing donor and acceptor substituents to suppress the thermodynamic and kinetic instability. Such modification is one of the typical procedure in physical organic chemistry to stabilized unstable electronic systems.

V-B-1 Crystal Structure of 2-Phenyl-3-hydroxyphenalenone

Jiro TOYODA, Kunio HATANAKA, Yasushi MORITA, and Kazuhiro NAKASUJI

3-Hydroxyphenalenone is an important component molecular skeleton for design stable neutral radicals. As a preliminary investigation, the crystal structure analysis of 2-phenyl-3-hydroxyphenalenone were performed. We found that there are hydrogen-bonds even though there exists bulky phenyl group at 2-position. Crystal data: $C_{19}H_{12}O_2$, M_w=272.30, triclinic, space group $P\bar{1}$, a=12.553, b=14.536, c=7.569 Å, α=90.76, β=99.06, γ=109.44°, V=1283.0 Å^3, Z=4, Final R=0.060.

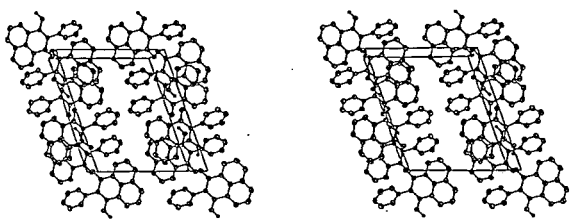

V-B-2 Theoretical Studies of CT Ferromagnets and Ferrimagnets: Metallocenium-TCNE Complexes

Kizashi YAMAGUCHI,[a] Mitsutaka OKUMURA,[a] Takeshi NORO,[a] and Kazuhiro NAKASUJI *([a]Hokkaido Univ.)*

An intermolecular orbital interaction theory has been applied to elucidate the mechanisms of spin alignments in the ferromagnetic or antiferromagnetic metallocenium(M)-TCNE complexes and other CT complexes. It is found that spin polarization and super-exchange interactions play important roles for the ferro- and antiferro-magnetic spin alignments, respectively. Ab initio calculations have been carried out for metal complexes.

V—C New Cooperative Proton-Electron Transfer (PET) Systems

From synthetic chemistry viewpoints, we have started to explore a new type of molecular materials having interesting chemical reactivities and physical properties, while searching for a new concept or a general strategy with interdisciplinary cooperation. Our particular attention in this research project is concentrated on the molecular materials which can exhibit the cooperative interactions between hydrogen bonding and charge transfer in the solid state. A typical example is a phase transition of benzoquinhydrone which can be regarded as a cooperative proton-electron transfer (PET) phenomenon. The final PET state can be characterized as a molecular assembly of *H-bonded neutral radicals.* We are now developing a general strategy to explore new molecular materials based on PET phenomena. A stepwise consideration leads to two reasonable molecular design strategies to realize such cooperative phenomena under milder conditions in the solid state: the exploration of (a) a quinone-hydroquinone pair with a smaller intermolecular CT gap and/or (b) an electronic modification to stabilize H-bonded neutral radicals. We are now improving the molecular level concept, designing, and synthesizing new molecular materials. Our fundamental efforts are concentrated in the exploration of a wide range of hydrogen-bonded charge transfer (HBCT) complexes, which might open a new way toward new molecular materials without restricting to PET systems.

V-C-1 Three Dimensional Molecular Structure of Unsymmetrical Proton-Electron Transfer (PET) System Containing Disufide Bond: 4-Hydroxyphenyldisulfide-Benzoquinone Complex (HPDS-BQ)

Kenichi SUGIURA, Jiro TOYODA, Hiroshi OKAMOTO, Kaoru OKANIWA, Tadaoki MITANI, Atsushi KAWAMOTO,[a] Jiro TANAKA,[a] and Kazuhiro NAKASUJI *([a]Nagoya Univ.)*

[*Angew. Chem. Int. Ed. Engl.*, **31**, 852 (1992)]

In order to develop unsymmetrical PET systems, we synthesized the proton-electron donors, **1-4**, which are composed of two phenol moieties connected by oxygen, sulfur, selenium, or disulfide. Their characteristics are as follows: (i) the exchange reaction can be suppressed by the chalcogen atoms inserted, and (ii) the twisted bond character of the hetero atoms affects the crystal packing. CT complexes of these donors with various quinone type acceptors were prepared. Crystal structure analysis for 1:1 CT complex, **5** (HPDS-BQ) and the spectroscopic data show that this complex is a unique hydrogen-bonded CT complex with a three dimensional molecular architecture. The data of the bond lengths and the IR stretching frequencies reflect the nonionic nature of HPDS-BQ. The CT transition between the hydroxyphenyl moiety and BQ appeared at 2.28 eV. HPDS-BQ displays a pressure dependent IR spectrum.

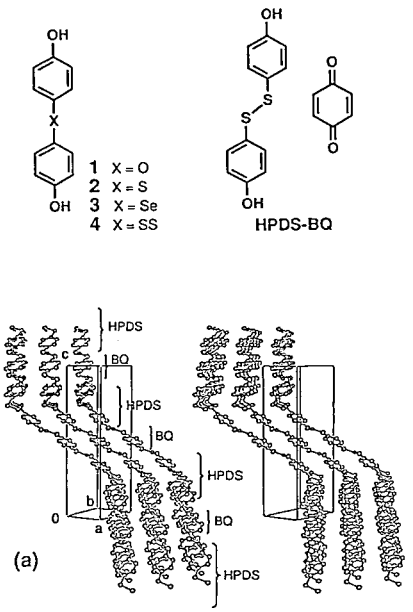

V-C-2 Crystal Structure of Hydrogen-Bonded Charge Transfer Complex Containing Water Molecule: [Bis(4-hydroxyphenylthio)-1,5-naphthalene]-Chloranil-H_2O

Kenichi SUGIURA, Jiro TOYODA, Kaoru OKANIWA, Tadaoki MITANI, and Kazuhiro NAKASUJI

One of the common features in the crystal structures of the PET systems is the existence of hydrogen bonding (H-bonding) chains and charge transfer (CT) interaction between the proton-electron donor and acceptor components. As component molecules for the additional examples of unsymmetrical PET systems, new proton-electron donors, **1-3**, were synthesized. Bis(4-hydroxylphenylthio)-1,5-naphthalene (**2**, HPTN) produced CT complex, HPTN-CHL-H_2O. The crystal structure analysis indicates the presence of alternated DA columns of the naphthalene moiety and chloranil and the hydrogen bonding ribbon between hydroxyphenyl moiety and water molecules. There found hydrogen-bonding between the hydroxyphenyl moieties and water molecule but no direct hydrogen-bonding between the donor and the acceptor.

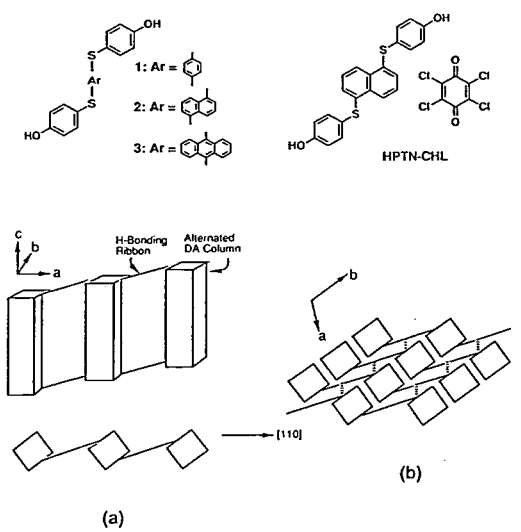

V-C-3 Synthesis and Properties of Benzoquinhydrones with Donor and Acceptor Substituents

Kenichi SUGIURA, Jiro TOYODA, and Kazuhiro NAKASUJI

The 86 derivatives of hydroquinones and quinones were prepared to investigate the basic physical properties concerning with the hydrogen-bonding and charge transfer (CT) interaction in benzoquinhydrone and their components. We found that the energy gaps between the HOMO and LUMO energies of the hydroquinones and quinones, respectively, are nearly constant in spite of the difference of the number and the kind of the substituents. A large number of the complexes with mono-, bis-, and tris-substituted derivatives were obtained. The investigation of O-H and C=O stretching frequencies indicated the presence of hydrogen bonding in the quinhydrones. The CT transition energies were found at around 1.9—2.3 eV. All these results indicate that the benzoquinhydones with donor and acceptor substituents are classified into the neutral CT complexes. Interestingly, benzoquinhydrones with methylchalcogeno groups possessed the lower CT transition energies, which might important for design quinhydrone with a smaller CT gap.

V-C-4 The Extended Conjugated Quinhydrones: Biphenoquinhydrones and Stilbenquinhydrones

Kenichi SUGIURA, Jiro TOYODA, and Kazuhiro NAKASUJI

In order to decrease the charge transfer gap in PET systems, we reported the design and synthesis of 1,5-dihalo-2,6-naphthoquinhydrones as the first examples of the extended quinhydrones. In this report, we synthesized bipheno- and stilben-quinhydrones. The extension of electronic system causes the lower frequency shift of O-H and C=O stretching frequencies for the hydroquinones and the quinones, respectively. The extension also causes the increase of HOMO energy level of the hydroquinones and the decrease of LUMO energy level of the quinones. Thus, the donor and acceptor abilities of proton and electron for the extended hydroquinones and quinones, respectively, are found to be enhanced. The extended conjugated quinhydrones were obtained by mixing the solution of the hydroquinone and quinone components as 1:1 complexes. The IR and electronic spectra showed the stronger H-bonding character and smaller CT gaps in the extended systems.

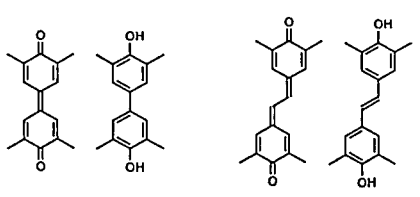

V-C-5 Crystal Structure of Nickel Complex with Modified Diaminoglyoxime Ligand

Jiro TOYODA, Tetsuji ITOH, Makoto TADOKORO, and Kazuhiro NAKASUJI

The fundamental importance of PET systems can be expanded to the electronic systems containing transition metals. We designed new such compound based on the bis(diaminoglyoxime)M skeleton. One of the modified bis(diaminoglyoxime)Ni complex crystallized. Crystal data: This complex contains no other molecules like solvent, which is fundamentally different from the case of the bis(diaminoglyoxime)M complexes.

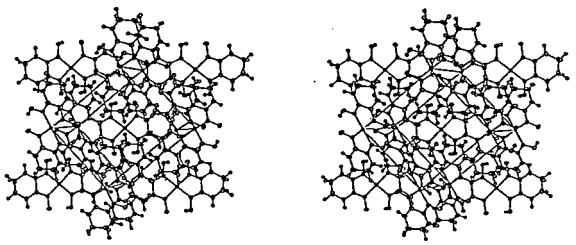

V-C-6 Synthesis and Physical Properties of Alkylthiobenzoquinhydrone

Kenichi SUGIURA, Jiro TOYODA, and Kazuhiro NAKASUJI

Long alkyl substituents as a side chain are known to exhibit a function of intermolecular interactions, molecular fastener effect, which can reduce the interplanar distance between the adjacent molecular skeletons. Since this effect can be considered a similar one to the addition of pressure on the materials, we investigated the effect of long alkylthio group to PET systems. We prepared the benzoquinhydrones with long alkylthio substituents, **1** (n=1–8). In the IR spectra, the frequencies of OH and C=O stretching vibration of the quinone skeleton shift to lower energy and those of C=C and C-C stretching vibration of the hydroquinone skeleton shift to higher energy with increasing the number of carbon atoms, n. Therefore, the benzoquinhydrones with long alkylthio groups showed a similar spectroscopic behavior to the addition of pressure with increasing the number, n.

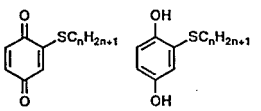

1 (n = 1 - 18)

V—D Transition Metal Oxide Clusters

Fairly many cubane-type oxide including hydroxide and alkoxide clusters have been synthesized so far, but in many cases the formation reactions were under thermodynamic control and the cluster framework could not have been predicted from reaction conditions. Serendipity provides a helping hand for the cubane-type cluster synthesis. It is important to overcome this lack of control and develop methodology for the rational synthesis of the clusters. The synthetic chemistry of metal oxide cubane-type cluster is in its infancy, but is developing gradually and showing potential importance for inorganic surface field. We have studied reactivity of the triple cubane-type cluster $[RhCp^*MoO_4]_4$ ($Cp^*=\eta^5$-C_5Me_5) toward small molecules.

V-D-1 Trishomocubane-Type Methoxide Cluster $[(RhCp^*)_2Mo_3O_9(OMe)_4]$ as a Potential Model for Partial Oxidation MeOH on MoO_3

Kiyoshi ISOBE, Yoshiki OZAWA *(IMS and Himeji Institute of Technology)*, **and Youngkyu DO** *(KAIST and IMS)*

The trishomocubane-type cluster $[(RhCp^*)_2Mo_3O_9(OMe)_4]$ (**1**) has been obtained from reaction of $[(RhCp^*)_4Mo_4O_{16}]$ with MeOH in the presence of p-hydroquinone.[1] The solid state of cluster **1** is quite stable in air at room temperature, but its integrity does not remain intact upon dissolution in CH_2Cl_2 and the quadruple cubane-type cluster comes down from the system. In addition, methanol and small amounts of formaldehyde are formed during the conversion of **1** at room temperature. We have also studied the behavior of **1** on heating. **1** was readily pyrolyzed; a typical product composition (pyrolysis at 386°C) methanol (56%), methyl formate (28%) dimethyl ether (12%), and acetone (4%). At 160°C the gas composition was similar to that at 386°C except that less methyl formate, less dimethyl ether, and more acetone were formed. Aromatic compounds were detected at higher temperature.

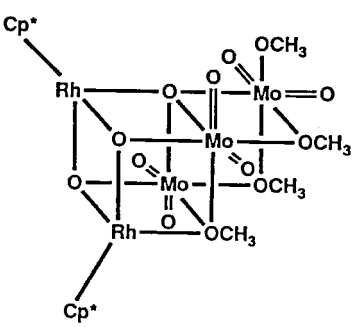

1

Klemperer, Goddard, and Edwards have proposed the different mechanisms of the oxidation of methanol on MoO_3, but they have suggested the same key species with the terminal Mo-OMe group. Inspection of the structure of **1** reveals that the overall methoxy conformation leads to close proximities (3.05–3.12 Å) between doubly bridged methoxy carbons and terminal Mo=O oxygens, indicating a possible short C-H···O intramolecular contact which is a trigger of the proton transfer to form CH_2O in CH_2Cl_2. Similar close proximities (3.13–3.21 Å) are also found between one of doubly bridging methoxy oxygen and methoxy carbon of triply bridged suggesting a non-redox methyl transfer between methoxy groups involved in the above pyrolysis.

Scheme I

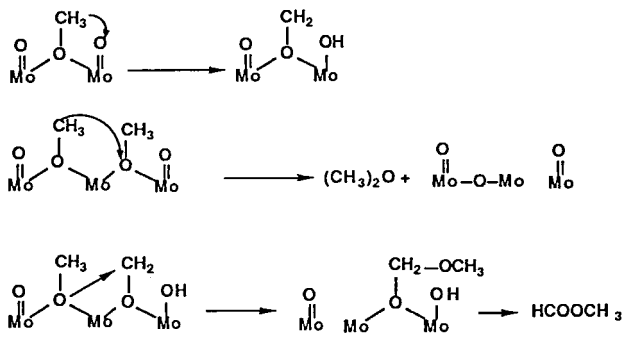

Thus the results of the pyrolysis and the structural data of **1** described above lend support to the mechanism with the bridging methoxy group as the key species for the formation of formaldehyde, dimethyl ether, and methyl formate (Scheme I). The formation mechanism of acetone is very interesting, but remain to be established.

Reference

1) Y. Do, X.-Z. You, C. Zhang, Y. Ozawa, and K. Isobe, *J. Am. Chem. Soc.*, **113**, 5892 (1991).

V-D-2 New Type Octamolybdate $[(RhCp^*)_2(SCH_3)_3]_4[Mo_8O_{26}]$ and Hexamolybdate $[(RhCp^*)_2(SCH_3)_3]_2[Mo_6O_{19}]$

Xi RIMO *(Grad. Univ. for Adv. Studies and IMS)*, **Bateer WANG** *(IMS and Inner Mongolia Norm. Univ.)*, **Koshiro TORIUMI** *(Himeji Institute of Technology)*, **Yoshiki OZAWA** *(IMS and Himeji Institute of Technology)*, **Takanori NISHIOKA, and Kiyoshi ISOBE**

Recently our group has synthesized some integrated-cubane type clusters. During the study of reaction of triple cubane-type cluster $[RhCp^*MoO_4]_4$ with CH_3SH, we discovered two poly oxometallates: an octamolybdate, $[(RhCp^*)_2(SCH_3)_3]_4[Mo_8O_{26}]$ (**1**) and a hexamolybdate $[(RhCp^*)_2(SCH_3)_3]_2[Mo_6O_{19}]$ (**2**). The octamolybdate has a new and intermediate structure among the other three well known octamolybdates α-, β-, and γ-$Mo_8O_{26}^{4-}$. The structure of the new octamer supports one of the proposed mechanisms for their interconversion.

The structures of the anion of **1** and the salt of **2** were shown in Figure 1 and Figure 2, respectively. The anion in complex **1** has an intermediate structure among α-, β-, and γ-$Mo_8O_{26}^{4-}$. In our new anionic octamer there are six molybdenum atoms linked by oxygen atoms to form a ring, but there are two sorts of molybdenum atoms among six ring metal atoms: four-coordinated and six-coordinated molybdenums. This structure consists of cubic closed packed (ccp) oxygens with molybdenums occupying tetrahedral and octahedral holes.

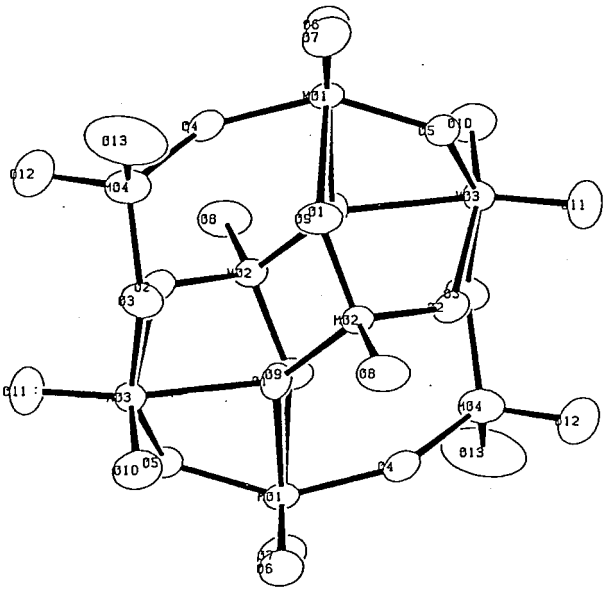

Figure 1. Perspective view of a new $Mo_8O_{26}^{4-}$ anion in **1**.

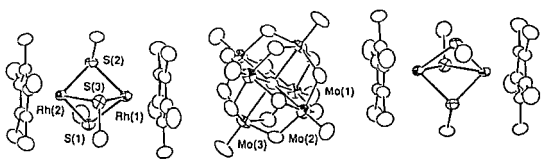

Figure 2. Perspective view of **2**.

V-D-3 Linear-type Tetranuclear Rh_2Mo_2 Complex $[(RhCp^*)_2Mo_2O_5(SCH_3)_6]$ Obtained from Reaction of Triple Cubane-type Cluster $[RhCp^*MoO_4]_4$ with CH_3SH

Xi RIMO *(Grad. Univ. for Adv. Studies and IMS)*, **Bateer WANG** *(IMS and Inner Mongolia Norm. Univ.)*, **Yoshiki OZAWA** *(IMS and Himeji Institute of Technology)*, **and Kiyoshi ISOBE**

Study of reactions and bonding of sulfur-containing complexes is a field of growing interest due to their importance in both the fundamental and applied chemistry. We previously studied the reaction of the triple cubane-type cluster $[RhCp^*MoO_4]_4$[1] with CH_3OH: the structure of the triple cubane framework was broken partly and we obtained an incomplete double cubane-type cluster $[(RhCp^*)_2Mo_3O_9(OMe)_4]$[2]. Having noted that CH_3SH is more reactive than CH_3OH, we have been prompted to investigate the reactivity of CH_3SH toward $[RhCp^*MoO_4]_4$. Consequently, the triple cubane framework was broken thoroughly and a sulfur-containing $[(RhCp^*)_2Mo_2O_5(SCH_3)_6]$ complex (**1**) was obtained.

The reactions may proceed as follows:

$$[RhCp^*MoO_4]_4 \cdot 2H_2O + 12CH_3SH \rightarrow 2[(RhCp^*)_2Mo_2O_5(SCH_3)_6] + 8H_2O \quad <1>$$

The structures of **1** is shown in Figure 1. Each molybdenum atom in the molecule forms a distorted octahedron by binding to two terminal oxygen atoms, one bridging oxygen atom, and three SCH_3 ligands. The Mo-S bond length which is trans to terminal oxygen is significantly longer than

other ones. The bond distance of Mo-Mo is 3.765(3) Å, which indicates no interaction between two molybdenum atoms. Each sulfur atom of SCH_3 ligands as a bridge to connect the two different metals-Mo and Rh. In addition the lone-pair electrons and methyl groups are oriented to certain directions. The complex is racemic in the crystals. The ^1H NMR signals of SCH_3in **1** are broad even at room temperature, but they become sharp at low temperatures. This is due to fluxionality of the SCH_3 ligands. Complex **1** shows two series of signals in its ^1H NMR and ^{13}C NMR spectra. This can be attributed to the existence of another isomer in solution.

References

1) Y. Hayashi, K. Toriumi, and K. Isobe, *J. Am. Chem. Soc.*, **110**, 3666 (1988).
2) Y. Do, X.-Z. You, C. Zhang, Y. Ozawa, and K. Isobe, *J. Am. Chem. Soc.*, **113**, 5892 (1991).

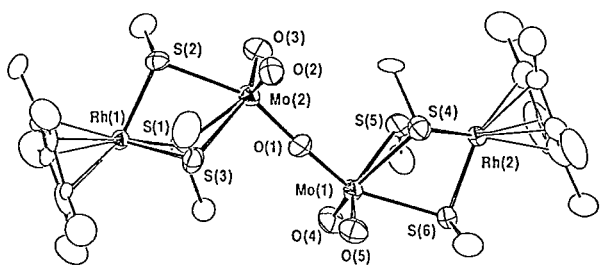

Figure 1. Perspective view of $[(RhCp^*)_2Mo_2O_5(SCH_3)_6]$ with selected interatomic distances (Å) and angles (°): Rh(1)···Mo(2) 3.520(3), Mo(1)···Mo(2) 3.765(3), Rh(2)-S(4) 2.362(6), Mo(1)-S(4) 2.720(7), Mo(1)-S(6) 2.553(6), Mo(1)-O(1) 1.86(1), Mo(1)-O(4) 1.71(2), Mo(1)-O(1)-Mo(2) 175.

V-D-4 Double Oxygen Bridge Tetranuclear Rh_2Mo_2 Complex $[(RhCp^*)_2Mo_2O_4(SCH_3)_6]$

Xi RIMO *(Grad. Univ. for Adv. Studies and IMS)*, **Bateer WANG** *(IMS and Inner Mongolia Norm. Univ.)*, **Yoshiki OZAWA** *(IMS and Himeji Institute of Technology)*, **and Kiyoshi ISOBE**

Reaction of the triple cubane-type cluster $[RhCp^*MoO_4]_4$ with CH_3SH gave $[(RhCp^*)_2Mo_2O_5(SCH_3)_6]$ (see V-D-3) and $[(RhCp^*)_2Mo_2O_4(SCH_3)_6]$ (**1**). Here we describe complex **1** which has the formal oxidation state of +5 in the molybdenum atom and the Mo-Mo single bond. The CH_3S ligand bridges between Mo^V and Rh^{III}.

A solution of $[RhCp^*MoO_4]_4 \cdot 2H_2O$ (0.35 g, 0.21 mmol) in CH_2Cl_2 (15 cm^3) was added to a solution of CH_3SH (3.0 cm^3, 15 mmol (about 30% in CH_3OH)) in CH_2Cl_2 (10 cm^3) at room temperature. After stirring for 30 min. the solvent was removed to give a mixture of orange powder which was separated by using a column of silica gel 60 and CH_2Cl_2:CH_3COCH_3=15:1 (by volume) as an eluent. The second fraction gave red solid **1** in a 9.2% yield (40 mg). **1** was recrystallized from CH_3CN and CH_2Cl_2 at room temperature.

The reaction may proceed as follows:

$$[RhCp^*MoO_4]_4 \cdot 2H_2O + 16CH_3SH \rightarrow 2[(RhCp^*)_2Mo_2O_4(SCH_3)_6] + 2CH_3SSCH_3 + 10H_2O$$

The structures of **1** is shown in Figure 1. The crystals also contain the racemic isomers. The short distance of Mo-Mo in **1** [2.564(1) Å] suggests the existence of single bond between two molybdenum atoms. The sharp NMR signals also provide evidence for the diamagnetic nature in **1**. The CH_3S ligands in **1** acts as a bridge to connect the two different metals-Mo and Rh. Three CH_3S ligands in the $RhCp^*(\mu\text{-}SCH_3)_3$ Mo moiety are chemically nonequivalent one another and show three signals in both ^1H and ^{13}C NMR spectra.

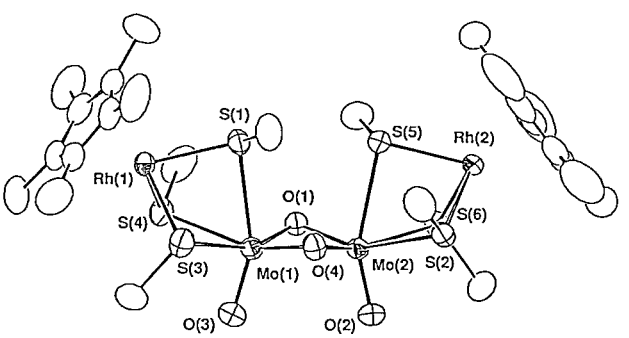

Figure 1. Perspective view of $[(RhCp^*)_2Mo_2O_4(SCH_3)_6]$ with selected interatomic distances (Å): Rh(1)···Mo(2) 3.466(1), Mo(1)-Mo(2) 2.564(1), Rh(1)-S(1) 2.351(2), Mo(1)-S(1) 2.736(2), Mo(1)-S(3) 2.583(2), Mo(1)-O(1) 1.951(5), Mo(1)-O(4) 1.918(2).

V—E Transition Metal Sulfide Compounds

The study of the reactions and bonding of sulfur-containing transition metal compounds is a field of wide importance and growing interest. The functionality of the M-S bond plays important roles in biological systems, in industrial hydrotreating catalysis, and in mineralogical processes. We have continued to elucidate the M-S bond character and to compare its chemistry with that of the M-O bond.

V-E-1 Novel Trinuclear μ-Methylene Rhodium Complex with Capping Sulfur Ligand: $[(RhCp^*)_3(\mu_2\text{-}CH_2)(\mu_3\text{-}S)](BF_4)_2$

Amelio VAZQUEZ DE MIGUEL *(University of Alcala of Henares and IMS)*, **Yoshiki OZAWA** *(IMS and Himeji Institute of Technology)*, **and Kiyoshi ISOBE**

Although air oxidation of $[Rh_2Cp^*_2(\mu_2\text{-}CH_2)_2(\mu_2\text{-}SH)]BF_4$ with the bridging SH ligand takes place to give the tetranuclear complex, $[[Rh_2Cp^*_2(\mu_2\text{-}CH_2)_2]_2(\mu_2\text{-}S_2)_2](BF_4)_2$, that of *trans*-$[Rh_2Cp^*_2(\mu_2\text{-}CH_2)_2(SH)_2]$ with the terminal SH ligand does not proceed. We report oxidation of *trans*-$[Rh_2Cp^*_2(\mu_2\text{-}CH_2)_2(SH)_2]$ with $AgBF_4$ and characterization of a product, $[(RhCp^*)_3(\mu_2\text{-}CH_2)(\mu_3\text{-}S)](BF_4)_2$ (**1**), which has a novel trinuclear rhodium framework.

trans-$[Rh_2Cp^*_2(\mu_2\text{-}CH_2)_2(SH)_2]$ reacts with $AgBF_4$ in THF to give **1** through an intermediate which shows two signals both in the μ-CH_2 (δ 8.08, 8.44) and the CH_3 of

Cp* (δ 2.01, 1.98) regions.

Recrystallization of **1** from CH_2Cl_2 afforded black plate crystals suitable for single crystal X-ray analysis. Crystal data of **1** are as follows: hexagonal, space group $P6_3$, a=11.430(2), c=15.743(2) Å, Z=2, Dx=1.746 g cm^{-3}, Dm=1.750 g cm^{-3}. Intensity data were collected of a Rigaku AFC-5 diffractometer with graphite-monochromated MoKα radiation in the $2\theta < 60°$ range. The structure was solved and refined by a block-diagonal least-squares technique. The current R value is 0.037 for 1054 independent absorption-corrected reflections. The cationic part of **1** has a triangular framework with the Rh-Rh single bond (2.824(1) Å) as shown in Figure 1. The S atom bridges between three Rh atoms with 2.239(3) Å of the Rh-S bond, and the μ-CH_2 ligand bridges one of the Rh-Rh bonds.

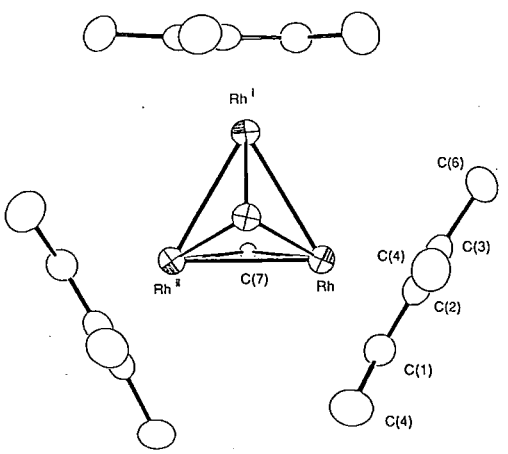

Figure 1. Perspective view of $[(RhCp^*)_3(\mu_2\text{-}CH_2)(\mu_3\text{-}S)]^{2+}$ with selected interatomic distances (Å) and angles (°): Rh-Rh^{i} 2.824(1), Rh-S 2.239(3), Rh-C(7) 2.20(2), Rh^{ii}-C(7) 2.17(2), Rh^{i}-C(7) 2.81(2), Rh-S-Rh^{i} 78.2(1), Rh-C(7)-Rh^{i} 80.6(6).

V-E-2 Synthesis, Structure, and Properties of Oxidized Hexamolybdenum Clusters $[(Mo_6X_7Y)X'_6]^{2-}$ (X=X'=Cl, Br; Y=S, Se)

Masahiro EBIHARA *(Gifu Univ.)*, **Kiyoshi ISOBE, Yoichi SASAKI** *(Tohoku Univ.)*, **and Kazuo SAITO** *(IMS and Graduate School, International Christian Univ.)*

[*Inorg. Chem.*, **31**, 1644 (1992)]

The synthesis, structure, and properties of $Mo_6(13+)$ species, which are obtained by the oxidation of $Mo_6(12+)$ $[(Mo_6X_7Y)X'_6]^{3-}$ (X=X'=Cl, Br; Y=S, Se), are reported. $(n\text{-}Bu_4N)_2[(Mo_6Cl_7S)Cl_6]$ crystallizes in the monoclinic space group $P21/n$ with a=18.542(2) Å, b=11.701(2) Å, c=12.806(2) Å, β=90.21 (1)°, V=2778.5(7) Å^3, and Z=2. $(n\text{-}Bu_4N)_2[(Mo_6Cl_7Se)Cl_6]$ crystallizes in the monoclinic space group $P21/n$ with a=18.571(2) Å, b=11.685(1) Å, c=12.845(1) Å, β=90.12 (1)°, V=2787.1(5) Å^3, and Z=2. $(n\text{-}Bu_4N)_2[(Mo_6Br_7Se)Cl_6]$ also crystallizes in the monoclinic space group $P21/n$ with a=18.740(2) Å, b=11.647(2) Å, c=13.030(2) Å, β=90.05 (1)°, V=2844.0(7) Å^3, and Z=2. The $Mo_6(12+)$ species $(n\text{-}Et_4N)_3[(Mo_6Cl_7Se)Cl_6]$ crystallizes in the tetragonal space group $P4_2/mnm$ with a=11.968(1) Å, c=16.804(2) Å, V=2406.8(4) Å^3, and Z=2. The Mo-Mo distances of the $Mo_6(13+)$ clusters (2.626(3) Å in $[(Mo_6Cl_7S)Cl_6]^{2-}$, 2.628(3) Å in $[(Mo_6Cl_7Se)Cl_6]^{2-}$, 2.653(3) Å in $[(Mo_6Br_7S)Cl_6]^{2-}$) are slightly longer than those of the corresponding $Mo_6(12+)$ species. Absorption peak positions in the 1800-nm (5320–6060 cm^{-1}) and 900-nm regions (10500–11200 cm^{-1}) are independent of the capping and terminal ligands, but those in the range 480–650 nm (15400–20400 cm^{-1}) depend on the ligand. Their ESR spectra at 77 K are axially symmetric ($g_\perp$=2.12–2.15, $g_\parallel$=2.05–2.07). The electronic structure is discussed on the basis of these data.

V—F Organic Synthesis with Lanthanoids

The fifteen elements from lanthanum to lutetium constitute a unique family of closely related elements. Recent progress on the utilization of such lanthanoids in organic synthesis has aroused a growing interest among organic chemists. For several years, we have also been working in this field by using samarium(II) reagent and developed a number of new synthetic reactions, in which a unique property of samarium(II) iodide, such as high oxidation potential, large ionic radius, high oxophilicity, etc., was found to play an important role. One of our current interest is the difference of reactivity which may be obtained by changing the central metal of a series of lanthanoid reagents in promoting organic reactions. In this project, we have studied on the relative catalytic activity of a variety of lanthanoid(III) compounds in some organic transformations.

V-F-1 Studies on the Catalytic Activity of Lanthanoids(III) Salts in the Glycosylation of Methoxyacetyl Glucoside Derivative

Junji INANAGA, Yasuo YOKOYAMA, and Takeshi HANAMOTO

A series of lanthanoid(III) chlorides and triflates were prepared and examined as a new catalyst for the glycosylation of methoxyacetyl 2,3,4,6-tetra-*O*-benzyl-D-glucoside. As shown in the graph, the triflates of some heavy lanthanides were found to have high catalytic activities. To our surprise, however, there seems to be no correlation between the catalytic activity and either the ionic radius or the oxophilicity of lanthanides. α-Methoxyacetyl function is essential for the lanthanide-involved chelate formation which is the activation step of the substrate: The corresponding acetyl glycoside did not react at all under the same conditions. When ytterbium(III) triflate was employed as a catalyst, the amount of it could be reduced to 0.005 equivalent to the glycosyl donor without considerable decrease of yield.

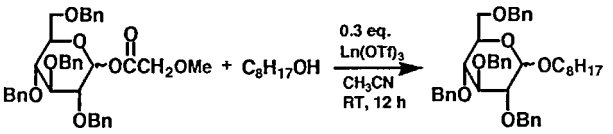

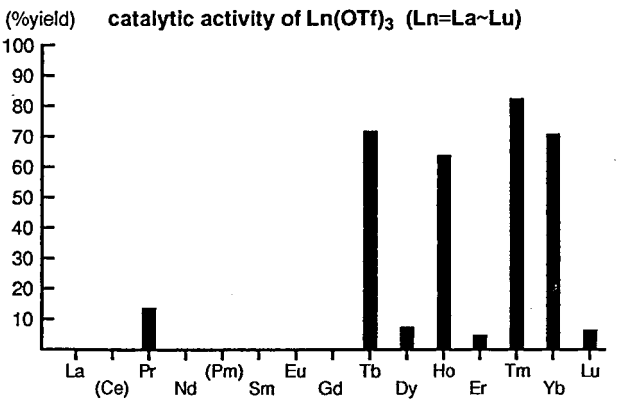

V-F-2 A Novel Catalytic Glycosylation of 1-Hydroxyglucose Derivatives with the Aid of Methoxyacetic Acid and Ytterbium(III) Triflate

Junji INANAGA, Yasuo YOKOYAMA, and Takeshi HANAMOTO

Glycosylation of 1-hydroxyglucose derivatives with alcohols is promoted by a catalytic amount of methoxyacetic acid and ytterbium(III) triflate. The reaction seems to involve the following three processes: (i) the esterification of methoxyacetic acid with an alcohol, (ii) the formation of the methoxyacetyl glycoside intermediate via transesterification, and (iii) the glycosylation accompanied by the liberation of methoxyacetic acid to be recycled as a catalyst. The above three reactions take place in one-pot and ytterbium triflate may work as a catalyst in each step. Although the lanthanide(III) catalyst works as a Lewis acid, water, which is produced as the reaction proceeds, does not deactivate the catalyst seriously thus permitting the non-stoichiometric use of the catalyst (0.1 equiv.). The use of molecular sieve 4A as a drying agent largely accelerates the reaction.

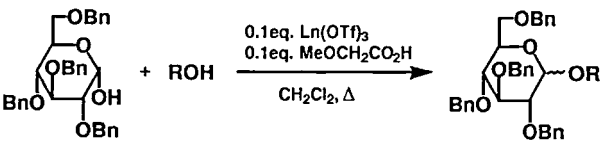

V-F-3 Methoxyacetate as a New Protective Group for the Hydroxy Functionality: Easy Formation and Selective Cleavage Catalyzed by Ytterbium(III) Triflate

Junji INANAGA, Yasuo YOKOYAMA, and Takeshi HANAMOTO

When a chemical reaction is to be carried out selectively at one reactive site in a multifunctional compound, other reactive sites must be temporarily blocked. For this purpose, esters have been widely used as useful protective groups for the hydroxy functionality. They can be cleaved at an appropriate stage usually by hydrolysis under basic conditions. As one of the ester-type protective gorups, methoxyacetate was newly introduced: The ester is easily prepared and selectively cleaved in the presence of another ester function in the molecule by the pivotal use of a lanthanide Lewis acid catalyst, ytterbium(III) triflate.

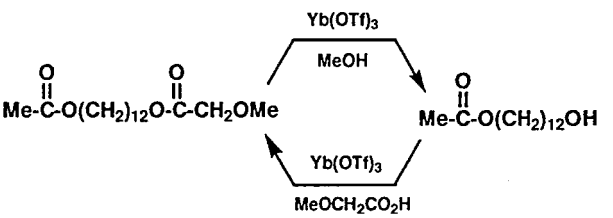

V—G Development of New Organic Reactions Based on the Design of Reaction Intermediates

The development of mild and efficient synthetic methods is a continuous scientific challenge offered by complex and unstable organic molecules. In this project, some novel organic transformations which are designed on the basis of new reaction intermediates have been developed.

V-G-1 Utility of Phosphonium Enolates as Synthetic Intermediates. A Novel Catalytic [3,3] Rearrangement of Allylic Acrylates

Takeshi HANAMOTO, Yoshiyasu BABA, and Junji INANAGA

[*J. Org. Chem.*, in press]

A novel catalytic [3,3] rearrangement of allylic acrylates was developed. The reaction proceeds under mild conditions with 1,8-diazabicyclo[5.4.0]undec-7-ene, chlorotriethylsilane (or chlorotrimethylsilane), and a catalytic amount of tricyclohexylphosphine (5—10 mol%) to give, after work-up, α-methylene-γ,δ-unsaturated carboxylic acids in good yields. The phosphonium ester enolate intermediate is proposed as a new precursor for the rearrangement: Nucleophilic attack of trialkylphosphine to the β-carbon of an allylic acrylate (**1**) followed by silylation of the resulting phosphonium enolate would produce the phosphonium ketene silyl acetal (**A**), which then undergoes a [3,3] sigmatropic rearrangement to give the new intermediate (**B**). The deprotonation of **B** by a base should afford the trialkylsilyl α-methylene-γ,δ-unsaturated carboxylate (**2**) with liberation of the trialkylphosphine to be recycled as a catalyst. The synthetic utility of this process is further demonstrated by converting a rearranged product to the corresponding α-methylene-γ-butyrolactone derivative.

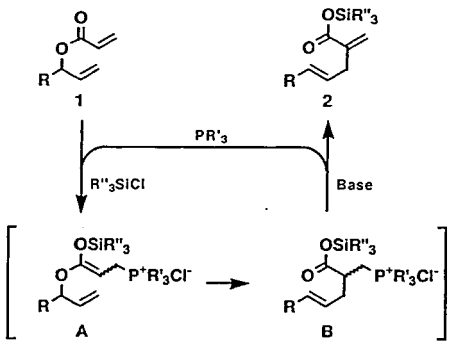

V-G-2 An Easy Access to Erythrose and Threose by a Sequence of Reactions — C1-Alkoxy Radical Fragmentation and Acid-Catalyzed Transacetalization

Junji INANAGA, Yuichi SUGIMOTO, Yasuo YOKOYAMA, and Takeshi HANAMOTO

[*Tetrahedron Lett.*, in press]

C1 carbon extrusion from easily available carbohydrates with desired stereochemistry at appropriate chiral centers may be a logical choice to obtain the corresponding lower carbohydrates which are sometimes expensive or rare in nature. In this approach, we developed a new reaction sequence: (i) the formation and the fragmentation of anomeric alkoxy radicals promoted by (diacetoxyiodo)benzene or lead tetraacetate in the presence of iodine catalyst; (ii) the acid-catalyzed furan ring formation. Thus, erythrose and threose derivatives were easily prepared from arabinose and xylose derivatives, respectively, by utilizing the above methodology.

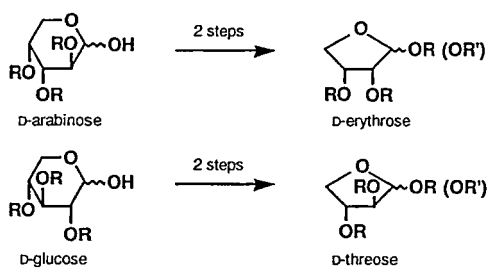

V-G-3 Methoxyacetyl Glycoside as a New Glycosyl Donor for the Zinc(II) Chloride-Promoted Glycosylation

Junji INANAGA, Yasuo YOKOYAMA, and Takeshi HANAMOTO

Methoxyacetyl glycosides, which are readily obtainable and storable at room temperature, are easily activated by zinc(II) chloride through five-membered chelate formation and react with a variety of nucleophiles such as primary, secondary, and tertiary alcohols, phenols, and thiols to give the corresponding glycosides in good yields.

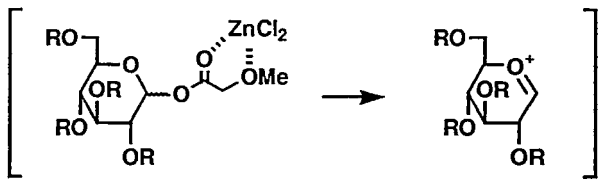

V-G-4 Heptadecafluorooctanesulfonic Acid-Catalyzed Stereoselective Glycosylation of Acyl Glycosides

Junji INANAGA, Yasuo YOKOYAMA, and Takeshi HANAMOTO

A new and efficient perfluorooctanesulfonic acid-catalyzed glycosylation has been developed. When the reactions were carried out by using acyl glycosides and either alcohols or thiols in acetonitrile, the corresponding β-glycosides were produced stereoselectively. On the other hand, α-glycosides were obtained predominantly by changing the solvent for ether.

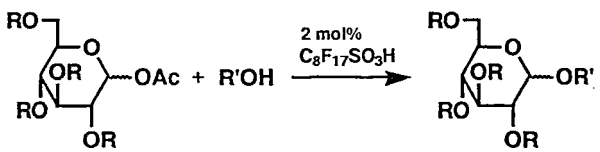

V—H Synthesis and Conformational Study of Multibridged [3n]Cyclophanes

[3$_6$](1,2,3,4,5,6)Cyclophane **1** is one of the final target molecules in the field of [3.3]cyclophane chemistry. This compound is a promising precursor to propella[3$_6$]prismane **2** since photochemical isomerization of **1** to **2** has been predicted based on molecular mechanics calculations[1] (Figure 1). Hexaprismane **3** is a theoretically and structurally intriguing compound, but its synthesis has not been accomplished yet. Therefore, if we succeeded in the synthesis of **1**, we would have a good chance of obtaining the first hexaprismane derivative **2**. The stereochemical features of **1** are also fascinating; six trimethylene chains are expected to undergo correlated inversion in solution (Figure 2).

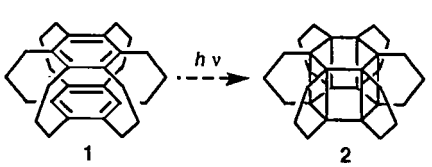

Figure 1. Predicted photochemical isomerization of **1** to hexaprismane derivative **2**.

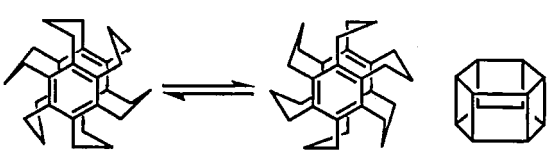

Figure 2. Predicted most stable conformation and correlated inversion process of the six trimethylene bridges of **1**.

V-H-1 Synthesis of [3$_4$](1,2,3,5)- and (1,2,4,5)Cyclophanes

Teruo SHINMYOZU, Shirou KUSUMOTO, Sachiyo NOMURA, Haruo KAWASE,* and Takahiko INAZU* *(*Kyushu Univ.)*

[*Chem. Ber.*, in press]

As a strategy for the synthesis of **1**, we chose the stepwise approach: stepwise introduction of additional trimethylene bridges to [3$_3$](1,3,5)cyclophane **6** by way of four- and five-bridged cyclophanes. In our efforts along these lines, we have synthesized the first tetra-bridged [3.3]cyclophanes, [3$_4$](1,2,3,5)- and (1,2,4,5)cyclophanes (**4** and **5**).

Taking advantage of the directing effect of the acetyl group of **7**, we were able to introduce a chloromethyl group in a pseudogeminal position (**8**). For the coupling reaction, we found that an acid-catalyzed reaction effected the cyclization (30% HBr in AcOH) to yield the desired ketone **9**. The Wolff-Kishner reduction of **9** afforded [3$_4$]cyclophane **4** (Scheme 1).

A similar directing effect of a methoxycarbonyl group of **10** led to the formation of pseudogeminally substituted bis(chloromethyl) compound **11**. Conversion of the chlorine atoms to the acetoxy groups, followed by $LiAlH_4$ reduction and bromination of the resultant tetra-ol with PBr_3 in $CHCl_3$ afforded bromide **12**. One-step TosMIC coupling reaction of **12** and subsequent acid hydrolysis afforded diketone **13**, which was converted into **5** by the Wolf-Kishner reduction (Scheme 2).

The electronic and charge-transfer spectra of **4**, **5**, and **6** in CH_2Cl_2 indicated that the π–π interaction was considerably dependent upon the number and substitution pattern of the bridges, and **5** showed the strongest CT interaction with TCNE among the [m.n]cyclophanes and multibridged cyclophanes.

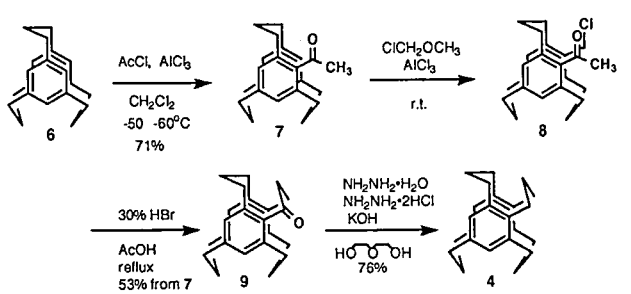

Scheme 1. Synthetic route to [3$_4$](1,2,4,5)cyclophane **4**.

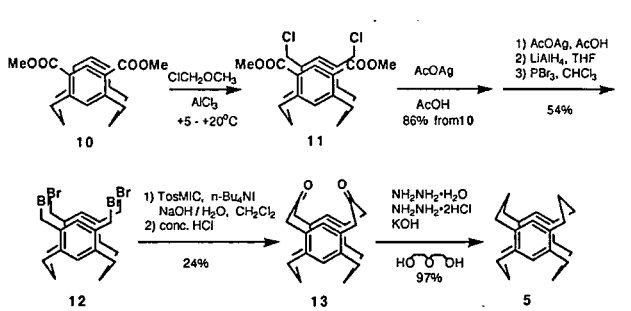

Scheme 2. Synthetic route to [3$_4$](1,2,4,5)cyclophane **5**.

V-H-2 Synthesis and Conformational Study of [3$_5$](1,2,3,4,5)- and [3$_6$](1,2,3,4,5,6)Cyclophanes

Teruo SHINMYOZU, Shirou KUSUMOTO, Yoichi SAKAMOTO,* and Takahiko INAZU* *(*Kyushu Univ.)*

The acid-catalyzed cyclization reaction described above is an especially efficient method for introducing a trimethylene bridge in a very crowded position since only the least bulky proton is needed for the reaction. By a similar series of reactions, we prepared [3$_4$]cyclophane **14** in which an acetyl and a chloromethyl groups were pseudogeminally substituted. The acid-catalyzed cyclization reaction was successfully applied to **14**, and the resulting ketone **15** was converted into **6** by the Wolff-Kishner reduction (Scheme 3). Introduction of the final trimethylene bridge to **6** and the conformational and photochemical studies of these compounds are now in progress.

Reference

1) E. Ōsawa, *Kagaku*, **44**, 200–201 (1989).

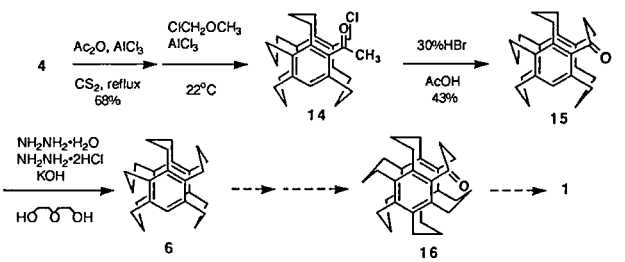

Scheme 3. Synthetic route to [3$_5$](1,2,3,4,5)- and [3$_6$](1,2,3,4,5,6)cyclophanes **6** and **1**.

V-H-3 A MNDO-PM3 Study on the Conformation of Multibridged [3$_n$]Cyclophanes

Teruo SHINMYOZU, Jerzy M. RUDZIŃSKI,* and Mayumi MATSUSHITA* *(*Fujitsu Kyushu System Engineering)*

The conformational potential energy surfaces of multibridged [3$_n$]cyclophanes (n=2–6) have been studied by the semi-empirical molecular orbital method (MNDO-PM3). The relative thermodynamic stabilities of possible conformers, their equilibrium populations, and the barriers for conformational interconversions were estimated, and the result was compared with experimental data. Generally a very good agreement was observed between calculated and observed structures and energetics.

V-H-4 A Conformational Study of [3.3]Metacyclophanes through Variable Temperature ^{1}H NMR and Optical Rotation

Katsuya SAKO,[a] Teruo SHINMYOZU, Hiroyuki TAKEMURA,[b] Masahiko SUENAGA,[b] and Takahiko INAZU[b] *([a]Nagoya Inst. Tech., [b]Kyushu Univ.)*

[*J. Org. Chem.*, in press]

Conformational behavior of 2,2,11,11-tetradeuterio-[3.3]metacyclophanes (**1-d$_4$**, **2-d$_4$**) has been studied by a variable temperature (VT) ^{1}H NMR method. In order to

simplify the interpretation of the ^{1}H NMR spectrum, four deuteriums were introduced at C-2 and C-11 positions of the trimethylene bridges of [3.3]metacyclophanes by reductive desulfurization of 2,11-bis(1,4-dithiabutane-1,4-diyl)-[3.3]metacyclophanes (**4**,**5**) with tri-*n*-butyltin deuteride. Our previous conformational study of tetradeuterio-1,4-dioxa[4.3.3]cyclophane (**3-d$_4$**) revealed that the temperature-dependent phenomenon in the ^{1}H NMR spectrum of **1** was ascribed to the inversion the trimethylene bridges (Figure 1). The work also suggested the presence of benzene ring inversion. To confirm this, optically active [3.3]metacyclophane chromium tricarbonyl complexes (−)- and (+)-**6** were prepared by means of the HPLC separation of racemic complex (±)-**6** using a chiral stationary phase. Racemization occurred when (−)- and (+)-**6** were decomplexed at 20°C. This result as well as the fact that the energy barrier ($\Delta G^{\neq}$) for the benzene ring inversion could not be detected by the VT NMR method indicated that the barrier is much lower than that of timethylene bridge inversion ($\Delta G^{\neq}$=11−12 kcal/mol). The most stable conformer of **1-d$_4$** and **2-d$_4$** is a syn(chair-chair), and the less stable conformer is estimated to be a syn(chair-boat) based on the ^{1}H NMR data.

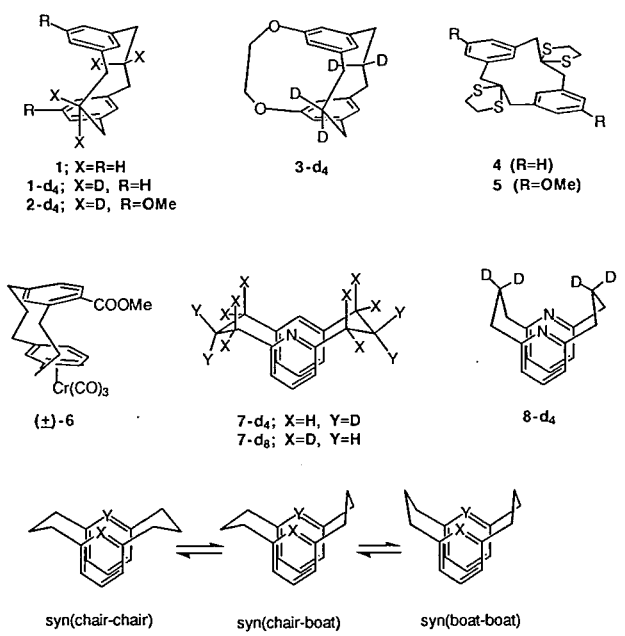

Figure 1. Conformational isomerism of [3.3]metacyclophanes **1** (X=Y=CH), **7**(X=CH, Y=N), and **8** (X=Y=N) *via* chair-boat type inversion of the trimethylene bridges.

V-H-5 A Conformational Study of [3.3](2,6)Pyridinophanes by Dynamic NMR Method

Katsuya SAKO,[a] Teruo SHINMYOZU, Hiroyuki TAKEMURA,[b] Masahiko SUENAGA,[b] and Takahiko INAZU[b]
([a]Nagoya Inst. Tech., [b]Kyushu Univ.)

[*J. Org. Chem.*, in press]

As an extension of the conformational study of [3.3]-metacyclophanes, variable temperature (VT) ^{1}H NMR spectra of [3.3](2,6)pyridinophanes have been studied. Previously the most stable conformer of [3.3]metacyclophane **1** in solution was identified as a syn(chair-chair), and the next stable isomer was expected to be a syn(chair-boat). The VT NMR study of [3]metacyclo(3)(2,6)pyridinophanes (**7-d$_4$** and **7-d$_8$**) revealed that the major [syn(chair-chair)] and minor [syn(chair-boat)] isomers exist with the population of 2:1 (−80°C, CD_2Cl_2). On the contrary, [3.3](2,6)pyridinophane **8-d$_4$** exists in an equilibrium mixture of syn(boat-boat) and syn(chair-boat) where the syn(boat-boat) is preferred [−110°C, CD_2Cl_2/CS_2 (3:2)]. The result indicates that the non-bonded interactions between an internal benzenoid proton or nitrogen lone pair(s) and trimethylene bridge protons decrease in magnitude as the sp^2 carbon bearing hydrogen in the benzene ring is replaced with sp^2 nitrogen with its lone pair. These interactions serve as a dominant factor for the determination of the relative stabilities of isomers. The energy barrier for trimethylene bridge inversion decreases in the following order: **1**>**7**>**8**.

V-H-6 Synthesis of Novel Cyclophane Host Molecules Constructed with [3.3]Metacyclophane Units

Teruo SHINMYOZU, Michiko YOKOI,[a] Junko KIKUMOTO,[a] Hiroe NONAKA,[a] Katsuya SAKO,[b] Hiroyuki TAKEMURA,[a] and Takahiko INAZU[a] *([a]Kyushu Univ., [b]Nagoya Inst. Tech.)*

[*Synthesis*, in press]

[3.3]Metacyclophane (**1**) exists in the syn geometry with the dihedral angle between two benzene rings being 25° in the crystalline state. Its preferred geometry in solution is also the syn. By taking advantage of the structural features of **1**, we designed to synthesize novel host molecules with cavities of various shapes and sizes **2**, **3**, **4**, and **5**. **2** has a ellipsoidal cavity which can accomodate small organic molecules like benzene, whereas **3** has a cubic π-electron-rich cavity of a similar size. The formation of π-prismand type complexes with metal cations is expected in **4**, while **5** has a much larger cavity. For the synthesis of these host molecules, we developed two new cyclization methods of [3^n]azacyclophanes by alkylation of trifluoroacetylated amines or cyanamide. By using these methods, we successfully synthesized the novel host molecules **2**-**5** and studied their inclusion properties.

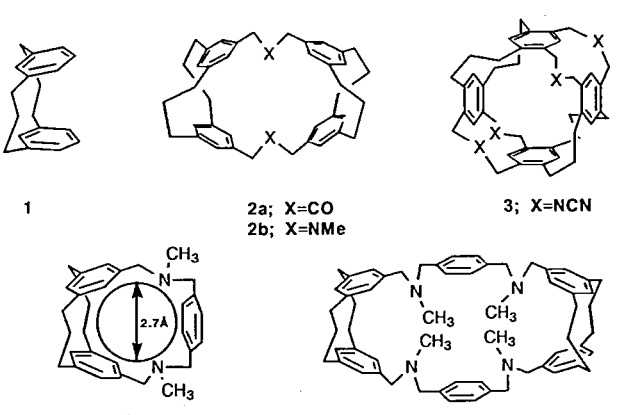

V—I Transannular π–π Interaction of (4n)π Systems

In cyclic conjugated planar systems, molecules with (4n+2)π-electrons are stabilized by delocalization of the π-system and called aromatic compounds. On the other hand, the π-delocalization causes an increase in the energy of the system in planar (4n)π monocyclic systems. These types of systems have been defined as antiaromatic. It is our interest to study how two π-systems mutually interact when they are overlapped each other in a close proximity. According to the frontier molecular orbital calculations, Greenberg *et al.* predicted a destabilizing π—π interaction in a (4n+2)π-(4n+2)π system, a stabilizing interaction in a (4n+2)π-(4n)π system, and greater stabilization in a (4n)π-(4n)π system than in the (4n+2)π-(4n)π system.[1] To verify these interesting predictions experimentally, we considered that [3.3]cyclophanes containing annulene rings must be the most suitable models since two π-systems in [3.3]cyclophane are located in the most optimal transannular distance and they are almost planar. [3.3]Cyclophane, therefore, permits exact evaluation of π—π interaction without interference of the strain effect.

V-I-1 Synthesis and Transannular π—π Interaction of [3.3]Cyclophanes Containing 1,6-Methano[10]-annulenes

Teruo SHINMYOZU, Tomonori MATSUNAGA,[a] Takahiko INAZU,[a] Jerzy M. RUDZIŃSKI,[b] and Mayumi MATSUSHITA[b] *([a]Kyushu Univ., [b]Fujitsu Kyushu System Engineering)*

As an initial step for this study, we planned to synthesize (4n+2)(4n+2)-cyclophanes (n > 2). First we undertook the synthesis of [3.3]cyclophanes containing 10π-monocyclic aromatics, Vogel's 1,6-methano[10]annulene **1**.[2] The precursor of cyclization reactions, 2,7-bis(bromomethyl)-1,6-methano[10]annulene **2** was prepared from **1** in four steps. The TosMIC coupling reaction of **2** and **3** afforded annulenophane **4** (Scheme 1). But a similar coupling reaction between **2** and TosMIC did not yield the desired **5** because of the instability of the annulene moiety of **5** to an acid, which was used in the reaction. We found that the cyanamide coupling method, which was developed for the synthesis of aza[3^n]cyclophanes, afforded the desired annulenophanes. The coupling reaction of **2** and cyanamide in a mixture of 50% NaOH aqueous solution and toluene in the presence of a phase-transfer catalyst at room temperature provided a mixture of the desired **6a** and **6b** in a ratio of 1.0:2.4 (Scheme 2), which were separated by HPLC and characterized. These compounds are the first example of [m.n]cyclophanes containing two annulene rings. Their transannular π—π interactions were studied based on the electronic spectra and theoretical calculations by the MNDO-PM3 method.

Synthesis of the model compounds **7** and **8** for the study of (4n)π interaction is currently under way.

References

1) A. Greenberg, J.F. Liebman, *"Strained Organic Molecules"*, Academic Press, New York, 1978, p.170.
2) E. Vogel, H.D. Roth, *Angew. Chem. Int. Ed. Engl.*, **3**, 228 (1964).

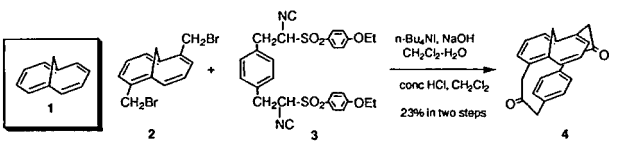

Scheme 1. Synthetic route to annulenophane **4**.

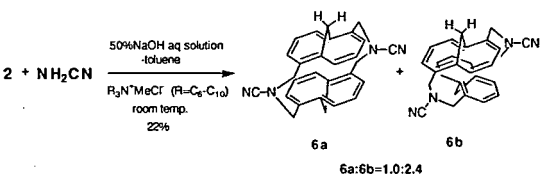

Scheme 2. Synthesis of annulenophanes **6a** and **6b** by the cyanamide coupling reaction.

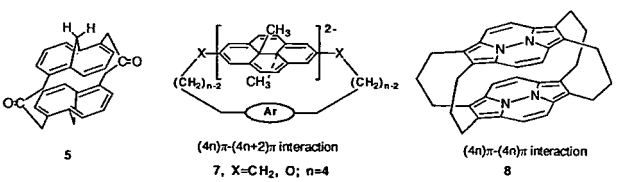

V—J Structure-Reactivity Relationship in the Gas Phase

Substituent effect linear free energy relationship has been used as an experimental tool for the exploration of mechanistic hypotheses in a wide variety of situation. It is of particular importance to elucidate real physical meaning of correlation results of the substituent effect analysis. Thermodynamic properties of organic ions in the gas phase can provide the most precious basis for this purpose because such data are absolutely free from difficulties arising from mechanistic complexities as well as solvent modification of the electronic effect of substituents. In addition, these data can be easily compared with theoretical calculations. In these several years, we have analyzed a series of substituent effects for the stability of benzylic carbocations in the gas phase using the Yukawa-Tsuno LArSR equation. It has been shown that the resonance demand (r) which is a measure of the degree of resonance stabilization of the positive charge into aryl π-system increases linearly with the decrease in stability of the carbocation. This revealed that the r value is characteristic of a carbocation itself. In this project, we have studied gas phase substituent effects of stabilities of negative ions to make intrinsic nature of resonance demand clear, and have carried out theoretical calculations of several benzylic cations.

V-J-1 Substituent Effects of Gas Phase Acidities. Intrinsic Resonance Demand of Negative Ions

Masaaki MISHIMA, Mizue FUJIO,* and Yuho TSUNO* *(*Kyushu Univ.)*

Several gas phase acidities of toluenes and anilines have been determined by measuring proton transfer equilibrium constants with a pulsed ion cyclotron resonance (ICR) spectrometer to complete data sets for the substituent effect analysis of gas phase acidities. Application of the LArSR Eq. 1 to a series of substituent effects using ordinary substituent constants determined in solution provided following results with satisfied precision; ρ=18.90 and r=0.61 for phenol, ρ=16.52 and r=0.99 for aniline, ρ=17.34 and r=1.14 for toluene, ρ=17.38 and r=0.74 for benzylnitrile.

$$\delta\Delta G^{\circ}_{acid} = \rho(\sigma^{\circ} + r\,\Delta\bar{\sigma}_R^{-}) \qquad (1)$$

Resonance demand of phenoxide ion is smaller in gas phase than in aqueous solution (r=1.00). Similar result was observed for acidities of anilines. The larger resonance demand in solution may be attributed to exalted resonance effect of para π-acceptor caused by hydrogen-bonding interaction with solvent as noted by Taft et al. Most importantly, the r value in gas phase was found to increase linearly with the decrease in stability of the parent anion (ring substituent=H) as shown in Figure 1. This situation is in accord with that observed for the stabilities of benzylic carbocation, supporting that the concept of varying resonance demand introduced into the LArSR equation is an essential requirement in the substituent effect analysis.

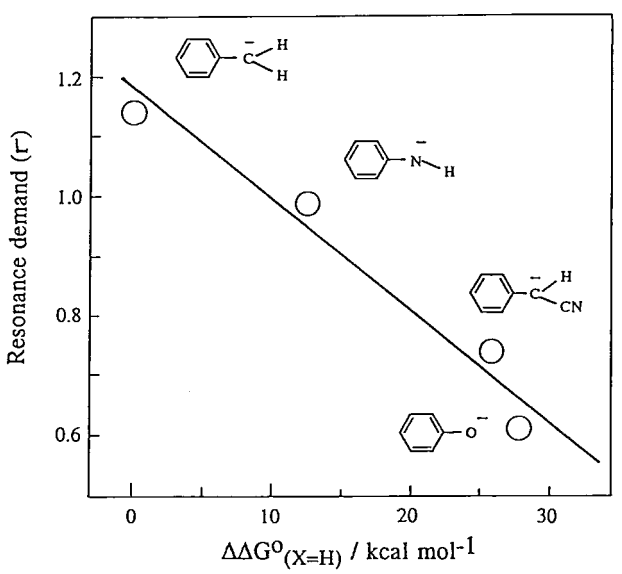

Figure 1. A linear relationship between resonance demand and relative stability of the parent anion.

V-J-2 Effect of the Twisted Nitro Group on Gas Phase Acidities of Benzoic Acid, Toluene, Aniline, and Phenol

Masaaki MISHIMA, Chul Hyun KANG *(Inha Univ. and IMS)*, **Chul HUH** *(Inha Univ. and IMS)*, **and Yuho TSUNO** *(Kyushu Univ.)*

Gas phase acidities have been determined for 3,5-dimethyl-4-nitro-1-Y-substituted benzenes (Y=COOH, CH_3, NH_2, and OH) and for the corresponding 4-H and 4-CN derivatives. Effect of the 4-nitro group on the acidity of 3,5-Me_2 system is reduced significantly in all Y-series compared with that of 3,5-H_2 system while the effect of the 4-cyano group is identical in both systems. The decreased effect of the nitro group in the 3,5-Me_2 system can be attributed to steric inhibition of resonance effect caused by twisting out of the coplanarity with the benzene π-ring. Interestingly, the degree of the decrease in effect of the nitro group was found to be constant at 22±2% for all Y-series regardless of the varying contribution of resonance effect involved in their acidities. This suggests that the system with the greater resonance demand has the smaller steric inhibition of resonance effect. In other words, the high ability of π-delocalization of negative charge into aryl π-system prevents the loss of the coplanarity. This is also consistent with the fact that the dihedral angle of twisting out of the coplanarity estimated from the present data with the aid of the LArSR analysis, 35° to 45°, is clearly smaller than that of the corresponding neutral molecules, 60° to 66°, based on spectroscopic data (UV, NMR, and X-ray).

V-J-3 Electron Affinities of 2,6-Dimethyl-4-substituted Nitrobenzenes. Substituent Effect on the Stability of Radical Anions

Masaaki MISHIMA, Chul Hyun KANG *(Inha Univ. and IMS)*, **and Yuho TSUNO** *(Kyushu Univ.)*

Electron affinities (EA) have been determined for a series of 2,6-dimethyl-4-substituted nitrobenzenes, where the nitro group is twisted out of the coplanarity with the phenyl ring, by measuring equilibrium constant of electron transfer reaction with a pulsed ICR spectrometer. EA of 2,6-dimethylnitrobenzene is significantly smaller than nitrobenzene by 5.7 kcal mol^{-1}. Nevertheless the substituent effect on the stability of the radical anion (**1**) was found to be in complete agreement with that of untwisted 4-substituted nitrobenzenes. This means that resonance demand (r) is identical for both radical anions. This situation is not consistent with the "resonance demand-stability relation" for the stabilities of ordinary anions reported in the previous section. Such difference in substituent effect behavior may be attributed to inherent nature of radical anion itself. That is, the present result suggests that the SOMO (singly occupied molecular orbital) of **1** bears not only π^*-character but also σ^*-character.

V-J-4 The Acidities of 4-Substituted Benzoic, Bicyclo[2.2.2]oct-1-yl and Bicyclo[2.2.2]oct-2-enyl Carboxylic Acids

Ilmar A. KOPPEL *(Tartu Univ.)*, **Masaaki MISHIMA, Leon M. STOCK** *(Univ. of Chicago)*, **Robert W. TAFT** *(Univ. of Calif., Irvine)*, **and Ronald D. TOPSOM** *(La Trobe Univ.)*

[*J. Phys. Org. Chem.*, in press]

Experimental gas phase acidities have been determined for a series of 4-substituted bicyclo[2.2.2]oct-1-yl carboxylic acids (**1**) and for a limited number of the corresponding bicyclo[2.2.2]oct-2-enyl carboxylic acids (**2**). Similar

acidities have been also determined for additional 4-substituted benzoic acids, allowing a comparison of field and resonance effects among the three series. Ab initio molecular orbital calculations for these series of acids confirm the conclusion that the aromatic acids display direct field and resonance effects, whilst the acidities in the aliphatic series acids are largely determined by direct field effects.

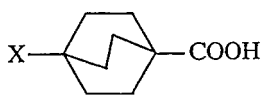

(1)

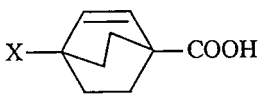

(2)

V-J-5 Theoretical Study on Resonance Demand of Carbenium Ions

Yoshihiro SAEKI, Kazuhide NAKATA,* Hideyuki NOMURA,* Masaaki MISHIMA, Mizue FUJIO,* Yuho TSUNO,* Kichisuke NISHIMOTO, and Toshio MATSUSHITA**** *(*Kyushu Univ. and **Osaka City Univ.)*

In order to clarify a relationship between resonance demand (r) determined empirically by substituent effect analysis and molecular structures the electronic and geometrical structures of various carbocations have been investigated by ab initio molecular orbital calculations. A linear relationship between the C1-C7 bond distance and the r value has been found for a series of benzylic carbocations, revealing that an r value can be regarded as a measure of double bond character between a cationic center carbon and the benzene ring. Furthermore, we have studied highly congested carbocation systems such as α-di-t-butylbenzyl and α-t-butyl-α-methylbenzyl cations. It has been shown that the dihedral angle of twisting out of the coplanarity with the benzene π-ring ($\angle$R1C7C1C6) is in complete agreement with that estimated from the r value of the LArSR analysis of the corresponding S_N1 solvolysis. These results offer further corroborating evidence for the validity of the LArSR analysis of the substituent effect.

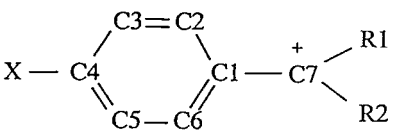

RESEARCH ACTIVITIES VI
Department of Vacuum UV Photoscience

VI—A Two-Color cm^{-1}-Resolution Threshold Photoelectron Spectroscopy for Studying Molecular Cations

In this Institute we have developed 'laser excite-state photoelectron spectroscopy' using REMPI (resonantly enhanced multiphoton ionization), and applied it to various jet-cooled molecules and molecular complexes [see, K. Kimura, *Adv. Chem. Phys.*, **60**, 161 (1985); *Intern. Rev. Phys. Chem.*, **6**, 195 (1987)]. Recently in this Institute we have further developed a compact cm^{-1}-resolution photoelectron analyzer, which collect threshold photoelectrons at several hundreds nanoseconds after each laser shot in our two-color experiments. (Such a threshold photoelectron technique is equivalent to so-called ZEKE photoelectron spectroscopy.)

In the present project, we have carried out two-color (n+1') REMPI experiments using our cm^{-1}-resolution photoelectron analyzer for studying low-frequency vibrational spectra of various jet-cooled molecular cations.

VI-A-1 REMPI Threshold Photoelectron Spectra of the *cis* and *trans* Rotational Isomers of Jet-Cooled *m*-Chlorophenol.

Martin C.R. COCKETT, Masahiko TAKAHASHI, Katsuhiko OKUYAMA, and Katsumi KIMURA

[*Chem. Phys. Lett.*, **187**, 250 (1991)]

The *cis* and *trans* rotational isomers of jet-cooled *m*-chlorophenol have been studied by two-colour (1+1') laser threshold photoelectron spectroscopy. The adiabatic ionization energy (I_a) for each isomer spectra was obtained from the positions of the respective zeroth vibrational peaks in the threshold photoelectron spectra. This yielded I_a values of 8.655 ± 0.001 eV for the *cis* isomer and 8.682 ± 0.001 eV for the *trans* isomer. Additionally, a provisional assignment of the vibrational structure observed in the ion current spectrum (S_1 state) and the threshold photoelectron spectra (D_0 state), has been made on the basis of comparison with the known ground state vibrational frequencies of the neutral molecule.

VI-A-2 Observation of Torsional Motion in the Ground-State Cation of Jet-Cooled Tolane by Two-Color Threshold Photoelectron Spectroscopy

Katsuhiko OKUYAMA, Martin C.R. COCKETT, and Katsumi KIMURA

[*J. Chem. Phys.*, **97**, 1649 (1992)]

High-resolution threshold photoelectron spectra of jet-cooled tolane ($C_6H_5-C\equiv C-C_6H_5$) have been obtained by two-color (1+1') resonantly enhanced multiphoton ionization via the S_1 state $\{^1B_{1u}(\pi\pi^*)\}$. From the threshold photoelectron spectra, the adiabatic ionization energy has been determined to be $I_a = 63917 \pm 3$ cm^{-1} (7.9243 ± 0.0004 eV). A vibrational progression due to trosional motion in the cation ground state was observed up to its fifth quantum level with a fundamental frequency of 54 cm^{-1}, showing small anharmonicity. From these results, we have evaluated the potential barrier height to the torsional motion to be 1980 ± 60 cm^{-1}. The threshold photoelectron spectra obtained via several S_1 vibronic levels exhibit dominant peaks due to the $\Delta v=0$ ionization transitions. This fact indicates that no significant change occurs in molecular structure upon photoionization with removal of the antibonding π electron from the S_1 state. Threshold photoelectron bands arising from formally forbidden odd quantum transitions in the torsional mode were also clearly observed with small intensities. The mechanism of the appearance of such a nontotally symmetric mode is discussed.

VI-A-3 Cation Vibrational Spectroscopy of *trans* and *gauche* *n*-Propylbenzene Rotational Isomers. Two-Color Threshold Photoelectron Study and *Ab Initio* Calculations

Masahiko TAKAHASHI and Katsumi KIMURA

[*J. Chem. Phys.*, in press]

In this paper, a full account of an earlier report [Takahashi, Okuyama, and Kimura, *J. Mol. Struct.*, **249**, 47 (1991)] on the cation vibrational spectra of *trans* and *gauche* *n*-propylbenzene, which were obtained by means of a two-color (1+1') multiphoton ionization threshold photoelectron technique is presented. The *trans* and *gauche* cations were separately produced by (1+1') multiphoton ionization resonant through the S_1 vibronic levels of *n*-propylbenzene in supersonic free jets in which both the *trans* and *gauche* isomers exist. From the observed threshold photoelectron spectra, adiabatic ionization energies are determined as I_a(*trans*)=70278 cm^{-1} (8.7134 eV) and I_a(*gauche*)=70420 cm^{-1} (8.7311 eV) with an accuracy of ± 8 cm^{-1} (± 1 meV). Furthermore, four benzene ring modes ($6b^+$, 1^+, 12^+, and $18a^+$) as well as several low-frequency torsional and bending modes have been identified which are sensitive to the relative conformations of the *n*-propyl group with respect to the benzene ring [(*trans*)$^+$: 82, 212, and 300 cm^{-1}; (*gauche*)$^+$: 46, 73, 207, and 252 cm^{-1}. The present vibrational assignments of the *trans* and *gauche* cations are based on a normal mode analysis performed for the *trans* cation by *ab initio* calculations. In the present work, this technique is demonstrated to be quite powerful for distinguishing the vibrational spectra of different cation isomers.

VI-A-4 Vibronic Coupling in the Ground Cationic State of Naphthalene: A Laser Threshold Photoelectron Spectroscopic Study.

Martin C.R. COCKETT, Hiroyuki OZEKI, Katsuhiko OKUYAMA, and Katsumi KIMURA

The two-colour (1+1') threshold photoelectron spectra of naphthalene in a supersonic free jet have been recorded via nine vibronic levels of the S_1 electronic state up to about 1420 cm^{-1} internal energy. The TES spectra recorded via vibronic levels having a_g symmetry show significant intensity in Δv=+1 transitions (in b_{1g} vibrations) indicating that the ionization transition gains significant intensity through a vibronic coupling mechanism between the two lowest doublet cationic states. The strongest departure from the expected Δv=0 propensity in the TES spectra occurs through excitation of the totally symmetric 8 mode having a_g symmetry indicating that a considerable displacement occurs along the normal coordinate of this 8 mode upon ionization from the S_1 state. The superior resolution of the threshold photoelectron technique over conventional photoelectron methods has allowed extremely accurate values for the fundamental vibrational frequencies of naphthalene in its ground cationic state to be determined and it has also allowed a more rigorous investigation of the vibronic coupling mechanism that occurs between the two lowest doublet cationic states. Moreover, an improved value for the adiabatic ionization energy of naphthalene of 65668 ± 5 cm^{-1} (8.1418 ± 0.0006 eV) has been determined.

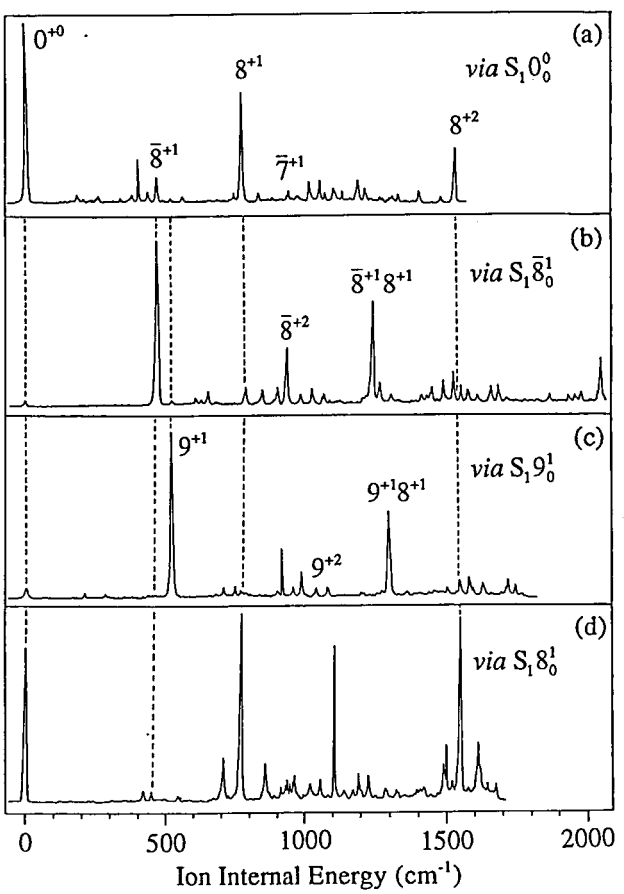

Figure 1. The two-colour (1+1') threshold photoelectron spectra of naphthalene recorded via the intermediate vibronic levels (a) $S_1 0_0^0$ (b) $S_1 \bar{8}_0^1$ (+436 cm^{-1}), (c) $S_1 9_0^1$ (+501 cm^{-1}), and (d) $S_1 8_0^1$ (+700 cm^{-1}). The bar above the vibrational mode number refers to a mode having b_{1g} symmetry and no bar refers to a_g symmetry.

VI-A-5 Absence of Photoelectron Spectroscopic Evidence for 'Proton Tunneling' in the Cation Ground State of Jet-Cooled Tropolone

Hiroyuki OZEKI, Masahiko TAKAHASHI, Katsuhiko OKUYAMA, and Katsumi KIMURA

[*J. Chem. Phys.*, **95**, 9401 (1991)]

From our high resolution REMPI threshold photoelectron measurements of jet-cooled tropolone, it has been found that no spectral doublet showing 'proton tunneling' in the cation ground state (D_0) is observed within an experimental accuracy of 2 cm^{-1}. The adiabatic ionization potential was obtained as I_a=68365 ± 5 cm^{-1}.

VI-A-6 Spectroscopic Studies on 'Proton Tunneling' in the Cation Ground State of 9-Hydroxyphenalenone (9-HPO)

Hiroyuki OZEKI, Masahiko TAKAHASHI, Katsuhiko OKUYAMA, and Katsumi KIMURA

In our recent paper, we showed the relative importance of geometric and electronic factors in determining the rate of proton tunneling in the cation ground state (D_0) of the tropolone molecule. The observed inhibition of proton tunneling was explained in terms of a large contribution from electronic effects. In order to investigate the applicability of this result to a similar molecular system, we chose the deuterated 9- hydroxyphenalenone (9-HPO-d) molecule.

Figure 1 shows threshold photoelectron spectra obtained via the S_1 0^+ and 0^- levels of 9-HPO-d. In each case the first band indicates the transition terminating on the lower and upper zeroth vibrational level, respectively. The difference in the total transition energies between the first bands shown in spectra (a) and (b) was observed to be 11 cm^{-1}, which represents the difference of tunneling splitting widths of the zeroth vibrational levels of the neutral ground (S_0) state and the D_0 state. In conjunction with the splitting width in the S_0 state, we can estimate the splitting width of the zeroth vibrational level to be 1 cm^{-1} (i.e. within our experimental accuracy).

The 9-HPO molecule has a rigid carbon skeletal framework and no large structural change affecting the rate of proton tunneling occurs upon ionization. π-electron removal results in the reduction of charge density of the ketonic oxygen and consequently weakens the strength of the intramolecular hydrogen bond. In other words, the inhibition of the proton tunneling in the D_0 state of 9-HPO can be explained in the same way as in the case of the tropolone molecule, for which electronic effects were found to be the dominating factor.

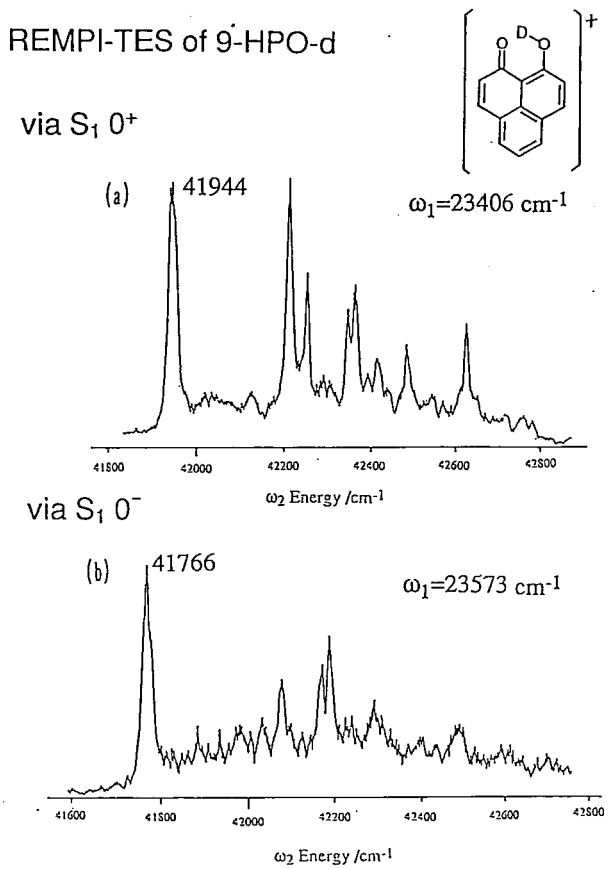

Figure 1. Threshold photoelectron spectra recorded by exciting the S_1 (a) 0^+ level and (b) 0^- level of 9-HPO-d.

VI-A-7 Two-Color (1+1') REMPI Threshold Photoelectron Study of 2-Hydroxypyridine

Hiroyuki OZEKI, Martin C.R. COCKETT, Katsuhiko OKUYAMA, Masahiko TAKAHASHI *(Tohoku Univ.)*, **and Katsumi KIMURA**

2-Hydroxypyridine (2-HP) adopts two isomeric forms in the gas phase, lactim (pyridine) and lactam (pyridone), which are distinguished by the location of a migrating proton. In addition to this, lactam form has at least two conformers in the S_1 state. The purpose of this study is to investigate the dynamic behavior of these various isomers in the cation ground state (D_0) by using high resolution threshold photoelectron spectroscopy combined with a REMPI technique.

Figure 1 shows threshold photoelectron spectra of the lactam form obtained via the S_1 origin of the two conformers. The total transition energies of the first bands in spectrum (a) and (b) are both found to be 68137 ± 5 cm^{-1}. This experimental result indicates that the molecular structure of the lactam form reverts to a single conformer in the D_0 state as is the case in the S_0 state.

We have also measured the ionization energy of the lactim form to be 72093 ± 5 cm^{-1} from a threshold photoelectron spectrum obtained via its S_1 origin. This information makes it possible to confirm the original assignments of the first and second photoelectron bands of 2-HP in the conventional He(I) photoelectron spectrum to the lactam form and the lactim form, respectively.

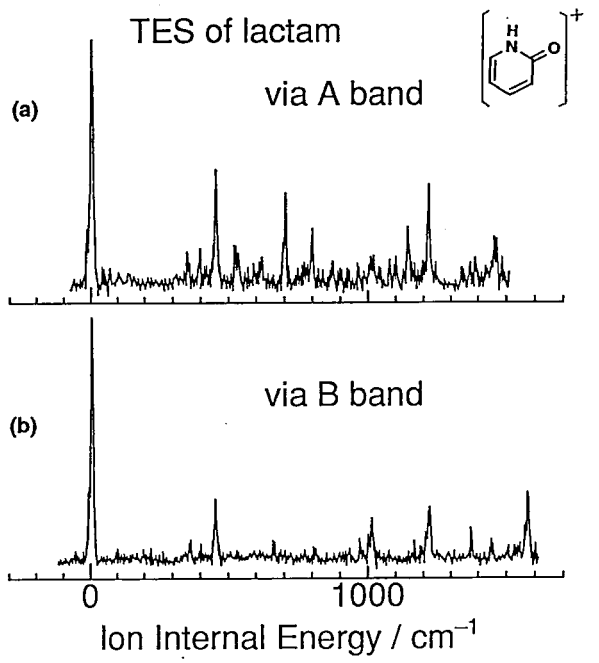

Figure 1. Threshold photoelectron spectra recorded by exciting the S_1 origin of each conformer of lactam.

VI-A-8 Vibrational Spectra of Aniline-Ar_n van der Waals Cations (n=1 and 2) observed by Two-Color "Threshold Photoelectron" [Zero Kinetic Energy (ZEKE)-Photoelectron] Spectroscopy

Masahiko TAKAHASHI, Hiroyuki OZEKI, and Katsumi KIMURA

[*J. Chem. Phys.*, **96**, 6399 (1992)]

Measurements of mass-selected ion-current and threshold photoelectron spectra of jet-cooled aniline-Ar_n van der Waals complexes (n=1 and 2) have been carried out with a two- color resonantly enhanced multiphoton ionization (REMPI) technique using a high-resolution threshold photoelectron analyzer developed in this laboratory. From our (1+1') REMPI experiments via the respective excited S_1 states, we have obtained photoelectron spectra with well-resolved vibrational progressions due to "low-frequency van der Waals modes" of the cations; ν_{vdW}=16cm^{-1} (n=1) and ν_{vdW}=11 cm^{-1} (n=2). From Franck-Condon calculations we have assigned these low-frequency vibrations to the "van der Waals bending" of the cations. We have also found that the angles of the van der Waals bonds in the cations are changed by 8.2 (n=1) and 8.8 (n=2) degrees with respect to the S_1 states. The adiabatic ionization potentials (I_a) of aniline and the aniline-Ar_n complexes (n=1 and 2) have been determined as 62268 ± 4 cm^{-1} (aniline), 62157 ± 4 cm^{-1} (n=1), and 62409 ± 4 cm^{-1} (n=2). Their shifts ΔI_a are 111 cm^{-1} (n=1) and 219 cm^{-1} (n=2) with respect to aniline. Spectral shifts due to complex formation have been observed for a total of 13 ring modes of the cations.

VI-A-9 Two-Color (2+1') Multiphoton Ionization Threshold Photoelectron Study of the Ar-NO van der Waals Complex: Observation of Intermolecular Vibrational Progressions of the Ar- NO^+ Cation

Masahiko TAKAHASHI

[*J. Chem. Phys.*, **96**, 2594 (1992)]

Two-color (2+1') multiphoton ionization high-resolution threshold photoelectron spectroscopy has been applied to the Ar-NO van der Waals complex in a supersonic free jet. The resonant ionization process studied may be expressed by Ar-NO ($X^2\Pi_{1/2}$, $v''=0$)+$2h\nu_1$→Ar-NO*($C^2\Pi$, v')+$h\nu_2$ →Ar-NO^+($X^1\Sigma^+$, v^+). Two strong anharmonic vibrational progressions have been observed in the threshold photoelectron spectra having frequencies of 79 and 94 cm^{-1}. These vibrations have been assigned to the intermolecular bending and stretching motions of the $(Ar\text{-}NO)^+$ complex cation. From the threshold photoelectron spectra, the adiabatic ionization potential of Ar-NO has been determined as 73869 ± 6 cm^{-1} (86 cm^{-1} higher than previously reported), and the dissociation energy of the $(Ar\text{-}NO)^+$ cation has been calculated as 951 cm^{-1}. The structural change of Ar-NO that occurs on photoionization has been calculated with the aid of simple Franck-Condon calculations, which suggest that the intermolecular bond distance of Ar-NO decreases by 1.03 Å, while the O-N-Ar angle decreases by 11.3°.

VI-A-10 Laser Threshold Photoelectron Spectra of the *cis* and *trans* Rotational Isomers of *p*-Dimethoxybenzene-Ar_n(n=0,1,2): Observation of the Intermolecular van der Waals Stretching and Bending Vibrational Modes in the Cation

Martin C.R. COCKETT, Katsuhiko OKUYAMA, and Katsumi KIMURA

[*J. Chem. Phys.*, *97*, 4679 (1992)]

The *cis* and *trans* rotational isomers of *p*-dimethoxybenzene-Ar_n(n=0,1,2) have been studied in a supersonic free jet by two-colour laser REMPI (resonance enhanced multiphoton ionization) threshold photoelectron spectroscopy. The two-colour (1+1') threshold photoelectron spectra recorded *via* the S_1 state of the *cis* and *trans* isomers of the 1:1 and 1:2 argon complexes reveal well resolved vibrational structure characteristic of the low frequency bending and stretching van der Waals vibrational modes. In the case of the *trans* isomer of the 1:2 complex, a very low frequency progression (11 cm^{-1}) in a non totally symmetric van der Waals bending mode appears in single quanta in the spectrum. The equivalent spectrum recorded for the *cis* isomer exhibits structure characteristic of van der Waals stretching modes as well as double quanta excitation in both totally symmetric and non totally symmetric van der Waals bending modes. The observation of single quantum excitation in formally forbidden van der Waals vibrational modes implies the possibility of a change in the overall symmetry of the complex in the ground cationic state when compared to that in the S_1 state. The adiabatic ionization energies (I_a) for the *cis* and *trans* isomers of *p*-dimethoxybenzene-Ar_n (n=0,1,2) were measured as 60774 ± 7 cm^{-1} (*cis*; n=0), 60687 ± 7 cm^{-1} (*cis*; n=1), 60509 ± 7 cm^{-1} (*cis*; n=2), 60563 ± 7 cm^{-1} (*trans*; n=0), 60479 ± 7 cm^{-1} (*trans*; n=1) and 60295 ± 7 cm^{-1} (*trans*; n=2).

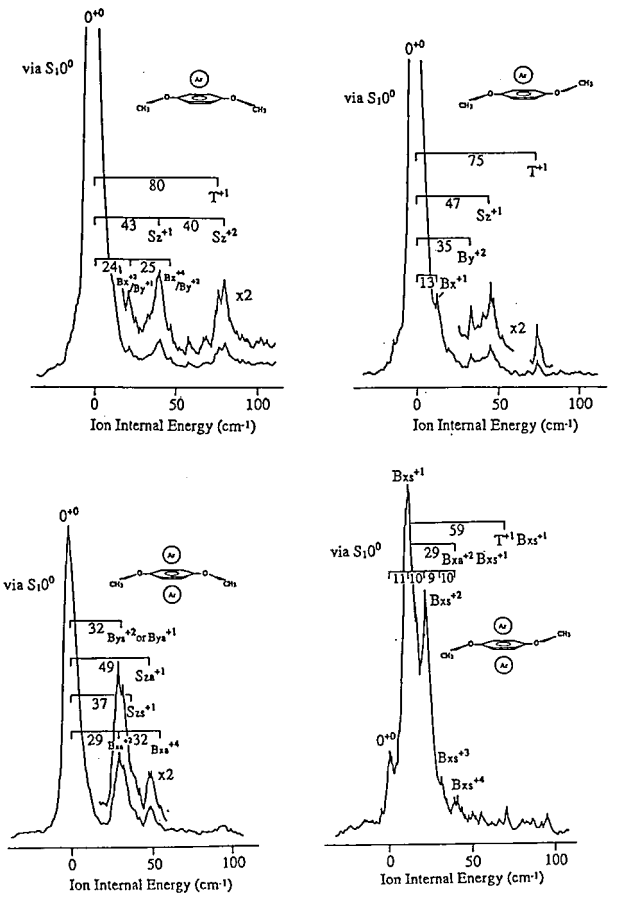

Figure 1. The two-colour (1+1') threshold photoelectron spectra recorded *via* the S_1 band origins of (a) *cis*- and (b) *trans*-*p*-dimethoxybenzene-Ar_n(n=1,2).

VI-A-11 A Study of Phenylacetylene (PA) and Styrene (ST), and Their Argon Complexes, PA-Ar and ST-Ar, with Laser Threshold Photoelectron Spectroscopy

John M. DYKE, Hiroyuki OZEKI, Masahiko TAKAHASHI, Martin C.R. COCKETT, and Katsumi KIMURA

[*J. Chem. Phys.*, in press (1992)]

In this work, the molecules styrene (ST) and phenylacetylene (PA), as well as their argon complexes ST-Ar and PA-Ar, have been investigated with (1+1') resonance enhanced multiphoton ionization (REMPI) threshold photoelectron spectroscopy (TES). The first adabatic ionization energies of ST, PA, ST-Ar and PA-Ar have been measured as 68267 ± 5 cm^{-1}, 71175 ± 5 cm^{-1}, 68151 ± 5 cm^{-1} and 71027 ± 5 cm^{-1}, respectively. For both ST-Ar and PA-Ar, the first photoelectron band shows structure in the lowest frequency van der Waals (vdW) bending mode in the ground ionic state, with ν_{vdW} being measured as 15 cm^{-1} in each case. For each molecule, excitation of a particular vibrational level of the S_1 state followed by ionization, allows structure in that mode to be observed in the

threshold photoelectron spectrum. This has been achieved for three modes in both styrene and phenylacetylene. The experimental ionic vibrational frequencies thus obtained, have been compared with those known for the S_0 and S_1 states.

VI-A-12 REMPI Spectroscopic Evidence for Pseudo Rotation in 3*s* Rydberg State of Tetrahydrofuran

Tatsuhisa KATO *(Kyoto Univ.)*, **Michio MATSUSHITA** *(Kyoto Univ.)*, **Tadamasa SHIDA** *(Kyoto Univ.)*, **Masahiko TAKAHASHI, Hiroyuki OZEKI, and Katsumi KIMURA**

The (2+1) resonant enhanced multiphoton ionization (REMPI) spectrum for tetrahydrofuran (THF) was observed under the collision free condition. The potential along the pseudo rotational coordinate in intermediate 3*s* Rydberg state was obtained as shown in Figure 1. The origin of 3*s* Rydberg state was observed at 50725.0 cm^{-1}, and the potential surface of the pseudo rotation has a double minimum shape with the barrier of 755 cm^{-1}. The large barrier to pseudo rotation in 3*s* Rydberg presented a sharp contrast to that in the ground state, which was reported by the far-infrared spectroscopic study, and showed a good correlation with the activation energy (E_a=577 cm^{-1}) of jumping between two minima of pseudo rotation potential for THF cation measured by an EPR spectroscopy in a matrix at low temperature.

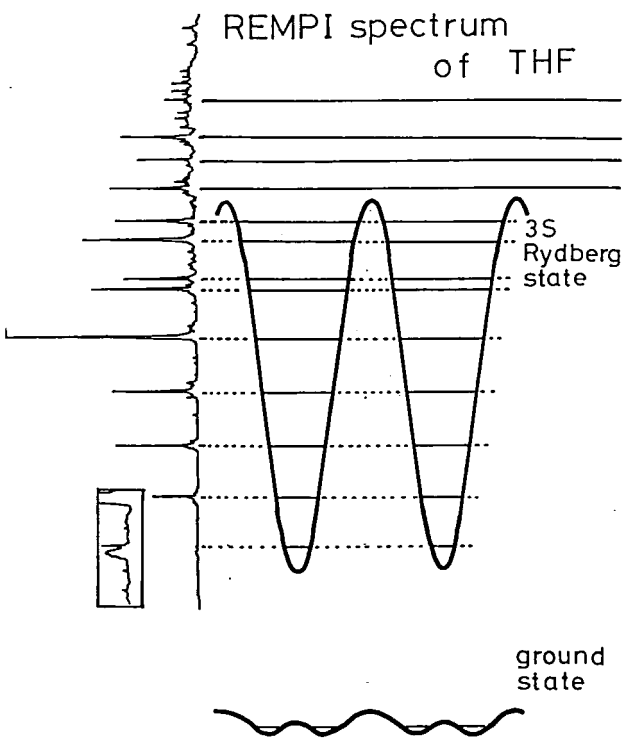

Figure 1. Approximate barrier to pseudo rotation and energy levels in 3*s* Rydberg state of tetrahydrofuran.

VI-A-13 Large-Amplitude Torsional Motion in Ground-State Cation of Jet-Cooled Biphenyl and 4-Fluorobiphenyl observed by Two-Color Threshold Photoelectron Spectroscopy

Katsuhiko OKUYAMA, Martin C.R. COCKETT, Hiroyuki OZEKI, and Katsumi KIMURA

In the series of *para* poly-phenylene compounds, large-amplitude torsional motion plays an important role in their molecular structure and photophysical properties. Biphenyl is the prototypical molecule in the series and has only one torsional mode. This mode is governed by the balance between the π electron conjugation and the *ortho* hydrogen repulsion. In the neutral ground state (S_0), the torsional motion has a large amplitude with an equilibrium torsional angle of $42 \pm 2°$.[1] After the establishment of the supersonic-jet technique, many spectroscopists[2] attempted to research the torsional motion of electronically excited biphenyl (S_1). It was found that the π electron conjugation of biphenyl becomes strengthened upon electronic excitation and its stable structure is planar. However, the mount of spectroscopic information available on the cation ground state (D_0) is poor. This state has an electron configuration described by the removal of one π electron from the neutral ground state configuration and consequently the degree of π electron conjugation will be significantly affected. In this manuscript we report the preliminary results obtained for the biphenyl cation observed by two-color threshold photoelectron spectroscopy. The results are shown in Figure 1. Although the spectrum is very noisy, we can identify the threshold photoelectron signal of biphenyl with confidence. The peak energy position observed is the 3220 cm^{-1} (0.4 eV) lower than the photoelectron onset reported by He(I) spectroscopy. The reason for noisy spectrum is due to the rapid energy-relaxation of the S_1 vibronic level used as the resonant state in the (1+1') two-color ionization process.

Reference

1) A. Almenpingen and O. Bastiansen, *K. Nor. Vidensk. Selsk. Skr.* **4**, 1 (1958).
2) Hoong-Sun Im and E. R. Bernstein, *J. Chem. Phys.* **88**, 7337 (1988).: J. Murakami, M. Ito, and K. Kaya, *J. Chem. Phys.* **74**, 6505 (1981).

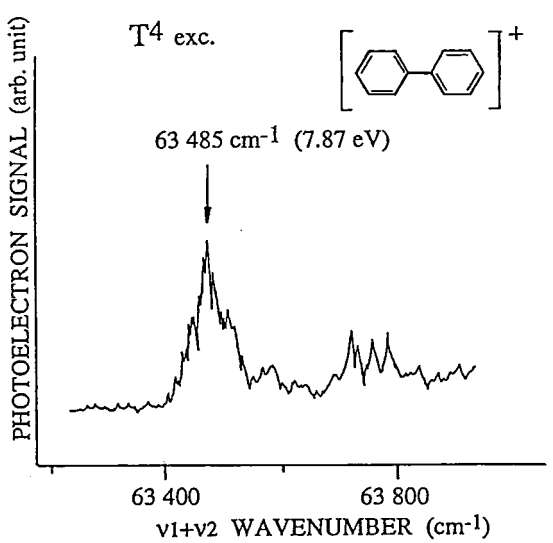

Figure 1. The two-color threshold photoelectron spectrum of jet-cooled biphenyl. This spectrum is obtained in resonance with the T^4 level in the S_1 state, assigned by Hoong-Sun Im and E. R. Bernstein.[2]

VI-A-14 Butterfly Motion in the Ground-State Cation of Jet-Cooled 1,2,4,5-Tetrafluorobenzene observed by Two-Color Threshold Photoelectron Spectroscopy

Katsuhiko OKUYAMA and Katsumi KIMURA

It is known that 1,2,4,5-tetrafluorobenzene in its lowest singlet excited state (S_1) undergoes a flexible butterfly motion in which the four fluorine atoms move out-of plane and in-phase with each other (this mode is named 11 according to the Wilson benzene-based numbering). Its motion is governed by a shallow double minimum potential in which the most stable conformation deviates from a planar one by $11 \pm 4°$ and the overtone frequency is 60 cm^{-1}. In contrast to the S_1 state, this motion in the neutral ground state (S_0) is a rigid vibration described by a harmonic potential for which the overtone frequency is 388 cm^{-1}.

On the basis of this research background, we are interested in investigating this motion in the cation ground state (D_0) and have applied two-color threshold photoelectron spectroscopy for this purpose. The resulting spectra shown in Figure 1 were recorded in resonance with the 0^0 and 11^2 levels in the S_1 state. The adiabatic ionization energy of this molecule was determined to be $75640 \pm 5 cm^{-1}$. Both spectra exhibit long vibrational progressions with a frequency interval of $366 cm^{-1}$ but provide different intensity distributions each other. These facts indicate that the vibrational progression obseved in the spectra is due to the 11 mode in the cation ground state and that 1,2,4,5-tetrafluorobenzene cation has a rigid molecular structure similar to that in the neutral ground state.

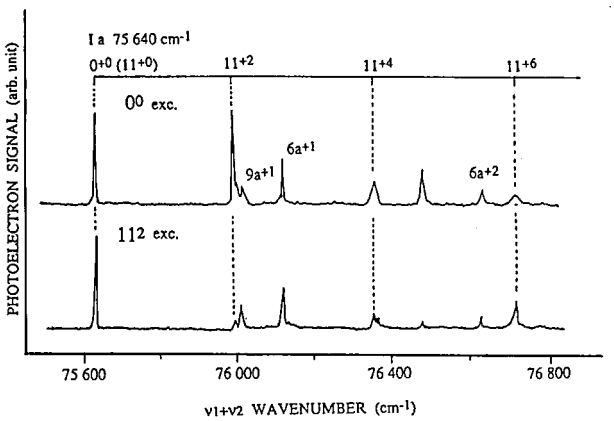

Figure 1. The two-color threshold photoelectron spectra of 1,2,4,5-tetrafluorobenzene. The upper figure is obtained in resonance with the 0^0 level in the S_1 state and the lower is the 11^2 level.

VI—B Synchrotron Radiation Researches of Molecules and Molecular Clusters: Photoionization and Photoelectron Spectroscopy

The use of synchrotron radiation is attractive for studying photoionization and photoelectron spectroscopy of gaseous atoms, molecules and molecular clusters produced in supersonic jets. For this purpose, we have been using two kinds of synchrotron-radiation photoionization apparatuses connected with the 750-MeV electron storage ring (called UVSOR) in this Institute. One is a molecular-beam apparatus on beamline BL2B2 [K. Kimura, Y. Achiba and H. Shiromaru, *Rev. Sci. Instrum.* **60**, 2205 (1989)], using a multi-stage differential pumping system without using any window materials between the molecular-beam apparatus and the storage ring. The other is an undulator- radiation PEPECO apparatus on beamline 3A2 [K. Okuyama, J. H. D. Eland and K. Kimura, *Phys. Rev.* **A 41**, 4930 (1990)], constructed to study doubly charge ions of gasous atoms and molecules as well as to perform coincidence measurements of two photoelectrons.

VI-B-1 Energy Partitioning in the Dissociation Reaction $Ar_3^+ \rightarrow Ar_2^+ + Ar$

Kenji FURUYA, Katsumi KIMURA, and Takato HIRAYAMA *(Gakushuin Univ.)*

[*J. Chem. Phys.*, **97**, 1022 (1992)]

Threshold-photoelectron photoion coincidence (TPEPICO) spectra of argon clusters ionized with synchrotron radiation have been observed, and the average kinetic energy of Ar_2^+, which originates from Ar_3^+, has been estimated. All the line shapes of the Ar_2^+ ion observed in the TPEPICO spectra have been appropriately simulated in terms of superposition of a sharp and a broad Gaussian function, where the sharp Gaussian function corresponds to ionization of the argon dimer Ar_2. The observed line shapes agree very well with the simulated ones, implying that the excess energy in the Ar_3 ionization is thermally or quasithermally partitioned to translational energy of the fragment species. From the average kinetic energies of Ar_2^+, it has been found that the percentage of excess energy in Ar_3^+, that is partitioned into the total translational energy of the fragment species, is dependent on the excitation energy. The percentage is slightly less than the value of 40% expected from statistical theory. It has also been found that complete dissociation of Ar_3^+ takes place in the excess energy range 0.3—1.1 eV.

VI-B-2 Photoelectron Spectra of Acetone and Acetone Dimer

Kenji FURUYA, Shunji KATSUMATA *(Iwaki Meisei Univ.)*, **and Katsumi KIMURA**

He(I) and threshold photoelectron spectra (PES and TPES) of acetone have observed in the region 122.0—130.0 nm. A comparison of PES and TPES has clarified the contribution of autoionization in the intensity distribution of TPES. Threshold-photoelectron photoion coincidence spectra of acetone dimer have been measured in the region 124.0—135.0 nm with an interval of 0.2 nm, and the dimer intensity in each spectrum obtained has been plotted against the excitation wavelength. The plot corresponds to the TPES of non-dissociative acetone dimer. In contrast to the PES and the TPES of acetone monomer, no vibrational

structure appears in the dimer spectrum. From the dimer spectrum, the ionization potential of acetone dimer has been estimated to be 9.21 ± 0.015 eV. The two major bands observed in the dimer spectra are assigned to the two electronic states resulting from the interaction between the electronic ground states of two kinds of dimer cations, (acetone)$^+$-acetone and acetone-(acetone)$^+$.

VI-B-3 Dissociation Dynamics of $CH_4{}^{+2}A_1$ State

Yasuhiro SAKAI *(Toho Univ.)*, **Kenji FURUYA, Toshinobu TAKAYANAGI** *(Sophia Univ.)*, **and Katsumi KIMURA**

We have measured threshold-photoelectron photoion coincidence (TPEPICO) spectra of CH_4 in the region of $^2A_1$ state and some Rydberg states converging to the $^2A_1$ state (53–58 nm) by ionizing with synchrotron radiation. In all of the TPEPICO spectra observed, CH_3^+ band has a shape almost rectangular, implying that CH_4^+ dissociates isotropically and the kinetic energy distribution of CH_3^+ is very narrow. Figure 1 shows the plots of the total kinetic energy resease (KER) in the dissociation reaction $CH_4^+ \rightarrow CH_3^+ + H$ estimated from the CH_3^+ band width in the TPEPICO spectra against the excitation energy. The bars indicated in Figure 1 do not express error, but express the upper and lower limits of the KER estimated. It has been reported that the ionization potential of CH_3 is 9.84 eV, and that the dissociation energy in the reaction $CH_4 \rightarrow CH_3 + H$ is 4.41 eV. Since the total KER estimated from the present experiments is about 2–3 eV, it is expected that the CH_3^+ produced in the CH_4^+ dissociation is in a electronically excited state. The candidate is ^3E or ^1E state (in C_{3v} symmetry) from the result of a photoelectron spectrum of CH_3. The narrow distribution of the total KER implies that the CH_3^+ is in a specific vibrational state of ^3E or ^1E electronic state.

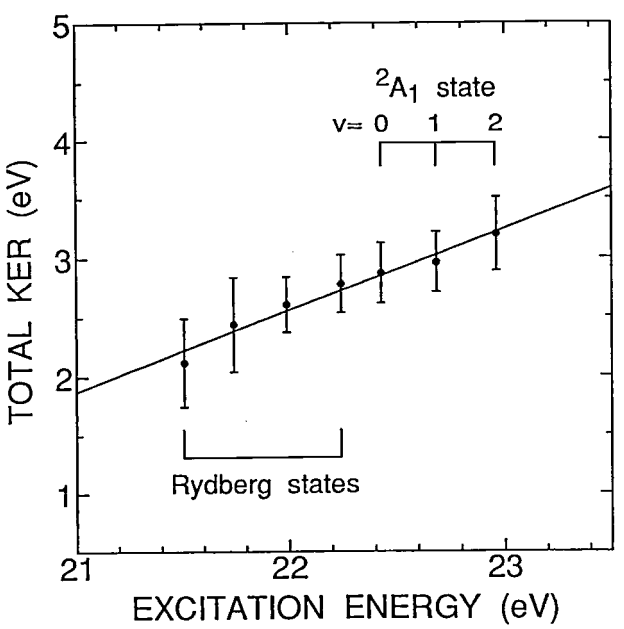

Figure 1. Plots of the total KER in the dissociation reaction $CH_4^+ \rightarrow CH_3^+ + H$ against the excitation energy. The bars express the upper and lower limits of the KER estimated.

VI-B-4 Improvement of the Photoelectron-Photoelectron Coincidence Spectrometer and the Development of a Program for Displaying the High-Resolution Three-Dimensional Spectrum

Katsuhiko OKUYAMA, Hisashi YOSHIDA, Eiken NAKAMURA, Makoto WATANABE, and Katsumi KIMURA

Recently we have obtained successful results concerning a single-photon double-photoionization process in Xe atom by means of a photoelectron-photoelectron coincidence (PEPECO) apparatus equipped with a magnetic-bottle time-of-flight (TOF) analyzer and using the monochromatic orbiting radiation from the 25-pole undulator on beamline 3A2 of UVSOR (K. Okuyama, J. H. D. Eland, and K. Kimura, *Phys. Rev.*, **A 41**, 4930 (1990)). In order to expand our field of research to molecular systems as well as investigating a double-photoionization process in greater detail, we have initiated a series of improvements on the PEPECO apparatus. Firstly, we have introduced a new rear mirror that provides a suitable focal position for our apparatus, which has made the photon density 20-times higher than previously and has increased the coincident rate. Secondly, the photoelectron flight length of the short TOF tube constructed on the opposite side of the main TOF tube has increased from 4 cm to 14 cm and a small turbo molecular pump has been introduced to pump the short TOF tube. These improvements have resulted in a significant improvement in spectral resolution. Finally, we have developed the program for displaying the high-resolution three-dimensional PEPECO spectrum. In this program a flame buffer memory for the graphic display is used as the histogram memory in the PEPECO spectrum. The development makes it possible to expand the dimension of the spectrum from 200×200×12 to 640×400×24 bits.

VI—C Molecular Beam Studies of Gas Phase and Surface Reaction Dynamics

In the present project we investigate dynamics of bimolecular reactions using a crossed molecular beams technique and also surface reaction dynamics using molecular beam-surface scattering techniques. Experimental data obtained in this project are angular and velocity distributions of the scattered species detected by a rotatory quadrupole mass spectrometer using a TOF technique as a function of reactant collision energy and, in the case of surface reactions, surface conditions such as substrate temperature, incident angle, and surface structure and coverage. We are interested in obtaining interaction energies between a molecule and a characterized surface in relation to the reactivities.

VI-C-1 Translational-Surface Vibrational Energy Transfer in the Collisions of Hyperthermal Xe with Hydrogen-Terminated Si(100) Surface

Aiichiro TSUKAHARA*, Tetsuo FUJIMOTO* *(*Nagoya Univ.)*, **Kiyohiko TABAYASHI, Mitsuhiko KONO, Haruhiko OHASHI, and Kosuke SHOBATAKE**

In order to seek the possibilities of using hyperthermal rare gas atoms to stimulate surface reactions we have studied translational-surface vibrational energy transfer processes in scattering of hyperthermal Xe atoms with hydrogen-terminated Si(100) surface. Experimentally time-of-flight (TOF) velocity distributions of Xe atoms scattered from the H-terminated Si(100) surface were measured. The hydrogen terminated Si(100) surface was prepared by a conventional method (Shiraki method). Hyperthermal Xe atom beams were produced by supersonic expansion of mixture gas of 0.5% in He and 0.3% in H_2 at varied nozzle temperatures. The nominal kinetic energies of Xe used are 1.64, 3.58, and 6.31 eV.

The incident angle of the Xe beam was kept at θ_i=75°. TOF spectra of scattered Xe atoms were measured at scattering angle θ_f=15, 22, 30, 45, 60, and 75° using a pseudo-random correlation chopper. The H-terminated Si(100) surface was kept at room temperature. For thermal atom-surface collisions it is known that the velocity component parallel to the surface does not change after scattering, especially for large incident angles. The TOF spectrum at each scattering angle was fitted to the contributions of three shifted-Maxwellian distributions. In Figure 1 the average energy for each component is plotted against θ_f. For the hyperthermal collisions, however, we find that a large fraction of the incident translational energy is lost due to energy transfer to vibrational motions of surface atoms. The energy accommodation coefficient defined as the energy remaining in the translational motion relative to the incident energy is found to be constant as 0.21 for three incident energies.

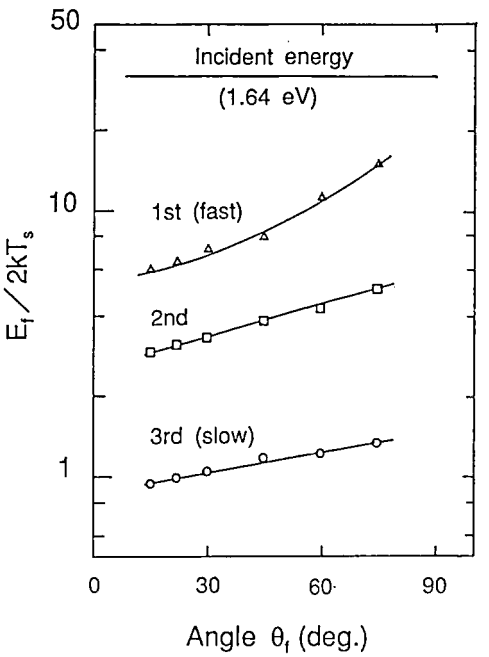

Figure 1. Translational energies of scattered Xe atoms for the first (fast), second, and third (slow) components vs. scattering angle θ_f at an incident collision energy of 1.64 eV. The energy is plotted in the units of $2kT_s$, where k is the Boltzmann constant and T_s is surface temperature kept at room temperature (298 K).

VI-C-2 Construction of a Molecular Beam-Surface Scattering Apparatus with an Electron Bombardment Ionization Mass Spectrometer Detector

Hiroshi YOSHIKAWA, Kouji ITO*, Tetsuo FUJIMOTO* *(*Nagoya Univ.)*, **Toshio HORIGOME**, Mitsukazu SUZUI**, Nobuo MIZUTANI**, Hisashi YOSHIDA**,** *(**Equipment Development Center)*, **Kiyohiko TABAYASHI, and Kosuke SHOBATAKE**

A molecular beam chemistry apparatus (MBC-II) used for crossed beams reactive scattering experiments is under modification into an ultrahigh vacuum apparatus equipped with a low energy electron diffraction (LEED) spectrometer and a rotatory mass spectrometer detector to study molecular beam-surface scattering processes and to seek possibilities of stimulated surface reactions by hyperthermal atom or molecule bombardment upon the adsorbed surfaces. Figure 1 shows a schematics of the apparatus under construction. Almost all parts are made by the in-house staff including a LEED spectrometer which was designed to fit to the chamber.

The apparatus consists of four regions; 1) a main chamber, 2) a rotatory mass spectrometer detector equipped with an electron bombardment ionizer, 3) a sample

characterization and scattering chamber, and 4) molecular beam source chambers. The scattering experiment will be carried out in the following: The hyperthermal supersonic beams of heavy atoms (i.e. Kr, Xe) and/or molecules (SF_6, CO) generated by a seeded beam technique is pulsed by a chopper disc and then goes into the sample chamber. The intensity of the molecules scattered from the well-characterized solid surface is measured as a function of scattering angle and flight time. The velocity distributions of the scattered species are measured.

In the cases of collision- or light excitation-induced surface reactions the angular and velocity distributions of the product species are measured using a time-of-flight technique. The detection of the products from synchrotron radiation stimulated surface reactions will be also attempted on this apparatus.

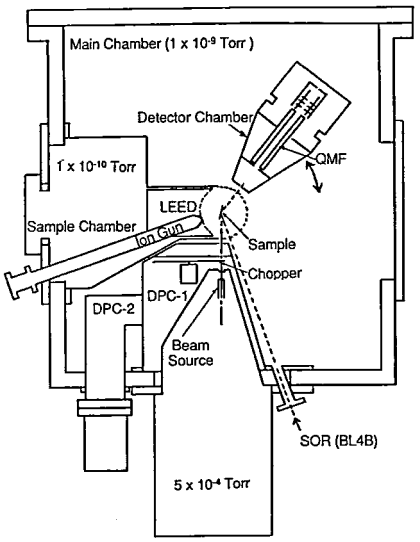

Figure 1. Schematics of a molecular beam-surface scattering apparatus equipped with a rotatory mass spectrometer detector.

VI—D Vacuum UV Photochemistry of Molecules and Clusters

In the present project we seek to obtain detailed information about, 1) photodissociation dynamics of simple molecules, 2) photodissociative excitation processes from highly excited molecules, and 3) photochemistry of excited van der Waals (vdW) molecules and clusters formed in a supersonic expansion. The techniques applied are absorption and fluorescence spectroscopies of gaseous molecules and vdW molecules on an apparatus constructed on the beam line BL2A of UVSOR facility. In particular we use fluorescence excitation, fluorescence polarization, and dispersed fluorescence spectroscopies to identify product species and obtain information on the dynamics of photochemical reactions.

VI-D-1 Photo-induced Processes of Cl_2 ($1^1\Sigma_u^+$) State Studied by VUV/UV-fluorescence Life-time Measurements.

Kiyohiko TABAYASHI, Mitsuhiko KONO, Atsunari HIRAYA *(UVSOR)*, **and Kosuke SHOBATAKE**

Photo-induced processes of excited Cl_2 in the presence of rare gas third atoms are of fundamental importance in connection with the studies on the excited state dynamics of Rg-Cl_2 van der Waals molecules. Here, VUV excitation light pulse with time duration of ca. 400 psec and high repetition rate of 90.1 MHz (multi-bunch operation of UVSOR) was successfully used for the time resolved fluorescence measurement of Cl_2/Rg in a gas cell.

A sample time-decay curve of the fluorescence intensity from Cl_2 ($1^1\Sigma_u^+$) and that of excitation light pulse are shown in Figure 1. Fluorescence of bound-free transition of Cl_2 ($1^1\Sigma_u^+$–$X^1\Sigma_g^+$) was collected in the region $180 < \lambda_{obs} < 200$ nm via VUV monochromator and detected with a multichannel plate detector. With excitation to vibronic state ($1^1\Sigma_u^+$, $31 < v' < 41$) under the single collision condition, a fast decay less than ~3 nsec was obtained by a simple deconvolution analysis. Relaxation to an intermediate $2^3\Pi_g$ fluorescent state is also directly measured by the present technique. These observations may assure a wide application of time-resolved measurements to the studies of photo-induced processes involving collisional reaction as well as inter- and intra-molecular energy transfer using SOR light source.

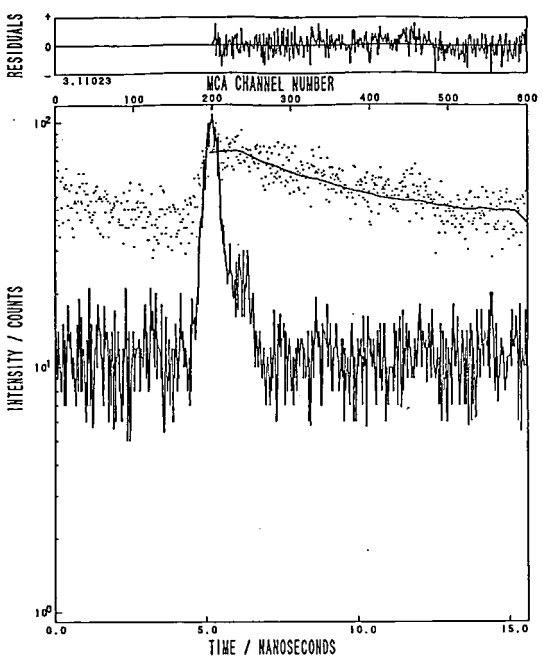

Figure 1. Time-decay curve of the Cl_2 ($1^1\Sigma_u^+$–$X^1\Sigma_g^+$) fluorescence with excitation at 1355 Å (upper trace) and excitation pulse response observed from scattered light (lower trace).

VI-D-2 Construction of a High Temperature Gas Cell for Absorption Spectral Measurements in the Vacuum UV Region

Hisato YASUMATSU*, Tamotsu KONDOW* *(Univ. of Tokyo)*, **Kaoru SUZUKI** *(Dept. of Electronic Structure)*, **Kiyohiko TABAYASHI, and Kosuke SHOBATAKE**

An absorption gas cell which can be operated at temperatures up to 750 °C has been constructed to measure absorption spectra in the vacuum UV region. The cell has been designed such that a) the gas cell itself is windowless and yet b) the effusive loss of solid samples from the sample reservoir can be minimized. The cell is made of stainless steel and has two well aligned channels (2 mm øX33 mm long each) at both ends of the gas reservoir (36 mm ø IDX60 mm long). The two channels and the gas reservoir were independently heated with sheath heaters and they were radiation-shielded with layers of thin stainless sheets in order to minimize a heat loss. The whole gas assemblies are held and suspended with stainless steel frame inside a vacuum chamber pumped by a 5000 *l*/s diffusion pump (Varian VHS-10).

The samples used were alkali cyanide compounds (NaCN, KCN, and CsCN). The transparent light intensity was measured using a light converter of sodium salicylate coating on the inner side of guartz window and with a photomultiplier tube (Hamamatsu R585). Due to the black body radiation from the gas cell, was observed a constant back ground light intensity which is independent of wavelength of the incident light. For example, we have measured the absorption spectrum of NaCN vapor at a cell temperature of 675°C. On top of broad bands peaked at 1135, 1255, and 1560 Å, one finds sharp bands due to CO gas in the cell, which is outgased from the cell body.

VI-D-3 Fluorescence Polarization Measurements of CN(B → X) Formed in the Photodissociative Excitation Process of ClCN

Mitsuhiko KONO, Kiyohiko TABAYASHI, and Kosuke SHOBATAKE

Photodissociative excitation process of ClCN forming $CN(B^2\Sigma^+)$ fragments in the wavelength region from 110 to 150 nm was studied using synchrotron radiation as a polarized light source. Figure 1 shows $CN(B^2\Sigma^+ \rightarrow X^2\Sigma^+)$ fluorescence spectra observed for polarized fluorescence parallel ($\mathbf{I}_\parallel$) and perpendicular ($\mathbf{I}_\perp$) to polarization vector of the incident light ranging from 108 nm to 130 nm. The degree of polarization calculated from the two intensities, $P=(I_\parallel-I_\perp)/(I_\parallel+I_\perp)$, is plotted against exciting light wavelength. The resolution of the incident light is 3.0 Å and the ClCN pressure was 20 mTorr. One finds that a) the degree of polarization is larger than 0.1 above 111 nm and b) there are undulatory structures around 116 nm and in the region from 120 to 126 nm. Compared with photodissociative excitation process of HCN and DCN molecules, the dissociation seems to proceed via very short-lived intermediates states, especially in the 117–130 nm region.

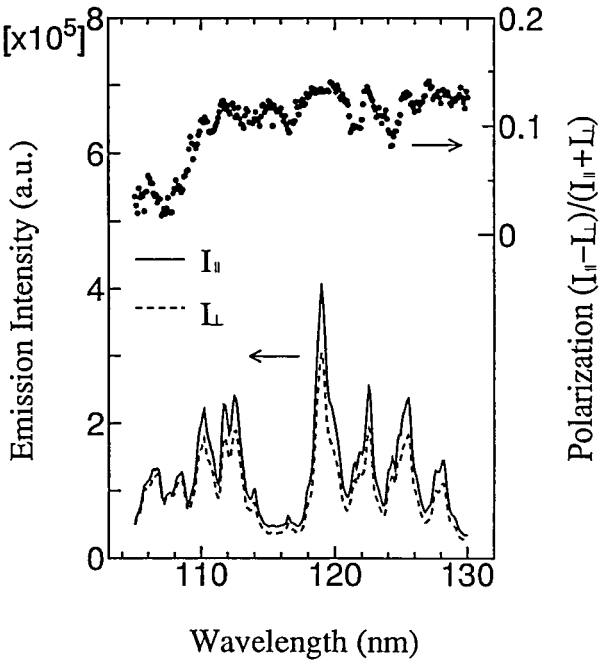

Figure 1. $CN(B^2\Sigma^+ \rightarrow X^2\Sigma^+)$ fluorescence excitation spectra observed for polarized fluorescence parallel ($\mathbf{I}_\parallel$) and perpendicular ($\mathbf{I}_\perp$) to polarization vector of the incident light ranging from 108 nm to 130 nm. The degree of polarization calculated from the two intensities, $P=(I_\parallel-I)/(I_\parallel+I_\perp)$, is plotted against exciting light wavelength. The resolution of the incident light is 3.0 Å and the ClCN pressure was 20 mTorr. Note that fluorescence intensities are not normalized to the incident light intensity.

VI-D-4 Vacuum Ultraviolet Absorption Spectra and Photodissociative Excitation of $CHBr_2Cl$ and $CHBrCl_2$

Toshio IBUKI *(Kyoto Univ. of Education)*, **Atsunari HIRAYA** *(UVSOR)*, **and Kosuke SHOBATAKE**

[*J. Chem. Phys.*, **96**, 8793 (1992)]

Photoabsorption and fluorescence excitation spectra of $CHBr_2Cl$ and $CHBrCl_2$ trihalomethanes were measured in the 106–200 nm region using synchrotron radiation as a light source. Main photoabsorption bands observed are assigned as the Rydberg transitions of the outer shell orbitals. In the photoexcitation of $CHBr_2Cl$ a diffuse emission band of $CHCl(\tilde{A}^1A'' \rightarrow \tilde{X}^1A')$ was observed in the 500–800 nm region. The radiative lifetime of the $CHCl(\tilde{A}^1A'')$ state was first determined to be 7.01 ± 0.25 μs. In the photolysis of $CHBrCl_2$ at 121.6 nm, the formation of CHCl $(\tilde{A}^1A'')$ and CCl_2 $(\tilde{A}^1B_1)$ radicals were observed. The fluorescence thresholds for $CHBr_2Cl$ and $CHBrCl_2$ start at 162 and 159 nm with the maximum yields of 5% and 11% at 122 and 119 nm, respectively.

VI—E Surface Molecular Dynamics Sensitive to the Structure of Reaction Sites

The structure of reaction sites is essential information for designing new functional catalyst surfaces. This should be analyzed through dynamic properties of surface processes, since it is not provided by structural information of non-reacting surface species. The spatial and velocity distribution of desorbing product molecules open new reaction dynamics sensitive to the structure. The spatial distribution depends on (a) the reactant density around the reaction site, (b) the arrangement of substrate atoms consisting the reaction site, and (c) the orientation. The velocity distribution is more sensitive to the site structure. We have succeeded in constructing a new apparatus for measurements of time-of-flight spectra of desorbing molecules during thermal desorption procedures. This method has advantages compared with molecular beam scattering technique, since it can be applied to a wide range of reactant coverages.

VI-E-1 Anisotropic Velocity Distribution of Desorbing Product in Carbon Monoxide Oxidation on Palladium (110)

Tatsuo MATSUSHIMA* *(*Hokkaido Univ.)*, **Kosuke SHOBATAKE, Yuichi OHNO, and Kiyohiko TABAYASHI**

[*J. Chem. Phys.*, **97**, 2783 (1992)]

A significant anisotropy was found in the velocity distributions of desorbing product CO_2 from Pd (110) surfaces. The velocity was measured by a cross-correlation time-of-flight technique combined with angle-resolved thermal desorption. Heating the coadlayer of CO with oxygen produces five peaks in the CO_2 formation spectrum; P_1- (around 420 K), P_2- (around 370 K), P_3- (around 300 K), P_4- (around 230 K), and P_5- (around 170 K). The translational temperature of each CO_2 is much higher than the corresponding surface temperature, and increases in the sequence of P_1-<P_2-<P_3-<P_4-<P_5-CO_2. It decreases rapidly with an increase in the desorption angle perpendicular to the surface trough and more slowly parallel to it. This anisotropy is correlated to the reaction site symmetry.

VI-E-2 Reaction Diagram of Carbon Monoxide and Oxygen on Palladium (100) and Angular Distribution of Reactive Carbon Dioxide Desorption

Yuichi OHNO, Tatsuo MATSUSHIMA* *(*Hokkaido Univ.)*, **Kosuke SHOBATAKE, and Hisakazu NOZOYE**** *(**Natl. Chem. Lab for Industry)*

[*Surf. Sci.*, **273**, 291 (1992)]

The co-adsorption structures of CO and oxygen on Pd(100) and the angular distribution of reactive CO_2 desorption were studied with angle resolved thermal desorption and low-energy electron diffraction. The CO_2 formation induced by heating the co-adlayer was extended to lower temperatures with an increase in the coverages, yielding five peaks; P_1- (~400 K), P_2-(~350 K), P_3- (~290 K), P_4- (~240 K), and P_5- (~150 K). A reaction diagram was constructed from the threshold coverages determined by the appearance of each CO_2 peak and the variation of LEED spot intensity. Each zone in the diagram is characteristic of separate domains of CO and oxygen, and different angular distribution of reactive CO_2 desorption.

VI—F Synchrotron Radiation Stimulated Surface Reactions

Study of synchrotron radiation (SR) stimulated surface reactions is a promising topic in fundamental science, because dynamical processes induced by the photostimulated core-electron excitations on surfaces are scarecely explored so far. This field is important also in applied science, since the fundamental study is expected to develop the new techniques for semiconductor processing such as SR stimulated etching and SR stimulated epitaxial growth.

VI-F-1 Fundamental Processes and Reaction Dynamics in Synchrotron Radiation Stimulated Semiconductor Processing

Tsuneo URISU, Haruhiko OHASHI, Kazuhiko MASE, and Kosuke SHOBATAKE

The aim of the present project is to clarify the detailed mechanism of the fundamental processes and the dynamics involved in SR stimulated semiconductor processing such as photoetching and photochemical epitaxial growth. To explore various problems in this field, we are now constructing a new apparatus consisting of five chambers: a sample loadlock chamber, a sample exchange chamber, a SR stimulated etching chamber, a SR-stimulated eptaxial growth chamber, and an analyser chamber. The sample such as Si(111) or Ge(111) surface is transfered from the atmosphere into ultra-high vacuum (UHV) via the loadlock chamber. Then, the surface is cleaned by heating and characterized by low-energy electron diffraction (LEED) in the sample exchange chamber. The cleaned sample is transfered to the etching chamber or the epitaxial growth chamber, where SR stimulated etching or SR stimulated epitaxial growth is carried out, respectively. The etching gasses such as Cl_2 or F_2, and epitaxial gases such as SiH_4, Si_2H_6, or GeH_4 are supplied from reactive gas supply systems. After the SR stimulated reaction, the sample is transfered into the analyser chamber and analyzed by the X-ray photoemission spectrometer. Developing in-situ and real-time measurement techniques for monitoring these reactions is also an important target of this project. The mechanism of the fundamental processes and the dynamics involved in SR stimulated reactions will be discussed on the basis of these observed data.

VI-F-2 Development of New Techniques for Synchrotron Radiation Stimulated Desorption

Kazuhiko MASE, Tsuneo URISU, Haruhiko OHASHI, and Kosuke SHOBATAKE

Desorption induced by electronic excitations has developed into an attractive topic in the field of surface science, as well as molecular physics, photochemistry, and surface technology, because it is one of the most fundamental dynamical processes on surfaces. SR stimulated desorption, however, were less investigated, because the brightness is much less than other photon sources such as laser. To clarify the mechanism of SR stimulated desorption, we started a project to develop a new device for the detection of the neutral molecules from surface. The apparatus under consideration is an UHV chamber equipped with a SR inlet port, sample manipulation system, sample cleaning system, LEED, gas inlet line, UV laser inlet and outlet windows, and time-of-flight (TOF) ion detection system. The neutral molecules desorbed from the surface is ionized by the focussed UV laser via multiphoton ionization processes. The ions are mass-selected and detected by the TOF system.

VI-F-3 Mechanisms of Synchrotron Radiation-Excited Etching Reactions of Semiconductor Materials

Haruhiko OHASHI, Akira YOSHIDA, Kiyohiko TABAYASHI, and Kosuke SHOBATAKE

[*Appl. Surf. Sci.*, in press]

Synchrotron radiation-excited etching of semiconductor materials including SiO_2 and SiC is studied to clarify the mechanisms of the etching processes. Synchrotron radiation (SR) was shone upon SiO_2 and SiC surfaces in the SF_6 atmosphere. The etch rates against SF_6 pressure and the cross sectional profiles of the etched surface were measured. From the results obtained it has been concluded that excitation of surface by SR is essential and is the rate-determining step when the etchant pressure is high enough. We have proposed a simple reaction model that the excitation of the outermost layer is essential in the SR-excited etching of insulator surface.

VI—G Study of Ion-Pair Formation in the Vacuum Ultraviolet Region Using Synchrotron Radiation

Ion-pair formation is a very common process in photoexcitation of molecules in the photon energy range of 10—50 eV in spite of the minor fraction of the oscillator strength in photoabsorption. We have demonstrated that the detection of the counterpart negative ions using synchrotron radiation is a sensitive probe to investigate the properties of Rydberg states lying in the vacuum ultraviolet. Here, measurements of the negative-ion efficiency curve for hydrocarbons are reported. Superexcited Rydberg states are discussed in terms of their spectroscopy and dynamics in predissociation.

VI-G-1 Ion-Pair Formation in Acetylene

Hideo HATTORI, Hiroaki YOSHIDA, Koichiro MITSUKE, Shinzo SUZUKI *(Tokyo Met. Univ.)*, **Takashi IMAMURA** *(Natl. Inst. Environ. Studies)*, **and Inosuke KOYANO** *(Himeji Inst. of Tech.)*

We have measured the photodissociation efficiency curve for negative ions produced from Acetylene and Ethylene on the beamline BL3B in the UVSOR facility. We detect C_2H^- and H^- produced from C_2H_2. In the case of C_2H^-[Figure 1(a)], the spectral features in 650—700 Å result from predissociation of the Rydberg states $2\sigma_u \rightarrow ns\sigma_g$, $nd\sigma_g$, and $nd\pi_g$. The C_2H^- efficiency decreases promptly with the decrease of the wavelength λ below 630 Å. In contrast, the efficiency curve of H^- in Figure 1(b) has a broad maximum at $\lambda \sim 580$ Å. It is likely that the Rydberg states $2\sigma_g \rightarrow np\sigma_u {}^1\Sigma_u$ and $2\sigma_g \rightarrow np\pi_u {}^1\Pi_u$ existing below 600 Å predissociate more preferentially into H^- than into C_2H^-.

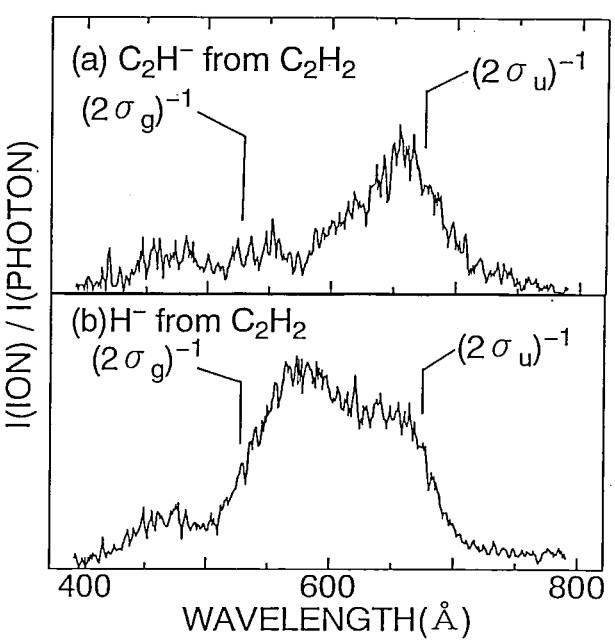

Figure 1. Photodissociation efficiency curves of (a) C_2H^- and (b) H^- produced from C_2H_2 taken at a wavelength resolution (FWHM) of 0.8 Å and wavelength intervals of 1 Å. The vertical ionization potentials for the $(2\sigma_u)^{-1}$ and $(2\sigma_g)^{-1}$ states of $C_2H_2^+$ are indicated.

VI-G-2 Ion-Pair Formation in Ethane

Hideo HATTORI, Hiroaki YOSHIDA, Koichiro MITSUKE, Shinzo SUZUKI *(Tokyo Met. Univ.)*, **Takashi IMAMURA** *(Natl. Inst. Environ. Studies)*, **and Inosuke KOYANO** *(Himeji Inst. of Tech.)*

Figure 1 shows the photodissociation efficiency curve of H^- produced from C_2H_6. Peaks in the region of 630–670 Å are assigned to the s-type Rydberg states converging to the $\tilde{C}^2A_{2u}$ state of $C_2H_6^+$. These transitions are accompanied by vibrational excitations in the C-H stretching mode, ν_1, and the C-C stretching mode, ν_3. The average spacings of the ν_1 and ν_3 progressions are respectively smaller and larger for the Rydberg states than for the electronic ground state of C_2H_6. This result suggests that the $2a_{2u}$ orbital may have the C-H bonding and C-C anti-bonding character. The broad peak at ~580 Å is considered to be attributed to the Rydberg state $2a_{1g} \rightarrow 3p$ converging to the $\tilde{D}^2A_{1g}$ state of $C_2H_6^+$ (vertical ionization potential=23.6 eV).

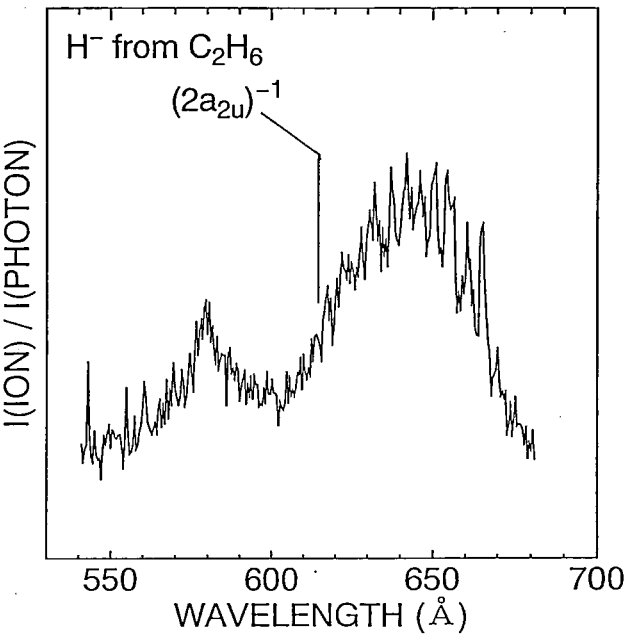

Figure 1. Photodissociation efficiency curve of H^- produced from C_2H_6 taken at a wavelength resolution (FWHM) of 0.8 Å and wavelength intervals of 0.5 Å. The vertical ionization potential for the $(2a_{2u})^{-1}$ state of $C_2H_6^+$ is indicated.

VI—H Positive Ion-Negative Ion Coincidence Spectroscopy Using Synchrotron Radiation

A new coincidence technique is developed for studying the ion-pair formation processes in the vacuum ultraviolet using synchrotron radiation. This technique utilizes the flight-time correlation of a pair of positive and negative ions produced by single photon excitation. The performance of our time-of-flight mass spectrometers is examined by observing ion pairs produced from homonuclear diatomic molecules: O^+ and O^- from O_2 and H^+ and H^- from H_2. We present here the basic design of the apparatus and the principles of operation.

VI-H-1 Positive Ion-Negative Ion Coincidence Spectroscopy —I— Experimental Technique

Koichiro MITSUKE, Hiroaki YOSHIDA, and Hideo HATTORI

[*Z. Phys.*, submitted]

Experiments are made by using synchrotron radiation emitted from beam line BL2B2 installed in the UVSOR storage ring. Figure 1 shows the schematic diagram of the time-of-flight mass spectrometer (TOFMS) and the data acquisition system. A sample gas is expanded into a beam expansion chamber from a nozzle of 100-μm diameter at temperature of 298±3 K and the stagnation pressure of 25 torr. The molecular beam is introduced through a conical skimmer into a photoionization chamber pumped to 10^{-6} torr when the beam is on. The molecular beam intersects at 90° with a monochromatized VUV photon beam at the photoexcitation region. We use a 1-m Seya-Namioka monochromator with a Pt-coated 2400-lines/mm grating (a blaze wavelength of 96 nm). The wavelength resolution is estimated to be 0.8 Å (FWHM) when both the entrance and exit slits are set to be 150 μm wide. Produced ions are accelerated by an electrostatic field applied in the perpendicular direction to axes of both molecular beam and photon beam. Positive ions are mass-separated by a single-field type of TOFMS, while negative ions by a double-field type. The positive-ion signal is fed into the start input of a time-to-amplitude converter and the negative-ion signal into the stop input. Flight-time difference thus obtained is accumulated in a multichannel analyzer. Upon detection of a positive ion, a gate pulse voltage is applied to grid G2 to prevent electrons from penetrating the flight tube beyond G2. Application of this gate pulse is found to be essential to attain high signal-to-noise ratio.

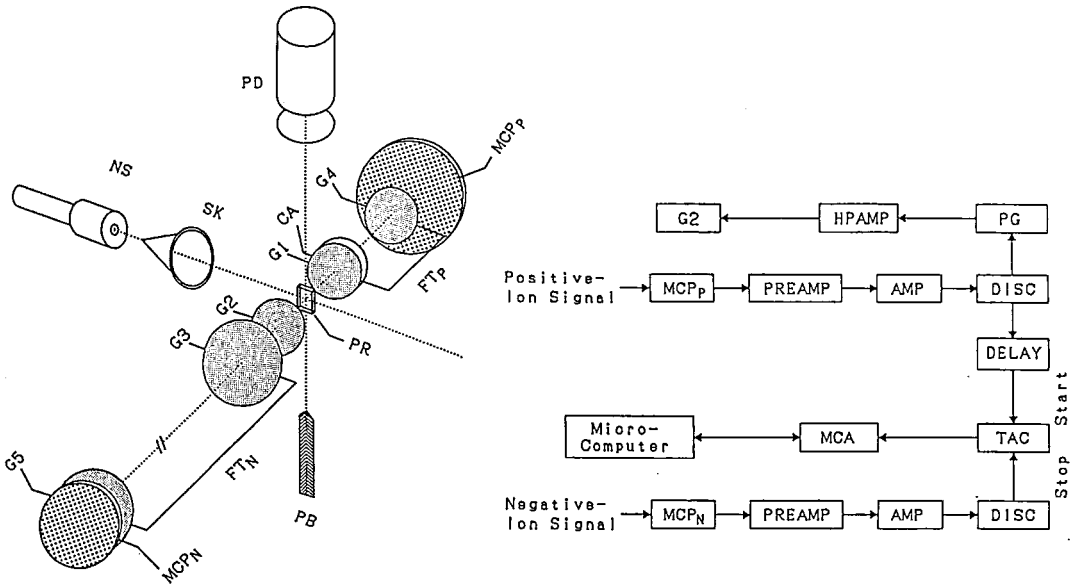

Figure 1. Schematic diagram of the time-of-flight mass spectrometers and data acquisition system for coincidence spectroscopy. (NS) nozzle source; (SK) conical skimmer; (PR) photoexcitation region; (PB) monochromatized photon beam; (PD) photon detector; (G1-G5) grids; (CA) capillary array plate; (FT_P) flight tube for positive ions; (FT_N) flight tube for negative ions; (MCP_P) microchannel plates for positive-ion detection; (MCP_N) microchannel plates for negative-ion detection; (PREAMP) pre-amplifier; (AMP) main-amplifier; (DISC) discriminator; (TAC) time-to-amplitude converter; (DELAY) delay circuit; (MCA) multichannel analyzer; (PG) pulse generator; (HPAMP) high-speed power amplifier.

VI-H-2 Positive Ion-Negative Ion Coincidence Spectroscopy —II— Ion-Pair Formation from O_2

Hiroaki YOSHIDA, Koichiro MITSUKE, and Hideo HATTORI

Figure 1 shows a coincidence spectrum of O^+ and O^- produced from O_2 at the photon wavelength of 709.5 Å (photon energy $E_{h\nu}$=17.47 eV). This energy is 0.2 eV distant from the threshold at 17.27 eV (717.8 Å) for the lowest ion-pair formation channel,

$$O_2(^3\Sigma_g^-) + h\nu \rightarrow O^+(^4S_u) + O^-(^2P_u).$$

The background count is ascribed to the false coincidence signals, mainly arising from the start input of O_2^+ ions and the stop input of electrons. The sharp peak observed at 14.2 μs is assigned to the coincidence peak due to the ion pair produced by a single photoexcitation event. This assignment is supported by the following corroborating evidence. First, we measure the flight times for O^+ and O^- separately from photoexcitation region to the detectors by applying a pulse voltage to grid G2: 3.8±0.3 μs for O^+ and 18.2±0.2 μs for O^-. The flight-time difference is estimated to be 14.4±0.5 μs, which is in good agreement with the position of the coincidence peak in Figure 1. Second, we get the photodissociation efficiency curve for the ion-pair formation process by scanning the photon wavelength. This curve can be compared with the efficiency curve of O^- measured by using molecular-beam photoionization apparatus on the beam line BL3B in the UVSOR facility. Several structures are commonly observed in the two curves.

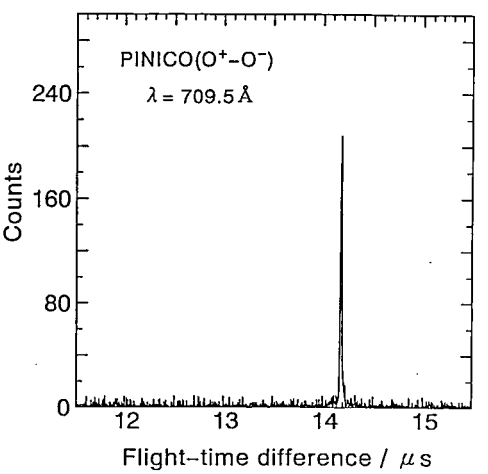

Figure 1. Coincidence spectrum of O^+ and O^- produced from O_2 measured at the photon wavelength of 709.5 Å.

VI—I Transition-State Spectroscopy by Photodetachment of Solvated Cluster Anions

Photodetachment spectroscopy of negative triatomic ions have been used by Neumark and coworkers to investigate the transition-state region of the corresponding neutrals in H-atom exchange reactions, X+HX → XH+X (X=Cl, Br, and I). In this project, we attempt to develop this methodology for photodetachment process of solvated cluster anions for the purpose of probing the transition-state region of chemical reactions in solution. Construction of the apparatus is nearing completion. We obtain time-of-flight (TOF) mass spectra of negative cluster ions and preliminary data of their photodetachment spectra.

VI-I-1 Mass Spectrometry of Positive and Negative Cluster Ions Using Beam-Modulated Time-of-Flight Method

Koichiro MITSUKE

Cluster ions are produced by electron impact on the gas jet just outside the nozzle and are mass-selected with a beam-modulated TOF mass spectrometer. Figure 1 shows TOF mass spectra of positive ions produced from CO_2 clusters and negative ions from N_2O clusters. In the latter spectrum, a series of $O^-(N_2O)_n$ are observed in addition to O^- and NO^-. Photoelectron spectrum of $O^-(N_2O)_n$ can be measured by synchronizing irradiation of a Nd:YAG laser with a pulsed voltage applied to the beam modulator.

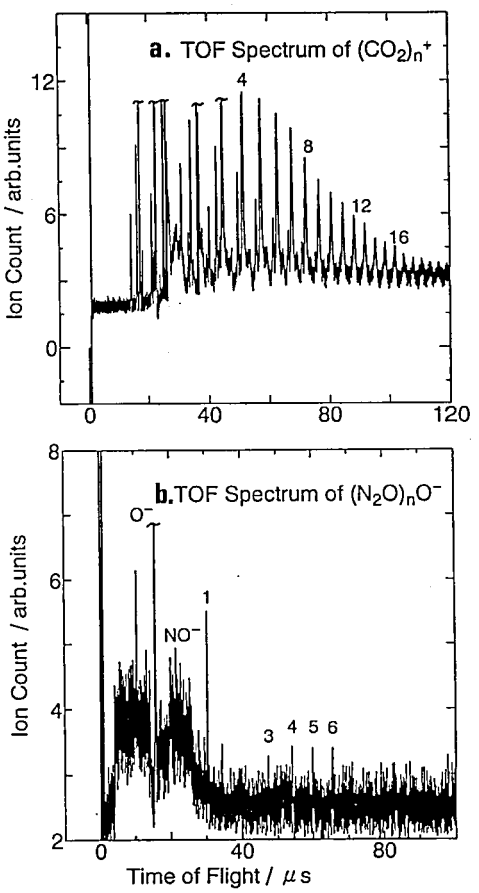

Figure 1. TOF mass spectra of (a) positive ions produced from CO_2 clusters and (b) negative ions from N_2O clusters.

VI—J Preparation and Characterization of Semiconductor Thin Films by New Excitation Processes

Crystalline and amorphous semiconductor thin films of high quality, especially prepared at low temperatures, are essential for the development of VLSI (Very Large-scale Integration) and new functional devices in the near future. Synchrotron radiation-assisted, plasma-activated, photo-excited CVD (Chemical Vapor Deposition) and fine fabrication processes are believed to be powerful in this field. We have been developing new semiconducting thin films and new devices by these excitation methods.

VI-J-1 Vacuum-ultraviolet-light-induced Defects in Hydrogenated Amorphous Silicon Films

Yoji SAITO* and Akira YOSHIDA *(*Toyohashi Univ. of Tech.)*

[*Philos. Mag. B*, **66**, 219 (1992)]

Hydrogenated amorphous silicon films are rapidly degraded by irradiation with vacuum-ultraviolet light from a synchrotron, as shown in Figure 1. The main light-induced defects are silicon dangling bonds as deduced from measurements of electron spin resonance. Defects creation is due to bond breaking of silicon-silicon bonds by excited electrons having a high energy. The value of the required activation energy (about 1 eV) has been obtained by studying the process of defect decay during thermal annealing.

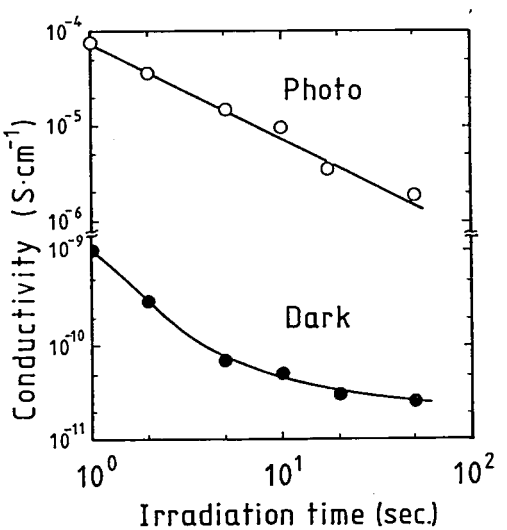

Figure 1. Photo- and dark-conductivity of a-Si:H film as a function of irradiation time.

VI-J-2 Optical Transitions in RF Sputtered $CuIn_xGa_{1-x}Se_2$ Thin Films

Toshiyuki YAMAGUCHI*, Jiro MATSUFUSA, and Akira YOSHIDA** *(*Wakayama College of Tech., **Toyohashi Univ. of Tech.)*

[*Jpn. J. Appl. Phys.*, **31**, L703 (1992)]

Thin films of $CuIn_xGa_{1-x}Se_2$ were produced over the entire range of $0<x<1$ by rf sputtering. The optical absorption coefficients of the $CuIn_xGa_{1-x}Se_2$ thin films were determined from the measured transmittance and reflectance in the wavelength range of 400 to 2000 nm. The optical absorption spectra for sputtered $CuIn_xGa_{1-x}Se_2$ thin films ($x \neq 0$) show three energy gaps, which are attributed to the fundamental edge, and band splitting by crystal-field and spin-orbit splitting, respectively. The primary transition energies exhibit bowing behavior expressed by the relationship $Eg=1.674-0.803X+0.130X^2$. The second and third energies are 0.06–0.08 eV and 0.22–0.27 eV above the primary transition energies, respectively.

VI-J-3 Thin Films of $CuInSe_2$ Prepared by RF Sputtering from Various Compositional Powder Targets

Toshiyuki YAMAGUCHI*, Jiro MATSUFUSA, and Akira YOSHIDA** *(*Wakayama College of Tech., **Toyohashi Univ. of Tech.)*

[*Solar Energy Mat.*, **27**, 25 (1992)]

$CuInSe_2$ thin films were prepared in the temperature range of 300–500°C by RF sputtering from powder targets, which were previously synthesized by reacting Cu, In, and Se in various ratios. The peaks from X-ray diffraction analyses were assigned to the planes of the $CuInSe_2$ chalcopyrite structure. The full width at half maximum of the (112) diffraction peak decreased with an increase in Cu/In ratio in the thin films. The photoelectron energies of the prepared thin films agreed with those reported for single crystalline $CuInSe_2$ from X-ray photoelectron spectroscopy measurements. The electronic conduction type and optical properties were found to change according to the Cu/In ratio in the thin films.

VI-J-4 Effect of Ar Laser-illumination upon ZnTe Growth in Atmospheric-pressure MOVPE

Mitsuhiro NISHIO*, Hiroshi OGAWA*, and Akira YOSHIDA *(*Saga Univ.)*

[*J. Cryst. Growth*, **115**, 284 (1991)]

ZnTe growth has been investigated, using (100), (110) and (111) Zn and Te substrates, by Ar^+-ion laser-assisted metalorganic vapor phase epitaxy at atmospheric pressure. For the (100)-oriented substrate, the growth rate of the epitaxial layer is dramatically enhanced under illumination. The quantum yield for forming ZnTe molecules by photons is calculated to be as high as about 3%. From the relationship between the transport rate of source material and the growth rate, it has been concluded that both the diethyltelluride and the dimethylzinc which are used as source materials become decomposed by illumination. On the other hand, for other substrate orientations, the effect of illumination upon the growth rate has been hardly observed. Hence, source gas molecules are effectively decomposed on the (100) surface under illumination. Epitaxial layers of good quality can be obtained at low substrate temperature by using the (100) substrate.

VI-J-5 Chemical Etching of Indium Nitride

Q.X. GUO*, Osamu KATO*, and Akira YOSHIDA *(*Toyohashi Univ. of Tech.)*

[*J. Electrochem. Soc.*, **139**, 2008 (1992)]

Indium nitride epitaxial layers were grown by microwave- excited metalorganic vapor phase epitaxy. Acid solutions are inappropriate for etching the surface of indium nitride, but alkaline etchants, such as aqueous KOH and NaOH solutions, give controllable etching rates. Smooth surfaces free from etch pits are thereby obtained. The temperature dependence of the etching rate is shown in Figure 1.

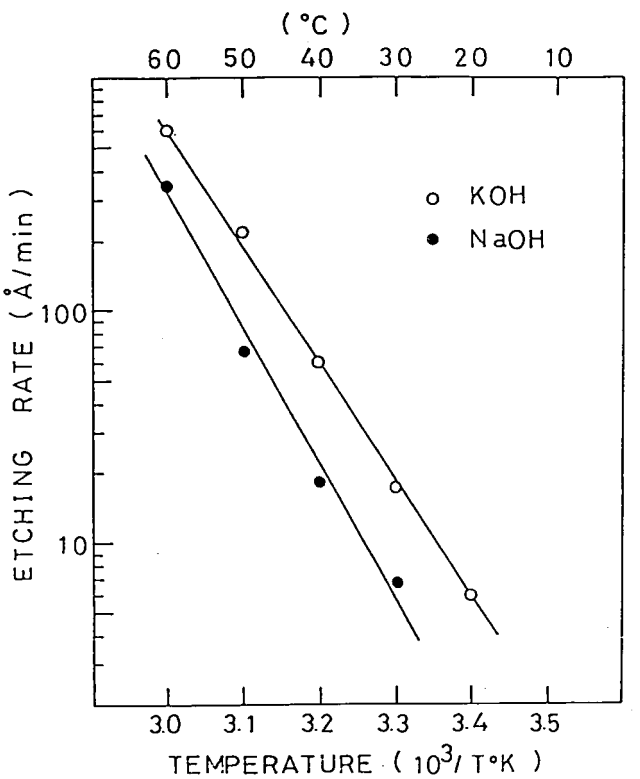

Figure 1. Temperature dependence of the etching rate

VI-J-6 Anisotropic and Damageless Etching of Single-crystalline Silicon Using Chlorine Trifluoride Molecular Beam

Yoji SAITO*, Masahiro HIRABARU*, and Akira YOSHIDA *(*Toyohashi Univ. of Tech.)*

[*J. Vac. Sci. Technol. B*, **10**, 175 (1992)]

At room temperature, anisotropic etching of both (100) and (111) oriented single-crystalline silicon substrates is successfully achieved, using a thermally excited ClF_3

molecular beam. The morphology of the etched surface is better than that using Cl_2. The etching rate is more than 50 A/min, and the ratio of etching rate of vertical direction to that of horizontal direction is more than eight. Process-induced damage in the metal-oxide-semiconductor device was not observed from the capacitance-voltage characteristic measurements.

VI-J-7 Plasmaless Etching of Silicon Using Chlorine Trifluoride

Yoji SAITO*, Osamu YAMAOKA*, and Akira YOSHIDA *(*Toyohashi Univ. of Tech.)*

[*J. Vac. Sci. Technol. B*, **9**, 2503 (1991)]

Silicon etching using ClF_3 gas has been carried out at various substrate temperatures from −20 to 120°C. The etching properties (etch rate, pressure effect, and surface morphology) depend remarkably on the temperature. Based on the mass spectroscopic measurements, SiF_4 is specified as a main product. The minor product SiF_2 is also found, and the ratio of the signal intensity of SiF_2 to that of SiF_4 decreases with temperature. From Auger electron analyses on the etched surface, the density of fluorine atoms on the surface decreases with increasing the temperature. It is concluded that the density of the fluorosilyl species greatly influences the etching reaction process.

VI—K Photochemistry of Organometallic Complexes Adsorbed on Solid Surfaces

Photochemistry of organometallic complexes adsorbed on solid surfaces has received increasing attention in recent years. The driving force behind this stems from its potential use in catalysis and microelectronics. Interest in the surface photochemistry also arises from the fact that its products are often quite different from those observed in gas phase or in liquid solution. We have studied the surface-chemistry and the photochemistry of metal carbonyls adsorbed on metal oxide powders and metals to investigate catalytic effects of the surface on a photochemical secondary process using infrared, X-ray photoelectron, and Auger electron spectroscopy.

VI-K-1 Spectroscopic Studies on Adsorption States of Iron Pentacarbonyl Adsorbed on Titanium Dioxide

Yuji UKISU, Shinri SATO, and Tadayoshi OHMORI

[*J. Molecular Catal.*, **78**, 287 (1993)]

Adsorption states and reactivity of $Fe(CO)_5$ adsorbed on TiO_2 (anatase) have been studied by FT-IR and UV-Visible diffuse reflectance spectroscopy. When the TiO_2 sample with a large surface area (50 m^2g^{-1}) is outgassed at temperatures above 373 K, adsorbed $Fe(CO)_5$ exhibits a marked increase in adsorption amount, a significant red-shift of IR bands in the C-O stretching region, and a new absorption band in the visible region. These phenomena are no longer observed on the TiO_2 sample oxidized in O_2 at 673 K followed by outgassing at room temperature. The surface of TiO_2 thus provides a different kind of adsorption sites for $Fe(CO)_5$ depending on its oxidation states. When the adsorbed $Fe(CO)_5$ on TiO_2 is exposed to NO, a substitution reaction of the carbonyl ligands with NO readily occurs at room temperature, whereas no such reaction takes place on silica and alumina. These results are discussed in terms of the electronic interaction between adsorbed $Fe(CO)_5$ and electron-donating sites of substrate.

VI-K-2 Mechanism of the Photolysis of Iron Pentacarbonyl Adsorbed on a Pt Surface

Shinri SATO and Yuji UKISU

[*Surf. Sci.*, in press]

Photolysis of $Fe(CO)_5$ adsorbed on a Pt surface was investigated by IR reflection absorption spectroscopy (IRAS), temperature-programmed desorption (TPD) technique, and X-ray photoelectron spectroscopy (XPS). Although no photoproducts are detected by IRAS, TPD and XPS spectra show that partly decarbonylated species is formed by irradiation and its Fe/CO ratio is approximately 1:4. Because IRAS is selectively sensitive to vibrational modes perpendicular to a metal surface, these results indicate formation of $Fe(CO)_4$ as an intermediate species with a square planar structure parallel to the surface. The intermediate $Fe(CO)_4$ species decomposes completely with rise in temperature up to 300 K. Such instability of the intermediate is responsible for the absence of $Fe_2(CO)_9$ or $Fe_3(CO)_{12}$ produced typically by the $Fe(CO)_5$ photolysis over insulator surfaces, in the gas or liquid phase, or in low temperature matrices.

VI-K-3 Photochemistry of Nickel Tetracarbonyl Adsorbed on Silica

Tadayoshi OHMORI, Yuji UKISU, and Shinri SATO

Photolysis of $Ni(CO)_4$ adsorbed on silica was investigated by IR spectroscopy. The photolysis was found to occur efficiently under IR illumination at around 2047 cm^{-1} which corresponds to the C-O stretching band of the carbonyl, while IR light with other frequencies, visible and near UV light give no appreciable effects upon the decomposition rate. The decarbonylation of $Ni(CO)_4$ is thus induced by vibrational excitation of the carbonyl group, although other metal carbonyls usually undergo photodissociation by UV illumination. Adsorbed $Ni(CO)_4$ decomposes to Ni metal via intermediate species $Ni(CO)_3$ and $Ni(CO)_2$, and the decarbonylation step from $Ni(CO)_4$ to $Ni(CO)_3$ was concluded to be rate-determining.

VI-K-4 IRAS, XPS, and TPD Study on the Adsorption and Decomposition of $Fe(CO)_5$ on Silver Surface

Shinri SATO, Yuji UKISU, Hisashi OGAWA*, and Yoshio TAKASU* *(*Shinshu Univ.)*

The adsorption and decomposition of $Fe(CO)_5$ on silver surface has been studied by infrared reflection absorption spectroscopy (IRAS), X-ray photoelectron spectroscopy (XPS), and temperature-programmed desorption (TPD) technique. TPD spectra showed that $Fe(CO)_5$ physisorbs at temperatures below 120 K on uncleaned silver surface while chemisorbed species is formed on the surface cleaned by Ar ion sputtering. The active sites for chemisorption may be defect sites produced by the sputtering. At lower coverage of adsorbed $Fe(CO)_5$ than monolayer, IRAS and XPS revealed that the chemisorbed species undergoes decarbonylation upon rising temperature to 182 K and converts into $Fe(CO)_4$ which has a planar structure parallel to the surface. The $Fe(CO)_4$ species undergoes conformation change with further rise in temperature and releases all the carbonyls at temperatures above 350 K. When physisorbed $Fe(CO)_5$ presents on the chemisorbed species, the $Fe(CO)_4$ species reacts weakly with the physisorbed species to form an adduct which decomposes at around 350 K. The intermediate species $Fe(CO)_4$ exhibits behavior very similar to $Fe(CO)_4$ species produced by the photolysis of $Fe(CO)_5$.

VI-K-5 Photochemistry of $Fe(CO)_5$ Adsorbed on Silver

Shinri SATO, Yuji UKISU, Hisashi OGAWA*, and Yoshio TAKASU* *(*Shinshu Univ.)*

The photolysis of $Fe(CO)_5$ on silver surface has been studied by infrared reflection absorption spectroscopy (IRAS), X-ray photoelectron spectroscopy (XPS), and temperature-programmed desorption (TPD) technique. $Fe(CO)_5$ physisorbs at temperatures below 150 K on uncleaned silver surface and undergoes photo-decarbonylation to form planar $Fe(CO)_4$ adsorbed in parallel to the surface. On the surface cleaned by Ar ion sputtering, $Fe(CO)_5$ chemisorbs on defect sites and thermally decomposes at temperatures above 350 K. The chemisorbed species photodecomposes releasing one carbonyl like the physisorbed species, but the product species is likely to react weakly with each other or with $Fe(CO)_5$ to produce an adduct species.

VI—L Studies on Catalysis for Automobile Exhaust and Energy Resources

The measures against global air pollution and the development of new energy resources instead of fossil fuel are current problems. Catalysts play important roles in the cleaning of exhaust gases from industrial factories and gasoline engines. We are now aiming the catalytic reduction of NO_X from diesel engines, and have recently found a new catalytic system hopeful for this purpose. A mechanistic study on the NO_X reduction is under progress in our laboratory. We have also studied a photocatalyst which converts light energy to chemical energy from the viewpoint of solar-to-chemical energy conversion.

VI-L-1 Activity Enhancement of Copper-containing Oxide Catalysts by Addition of Cesium in the Reduction of Nitric Oxide

Yuji UKISU, Shinri SATO, Gyo MURAMATSU*, and Kiyohide YOSHIDA* *(*Riken Co. Ltd.)*

[*Catal. Lett.*, **16**, 11 (1992)]

Catalytic reduction of nitric oxide in the presence of propylene and oxygen over alumina and copper-containing oxide catalysts has been studied. Optimum temperature for this reaction is dependent upon the composition of catalysts; ca. 640 K on $Cu\text{-}Cs/Al_2O_3$, ca. 680 K on Cu/Al_2O_3, and ca. 780 K on Al_2O_3. IR spectroscopic measurements show that an isocyanate (—NCO) intermediate formed on $Cu\text{-}Cs/Al_2O_3$ is more reactive with NO to give N_2 than the intermediate produced on Al_2O_3 and Cu/Al_2O_3. Electron donation from Cs to Cu may activate the intermediate.

VI-L-2 Influence of Hydrocarbons and Water on the NO_X Reduction over Copper-containing Oxide Catalysts

Yuji UKISU, Shinri SATO, Gyo MURAMATSU*, and Kiyohide YOSHIDA* *(*Riken Co. Ltd.)*

[*Appl. Catal.*, submitted]

Behavior of an isocyanate intermediate (—NCO) formed during catalytic NO_X reduction has been studied on alumina-supported Cu-Cs oxide catalyst in the presence of oxygen and hydrocarbons (propylene, acetylene, propane, and n-heptane) using infrared spectroscopy. While a reaction involving NO, O_2, and acetylene needs some heat treatment to produce the isocyanate species on the catalyst, no heat treatment is required in a NO/O_2/propylene or n-heptane system. No isocyanate intermediate is formed in a NO/O_2/propane system by an ordinary procedure. Adsorbed water on the catalyst surface is found to suppress formation of the isocyanate species, and this inhibition effect of water is smaller in the acetylene or n- heptane containing system than in the propylene containing system. These results are discussed with reference to the results of the practicadl NO_X reduction.

VI-L-3 Photochemical Diode of TiO_2 Film Prepared on SnO_2 Film

Hisato KOSHIBA*, Noriyoshi KAKUTA*, Akifumi UENO*, and Shinri SATO *(*Toyohashi Univ. of Tech.)*

TiO_2 film was prepared on a half part of a SnO_2-coated quartz plate by a spin-on process of TiO_2 sols, and the

other part of the SnO_2 film was coated with Pt by sputtering. When this device is immersed in an aqueous alcoholic solution and illuminated with UV light, gas evolution is observed both at TiO_2 and Pt parts. Mass spectrometric analysis shows that H_2 and CO_2 are produced. This kind of a device is called a photochemical diode. In the present device, TiO_2 film is thought to work as a photoanode at which photogenerated holes oxidize alcohol to produce CO_2, while Pt film functions as a cathode at which electrons supplied from the illuminated TiO_2 film through the SnO_2 film reduce water to evolve H_2. Success in the photochemical diode of TiO_2 film indicates that photogenerated electrons and holes can be separated at TiO_2 film, and the electrons can move to Pt film, even though the TiO_2, Pt, and SnO_2 films consist of small particles. The yield of hydrogen was increased by the addition of NaOH to the solution, whereas the addition of HNO_3 gave no effects. The role of NaOH is not clear at present.

RESEARCH ACTIVITIES VII
Coordination Chemistry Laboratories

All the staff of the laboratory of Synthetic Coordination Chemistry were renewed after the two year term. Professor Yoshihiko Kushi and associate professor Fumio Kawaizumi of the laboratory finished their term and returned to Osaka University and Nagoya University, respectively, the latter still continuing his contribution to the Coordination Chemistry Laboratories (CCL) as an adjunct associate professor of the laboratory of Complex Catalysis. Together with them, Dr. Tatsuya Kawamoto and Dr. Matsuo Nonoyama also moved back to their original universities (Osaka University and Nagoya University, respectively). We sincerely thank their cooperation during these two years. Instead of them professor Yutaka Fukuda of Ochanomizu Women's University and associate professor Kiyoshi Sawada of Niigata University have been appointed to be the new members of the laboratory of Synthetic Coordination Chemistry. Dr. Hikaru Ichida of the University of Tokyo and Dr. Keiichi Sato of Niigata University came with them as the research associates of the laboratory. Professor Hisanobu Ogoshi has chaired the adjunct professor of the laboratory of Complex Catalysis to cooperate with associate professor Kawaizumi for two years. Mr. Noriyuki Suzuki, who graduated from the University of Tokyo and was working in the Showa Denko Co. Ltd., has been appointed to be a research associate of the laboratory of Functional Coordination Chemistry since October, 1991. Moreover, Mr. Tetsunori Mizukawa has moved from Moji Agriculture, Forestry and Fishery Center for Consumer Science of the Ministry of Agriculture, Forestry and Fishery to the same laboratory as a technical associate from April, 1992. Thus, the laboratory of Functional Coordination Chemistry has now the full staff. Dr. Ryo Miyamoto of Tohoku University has joined us as an IMS fellow from this June. Dr. Viktor Denisov of St. Petersburg University, Russia has been invited by CIBA-GEIGY Foundation (Japan) for the Promotion of Science to work with associate professor Takahashi of the laboratory of Functional Coordination Chemistry for one year from May. Dr. Denis Kondakov from St. Petersburg University, who has been invited by JSPS, has also joined Takahashi's group since this June. Miss Daniele Choueiri, a graduate student of Purdue University, stayed in the laboratory of Functional Coordination Chemistry for 2 months from the middle of June. Thus, CCL had five foreign scientists in the summer of 1992, including Dr. Támas Radnai of the Hungarian Academy of Sciences (laboratory of Complex Catalysis), Dr. Christophe Rousset of Purdue University, USA (laboratory of Functional Coordination Chemistry), who have stayed with us for one year and both of them left CCL at the end of August, 1992. Besides these visitors to CCL, Dr. Kiyohiko Nakajima, research associate of the laboratory of Complex Catalysis, moved to Aichi University of Education with promotion to an associate professor. We thank his cooperation since 1986.

The number of the staff and coworkers in CCL remarkably increased compared with that in 1984 when CCL was established. The total numbers of the members of CCL since 1984, including regular staff members, IMS fellows, invited foreign scientists, students of the Graduate University of Advanced Studies, graduate students from other universities and visiting scientists from companies and universities, are listed in Table 1. The increase in the number of members leads to not only an increase in the number of publications from CCL, but also an increased ratio of publications to members. We are hoping that we will be able to realize the dream of the establishment of a new national institute for coordination chemistry in the near future on the basis of the activity of CCL and efforts of coordination chemists of Japan.

Table 1. Number of Members of the Coordination Chemistry Laboratories.

Year	Laboratory				Total
	Synthetic Coordination Chemistry	Complex Catalysis	Functional Coordination Chemistry	Coordination Bond[a]	
1984	5	4	–	–	9
1985	6	5	–	–	11
1986	9	4	–	2	15
1987	9	3	–	2	14
1988	10	7	–	2	19
1989	12	11	–	2	25
1990	6	7	3	2	18
1991	6	7	6	2	21
1992	6	7	17	2	32

[a] Adjunct professor and adjunct associate professor only

VII—A Developments of Diastereoisomers of Metal Complexes Having Various Combinations of Chiral Elements

A series of metal complexes with various chiral elements as building blocks were synthesized. The reaction products between these metal complexes have also been studied. The molecular and crystal structures of them were detremined. The detailed comparison between those structures revealed sometimes the origin of the diastereoselectivities in these systems.

VII-A-1 Helically Chiral Trinuclear Complexes with Ferrocene Group

Tatsuya KAWAMOTO and Yoshihiko KUSHI

[*J. Chem. Soc. Dalton Trans.*, 1992, in press.]

The reaction between M^{2+} (where M=Ni, Zn and Pd) and 2—(ferrocenyl)benzothiazoline in ethanol affords the trinuclear complexes [Ni(fabt)$_2$], [Zn(fabt)$_2$] and [Pd(fabt)$_2$] (Hfabt=2—N—(ferrocenylmethylideneamine)benzenethiolate). Interaction of [Ni(fabt)$_2$] or [Zn(fabt$_2$] with $HgCl_2$ gives the complex trans-[Hg(fabt)$_2$]. IR, NMR, UV/VIS spectra and CV data are given. The X-ray crystal structures of [Ni(fabt)$_2$] and [Pd(fabt)$_2$] show a helical geometry, which is also confirmed for a distorted tetrahedral [Zn(fabt)$_2$] complex.

VII-A-2 Carbon-carbon Bond Formation in Helical Nickel(II) Complex

Tatsuya KAWAMOTO and Yoshihiko KUSHI

[*Chem. Lett.*, 893 (1992)]

The reaction of 2-phenylbenzothiazoline with nickel(II) acetate tetrahydrate leads to cis-bis[2-N-(phenylmethylideneamine)benzenethiolato] nickel(II)(complex (1)) and two ligands in this complex (1) are joined through a C-C bond to form a complex having two chiral centers(complex (2)). The X-ray structural analysis of the complex (2) establishes the bond patterns of the delocalized ligand.

VII-A-3 Crystal and Molecular Structure of Tetrapalladium Cluster with a C,N,S—Tridentate Ligand

Tatsuya KAWAMOTO and Yoshihiko KUSHI

[*Chem. Lett.*, 1057 (1992)]

The ligand 2-(1-naphthyl)benzothiazoline, 1-nabz, reacts with palladium(II) acetate to yield, in addition to the expected bis[2-N-(1-naphthylmethylideneamine) benzene-thiolato]palladium(II), a minor by-product tetrakis[2-N-(1-naphthylmethylideneamine)benzenethiolato-C$^{\theta}$, N, S] tetrapalladium(II) complex having a composition $C_{68}H_{44}N_4Pd_4S_4$. The novel structure of the tetramer complex is established by X-ray diffraction.

VII-A-4 Rotamers of 1-Phenylethylamine Ligands in (R, S)-and (S, S)-trans-Bis(succinimidato)bis(1-phenylethylamine) palladium(II) Complexes

Hiroshi SHIMOMURA*, Seiko KOMORITA*, Hiro KUMA*, and Yoshihiko KUSHI *(*Osaka University)*

[*Chem. Lett.*, 913 (1992)]

Both trans-[Pd(succim)$_2$(R-phenea)(S-phenea)] and trans-[Pd(succim)$_2$(S-phenea)$_2$], where succim=succinimidate anion and phenea=l-phenylethylamine, were prepared and their crystal structures were determined by X-ray analysis. Three different staggered rotamers around the N-C bond of the phenea ligands have been found.

VII-A-5 Rotamers of 1-Phenylethylamine Ligands in trans-Bis(cyclicimidato)bis(1-phenylethylamine) copper(II) Complexes

Hiroshi SHIMOMURA*, Seiko KOMORITA*, Hiro KUMA*, and Yoshihiko KUSHI *(*Osaka University)*

[*Inorg. Chim. Acta*, 1993, in press.]

Three [CuN4] type complexes, red trans-[Cu(3,3-dmgluim)$_2$(R-phenea)$_2$] (1), blue trans-[Cu(hyd)$_2$(R-phenea)$_2$] (2), and blue trans-[Cu(succim)$_2$ (S-phenea)(R-phenea)] (3), were prepared and their crystal structures were determined. In (1), the coordination geometry is planar, and the intermolecular hydrogen bonds are formed between the NH_2 of phenea and O(CO) of the six-membered cyclic imidate. In (2) and (3), the geometry are flattened tetrahedral and intramolecular hydrogen bonds are formed. Three different staggered forms of and one eclipsed form of the rotamers on the phenea ligands have been found in these systems.

VII—B Syntheses, Structures and Functions of Chromotropic Complexes

VII-B-1 Synthesis of Fe(II) complexes with aminomethylpyridine derivatives and their spin-crossover phenomena in solution

Kayoko KASAI, Yuichi MASUDA *(Ochanomizu Univ.)*, **Hikaru ICHIDA, Keiichi SATO, and Yutaka FUKUDA**

We have synthesized new ligands, 1,1,1-tris(2-aminomethylpyridylmethyl)propane(AMPMP) and its oxidized form (tris(diimine)-type(AMPMP-6H) chelating reagent). These ligands are hexadentate so that they can form stable complexes with Fe(II), among which the complex with the former ligand shows typical spin-crossover transition in solution and the latter one is not a spin-crossover but a low-spin complex at room temperature. We have studied thermodynamic properties of these complexes in solution and their solvent dependent spin-transition phenomena by means of NMR and electronic spectral measurements and compared these results with the data of simple bidentate aminomethylpyridine(AMP)-Fe(II) complex reported before.

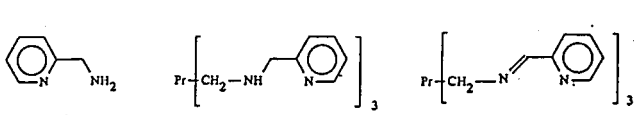

AMP AMPMP AMPMP-6H

VII-B-2 Mixed ligand complexes as anion sensing materials

Noriko SATO *(Toshiba Corp.)* **and Yutaka FUKUDA**

[*Chem. Lett.*, 399 (1992)]

The mixed ligand nickel(II) chelate, [Ni(dike)(diam)]X where dike=β-diketonate anion, diam=N-alkylated ethylenediamine, and X=an anion such as perchlorate or tetraphenylborate, show characteristic thermochromism and solvatochromism in certain donor solvents. The mechanism of this chromotropism is the structural change between the square planar coordination(Sp) and the octahedral structure(Oh) with two solvent molecules, i.e., the original complex is coordination unsaturation. This led us to expecting that these square planar chelates could exist as an equilibrium mixture between Sp and Oh in an inert solvent if coordinating anions (in this case, a monohydrogenphosphate anion) were introduced instead of solvent molecules. Ion-sensing electrodes containing these metal complexes have been constructed, among which the electrode with the perchlorate complex responds to the monohydrogenphosphate anion but in the case of tetraphenylborate electrode there is no response to the anion.

VII-B-3 Synthesis of dinuclear complexes composed by mono-nuclear mixed ligand complexes

Kasumi YAMADA *(Ochanomizu Univ.)* **and Yutaka FUKUDA**

[*Acta Cryst. Sect. C48*, 1992, in press]

Some dinuclear complexes composed with the building unit of Ni(II) mixed ligand complex cation ([Ni(tmen)(acac)]$^+$) have been obtained, where tmen=N,N,N',N'-tetramethylethylenediamine, acac=acetylacetonate and a bridging ligand such as oxalate(ox) or pseudohalide anions; i.e., [(tmen)(acac)Ni(ox)Ni(acac)(tmen)], [(tmen)(acac)Ni$(X)_2$Ni(acac)(tmen)] where X=NCS^-, NCO^- or N_3^-. From the synthetic point of view, the important properties of the complex as the starting materials to form dinuclear complexes are also due to the coordination unsaturation. These dinuclear complexes thus obtained show intermetallic interaction, i.e., anti-ferromagnetic interaction. In addition to these dinuclear complexes, we could obtain accidentally one more curious dinuclear complex which contains a carbonate anion as the bridging group coming from atmospheric CO_2. From the crystal structure data, there are two complex species in the same unit cell which are mono-nuclear species [Ni(acac)(tmen)(H_2O)(MeOH)]$B(Ph)_4$ and dinuclear one [(tmen)(acac)Ni(CO_3)Ni(acac)(tmen)].

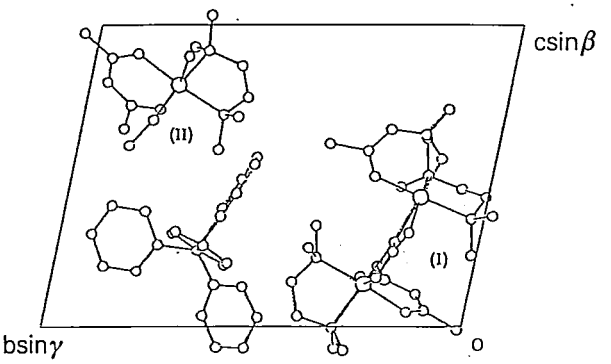

Figure 1. Crystal structure of the complex [Ni(tmen)(acac)(H_2O)(MeOH)]BPh_4[[Ni(acac)(tmen)]$_2(CO_3)$] viewed along the a axis.

VII—C Thermodynamic and Molecular Approach to the Solute-Solvent Interaction in Solutions

The solute-solvent interactions in solutions were studied from the macroscopic and microscopic points of view. This year effort was devoted to establish a way of statistical mechanical calculation which enables us to express the partial molar volume of solute V_2^0 in terms of interaction potentials working between the atoms of which solute and solvent molecules are consisted.

VII-C-1 A Simple Method for the Evaluation of Enthalpy of Proton Dissociation in Water

Motoharu TANAKA*, Hiroyasu NOMURA*, and Fumio KAWAIZUMI *(Nagoya Univ. and IMS) (*Nagoya University)*

[*Bull. Chem. Soc. Jpn.*, **64**, 510 (1992)]

A method is proposed for evaluating the ΔH° value for the proton dissociation of an acid HB from the temperature dependence of the dissociation constant Ka: Instead of differentiating the pKa(=-log Ka) value of acid HB with respect to temperature, we select an appropriate acid HA as a reference and plot the quantity X=pKA(HB)−pKa(HA) as a function of reciprocal temperature. The plot was found to be linear with sufficient accuracy for most non-chargaed or negatively charged acids, for which pKa itself is a complex function of temperature. ΔH° values are thus readily evaluated by linear least-squares fitting. The theoretical background is discussed.

VII-C-2 Effects of Molecular Conformation on the Packing Density in the Liquid State. 3. Partial Molar Volume Differences of Cis and Trans Conformers at Infinite Dilution

Masaharu OHBA *(Kawaijuku Educational Institution)*, **Hiroyasu Nomura** *(Nagoya Univ.)*, **and Fumio KAWAIZUMI** *(Nagoya Univ. and IMS)*

[*J. Phys. Chem.*, **96**, 5129 (1992)]

Starting from the PY-like integral equation of RISM-1 type and using the Kirkwood-Buff theory, we evaluated the differences in the partial molar volumes of solute V_X^0 of cis and trans isomers. The system investigated consists of a tetratomic A-B-B-A fused hard sphere and a single hard sphere both of which are considered as solvent or solute. To compare the evaluated values with the actual values, the V_X^0 's were determined for cis-and trans-decahydronaphthalene dissolved in such solvents as carbon tetrachloride, hexane, and benzene, etc., as well as for hexane and *p*-dioxane in cis-and trans-decahydronaphthalene. The

evaluation and experimental results have agreed in the relation that V_X^0(trans) > V_X^0(cis) and also in the magnitude of their differences. Clear correlation was observed between the isothermal compressibility of the solvent and the quantity V_X^0−V, where V is the molar volume of solute decahydronaphthalene.

VII-C-3 Partial Molar Volumes of Halogeno Complexes of Platinum and Palladium in Aqueous Solutions and Differences in Volume between Tetra-and Hexa-coordinated Forms

Fumio KAWAIZUMI *(Nagoya Univ. and IMS)*

[*J. Chem. Soc., Faraday Trans.*, (1992)]

From the density data measured for dilute aqueous solutions of $K_2[PtX_4]$ $K_2[PtX_6]$ $K_2[PdX_4]$, and $K_2[PdX_6]$ (X=Cl,Br or SCN), the partial molar volumes V_2^0 of these complexes were determined at 298.15 K. The values $V_2^0(K_2[MX_4])$ and $V_2^0(K_2[MX_6])$ are roughly predictable by combining respectively the V_2^0 values for $K_2[MX_4]$ and $K_2[MX_6]$ and the difference between V_2^0(MX) and V_2^0(KCl). Platinum and palladium complexes have quite similar $V_2{}^0$, but the $V_2{}^0$, values for the latter are larger by 1.7-1.9 cm^3mol^{-1} than the former values. The amount of increase of V_2^0 with change of coordination number from four to six was compared with the V_2^0 values of the ions Cl^-, Br^- and SCN^-. For the hard ion Cl^-, the degree of volume increase was largely smaller than for the soft ions Br^- and SCN^-.

VII—D Structures and Thermodynamics of Ionic and Molecular Ensembles in Solution

The interaction of ion-ion and ion-molecule in solution has been studied for various kinds of systems of complex formation and solvents. The weak interactions such as ion-pair, intermolecular, and solvation, play an important role to determine the general feature of thermodynamics and structures of complexes in solution. The studies of transfer phenomena between two phases are also important to understand the reactions in homogeneous solution.

VII-D-1 Protonation Equilibria of Nitrilotris (methylenephosphonato)-and Ethylenediaminetetrakis(methylenephosphonato)-Complexes of Scandium, Yttrium, and Lanthanoids

Kiyoshi SAWADA, Misao KURIBAYASHI*, Toshio SUZUKI*, and Hiroshi MIYAMOTO* *(*Niigata Univ.)*

[*J. Solution Chem.*, **20**, 829 (1991)]

The protonation equilibria of nitrilotris(methylenephosphonic acid) (NTMP, H_6L) and ethylenediaminetetrakis(methylenephosphonic acid) (EDTMP, H_8L) complexes of scandium, yttrium, and lanthanoids have been studied potentiometrically at 25.0°C and at an ionic strength of 0.1 mol dm^{-3} KNO_3. The first protonation constants of NTMP complexes of lanthanoids, K_{MHL}, decrease with decreasing of the ionic radius of the lanthanoid (log K_{MHL}=7.82 (La^{3+}) −6.90 (Lu^{3+})) and show a so-called "Tetrad effect". The second protonation constants, K_{MHL}, change very little with the lanthanoid metal ions (log K_{MH2L}=5.3 −5.7). These results suggest that, in the first protonation process in ML, the proton attacks the nitrogen of NTMP rupturing the M—N of $M(ntmp)^{3-}$, and that the second protonation occurs on the free O^- of phosphonate group coordinating to the metal ion. The pattern of the change in the protonation constants of the EDTMP complexes with the atomic number of the lanthanoid is quite different from that of the NTMP complexes. This fact indicates that the manner of protonation of the EDTMP complexes differs from that of NTMP complexes. The protonation constants of yttrium complexes of NTMP and EDTMP agree with those of lanthanoid complexes, whereas those of scandium complexes deviate from the values predicted from its ionic radius.

VII-D-2 Structure and NMR Behavior of Cobalt(III)-polyamine Complexes of Nitrilotris(methylenephosphonate) in Aqueous Solution

Kiyoshi SAWADA, Katsuhiro UEHARA*, and Toshio SUZUKI* *(*Niigata Univ.)*

The complex formation of the nitrilotris(methylenephosphonate)(NTMP) with cobalt(III)-polyamine complexes has been investigated by means of NMR spectroscopy. P-31 NMR spectra of the reaction mixture were measured at 0°C as a function of pH. The analysis of the pH dependence of P-31 NMR signals revealed that two types of complexes were formed by the reaction of cis-$[Co(en)_2Cl]_2^+$ with NTMP: O-monodentate complex and O, O-bidentate complex having a eight membered chelate ring. The protonation constants and P-31 NMR chemical shifts of each complex were evaluated and the structures of these complexes were estimated. The NMR data of the NTMP complexes of cis-$[Co(en)_2(NH_3)Cl]^{2+}$ supports the structure of O-monodentate complex. The reaction of mer-$[Co(dien)(H_2O)_3]^{3+}$ with NTMP forms the facial and meridional forms of O,N,O-tridentate complexes.

VII-D-3 Thermodynamic Study of Steric Effect on the Formation of Tetrahedral Pyridine Base Complexes of Cadmium Halides.

Kiyoshi SAWADA, Keiichi SATOH, Chikako HONDA*, Tomoe ISHIYAMA*, and Toshio SUZUKI* *(*Niigata Univ.)*

[*J. Chem. Soc., Dalton*, in press]

The formation of tetrahedral complexes of cadmium halide with methyl-substituted pyridine (R-py)[R-py=pyridine, 3-methyl-, 4-methyl-, 2-methyl-, 2,4-dimethyl-, 2,6-dimethyl-, 2,4,6-trimethyl-pyridine] and the steric effect of

methyl substituent of pyridine on the formation of the complexes in 1,2-dichloroethane were studied by means of liquid-liquid extraction at 25.0°C. The formation of pyridine base complexes from the tetrahedral tri-*n*-octylphosphine oxide(topo) complex is written as:

$$[CdX_2(topo)_2] + R{-}py \overset{\beta_1}{\rightleftharpoons} [CdX_2(topo)(R\text{-}py)] + topo \quad (i)$$

$$[CdX_2(topo)_2] + 2R{-}py \overset{\beta_2}{\rightleftharpoons} [CdX_2(R\text{-}py)_2] + 2\ topo \quad (ii)$$

where X refers to Cl^- or Br^- ion. The logarithmic formation constants, log β_1 and log β_2, of the complexes having no steric hindrance show a good linear free energy relation ship with pKa of the conjugate acid of the pyridine base. The formation constants of the 2- and 2.6-substituted pyridine complexes are lowered by the steric hindrance of the substituent. Thermodynamic parameters of the formation of bispyridine complex, $CdX_2(R{-}py)_2$, were determined from the temperature dependence of the formation constants. In the case of the bromo complex, the formation of pyridine complex is enthalpy driven and the increase in the formation constant with the increase in pKa responsible to the increase in enthalpy $-\Delta H$. The decrease in the formation constant by sterically hindered complex is predominantly caused by the decrease in entropy, i.e., the decrease in a freedom of rotation of the coordinating pyridine. The formation of bispyridine complex of cadmium chloride is entropy driven and the steric effect is caused by the decrease in both of enthalpy and entropy terms.

VII-D-4 Thermal Properties of Mixed-Ligand Complexes of Transition Metal Chlorides Containing Substituted Pyridines

Kiyoshi SAWADA, Yasuhiro SHIRAKURA*, Yoshio MASUDA*, and Toshio SUZUKI* *(*Niigata Univ.)*

Thermal decomposition of the crystals of the substituted pyridine adducts of cadmium chloride, $CdCl_2(R{-}py)_n$, has been investigated by the methods of TG, DTA, DSC and XRD. The decomposition reaction is written as: $CdCl_2(R{-}py)_4 \rightarrow CdCl_2(R\text{-}py)_2 \rightarrow CdCl_2(R\text{-}py) \rightarrow CdCl_2(R\text{-}py)_{2/3} \rightarrow CdCl_2$. This scheme was confirmed by the elementary analysis of the compounds decomposed at constant temperatures. The XRD profiles of the complexes thermally decomposed are essentially same as those of the complexes crystallized from ethanolic solution. The patterns of TG and DTA curves of former complexes is almost the same as those of latter one. The enthalpy of the decomposition was discussed by the comparison with the cycle through a dissolution of the complexes with tetrabutyl ammonium chloride into 1,2—dichloroethane.

VII-D-5 Liquid-Liquid Extraction of Alkali and Alkaline-Earth Metals with Non-ionic Surfactant Having a Poly(oxyethylene) Chain (Triton X-100)

Kiyoshi SAWADA, Yoichi KIKUCHI, and Toshio SUZUKI*** *(*Niigata Univ., **Iwate Univ.)*

[*Anal. Chim. Acta*, **256**, 311 and **264**, 65 (1992)]

The ion pair extraction of poly(oxyethylene) alkylphenyl ether (Triton X-100) complexes of alkali metal ions (M^+) with picrate ion (Pic^-) in to 1,2-dichloroethane (1,2-DCE) was studied. The results of vapour pressure osmometry suggest a partial dissociation of the ion pair in 1,2-DCE. Quantitative analysis of the extraction data revealed the extraction of the ion pair of Triton X-100-alkali metal ion with picrate ion and dissociation of the ion pair. The thermodynamic constants of the extraction and the dissociation of the ion pair was evaluated by taking into consideration the activity coefficients of ionic species in aqueous and 1,2-DCE phases. The extraction constants of large metal ions, rubidium and caesium, are almost the same as that of potassium ion, where as those of sodium and lithium ions decrease with decrease in the ion size. The effect of the size of the alkali metal ions on the Triton X-100 extraction system is less important than that on the 18-crown-6 extraction system. The dissociation constants of the ion pair were almost the same irrespective of the kind of alkali metal ion, and the interionic distance of the ion pair between the cationic complex and picrate ion was estimated to be 6 A.

The extraction equilibria of alkaline earth metal ions (M^{2+}) are interpreted by the extraction of the ion pair, $[SM^{2+} \cdot (Pic^-)_2]$, and the dissociation of the ion pair into $[SM^{2+} \cdot (Pic)]$ and Pic^- in 1,2-DCE. The extraction constant increases in the order of $Ca^{2+} < Sr^{2+}, Ba^{2+}$. This order is explained by the magnitudes of the formation constants of the alkaline—earth—metal ion complexes with Triton X-100 in aqueous phase. The dissociation constant of the ion pair is almost constant for the alkaline earth metal ions.

VII-D-6 The Solvent Extraction and Dissociation of the Ion Pair of Alkali Metals Complex of Monodisperse Poly(oxyethylene) Derivatives with Picrate Ion.

Kiyoshi SAWADA, Yoichi KIKUCHI*, Toshio SUZUKI* *(*Niigata Univ., **Iwate Univ.)*

[*Bull. Chem. Soc. Jpn.*, **65**, 1506 (1992)]

The ion pair extraction of the alkali metal ion complex of poly(oxyethylene) monododecyl ethers (DEOn: n=4, 6, and 8, where n refers to the number of the oxyethylene unit) with picrate ion into 1,2-dichloroethane (1,2-DCE) has been studied by means of a vapour pressure osmometry and a solvent extraction. The extraction equilibria have been interpreted by taking into consideration the ion pair dissociation in 1,2-DCE. Thermodynamic constants of the extraction and the dissociation of the ion pairs have been evaluated from a quantitative analysis of the extraction data. The extractability of the alkali metal ion increase in the order $Li^+ < Na^+ < Cs^+ < K^+$, irrespective of the number of oxyethylene unit of DEOn. The formation constant of the DEOn-alkali metal ion complex in the aqueous phase. The formation constants of the DEOn-alkali metal ion complex both in the aqueous phase and in 1,2-DCE increase with the increase in the number of EO unit. the interionic distance between the cationic complex and picrate ion of the ion pair was estimated from the dissociation constant in 1,2-DCE.

VII-D-7 Adsorption of Phosphate on Vaterite.

Kiyoshi SAWADA, Shoji YOSHIDA*, and Toshio SUZUKI* *(*Niigata Univ.)*

[*J. Chem. Soc., Faraday Trans.*, in press]

The adsorption of orthophosphate on the vaterite surface was investigated at 25.0°C. The adsorption obeys the Henry adsorption isotherm at low phosphate concentration and the Freundlich adsorption isotherm at high concentration. The unprotonated phosphate ion is adsorbed on vaterite forming a negatively charged ion pair with accompanying calcium ion, $Ca^{2+} \cdot PO_4^{3-}$. The adsorption of negatively charged species is attributed to the positive charge of vaterite surface. A part of the adsorbed PO_4^{3-} ion is irreversibly incorporated into the vaterite lattice. From the temperature dependence of distribution ratio (15—45°C) the enthalpy change of the adsorption of the ion pair was evaluated to be almost zero.

VII-D-8 High Sensitive Spectrophotometer System Coupled with Solvent Extraction/Continuous Phase Separation.

Keiichi SATOH, Yoichi KIKUCHI, Hideji SATOH*, Toshio SUZUKI*, Kiyoshi SAWADA** *(*Niigata Univ., **Iwate Univ.)*

[*Bunseki Kagaku*, **40**, T119 and T167 (1991)]

High sensitive spectrophotometer system has been developed for a low-absorbance measurements. The use of a flow through absorbance cell fixed in a cell compartment and a data treatment with an external microcomputer makes possible to read out an absorbance of 0.0001 as a significant figure. The high sensitive continuous solvent extraction spectrophotometry was achieved by the introduction of phase separator. These systems were applied for the analysis of complex formation equilibria, the liquid-liquid extraction measurements, and the determination of trace amounts of metals in natural waters.

VII—E Cyclometallation of Heterocyclic Aromatic Compounds

Cyclometallation occurs easily for benzene derivatives suitably substituted with donor groups giving metallaheterocycles. The metallaheterocycles are often useful intermediates for organic and organometallic synthesis. Cyclometallated benzene derivatives are now numerous but heterocyclic aromatic compounds cyclometallated are so far very scanty. This research aims to gain an insight into cyclometallation of heterocyclic aromatic compounds. We have found that an N,N-dimethylthio (or seleno) carbamoyl group is a substituent which facilitates cyclometallation of thiophene and furan rings with platinum metals.

VII-E-1 Cyclometallation of N,N-Dimethylfuran-2 (and 3) - carboselenoamide with Palladium(II), Rhodium(III), and Ruthenium(II)

Matsuo NONOYAMA and Kiyoko NONOYAMA *(Konan Junior College)*

[*Polyhedron*, **10**, 2265 (1991)]

Newly prepared N,N-dimethyl-furan-2(and 3)-carboselenoamide (abbreviated as H(C-E), or as Hafs and Hbfs, respectively) is cyclopalladated with lithium tetrachloropalladate in methanol to give PdCl (C-E), which reacts with tri-n-butylphosphine (PBu_3) and 4-t-butylpyridine (tbp) to give the adducts PdCl (C-E) (PBu_3) and PdCl (C-E) (tbp), respectively. The iodo analogues are also prepared. Spectroscopic characterization reveals that the furan ring of H(C-E) is cyclopalladated and the Se atom of the selenoamide group is coordinated to form a five membered palladaselenaheterocycle. The cyclopalladation of Hbfs occurs exclusively at the positon 2 of the furan ring. The two selenoamides are cyclorhodated with trichlorobis (tri-n-butylphosphine) rhodium(III) in refluxing toluene to give $RhCl_2$ (C-E)$(PBu_3)_2$. The bromo analogues are similarly obtained. Hbfs is similarly cycloruthenated with dichlorotricarbonylruthenium(II) in refluxing 2-methoxyethanol to afford RuCl (bfs) $(CO)_2$ but Hafs is not cycloruthenated in the same conditions. This fact suggests that Hbfs is more reactive toward cyclometallation than Hafs.

VII-E-2 Cyclopalladated N,N-Dimethylthiophene-2- and -3-carboselenoamide Derivatives

Hiroyuki MIZUNO*, Masakazu KITA*, Matsuo NONOYAMA, and Junnosuke FUJITA* *(*Nagoya Univ.)*

[*Inorg. Chim. Acta*, **202**, 183 (1992)]

N,N-Dimethylthiophene-2- and -3-carboselenoamides, abbreviated as Hats and Hbts, respectively were easily obtained by the reaction of the corresponding carboxamide with phenyldichlorophosphine selenide. Hats and Hbts reacted with lithium tetrachloropalladate in methanol to give $[PdCl(ats)]_2$ and $[PdCl(bts)]_2$, respectively. Several derivatives of the two were prepared with ligands (L) such as pyridine (py) or tri-n-butylphosphine (PBu_3). The new compounds were characterized spectroscopically and the structures of $[PdCl(bts)(PBu_3)]$ and [PdCl(ats)(tbp)] (tbp=4-tert-butylpyridine) were determined by X-ray analysis. The former was shown to be a trans-(C, Cl) isomer, while the latter a cis-(C, Cl) one where C represents the palladated carbon atom. Hats was palladated at the position 3 of the thiophene ring and Hbts exclusively at the position 2 of the ring. The selenoamide group was coordinated through the selenium atom to form a five-membered palladaselenaheterocycle. The trans influence of a trans donor was reflected on the Pd-Se bonds: 2.4147 (8) Å (trans to PBu_3) in $[PdCl(bts)(PBu_3)]$ and 2.359(1) Å (trans to Cl) in [PdCl(ats)(tbp)].

VII-E-3 Cyclorhodation of N,N-Dimethylthiophene-2(and 3)-carbothio (and seleno) amide

Matsuo NONOYAMA and Keinosuke SUZUKI *(Nagoya Univ.)*

[*Syn. React. Inorg. Met.-Org. Chem.*, in press]

Reactions of $RhCl_3(PBu_3)_2$ (PBu_3=tri-n-butylphosphine) with the four title amides (HA) gave the complexes, $RhCl_2(A)(PBu_3)_2$, where the thiophene ring was metallated at position 3 or 2 to form a five membered rhodathia (or selena) heterocycle accompanied with amide-S or -Se coordination. The two PBu_3 ligands were mutually trans in the octahedral complexes. Reactions of $RuCl_2(CO)_3$ with these amides gave $RuCl_2(CO)_2(HA)_2$ except for N,N-dimethylthiophene-3-carbothioamide which gave $RuCl(A)(CO)_2$ containing a ruthenathiaheterocycle. In $RuCl_2(CO)_2(HA)_2$ HA was not cyclometallated and coordinated only through the amide S or Se atom.

VII—F Structure of Liquids

VII-F-1 Intramolecular and Liquid Structures of Tetramethylurea Studied by Means of X-Ray Diffraction

Támas RADNAI* *(*Hungarian Acad. Sci. and IMS)* **and Hitoshi OHTAKI**

[*Z. Naturforsch.*, **47a**, 1003 (1992)]

The intramolecular and liquid structures of tetramethylurea (TMU) were investigated by the liquid x-ray diffraction method. It is confirmed that in the liquid state the four methyl groups are out of the plane which is constructed by the O, C, and the two N atoms, the molecular structure being similar to what had been found in the gas phase. All structural parameters are in good agreement with those of TMU determined in the gas phase and with those of amide derivatives in liquid. The liquid structure is characterized by a random distribution of molecules as predominant, but a weak molecular ordering specific to approximately 2 intermolecular nonbonding Me...O distances at 340 pm is proposed.

VII—G Structures of Solvated Metal Ions and Complexes in Solution

VII-G-1 X-Ray Diffraction Studies on the Structure of the Tri- and Tetrathiocyanatomanganate(II) Complexes and Solvated Lithium Ion in *N,N*-Dimethylformamide

Támas RADNAI* *(*Hungarian Acad. Sci. and IMS)*, **Shin-ichi ISHIGURO**** *(**Tokyo Inst. Technol.)*, **and Hitoshi OHTAKI**

[*Bull. Chem. Soc. Jpn.*, **65**, 1445 (1992)]

The structure of the tri- and tetrathiocyanato-*N*-manganate(II) complexes in *N,N*-dimethylformamide (DMF) solution was determined by the solution X-ray diffraction method at 25°C. The most probable structure of the tri-complex is octahedral with additional three DMF molecules in the first coordination sphere, while the tetra-complex is tetrahedral. The Mn-O and Mn-N bond lengths were determined to be 220 pm in both complexes. The structure of the octahedrally solvated lithium ion $[Li(dmf)_6]^+$ with the Li-O bond length of 195 ppm was also determined in an LiSCN solution of DMF.

VII-G-2 EXAFS and X-Ray Diffraction Studies on the Structure of the Tetrathiocyanatocadmate(II) Complex in Dimethyl Sulfoxide

Kazuhiko OZUTSUMI* *(*Univ. Tsukuba)*, **Toshiyuki TAKAMUKU**, Shin-ichi ISHIGURO**** *(**Tokyo Inst. Technol.)*, **and Hitoshi OHTAKI**

[*Bull. Chem. Soc. Jpn.*, **65**, 2104 (1992)]

The structure of the tetrathiocyanatocadmate(II) complex in dimethyl sulfoxide (DMSO) has been studied by the EXAFS (extended X-ray absorption fine structure) and solution X-ray diffraction methods. It has been revealed that the tetrathiocyanatocadmate(II) complex has a five-coordinate structure with an additional DMSO molecule. The structure in DMSO is different from that in water and *N,N*-dimethylformamide, in which no solvent molecule coordinates to the central metal ion. It has also been seen that the coordination mode of the thiocyanate ions in the tetrathiocyanatocadmate(II) complex changes depending on the source of thiocyanate ions due, probably, to different hydrogen bonding abilities of the N-and S-sites of the thiocyanate ion with the counter cations, i.e., the $[Cd(NCS)_3(SCN)(dmso)]^{2-}$ and $[Cd(NCS)_4(dmso)]^{2-}$ complexes are formed in solutions containing NH_4SCN and $(C_2H_5)_4NSCN$, respectively. The Cd-N, Cd-S, and Cd-O bond lengths within $[Cd(NCS)_3(SCN)(dmso)]^{2-}$ are 222(1), 262(1), and 234(1) pm, while the Cd-N and Cd-O bond lengths within $[Cd(NCS)_4(dmso)]^{2-}$ are 223(1) and 239(2) pm, respectively.

VII-G-3 Density Functional Calculations on the Geometries and Dissociation Energies of $[M(H_2O)_6]^{2+}$ Ions. M^{2+} = Cr^{2+}, Mn^{2+}, Fe^{2+}, Co^{2+}, Ni^{2+}, Cu^{2+}, and Zn^{2+}

Kenji WAIZUMI, Hitoshi OHTAKI, Hideki MASUDA* *(*Nagoya Inst. Technol.)*, **Nobuhiro FUKUSHIMA**, and Youichi WATANABE**** *(**Cray Research Japan)*

[*Chem. Lett.*, 1489 (1992)

Full geometry optimizations have been carried out on high-spin hexaaqua complexes of Cr^{2+}, Mn^{2+}, Fe^{2+}, Co^{2+}, Ni^{2+}, Cu^{2+}, and Zn^{2+} by the local spin density functional method with non-local corrections using Gaussian-type basis sets. The octahedral molecular arrangement around the Mn^{2+}, Ni^{2+}, and Zn^{2+} ions optimized were regular, whereas those around the Cr^{2+}, Fe^{2+}, Co^{2+}, and Cu^{2+} ions were distorted with significant differences in the three kinds of M-O distances. The Jahn-Teller distortion for the Fe^{2+} and Co^{2+} complexes was firstly found in the field of

computational geometry optimization.

VII-G-4 Structure of Divalent Transition-Metal Complexes at Consecutive Step of Interaction with Halide and Thiocyanate Ions in Solution

Hitoshi OHTAKI

[*J. Indian Chem. Soc.*, in press]

All of the solvated ions discussed here, except for those in HMPA, have the octahedral structure and the final products of the complexes are tetrahedral. Structural changes occurring at the stepwise formation of the transition-metal complexes with halide and thiocyanate ions in aqueous and nonaqueous solutions are discussed on the basis of spectroscopic, calorimetric and solution X-ray diffraction data. The structures of some of the complexes $[MX_n]^{(2-n)+}$ (n=1–4) are determined by the solution X-ray diffraction method and the bond-length variations through the structural changes are shown. The step where the structure changes from octahedral to tetrahedral is thus shown from thermodynamic data, absorption spectra and structural analyses of the complexes. The importance of structures and properties of solvents in the complex formation reactions is especially emphasized.

VII—H Crystal Structure of Metal Complexes

VII-H-1 X-Ray Structural Studies of $FeCl_2 \cdot 4H_2O$, $CoBr_2 \cdot 4H_2O$, $NiCl_2 \cdot 4H_2O$ and $CuBr_2 \cdot 4H_2O$. *cis/trans* Selectivity in Transition Metal(II) Dihalide Tetrahydrate

Kenji WAIZUMI, Hideki MASUDA* *(*Nagoya Inst. Technol.)*, **and Hitoshi OHTAKI**

[*Inorg. Chim. Acta*, **192**, 173 (1992)]

Crystal structures of $FeBr_2 \cdot 4H_2O$ (**1**), $CoBr_2 \cdot 4H_2O$ (**2**), $NiCl_2 \cdot 4H_2O$ (**3**) and $CuBr_2 \cdot 4H_2O$ (**4**) have been determined by the X-ray diffraction method. **1** crystallizes in the monoclinic form with the space group $P2_1/a$ having the unit cell dimensions of a=8.730(2)×10², b=7.239(1)×10², c=6.149(2)×10² pm, β=110.72(2)°, V=363.5×10⁶ pm³ and Z=2; **2** monoclinic, $P2_1/a$, a=8.581(5)×10², b=7.143(4)×10², c=6.180(2)×10² pm, β=110.29(4)°, V=355.3×10⁶ pm³ and Z=2; **3** monoclinic, $P2_1/a$, a=13.378(3)×10², b=9.301(3)×10², c=5.988(1)×10² pm, β=126.45(1)°, V=599.4×10⁶ pm³ and Z=4; **4** monoclinic, $P2_1/a$, a=12.013(3)×10², b=7.330(4)×10², c=4.116(2)×10² pm, β=105.44(3)°, V=349.3×10⁶ pm³ and Z=2. The hexa-coordinated geometry around the Fe^{2+} and Co^{2+} ions in **1** and **2**, respectively, is a distorted *trans*-octahedron with four aqua oxygens at the equatorial position and two Br^- ions at the axial position, whereas the hexa-coordinated central Ni^{2+} ion in **3** has a distorted *cis*-octahedral geometry with three aqua oxygens and one Cl^- ion at the equatorial position and one aqua oxygen and one Cl^- ion at the axial position. The central Cu^{2+} ion in **4** has an axially elongated octahedral form with two Br^- ions and two aqua oxygens at the equatorial position, and two Br^- ions belonging to the adjacent units locate at the axial position of the copper(II) ion. The remaining two water molecules in the compound are situated outside the coordination sphere of the copper(II) ion and are connected to the water molecule in the coordination sphere of a copper(II) ion with a Br^- ion in an adjacent copper(II) complex by hydrogen bonds. The *cis/trans* selectivity in the transition metal(II) dihalide tetrahydrate complexes is discussed in terms of the electronic configuration of the central metal(II) ions, the repulsive interaction between halide ions due to the steric effect, and the effect of hydrogen bonds.

VII-H-2 Structure of $2RbCl \cdot CuCl_2 \cdot 2H_2O$

Kenji WAIZUMI, Hideki MASUDA* *(*Nagoya Inst. Technol.)*, **Hitoshi OHTAKI, Kim A. BURKOV**, and Ludmila CHERNYKH**** *(**St. Petersburg Univ. and IMS)*

[*Acta Crystallogr.*, **C48** 1374 (1992)]

Copper(II) dirubidium tetrachloride dihydrate, M_r=412.32, tetragonal, $P4_2/mnm$, a=7.596(2), c=8.027(3) Å, V=463.1(2) Å³, Z=2, D_x=2.957 Mg m⁻³, $\bar{\lambda}$(Mo$K\alpha$)=0.71073 Å, μ=13.63 mm⁻¹, F(000)=382, T=293 K, $R(F)$=0.039 for 277 independent reflections with $|F_o| > 3\sigma|F_o|$. The Cu^{2+} ion has a distorted octahedral coordination consisting of two Cl(1) ions at 3.000 (3) Å, two Cl(2) ions at 2.257(3) Å and two water molecules at 1.969(8) Å at the equatorial positions of the square plane. Each of the water molecules is trigonally coordinated and forms two equivalent O-H···Cl(1) hydrogen bonds with an O···Cl(1) length of 3.130(7) Å. Four Cl(1) and four Cl(2) ions form a distorted cube around the Rb^+ ion with Rb-Cl(1) and Rb-Cl(2) lengths of 3.367(2) and 3.380 (2) Å, respectively.

VII—I Molecular Dynamics Simulations of Electrolyte Solutions

VII-I-1 Dissolution and Nucleation Phenomena of Salts in Water. Molecular Dynamic Approaches and Supporting Solution X-Ray Diffraction Measurements

Hitoshi OHTAKI

[*Pure & Appl. Chem.*, **65**, 203 (1993)]

Molecular dynamics (MD) simulations have been demonstrated to elucidate the dissolution and nucleation phenomena at a molecular level for a variety of alkali halide salts in water at 25°C. Within 12 to 20 ps anions in the LiCl, NaCl and CsF crystals have dissolved, but dissolution of cations has not been observed within the same time period. For KCl, NaF, and KF crystals which have cations and anions with similar size, no ions have dissolved within

20 ps, although the crystal lattice has significantly distorted. Thus, the rate of dissolution of ions is lower in crystals having the cations and anions with a similar size than in those with different sizes. In supersaturated aqueous solutions of NaCl and CsF ionic microclusters are formed which might be regarded as embryoes of nuclei of crystals. According to solution X-ray diffraction measurements of almost saturated aqueous solutions of NaCl (6.18 mol (kg H_2O)$^{-1}$) and KCl (4.56 mol (kg H_2O)$^{-1}$), 1:1 ion pairs are formed. On the other hand, ion clusters with the average coordination numbers of the cation-anion pairs, n_{MX}, of 2.29 and 3.33 are formed in KF (16.15 mol (kg H_2O)$^{-1}$) and CsF (31.96 mol (kg H_2O)$^{-1}$) solutions, respectively, the results being in good agreement with those obtained by the MD simulations.

VII-I-2 Molecular Aspects on the Dissolution and Nucleation of Ionic Crystals in Water

Hitoshi OHTAKI

[*Adv. Inorg. Chem.*, in press]

Dissolution and nucleation phenomena and the process of crystal growth of various salts in water have been discussed on the molecular level on the basis of X-ray diffraction data on solutions and crystals and results of MD simulations for the systems of alkali halides, calcium chloride hydrates, cohalt(II) chloride hydrates, and $M^{I}Cl \cdot MgCl_2$ hydrates with various alkali metal ions (M^{I}). Easy crystallization and rapid crystal growth have been discussed in connection with the similarity of structures of the constituent complexes in crystal with those in solution.

VII—J Developments of Novel Multi-functionalized Macrocyclic Compounds and Their Metal Complexes

Novel macrocyclic polyamines have been synthesized by renovating the classical structure of macrocyclic polyamines. Their metal complexes well mimic metal enzymes and act as excellent metal catalysts for a variety of interesting transformations of organic compounds.

VII-J-1 A Versatile Macrocyclic [12]aneN$_3$ for Interconversion of Tetrahedral and Trigonal Bipyramidal Zinc(II) Complexes. Relevance to Four- ⇌ Five-Coordinate Geometries of Zinc(II) in Carbonic Anhydrase

Eiichi KIMURA *(Hiroshima Univ. and IMS)*, **Tohru KOIKE, Mitsuhiko SHIONOYA** *(Hiroshima Univ.)*, **and Motoo SHIRO** *(Rigaku Corporation)*

[*Chem. Lett.*, 787 (1992)]

Carbonic anhydrases (CA) are a family of zinc enzymes that contain Zn^{II}-(imidazole)$_3$ complexes at the active centers. Thiocyanate anion, SCN^- is one of the typical CA inhibitors, which is due to the strong binding to the Zn^{II} ion. Recent X-ray crystal analysis of the SCN^- binding to CA showed the Zn^{II} ion in an ill-defined five-coordinate complex with SCN^- and a water.

Recently, we have discovered that a tetrahedral Zn^{II}-OH_2 triamine complex **1** with a 12-membered macrocyclic triamine ([12]aneN$_3$) is a good model for the active center of CA. Of particular interest was the similarly strong affinity of **1** to SCN^- ion into **2** (log$K$=2.4). X-Ray analysis of Zn^{II}[12]aneN$_3$(NCS)$_2$, **3**, has shown a *five-coordinate structure* with two bound SCN^- ions. The Zn^{II} ion is 0.095 Å above the N(1),N(5),N(16) trigonal plane to an apical SCN^- ion. The equatorial Zn-NCS-bond length is very short (Zn-N(16)2.012(3)Å) and the Zn-N-C angle is more linear (Zn-N(16)-C(17) 171.3(3)°C), and the apical Zn-NCS^- bond length is longer (Zn-N(13) 2.119(3)Å) and the Zn-N(13)-C(14) angle is bent at 152.2(3)°. This fact implies that the five-coordinate, trigonal bipyramidal structure is one of the *intrinsic properties* of Zn^{II} ion, where a strong σ donating ligand such as SCN^- comes at an equatorial position. The infrared CN stretching frequencies ν_{CN} of 2107 and 2062 cm^{-1} are assigned to the equatorial shorter N≡C length of 1.143(4)Å and the apical N=C length of 1.152(5)Å, respectively. The strong binding of the first incoming NCS^- ion would break the [*up,up,up*] configuration set for the tetrahedral geometry. **3** exhibited only three ^{13}C NMR signals assigned to two kinds of CH_2 and one SCN^- ion, and symmetrical ^1H NMR signals in MeOH at 27°C, indicating the fast equilibrium for **3** ⇌ **2** (or the H_2O-less, four-coordinated complex). The 12-membered macrocyclic triamine complex is thus well illustrating the four- ⇌ five-coordinate transformation of Zn^{II} in the enzyme.

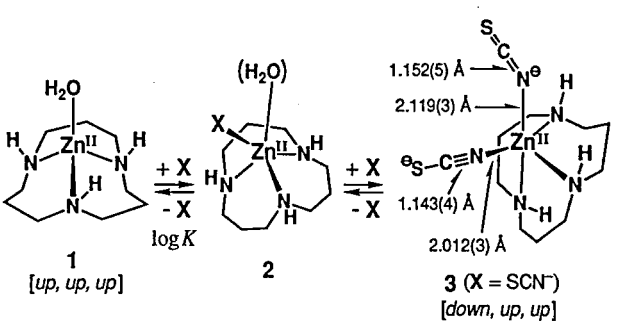

VII-J-2 The Gold(III)-Cyclam Complexes. X-ray Crystal Structure and a Useful Macrocyclic Effect on Reduction of Gold(III) for Development of New Gold Metal Plating

Eiichi KIMURA *(Hiroshima Univ. and IMS)*, **Yasuhisa KUROGI, Tohru KOIKE, Mitsuhiko SHIONOYA** *(Hiroshima Univ.)*, **and Yoichi IITAKA** *(Nishi-Tokyo Univ.)*

[*J. Coord. Chem.* in press]

X-Ray crystal structure of Au^{III}-cyclam complex **1** shows a four-coordinate square-planar N_4 geometry with *trans* III conformation (or *RRSS* configuration) of cyclam and an

average Au^{III}-N bond distance of 2.04 Å. A block-diagonal-matrix least-squares refinement yielded a final R value of 0.069 for 2463 independent reflections. Crystals of $\mathbf{1} \cdot (NO_3)_{1.5}(ClO_4)_{1.5} \cdot H_2O$ ($C_{10}H_{26}N_{5.5}O_{11.5}AuCl_{1.5}$) are triclinic, space group P1 with a=15.148(8)Å, b=8.668(5)Å, c=8.267(5)Å, α=109.17(6)°, β=101.08(5)°, γ=82.08(4)°, V=1003(1) Å^3, d_{calcd}=2.177 g cm^{-3}, and Z=2. The reduction potential for Au^{III} in **1** to Au^0 metal deposit varies with pH: −0.16V vs SCE (pH 1.0) to −0.55 V (pH 9.0) at I=0.50 ($NaClO_4$) and 259°C according to the degree of cyclam NH deprotonation. The macrocyclic gold(III) complex **1** has been found to posses very useful electrochemical properties for a novel gold-plating agent.

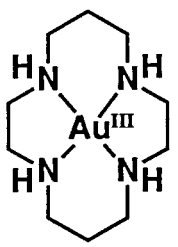

1

VII-J-3 The First Anionic Sulfonamide-Binding Zinc(II) Complexes with a Macrocyclic Triamine: Chemical Verification of the Sulfonamide Inhibition of Carbonic Anhydrase

Tohru KOIKE *(Hiroshima Univ.)*, **Eiichi KIMURA** *(Hiroshima Univ. and IMS)*, **Ikushi NAKAMURA, Yukie HASHIMOTO** *(Hiroshima Univ.)*, **and Motoo SHIRO** *(Rigaku Corporation)*

[*J. Am. Chem. Soc.*, **114**, 7338 (1992)]

Roles of Zn^{II} in zinc enzymes (e.g. carbonic anhydrase (CA)) have been discussed mostly on the basis of enzymatic studies. Chemical verification of these conclusions, or the bridging of the biochemical chemical facts about the zinc(II), has received little attention. The greatest challenge rests with the design of appropriate ligands mimicking the biological zinc environments. We have discovered that a 1:1 Zn^{II}-[12]aneN$_3$ complex **1** serves as the best structural as well as functional model for the active center of CA.

A zinc(II) complex with 1-(*p*-toluenesulfonamidopropyl)-1,5,9-triazacyclododecane, **2** has been synthesized as a model for sulfonamide inhibition of CA. X-ray crystal structure analysis of **2** showed a distorted tetrahedral structure, where a strong interaction is revealed between Zn^{II} and the sulfonamide anion. This intramolecular sulfonamide N^-binding to Zn^{II} completely inhibits formation of the Zn^{II}-OH^- species, which, as a model for CA active site, was previously shown to be formed with [12]aneN$_3$ and possess a strong nucleophilicity in ester hydrolysis or acetaldehyde hydration. The new complex **2** has no activity in 4-nitrophenyl acetate (NA) hydrolysis. Thus, **2** is shown to be a good chemical model for the strong sulfonamide inhibition of CA. Intermolecular interaction of **1** with HCO_3^- (a CA substrate), *p*-toluenesulfonamide, 4-nitrobenzenesulfonamide, and acetazolamide (a most potent CA inhibitor) was quantitatively determined by inhibition kinetics in NA hydrolysis. The intermolecular inhibition was caused by $ArSO_2NH^-$ or HCO_3^--binding to **1** and the inhibition order was acetazolamide ($\log K_i$=3.6) > HCO_3^-(2.8) > 4-nitrobenzenesulfonamide (2.6) > *p*-toluenesulfonamide (2.4). The apparent sulfonamide affinities (K_i at pH 8.4) to **1** are parallel with those reported for CA, and thus our model study provides the first chemical evidence of strong acetazolamide-binding to Zn^{II} in CA.

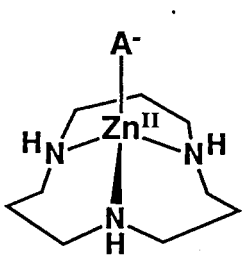

1

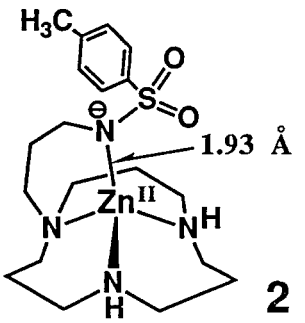

2

VII-J-4 The pH-Dependent Coordination Mode of New Bleomycin Synthetic Analogues with Copper(II), Iron(II), and Zinc(II)

Eiichi KIMURA *(Hiroshima Univ. and IMS)*, **Hiromasa KUROSAKI, Yasuhisa KUROGI, Mitsuhiko SHIONOYA** *(Hiroshima Univ.)*, **and Motoo SHIRO** *(Rigaku Corporation)*

[*Inorg. Chem.*, **31**, 4314 (1992)]

The new simplified bleomycin (BLM)-mimic ligands $\mathbf{L}_1$ and $\mathbf{L}_2$ (=a carbamide attached $\mathbf{L}_1$) have been synthesized to study pH-dependent coordination chemistry. Comparison of the protonation constants for $\mathbf{L}_1$ (9.8, 7.3, and 5.6 at 25°C, I=0.2 ($NaClO_4$)) and $\mathbf{L}_2$ (7.8, 6.9, and 3.7) reveals the significance of the carbamide group which is applied to the primary function of the corresponding carbamide of the β-aminoalanine portion in BLM. The pH-dependent complexation behaviors of $\mathbf{L}_1$ and $\mathbf{L}_2$ with Cu^{II}, Fe^{II}, and Zn^{II} were studied with pH-metric titrations. The X-ray crystal study of $[Cu^{II}(H_{-1}\mathbf{L}_2)]^+$ as perchlorate salts proves the 5-coordinate, square-pyramidal complex structure. Final R and R_w values were 0.056 and 0.084, respectively: $C_{15}H_{20}N_7O_2Cu \cdot ClO_4 \cdot H_2O$, triclinic, space group P_1 with a=9.566(1), b=13.760(1), c=8.504(1)(Å), α=105.13(1)°, β=101.14(1)°, γ=98.84(1)°, ρ_c=1.640 (g cm^{-3}) for Z=2, V=1035.4(2)(Å^3).

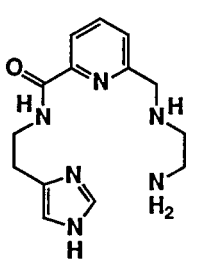

$\mathbf{L}_1$

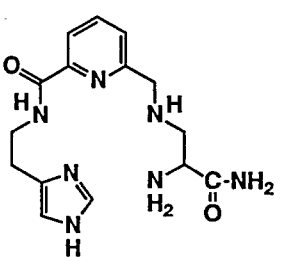

$\mathbf{L}_2$

VII-J-5 A New Nickel(II) Cyclam Complex Covalently Attached to Ru(phen)$^{2+}$. A New Candidate for the Catalytic Photoreduction of Carbon Dioxide

Eiichi KIMURA *(Hiroshima Univ. and IMS)*, **Xianhe BU, Mitsuhiko SHIONOYA, Senji WADA, and Shinobu MARUYAMA** *(Hiroshima Univ.)*

[*Inorg. Chem.*, **31**, 4542 (1992)]

A bifunctional supramolecular complex $Ru(phen)_2(phen\text{-}cyclam\text{-}Ni)(ClO_4)_4$ (**1**)(phen-cyclam=1-(1',10'-phenanthrolin-5'-ylmethyl)-1,4,8,11-tetraazacyclotetradecane) has been newly synthesized, and its spectroscopic, redox properties and catalytic behavior in the phtoreduction of CO_2 have been examined. The new binuclear complex **1** is shown to be an interesting hybrid molecule composed of a $Ru(phen)_3^{2+}$ (phen=1,10-phenanthroline) subunit, which acts as a photosensitizer, and a $Ni(cyclam)^{2+}$ catalytic reduction site.

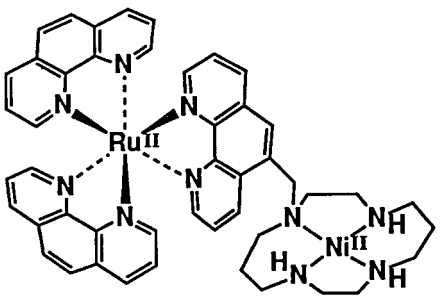

1

VII-J-6 A Model for Catalytically Active Zinc(II) Ion in Liver Alcohol Dehydrogenase: A Novel "Hydride Transfer" Reaction Catalyzed by Zn^{II}-Macrocyclic Polyamine Complexes

Eiichi KIMURA *(Hiroshima Univ. and IMS)*, **Mitsuhiko SHIONOYA, Ayumi HOSHINO, Takuya IKEDA, and Yuko YAMADA** *(Hiroshima Univ.)*

[*J. Am. Chem. Soc.*, in press]

The role of Zn^{II} ion at the active center of liver alcohol dehydrogenase has been well-defined for the first time by the comparative studies of Zn^{II}-[12]aneN$_3$, **1**([12]aneN$_3$= 1, 5, 9-triazacyclododecane, L_1), Zn^{II}-[12]aneN$_4$, **2** ([12]aneN$_4$=1, 4, 7, 10-tetraazacyclododecane,L_2), Zn^{II}-[14]aneN$_4$, **3** ([14]aneN$_4$=1,4,8,11-tetraazacyclotetradecane, L_3), and Zn^{II}_{aq}, **4.** Variations in Zn^{II} acidity and coordination environment in these complexes result in varying degrees of catalytic activity in the reduction of *p*-nitrobenzaldehyde and an NAD^+ model compound with alcohols as the "hydride" sources (e.g., 2-PrOH) to *p*-nitrobenzyl alcohol and the corresponding NADH model compound, respectively. Among Zn^{II} species tested, the Zn^{II} complex of macrocyclic triamine [12]aneN$_3$, **5**, $(L_1\text{-}Zn^{II}\text{-}OH)_3 \cdot (TfO)_3 \cdot TfOH$ (TfOH (TfO=CF_3SO_3-), was by far the most effective catalyst: *p*-nitrobenzyl alcohol was obtained from *p*-nitrobenzaldehyde in 7820 % yield (based on [Zn^{II}]) in the presence of **5** (0.8 mol %) in refluxing 2-PrOH for 24 h. The Zn^{II} complex **5**, also promotes the "hydride transfer" from 2-PrOH to an NAD^+ model compound, *N*-benzylnicotinamide chloride, to yield the 1,4-adduct, *N*-benzyl-1, 4-dihydronicotinamide exclusively. It is concluded, from the comparison of **5** with other Zn^{II} complexes of [12]aneN$_4$ and [14]aneN$_4$, that the most acidic and coordinatively least saturated Zn^{II} in L_1 catalytically generates Zn^{II}-alkoxide complex to facilitate the "hydride transfer" to the "hydride" acceptor on the Zn^{II} coordination sphere. The present study provides the first chemical model illustrating the significance of the Zn^{II} acidity and the steric requirement around Zn^{II} coordination sphere in the "hydride transfer" reaction (from alcohol) catalyzed by Zn^{II}-containing alcohol dehydrogenases (ADH).

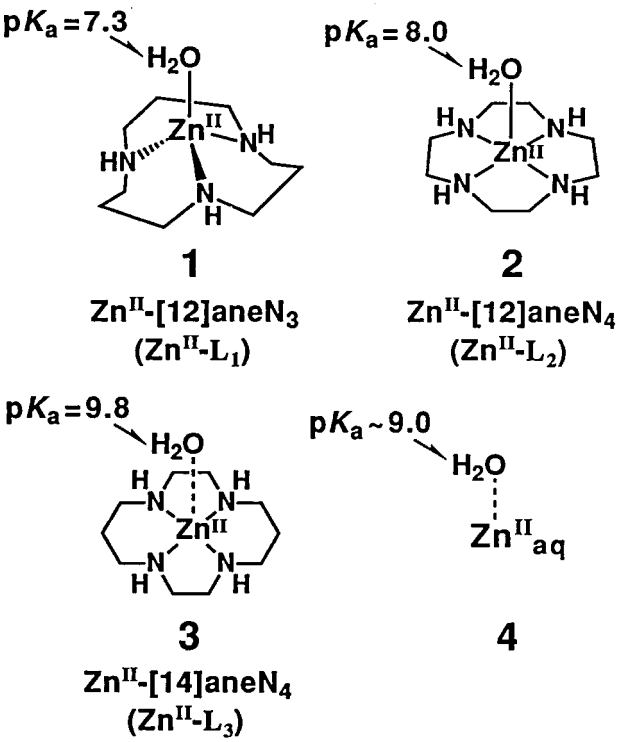

1 Zn^{II}-[12]aneN$_3$ (Zn^{II}-L_1)

2 Zn^{II}-[12]aneN$_4$ (Zn^{II}-L_2)

3 Zn^{II}-[14]aneN$_4$ (Zn^{II}-L_3)

4

VII-J-7 Inversion of DNA Helicity Induced by Zinc(II)-Macrocyclic Polyamine Complexes

Mitsuhiko SHIONOYA *(Hiroshima Univ.)*, **Eiichi KIMURA** *(Hiroshima Univ. and IMS)*, **Hiromi HAYASHIDA** *(Hiroshima Univ.)*, **Gabor PETHO, and Luigi G. MARZILLI** *(Emory Univ.)*

[*Supramolecular Chemistry* in press]

Exposure of synthetic polynucleotide poly(dG-dC) · poly(dG-dC) to a zinc(II) complex of macrocyclic tetraamine, [12]aneN$_4$ or cyclen (=1,4,7,10-tetraazacyclododecane), produces a dramatic change in its circular dichroism (CD) in H_2O at pH 7.2 and 24°C: the CD spectrum of the initial B form changes to the spectrum characteristic of Z form (or a non-Z structure with left-handed helix) at very low concentrations ([Zn^{II}]/[base pair] in molar basis < 1). By contrast, Zn^{II}-[12]aneN$_3$ ([12]aneN$_3$=1,5,9-triazacyclododecane) and Zn^{II}-cyclam (cyclam=1,4,8,11-tetraazacyclotetradecane) do not significantly affect such a topological change of the polynucleotide even at much higher concentrations. An increase in Na^+ ionic strength nullified

the effect of Zn^{II}-cyclen on the CD spectrum, indicating an outside interaction (electrostatic and/or hydrogen bonding) of the DNA model. This study illustrates the significance of the macrocyclic ligand structure around Zn^{II} ion for the specific interaction with DNA.

VII—K Bioinorganic Studies on Metalloporphyrins

New chiral porphyrins and electron-deficient porphyrins have been synthesized and characterized by molecular spectroscopies. Some metalloporphyrins showed effective catalytic oxidation of olefins and specific binding with nucleobases.

VII-K-1 New Mode Complexation of Porphyrin with Nucleobase

Hisanobu OGOSHI *(Kyoto Univ. and IMS)*, **Hitoshi HATAKEYAMA** *(Kyoto Univ.)*, **Jun KOTANI** *(Kyoto Univ.)*, **Ayato KAWASHIMA** *(Kyoto Univ.)*, **and Yasuhisa KURODA** *(Kyoto Univ.)*

[*J. Am. Chem. Soc.*, **113**, 8181 (1991)]

Molecular recognition of nucleosides using porphyrin derivatives was investigated, It was found that porphyrin Zn(II) complexes bound 3',5'-bis(O-triisopropylsilyl) deoxyribonucleosides via coordination interaction except the thymine derivative. Among porphyrin derivatives investigated as a host molecule, 5,15-bis(2-hydroxy-1-naphthyl) octaethylporphyrin, 1, was demonstrated to bind adenine via simultaneous double hydrogen bondings without the assistance of coordination interaction. Thus, its Zn complex acts as "both sides receptor" which recognizes two adenine molecules using hydrogen bonds with OH groups and coordination on a Zn atom. Its association constant for 9-ethyladenine, 41000 M^{-1}, is shown to be one of the largest value ever reported for the artificial adenine receptors. Taking account of wide variety of functions of porphyrin complexes, the present new 1:2 complex of 1Zn with adenine derivatives is expected to offer unique applications both for the nucleoside recognition and for its reactions.

VII-K-2 Olefin Oxidation Catalyzed by Electron Deficient Metallo-Porphyrin

Hisanobu OGOSHI *(Kyoto Univ. and IMS)*, **Yasuhiko SUZUKI** *(Kyoto Univ.)*, **and Yasuhisa KURODA** *(Kyoto Univ.)*

[*Chemistry Lett.*, 1548 (1991)]

Olefin oxidations catalyzed by Ge or Mn complexes of 2,4,6,8-tetratrifluoromethyl-1,3,5,7-tetraethylporphyrin(TFTEP) using iodosobenzene as oxidant were investigated, The electron deficient character of TFTEP which has four trifluoromethyl groups is clearly shown by its redox potential. For example, the redox potential of TFTEP · Mn is 10 times faster than that catalyzed by OEP · Mn. In contrast with these different properties between OEP and TFTEP, the relative reactivities of various types of olefins towards epoxidation catalyzed by these porphyrins are found to be quite similar. Furthermore, the exo/endo product ratio in the norbornene epoxidation catalyzed by TFTEP is practically same with that by OEP and the ratio seems to be affected only by the central meta. These results shows that the electronic effect in porphyrin ring does not seriously affect the selectivity of norbornene oxidations.

VII-K-3 Selective Syntheses of Unsymmetrical meso-Arylporphyrins

Tadashi EMA *(Kyoto Univ.)*, **Yasuhisa KURODA** *(Kyoto Univ.)*, **and Hisanobu OGOSHI** *(Kyoto Univ. and IMS)*

[*Tetrahedron Lett.* **32**, 4529 (1991)]

A selective synthetic route to unsymmetrical meso-arylporphyrins is described. The synthetic strategy for the target unsymmetrical porphyrins belonging to C_{2V} symmetry is based on the pyrrylcarbinol method as the key coupling reaction. The coupling of 5,5'-biscarbinoldipyrrylmethane bearing two aryl groups on carbinol carbons with 5,5'-unsubstituted dipyrrylmethane in a [2+2] way gave the desired unsymmetrical porphyrin exclusively. Three different porphyrins are synthesized by this method and all products are characterized by ^{1}H-NMR, FABMS and UV-Vis Spectra. Among the porphyrins obtained in this method, 5,15-diphenyl-10-p-chlorophenyl-2,3,17,18-tetraethylporphyrine is the new type of porphyrin which have not ever been synthesized. Spectroscopic and redox behaviors of this new porphyrin show a hybrid character of TPP and OEP. The present new synthetic route is expected to be widely applicable to syntheses of unsymmetrically substituted porphyrins.

VII-K-4 Iron(III) Porphyrins Substituted with Highly Electron-Withdrawing CF_3 Group: Electronic Absorption MCD, and EPR Spectral Study

Tetsuhiko YOSHIMURA *(Nagoya Univ. Technol.)* **Hiroo TOI** *(Nagaoka Univ. Technol.)*, **Shinji INABA** *(Nagaoka Univ. Technol.)*, **and Hisanobu OGOSHI** *(Kyoto Univ. and IMS)*

[*Inorganic Chemistry*, **30**, 23 (1991)]

Electronic absorption, MCD, and EPR spectra of iron (III) complexes of etioporphyrin I and electron-deficient porphyrins with one, two, or four CF_3 groups at pyrrole β-positions of the porphyrin have been measured. The overall equilibrium constants of the reaction of the iron(III) porphyrin chloride with imidazole and 1-methylimidazole were evaluated from the electronic spectral changes on addition of the bases. The equilibrium constants for imidazole have a slight tendency to decrease with the number of CF_3 group, and those for 1-methylimidazole have a marked such tendency. The effects of highly electron-withdrawing substituents at the porphyrin periphery were revealed more obviously in the MCD spectra of the (porphyrinato)iron(III) chloride than in the electronic spectra. MCD spectral results indicated that the Soret region is sensitive to minor changes in the redox potential of the porphyrin. In the EPR

spectra of both low-spin complexes with imidazole and 1-methylimidazole, the g anisotropy was apparently lowered and the tetragonality m/o was increased with an increase in the number of CF_3 groups. The rhombicity R/u for CF_3-substituted porphyrin complexes was larger than that for the unsubstituted analogues. These EPR spectral results were discussed in relation to the electron-withdrawing ability of peripheral substituents.

VII-K-5 Bis(1-methylimidazole)iron(II) Complex of Porphyrins Substituted with Highly Electron-Withdrawing CF_3 Groups: Electronic Spectra with Split Q-Bands and MCD Spectra with Unusual Features

Tetsuhiko YOSHIMURA *(Nagaoka Univ. Technol.)*, **Hiroo TOI** *(Nagaoka Univ. Technol.)*, **Shinji INABA** *(Nagaoka Univ. Technol.)*, **and Hisanobu OGOSHI** *(Kyoto Univ. and IMS)*

[*Bull. Chem. Soc. Jpn*, 65 (1992)]

The Bis(1-methylimidazole)iron(II) complexes of porphyrins substituted with one, two, or four CF_3 groups at pyrrole β-positions of a porphyrin have been studied by electronic absorption and magnetic circular dichroism(MCD) spectroscopies. The splittings of Q-Bands observed in the electronic spectra of the complexes may arise ration of absorption intensity ($\varepsilon(\alpha)/(\varepsilon(\beta))$ decreased with an increase of the number of CF_3 group, suggesting the decrease of a splitting in HOMOs. The MCD spectra of the bis(1-methylimidazole)iron(II) porphyrin complexes were markedly sensitive to the porphyrin peripheral substituents. The MCD spectra in Soret region successively changed in shape with the number of CF_3 group on porphyrin periphery and consequently were apparently inverted in sign, which can be explained by the shift of maximal wavelength accompanied by a change in intensity.

VII-K-6 Molecular Recognition of Quinones: Two Point Hydrogen-Bonding Strategy for the Construction of Face-to-Face Porphyrin-Quinone Architectures

Yasuhiro AOYAMA *(Nagaoka Univ. Technol.)*, **Masumi ASAKAWA** *(Nagaoka Univ. Technol.)*, **Yuichi MATSUI** *(Nagaoka Univ. Technol.)*, **and Hisanobu OGOSHI** *(Kyoto Univ. and IMS)*

[*J. Am. Chem. Soc.*, **113**, 6233 (1991)]

5, 15-cis-Bis(hydroxy-1-naphthyl)octaethylporphyrin, 1, in chloroform selectively binds p-quinones via two-point hydrogen-bonding interaction between the two, convergent hydroxyl groups of host 1 and two carbonyl moieties of guest quinone. Upon complexation the ^1H NMR resonance and IR absorption for the OH groups undergo a characteristic downfield shift and a shift to lower wavenumber, respectively. The variation in the binding constants, K, suggests that the strength of hydrogen bonds, direct porphyrin-quinone interaction apparently of a charge-transfer type, and the steric effects of methoxy substituents are important factors. The resulting 1-quinone adducts have an estimated face-to-face separation of as short as 3A and exhibit porphyrin-quinone π-π interaction as revealed by UV/visible spectroscopy; the longest wavelength absorption band of 1 undergoes either a blue shift or a red shift depending on the electronic property of bound quinone. In addition the adducts are rendered completely nonfluorescent as a result of an efficient, intracomplex electron transfer from photoexited 1 to bound quinone.

VII—L Structure and Chemical Properties of Transition Metal Complexes Relevant to Homogeneous Catalysis

Many synthetic organic reactions catalyzed by transition metal complexes involve organotransition metal complexes as the key intermediates. Structures and fundamental reactions of the transition metal complexes were elucidated by means of X-ray kinetic measurement.

VII-L-1 Palladium and Platinum Complexes with π-Allyl and Carbonato Ligands.

Fumiyuki OZAWA*, Tae-il SON*, Kohtaro OSAKADA, and Akio YAMAMOTO* *(*Tokyo Inst. Tech.)*

[*Organometallics*, **11**, 171 (1992)]

Palladium complex catalyzed functionalization of allyl carbonates has been extensively utilized in synthetic organic chemistry. However, there have been few studies on the intermediate π-allyl(carbonato)palladium complexes. Reaction of a Pd(0) complex with PMe_3 ligands, generated in situ by reaction of $PdEt_2(PMe_3)_2$ with styrene, with allyl alkyl carbonate gives palladium complexes both with π-allyl and alkylcarbonato ligands. The alkyl carbonato ligands readily undergo hydrolysis by trace amount of water contained in the solvent to give hydrogen carbonato ligand. Structure of a π-allylpalladium hydrogen carbonato complex was determined by X-ray crystallography. Reaction of CO with the allylpalladium complexes gives butenoate ester and ether as the products. Properties of π-allylplatinum complexes were also investigated.

VII-L-2 Oxidation and Reduction of Polyaniline.

Doo-Kyong MOON*, Kohtaro OSAKADA, and Takakazu YAMAMOTO* *(*Tokyo Inst. Tech.)*

[*Chem. Lett.*, 1633 (1991) *Macromolecules* in press]

Polyaniline molecule has several possible structures depending on the oxidation state. Oxidation of reduced polyaniline (PLM) using O_2 or H_2O_2-Fe catalyst gives partially oxidized polyaniline (PEM) very cleanly. Kinetic study was carried out by measurement of the absorption spectra of the

reaction mixture. Reaction of O_2 with PLM obeys simple first-order kinetics both to the polymer concentration and to oxygen while the reaction using H_2O_2 in the presence of Fe catalyst agrees with Michelis-Menten kinetics. These results were interpreted by assuming the probable radical intermediates in the oxidations. These oxidation reactions were extended to H_2O_2 oxidative polymerization of aniline derivatives to give substituted polyanilines that have not been obtained in high yields.

VII—M Synthesis of Optically Active Complexes and their Catalytic Properties

The enantioselective synthesis of organic compounds using chiral transition metal complexes has received attention. We are interested in the asymmetric epoxidation of olefins and oxidation of prochiral sulfides. In this project, the synthesis of new optically active complexes and their catalytic porperties are investigated.

VII-M-1 Structure of Two Geometrical Isomers of Dioxo[*(S)-N*-salicylidene-3-aminopyrrolidine]vanadium(V)

Kiyohiko NAKAJIMA, Nobuko TOKIDA*, Masaaki KOJIMA, and Junnosuke FUJITA*** *(*Nagoya Univ., **Okayama Univ.)*

[*Bull. Chem. Soc. Jpn.*, **65**, 1725 (1992)]

Dioxo[*(S)-N*-salicylidene-3-aminopyrrolidine]vanadium(V) was prepared and the crystal structure was determined by the X-ray method. Two geometrical isomers are in a unit cell. For each isomer, the coordination polyhedron is a distorted square pyramid, and the two isomers differ from each other with respect to the mutual disposition of the basal chelate ligand and the apical V=O group. These two isomers are interconvertible in solution and the equilibrium between the isomers varies with the kind of solvent.

VII—N Chemical Simulation of Biological Nitrogen Cycle and Carbon Dioxide Fixation

The amount of inorganic nitrogen compounds on earth is regulated by the nitrogen cycle, which consists of N_2 fixation, nitrification, assimilatory and dissimilatory reduction of NO_3^-. The pathways for those biological multi-electron redox reactions have not been solved completely. There are, in particular, great arguments against the pathway of NO_2^- to N_2 by nitrite reductases containing heme and copper proteins. Despite of a strong affinity of NO for heme proteins, NO evolves during the turnover. Furthermore, the process of the N-N bond formation of N_2O as the precursor of N_2 is still unresolved. Copper or iron complexes having an ability of catalyzing dissimilatory reduction of NO_2^- to N_2 via NO and N_2O in H_2O, therefore, are of great interest from the viewpoints of the elucidation for biological NO_2^- reduction. In green plants and photosynthetic bacteria, carbon dioxide is fixed to carbonyl carbons of organic molecules to form α-hydroxy of α-keto acids as the precursor of glucose and α-amino acids, although it is not clear whether CO_2 or substrates are activated by enzymes. To simulate those reactions by artificial CO_2 fixation may give clues to disclose the evolution of biological CO_2 fixation.

VII-N-1 Characterization of Formyl- and Hydroxymethyl Ru(II) Complex as Precursors for Methanol Formation

Hirotaka NAGAO, Tetsunori MIZUKAWA, Hiroaki TANAKA, and Koji TANAKA

There has been growing interest in activation and utilization of CO_2 as well as CO by using homogeneous catalysts. A variety of transition metal complexes have proved to be active electro- and photochemical CO_2 reduction affording CO and/or HCOOH. Multi-electron reduction products such as CH_3OH and CH_4, however, have not been obtained in those CO_2 reduction catalyzed by homogeneous catalysts. The reactions of $[Ru(bpy)_2(CO)_2](PF_6)_2$ **(1)** and $[Ru(bpy)(trpy)(CO)](PF_6)_2$**(2)** (bpy=2,2'-bipyridine; trpy= 2,2': 6,2"-terpyridine) with 1 equiv of $NaBH_4$ gave $[Ru(bpy)_2(CO)(CHO)]^+$ and $[Ru(bpy)(trpy)(CHO)]^+$ with evolving a small amount of CO in CH_3CN/H_2O at −30°C, and methanol was produced in the solution (5 and 12% based on the complexes) upon heating the reaction mixtures. The yields of methanol increased to 50 and 100%, when **2** was treated with 2 and 4 equiv of $NaBH_4$. As the precursor for the formation of methanol, $[Ru(bpy)_2(CO)(CH_2OH)](PF_6)$ was isolated in the reaction of **1** with $NaBH_4$, and the molecular structure was determined by X-ray analysis (Figure 1). In addition, the electrochemical reduction of CO_2 by **2** under protic conditions produced not only CO and HCOOH but also methanol. These results can be explained by a successive reduction of CO_2 ligated to Ru to methanol through the Ru-C(O)OH, Ru-CO, Ru-CHO, and Ru-CH_2OH moieties.

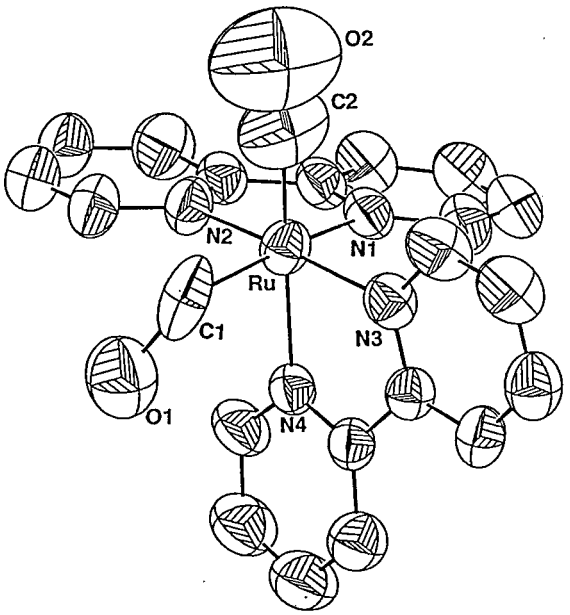

Molecular structure of $[Ru(bpy)_2(CO)CH_2OH]^+$.

VII-N-2 Denitrification of NO_2^- on a Copper Site in Water

Nobutoshi KOMEDA*, Ryo MIYAMOTO, Hirotaka NAGAO, Gin-ya ADACHI*, Masatatsu SUZUKI, Akira UEHARA**, and Koji TANAKA** *(*Osaka Univ. **Kanazawa Univ.)*

Denitrification of NO_2^- by nitrite reductase containing heme and copper proteins is the key reaction of the nitrogen cycle. There are controversies about the precursors of NO and N_2O evolution in the pathway from NO_2^- to N_2O. A nitrito complex $[Cu(tpa)(ONO)](PF_6)$ (Figure 1) prepared by the reaction of $[Cu(tpa)(H_2O)]^{2+}$(tpa= $(2-C_5H_4NCH_2)_3N$) with $NaNO_2$, exist as an equilibrium mixture with $[Cu(tpa)(NO_2)](PF_6)$ in solutions. A controlled potential electrolysis of an aqueous solution (pH 7.0) containing $[Cu(tpa)(H_2O)](ClO_4)_2$ and $NaNO_2$ catalytically produced NO, N_2O, and N_2 at -0.40 V (vs. Ag/AgCl) without decomposition of the complex. The present denitrification is initiated by reduction of $[Cu(tpa)(ONO)]^+$ and $[Cu(tpa)(NO_2)]^+$ in H_2O, and NO evolution can be account for the Cu-O bond cleavage and lability of the Cu-ON bond resulting from the removal of the bound- or terminal-oxygen in the Cu-ONO moiety. Free NO thus formed will form a nitrogen-bound nitrosyl adduct, $[Cu(tpa)(NO)]^{2+}$, which also is formed in the reduction of $[Cu(tpa)(NO_2)]^+$ in H_2O without the Cu-NO bond cleavage, because of the removal of the terminal-oxygen of the Cu-NO_2 moiety. Thus, $[Cu(tpa)(NO)]^{2+}$ is the obligatory intermediate in the present denitrification of NO_2^- in H_2O.

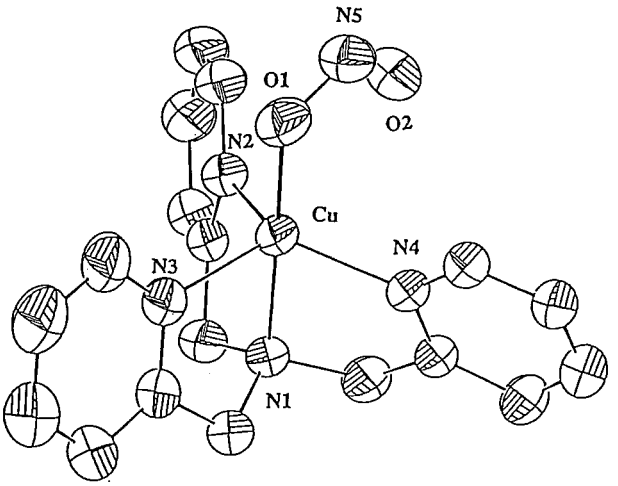

Molecular structure of $[Cu(tpa)(ONO)]^+$.

VII-N-3 Electrochemical Carbon Dioxide Fixation to Thioesters Catalyzed by $[Mo_2Fe_6S_8(SEt)_9]^{3-}$

Nobutoshi KOMEDA*, Hirotaka NAGAO, Tatsuji MATSUI*, Gin-ya ADACHI*, and Koji TANAKA* *(*Osaka Univ.)*

[*J. Am. Chem. Soc.*, **114**, 3625 (1992)]

A controlled potential electrolysis at −1.55 V *vs.* SCE of CO_2-saturated CH_3CN containing $(Et_4N)_3[Mo_2Fe_6S_8(SEt)_9]$, $CH_3C(O)SEt$, Bu_4NBF_4, and molecular sieves 3A as a desiccant produced $CH_3C(O)COO^-$ with current efficiency 27%. Similar electrolysis using $C_2H_5C(O)SEt$ and $C_6H_5C(O)SEt$ also catalytically afforded $C_2H_5C(O)COO^-$ and $C_6H_5C(O)COO^-$ with current efficiency 49 and 13%, respectively. Those reactions are strongly inhibited by the presence of not only H_2O but also excess EtS^-. Strong acylating agents such as acetyl chloride, acetic anhydride, acetyl sulfide, and acetylimidazole in place of $CH_3C(O)SEt$ caused decomposition of $[Mo_2Fe_6S_8(SEt)_9]^{3-}$ and no $CH_3C(O)COO^-$ was formed under the same electrolysis conditions.

VII-N-4 Stabilization of Superoxide Form of an Fe_4S_4 Cluster in Aqueous Media

Hide KAMBAYASHI, Masami NAKAMOTO*, S.-M. PENG, Hirotaka NAGAO, and Koji TANAKA** *(*Osaka Municipal Technical Research Institute, **National Taiwan Unv.)*

4Fe-iron sulfur proteins operate among three different oxidation states, $[Fe_4S_4]^+$, $[Fe_4S_4]^{2+}$, and $[Fe_4S_4]^{3+}$. Ferredoxins (Fd) exhibit the $[Fe_4S_4]^{+/2+}$ redox couple around −0.7 V *vs.* SCE, while high potential iron-sulfur proteins (Hp) show the $[Fe_4S_4]^{2+/3+}$ couple around 0 V at pH7. Stability of the $[Fe_4S_4]^{3+}$ state of Hp_{OX} has been explained in terms of protection of the Fe_4S_4 core from water attack by hydrophobic protein environments around Fe_4S_4 cores. Adamantanethiolate ligated Fe_4S_4 cluster, $[Fe_4S_4(SAd)_4]^{2-}$, exhibits two stable $[Fe_4S_4]^{+/2+}$ and $[Fe_4S_4]^{2+/3+}$ redox couples in dry DMF and aqueous PDAH solutions (PDAH=Poly[2−(dimethylamino)hexanamide]), and protons participate in those redox reactions in the latter, while it undergoes an irreversible oxdation in the presence of a small amount of H_2O in DMF (3 vol%). Unusual

hydrolysis reaction of $[Fe_4S_4(SAd)_4]^-$ in H_2O and H_2O/DMF solutions can be account for depression of dissociation of the terminal AdS^- ligand due to the insolubility in H_2O rather than hydrophobic spheres around the $[Fe_4S_4]^{3+}$ core. In accordance with this, midpoint potentials of some Hp proteins in Reiske center shift by −0.06 V/pH, as similar to the present study. In addition, X-ray crystal structure of $(Ph_4As)_2[Fe_4S_4(SAd)_4]$ (Figure 1) reveals that the cluster has open space for coordination of the solvent molecules to the Fe_4S_4 core.

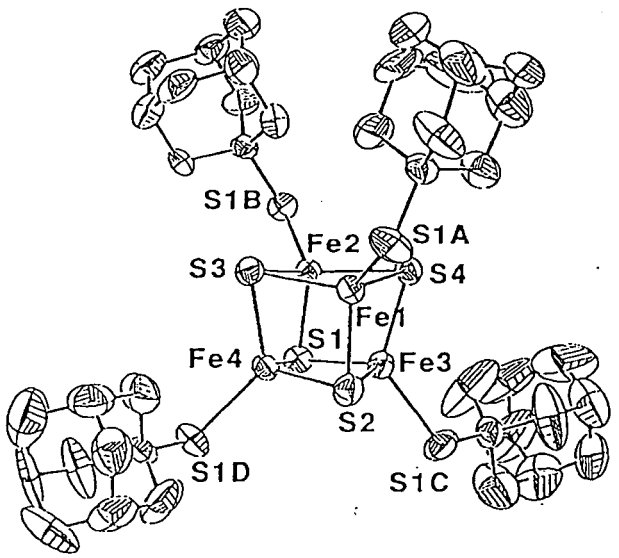

Figure 1. Molecular structure of $[Fe_4S_4(SAd)_4]^{2-}$.

VII-N-5 Comparative Study on Crystal Structures of $[Ru(bpy)_2(CO)_2](PF_6)_2$, $[Ru(bpy)_2(CO)(C(O)OCH_3)]B(C_6H_5)_4 \cdot CH_3CN$, and $[Ru(bpy)_2(CO)(\eta^1\text{-}CO_2)] \cdot 3H_2O$ (bpy=2,2'-bipyridyl)

Hiroaki TANAKA, Biing-Chiau TZENG*, Hirotaka NAGAO, Shie-Ming PENG*, and Koji TANAKA*
*(*National Taiwan Univ.)*

Since the first characterization of $Ni(PC_{y3})_2(\eta^2\text{-}CO_2)$, a variety of CO_2-metal complexes with η^1-, η^2-, μ^2-, and μ^3-CO_2 modes have been prepared. As expected from the rapid interconversions among $[Ru(bpy)_2(CO)_2]^{2+}$, $[Ru(bpy)_2(CO)(C(O)OH)]^+$, and $[Ru(bpy)_2(\eta^1\text{-}CO)(CO_2)]$ in H_2O, the η^1-CO_2 mode may be more suitable than others as an active species in the reduction of CO_2 affording CO and HCOOH. We have determined the molecular structures of $[Ru(bpy)_2(CO)_2](PF_6)_2$, $[Ru(bpy)_2(CO)(C(O)OCH_3]B(C_6H_5)_4 \cdot CH_3CN$ as a model complex of $[Ru(bpy)_2(CO)(C(O)OH)]^+$, and $[Ru(bpy)_2(CO)(\eta^1\text{-}CO_2)] \cdot 3H_2O$ by X-ray analysis (Figure 1). The fact that the Ru-$C(O)OCH_3$ bond distance for $[Ru(bpy)_2(CO)(C(O)OCH_3)]^+$ is shorter than the Ru-CO_2 one for $[Ru(bpy)_2(CO)(CO_2)]$ suggests that the multi-bond character of the Ru-CO_2 bond is not larger than the Ru-$C(O)OCH_3$ bond. One extra electron-pair produced by dissociation of a terminal proton of $[Ru(bpy)_2(CO)(C(O)OH)]^+$ may be mainly localized in the CO_2 ligand in $[Ru(bpy)_2(CO)(CO_2)]$ rather than delocalized over the $RuCO_2$ moiety. The existence of the extended three dimensional network of hydrogen bondings between the CO_2 ligand and three hydrated water molecules for $[Ru(bpy)_2(CO)(CO_2)] \cdot 3H_2O$, therefore, compensates the increase in the electron density of the CO_2 moiety.

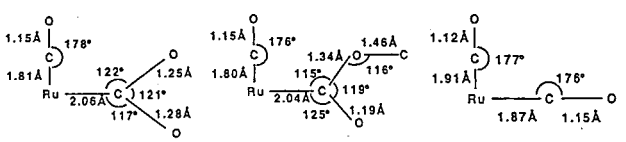

Figure 1. Bond distances and angles for the Ru(CO)(CO_2), Ru(CO)(C(O)OCH_3), and Ru$(CO)_2$ moieties.

VII—O Development of Highly Selective Reactions Using Early Transition Metal Complexes

Highly selective bond formation reactions have been investigated using early transition metal complexes, especially zirconium complexes. Zirconium alkene complexes can be easily prepared and these species led us not only stoichiometric but catalytic highly selective C-C, C-Si, C-H, C-X bond formation reactions.

VII-O-1 Hydrosilation Reactions Catalyzed by Zirconium Complexes

Tamotsu TAKAHASHI, Maki HASEGAWA*, Noriyuki SUZUKI, Masahiko SABURI*, Christophe J. ROUSSET and Ei-ichi NEGISHI**** *(*Tokyo Univ. **Purdue Univ.)*

[*J. Am. Chem. Soc.*, **113**, 8564, (1991)]

We investigated zirconium catalyzed hydrosilation reactions of alkenes and X-ray structure of a novel hydrosilated zirconocene dimer $[Cp_2Zr(H)(HSiPh_2)]_2$ with bridged hydride ligands, which was obtained as a stable complex from the reaction mixture of the zirconium catalyst and H_2SiPh_2. The hydrosilation reactions of alkenes proceeded in good yields (70—80%) with high regioselectivity (>98%).

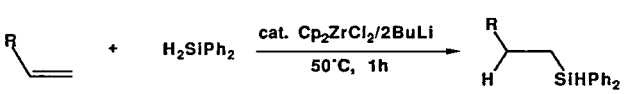

R = C_8H_{17} 73%
Ph 78%

In the presence of an excess of H_2SiPh_2 or $H_2SiMePh$ a novel zirconocene dimer complex $[Cp_2Zr(\mu\text{-}H)(HSiPh_2)]_2$ or $[Cp_2Zr(\mu\text{-}H)(HSiPh_2)]_2$ was obtained from the reaction mixture. This complex can be considered as an oxidative addition product of H_2SiPh_2 or $H_2SiMePh$ to zirconocene species "Cp_2Zr".

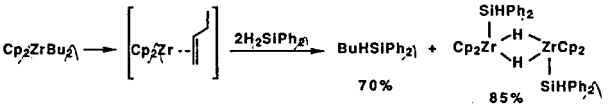

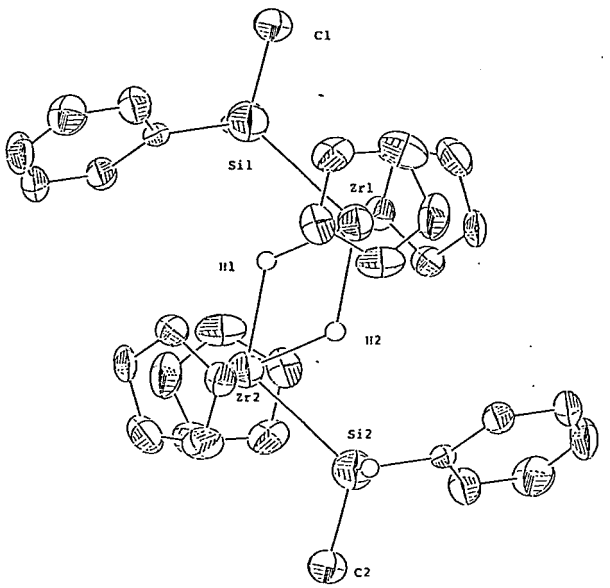

Perspective view of $[Cp_2ZrH(SiHMePh)]_2$.

VII-O-2 Novel Head-to-Tail Alkyl-Alkene Coupling via Zirconium Catalyzed Reactions of Alkylmagnesium Derivatives with Monosubstituted Alkenes

Christophe J. ROUSSET*, Ei-ichi NEGISHI*, Noriyuki SUZUKI, and Tamotsu TAKAHASHI, *(*Purdue Univ.)*

[*Tetrahedron Lett.*, **33**, 1965 (1992)]

The reaction of monosubstituted alkenes with alkylmagnesium derivatives catalyzed by Cp_2ZrCl_2 or related zirconocene derivatives provides head-to-tail alkyl-alkene or alkene-alkene coupling products, about 50% of which are 2,5-dailkyl-4-pentenylmagnesium halides.

VII-O-3 Zirconium Mediated Regioselective Carbon-Carbon Bond Formation Reactions

Tamotsu TAKAHASHI, Noriyuki SUZUKI, Maki HASEGAWA*, Yu NITTO*, Koichiro AOYAGI*, and Masahiko SABURI* *(*Tokyo Univ.)*

[*Chem. Lett.*, 331 (1992)]

Reactions of zirconocene-alkene complexes with aldehydes gave alcohols as coupling products after hydrolysis. The carbon-carbon bond formaton proceeded at Cl carbon of alkenes, in sharp contrast to the reactions of alkene-alkene coupling on zirconium. A similar alcohol was also obained by the reaction of zirconacyclopentane with aldehyde after hydrolysis. Treatment of $(C_5Me_5)_2ZrEt_2$ with styrene gave 2-phenylbutane after hydrolysis contrary to the case of Cp_2ZrEt_2 which afforded 1-phenylbutane.

VII-O-4 Monohalogenation of Zirconacyclopentane Complexes via Alkylalkoxyzirconocene

Tamotsu TAKAHASHI, Koichiro AOYAGI, Ryuichiro HARA, and Noriyuki SUZUKI

[*Chem. Lett.*, 1693 (1992)]

Zirconacyclopentane complexes have been selectively prepared by alkene-alkene coupling or non-conjugated diene cyclization coupling on zirconium. From the point of view of organic synthesis, functionalization of the coupling products on zirconium is also important and attractive. Although many reactions of zirconacyclopentanes with reagents such as I_2, Br_2, H^+, D^+, O_2, $SeCl_2$, Ph_2SnCl_2, S_2Cl_2 and CO have been investigated, most of the products were di-functionalized compounds or cyclized compounds. Selective mono-functionalization of zirconacyclopentanes is very rare.

We investigated this type of transformation and we found a new method to produce monofunctionalized coupling products with high stereoselectivities as follows. Treatment of trans-3,4-diethylzirconacyclopentane complex, which was a selective butene-butene coupling product on zirconium, with methanol followed by bromine gave selectively monobromination product, 2-ethyl-3-methyl-1-bromopentane, in 89% yield with high stereoselectivity. Similarly, non-conjugated diene cyclization products on zirconium were also selectively converted into monohalogenated compounds. These selective monohalogenations proceeded via alkylalkoxyzirconocene complexes.

VII-O-5 Factors Affecting the Unusual Reactivity Order in the β-Hydrogen Abstraction of Dialkylzirconocenes

Ei-ichi NEGISHI*, Thinh NGUYEN*, John P. MAYE*, Daniele CHOUEIRI*, Douglas R. SWANSON*, Noriyuki SUZUKI, and Tamotsu TAKAHASHI, *(*Purdue Univ.)*

[*Chem. Lett.*, 2367 (1992)]

Competitive β-hydrogen abstraction of "mixed" dialkylzirconocene and kinetic measurements of decomposition of methyl(alkyl)zirconocenes reveal unexpected relative reactivity of alkyl groups as β-hydrogen donors, such as *s*-Bu > *t*-Bu > Et > *n*-Bu > *i*-Bu, which correlate well in most cases with the reactivity order of: β-methyl > β-methylene > β-methine. Some mechanistically crucial features of the reaction are also discussed.

VII—P Chemistry of Polynuclear Metal Complexes

Cooperative phenomena based on direct or indirect metal-metal interaction in polynuclear metal complexes give rise to interesting and sometimes useful chemistry. And a polynuclear complex often exhibits unique reactivity with the use of polymetallic reaction site. We are trying to synthesize new polynuclear metal complexes with the cooperative metal-metal interaction to develop chemistries along such a line.

VII-P-1 Tri- and Tetra-Nuclear Platinum(II) Cluster Complexes Having Novel Triangular Core

Tadashi YAMAGUCHI *(Tohoku Univ.)*, **Nozomu NISHIMURA** *(Tohoku Univ.)*, **and Tasuku ITO** *(Tohoku Univ. and IMS)*

Tetranuclear Pt(II) complex $[Pt^{II}_4(\mu\text{-}CH_3COO)_8]$ **(1)** undergoes two step cluster core rearragement when reacts with bulky chelate ligand such as dimethylglyoxime (dmg) or cyclohexanedionedioxime (cdo) (Scheme 1), giving tetra-nuclear intermediate **(2a and 2b)** and tri-nuclear complex **(3a and 3b)** as a final product. The formal oxidation state of Pt's in **2a, 2b, 3a**, and **3b** remained unchanged in the +2 state. X-ray analysis of **2a** disclosed that the compound consists of two basic units: the one is a Pt_3 triangular portion, each Pt having distorted octahedral geometry, and the other is a mononuclear portion with square-planar coordination geometry. There exist direct Pt-Pt bonds within the triangular skeleton (2.54-2.67 Å). ^{1}H-, ^{13}C-, and ^{195}Pt-NMR of **2a, 2b, 3a**, and **3b** along with elemental analyses and FAB mass data gave unambiguous structural assignment. The proposed triangular trinuclear structure for **3a** is shown in Figure 1. EHMO calculation for a triangular model compound, in which all the methyl groups in **3a** are replaced by hydrogens, shows the presence of three Pt-Pt single bonds between neighbouring Pt atoms in the triangular framework. To our knowledge, the present complexes are the first compound with triangular cluster core unit of Pt(II).

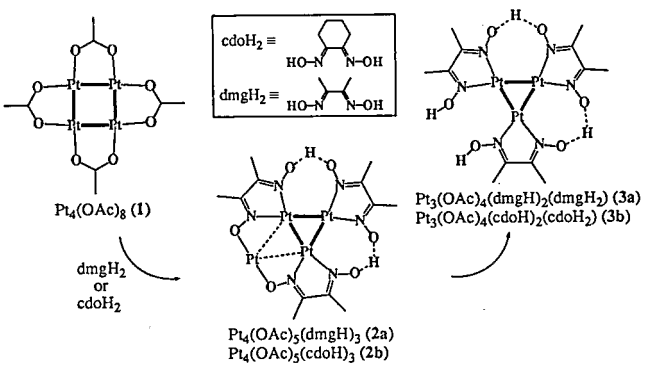

Scheme 1. (The out-of-plane ligands are omitted for clarlity).

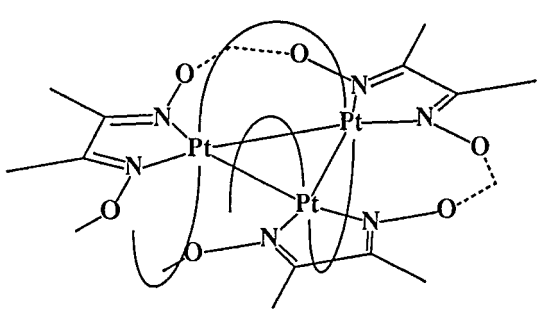

Figure 1. Proposed structure for $Pt_3(CH_3COO)_4(dmgH)_2(dmgH_2)$ **(3a)**.

VII-P-2 Mixed Chromium(III)-Ruthenium(III) Trinuclear Complex, $[CrRu_2(\mu_3\text{-}O)(\mu\text{-}CH_3COO)_6(pyridine)_3]^+$

Yoichi SASAKI *(Tohoku Univ.)*, **Yukihiro YOSHIDA** *(Tohoku Univ.)*, **Akihiro OHTO** *(Tohoku Univ.)*, **Ayako TOKIWA** *(Tohoku Univ.)*, **Tasuku ITO** *(Tohoku Univ. and IMS)*, **Hanako KOBAYASHI** *(Toin Yokohama Univ.)*, **Norikiyo URYU** *(Nagasaki Univ.)*, **and Iwao MOGI** *(Tohoku Univ.)*

The titled new mixed Cr-Ru complex has been prepared. It is a first example of the trinuclear complex containing two kinds of metal ions with both different rows and groups. The magnetic moment (μ_{eff}) is essentially temperature independent (3.5 BM) in the range above ca. 20 K, and decreases below 20 K (Figure 1). Its cyclic voltammogram in CH_3CN shows two reversible oxidation ($E_{1/2}$ =+1.64, +0.78 V vs Ag/Ag^+) and one reversible reduction ($E_{1/2}$=−0.68 V) waves. All the redox processes are localized at the Ru_2O moiety. Cr(III) ion in the trinuclear complex acts as if an isolated ion and two Ru(III) ions are effectively coupled. The Cr-Ru interaction is less significant as compared with the Ru-Ru one.

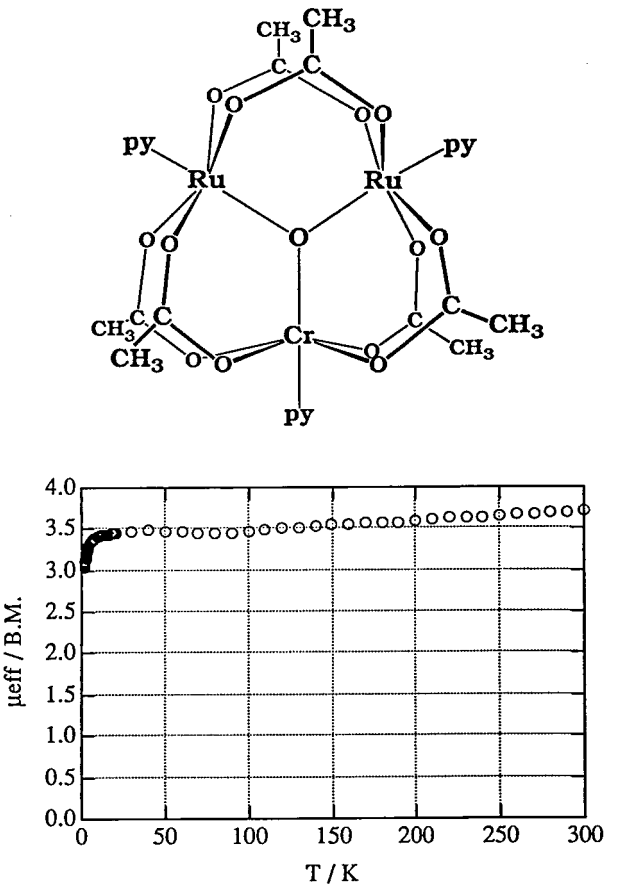

Figure 1. Structure and magnetic moment (μ_{eff}) of $[CrRu_2(\mu_3\text{-}O)(\mu\text{-}CH_3COO)_6(pyridine)_3]^+$.

VII-P-3 Multi-Step Redox Behavior of Oxo and Acetato-Bridged Ruthenium and Rhodium Trinuclear Complexes Having Redox-Active Ligand, *N*-Methyl-4,4'-Bipyridinium Ion

Masaaki ABE *(Tohoku Univ.)*, **Yoichi SASAKI** *(Hokkaido Univ.)*, **Yasuko YAMADA** *(Nara Women's Univ.)*, **Keiichi TSUKAHARA** *(Nara Women's Univ.)*, **Shigenobu YANO** *(Nara Women's Univ.)*, **and Tasuku ITO** *(Tohoku Univ. and IMS)*

Aiming at metal complex having variegated multi-step and multi-electron redox behavior, new oxo and carboxylato-bridged ruthenium, rhodium, and ruthenium-rhodium mixed-metal trinuclear complexes with redox-active ligand (*N*-methyl-4,4'-bipyridinium ion=mbpy$^+$), $[M_3(\mu_3\text{-O})(\mu\text{-}CH_3CO_2)_6(mbpy^+)_3]^{4+}$ (M_3=Ru_3, Ru_2Rh and Rh_3), have been synthesized. Cyclic voltammogram of "Ru_3" complex in 0.1 M $(n\text{-}C_4H_9)_4NPF_6$ -acetonitrile solution (Figure 1) shows reversible multi-step redox waves in the range from +2.0 to −2.8 V vs Ag/Ag$^+$, which include four "Ru_3O" core-based one-electron processes (+1.71, +0.73, −0.25, −1.66 V: Ru_3(III,IV,IV) to (II,II,III)) and two sets of ligand-based processes (−1.16 to −1.29 V: 3mbpy$^{+/\bullet}$; −1.92 to -2.02 V: 3mbpy$^{\bullet/-}$). Splitting of ligand-based waves of "Ru_3" and "Ru_2Rh" comes mainly from electronic interactions between the ligands through MO arising from dπ (metal)−pπ(μ_3-O) interactions in the trinuclear core. However, "Rh_3" analogue exhibits no such splitting. These features can be qualitatively explained on the basis of electron contents within the MO of each trinuclear core.

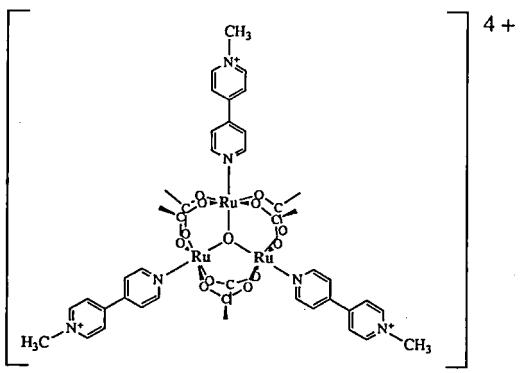

$[Ru^{III}_3(\mu_3\text{-O})(\mu\text{-}CH_3CO_2)_6(mbpy^+)_3]^{4+}$

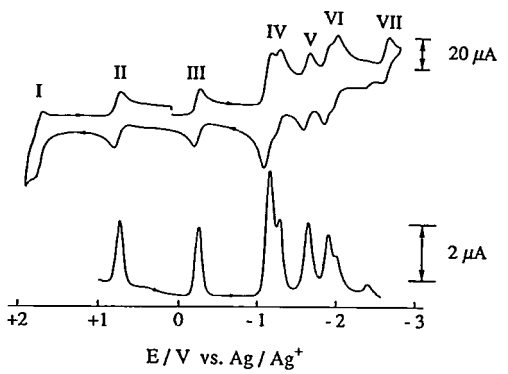

Figure 1. Cyclic-(top) and differential-pulse(bottom) voltammogram in 0.1 M $(n\text{-}C_4H_9)_4NPF_6$ -acetonitrile solution of $[Ru_3(\mu_3\text{-O})(\mu\text{-}CH_3CO_2)_6(mbpy^+)_3]^{4+}$. Scan rate=100 mVs^{-1} for CV and 20mVs^{-1} for DPV.

VII-P-4 Photosubstitution of Carbonyl Ligand in $[Ru_3(\mu_3\text{-O})(\mu\text{-}CH_3COO)_6(CO)(L)_2]$ (L=pyridine, 4-cyanopyridine, methanol) in Acetonitrile and Application to the Syntheses of Nitrosyl and Phosphine Complexes.

Hiroaki KIDO *(Tohoku Univ.)*, **Daisuke AKASHI** *(Tohoku Univ.)*, **Yoichi SASAKI** *(Hokkaido Univ.)*, **and Tasuku ITO** *(Tohoku Univ. and IMS)*

$[Ru_3(\mu_3\text{-O})(\mu\text{-}CH_3COO)_6(CO)(py)_2]$ (py=pyridine) (**1**) undergoes photo-substitution at the carbonyl ligand in deaerated CH_3CN upon ultraviolet irradiation to yield $[RU(CH_3CN)py_2]$ (**2**) (RU=$Ru_3(\mu_3\text{-O})(\mu\text{-}CH_3COO)_6$). The reaction in the presence of large excess of free pyridine affords $[RU(py)_3]$(**3**). Complex **3** is formed stepwise via **2**. The first-order rate constant of the reaction was constant irrespective of the absence or presence of free pyridine, and was independent of the pyridine concentration and the kind of solvents (acetone or benzene). The quantum yield was 0.012 at 308 nm. Photo-generated **2** reverts to the original carbonyl complex (**1**) when reacts with an excess of CO in solution in the dark. Dependence of the decarbonylation rate on the irradiation wavelength for $RU(CO)L_2$(L=py, 4-cyanopyridine(cpy), and CH_3OH) disclosed that absorption band near 300 nm is responsible for the reaction. This band is assigned to the cluster-to-ligand(CO) charge transfer. The photo-decarbonylation proceeds by the dissociative mechanism. Preparative applications of the reaction gave new monomers, $[RU(NO)py_2]$ and $[RU\{P(C_6H_5)_3\}py_2]PF_6$, and the known dimer $[\{RUpy_2\}_2(\mu\text{-pyrazine})](PF_6)_2$ in one step.

VII—Q Study of Dinuclear and Polynuclear Metal Complexes

There are many polynuclear metalloproteins in biological system, whose functions are mainly associated with the redox reactions. In order to synthesize model complexes for polynuclear metalloproteins, we have developed various types of polynucleating ligands which can control oxidation state (including redox potential) of individual metal ions by the steric and electronic effects of ligand environment.

VII-Q-1 Synthesis and Characterization of a Novel Tetranuclear Iron (II,III,II,III) Mixed Valence Complex: the Reaction Product of Dinuclear Iron (II,II) Complex with Molecular Oxygen

Hideki SUGIMOTO*, Yoshihito HAYASHI*, Masatatsu SUZUKI *(Kanazawa Univ. and IMS)*, **and Akira UEHARA*** *(*Kanazawa Univ.)*

Reaction of an ethanol solution containing HMe_4-tpdp (0.5 mmol), $Fe(BF_4)_2 \cdot 6\,H_2O$ (1 mmol), Et_3N (0.5 mmol), and Bu_4NF (0.5 mmol) with molecular oxygen (0.125 mmol) gradually oxidizes a half of iron(II) ion to give a novel tetranuclear mixed valence (II,III,II,III) complex $[Fe_4(Me_4\text{-tpdp})_2(OH)_2F_2(H_2O)_2](BF_4)_4$ as shown in Figure 1, where HMe_4-tpdp is 1,3-bis[bis(6-methyl-2-pyridylmethyl)amino]-2-propanol. The complex cation which possesses an inversion center consists of two alkoxo-bridged dinuclear units which are connected by two F^- ions to form a bilayered structure (a box structure). The oxidation states of Fe1 and Fe2 can be assigned to be three and two by the comparison of the bond distances around iron atoms. Hydroxide ion is coordinated to iron(III) moiety and water to iron(II) moiety. Mössbauer spectra at 77 K and 300 K indicate the presence of iron(II) and Iron(III) ions in an equimolar amount. These results suggest that the valence states of iron1 and iron2 are firmly trapped so that the complex belongs to the so called class I mixed valence system.

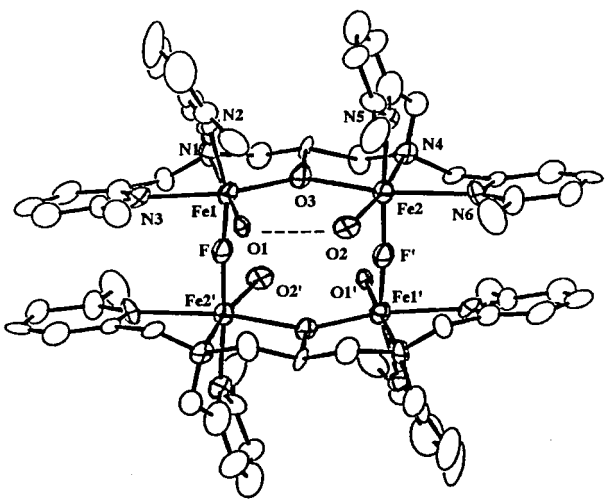

Figure 1. Molecular structure of $[Fe_4(Me_4\text{-tpdp})_2F_2(OH)_2(H_2O)_2]^{4+}$.

VII-Q-2 Syntheses, Characterization, and Redox Behavior of Dinuclear Di(μ-oxo)dimanganese (III,IV) and (IV,IV) Complexes with Coordinated Imidazole Groups.

Sigeki MIYAKAWA*, Yoshihito HAYASHI*, Masatatsu SUZUKI *(Kanazawa Univ. and IMS)*, **and Akira UEHARA*** *(* Kanazawa Univ.)*

Dinuclear di(μ-oxo)Mn_2(III,IV) complexes, $[Mn_2(N_4\text{-}py_2his)_2(O)_2](ClO_4)_3 \cdot 4H_2O$ (**1**) and $[Mn_2(N_4\text{-}py_2im)_2(O)_2](ClO_4)_3 \cdot 2H_2O$ (**2**), and dinuclear di(μ-oxo)Mn_2(IV, IV) complex, $[Mn_2(N_4\text{-}pyim_2)_2(O)_2](ClO_4 \cdot 4H_2O$ (**3**) with imidazole groups were synthesized as models for manganese cluster in OEC, and the crystal structure of **3** was determined by X-ray structure analysis. The pKa_1 of the coordinated imidazole group of **1** and **2** in the (IV,IV) oxidation state are estimated to be 6.2 and > 11, respectively, by cyclic voltammetry. Such a significant difference of pKa_1 implies that the imidazole group in **1** is a much stronger donor than that in **2**. Cryomagnetic measurement of **1** and **2** revçeals that antiferromagnetic interaction is present between Mn(III) and Mn(IV) ions with J values of -150 cm^{-1} and -85 cm^{-1}, respectively. This large difference in the antiferromagnetic interaction may be interpreted in terms of the donor strength of the imidazole groups : a stronger donor weakens the bridging Mn-oxo bonds which mediate antiferromagnetic interaction, resulted in a weak antiferromagnetic interaction in **1**.

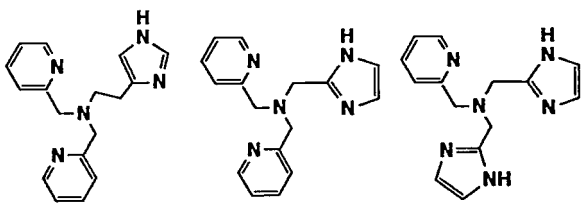

Figure 1. Ligands.

VII-Q-3 Mono and Dinuclear Copper(I) Complexes: Syntheses and Reaction with Molecular Oxygen

Kounosuke UOZUMI*, Yoshihito HAYASHI*, Masatatsu SUZUKI *(Kanazawa Univ. and IMS)*, **and Akira UEHARA*** *(*Kanazawa Univ.)*

New tri-and hexadentate ligands (Figure 1), and their mononuclear and dinuclear copper(I) complexes were synthesized as models for Hemocyanin, $[Cu(N_3\text{-}Me_2py)(CH_3CN)]^+$(**1**), $[Cu_2(Me_4\text{-tpbn})(CH_3CN)_2]^{2+}$ (**2**), and $[Cu_2(Me_4\text{-tpxyl})(CH_3CN)_2]^{2+}$ (**1**). Reaction of **1** with molecular oxygen in acetone or dichloromethane at -70°C changes a color from pale yellow to intense brown and several new absorption bands appears at 350 nm (ε=ca. 20000), 400 nm (shoulder), 450 nm (shoulder), and 600 nm (ε=ca. 700). Warming the brown solution upto -20°C causes a decomposition of the oxygenated complex with a color change to blue green. A simiar spectral behavior is also observed for **1**. These absorption spectra resemble those of oxyhemocyanin and Kitajima's complexes with μ-η^2:η^2 peroxo group. ^1H NMR reveals that the oxygenated species is diamagnetic. Reaction of **3** with molecular oxygen in the same conditions dose not shown any evidence of the formation of an oxygenated species and irreversible oxidation of the complex occurs to give copper(II) complex $[Cu_2(Me_4\text{-tpxyl})(OH)_2]^{2+}$.

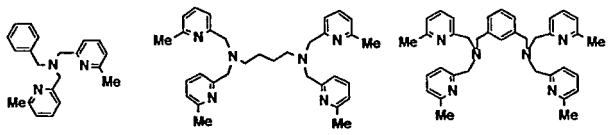

Figure 1. Ligands.

VII-Q-4 Dinuclear Cobalt(II,II) Complexes with an Unsymmetrical Dinucleating Ligand: Syntheses and Reaction with Molecular Oxygen

Takayuki KAYATANI*, Yoshihito HAYASHI*, Masatatsu SUZUKI *(Kanazawa Univ. and IMS)*, **and Akira UEHARA*** *(* Kanazawa Univ.)*

Dinucear metal complexes with sterically and electronically controlled environment are expected to bind molecular oxygen. A new unsymmetrical dinucleating ligand (tpdb) which is a hybrid one of tpdp and tmdp (Figure 1) and dinuclear cobalt(II,II) complexes $[Co_2(tpdb)(RCOO)]^+$ (RCOO=CH_3COO and C_6H_5COO) were synthesized to investigate how the bridging skeleton of the dinucleating ligand influences the oxygen affinity and reversibility. The complexes reversibly bind molecular oxygen to form μ-peroxo complexes in acetonitrile. The oxygen affinities of the tpdb complexes are larger than that of the tpdp complex. The result may be interpreted in terms of a difference between the steric effect of the bridging skeleton of tpdp and tpdb (metal-metal distances and the mutual arrangement of metal ions.)

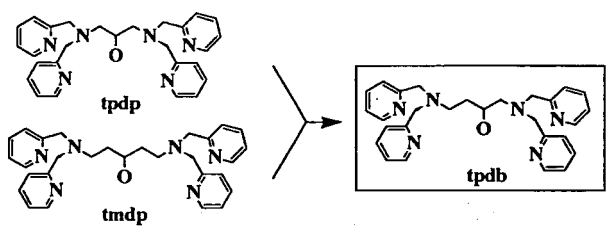

Figure 1. A hybrid Ligand (tpdb).

VII-Q-5 Syntheses and Characterization of Novel Linear Tetranuclear Manganese(II,III,III,II) and (II,III,IV,II) Complexes with Di(μ-oxo)Mn_2core

Hisano KAWASAKI*, Yoshihito HAYASHI*, Masatatsu SUZUKI *(Kanazawa Univ. and IMS)*, **and Akira UEHARA*** *(* Kanazawa Univ.)*

Novel linear tetranuclear manganese(II,III,III,II) and (II,III, IV,II) complexes with di(μ-oxo)Mn_2 core were prepared, $[[Mn_2(tpdp)(H_2O)_2(O)]_2](ClO_4)_4$ **(1)** and $[[Mn_2(tpdp)(H_2O)_2(O)]_2](ClO_4)_5$**(2)**, where HMe_2-tpdp is N,N-bis(6-methyl-2-pyridyl-methyl)-N',N'-bis(2-pyridyl-methyl)-1,3-diamino-2-propanol and the crystal structure of the complex **1** was determined by X-ray structure analysis. The complex **3** consists of di (μ-oxo)Mn_2(III,III) unit to which two manganese(II) ions are linked by the alkoxo bridges of Me_2-tpdp, forming a linear tetranuclear structure (Figure 1).

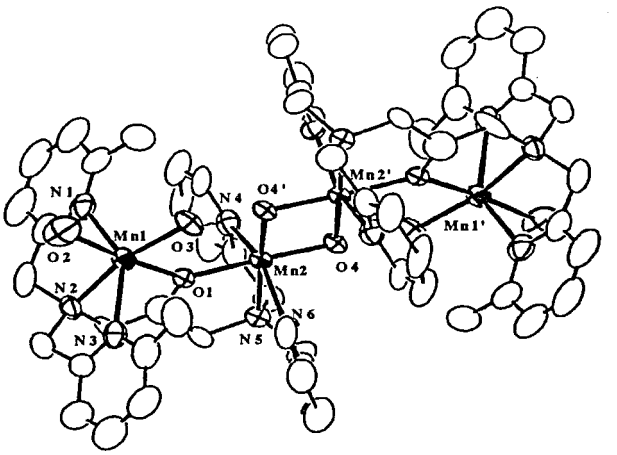

Figure 1. Molecular structure of $[[Mn_2(Me_2\text{-tpdp})(H_2O)_2(O)]_2]^{4+}$.

VII-Q-6 Dinuclear Iron(II,II) Complexes with an Unsymmetrical Dinucleating Ligand: Syntheses and Reaction with Molecular Oxygen

Takayuki KAYATANI*, Yoshihito HAYASHI*, Masatatsu SUZUKI *(Kanazawa Univ. and IMS)*, **Akira UEHARA*** *(* Kanazawa Univ.)*, **Yasuhisa MIZUTANI, and Teizo KITAGAWA**

A new unsymmetrical dinucleating ligand (Me_2-tpdp) which is a hybrid one of tpdp and Me_4-tpdp (Figure 1) and its dinuclear iron(II,II) complex $[Fe_2(Me_2\text{-tpdp})(CF_3COO)]^+$ were synthesized to study the influence of the unsymmetrical environments around two iron ions. The complex reacts with molecular oxygen to form μ-peroxo species in acetone or acetonitrile at −40°C. In contrast to the corresponding Me_4-tpdp complex, reversible oxygenation is not observed by bubbling of Ar gas. The oxygenated species exhibits an absorption band at 603 nm (ε=ca. 1600), which can be assigned to the charge transfer transition from μ-peroxo group to Fe^{3+}. Formation of a peroxo species is confirmed by Resonace Raman spectrum. The spectrum shows two Fe-O stretching bands, suggesting an unsymmetrical bridging coordination of peroxo group to two iron(III) ions.

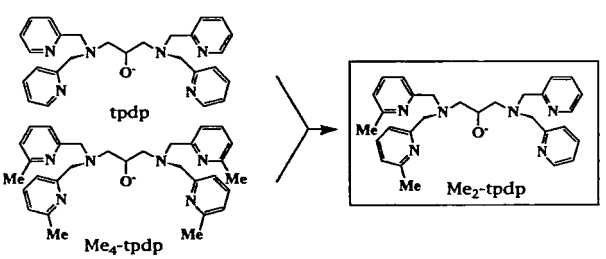

Figure 1. A hybrid Ligand (Me_2-tpdp).

RESEARCH ACTIVITIES VIII
Computer Center

VIII—A Theoretical Investigations of Structures and Properties of Molecular Assemblies

Structures and properties of molecular clusters, liquids, solutions and solids are studied using the molecular dynamics and the Monte Calro technique. A new intermolecular potential function for the molecular simulations is developed based on the ab initio molecular orbital theory.

VIII-A-1 Theoretical Study of Structure and Thermodynamic Properties of Liquid Hydrogen Fluoride

Kazuhiko HONDA, Kazuo KITAURA, and Kichisuke NISHIMOTO *(Osaka City Univ.)*

Monte Calro (MC) simulations for liquid hydrogen fluoride (HF) were carried out using a new type of intermolecular potential function. The bonding energy distribution function was found to have three peaks corresponding to the distributions of molecules which have one, two and three hydrogen bond with neighbors. (Figure 1) A partition function of liquid HF was derived referring to the results of MC simulations, where a simple Hamiltonian consisting of harmonic oscillators and hydrogen bond energies was employed. The thermodynamic properties calculated by the partition function reasonably reproduced the experimental data. Moreover, the effects of hydrogen bondings on various thermodynamic properties were revealed based on the partition function.

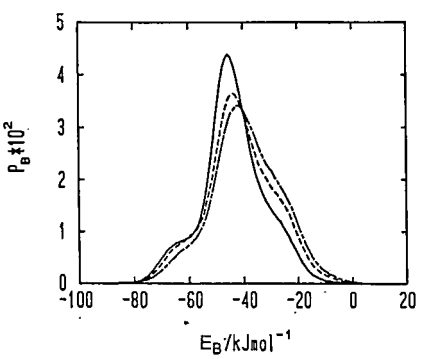

Figure 1.

VIII-A-2 A Study on GABA and Their Analogues with the Molecular Orbital Method

Mitsunori TSUDA *(Mie Univ.)* **and Kazuo KITAURA**

GABA is a major neurotransmitter in the central nervous system. The analyzed data of these compounds by the ab initio method were compared with those by the experimental methods. 1) The structure of GABA and GABA analogues calculated by the ab initio method agreed well with experimental data. 2) For GABA and GABA analogues, the amino group was proved to be the major active site. The electrostatic potentials (Figure 1) around the amino group seems to be related to their biological activity. 3) The difference in the electrostatic potentials between the recoptor binding molecules and the neuronal uptake molecules suggest that the structure of post-synaptic receptors might differ from that of uptake receptors. This finding suggests that there are at least two GABA-A receptors. 4) GABA molecules seem to have high potentiality to bind to the two receptors, since they are highly flexible and can readily change their comformation.

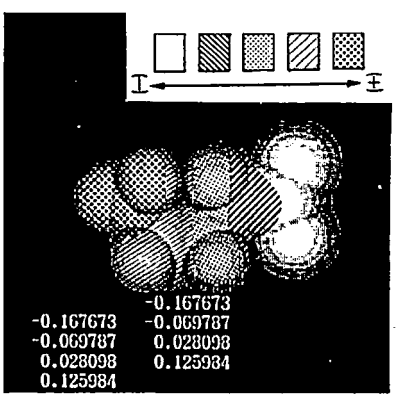

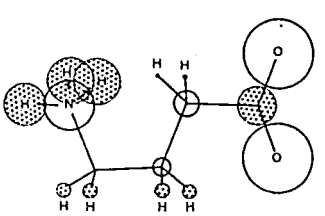

Figure 1.

Chemical Materials Center

VIII—B Preparation and Properties of Novel Heterocyclic Compounds

Heterocycles containing sulfur or nitrogen atoms are useful as components of organic conductors because heteroatoms in their rings are helpful to stabilize ions or ion-radical species, and extended π-conjugation decreases Coulombic repulsion. In addition intermolecular interactions caused by heteroatom contacts can be expected to form unique molecular assemblies. In

this project novel electron acceptors and donors based on heterocycles were synthesized and their properties including those of the charge-transfer complexes or ion-radical salts were investigated.

VIII-B-1 Structure and Redox Reactions of Tricyclic Pyridinium N-Imines

Yoshiro YAMASHITA, Shoji TANAKA, and Masaaki TOMURA

[*Heterocycles*, **33**, 47 (1992)]

Although pyridinium N-imines having no electron withdrawing group at the imino position are usually unstable, tricyclic pyridinium N-imines **1a-c** were isolated as stable solids. The X-ray structural analysis of **1a** revealed characteristics of the structure with the N-N bond distance of 1.34 Å. Studies on the redox reactions demonstrated that **1a-c** and quinolinium N-imine **2** are electron donors and they were oxidized with nitrosonium tetrafluoroborate.

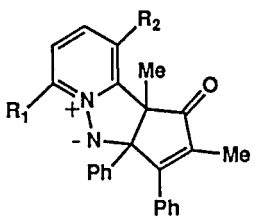

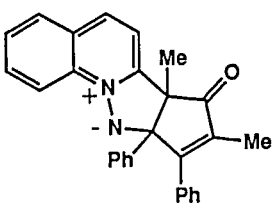

2

1a; R_1=R_2=H
1b; R_1=H, R_2=Me
1c; R_1=R_2=Me

VIII-B-2 Tetracyanoquinodimethanes Fused with 1,2,5-Thiadiazole and Pyrazine Units

Yoshiaki TSUBATA*, Takanori SUZUKI*, Yoshiro YAMASHITA, Toshio MUKAI*, and Tsutomu MIYASHI* *(*Tohoku Univ.)*

[*Heterocycles*, **33**, 337 (1992)]

1,2,5-Thiadiazolopyrazino-TCNQs **1a-d** were prepared by the condensation of the corresponding quinones with malononitrile in the presence of $TiCl_4$ and dry pyridine. They underwent reversible four-stage one-electron reduction and gave conductive CT complexes with some donors. The X-ray structural analysis of the unsubstituted derivative **1a** revealed that the coplanar "sheet-like network" was formed by interatomic contacts of S--N-C and H--N-C in crystal.

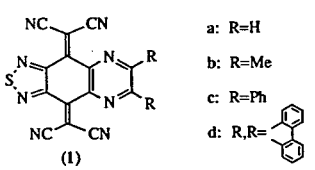

(I)

a: R=H
b: R=Me
c: R=Ph
d: R,R=

VIII-B-3 5,8-Bis(1,3-dithiol-2-ylidene)-4,7-dihydro-2,1,3-benzothiadiazoles. Novel Electron Donors Affording Organic Metals

Yoshiro YAMASHITA, Shoji TANAKA, Kenichi IMAEDA, Hiroo INOKUCHI, and Mizuka SANO* *(*International Christian Univ.)*

[*Chem. Lett.*, 419 (1992)]

The title compounds **1a-d,** tetrathiafulvalene (TTF) analogues with a quinoid structure fused with a 1,2,5-thiadiazole ring, were prepared using a Witting-Horner reaction and a retro-Diels-Alder reaction. The cyclic voltammetry showed that they are stronger electron donors than TTF in spite of the presence of the electron-withdrawing heterocycle. The X-ray structural analysis of **1d** revealed that the molecule is almost planar and short contacts between the S of the dithioles and the N of the thiadiazole exist. The tetramethyl derivative **1b** gave highly conducting cation radical salts showing metallic temperature dependence down to 100 K.

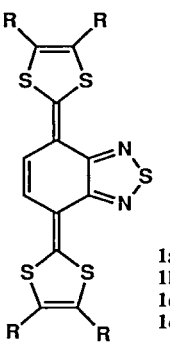

1a; R=H
1b; R=Me
1c; R,R=SCH_2CH_2S
1d; R,R=benzo

VIII-B-4 Tetrathio-Derivatives of *p*-Quinodimethanes Fused with Selenadiazole Units: A Novel Type of Electron Donors

Yoshiro YAMASHITA, Shoji TANAKA, and Masaaki TOMURA

[*Phosphorous, Sulfur, and Silicon*, **67**, 327 (1992)]

Novel electron donors **1a-d** which are TTF analogues with a quinoid structure containing fused-selenadiazole rings were synthesized from 2,1,3-benzoselenadiazole-4,7-dione similarly to the thiadiazole counterparts. Their cyclic voltammograms showed that they are strong electron donors. The differences between the first and second oxidation potentials are much smaller than that for TTF, indicating that on-site Coulombic repulsion in **1** is decreased due to the extended π-conjugation. A PF_6 salt of **1b** [σ=100 S cm^{-1} at room temperature, D:A=2:1] showed metallic temperature dependence down to 100 K.

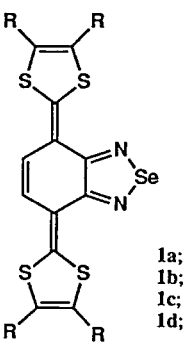

1a; R=H
1b; R=Me
1c; R,R=SCH_2CH_2S
1d; R,R=benzo

VIII-B-5 Clathrate Formation and Molecular Recognition by Novel Chalcogen-Cyano Interactions in Tetracyanoquinodimethanes Fused with Thiadiazole and Selenadiazole Rings

Takanori SUZUKI*, Hiroshi FUJII*, Yoshiro YAMASHITA, Chizuko KABUTO*, Shoji TANAKA, Masako HARASAWA*, Toshio MUKAI*, and Tsutomu MIYASHI* *(*Tohoku Univ.)*

[*J. Am. Chem. Soc.*, **114**, 3034 (1992)]

The intermolecular contacts between chalcogen atoms and cyano lone pairs were found to stabilize the crystalline state by electrostatic interaction. This interaction causes the formation of various types of inclusion lattices in the charge-transfer (CT) crystals of **1-3**. By using highly selective formation of CT crystals with substituted aromatic hydrocarbons, particular isomers such as *p*-xylene or 2,6-dimethylnaphthalene (2,6-DMN) could be separated from the corresponding isomer mixtures. Lattice-related interaction plays a more significant role than molecular orbital interaction in the observed selectivity for para-disubstituted benzenes. However, the latter interaction is important for the recognition of 2,6-DMN from the 2,7 isomer.

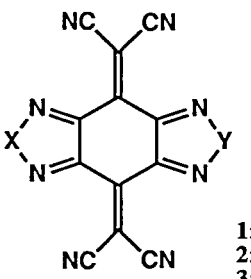

1: X=Y=S
2: X=S, Y=Se
3: X=Y=Se

VIII-B-6 Tetrathienylethylenes, a New Class of Electron Donors — Dications Twisted by 90° Stabilized by Formation of Polymethine Units

Takanori SUZUKI*, Hiroaki SHIOHARA*, Masayuki MONOBE*, Tomoo SAKIMURA*, Shoji TANAKA, Yoshiro YAMASHITA, and Tsutomu MIYASHI* *(*Tohoku Univ.)*

[*Angew. Chem, Int. Ed. Engl.*, **31**, 455 (1992)]

In view of the stabilization of a carbenium ion by thiophene ring, we designed tetrathienylethylenes **1** as a new class of electron donors. Tetramethyl- (**1b**, E^{OX}=+0.70 V) and tetrakis(methylthio) derivative (**1c**, E^{OX}=+0.55 V) underwent reversible one-wave two-electron oxidation. The molecular geometries of **1b** and $\mathbf{1c}^{2+}$ were determined by X-ray structural analyses. Neutral **1b** possesses a planar trans-diethylethylene structure substituted with two thiophene rings orthogonal to the molecular plane. On the other hand, the molecular geometry of $\mathbf{1c}^{2+}$ is remarkably different from that of **1b**, where the two molecular halves are perpendicularly twisted around the central ethylene bond.

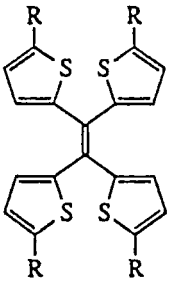

1a: R = H
1b: R = Me
1c: R = SMe

VIII-B-7 Preparation and Properties of Poly-4-(1,3-dithiol-2-ylidene)-4H-cyclopenta[2,1-b;3,4-b']dithiophene and Its Derivatives

Masatoshi KOZAKI, Shoji TANAKA, and Yoshiro YAMASHITA

[*J. Chem. Soc., Chem. Commun.*, in press]

1,3-Dithiole compounds **1a-d** were prepared in 65—98% yields using a Witting-Horner reaction. The X-ray structural analysis of the benzo derivative **1c** revealed that the molecule is planar. Cyclic voltammograms of **1** showed irreversible oxidation waves. Their oxidation potentials are significantly lower than that for bithiophene. Polymers **2** were prepared by the electrolytic oxidation of the corresponding monomers **1**. Conductivities of **2a,c,d** were 4.1×10^{-1}, 4.4×10^{-1}, and 1.4 S cm^{-1} in the doping state, respectively. The doping states were stable and conductivities did not change after storage in air for a month. Another advantage of this system is that substituents are easily introduced to modify characters of the polymers. We have succeeded in preparing derivatives **2f-h** containing long alkyl chains.

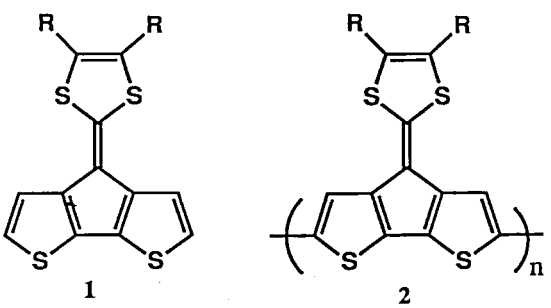

a: R=H
b: R=Me
c: R=benzo
d: R=SMe
e: R=CO_2Me
f: R=$S(CH_2)_3CH_3$
g: R=$S(CH_2)_5CH_3$
h: R=$S(CH_2)_9CH_3$

VIII-B-8 Narrow Band Gap Conjugated Polymers Containing Thieno[3,4-c][1,2,5]thiadiazole Units

Shoji TANAKA, Masaaki TOMURA, and Yoshiro YAMASHITA

One approach to obtain narrow band gap polymers is offered by mixing together the repeat units of polymer with significantly different electronic structures. In this framework we have designed a new class of periodic copolymer

2a containing nonclassical condensed thiophene, thieno-[3,4-c][1,2,5]thiadiazole, units. In order to elucidate the factors determining the electronic structure of this type of conjugated system, we have prepared and characterized the related copolymers **2b-c**. The monomers **1b-c** were synthesized by a cross-coupling reaction of 4,6-dibromothieno[3,4-c][1,2,5]thiadiazole with 5-MgBr-2,2'-bithienyl or 2-ZnCl-1-methylpyrrole catalyzed by $Ni(dppp)Cl_2$. The electrochemical oxidation of the monomers afforded the copolymers **2b-c**. The cyclic voltammograms revealed that the monomer **1b** has higher HOMO and LUMO energies compared with **1a**. This reflects on the doping behavior of the polymers: the p-doping state of **2b** is well stabilized, while its n-doping state is significantly destabilized in comparison with the doping state of **2a**. The monomer **1c** has a lower HOMO-LUMO separation compared to **1a** due to the more extended π-system. The optical and electrochemical investigations, however, showed that the band gap values of the polymers increase going from **2a** to **2c**. This result suggests that copolymers with a higher percentage of the thienothiadiazole will be desirable for the reduction of band gap value.

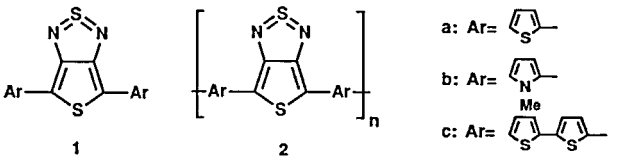

1 2

Instrument Center

VIII—C Studies of Solvated Metal Clusters

Solvated metal ions and metal cluster ions afford a particularly interesting collection of systems for study because they bridge the gap between bare, isolated ions and ionic solids and electrolyte solutions. From the point of view of cluster chemistry, the question of charge delocalization, the formation of solvation shells, and the interaction of solvent with metal surfaces appear especially attractive.

In this project we investigate the photoionization and photodissociation processes of various kinds of solvated metal atom (ion) clusters to unveil the microscopic aspect of solvation.

VIII-C-1 Photoionization Study on $Cs(CH_3CN)_n$ Clusters

Keizo TSUKAMOTO, Masaomi SANEKATA, Fuminori MISAIZU, and Kiyokazu FUKE

Cesium atom solvated with acetonitrile molecules, $Cs(CH_3CN)_n$, is studied by single-photon laser ionization and time-of-flight mass spectroscopy. The solvated Cs atom clusters were produced by pick-up type cluster source. In this source, Cs-atom beam produced from a pulse valve heated to about 350°C were crossed with the CH_3CN cluster beam formed by expansion from another pulse valve. The $Cs(CH_3CN)_n$ clusters were formed by subsequent multiple collisions and were ionized by irradiation with an output of a tunable dye laser. Ionization potentials (IPs) of the clusters with n=1—21 are determined from the ionization efficiency curves obtained by scanning the photon energy.

Figure 1 shows photoionization efficiency curves near threshold for $Cs(CH_3CN)_n$ with n=1—14. The efficiency curves show anomalous change with increasing cluster size: The rise for n=4—6 are found to be as steep as that for n=1, while those for n=2, 3, and for n≧7 are much less steep. These results suggest that the differences in the geometry of neutral and ionic clusters for n=4—6 are much closer than those for n=2 and 3. The IPs for n≦11 determined from these curves also show the alternative feature: IPs for n=4—6 are higher than those for n=2 and 3. On the other hand, the successive binding energy of acetonitrile to cesium ions has been found to decrease smoothly with n up to 5.[1] Therefore, the present results suggest that the ground-state geometry of these clusters changes anomalously with increasing n because of the large dipole moment of the CH_3CN molecule. To gain further insight into details of the geometrical change, it seems necessary to carry out theoretical calculations based on Monte Carlo simulation.

Reference

1) W.R. Davidson and P. Kebarle, *J. Am. Chem. Soc.* **98**, 6125 (1976).

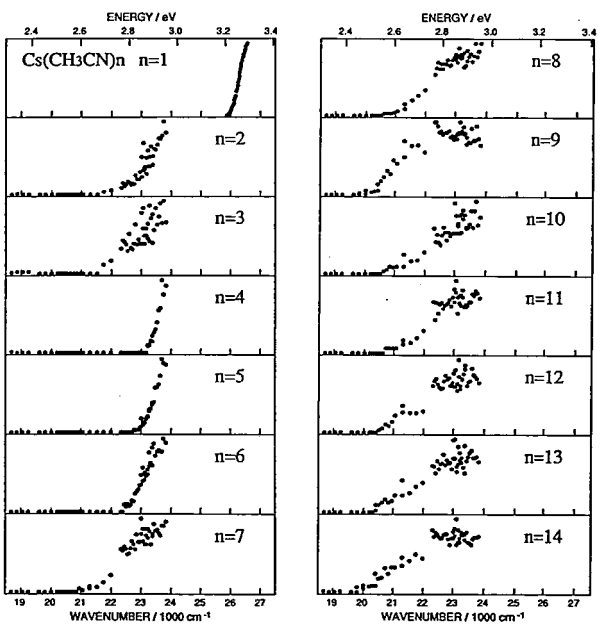

Figure 1. Photoionization efficiency curves of the $Cs(CH_3CN)_n$ clusters with n=1—14.

VIII-C-2 Construction of an Apparatus for Photoelectron Spectroscopy of Mass-Selected Cluster Anions

Fuminori MISAIZU, Keizo TSUKAMOTO, Masaomi SANEKATA, and Kiyokazu FUKE

Negative-ion photoelectron spectroscopy is one of the most useful techniques to obtain size-dependent information about the electronic structure of clusters. In order to apply this method to the clusters of metal atoms solvated with up to more than one hundred solvent molecules, the apparatus as shown in Figure 1 has been constructed.

The system consists of three-stage differentially evacuated chambers which contains a laser vaporization cluster beam source, time-of-flight mass spectrometer, and magnetic bottle-type time-of-flight photoelectron spectrometer. Negative ions directly produced in the source are extracted by pulsed electric fields at right angles in the first chamber. The ions of a given mass are isolated by ejection of all other ions from the beam by using another pulsed electric field after flying 60 cm. Then the ions are decelerated by pulsed switching method and focussed by Gustafsson-Lindholm-type electrostatic lenses at the entrance of the photoelectron spectrometer. The magnetic-bottle photoelectron spectrometer has an advantage that electrons emitted over 4π steradian form a beam by magnetic mirror effect and magnetic parallelization. Because of this high collection efficiency, the spectrometer is expected to be suitable for the study of clusters. The ion-pair state of the solvated alkali-metal-atom clusters will be examined as a function of the number of solvent molecules by this apparatus. This study will provide information related to the formation and stability of solvated electron in the bulk solution.

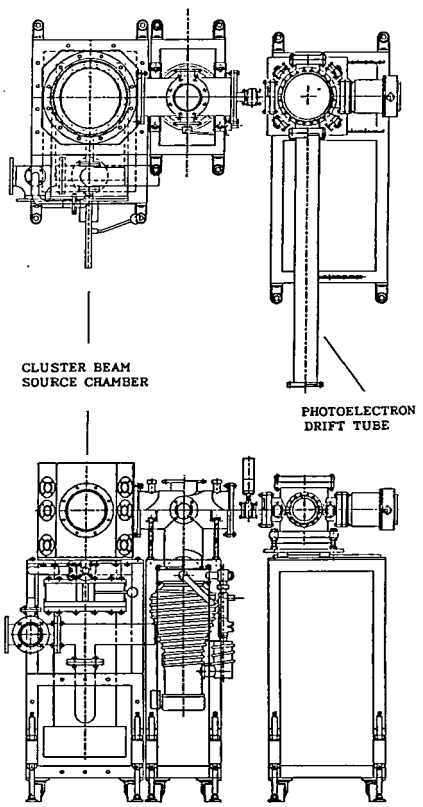

Figure 1. Drawing of the apparatus.

VIII-C-3 Intracluster Reaction in the Formation of Mg^+-Water and Ca^+-Water Clusters

Fuminori MISAIZU, Masaomi SANEKATA, Keizo TSUKAMOTO, and Kiyokazu FUKE

A pick-up type cluster source coupled with a laser vaporization method was used to produce ionic clusters which contain an alkaline-earth-metal atomic ion, M^+ (M=Mg and Ca), with water clusters. Both $MOH^+(H_2O)_m$ and $M^+(H_2O)_n$ ions are produced efficiently with pronounced size dependence: For the Mg^+ ion, the former ions are produced for $5 \leqq m \leqq 14$, while the latter ions are for $n \leqq 5$ and $n \geqq 15$. For the Ca^+ ion, these ions are observed for $4 \leqq m \leqq 12$ and $n \leqq 5$ and $n \geqq 13$, respectively as shown in Figure 1. The results suggest that the hydration process including an energy redistribution and evaporation competes with a hydrogen elimination reaction within nascently produced cluster ions. We also investigated the ion distribution in the Mg^+/Ca^+-deutrated water clusters. In these cases, the ions with $5 \leqq m \leqq 13$, $n \leqq 6$ and $n \geqq 14$ were observed for Mg^+-D_2O clusters, and those with $4 \leqq m \leqq 11$, $n \leqq 5$ and $n \geqq 12$ for Ca^+-D_2O systems. The $CaOH^+$ ion is unstable with respect to Ca^+, however, $CaOH^+(H_2O)_n$ becomes more stable than $Ca^+(H_2O)_n$ with increasing n, because the hydration energy of the $CaOH^+$ ion (1.49 eV) is larger than that of Ca^+ (1.21 eV). The difference between H_2O and D_2O probably indicates that the dissociation reaction, $Ca^+(H_2O)_n \rightarrow CaOH^+(H_2O)_m + H + (n\text{-}m\text{-}1)H_2O$, includes a tunneling process. In contrast, the fact that the $Ca^+(H_2O)_n$ is dominantly produced for $n \geqq 13$ should be explained by the dynamic effect of the reaction in addition to the energetics. One possibility is that, with increasing n, the dissociation of the O-H bond is suppressed or, even if dissociates, the hydrogen atom is confined within the cluster, because the water molecules in the second shell play the role of solvent cage.

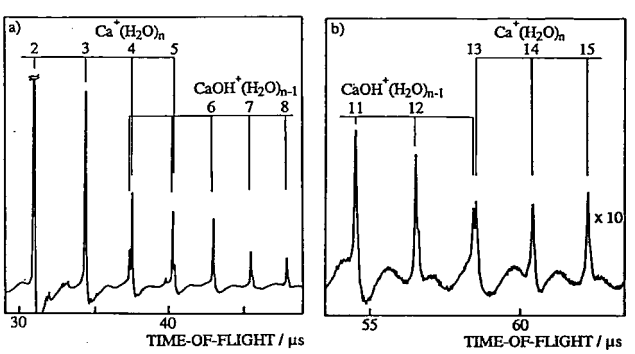

Figure 1. Portions of the mass spectrum of the $Ca^+(H_2O)_n$ and $CaOH^+(H_2O)_{n-1}$ cluster ions directly produced in the laser-vaporization source. a) n=2–8. b) n=11–15.

VIII-C-4 Photodissociation Spectroscopy of $Mg^+(H_2O)_n$

Fuminori MISAIZU, Masaomi SANEKATA, Keizo TSUKAMOTO, Kiyokazu FUKE, and Suehiro IWATA *(Keio Univ.)*

[*Z. Phys. D*, in press]

Electronically excited states of $Mg^+(H_2O)_n$ with n up to

5 have been studied by photodissociation technique. Cluster ions were produced by laser vaporization and mass separated by time-of-flight mass spectrometer (TOFMS). At the end of the first drift region of the reflectron-type TOFMS, photolysis laser was irradiated to cluster ions with a given size, and the photofragment ions were detected after mass-analyzed in the reflection and the second drift regions. Total intensity of the fragment ions was recorded as a function of photolysis wavelength.

Figure 1 shows dissociation spectra of $Mg^+(H_2O)_n$ for n=1–5. Details of the dissociation mechanism are described in VIII-C-5. For n=1 and 2, the observed absorption bands are assigned to the ^2P-^2S type transitions localized on the Mg^+ ions; the ^2P state of free Mg^+ ion arised from the excitation of an s electron to p orbitals is splitted into three levels as a result of interaction of the ion with water molecules. In contrast, the energy splittings of these transitions are found to become small for n=3–5. According to the recent results of the ab initio calculation,[1] up to three water molecules directly coordinate to the Mg^+ ion, and the second solvation layer is formed from the fourth water ((3+1) structure). Narrowed splitting in the three transitions is consistent with the theoretical prediction that the equilibrium structure of $Mg^+(H_2O)_3$ is C_3 symmetry in which three equivalent waters coordinate to Mg^+. The similarity of the dissociation spectrum for n=4 to that for n=3 implies that the effect of the fourth water on the electronic structure of the $Mg^+(^2P)$ ion is substantially small, which supports the (3+1) structure predicted theoretically. For n=5, the absorption band is found to be extended to about 14000 cm^{-1}. This tail in the low energy region may indicate the existence of the isomer like (4+1), in addition to the (3+2) structure.

Reference

1) C.W. Bauschlicher, Jr. and H. Partridge, *J. Phys. Chem.* **95**, 9694 (1991).

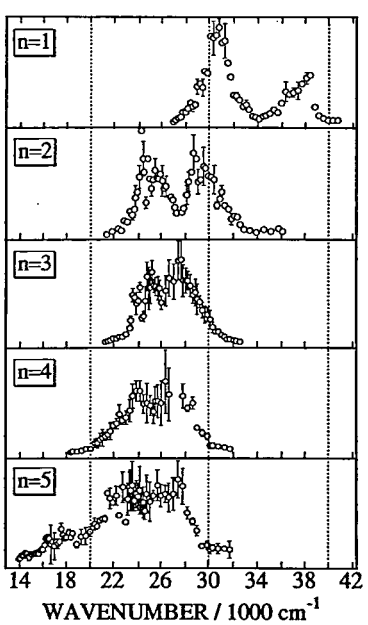

Figure 1. Photodissociation spectra of $Mg^+(H_2O)_n$ for n=1–5. These spectra were obtained from the total yield of the fragment ions. The dissociation cross sections are normalized at their peaks.

VIII-C-5 Photoinduced Intracluster Reaction of $Mg^+(H_2O)_n$ Ions

Fuminori MISAIZU, Masaomi SANEKATA, Keizo TSUKAMOTO, Kiyokazu FUKE, and Suehiro IWATA
(Keio Univ.)

[*Z. Phys. D*, in press]

In the photodissociation of mass-selected $Mg^+(H_2O)_n$ cluster ions, the intracluster reaction process to produce $MgOH^+(H_2O)_m$ by loss of hydrogen atom has been observed in addition to the evaporation process of H_2O molecules. For n=1, following dissociation processes are observed:

$$Mg^+(H_2O) + h\nu \rightarrow Mg^+ + H_2O : \text{evaporation}$$
$$\rightarrow MgOH^+ + H : \text{intracluster reaction}$$

The branching ratio of these two processes is found to be almost constant for the photolysis wavelength of 250–370 nm. In contrast, the fraction to produce $MgOH^+(H_2O)$ and $MgOH^+$ from $Mg^+(H_2O)_2$ has been found to show characteristic dependence upon the photolysis wavelength. Figure 1 shows yield spectra of the fragment ions, $MgOH^+(H_2O)$, $Mg^+(H_2O)$, and $MgOH^+$, formed from $Mg^+(H_2O)_2$. The branching fraction of the $MgOH^+$ ion gradually increases with increasing photon energy from 27000 to 32000 cm^{-1}. Moreover, below 29000 cm^{-1}, the $MgOH^+$ ion has found to be produced by two-photon absorption, though by one-photon process above this photon energy. Thus we concluded that this energy corresponds to the threshold energy for the formation of $MgOH^+$.[1] In contrast, the spectrum of the $MgOH^+(H_2O)$ yield shows a marked difference with those of other fragments: the intensity of the 30300-cm^{-1} band (2^2A, 2^2B-1^2A transitions) is three times stronger than that of the 25000-cm^{-1} band (1^2B-1^2A transition). This result implies that the fraction of the reaction process to produce $MgOH^+(H_2O)$ increases with increasing excitation energy. To gain further insight into the reaction process, we are conducting similar photodissociation experiments on large $Mg^+(H_2O)_n$ clusters.

Reference

1) F. Misaizu, M. Sanekata, K. Tsukamoto, K. Fuje, and S. Iwata, *J. Phys. Chem.* **96**, 8259 (1992).

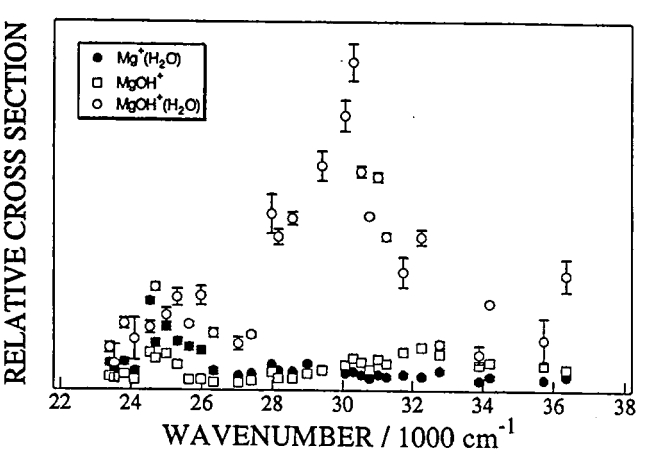

Figure 1. Photofragment ion yield spectra of $Mg^+(H_2O)$, $MgOH^+(H_2O)$, and $MgOH^+$ from the $Mg^+(H_2O)_2$ ion.

VIII-C-6 Photodissociation Spectroscopy of $Ca^+(H_2O)$

Masaomi SANEKATA, Fuminori MISAIZU, Keizo TSUKAMOTO, and Kiyokazu FUKE

In this work, we extend our studies on the photodissociation spectroscopy of alkali-earth metal atom ion solvated with water molecules.[1] We have investigated the photodissociation spectrum of $Ca^+(H_2O)$.

Ca^+ ion has a strong ^2P-^2S electronic transition at 25303 cm^{-1} with spin-orbit splitting of 222 cm^{-1} and a forbidden ^2D-^2S transition located at 11000 cm^{-1} below the above transition. Weakly bound complexes containing Ca^+ are expected to absorb near this resonance line with spectral shifts and electronic multiplets arising from metal ion solvation. Figure 1 shows a photodissociation spectrum of $Ca^+(H_2O)$, obtained by monitoring the yield of the photofragment ion (Ca^+) with the photolysis wavelengths of 347.5–490 nm. Five absorption bands, which are located at 21900, 23500, 24700, 26300, and 28200 cm^{-1}, are observed in this spectrum. Both of the two lower energy bands have a doublet feature with an energy spacing of ca. 300 cm^{-1}. The three bands observed at 21900, 23500, and 26300 cm^{-1} are assignable to the excitations to the states mostly have p character, because of its doublet feature and large absorption cross sections. On the other hand, vertical excitation energies and relative absorption cross sections of $Ca^+(H_2O)_n$ (n=1 and 2) have been calculated by ab initio method.[2] The calculated values are also shown in Figure 1 by sticks. The energies for the two low-lying transitions agree well with the theoretical results. However, as for the highest energy band in Figure 1, large discrepancy is found between the experimentally observed peak and theoretical prediction. This discrepancy may be attributed to the overestimation of the p-d mixing in the calculation. The two remaining bands at 24700 and 28200 cm^{-1} cannot be assigned decisively at present. We are conducting similar photodissociation experiments on larger $Ca^+(H_2O)_n$ clusters.

References

1) F. Misaizu, M. Sanekata, K. Tsukamoto, K. Fuke, and S. Iwata, *J. Phys. Chem.* **96**, 8259 (1992).
2) C.W. Bauschlicher, Jr., M. Sodupe, and H. Partridge, *J. Chem. Phys.* **96**, 4453 (1992).

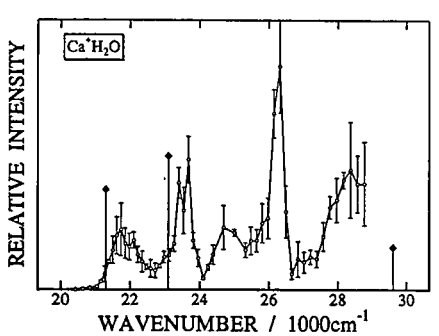

Figure 1. Photodissociation spectrum of $Ca^+(H_2O)$. The spectrum exhibits the photofragment Ca^+ ion signals normalized by laser fluences as a function of photon energy. Sticks in the figure show the theoretical excitation energies and relative transition intensities determined recently.[2]

VIII-C-7 Formation of Alkali Halide Cluster Ions Solvated with Water

Fuminori MISAIZU, Masaomi SANEKATA, Keizo TSUKAMOTO, and Kiyokazu KUKE

In the investigation of the solvation dynamics, it is important to know the incipient dissolution process of salts in aqueous solution. For the first step of this study, hydrated alkali halide cluster ions have been produced and studied by mass spectroscopy. For bare alkali halide clusters, positive ions of the form $M_nX_{n-1}^+$ (M: metal atom, X: halogen atom) are dominantly produced because of their stability; they are considered to be composed of n M^+ and $(n-1)X^-$ ions with no excess electrons or holes. The size distribution of these clusters is also explained by the stability of filled cubic lattice structures. For example, the $Na_nX_{n-1}^+$ ions are most abundant at n=14 (3×3×3), 23 (3×3×5), and so on.

Sodium halide cluster ions, Na_nX_{n-1} (X=Cl and I), were directly produced by laser irradiation to a rotating sample disk. The hydrated cluster ions were formed by the subsequent collision with water vapor in a fast flow cell (50-mm length) placed at the exit of the nozzle. Figure 1 shows the mass spectrum of $Na_nI_{n-1}(H_2O)_m^+$ cluster ions directly produced in the source. Up to 7 water molecules are found to be attached to the $Na_nI_{n-1}^+$ ions. Among these, the average number of water molecules, $\bar{m}$, is highest for the ions with n=3 and gradually decreases with increasing n. Furthermore, $\bar{m}$ for the filled cubic ions (n=14 and 23) is found to be smaller than those for ions with neighboring n values. The latter result indicates that, as a result of interaction with water molecules, the ions with lattice defects are more stabilized than those of filled cubic structures. This fact may also imply that the water molecules coordinate preferentially on the defect site.

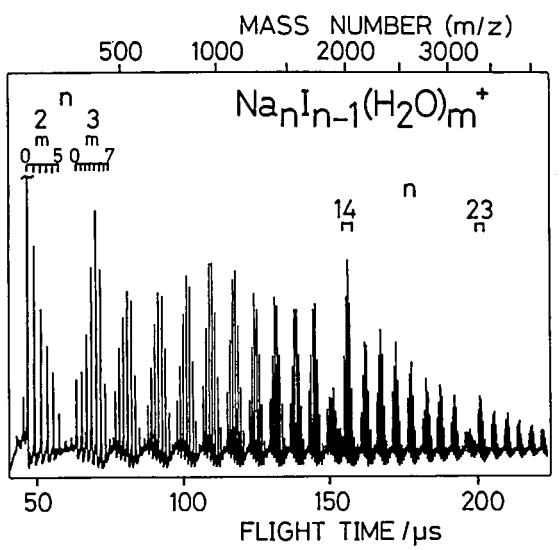

Figure 1. Time-of-flight mass spectrum of $Na_nI_{n-1}(H_2O)_m^+$ cluster ions directly formed in the cluster source.

VIII—D Physical Properties of Semiconductor Clusters

The study of structures and properties of small elemental clusters has been an extremely active area of current research. Particularly, the covalently bonded semiconductor clusters such as silicon clusters have attracted considerable attention. In the past several years a considerable amount of experimental and theoretical effort has been expended in the study of these clusters, but the complexity and variety of bonding modes that exist in these clusters has not been recognized. To gain further insight on the physical properties of small silicon clusters, we have studied the photoionization process of these clusters using a vacuum ultraviolet (VUV) laser.

VIII-D-1 Generation of VUV Radiation by High-Order Anti-Stokes Raman Scattering

Kiyokazu FUKE, Keizo TSUKAMOTO, Fuminori MISAIZU, and Masaomi SANEKATA

The VUV laser radiation has generated by anti-Stokes (AS) conversion of narrow-bandwidth UV radiation at 193 nm in hydrogen and deuterium. A schematic of experimental setup for VUV generation is shown in Figure 1. For the generation of narrow-bandwidth radiation around 193 nm, the second harmonic of a Rhodamine 6G dye laser pumped by a Nd:YAG laser is applied. The dye laser output is typically 100 mJ at 568 nm and yields the second harmonic output up to 20 mJ. This output is focussed into a first Raman cell-a 30 cm long stainless steel tube-by an f=20 cm plano-convex lens. The radiation leaving the cell is dispersed by a quartz Perin-Broker prism. For the optimum H_2 pressure of approximately 10 atm, the energy of the fourth AS component at 193 nm is typically 6 μJ. We used a Lambda-Physik LPX 110i as an amplifier into which the fourth AS-component is injected. The ArF amplifier is used in a double pass configuration. The energy from the net system is on the order of 10 mJ. The amplified radiation is focused into a second Raman cell via an f=15 cm suprasil lens. The radiation leaving the cell through an MgF_2-window into a vacuum vessel is dispersed by a LiF 30° prism. H_2 and D_2 are used as a nonlinear medium in the second Raman cell. For the optimum H_2 (D_2) pressure of approximately 8 atm, the Stokes component of up to seventh order and AS of up to fourth order are generated. Although we did not measure the energy of AS components, it is estimated to be on the order of 10 μJ, down to the shortest wavelengths (fourth AS component at 146 nm); we estimated the energy from the signal intensity of silicon cluster ions produced in the photoionization experiments described in the following topic.

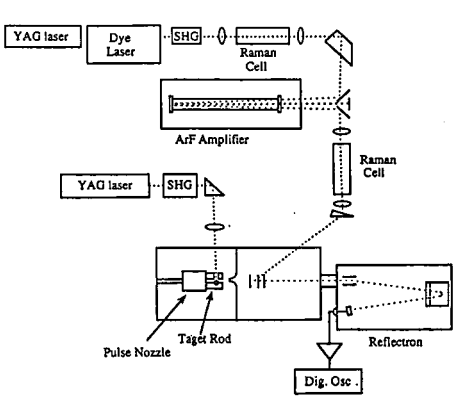

Figure 1. Experimental setup for VUV generation and photoionization study.

VIII-D-2 Photoionization of Small Silicon Clusters: Ionization Potentials for Si_2 to Si_{40}

Kiyokazu FUKE, Keizo TSUKAMOTO, Fuminori MISAIZU, and Masaomi SANEKATA

[*Z. Phys. D*, in press]

Photoionization thresholds of Si_n (n=2—40) were examined by a vacuum ultraviolet (VUV) laser (5.7—8.5 eV) described in VIII-D-1. Silicon clusters were synthesized in flowing He gas by pulsed-laser vaporization of a silicon rod, and photoionized with the VUV laser in a supersonic beam. Cluster ions thus produced were mass analyzed by a reflectron-type time-of-flight mass spectrometer.

The photoionization mass spectrum produced at 8.49-eV (H_2, AS-4) excitation predicts that Si_{10} is much more stable than its neighbors, while Si_{17}, Si_{20}, and probably Si_{13} are less stable in the neutral ground state. The photoionization mass spectra were also recorded at 7.97 (H_2, AS-3), 7.46 (H_2, AS-2), 7.17 (D_2, AS-2), 6.94 (H_2, AS-1), 6.80 (D_2, AS-1), 6.42 (193 nm), 6.05 (D_2, S-1), 5.91 (H_2, S-1), 5.68 (D_2, S-2)-eV photon energies, respectively. The ionization threshold energies for Si_n (n=2—40) deduced from these spectra are summarized in Figure 1. These constitute a set of upper bounds to the true adiabatic Si_n ionization potentials. A strong threshold energy dependence on cluster size is observed, featuring major maxima at n=10 and 20. The magic behavior at n=10 is consistent with the results of the experimental and theoretical studies reported previously.

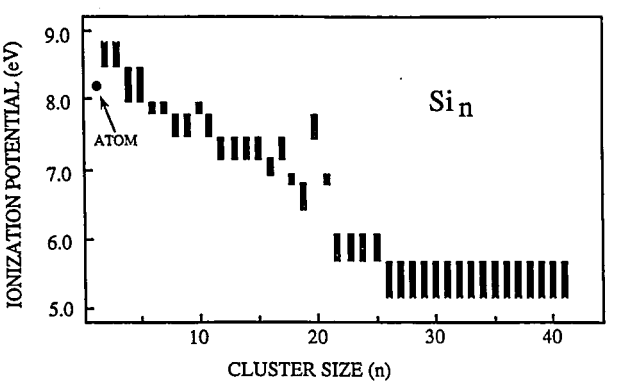

Figure 1. The ionization potentials of silicon clusters plotted vs cluster size. The IPs were determined from the phtoionization mass spectra produced at various Stokes and anti-Stokes lines (see the text) of narrow-bandwidth 193-nm radiation in high pressure H_2 and D_2 gases.

VIII—E Interatomic Potentials and Inter- and Intra-Multiplet Relaxation of the Excited Group IIB Metal Atoms

The collisional quenching of electronically excited metal atoms has been the subject of extensive studies because of its importance in photophysics and photochemistry. In the present project we seek to obtain more detailed information about the dynamics of deactivation processes of the excited group IIB metal atoms.

VIII-E-1 Intersystem Crossing and Intramultiplet Mixing of Excited Zn Atoms by Xe

Hironobu UMEMOTO, Toshiharu OHNUMA, Hiroyuki IKEDA, Shigeru TSUNASHIMA, Kazuya KUWAHARA *(Tokyo Inst. of Tech.),* **Fuminori MISAIZU, and Kiyokazu FUKE**

[*J. Chem. Phys.*, **97**, 3282 (1992)]

The intersystem crossing of $Zn(4^1P_1)$ and the intramultiplet mixing of $Zn(4^3P_1)$ by Xe were examined by using pulsed laser techniques. The following thermally averaged cross sections were obtained:

$Zn(4^1P_1) + Xe \rightarrow Zn(4^3P_2) + Xe$: 3.4,
$Zn(4^1P_1) + Xe \rightarrow Zn(4^3P_1) + Xe$: 0.4,
$Zn(4^1P_1) + Xe \rightarrow Zn(4^3P_0) + Xe$: <0.01,
$Zn(4^3P_1) + Xe \rightarrow Zn(4^3P_2) + Xe$: 12.0×0^{-3},
$Zn(4^3P_1) + Xe \rightarrow Zn(4^3P_0) + Xe$: 6.3×10^{-3},

in units of 10^{-16} cm^2. The magnitude of these cross sections can be correlated with the nature of the potential curves involved. Quantum mechanical calculations were carried out within a close-coupling treatment to evaluate these cross sections. The above experimental results could well be reproduced by quantum calculations when suitable potential energy curves were assumed. The close-coupling calculation also shows that the non-adiabatic transition from the singlet state to the triplet state is localized at the crossing point of the potential curves of the $^3P_1$ and $^3P_0$ states.

VIII—F Studies of Ultrafine Particles

The magnetic properties of ultrafine MnF_2-IV (metastable phase) particles are studied by ESR. It is confirmed by the size dependence of the critical exponent for ΔH that the decrease of T_N is due to decrease of the average coordination number in a particle. The nature of the spin ordering in finite system is now investigating.

VIII-F-1 Size Dependence of Critical Exponent for ESR Linewidth Observed in Ultrafine MnF_2-IV (metastable phase) Particles

Shunji BANDOW

The critical exponent of the ESR linewidth via reduced temperature are investigated for several sizes of particles. The result is shown in Figure 1. It is found that the critical exponent for ΔH become small in absolute value in the particle size less than *ca.* 3 nm. Although it is constant for the particles larger than 3 nm, the Néel temperature decreases linearly with a function of inverse of the volume of particle.[1] In general, the critical exponent is not changed by the total coupling strength per spin, but is sensitive to topological and spin dimensionality only.[2] This fact suggests that the decrease of T_N is due to the decrease of the average coordination number $\bar{z}$ given by the ratio of the total number of bonds to the number of atoms in a particle: Since the coordination number of surface atoms is smaller than that of inside atoms in a particle, $\bar{z}$ is smaller than z. Hence, it is not necessary to consider the change of the magnitude of exchange integral or the crystallographical phase transition; the decrease of T_N is purely due to the size effect of particles.

References
1) S. Bandow and K. Kimura, *IMS Ann. Rev.*, 188 (1990).
2) K.G. Wilson, *Sci. Am.*, **241** (2), 140 (1979).

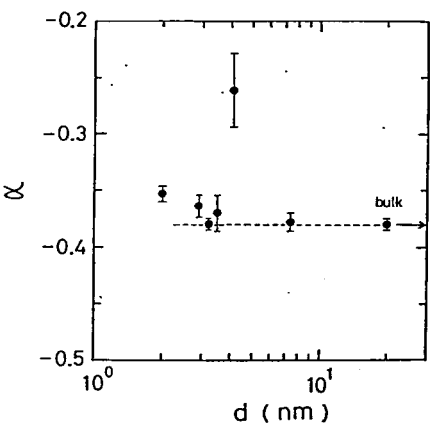

Figure 1. Size dependence of critical exponent α. The α is constant in the particles larger than *ca.* 3 nm.

VIII—G Formation and Physical Properties of Fullerenes and Metallofullerenes

The collection method for the soot including fullerenes and metallofullerenes is investigated for the purpose to study the new fullerenes composite. It is found that the metallofullerenes are air sensitive and therefore the anaerobic sampling is important to find the new metallofullerenes.

VIII-G-1 Collection Technique under Anaerobic Condition for Fullerenes/or Metallofullerenes Produced by the Gas-Flow Arc Discharge Method

Shunji BANDOW, Naoki TANAKA*, and Hisanori SHINOHARA* *(*Mi'e Univ.)*

The fullerenes/or metallofullerenes are usually extracted from the gas evaporated soot gathered from the wall of the vacuum chamber under aerobic condition. In such collection method, it is hard to avoid the oxidation effect. Especially for the metallofullerene, it seems to be a serious damage. Hence, we developed the new collection method for soot trap simultaneously with the extractive solution.

First we checked the helium flow condition for guiding the soot from the preparation chamber to the collection chamber (see Figure 1 in ref. 1). The He pressure in the chamber was fixed at 1.33×10^4 Pa and the flow rate of it was changed. The Yield of soot guided to the collection chamber was checked by the ratio of soot weight in the collection chamber to the whole soot generated. The result of the collection yield are shown in Figure 1 for each part in collection chamber. By selecting the suitable flow rate, it is possible to guide the soot to the collection chamber and to trap nearly whole soot guided at there. The solution trapping was also checked by inletting the toluene vapor to the gas stream. Nearly all of the soot guided to the collection chamber can be trapped and be gathered into the sample bottle attached at the bottom of the collection chamber only by removing liquid nitrogen. The solution in it is syringed out by the Luar-lock type syringe and filtered. This trapping method is useful to the air sensitive species since all of the sample handling processes can be done under anaerobic condition.

Reference

1) N. Mizutani, *et al., IMS Ann. Rev.*, 125 (1991).

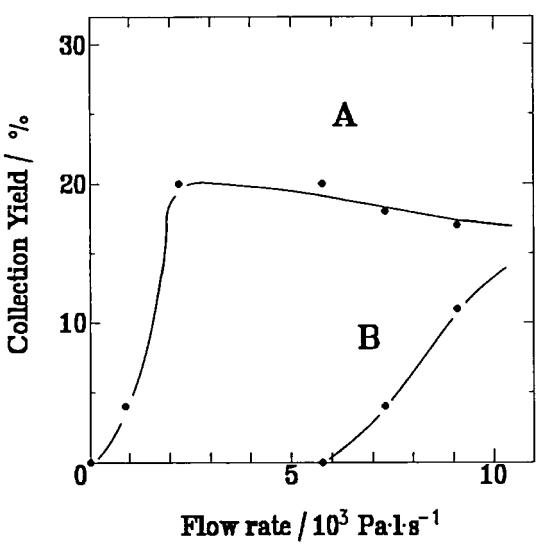

Figure 1. Collection yield of the soot guided to the collection chamber. The experimental conditions are as follows: He pressure is 1.33×10^4 Pa and the DC arc current density 2.5 A/mm^2. The collection yield was characterized by the weight ratio of the soot attached at collection chamber to the whole soot generated. **A** in the figure is the outer cylinder part in collection chamber and **B** the inner cylinder.

VIII-G-2 Anaerobic Sampling and Characterization of Lanthano-Fullerenes: Extraction of LaC_{76} and Other LaC_{2n}

Shunji BANDOW, Hiroshi KITAGAWA, Tadaoki MITANI, Hiroo INOKUCHI, Yahachi SAITO*, Hiroki YAMAGUCHI*, Naoyuki HAYASHI*, Hiroyasu SATO*, and Hisanori SHINOHARA* *(*Mi'e Univ.)*

[*J. Phys. Chem.*, **96**, 9609 (1992)]

Several new types of lanthano-fullerenes including LaC_{76} have been produced and extracted by a newly developed fullerene arc-generator equipped with an *anaerobic* (air-free) sampling and extraction mechanism of metallofullerenes. Other than the reported LaC_{82}, at least three different lanthanum metallofullerenes have been extracted by toluene and observed by ESR and mass spectrometry under anaerobic sampling conditions. The newly extracted lanthano-fullerenes exhibit equally-spaced octet ESR lines of equal signal intensities with different hyperfine coupling constants (0.44 G, 3.15 G, 2.12 G) and *g*-values (2.0043, 2.0042, 2.0010) as shown in Figure 1 *c* to *e*, respectively. Furthermore, these lanthano-fullerenes are found to be air sensitive, and the corresponding ESR signal intensities are decreased drastically to less than 5% of the original intensities when the samples are exposed to air for 5 days. The probable candidates for these fullerenes are presented including LaC_{76} and LaC_{84}.

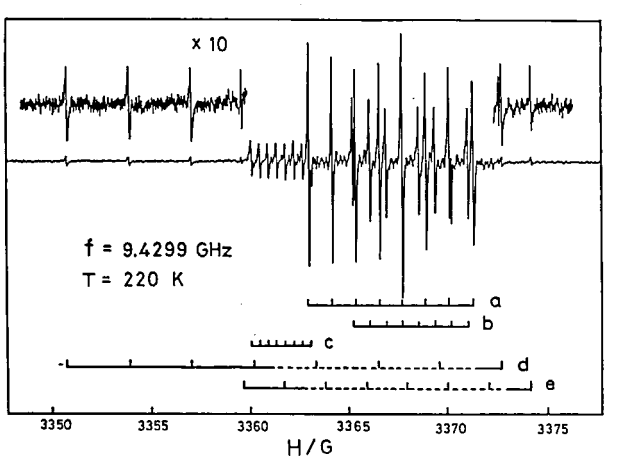

Figure 1. ESR spectra of lanthanum metallofullerenes extracted by toluene under anaerobic condition. The spectra *a* and *b* are already reported as LaC_{82} and its isomer, respectively, and *c* to *e* are the new ESR spectra found in this study.

Low-Temperature Center

VIII—H Ferromagnetic Interactions in Molecular Crystals

The study of the ferromagnetic intermolecular interaction in organic molecular solids should bring us important knowledge, not only to the establishment of molecular ferromagnet but also to the understanding about radical reactions. In the present project, we investigate the factors controlling ferromagnetic and antiferromagnetic behaviors in the solids.

VIII-H-1 α-Nitronyl Nitroxide Cation Radicals

Kunio AWAGA, Tamotsu INABE, Umpei NAGASHIMA, Takayoshi NAKAMURA*, Mutsuyoshi MATSUMOTO*, Yasujiro KAWABATA*, and Yusei MARUYAMA *(*National Chemical Laboratory for Industry)*

[*Chem. Lett.*, 1777 (1991)]

X-Ray crystal analysis and magnetic measurements have been carried out on the first *cation* radical salt of α-nitronyl nitroxide, 2-(4-*N*-R-pyridinium)-4,4,5,5-tetrametyl-4,5-dihydro-1*H*-imidazol-1-oxyl 3-*N*-oxide iodide (with R= methyl (**1**) and ethyl (**2**)), suggesting the separation between the spin and the charge density population, and revealing the strong antiferromagnetic intermolecular interaction of J_{AF}/k_B=149 K in **1**.

VIII-H-2 Ferromagnetic Intermolecular Interaction and Crystal Structure of the *p*-Pyridyl Nitronyl Nitroxide Radical

Kunio AWAGA, Tamotsu INABE, and Yusei MARUYAMA

[*Chem. Phys. Lett.*, **180**, 327 (1992)]

X-ray crystal analysis and magnetic measurements reveal the ferromagnetic linear chain with J_F/k_B=0.27 K in an α-nitronyl nitroxide, 2-(4-pyridyl)-4,4,5,5-tetramethyl-4,5-dihydro-1*H*-imidazol-1-oxyl 3-*N*-oxide.

VIII-H-3 Ferromagnetic and Antiferromagnetic Intermolecular Interactions in the Two-Dimensional Triangular Lattice of the *m*-*N*-Methylpyridinium Nitronyl Nitroxide Cation Radical

Kunio AWAGA, Tamotsu INABE, Takayoshi NAKAMURA*, Mutsuyoshi MATSUMOTO*, and Yusei MARUYAMA *(*National Chemical Laboratory for Industry)*

[*Chem. Phys. Lett.*, **195**, 21 (1992)]

An α-nitronyl nitroxide cation radical, 2-(3-*N*-methylpyridinium)-4,4,5,5-tetramethyl-4,5-dihydro-1*H*-imidazol-1-oxyl 3-*N*-oxide (*m*-MPYNN), has been found to possess quite an unique structure and magnetic properties: the molecules are manifested as dimers with a very short intermolecular contact between the NO group and the pyridinium ring, and the dimer units form an organic 2-D triangular lattice. It includes both the ferromagnetic and antiferromagnetic intermolecular interactions.

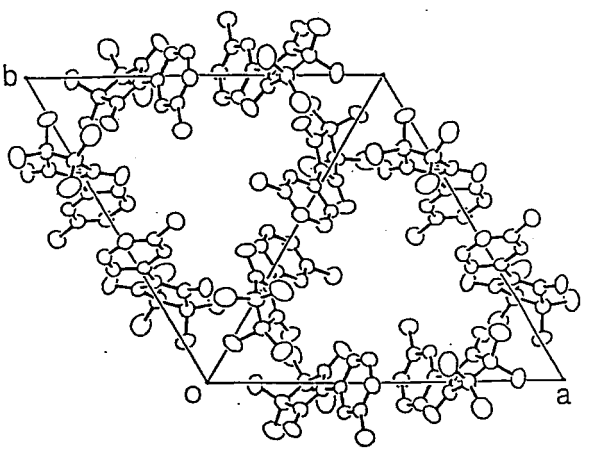

Figure 1. Triangular lattice in the crystal of *m*-MPYNN.

Equipment Development Center

VIII—I Activities of Division of "IMS Machines"

Equipment Development Center has the division for construction of so-called "IMS Machines", which are designed on the basis of ideas and/or proposals from members in the Institute for Molecular Science. New technologies required for their constructions are developed by the stuff of this division with an introduction of recently developed engineering and in collaboration with researchers of other institutes, universities and facilities of industries. The main aim of these activities is to expand a technical capability of this center, intending a development of future technology of the molecular science.

In this fiscal year, 1991, the project themes of IMS Machines selected from eight proposals are listed below. Their constructions were successfully executed as described separately.

1. **Fast-Scan Cyclic Voltammetry with Ultra-Microdisk Electrode**
(Hisashi YOSHIDA, Shuji ASAKA, and Koji TANAKA)
2. **Ultra-High-Vacuum and Low-Temperature Sample Transfer System for XPS**
(Norio OKADA, Toshio HORIGOME, Shuji ASAKA, and Shunji BANDOW)
3. **High-Sensitivity and High-Resolution Multi-Channel FT Spectrometer**
(Satoshi TAKAHASHI, Jeung Sun AHN, and Shuji ASAKA)

For fiscal year of 1992, three themes listed below were newly selected as IMS Machines, together with two themes renewed and three for surveying, out of 17 proposals. Their design is under way.

1. Fast Stabilizer for Fabry-Perot Interferometer
(Kazuo HAYAKAWA, Tatsuhisa KATO, and Shuji ASAKA)
2. Liquid Helium Auto-Supply System
(Hisashi YOSHIDA, Koichi SUZUI, Keiichi HAYASAKA, Kiyonori KATO, Takashi TAKAYAMA, and Shuji ASAKA)
3. Infra-Red Cryostat Windows
(Equipment Development Center)
[Renewed]
1. Multi-Channel Spectroscopic System in Mid-IR
(IMS Machine Division)
2. Ultra-High-Vacuum and Low-Temperature Sample Transfer System for XPS
(Norio OKADA, Toshio HORIGOME, Shuji ASAKA, and Shunji BANDOW)
[For surveying]
1. High-Resolution Technologies of STM/AFM in UHV
(proposed by Kosuke SHOBATAKE, Department of Vacuum UV Photoscience)
2. Wire Bonder for Minute Crystals
(proposed by Kiyonori KATO, Low temperature Center)
3. Fractional Mass Separator
(proposed by Yusei MARUYAMA, Department of Molecular Assemblies)

The construction of the IMS Machines is successfully executed in 1991. Among them the results of the two themes are ready to be opened to public. The following are brief reports of them.

VIII-I-1 Fast-Scan Cyclic Voltammetry with Ultra-Microdisk Electrode

Cyclic voltammetry with a fast voltage scan is expected to be useful to study reactions of short-lived radical ions from the aspect of redox potentials. The response speed of cyclic voltammograph systems now commercially available is, however, limited to 10,000 V/sec, which is not sufficient for the present research.

We have newly developed an ultra-fast cyclic voltammograph system for the purpose above. The constructed system consists of a wave-form generator, a potentiostat, a current-to-voltage converter, and a digital oscilloscope. These elements are controlled by a small computer.

Main features of the constructed apparatus are the following.

(1) The total system response is 60,000 V/sec.
(2) Computer-controlled wave generator enables any type of wave-forms in voltage scanning.

As to (1), the evaluation result of the system response for three different voltage scans is shown in Figure 1. The test sample is 9-methyl-anthracene solution, and the working electrode is a platinum disk of 10 μm in diameter. The constructed electronic circuit itself has a speed of 1,000,000 V/sec, and it was found that the use of a smaller electrode will further improve the total system response. Improvement with specially made microelectrodes (2 ~ 0.6 μm) is under way.

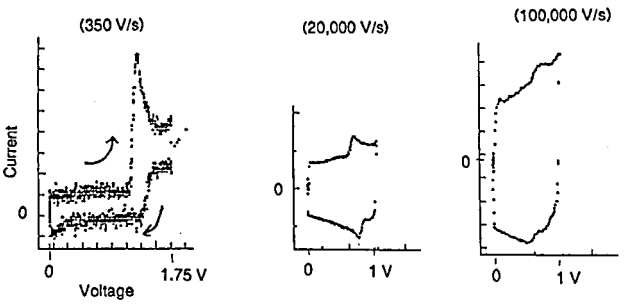

Figure 1. Cyclic voltammographs for three different voltage scanning speeds.

VIII-I-2 Ultra-High-Vacuum and Low-Temperature Sample Transfer System for XPS

In XPS apparatus now available a measurement, for example, in organic crystals is very difficult. This is because the high vacuum in the device will degrade the sample surface or even evaporates them up during measurements due to relatively high vapor pressures of such materials.

We have developed a sample transfer mechanism for ESCA system (VG corp.) in the Instrument Center available down to liquid helium temperature to solve the above mentioned drawback.

Main features of the present apparatus are the following:

(1) The sample mount can be cooled down to around liquid helium temperature.
(2) The sample temperature can be precisely controlled.
(3) In a same system cooling by liquid nitrogen is possible according to temperature range needed.
(4) A transfer tube for the coolant that is disassembled into two parts and a Z-axis bellow stage with a shrinkable guide are adopted. An easy operation of the system is realyzed.

Mechanism design is completed as shown in Figure 1, and the construction is being executed as the renewed theme for 1992.

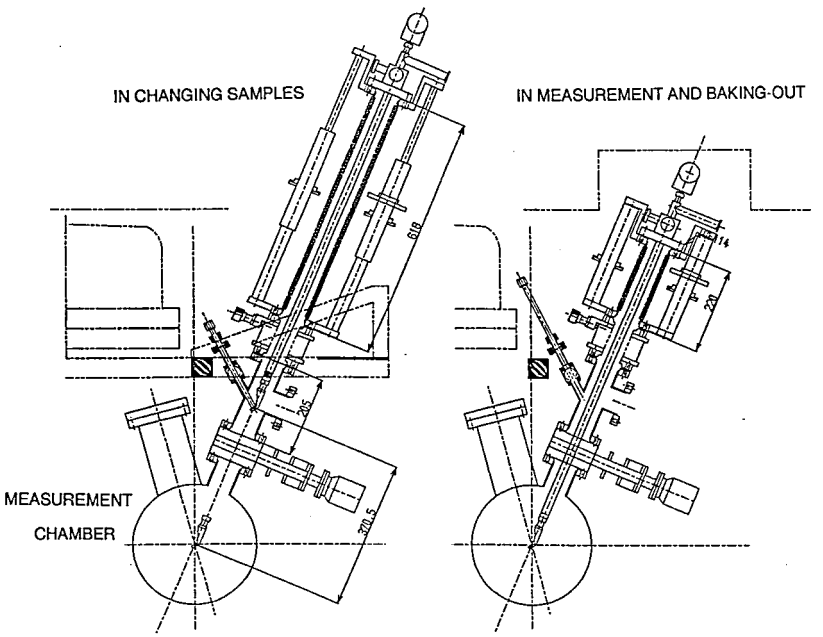

Figure 1. Design of UHV Sample Transfer System.

VIII—J Development of Experimental Devices

VIII-J-1 Pulse Generator for the Time-of-Flight Mass Spectrometer

Koichi UCHIYAMA

To pick out a needed ion from many ions in time-of-flight mass spectrometer (TOFMS), we made a pulse generator. Figure 1 shows the block diagram of the pulse generator. The power MOSFET (2SK1317, HITACHI) was used as the switching element for high voltage. In order to obtain fast switching by the FET, the MOS driver (DS0026, NS) was employed. Furthermore, the MOS drivers in the high-voltage parts, which are illustrated with two dashed blocks in Figure 1, were floated by the photo isolators (HCPL-2400, HP). The pulse generator was composed of two pulse generating circuits in order to control the magnitudes of two high-voltage pulses independently. For this reason, the output from one pulse generating circuit may be affected by the parasitic diode of the power MOSFET in the other circuit. To prevent such trouble, a diode was located between the HV power supply and the FET in each circuit.

The obtained pulse is shown in Figure 2. The pulse has the rising time of 200 nsec and the amplitude of 1.2 kV.

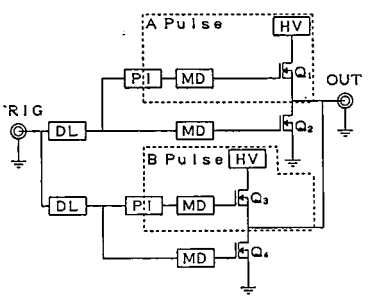

Figure 1. The block diagram of the pulse generator.

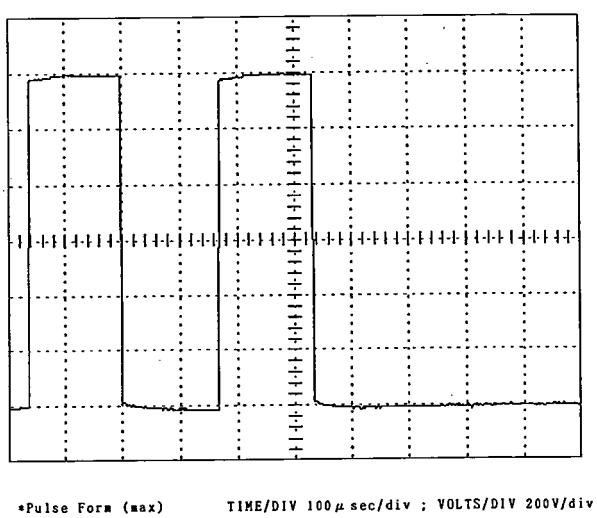

Figure 2. The output pulse form of the pulse generator.

VIII—K New Materials Research

Development of the technologies for new materials research is one of the most important subjects of Equipment Development Center. The policy of this activities is to achieve the project in collaboration with technicians and researchers in other facilities and departments in IMS. At present, the project of production and supply of C_{60}-related materials is going on.

VIII-K-1 Preparation, Separation, and Purification of C_{60}, C_{70}, and Higher Fullerenes

Masaaki NAGATA, Nobuo MIZUTANI, Shunji BANDOW, Yusei MARUYAMA, Hiroshi KITAGAWA, and Tadaoki MITANI

The efficient macroscopic syntheses of gram quantities of C_{60}, C_{70}, and higher fullerenes have been a flurry of interest in the new class of closed-caged carbon molecules. In the "Fullerene Factory" of IMS, several improvements in the method of preparation of fullerenes have been performed, which gives much larger amounts and higher purities than previously reported.

Figure 1 shows a schematic diagram of the Fullerene Factory in IMS. The carbon soot containing fullerenes was generated by a plasma discharge. The fullerene generator consists of two parts, preparation and collection chambers. The production of fullerenes is carried out under the helium flow condition (100 torr., 20—30 *l*/min.). In this way, we obtained a 20% yield of total carbon soot in the collection chamber, where the soot can be collected under anaerobic condition. Crude toluene-soluble products were extracted from the carbon soot by a special designed Soxhlet extractor for 24 hours. A fully integrated, automated, large-scale preparative HPLC system (Shodex AUTOPREP-50 with KF-801) was used to separate several kinds of fullerenes from concentrated extracts. Toluene was used as a eluted solution because of good solubility less adsorptivity compared with other solution. Its flow rate and auto-injection amount were 30 *ml*/min. and 40 *ml*, respectively. The absorption spectra (190—800 nm) can be measured *in situ* by a photo-diode array UV-VIS detector for the HPLC. Two or three recycle passes achieved complete separation (>99.5%) of C_{60} and C_{70}. In the Fullerene Factory, 5 g of C_{60} and 2 g of C_{70} with a purity of more than 99.5% can be obtained per week. Separations of higher fullerenes are indispensable and in progress.

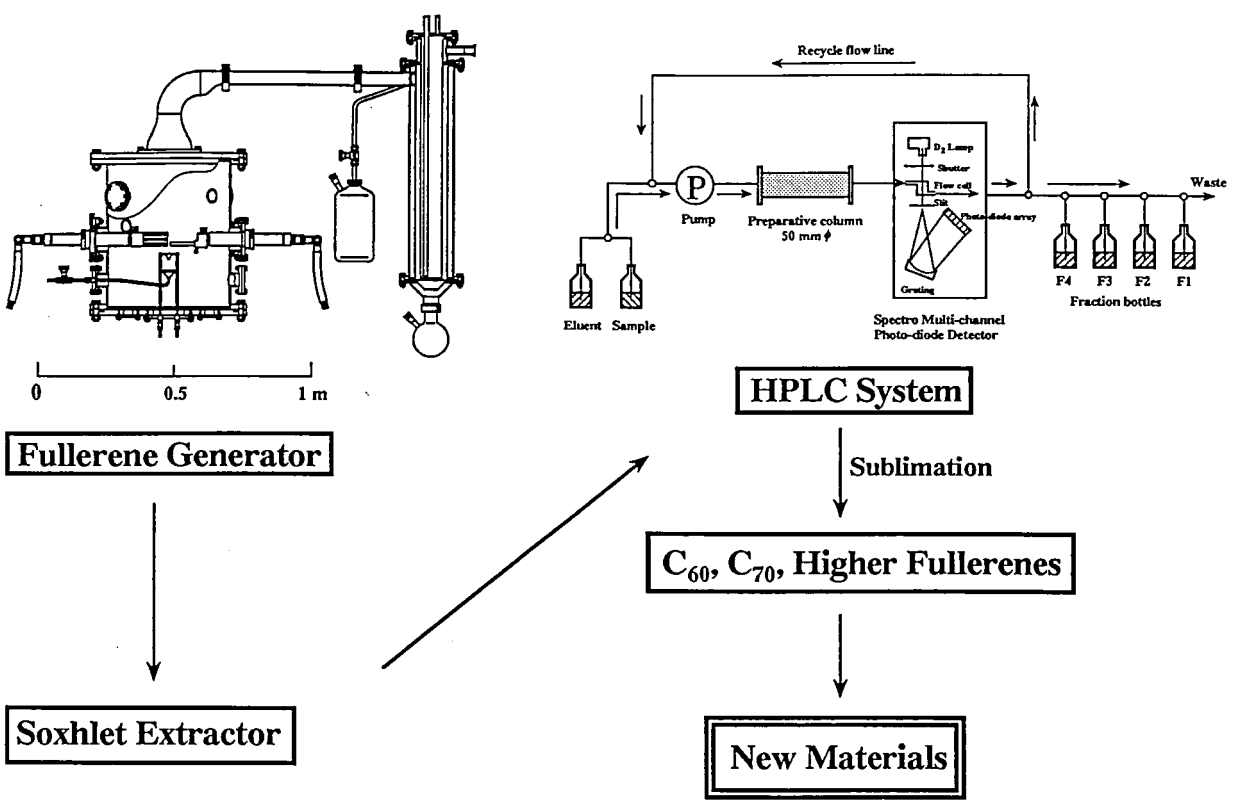

Figure 1. Schematic diagram of the Fullerene Factory in IMS.

VIII—L Studies of Halogen-Bridged Mixed-Valence Systems

Halogen-bridged one-dimensional (1-D) mixed-valence transition-metal complexes have been investigated intensively as a proto-type of 1-D electron-lattice coupling system. Recently, the interest of the photo relaxation process from a dynamical behavior of lattice-relaxed excitations such as a soliton or a polaron. The characteristic feature of the complexes is that their physical properties are strongly dependent on the species of the constituent metal, bridging halogen, and counter ion.

VIII-L-1 Photo-Generation of Solitons and Polarons in the 1-D Halogen-Bridged Metal Complexes

Hiroshi OKAMOTO*, Tadaoki MITANI, Koshiro TORIUMI, and Masahiro YAMASHITA***** *(*RISM, Tohoku Univ., **Himeji Inst. of Tech., ***Nagoya Univ.)*

[*Synth. Metals.*, in press]

The photo-induced IR absorption spectra of the halogen-bridged metal complexes have been measured on single crystals with different dimensionalities of chain structures. A decrease of the interchain coupling *via* the hydrogen-bonds leads to an appearance of a new band, which is attributable to photo-generation of solitons. The structures assigned to photo-generated polarons are rather insensitive to the interchain coupling. From the excitation spectra of the photo-induced absorption signals, it has been found that the exitonic effect completely quenches photo-generation of these gap states.

VIII-L-2 Control of CT Instability in 1-D Mixed-Valence Systems

Hiroshi OKAMOTO*, Koshiro TORIUMI, Tadaoki MITANI, and Masahiro YAMASHITA***** *(*RISM, Tohoku Univ., **Himeji Inst. of Tech., ***Nagoya Univ.)*

[*Mol. Cryst. Liq. Cyst.*, **218**, 247 (1992)]

Control of the amplitude of CDW has been made by making use of chemical modifications in the halogen-bridged metal complexes. The dynamics of the spin soliton originated from the CT instability is discussed on the basis of the results of the ESR measurements on the complexes belonged to the group near the boundary between the mixed-valence state and the mono valence state.

VIII-L-3 Electrical Conductivity of the Perovskite-Type Mixed-Valence Compound $Cs_2Au_2I_6$ under High Pressures and Low Temperature

Hiroshi KITAGAWA, Norimichi KOJIMA*, Hiroki TAKAHASHI, and Nobuo MORI**** *(*Kyoto Univ., **ISSP)*

[*Synth. Met.*, in press]

$Cs_2Au_2X_6$(X=Cl,Br,I) is known as a three-dimensional Au^{I}-Au^{III} mixed-valence system. We had shown that $Cs_2Au_2I_6$ undergoes a pressure-induced first-order phase transition at 5.5 GPa and room temperature. As the pressure is increased up to the transition pressure, the geometries of $Au^{I}I_6$ and $Au^{III}I_6$ octahedra become more equivalent. When those are equivalent and the electronic structure of Au approaches a d^9 valence state ($I4/mmm \rightarrow P4/mmm$), the lowering in symmetry of AuI_6 octahedra is caused by the Jahn-Teller effect.

The electrical conductivity of single crystal $Cs_2Au_2I_6$ has been investigated under high pressures (0—8 GPa) and low temperature (4.2—300 K). Strongly pressure-dependent resistivity anomalies have been observed under hydrostatic pressure condition. Drastic resistance jump has also been observed around 5 GPa, which may be interpreted in terms of the "band Jahn-Teller" transition or the CDW transition (Figure 1).

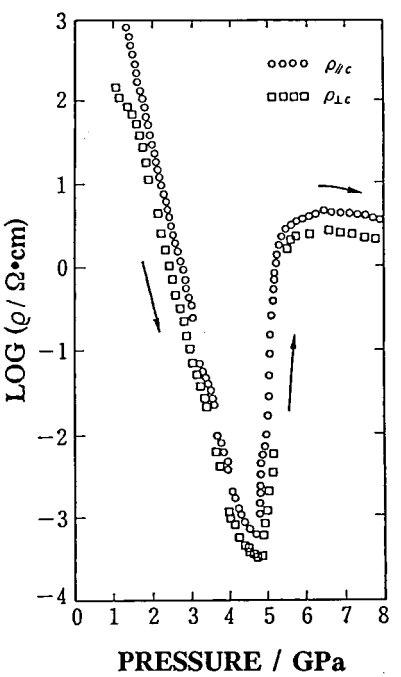

Figure 1. Pressure dependence of the resistivity parallel and perpendicular to the c-axis at room temperature.

VIII—M Studies of H-Bonded CT Complexes

The dynamics of hydrogen bond (H-bond) in solids has been a subject of prolonged interest, and a great deal of spectroscopic data of the H-bond has been accumulated. Nevertheless, there remain many foudational problems when the proton is dynamically correlated with electrons, particularly with regard to the quantum-mechanical dynamics of proton in H-bonded condense phases. Unquestionably, this is a reflection of the cooperation of H-bond with electron and lattice systems through a unique interaction in solids. The subject of this study is to elucidate the cooperation of proton-electron and proton-lattice in CT complexes.

VIII-M-1 A New Two-Band System of *d* and π with Interband H Bridges

Hiroshi KITAGAWA, Hiroshi OKAMOTO*, Tadaoki MITANI, and Masahiro YAMASHITA** *(*RISM, Tohoku Univ., **Nagoya Univ.)*

[*Mol. Cryst. Liq. Cryst.*, in press]

A two-band system of *d* and π with interband H bridges (Figure 1) provides a unique opportunity for construction of novel molecular assemblies, in which many electronic systems are combined *via* H-bond system. When the partial CT occurs between the chains, *d* holes (or electrons) in the metal-complex chains and π electrons (or holes) in the organic acceptor (donor) chains are expected to show a

unique cooperation through the interchain H bonds. As the first demonstration of this system, we have investigated single crystals of [M(H_2DAG)(HDAG)]TCNQ(M=Ni,Pd, Pt). These complexes consist of segregated stacks of bis(oxamidoximato)M(II) complex donors and TCNQ acceptors, whose chains are connected to each other by interchain H bonds. From the results of optical and transport measurements, the TCNQ stack of each salt exhibits a partial oxidation state and mainly contributes to the high conductivity around room temperature. The semiconducting behavior in the low-temperature region may arise from strong electron-lattice (or-proton) interaction; the CN stretching mode shows a characteristic temperature dependence below the temperature of the metal-to-semiconductor transition.

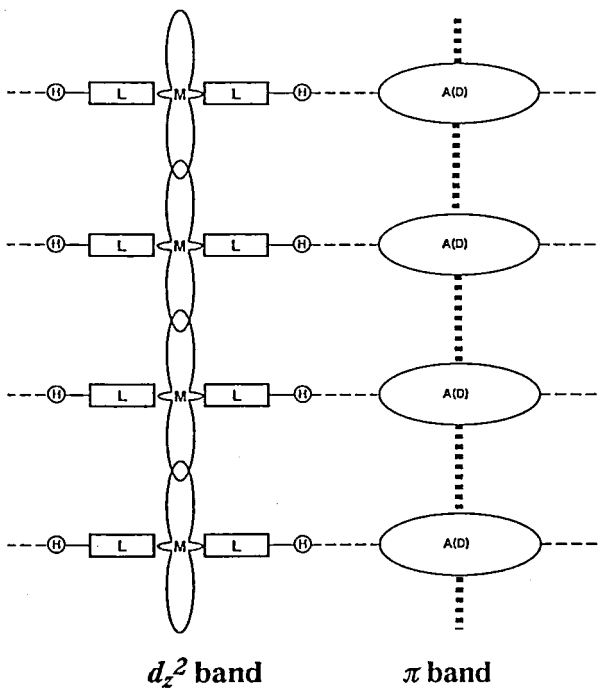

Figure 1. Two-band system of d_{z^2} and π bands with interband H bridges.

VIII-M-2 X-Ray Photoelectron Spectroscopic Study of H-Bonded CT Complexes

Hiroshi KITAGAWA, Hiroshi OKAMOTO*, Tadaoki MITANI, and Masahiro YAMASHITA** *(*RISM, Tohoku Univ., **Nagoya Univ.)*

[*Synth. Met.*, in press]

The results of optical and electrical resistivity measurements on [M(H_2DAG)(HDAG)]TCNQ (M=Ni,Pd,Pt, H_2DAG=diaminoglyoxime) show unusual behavior around 250 K. In order to investigate the oxidation states of the transition-metal-complex chain and the organic acceptor (TCNQ) chain, we have measured the X-ray photoelectron spectra in the temperature range 165–300 K on a VG ESCA MKII electron spectrometer.

Figure 1 shows the XPS spectra in the Pt 4*f* region of the Pt salt at r.t. and 165 K. The observed spectrum at room temperature shows a typical Pt^{II} doublet structure, while, at 165 K, it was resolved into two doublet structures for Pt^{II} and Pt^{IV}, the latter ionizing at higher energy. The intensity ratio of Pt^{II} and Pt^{IV} components is almost 1.0. These results indicates that the valence state of Pt in [Pt(H_2DAG)-(HDAG)]TCNQ changes from II to II-IV mixed-valence state below about 250 K. The transformation of the valency was also observed for the Pd salt but not for Ni salt.

We have also measured the absorption spectra at 77 K of [Pt(H_2DAG)(HDAG)]TCNQ using the same sample batch as used for the XPS measurement. Comparing with the spectra of TCNQ salts, the bands in the region of 2–4 eV are assigned to be intramolecular excitations in TCNQ molecules. While two bands at 2.1 and 3.5 eV were observed at room temperature, new two additional peaks at 2.4 and 3.2 eV were observed at 77 K. This suggests that the partial oxidized state of TCNQ stacks varies remarkably with decreasing temperature. From the experimental results of XPS and optical measurements, it may be reasonable concluded that the charge transfer occurs from the transition-metal-complex donor chain to the TCNQ acceptor one below about 250 K. These anomalous phenomena described above require further detailed researches.

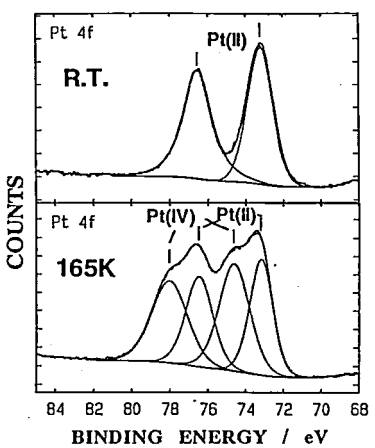

Figure 1. XPS spectra in the Pt 4*f* region of the Pt salt at room temperature (above) and 165 K (below).

VIII-M-3 Infrared Spectroscopy of One-dimensional Hydrogen-bonded System

Taro SEKIKAWA *(Univ. of Tokyo and IMS)*, **Tadaoki MITANI, Keisuke MIYAKUBO** *(Osaka Univ.)*, **and Sadamu TAKEDA** *(Osaka Univ.)*

Potassium Hydrogen Acetylenedicarboxylates make the infinite chains linked together by short (2.445 Å) hydrogen bonds. They are expected to have a solitary excitation from NMR. To examine the validity of the model, the temperature and pressure dependence of infrared spectra are measured. Especially the pressure dependence provides new knowledge of hydrogen bonds of the system, because the length of the hydrogen bonds are shorten under the higher pressure. The results of the measurements show that the anharmonic coupling due to the hydrogen bonds plays important roles in forming the absorption spectra. It explains the shift and the broadening of the (O-H) stretching mode and the temperature dependence of the line width of the (C=O) stretching mode. The relation between the anharmonic coupling and the formation of soliton is under consideration.

VIII-M-4 Intra- and Inter-Molecular Charge Transfer Interactions in H-Bonded DTPP Crystals

Kaoru OKANIWA, Hiroshi OKAMOTO*, Tadaoki MITANI, Tamotsu INABE, Jiro TOYODA, Yasushi MORITA, Kazuhiro NAKASUJI, Hiroshi YAMAMOTO***, Takashi DENO***, and Seiji HONMA*****
*(*RISM, Tohoku Univ., **Hokkaido Univ., ***Ciba-Geigy Japan Ltd.)*

[*Mol. Cryst. Liq. Cryst.*, **216**, 241 (1992)]

The spectra of polarized reflectivity and excitation of photoconductivity of β-DTPP crystal have been measured. Highly efficient photoconductivities were observed along the both directions of the stacking of the molecules and the intermolecular H-bond. These excitation spectra are considerably different and depend on the direction of applied electric field. These photoconducting properties are discussed in terms of charge transfer interaction along stacking axis and the electron-proton interactions.

Ultraviolet Synchrotron Orbital Radiation Facility

VIII—N Development of UVSOR Light Source

VIII-N-1 Control of the Bunch Length of Electron Beam on the UVSOR Storage Ring

Hiroyuki HAMA, Shiro TAKANO *(RIKEN)*, and Goro ISOYAMA

An experimental study to make the bunch length of the electron beam short is in progress on the UVSOR storage ring by means of reducing a momentum compaction factor α. An extremely short bunch of electrons in a storage ring will not only extend the region of time-resolved experiments with synchrotron radiation (SR) but also enhance gain of free electron laser because the peak current in the bunch becomes higher for the same average beam current. Furthermore, a spontaneous coherent SR may be hopefully detected. The longitudinal bunch length is proportional to the square root of α. Since α is proportional to the integral of dispersion function η in the bending magnets, we vary the dispersion function so that positive and negative parts of η cancel out to reduce α.

The experiment has been carried out in the single-bunch mode at an electron energy of 600 MeV. According to a model calculation, we changed excitation currents of quadrupole magnets synchronously, after the beam injection, to vary α while the betatron wave numbers were maintained to be close to the regular operating point. In order to determine α, the synchrotron oscillation frequency f_S was measured, which is proportional to the square root of α. The horizontal beam displacement was also measured as a function of the RF frequency, which is related to α as $\Delta x=(\eta_{PM}/\alpha)\times(\Delta f_{RF}/f_{RF})$, where η_{PM} is a dispersion function at a position monitor. Figure 1 shows the measured momentum compaction factors of first order α_1 and second order α_2 at several operating points specified by η in the long straight section. The experimental values are in good agreement with the model calculation. In the very low α region, it was found out that effect of the second order term in the momentum compaction factor α_2 revealed itself, then the beam lifetime became short. It turned out that the effect of α_2 was able to be compensated with focusing sextupole magnets. The lowest α obtained so far is 0.00025. The bunch length was measured using a streak camera at a very low beam current of less than 0.1 mA. In Figure 2, the bunch length is plotted as a function of f_S which was measured simultaneously with the bunch length. The bunch length is almost proportional to the synchrotron oscillation frequency over the wide range, as predicted by theory. The bunch length is successfully shortened down to ~30 ps (twice the standard deviation), which is approximately one tenth of the bunch length at the regular operating point. The correction of higher order effects in very low α operation and the bunch lengthening at higher beam current are under investigation.

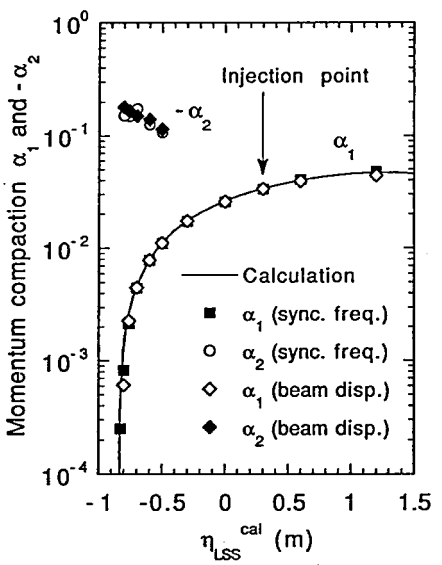

Figure 1. Measured first order α_1 and second order α_2 in the momentum compaction factor as a function of the dispersion function in the long straight section η_{LSS}^{cal}.

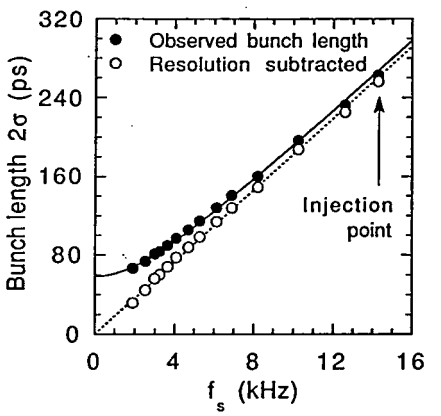

Figure 2. Measured bunch length as a function of the synchrotron oscillation frequency.

VIII-N-2 Free Electron Laser Experiments on the UVSOR Storage Ring

Shiro TAKANO *(Institute of Physical and Chemical Research)*, **Hiroyuki HAMA, and Goro ISOYAMA**

An experimental study of a free electron laser (FEL) is in progress on the UVSOR storage ring. As the initial step, an FEL gain was measured with a conventional undulator at a wavelength of 488 nm to be 8×10^{-4} for the beam current of 10 mA/bunch. Since the FEL gain is marginal to achieve lasing, we have remodeled the undulator into an optical klystron (OK) in order to make the gain as high as possible. The OK consists of two identical undulator sections, each of which has the period length of 11.1 cm and the number of periods of 8, and a dispersive section of 37 cm long. In order to measure the gain, the storage ring is operated in the single-bunch mode at the energy of 500 MeV. We use an argon ion laser as an external coherent light source and a lock-in amplifier to detect the intensity of gain signal detected with a silicon photodiode as well as its phase. Figure 1 shows the gain measured as a function of N_d, which is the number of light wavelengths passing over an electron in the dispersive section. The measured peak gain is 0.4% for the beam current of 10 mA/bunch, which is in good agreement with the theoretical peak gain calculated to be 0.5%.

An optical resonator used for the oscillation experiments consists of a pair of spherical mirrors separated by a distance of 13.3 m, which is a quarter of the circumference of the storage ring. The mirrors coated with dielectric multilayer are put in vacuum chambers, each of which is mounted on a 5-dimensional stage in the atmosphere in order to adjust the transverse and the longitudinal positions as well as tilt angles of the mirrors. In oscillation experiments, the storage ring is operated in a two-bunch mode with equal bunch spacing in order to ensure that the light pulse interacts with the electron bunch in every round trip in the cavity. The geometrical axis of the optical cavity is aligned with the electron beam in the OK by using spontaneous radiation. The cavity length is precisely tuned by observing the time profile of spontaneous radiation stored in the cavity with a streak camera so that the width of the temporal profile is minimized. We started the oscillation experiments with a beam current of more than 20 mA/bunch. The first lasing was obtained at a wavelength of 456 nm on March 8, 1992. Figure 2 shows evolution of radiation spectra measured with a monochromator as a function of the beam current. Lasing can be clearly seen in the upper two panels. The wavelength could be varied over the range from 430 to 480 nm. The line width of the laser is approximately 0.2 nm. When the rf frequency is adjusted, which is equivalent to tuning of the cavity length, to give the maximum output power, the macro pulsed structure appears with the typical repetition period of 7 ms. When the rf frequency is detuned, the CW mode operation is obtained. The peak power in micro pulses is roughly estimated to be at least 0.8 W at the beam current of 23 mA/bunch.

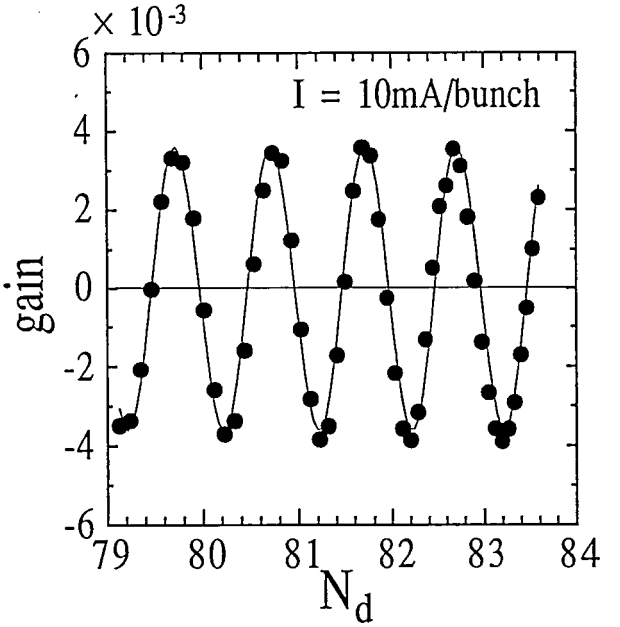

Figure 1. FEL gain with the OK as a function of N_d. The measured gain is denoted by the solid circles, and the theoretical gain by the solid line, which is calculated from the measured spectrum of spontaneous radiation with Madey's theorem.

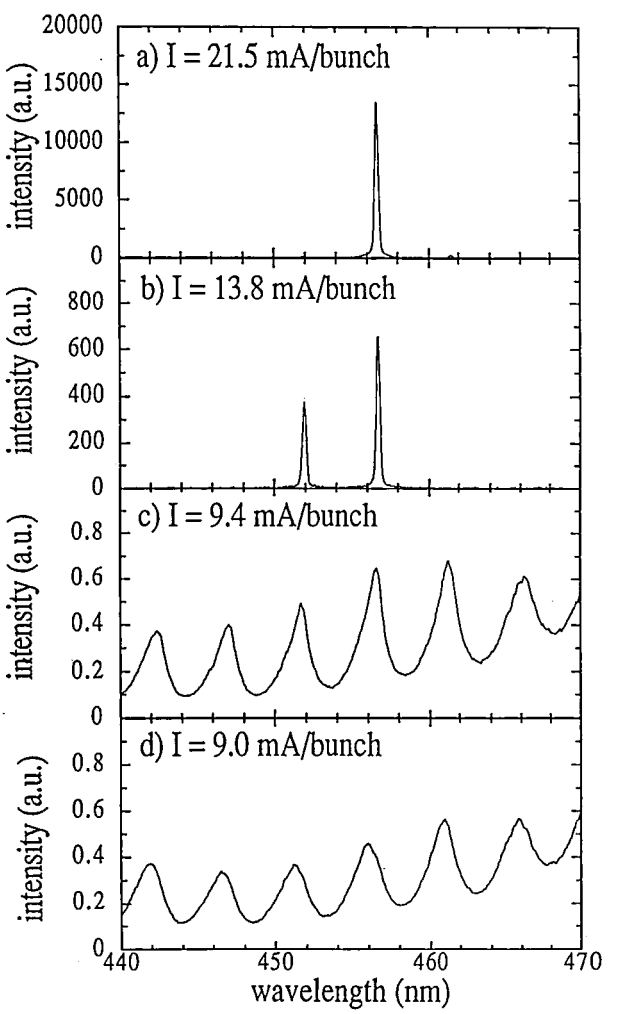

Figure 2. Spectral evolution of radiation from the FEL as a function of the beam current. Lasing Lines are clearly seen in he upper two panels. The lower two panels show spectra just above and below the lasing threshold, respectively.

VIII—O Development of Beamlines and Equipment for UVSOR

VIII-O-1 Test of Holographic SiC Gratings for High-Power Synchrotron Radiation

Eiji ISHIGURO *(Osaka City Univ. and IMS)*, **Hideki MAEZAWA** *(KEK)*, **Makoto SAKURAI** *(NIFS)*, **Mihiro YANAGIHARA** *(Tohoku Univ.)*, **Makoto WATANABE, Masaru KOEDA*, Tetsuya NAGANO*, Kazuo SANO*** *(*Shimadzu Corp.)*, **Yasuhiro AKUNE**, and Kichiya TANINO**** *(**Nippon Pillar Packing Corp.)*

High heat load resistivity is required for diffraction elements in grating monochromators which will be installed into VUV and Soft X-ray beam lines of a high-brilliance next-generation storage ring. Recently, SiC gratings have been fabricated by two different methods; one was a SiC based grating mechanically ruled on gold surface[1] and the other a holographic ion-beam etched SiC grating[2]. The former was found to withstand high power beams emitted from an undulator, although a slight deformation of the Au film was observed. The latter was manufactured by reactive ion-beam etching (RIBE) in CHF_3+Ar mixture with the aid of photoresist as mask against etching. Although the diffraction efficiency was not sufficiently high in the soft X-ray region, the scattered light component was quite low. The purpose of the present paper is to give results of an irradiation test for the ion-beam etched SiC gratings.

Polycrystalline CVD-SiC in which individual grains were strongly oriented to the (220) plane was used as a substrate of the grating. Diffraction efficiencies were measured by using a PGM installed to the BL5B beam line of UVSOR. The efficiency of the +1 order was 5 to 20% in the region between 17 Å and 300 Å. Irradiation test for the SiC gratings was performed by using intense radiation of power density of 2.7 W/mm^2 emitted from a multipole wiggler installed into the 2.5- GeV Photon Factory ring. The results are shown in Figure 1. No visible damages was observed for the uncoated SiC grating after the irradiation, while a remarkable deformation of the deposited Au layer was observed for the grating coated with Au.

References

1) T. Kita, T. Harada, H. Maezawa, Y. Muramatsu and H. Namba, *Rev. Sci. Instrum.* **63**, 1424 (1992).
2) E. Ishiguro, K. Yamashita, H. Ohashi, M. Sakurai, O. Aita, M. Watanabe, K. Sano, M. Koeda and T. Nagano, *Rev. Sci. Instrum.* **63**, 1439 (1992).

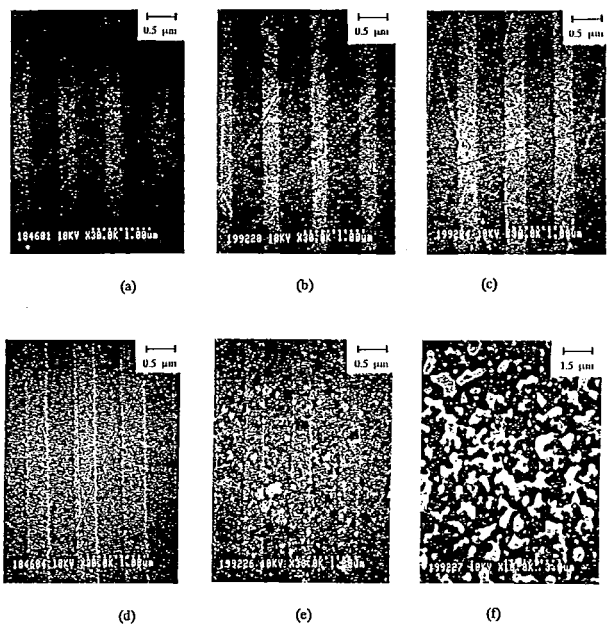

Figure 1. SEM photographs of a non-coated SiC grating (a)before irradiation, (b)after irradiation for 4 min and (c)after irradiation for 40 min, and those of a grating coated with Au of 200 Å thickness (d)before irradiation, (e)after irradiation for 4 min and (f)after irradiation for 40 min.

VIII—P Researches by the Use of UVSOR

VIII-P-1 X-Ray-Absorption Near-Edge Structure of Solid Rare Gases

Atsunari HIRAYA and Makoto WATANABE

X-ray absorption near-edge structure (XANES) of solid rare gases was recorded for Ne K-edge, Ar K-edge, Kr L-edge, and Xe M-edge using transmission method at double crystal monochromator beamlines BL1A and BL7A. Observed peak positions in XANES are analyzed by a model based on the Natoli's multiple-scattering theory which predicts linear correlation of the XANES peak energy from a bound state just below the edge with inverse-square of interatomic distances R. As shown in the K-edge XANES spectrum of solid Ne (Figure 1), correlation plot of XANES peak energy versus R^{-2} shows good linearity and intersect at the first peak which is the excitonic band just below the edge. Similar correlation plots for all other solid rare gases also show good correlation between XANES peak energy and interatomic distances, which implies validity of the Natoli's model for solid rare gases.

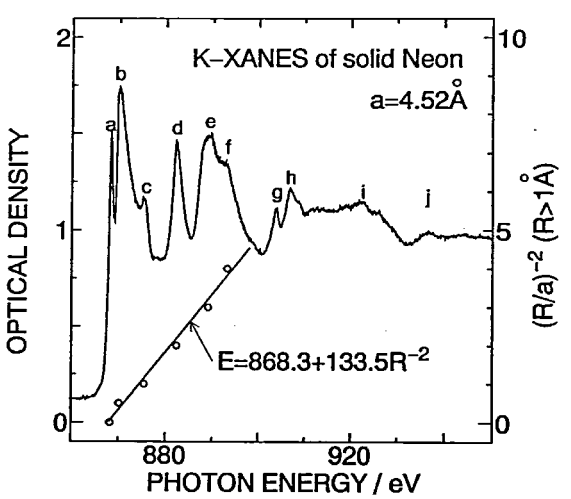

Figure 1. Ne K-edge XANES spectrum and correlation plot between XANES peak energy and R^{-2}. Values of R are the distances from central atom to the fcc lattice points (peaks b, c, d, and f) and to the (111) lattice plane (peak e). Peaks above 900 eV (g—j) correspond to the two-electron excited state.

VIII-P-2 Photo-stimulated Desorption Study of Ground and Excited State Alkalis from Alkali Halides by Using Synchrotron Radiation

Sayumi HIROSE and Masao KAMADA

Photo-stimulated desorption (PSD) of ground- and excited-state alkali atoms from alkali-halide crystals was investigated by using synchrotron radiation. The intensity of the desorbed excited-state alkali atoms showed the substance dependence which was reverse to that of ground-state alkali atoms. The desorption yield of excited-state alkali atoms peaked around room temperature, while that of ground-state alkali atoms increased as the temperature was increased. Moreover, the nano-second time response of PSD of excited-state sodium atoms was first observed on NaCl, which was faster by several orders times than the time response of ground-state alkali desorption. It is concluded that PSD from alkali halides is very different between ground- and excited-state alkali atoms.

VIII-P-3 Adsorption of K on the Si(100) and Si(111) Surfaces: Core-level Photoemission Study

Shin-ichiro TANAKA and Masao KAMADA

The adsorbed states of K atoms on the Si(100)(2×1) and Si(111)(7×7) surfaces were investigated by the use of the core-level photoemission spectroscopy. Experiments were performed using a 'grasshopper' monochromator and a double-pass CMA on BL2B1 at UVSOR. Peak positions of 3p emission from the adsorbed K atoms vary as a function of coverages. In the case of Si(100)/K, the binding energy of K3p level is nearly constant at low coverages, and becomes smaller at high coverages. The shift at saturation coverage is ~0.3 eV. In the case of Si(111)/K, the K3p peaks shift by ~0.4 eV to higher binding energy at low coverages, and reversely shift by ~0.9 eV to lower binding energy at high coverages. The additional band bending induced by the adsorption of K atoms was also measured, and was found to be different between Si(100)/K and Si(111)/K. These results reveal that there is a significant difference between the Si(100)(2×1) and Si(111)(7×7) surfaces interacting with K atoms.

RESEARCH FACILITIES

For the sake of brevity the present issue includes only the newly installed facilities and the activities since September 1991. Concerning the activities and facilities before September 1991, please refer to older IMS Annual Review issues (1978 ~ 1991).

Computer Center

The main computers at the Center are a supercomputer HITAC S-820/80 and a main-frame computer HITAC M-680H. The computers are linked to international networks through Tokyo University International Science Network (TISN). About 40% of the computer time is used by the research staff at IMS, and the remaining 60% is given out as research grants to scientist outside the Institutes in molecular science and related field. As of March 1992, the number of project group was 271, consisting of 781 users.

A system for making video movies has been adopted to S-820/80. Using this system, one can make video movies of one minute long in one job on S-820/80. The system is especially usefull for the visualization of molecular dynamics simulations.

The library programs of the Center amount to 723. Among them, about 200 programs can be executed immediately. Recent additions include GAUSSAN 90 and FLEX32 (a program for generating confomers). The Quantum Chemistry Literature Database (QCLDB) has been developed by the Center in collabolation with the QCDB group. The database, CMQCA, IR2, STERIC, and QCBDB are also available at the Center.

Chemical Materials Center

The Chemical Materials Center plays an important role in the synthesis and purification of chemical substances in IMS. The scientists and technical associates of this facility support other people in IMS to carry out the above works. Upon request, technicians carry out elemental and mass spectrometric analyses of new compounds prepared at IMS. They also carry out their own researches on synthesis of new interesting compounds, developments of new selective chemical transformations, elucidation of reaction mechanisms, and application of new methodologies developed in IMS to the analysis of chemical substances and reactions.

Instrument Center

For the efficient use of instruments, the Center is equipped with various types of instruments for general use.[1] Three instruments have been newly installed in 1991.

(1). Excimer Laser Pumped Dye Laser (Lambda Physik LPX 105i, LPD3002)

The excimer laser generates a pulse with pulse energy of 150 mJ/pulse at 308 nm (XeCl) and with repetition rate up to 50 Hz. Coupled with the excimer laser, the dye laser is operated in the tuning ranges of 320—970 nm in fundamentals and 205—335 nm in frequency doubling.

(2). Excimer Laser (Lambda Physik LPX 205i)

The excimer laser generates a pulse with pulse energy of 380 mJ/pulse at 308 nm (XeCl), pulse width of 28 ns, and with repetition rate up to 50 Hz.

(3). ESR spectrometer (BRUKER ESP 300E)

Electron spin resonance spectrum can be measured both in the X- (9 GHz) and Q-band (34 GHz) regions in the temperature range of 4.2-700 K. All the spectrometer functions are managed by a 32-bit computer.

Reference

1) *List of Instruments*, No.8, IMS Instrument Center (1992).

Low-Temperature Center

The supplied amount of liquid helium in 1991 was 21,289 *l* (17,662 *l* in 1990).

The liquid nitrogen automated supply system was improved by introducing a personal computer (PC-9800 series) to save every data on take-out process; date, time, group code, personal code, vessel code, system code and quantity.

Equipment Development Center

A number of research instruments have been designed and constructed by making use of the mechanical, electric and glass-blowing technologies at this Facility. Representative instruments developed during this fiscal year of 1991 are listed below.

Large-Size Cold Shield
Linear-Motion Gas-Doser in UHV Chamber
UHV Sample Transfer System
Precision Spinner for UVRR Spectroscopic Studies of Small Protein Sample Volumes
Apparatus for Photoelectron Time-of-Flight Spectroscopy of Cluster Ions
Cryostat for Measurement of Thermoelectromotive Force
UHV Chamber for Laser Trapping Experiment
Liquid N_2-Cooled Discharge Nozzle Source
Focusing Magnet for Electron Gun
Variable Laser-Beam Attenuator
Free Port Beamline at UVSOR
Sputtering Ion Gun
Two-Dimensional Photon Counter Utilizing CCD Camera
Pulse Generator for the Time-of-Flight Mass Spectrometer
Valve Driver for Molecular Beam Source
Two-Channel Programmable Gate Pulser
Three-Phase Motor Controller
Discharge Tube with Water Jacket for Light Analysis
Several Types of Cells Made of Pyrex and Quartz
Discharge Chamber for Producing Fullerenes

Division of IMS Machines

Equipment Development Center has the division of IMS Machines. Activities of this division is described in detail in the research activities section.

Ultraviolet Synchrotron Orbital Radiation Facility

The UVSOR light source is usually operated at an electron energy of 750 MeV with an initial current of 200 mA and a beam lifetime of about 200 min. The control system of the accelerators was replaced with a new computer control system. Four beamlines have been newly constructed or are under construction. They are BL4B for photo-assisted etching, BL5A for spin polarized photoelectron spectroscopy, BL6B for far-infrared microspectroscopy, and BL8B1 equipped with a grazing incidence monochromator for soft X-ray spectroscopy.

SPECIAL RESEARCH PROJECTS

IMS has special research projects supported by national funds. Three projects presently in progress are:

(1) Development and evaluation of molecular synergistic systems and their application to chemical energy conversion (1990–).

(2) Materials science on molecular devices (1990–).

(3) Molecular science of primordial chemical evolution and selforganization (1987–1991).

These projects are being carried out with close collaboration between research divisions and facilities. Collaborators from outside also make important contributions. Research fellows join these projects. The results in 1991 are reviewed in this report.

(1) Development and Evaluation of Molecular Synergistic Systems and their Application to Chemical Energy Conversion

(1) Studies on Dynamical Processes of Highly Excited Atoms and Molecules
(2) Studies of Laser Cooling and Trapping of Atoms

Norio MORITA, Asuka FUJII, and Mitsutaka KUMAKURA

The decay dynamics of the superexcited $7f$ Rydberg state (v=1) of NO molecule has been investigated with laser multiphoton excitation methods. Not only NO^+ ions generated by autoionization but also fragment nitrogen atoms produced by predissociation have been directly probed. As a result, it has been found that the decay process in the $7f$ state is mainly governed by predissociation due to *direct* coupling with the dissociative Σ^+ valence states, such as $A'^2\Sigma^+$ and $I^2\Sigma^+$ (see II-B-1).

In addition, the competing process between rotational autoionization and predissociation in high np Rydberg states ($n \geq 23$, v=0, N^+=12) of NO has also been studied with laser multiphoton excitation methods. In this study, it has been concluded that, in comparison with predissociation, rotational autoionization makes only minor contribution to the decay process of the high np Rydberg states (see II-B-2).

On the other hand, theoretical calculation for the spectra of doubly excited states of Ca atom so far experimentally observed has been continued by using the non-iterative eigenchannel R-matrix method and multichannel quantum defect theory. The calculated energy region has been extended up to −0.04 a.u. (just below the 9s ionization threshold) from the double ionization threshold (see II-B-3).

Laser trapping of helium atoms has been successfully achieved. With doubly resonant trapping scheme using infrared and visible lasers (see figure 1), the trapped helium atoms, which are confined in a sphere with a diameter of 1–2 mm, have been easily observed with naked eyes. Since this is the first demonstration of the doubly resonant trapping scheme, its characteristics have been investigated in detail (see II-C-1). However, the vacuum chamber used in this trapping experiment is not available for the ultrahigh vacuum condition, so that the number of trapped atoms has been limited by the collision with residual gases. We have, therefore, constructed a new chamber that can be evacuated to ultrahigh vacuum. With this chamber, it can be expected that the lifetime as well as the number of trapped atoms increase by three orders of magnitude and this improvement allows us to carry out various interesting experiments.

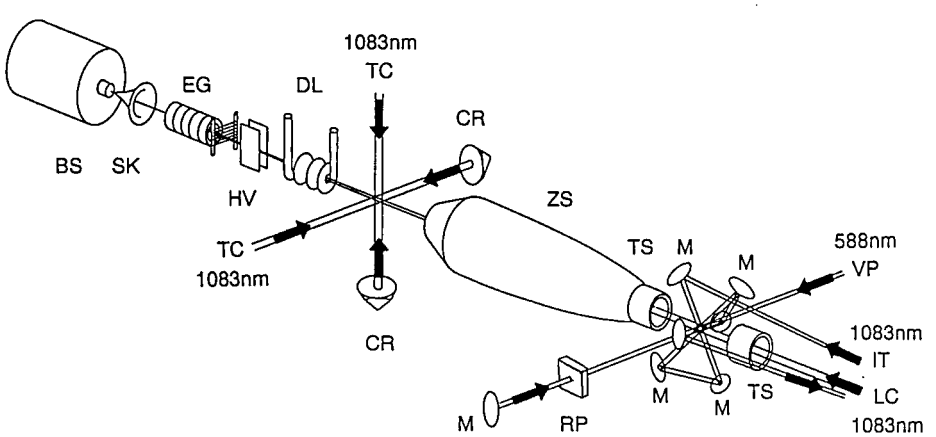

Figure 1. Schematic diagram of the experimental setup for laser trapping of helium atoms. BS: liquid-nitrogen-cooled nozzle, SK: skimmer, EG: electron gun, HV: high-voltage electrodes, DL: helium discharge lamp, TC: beam-collimation laser, CR: corner reflector, ZS: Zeeman-tuning solenoid, TS: solenoid for trapping, LC: deceleration laser, IT: infrared trapping laser VP: visible probe laser, RP: $\lambda/4$-retardation plate, M: mirror.

Mechanism of Oxygen Activation by Cytochrome Oxidase in a Respiratory Chain

Teizo KITAGAWA, Takashi OGURA, Satoshi TAKAHASHI, Shun HIROTA, and Shinya YOSHIKAWA *(Himeji Inst. Tech.)*

Cytochrome oxidase is the terminal enzyme of the respiratory electron transfer chain of aerobic organisms. This enzyme contains two heme A groups (Fe_A and Fe_B) and two copper ions (Cu_A and Cu_B) as the redox active metal centers and couples the dioxygen reduction reaction with proton translocation across the membrane. A functional unit containing the Fe_A and Cu_A ions serves as an electron transfer protein from cytochrome *c* to another functional unit containing the Fe_B-Cu_B binuclear dioxygen reducing site. A mechanism of dioxygen reduction by the Fe_B-Cu_B is a current topic of spectroscopic studies. We investigated reaction intermediates present in the time interval between 0.1 and 5.4 ms following initiation of the reaction by using time-resolved resonance Raman spectroscopy combined with our original Artificial Cardiovascular System. We succeeded in resolving an oxygen isotope-sensitive band of intermediates at 788 cm^{-1} into two components at 804 and 785 cm^{-1} by using a monochromator with higher resolution. The latter was shifted to 796 cm^{-1} in D_2O, while the former was insensitive to deuteration of the protein. Temperature dependence experiments clarified that the two bands arose from different intermediates. Experiments with $^{16}O^{18}O$ suggested that the 785 and 804 cm^{-1} bands were assigned to the Fe-O stretching of the Fe^{III}-O-O-H intermediate and the Fe^{IV}=O stretching of the Fe^{IV}=O intermediate of Fe_{a3}, respectively.

In order to develop a new method for probing the Cu_A site, a Raman system using a CCD (Charge Coupled Device) detector and Ti-supphire laser was constructed. The spectra of cytochrome oxidase excited at 830 nm yielded the amido bands and side chain modes of aromatic residues of protein irrespective of the oxidation state. However, additional Raman bands were observed around 330 cm^{-1} only for the oxidized enzyme, and were assigned to Cu_A-S(Cys) and Cu_A-N(His) stretching modes on the basis of deuteration sensitivity. Dependence of the Cu_A-associated bands on the presence of cytochrome *c* and also on the redox state of the Fe_B-Cu_B were examined.

Development of Non-Linear Spectroscopy for Studies on Ultrafast Phenomena

Ryoji INABA *(Univ. of Tokyo and IMS)*, **Vaclav KUBECEK, Shigeichi KUMAZAKI, Keisuke TOMINAGA, Keith A. NELSON** *(MIT)*, **Arkadiy YARTSEV, and Yutaka NAGASAWA** *(Graduate Univ. for Advanced Research)*

1) We have improved the time-resolution of femtosecond fluorescence up-converter to sub-hundred femtosecond region. The signal-to-noise ratio was also greatly improved. The details of the reconstruction of the system is described in III-F. With this system a detailed analyses of femtosecond electron transfer process which we found last year can be made. This is described in III-B. A new type of electron transfer reaction beyond "solvent controlled reaction" has been discovered.

2) Femtosecond CARS system was extensively applied to the studies of molecular dynamics of neat liquid systems and solution systems. Nature of vibrational dephasing processes has been clarified in mono-nitriles and α, ω-dinitriles. Vibrational dephasing processes in J-aggregate dyes has been studied for the first time. Details are described in III-D.

3) A passive negative feedback-controlled mode-locked Nd:glass laser using a GaAs wafer as an intracavity limiter was constructed. With its stable, high-power, and long pulse trains, it will be useful as an excitation source for an optical parametric oscillator.

Picosecond Reaction Dynamics of Excited Molecules in Clusters

Hrvoje PETEK, Prem B. BISHT, Bongsoo KIM, and Keitaro YOSHIHARA

While the understanding of reaction dynamics in isolated molecules has greatly advanced in recent years, similar progress in understanding of reaction dynamics in solution awaits development of more powerful experimental and theoretical techniques. A fruitful approach for studying condensed phase reactions is to investigate well characterized solvent-solute clusters under supersonic molecular beam conditions. This approach is particularly useful because it can reveal specific solvent-solute interactions that are otherwise obscured, and because such well characterized systems can be modeled by theoretical methods. We have investigated the exciplex formation in van der Waals clusters containing electron donor and acceptor molecules. For instance in anthracene-dimethylaniline complex two different isomers result in exciplex formation upon the excitation of the anthracene chromophore. However, the rates of exciplex formation are ~60 fs and > 10 ps. This shows that specific interactions, which can be easily probed in clusters, are extremely important in solution phase chemistry. Also, using multiphoton ionization spectroscopy in supersonic expansions, it has been possible to find a number of new electronic states and determine ionization thresholds of Cs_2, Cs_3, Rb_2, CsRb, and other alkali metal clusters.

Studies of Laser-Induced Photochemistry on Solid Surfaces

Yoshiyasu MATSUMOTO and Kyoichi SAWABE

Physical and chemical processes induced by photon irradiation on adsorbed molecules on solid surfaces are not only fundamentally interesting, but also practically important for industrial applications, such as the fabrication of catalysts and electronic devices. We have investigated photochemistry of nitrous oxide adsorbed on a Pt(111) surface. First, the adsorbed structure of N_2O was clarified by LEED; one monolayer of N_2O has a (3×3) structure with a fractional coverage of 4/9 ML. Second, it was found that adsorbed N_2O is dissociated with the irradiation of 193 nm photons to produce effectively oxygen adatoms on the

surface. Although maximum oxygen coverage is 0.25 ML attainable by a saturation exposure of Pt(111) to O_2 in ultra-high vacuum at a temperature below 300 K, high coverage of oxygen adatoms up to 0.75 ML was formed by photodissociation of adsorbed N_2O. This is useful in expanding a dynamic range of oxygen concentration in reaction kinetics studies. Third, since the dependence of photodissociation yield on photon polarization and incident angle is in good agreement with that of the bulk absorption predicted from classical electrodynamics, the substrate excitation is mostly responsible for the primary step of the photochemistry of N_2O on Pt(111).

Development of New Asymmetric Auxiliaries, Ligands, and Catalysts for Remote Asymmetric Inductions

Junji INANAGA, Takeshi HANAMOTO, and Yuichi SUGIMOTO

Asymmetric synthesis is one of the most important subjects in organic chemistry. In general, as the reaction center becomes closer to the chiral center, the better stereoselection can be expected. In this sense, therefore, stereocontrol at a remote position from the chiral center is usually difficult and of intense current interest. Our approach for this problem is based on the idea that asymmetric space-expansion by introducing bulky aromatic rings into optically active compounds at suitable positions would be effective for remote asymmetric inductions. According to the concept, *trans*-2,5-bis(*m*-terphenylethynyl)-pyrrolidine was designed as a core structure of some chiral auxiliaries, ligands, and catalysts. In this project, we have synthesized its analogue, *dl-trans*-2,5-bis(*m*-terphenylethynyl)-isoindoline hydrochloride, in five steps: *o*-Phthalaldehyde was treated with excess amount of lithium acetylide and the resulting bis-propargylic alcohol was mesylated and then cyclized with *p*-methoxybenzylamine to give a mixture of *cis*-and *trans*-2,5-bis(ethynyl)-isoindoline. Introduction of *m*-terphenyl unit by the palladium-catalyzed aryl-alkynyl cross-coupling reaction followed by the removal of *p*-methoxybenzyl group from the nitrogen atom afforded the desired product. Optical resolution of the chiral amine and its use in asymmetric reactions are under way.

External Magnetic Field Effects upon Chemical Reactions

Minoru SUMITANI *(Shizuoka Inst. of Sci. and Tech. and IMS)*, **Kaoru SUZUKI, and Saburo NAGAKURA** *(Grad. Univ. for Adv. Studies)*

In order to clarify the mechanism of the magnetic field effects on the emission intensity of NO in the $B^2\Pi$ state produced in chemical reaction, this state was produced by direct laser excitation from the NO $X^2\Pi$ state. It is not easy, however, to produce NO(B) in the low vibrational states under present concern, since the Franck-Condon factors between these states and NO(X, v=0) are known to be small. Therefore, photodissociation of N_2O by an ArF laser was used to produce NO(X) in the vibrationally excited states, where the Franck-Condon factors are much more favorable in producing NO(B) in low vibrational states. Then, a dye laser was used to excite NO(X, v'') to NO(B) in various vibrational states and the magnetic field effects on the fluorescence intensities was measured. Contrary to our expectation, no magnetic field quenching was observed for NO(B, v=0, 1, 2). Direct excitation to NO(B, v=7) was also tried by an ArF laser, but no magnetic field quenching was observed in this case, either. In conclusion, there is no magnetic field effects on the deactivation processes of NO(B).

A new experimental flow apparatus was constructed to investigate possible effects due to chemical species produced in discharge used in the production of NO(B) in the previous experiments. No magnetic field effects were observed in various discharge conditions and the positions of observation, either. Therefore, chemical species such as electrons, O, N, N_2, and NO are concluded to have minor contributions, if any, to the magnetic field effects on the NO B-X fluorescence.

It is now clear that other reaction channels of the $N(^4S)+O(^3P)$ system have to be investigated in more detail to reach a final conclusion of the mechanism of the magnetic field effects on the β band emission of NO.

Molecular Beam Study of Surface Reaction Dynamics

Haruhiko OHASHI, Hiroshi YOSHIKAWA, Aiichiro TSUKAHARA*, Tetsuo FUJIMOTO* *(*Nagoya Univ.)*, **Kiyohiko TABAYASHI, and Kosuke SHOBATAKE**

In the present project we have been studying the etching reactions of semiconductor (Si and SiO_2) surfaces stimulated by synchrotron radiation and other surface reactions which occur on metal surfaces, for the purpose of clarifying their dynamics and further finding ways to control surface reactions. Molecular beam techniques are applied since the state selection of the reactants is relatively easily done under the ultra-clean conditions. Three research projects are under investigation: 1) As to the synchrotron radiation excited etching reactions of SiO_2, SiC, and poly-Silicon surfaces we are clarifying the mechanisms, the results of which are summarized in **VI-F-3**. At present we have been trying to detect the desorbed species from the surface using a mass spectrometer detector; 2) We are obtaining fundamental information on how much energy transfers to vibration motion of surface atoms when a hyperthermal atom collides with solid surface using a time-of-flight technique on a modified molecular beam chemistry apparatus (see **VI-C-1**). We have found that, for the collisions of Xe atoms with hydrogen atom-terminated Si(100) at translational energy ranging from 1.64 to 6.3 eV, almost 80% of the incident energy is lost to surface vibration. 3) A smaller molecular beam chemistry apparatus (Model MBC-II) is being modified in order to make it possible to carry out molecule-surface scattering experiments under ultrahigh vacuum conditions (see **VI-C-2**). A rotatary mass spectrometer detector with a new design is under construction and the modification is near completion.

High-Brightness cm^{-1}-Resolution Threshold Photoelectron Spectroscopy for Cation Spectroscopy of Molecules

Katsumi KIMURA, Katsuhiko OKUYAMA, Masahiko TAKAHASHI, Hiroyuki OZEKI, and Martin C.R. COCKETT

Excited-state photoelectron spectroscopy combining a UV/visible pulse laser technique and a supersonic molecular beam technique has been developed in this Institute since 1980 (Kimura *at al., IMS Annual Review,* 1980–1991). The method which is often called "MPI or REMPI photoelectron spectroscopy" has made it possible to study dynamic behavior of excited-state molecular species which include nonradiative electronic states. Photoelectron spectra originating from various molecular excited states have been investigated from photophysical and photochemical points of view. The information deduced from excited-state photoelectron spectra has been found to be unique and important.

Recently we have developed a compact high-resolution high-brightness threshold photoelectron analyzer with which threshold photoelectrons are collected with a resolution of 1–2 cm^{-1} as a function of laser wavelength. The technique is equivalent to so-called ZEKE (zero kinetic energy) electron spectroscopy. In this project, we have further applied this threshold photoelectron analyzer to two-color (n'+1) REMPI experiments of various kinds of molecules and molecular complexes in supersonic free jets.

(2) Materials Science on Molecular Devices

d-π Interaction in Molecular Metals

Kyuya YAKUSHI, Hideo YAMAKADO, Akito UGAWA, and Kentaro IWASAKI

We have undertaken a systematic study on the solid molecular systems in which transition metals are embedded in a π-conjugated system from the viewpoint of the future design of the superconducting material. The most attractive materials are the one-dimensional solid based on phthalocyanine molecules. Through the systematic study of phthalocyanine radical salts, we have elucidated that $CoPc(AsF_6)_{0.5}$ has a unique double- chain structure where a half-filled Hubbard-type Co chain (*d*-orbital) and a quarter-filled Pc chain (π-orbital) are linked by an exchange interaction. This year we have further confirmed this result by the observation of the temperature-dependent thermoelectric power (see IV-A-2). However, it is not still clear that the *d*-π exchange interaction plays an essential role in determining the electronic structure of this material. Further studies are in progress including other phthalocyanine salts.

Coupled Proton and Electron Transfer in the Crystals of Salicylideneaniline Derivatives and their Complexes

Tamotsu INABE, Hironori OGATA, Naomi HOSHINO *(Hokkaido Univ.)*, **Kaoru OKANIWA, Hiroshi OKAMOTO, Tadaoki MITANI, Sadamu TAKEDA** *(Osaka Univ.)*, **and Yusei MARUYAMA**

Our interest in this particular area of research on molecular devices lies in the possibility of furnishing molecular assemblies with novel physical properties through an appropriate modification of the constituent molecules. Proton-transfer process was chosen as the molecule-based function, and its coupling to the assembly-based properties has been investigated. A framework of salicylideneaniline has such a function of intramolecular proton transfer. The thermochromic behavior observed in many of the derivatives gives a clue for changes in the π-electron state accompanying the proton transfer. Thus, the work has been devoted to the crystal structure determination at varied temperature and elucidation of possible cooperation in proton- and electron-transfer processes in the crystal of these compounds by means of optical measurements. Since the assembly-based properties depend largely on the intermolecular interaction, some derivatives have been employed as a donor component of the charge-transfer complexes with various acceptors in order to introduce stronger intermolecular interaction. The structural and optical studies of the complexes have provided the information about the correlation between the proton motion and the electronic state, which suggests possibilities of constructing a novel type of electrical conductors. Similarly, the structures and the optical, electrical, and magnetic properties of some charge-transfer complexes with intermolecular hydrogen-bonds have been studied. The donors are 1,6-pyrenediamine, 3,3',5,5'-tetramethylbenzidine, and 3,3'-dimethylbenzidine, and the acceptors are derivatives of *p*-benzoquinone and derivatives of TCNQ. Depending on the donor-acceptor combination and on the crystal morphology, the complexes show a variety of charge transport behaviors. Some of the details are given in Section IV- .

Fabrication of Novel Organic Molecular Assemblies with the Use of the Molecular Beam Epitaxy Technique

Yusei MARUYAMA, Hajime HOSHI, Naoki NAKAMURA *(Toyota Motor Corp. and IMS)*, **and Tamotsu INABE**

In order to prepare new materials which could be useful for molecular devices elements, we have started to design and fabricate ultra-thin organic multi-layered systems. In the first place, we have prepared ultra-thin single component phthalocyanine thin films to investigate epitaxial growth conditions on alkali halide single crystals. Fairly well oriented, uni-or bi-directionally, crystalline films are obtainable on the alkali halide substrates. Based on this kind of mono-film, we are going to fabricate a multi-layered system.

The SHG and/or THG of the films are investigated

from the view point of the molecular structure and the epitaxy or orientation of the films.

Fabrication of High T_C Metal Oxide-Superconducting Films by Layer-by-Layer Deposition from Multi-electron-Beam Gun Sources

Toshifumi TERUI and Yusei MARUYAMA

Successive deposition of each component of metal oxides has been undertaken to achieve the layer-by-layer construction for high T_C oxide superconductors. The high vacuum evaporation machine is equipped with three electron-beam guns and it can be operated under a differential pumping when oxygen inclusion is required. As an initial trial, La-Sr-Cu-O system is now investigated.

Ferromagnetism in Organic Molecular Solids

Kunio AWAGA and Yusei MARUYAMA

The study of ferromagnetic interaction in organic molecular solids is basically important to develop organic ferromagnets. We have chosen single crystal systems of organic radicals in which the ferromagnetic interaction is involved and of which structure can be well defined. Details of the work are described in VII- section.

Novel Electron Donors and Acceptors Containing Fused-Heterocycles

Yoshiro YAMASHITA, Shoji TANAKA, and Masaaki TOMURA

Electron donors and acceptors containing fused heterocycles such as thiadiazole and pyrazine are of interest since the presence of the fused heterocycles enlarges the π-electron ring system to decrease Coulombic repulsion. Intermolecular interactions leading to multi-dimensional structures can be also expected by heteroatom contacts. We have now prepared several novel compounds containing a fused [1,2,5]thiadiazole or a pyrazine ring. For example, 4,7-bis(1,3-dithiol-2-ylidene)-4,7-dihydro-2,1,3-benzothiadiazoles which are tetrathiafulvalene (TTF) analogues with a quinoid structure were prepared. The selenadiazole analogues were also synthesized. They were stronger donors than TTF in spite of the presence of an electron-withdrawing heterocycle. The tetramethyl derivatives gave highly conducting cation radical salts showing metallic temperature dependence down to 100 K. As strong electron acceptors, 1,2,5-thiadiazolopyrazino-tetracyanoquinodimethanes were prepared. They underwent reversible four-stage one-electron reduction and gave highly conductive CT complexes with donors. Details of these works are described in VIII-B section.

Creation of Helical Polynuclear Metal Complexes

Yoshihiko KUSHI *(Osaka Univ. and IMS)* **and Tatsuya KAWAMOTO** *(Osaka Univ. and IMS)*

In the current efforts to combine Werner type metal complexes with typical organometallic groups to develop new efficient catalysis systems, we have succeeded in the synthesis of a number of novel helical trinuclear hetello-metallo-complexes and found redox-active metal centers in these systems.

Dynamics of Solvated Metal Cluster Ions

Kiyokazu FUKE and Fuminori MISAIZU

Metal ions are intimately involved in chemistry and biochemistry and play a crucial role in many reactions. Although there has been extensive progress in the thermodynamic and kinetic studies of solvated metal ions, the study of microscopic aspect of solvation dynamics has been rather limited. Spectroscopic studies of the solvated metal ion clusters as a specific function of cluster size can provide detailed information on energetic and dynamics of solvation. The advent of mass spectrometer and metal cluster beam techniques in conjunction with laser probes now allow an attack on the problem for the solvation of metal ions and metal cluster ions through studies that probe energy levels and dynamical processes occurring in solvated metal clusters.

In the present research project, we have investigated the photoionization of cesium atom solvated by polar solvents such as acetonitrile relating with the excess electron in bulk fluids (see VIII-C-1). We have constructed a magnetic-bottle type photoelectron spectrometer for the investigation of the electronic structure of solvated metal atom clusters (see VIII-C-2). We are also studying the photoionization and photodissociation of water clusters involving the Group II and III metal atoms in order to obtain information about the cluster-size dependence of geometrical and electronic structures, and its reactivities. The details are described in VIII-C-3, 4, 5, 6, and 7.

New Development of Electron-Proton Cooperation Systems

Tadaoki MITANI and Hiroshi KITAGAWA

The electron-proton cooperation in solids has many possibilities for creation of novel functional H-bonded networks as an extension of conventional electronic systems. [*T. Mitani, Mol. Cryst. Liq. Cryst.*, **171**, 343 (1989)] Accumulation of detailed knowledge of the interrelationship between material elements and the cooperative interaction during recent two years made it possible to propose a new principle for design of novel H-bonded materials, which show new types of optical, magnetic, and conducting properties. As a first step of experimental confirmation of our proposal (*cf.* **VIII**-M-1, 2), [M(H_2DAG)(HDAG)]TCNQ (M=Ni, Pd, Pt, and H_2DAG: diaminoglyoxime) single crystals have been investigated by optical, vibrational and XPS measurements. The H-bonded networks composed of the d_{z^2} electronic state of the metal (M) chain, the π-electronic state of acceptor (TCNQ) stack, and the interchain H-bonds show unusual behaviors upon temperature changes. Both of the electronic states seem to be unstable with respect to the instability of 1-D systems and to correlate through the CT interaction *via* the interchain H-bonds. Experimental data suggest that our proposal promises to be a frontier work of novel H-bonded

systems. These efforts, we believe, lead to establishment of a new scientific field of "proto-electronics". More advanced investigations are under way for detailed analysis of the extraordinary phenomena of these systems.

Exploration of New Cooperative Proton-Electron Transfer (PET) Systems

Kazuhiro NAKASUJI, Jiro TOYODA, and Yasushi MORITA, Kenichi SUGIURA, Tetsuji ITOH, Kunio HATANAKA, and Makoto TADOKORO

Search for new molecular materials based on cooperative interactions between hydrogen bonding and charge transfer in the solid state has been actively continued. 1,4-Benzoquinhydrone undergoes a phase transition under pressure. The phase transition can be regarded as a cooperative proton-electron transfer (PET) phenomenon. The final PET state can be characterized as a molecular assembly of *H-bonded neutral radicals.* We are now developing a general strategy to explore new molecular materials based on PET phenomena. As a first step toward PET systems, we are now exploring he hydrogen-bonded charge transfer (HBCT) complexes. The stepwise consideration leads to two reasonable molecular design strategies to realize such cooperative phenomena under milder conditions in the solid state: the exploration of (a) a quinone-hydroquinone pair with a smaller intermolecular CT gap and/or (b) an electronic modification to stabilize H-bonded neutral radicals. As a former approach (a), we have already reported the synthesis and solid state properties of naphtho-, bipheno-, and stilben-quinhydrone as the extended conjugated quinhydrone. We found cooperative phenomena between H-bonding and CT interaction. The design and synthesis of heterocyclic conjugated quinhydrones are now actively performed. As a latter approach (b), the prototype, benzoquinhydrone, is modified by introducing the electron donor and the acceptor substituents. Although such a modification prevents the formation of the quinhydrone type complexes, this time we obtained a large number of the complexes with mono-, bis-, and tris-substituted derivatives. We also started to obtain PET systems containing transition metals. Clearly, the realization of the final PET state is extremely hard, but the exploration of a wide range of HBCT complexes might open a new way toward new molecular materials.

(3) Molecular Science of Primordial Chemical Evolution and Self-organization

Wavelength-Dependence of Relative Cross Section of Photo-Induced pH Oscillation in $Fe(CN)_6^{4-}$/H_2O_2/H_2SO_4 System: Irradiation of $Fe(CN)_6^{4-}$ before Mixing

Yoshihito MORI and Ichiro HANAZAKI

[*J. Phys. Chem.*, **96**, 9083 (1992)]

Photo-induced pH oscillation of the $Fe(CN)_6^{4-}$/H_2O_2/H_2SO_4 system has been observed. Irradiation of the stock solution of $Fe(CN)_6^{4-}$ induces oscillation and this has been taken as an evidence for that $HFe(CN)_6^{3-}$ is the primary absorber.[1] To re-examine this proposal, we have determined the wavelength-dependence of relative cross section for the irradiation of the $Fe(CN)_6^{4-}$ solution in a pre-reactor before mixing (Figure 1). The spectrum of the relative cross section coincides well with the absorption spectrum of the $Fe(CN)_6^{4-}$ solution in the pre-reactor. The primary photochemical process is thought to be the photoaquation of $Fe(CN)_6^{4-}$ to yield $Fe(CN)_5(H_2O)^{3-}$. Although the ratio of $[HFe(CN)_6^{3-}]/[Fe(CN)_6^{4-}]$ depends on pH of the solution, the yield of the photoaquation is independent of pH. These suggest that the primary absorber is $Fe(CN)_6^{4-}$ rather than $HFe(CN)_6^{3-}$. Moreover, as described elsewhere in this annual review, the primary absorber is not only $Fe(CN)_6^{4-}$ but also $Fe(CN)_6^{3-}$.

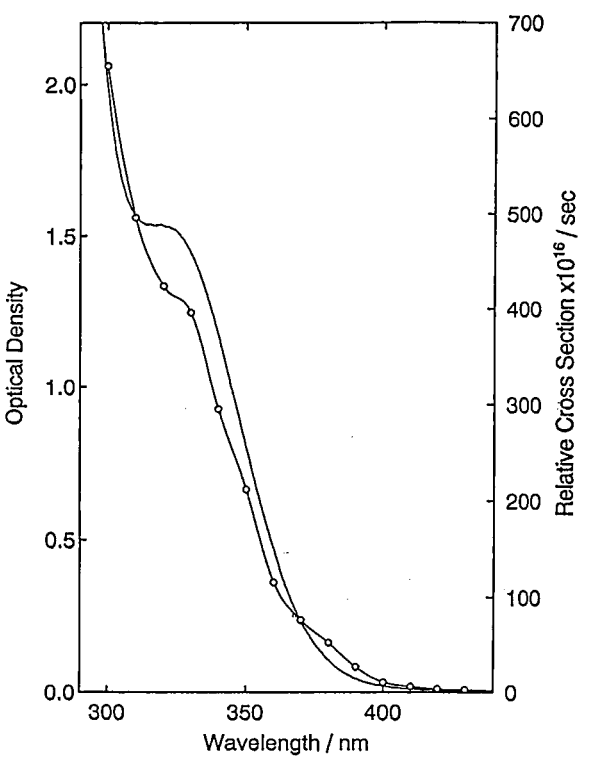

Figure 1. Wavelength-dependence of relative cross section.
Open circles: relative cross section; solid curve: absorption spectrum of the 9.90 mM solution of $Fe(CN)_6^{4-}$.
$[Fe(CN)_6^{4-}]_0$=3.30 mM, $[H_2O_2]_0$=50.0 mM, $[H_2SO_4]_0$=0.900 mM, residence time in a main reactor=368 s, and T=25.0±0.1°C.

References

1) Rábai et al., *J. Am. Chem. Soc.*, **111**, 8271 (1989).

Asymmetric Coupling Stabilizes the Out-of-Phase Mode: Experimental Evidence in the Belousov-Zhabotinsky Reaction

Minoru YOSHIMOTO *(Nagoya Univ.)*, **Kenichi YOSHIKAWA** *(Nagoya Univ.)*, **Yoshihito MORI, and Ichiro HANAZAKI**

[*Chem. Phys. Lett.*, **189**, 18 (1992)]

The Belousov-Zhabotinsky reaction was studied for the system with two continuous-flow stirred tank reactors coupled to each other through mass transfer. The coupling strength was quantitatively controlled by changing the flow rate between the reactors with a peristaltic pump. Figure 1 shows the phase diagram. It became clear that when the coupling between the reactors was symmetric, synchronization or entrainment with the in-phase mode was quite stable. On the other hand, the parameter space, or the basin, of the out-of-phase mode became greater with "asymmetric" coupling. Such an experimental trend is discussed in relation to the results of numerical simulations on coupled nonlinear differential equations.

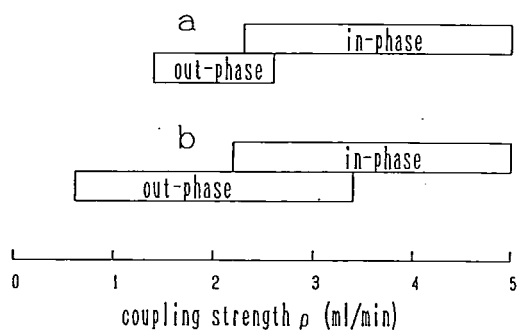

Figure 1. Phase diagram for the synchronization in the experimental coupled oscillators as a function of the coupling strengtrh ρ: (a) Symmetric coupling; (b) asymmetric coupling.

How do the Nonequilibrium Effects Associated with a Thermally Activated Chemical Reaction Scale if the Rate Constant Tends to Zero?

Jerzy GORECKI

[*Polish Journal of Chemistry*, **66**, 1183 (1992)]

The reactive cross section for a thermally activated chemical reaction strongly depends on the energy of colliding molecules. Therefore such a reaction may create a nonequilibrium energy distribution for molecules of reactant. In this paper phenomenological kinetic equations are used to derive the scaling rule for the strength of nonequilibrium effect in the case in which the rate constant tends to zero. The calculations are presented for the line-of-centers model for a chemical reaction. The results are compared with molecular dynamics simulations and with the analytical formula coming from the Boltzmann equation approach.

Direct Observation of a Nonequilibrium Velocity Distribution Function in a System with a Thermally Activated Chemical Reaction

Jerzy GORECKI and Byung Chan EU *(McGill University)*

[*J. Chem. Phys.*, in press]

The velocity distribution functions for the reactant and product of a thermally activated reaction A+A → B+B are calculated from molecular dynamics simulations. The results are compared with a simple phenomenological theory, which assumes that the temperature of the reactant A may be different from the temperature of the system as a whole. Good agreement between the two methods is observed.

On a Simple Phenomenological Description of the Nonequilibrium Effects Generated by a Binary, Thermally Activated Chemical Reaction

Jerzy GORECKI, Byung Chan EU*, and David RONIS* *(*McGill University)*

[Submitted to *J. Chem. Phys.*]

Recent molecular dynamics simulations of systems with a thermally activated chemical reaction have shown that nonequilibrium effects may significantly decrease the rate of a model reaction. A simple phenomenological formalism has been developed to describe the observed effects. We consider a unidirectional, thermally activated chemical process:

$$A + A \rightarrow B + B$$

for which the mechanical energy of colliding molecules is not changed during reactive collisions. We assume that the velocity distribution function for reactant A may be described by a Maxwellian, corresponding to a temperature T_A, which may be different than the temperature of the whole system. The phenomenological equations describing the time evolution of concentration [A], and T_A are derived and the results are compared with molecular dynamics simulations for a model thermally activated reaction of hard spheres. Good agreement between both methods have been obtained for a wide range of activation energies and system densities (Figure 1). We have found it quite surprising that the concept of temperature may be applied to systems in which a strong nonequilibrium effects is created by a very fast chemical reaction.

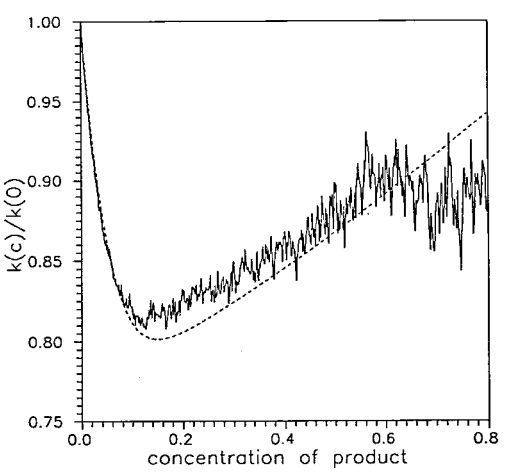

Figure 1. The nonequilibrium rate constant for the line-of-center model of a chemical reaction; comparison of the molecular dynamics simulations (dashed line) with the results obtained from phenomenological equations (solid line). The activation energy is $3K_BT$ and the packing density 0.508.

Solvation Structure and Properties of Ions in Supercritical Water

Hitoshi OHTAKI, Támas RADNAI* *(*Hungarian Academy of Sciences and IMS)*, **Yusuke TAMURA, and Kenji WAIZUMI**

An X-ray diffractometer with a high pressure-high temperature cell made of beryllium has been constructed and the structure of water near the supercritical condition has been studied by using the equipment. The temperature range examined was from room temperature to 200°C under various pressures which were changed from 1 to 2000 atmospheric pressures. Samples under the following conditions have been investigated: (1) t=(22 ± 1)°C, p=1 bar (1 bar=1.00×10^5 Pa), (2) t=(22 ± 1)°C, p=(300 ± 5) bar, (3) t=(22 ± 1)°C, p=(500 ± 5) bar, (4) t=(22 ± 1)°C, p=(1000 ± 5) bar, (5) t=(22 ± 1)°C, p=(2000 ± 30) bar, (6) t=(98 ± 5)°C, p=(3 ± 1) bar, (7) t=(206 ± 5)°C, p=(3 ± 1) bar, (8) t=(95 ± 5)°C, p=(100 ± 5) bar, (9) t=(195 ± 5)°C, p=(500 ± 5) bar. In Figure 1 preliminary results for experimental pair-correlation functions $g(r)$ of samples (1), (3) and (4) are shown. The curve of sample (1) was compared with that examined by Narten and Levy (*J. Chem. Phys.*, **55**, 2263 (1971)), which was carried out at 20°C under 1 atmospheric pressure.

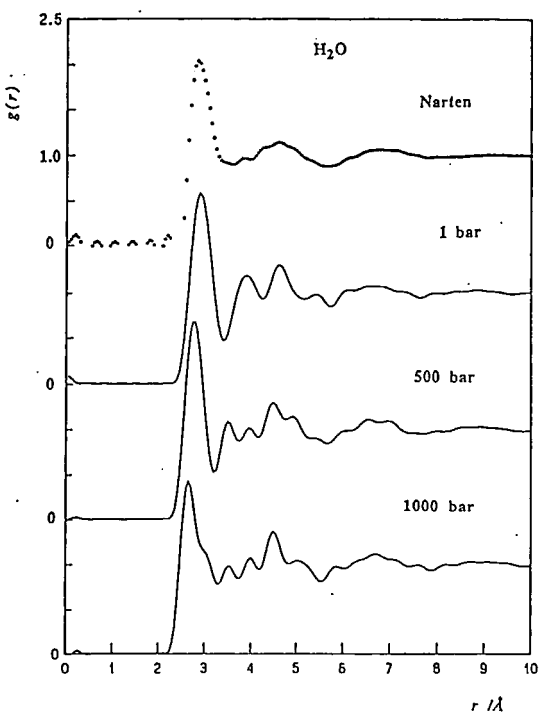

Fig. 1. Pair correlation functions $g(r)$ of water under various pressures at 22°C. The $g(r)$ curve obtained by Narten and Levy is shown for comparison.

Conversion of Carbon Dioxide to Organic Compounds and Reduction of Nitrite Catalyzed by Metal Complexes

Koji TANAKA, Hirotaka NAGAO, Tetsunori MIZUKAWA, Ryo MIYAMOTAO, Hiroaki TANAKA, Hide KAMBAYASHI, and Nobutoshi KOMEDA *(Osaka Univ.)*

A variety of transition metal complexes have proved to be active in electro- and photo-chemical CO_2 reduction affording CO and/or HCOOH. We are investigating reactivities of CO_2 activated on metal and sulfur ligands. Successive reduction of CO_2 to CH_3 through COOH, CO, C(O)H, and CH_2OH moieties can be expected in the former. The latter, on the other hand, may enable to change the intra-molecular polarization of CO_2 as observed in biological CO_2 fixation. The comparative study on the reactivity of CO_2 activated in those systems may lead to not only the elucidation of the evolution of biological CO_2 fixation but also the utilization of CO_2 as a Cl building block.

Denitrification by nitrite reductases containing heme and copper proteins plays fundamental roles in nitrogen cycle. Despite of intensive studies on the enzymatic reactions, the mechanism for NO and N_2O evolution in the reduction of NO_2^- by nitrite reductases have not been clarified so far. Elucidation of the reaction mechanism may greatly serve to decrease in the evolution of those environmental pollutants resulting from denitrification of artificial fertilizers in soils. We are studying on the reaction mechanism of denitrification of NO_2^- in H_2O by using copper complexes.

Carbon-carbon Bond Activation and Skeleton Transformation Reactions

Tamotsu TAKAHASHI, Yu NITTO *(Tokyo Univ.)*, **Masahiko SABURI** *(Tokyo Univ.)*, **and Noriyuki SUZUKI**

Carbon-carbon bond activation and selective transformation is very attractive target in chemistry. We have investigated this type of new transformation reactions using zirconium complexes. We found α,α'-dimethylzirconacyclopentane compound, prepared in situ from Cp_2ZrCl_2 and di-Grignard reagent, was selectively converted into β,β'-dimethylzirconacyclopentane in THF at room temperature. This reaction proceeded via β,β'-C-C bond activation reaction. Other metal complexes have been investigated for this transformation reaction. Only hafnium compound showed similar reactivity. Pd, Pt, Ti, Ni, and Nb, complexes did not give clear results. This reaction can be called selective skeleton rearrangement.

We turned our attention from this skeleton rearrangement to replacement of carbon atom of skeleton by heteroatoms. Similar system was also used for this reaction. Addition of aldehyde to zirconacyclopentane in THF at room temperature gave oxazirconacyclopentane. This mechanism involved Cβ-Cβ' bond activation of zirconacyclopentane, replacement of one of two alkenes on zirconium by aldehyde, and C-C bond formation between alkene and aldehyde on zirconium.

OKAZAKI CONFERENCES

"Okazaki Conferences" are principal symposia at IMS, which are held on the subjects related to the "Special Research Projects". They are held two or three times a year, with a moderate number of participants around 50, including several invited foreign speakers. The formal language for the conference in Engligh. Outlines of the forty-first, forty-second, and forty-third conferences are as follows.

The Forty-first Okazaki Conference

Interfacing the Theoretical and Physical Organic Chemistry in the Study of an Organic Reaction Process *(September 30 – October 2, 1991)*

Organizers: J. HAYAMI *(Kyoto Univ.)*, **K. NISHIMOTO** *(Osaka City Univ.)*, **R. NOYORI** *(Nagoya Univ.)*, **K. MOROKUMA** *(IMS)*, **and Y. TSUNO** *(IMS)*
Invited Speakers: J.F. BUNNETT *(Univ. of Calif., Santa Cruz, U.S.A.)*, **R.A. MORE O'FERRAL** *(Univ. College, Dublin, Ireland)*, **A. PROSS** *(Ben-Gurion Univ., Negev., Israel)*, **J.P. RICHARD** *(Univ. of Kentucky, U.S.A.)*, **and I.H. WILLIAMS** *(Univ. of Bath, U.K.)*

Fifty-one leading physical organic chemists (14 from abroad and 37 domestic) with 35 molecular scientist in IMS gathered to discuss the titled subject. The Conference was organized so that the discussions were focused on the following three faces. (1) Structure and dynamic properties of reactive intermediates, (2) The transition state structure and the structure-reactivity relationships. (3) Solvation and desolvation behavior in the progress of the reaction process. In addition to five invited lectures by eminent speakers, six contributed talks were presented by participants from abroad. Namely, **Y. APELOIG** *(Tech.-Israel Inst. of Tech., Israel)*, **A.J. KRESGE** *(Univ. of Toronto, Canada)*, H.F. KOCH *(Ithaca Coll., U.S.A.)*, **H.-U. SIEHL** *(Univ. of Tubingen, Germany)*, **M. SPERANZA** *(Univ. of Tuscia, Italy)*, and **T.T. TIDWELL** *(Univ. of Toronto, Canada)*. Also contributed were 12 domestic talks and 22 poster presentations. Many of the presentations furnished the audience with the latest unpublished results that certainly need cooperation between the experimentalists and theoreticians and led to the important discussions that resulted in several new joint researches among the participants. Organizers and participants all believe that the Conference wa successful in establishing new insights into the organic reaction processes.

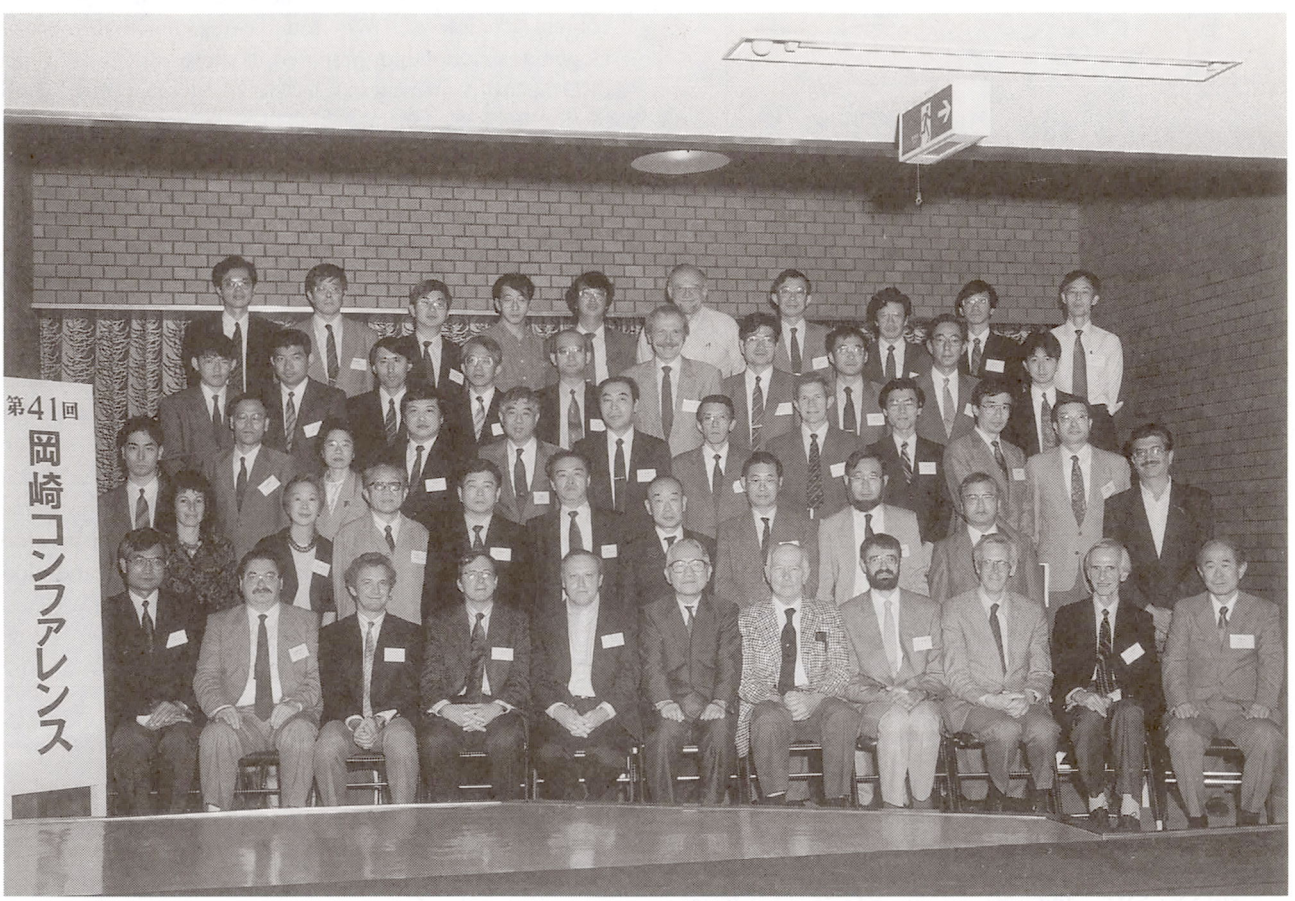

The Forty-second Okazaki Conference

Molecular Science: Current Status and Future Prospects *(January 7 – 9, 1992)*

Organizers: H. INOKUCHI *(IMS)*, **H. NAKAMURA** *(IMS)*, **K. SHOBATAKE** *(IMS)*, **and I. HANAZAKI** *(IMS)*

Invited Sperkers: R.M. NOYES *(Univ. of Oregon, U.S.A.)*, **Z. HERMAN** *(J. Heyrovsky Inst. Phys. Chem. & Electrochem., Czechoslovakia)*, **W.H. MILLER** *(Univ. of Calif. & Lawreuce Berkeley Lab., U.S.A.)*, **M. INOKUTI** *(Argonne Natl. Lab., U.S.A.)*, **C.T. CHANG** *(Inst. of Atom. & Molec. Sci., Rep. of China)*, **and M.S. JHON** *(Center for Molec. Sci., KAIST, Korea)*

This conference was proposed for discussing the current status and future prospects of molecular science in various fields of molecular science. Scientists from U.S.A., Europe and Asian countries were invited to introduce the present status of molecular science in their countries as well as detailed analyses of various sub-fields of molecular science by Japanese participants. The conference was successful particularly in exchanging information on the molecular science in various countries.

The Forty-Third Okazaki Conference

New Development of Laser Photoelectron Spectroscopy *(March 10 − 12, 1992)*

Organizer: K. KIMURA and K. SHOBATAKE *(IMS)*
Invited Overseas Speakers: R.N. COMPTON *(Oak Ridge National Lab.)*, **P.M. JOHNSON** *(State Univ. of New York at Stony Brook)*, **K. MÜLLER-DETHLEFS** *(Technical Univ. of München)*, **M.G. WHITE** *(Brookhaven National Lab.)*, **H.O. LUTS** *(Univ. Bielefeld)*, **K.H. BOWEN** *(Johns Hopkins Univ.)*, **and J.M. DYKE** *(Univ. of Southampton)*

The conference was organized to discuss recent development of laser photoelectron spectroscopy as well as its related topics including laser excitation and ionization spectroscopy. Topics discussed are the following: (1) very high-resolution cation spectroscopy of jet-cooled molecules and van der Waals complexes by means of laser photoelectron spectroscopy, (2) photoelectron spectroscopy of laser excited molecules and van der Waals complexes, (3) laser ionization MPI ion-current and mass spectroscopy of jet-cooled molecules and molecular clusters, (3) photodetachment spectroscopy of molecular cluster anions, (4) laser ionization spectroscopy of solid states. The conference consisted of 19 invited talks (overseas and domestic) and 11 poster presentations. The total number of participants were 62.

JOINT STUDIES PROGRAMS

As one of the important functions of an inter-university research institution, IMS undertakes joint studies programs for which funds are available to cover research expenses as well as travel and living expenses of individuals. The proposals from domestic scientists are reviewed and controlled by the inter-university commitee. The programs are carried out under one of five categories:

1) Joint Studies on special projects (a special project of significant relevance to the advancement of molecular science can be carried out by a team of several groups of scientists).
2) Research Symposia (on timely topics in collaboration with both outside and IMS scientists).
3) Cooperative Research (carried out in collaboration with both outside and IMS scientists).
4) Use of Facility (the Computer Center, Instrument Center and other research facilities at IMS are open to all researchers throughout the country).
5) Joint studies programs using UVSOR facilities.
   a) Special Project, b) Cooperative Research, c) Use of UVSOR Facility.
   In the fiscal year 1991, numbers of joint studies programs accepted amounted to 2, 10, 115, and 300 for categories 1)—4), respectively 3, 32 and 111 for 5a)—5c), respectively.

1) Special Projects

Static and Dynamic Solvent Effects in Elementary Reactions

Contributors: **Okitsugu KAJIMOTO** *(Kyoto Univ.),* **Tadamasa SHIDA** *(Kyoto Univ.),* **Hisanori SHINOHARA** *(Mie Univ.),* **Masaru NAKAHARA** *(Kyoto Univ.),* **Nobuyuki NISHI** *(Kyusyu Univ.),* **and Kritaro YOSHIHARA**

This research project aims at the molecular-level understanding of both static and dynamic solvent effects by means of recently developed techniques such as molecular beam, supercritical solution and pico-second Raman spectroscopy.

1. Solvent Dynamics Studied by Pico-second Raman Spectroscopy

In order to obtain more specific and local information of solvent dynamics, time-dependent Raman spectroscopy was selected as one of the main subject of this project. However, the original plan using Cu-vapor laser as a pump laser for the amplification of ps laser pulse faced much difficulty due to the instability of the Cu-vapor laser. This year, we completely changed the ps-system to improve the stability.

An output of a mode-locked Ti: Sapphire lasr pumped by an Ar ion laser was amplified using a single stage amplifier pumped by a high-repetition Nd:YAG laser. The frequency-doubled photons were used for exciting reactant molecules while the photons of fundamental frequency were utilized for the resonance Raman spectroscopy.

Since the solvent dynamics in supercritical fluid is a target of this project, the Raman spectra of acetone in several supercritical fluids were measured as a preliminary test. As shown in Figure 1, the CO stretching vibration shows considerable red-shift in supercritical CF_3H whereas the shift becomes less significant in CF_3Cl and Ar. The hydrogen bonding between CO--HCF_3 causes the red-shift and the effect on the CO stretching increases with increasing fluid density.

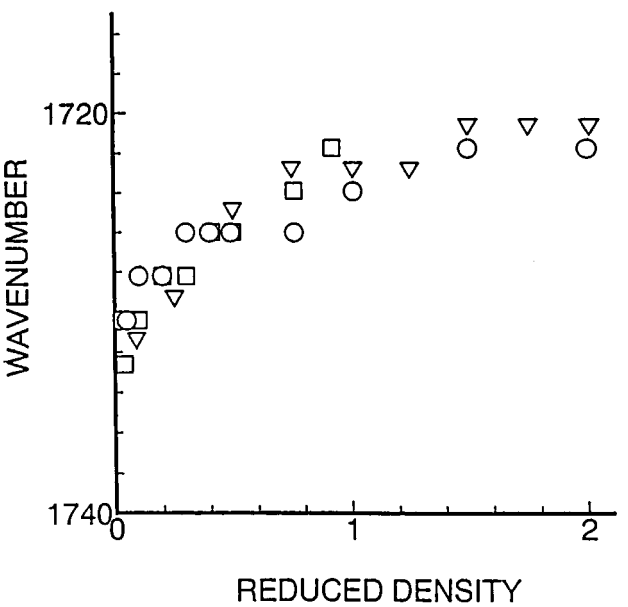

Figure 1. The CO stretching frequency of acetone in super-critical CF_3H as a function of fluid density

2. Rotational Coherence Measurements for Solvated van der Waals Complexes

For the detailed discussion of environmental effects in van der Waals complexes, the unambiguous information of their structure is essential. In our previous report of the polar excited state formation in bianthryl-acetone complex, we suggested that the location of the solvent molecules are quite important for the reaction to occur. One of the best method to explore the structure of heavy molecules is the measurement of rotational coherence. Figure 2 shows the rotational coherence profile for a bare bianthryl molecule. From the observed recurrence period (3.2 ns) we can determine the rotational constants of the molecule and hence estimate its structure.

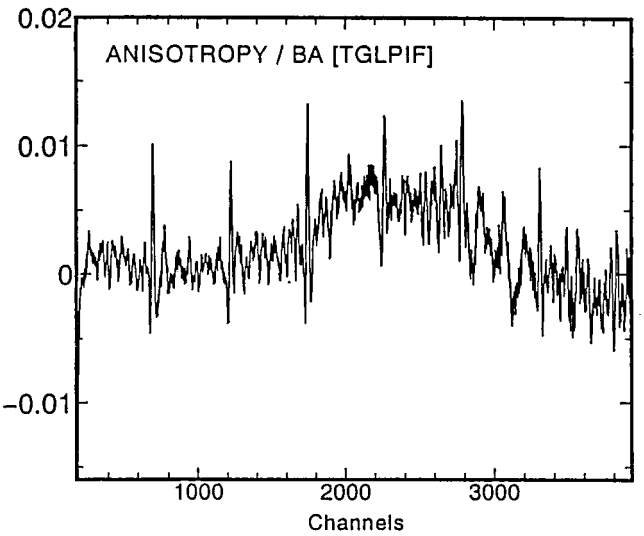

Figure 2. The rotational coherence signal of bare bianthryl.

3. Hydrogen Abstraction in a Matrix Cage

The γ radiolysis of an acetal in freon matrix produced a methyl radical and a carbonium ion, and successive hydrogen abstraction by the methyl radical occurs within a matrix cage. Since the deuterium substitution of acetal at various position considerably affects the rate of hydrogen/deuterium abstraction, the reaction must proceeds by the tunneling mechanism.

4. Binding Energy and the Structure of the Benzene Cluster Ions

The absorption spectra of mass-selected benzene cluster ions were obtained using the depletion of the cluster mass signal on the photolysis at various wavelength. In addition to the local excitation bands at 430 and 580 nm, intense and broad charge resonance band is observed around 900 nm. From these spectra, the average binding energy between benzene moieties were estimated as a function of cluster size. The result shows that the dimer ion forms the core of the cluster and other benzene molecules surround the core as solvent molecules.

Studies on Photo-responsive Chemical Oscillators

Coordinators: **Kenichi YOSHIKAWA** *(Nagoya Univ.)*, **Ichiro HANAZAKI** *(IMS)*, **Kazuo KITAHARA** *(Tokyo Inst. Tech.)*, **Takeko MATSUMURA** *(Nara Educ. Univ.)*, **Hiroyuki NAGASHIMA** *(Shizuoka Univ.)*, **Tetsuo UEDA** *(Nagoya Univ.)*, **Hidetoshi MIIKE** *(Yamaguchi Univ.)*, **and Tomohiko YAMAGUCHI** *(Natl. Chem. Lab. Ind.)*

In non-linear open systems, chemical reactions show sometimes an oscillating time evolution as well as a spatial pattern formation, which are due to the system's intrinsic nonlinearity. These phenomena have also been interesting for their close relationship to biological phenomena. This year, we continued to study the photoirradiation-induced inhibition and induction of chemical oscillations. In particular, we have given a general definition of the cross section for the light-induced inhibition and induction of oscillation on the basis of the bifurcation points between the steady and oscillatory states of the nonlinear chemical systems. The photoinduced inhibition and induction of chemical oscillations have been investigated extensively for the Belousov-Zhabotinsky (BZ), Briggs-Rauscher systems and the $Fe(CN)_6^{4-}/H_2O_2$ system on the basis of the newly defined cross section and its dependence on the irradiation light wavelength. Among them, the BZ system is interesting since a variety of metal complexes can act as a catalysts in the chemical oscillation. In view of the important role of the light absorption by the metal complex as the primary process of light effects, it is interesting to compare the irradiation effect for various catalysts. Accordingly, we have succeded in synthesizing various types of metal complexes which differ slightly in the redox potential, and are going to compare the efficiency of light-induced inhibition of oscillation.

Spatial pattern formation and its dynamics are another point of interest and have extensively studied. They include the interaction of chemical waves with the hydrodynamic flow, the simulation calculation on the pattern formation, and the interaction of chemical oscillator systems.

Electronic Relaxation and Reaction of Electronically Excited Metal Atoms

Coordinators: **Shigeru TSUNASHIMA** *(Tokyo Inst. of Tech.)*, **Suehiro IWATA** *(Keio Univ.)*, **Shunzo YAMAMOTO** *(Okayama Univ.)*, **Kazuo KASATANI** *(Fukuoka Women's College)*, **Kaoru YAMANOUCHI** *(Tokyo Univ.)*, **Hironobu UMEMOTO** *(Tokyo Inst. of Tech.)*, **Nobutaka NAMBU** *(Keio Univ.)*, **Fuminori MISAIZU, and Kiyokazu FUKE**

In order to understand reaction dynamics, the information on the reaction rates as well as the product state distributions are inevitable. In the present projects, both full- and half-collision processes of excited metal atoms are studied by employing pulsed laser techniques. In the half-collision studies, pico second spectroscopic studies are planned. Theoretical approaches also play important roles in the present project.

1. Nascent Internal Energy Distributions of Diatomic Products Produced in the Reaction of $Zn(4^1P_1)$ with Simple Molecules

The reaction between water and zinc in the excited 4^1P_1 state is studied. The nascent rotational and vibrational state distributions of the diatomic products, ground sate ZnH and OH, are measured. The joint probabilities for the pair products, ZnH and OH, are going to be determined. Since water is corrosive to hot zinc surfaces, a flow system combined with a pulsed valve is developed by the collaboration with Instrument Center of IMS. The reactions with alkane hydrocarbons and hydrogen halide are also going to be tried.

2. Half Collision Processes of Excited Cd Atoms

The half collision processes of excited Cd atoms and H_2 are going to be studied under beam conditions. The real time measurement of the dynamical behavior of short-lived species such as electronically excited CdH_2 complexes are going to be carried out. The ground state CdH_2 complexes can be formed in a super sonic expansion. These species are excited to the lowest singlet or triplet excited states by a tunable dye laser. The photofragments as well as the excited CdH_2 complexes are probed by using a nano- or pico-second lasers.

3. Theoretical Studies for the Dynamical Behaviors of the Transition States

Theoretical studies are important to characterize the reaction dynamics, especially at the transition regions. Both adiabatic and non-adiabatic processes are going to be investigated theoretically. The potential energy surfaces are evaluated by an ab initio method. The probabilities to pass through the transition regions as well as those for the surface hopping are calculated.

2) Research Symposia

1. Specific Properties of the Coordination Sphere of Metal Complexes at the Transfer and Arrangement of Electrons, Spins, Ions, and Molecules
   (September 6th, 1991)
   Organizer: H. Ohtaki
2. Applications of Molecular Beam Techniques to the Study of Chemical Reaction Dynamics
   (December 12th–13th, 1991)
   Organizer: I. Kusunoki
3. Theoretical Methods for the Dynamics of Atoms, Molecules and Nuclei and Related Subjects
   (December 13th–14th, 1991)
   Organizer: S. Watanabe
4. Reactions and Dynamics of Molecular Clusters
   (December 24th–25th, 1991)
   Organizer: M. Ito
5. Dynamical Behavior of Molecular Solids under High Pressure
   (February 6th, 1992)
   Organizer: H. Inokuchi)
6. Symposium on Conductivity and Magnetism of Organic and Inorganic Molecular Crystals
   (April 2nd, 1992)
   Organizer: H. Yakushi
7. Molecular Arrangements in Liquids and Liquid Mixtures
   (April 28th, 1992)
   Organizer: H. Ohtaki
8. Physical Chemistry Meeting for Young Molecular Scientists
   (May 16th, 1992)
   Organizer: S. Nonose
9. Rational Design of Complex-Reaction Site by Using Structurally Regulated Multi-Centered Ensemble of Metal Ions
   (June 25th–27th, 1992)
   Organizer: M. Ichikawa
10. Pursuit of Temporal and Spatial Changes of Material by Vibrational Spectroscopy
    (June 29th–July 1st, 1992)
    Organizer: S. Nakajima

3) Cooperative Research

This is one of the most important programs IMS undertakes for conducting its own research of the common interest to both outside and IMS scientists by using the facilities at IMS. During the first half of fiscal year of 1991 ending on September 30, 54 outside scientists including 1 invited collaborated with IMS scientists; and during the second half of the fiscal year, 59 outside scientists and 1 invited scientists worked in collaboration with IMS scientists, the names and the affiliations of these collaborators are found in the Research Activities.

4) Use of Facility

The number of projects accepted for the Use of Facility Program of the Computer Center during the fiscal year of 1991 amounted to 213 (623 users) and the computer time spent for these projects is 9139 hours (converted to the HITAC M-680H time), and amounted to 62% of the total annual CPU time used.

Eighty seven projects (154 users) were accepted for the Use of Facility Program of the Instrument Center during the fiscal year of 1991.

5) UVSOR

In the UVSOR Facility with the 750 MeV electron storage ring, there are nineteen beam lines available for synchrotron radiation research (see "Activity Report" UVSOR, 1992), one beam line which belongs to the Institute of Nuclear Fusion Science. The Experimental facility of each beam line in introduced in the newly edited pamphlet "OUTLINE OF UVSOR". The Japanese and English versions are available through UVSOR facility. Under the following programs, a number of SR studies have been carried out by many users outside and inside IMS: a) the UVSOR Special Projects, b) the UVSOR Cooperative Research Projects, c) the UVSOR Invited Research Projects, and d) the Use-of-UVSOR Projects. Furthermore, the 11th UVSOR User's Symposium was held at Okazaki during the period December 13—14, 1991.

5-a) UVSOR Special Project

Development of the Infrared and Far-infrared Spectroscopy Using Synchrotron Radiation

Coordinators: **Kyuya YAKUSHI, Akito UGAWA, Hideshi ISHII*, Tadaoki MITANI, Hiroshi OKAMOTO, Takao NANBA**, Makoto WATANABE, and Kusuo SAKAI** (**Univ. of Tokyo, **Kobe Univ.)*

Application of Synchrotron Radiation (SR) has been

performed at the beamline BL-6A1 of the UVSOR facility in IMS. We are planning and conducting three projects for the use of infrared region of SR using the characteristic natures of SR such as a high collimation, high brilliance, wide-range tunability, and pico-second pulse width. (1) The former three natures are the ideal properties as the light source of a microspectrophotometric apparatus. We are constructing a microspectrophotometer to measure optical reflectivity of a small (~ 20 μm) single crystal in the wide range (50 cm^{-1}—13000 cm^{-1}). This apparatus will be mainly used for the study of organic conductors and superconductors. (2) The last property of SR is appropriate to the time-resolved spectroscopy. Delay-time modulation spectrometer has been designed and constructed using the pico-second light pulse of SR synchronized with a cw mode-locked Nd-YAG laser. This method is applied to the transient photo-induced absorption spectroscopy in the infrared region by combining with FT-IR to increase the sensitivity. (3) The future plan is the grazing-angle infrared spectroscopy for the surface absorbed molecules. This optical system uses also the high collimation and high brilliance of SR.

5-b) UVSOR Cooperative Research Projects

Under this joint-study program, many synchrotron radiation experiments have been carried out with the beam lines of in-house staff in cooperation with scientists who were invited from other institutions. The total number of the projects in this category was 27 in the fiscal year of 1991.

5-c) The UVSOR Invited Research Projects

Under this joint-study program, several scientists were invited from other institutions to help for construction of new beam lines and improvement of the UVSOR storage ring and others. The total number of the projects in this category was 5 in the fiscal year of 1991.

5-d) The Use-of-UVSOR Projects

Ten out of the total of nineteen UVSOR beam lines are available for general users outside and inside IMS for their synchrotron radiation studies in the field of molecular science. The total number of the projects in this category was 111 in the fiscal year of 1991.

FOREIGN SCHOLARS

Visitors from abroad play an important role in research activities and are always welcome at IMS. The following is the list of foreign scientists who visited IMS in the past year (Aug. 1991 — July 1992). The sign *1 indicates an attendant to an Okazaki Conference, *2 an IMS or Japan Society for the Promotion of Science Invited Foreign Scholar, *3 an IMS councillor, *4 an IMS visiting scientist, and *5 an IMS adjunct professor or associate professor from abroad (period of stay is from 9 to 12 months). Scientists who wish to visit IMS under programs *2 and *5 are invited to make contact with an IMS faculty in a related field.

Dr. J. L. Anchell *2	Univ. Utah	(USA)	Mar. 1991 - May 1992
Dr. J. Moc*2	Univ. Wraclaw	(Poland)	Mar. 1991 -
Dr. D.G. Musaev*2	Inst. New Chem. Problems	(Russia)	Apr. 1991 -
Dr. V. Kubecek*5	Tech. Univ. of Praha	(Czechoslovakia)	- Aug. 1991
Dr. N.J. Fitzpatrick*4	Univ. Coll. Dublin	(Ireland)	- Aug. 1991
Prof. B.H. Boo*2, *4	Chungnam Natl. Univ.	(Korea)	- Aug., Oct. - Nov. 1991, Jan., Jul. - Aug. 1992
Dr. S. Lee*4	Kyung Hee Univ.	(Korea)	Jun. - Aug. 1991, Jan. - Feb., Jun - Jul. 1992
Dr. Zhongfang Liu*4		(China)	Aug. 1991 -
Prof. B.H. Schlegel	Wayne State Univ.	(USA)	Sep. 1991
Prof. June-Rong Chen	Synchrotron Radiation Reasearch Center	(Taiwan)	Sep. 1991
Prof. N. Moiseyev	Israel Tech. Univ.	(Israel)	Sep. 1991
Prof. J.M. Hicks	Georgetown Univ.	(USA)	Sep. 1991
Prof. J.R. Huber	Univ. of Zurich	(Switzerland)	Sep. 1991
Prof. Beck Sim Lee*4	Univ. Sci. Malaysia	(Malaysia)	Sep. - Oct. 1991
Prof. M.R. Willis	Univ. of Nottingham	(UK)	Sep. - Oct. 1991
Prof. J.F. Bunnett*1	Univ. of California, Santa Cruz	(USA)	Sep. - Oct. 1991
Prof. R.A. More O'Ferrall*1	Univ. Coll. Dublin	(Ireland)	Sep. - Oct. 1991
Prof. A. Pross*1	Ben-Gurion Univ., Negev	(Israel)	Sep. - Oct. 1991
Prof. J.P. Richard*1	Univ. of Kentucky	(USA)	Sep. - Oct. 1991
Prof. I.H. Williams*1	Univ. of Bath	(UK)	Sep. - Oct. 1991
Prof. Y. Apeloig*1	Tech.-Israel Inst. of Tech.	(Israel)	Sep. - Oct. 1991
Prof. A.J. Kresge*1	Univ. of Toronto	(Canada)	Sep. - Oct. 1991
Prof. H.F. Koch*1	Ithaca Coll.	(USA)	Sep. - Oct. 1991
Prof. H.-U. Sielh*1	Univ. of Tubingen	(Germany)	Sep. - Oct. 1991
Prof. M. Speranza*1	Univ. of Tuscia	(Italy)	Sep. - Oct. 1991
Prof. T.T. Tidwell*1	Univ. of Toronto	(Canada)	Sep. - Oct. 1991
Dr. Y. Chang*1	Univ. of Toronto	(Canada)	Sep. - Oct. 1991
Mr. P. Groarke*4	Univ. Coll. Dublin	(Ireland)	Sep. - Dec. 1991, Mar. 1992
Dr. C.J. Rousset*2	Purdue Univ.	(France)	Sep. 1991 -
Dr. F. Maseras*4	Univ. Autonoma Barcelona	(Spain)	Sep. 1991 -
Dr. G.S. Lodha*4	Centre Advanced Tech., Indore	(India)	- Oct. 1991
Prof. V. Aquilanti*2	Univ. of Perugia	(Italy)	Oct. 1991
Prof. A.Vazquez. de Miguel	Alcala de Henares Univ.	(Spain)	Oct. 1991, Apr. 1992
Prof. M. Gala	Alcala de Henares Univ.	(Spain)	Oct. 1991
Prof. D. Neumark	Univ. of California, Berkeley	(USA)	Oct. 1991
Prof. M. Okumura	California Inst. of Tech.	(USA)	Oct. 1991
Prof. R. Parson	Univ. of Colorado	(USA)	Oct. 1991
Prof. L. Philips	Baker Lab., Cornell Univ.	(USA)	Oct. 1991
Dr. D. Ray	Mol. Sci. Res. Center, Pacific Northwest Lab.	(USA)	Oct. 1991
Prof. N. Sibert	Univ. of Wisconsin	(USA)	Oct. 1991
Prof. J.A. Cina	James Franck Inst., Univ. of Chicago	(USA)	Oct. 1991
Prof. D.W. Pratt	Univ. of Pittsburgh	(USA)	Oct. 1991
Prof. L. Butler	Univ. of Chicago	(USA)	Oct. 1991
Prof. R.D. Coalson	Univ. of Pittsburgh	(USA)	Oct. 1991
Prof. K. Ervin	Univ. of Nevada	(USA)	Oct. 1991
Prof. J.H. Frederick	Univ. of Nevada	(USA)	Oct. 1991

Dr. S.M. George	Stanford Univ.	(USA)	Oct. 1991
Prof. C.C. Martens	Univ. of California	(USA)	Oct. 1991
Prof. B. Jackson	Univ. of Massachusetts	(USA)	Oct. 1991
Prof. G.M. Nathanson	Univ. of Wisconsin	(USA)	Oct. 1991
Prof. C. Taliani	Inst. of Spectrosc., CNDR	(Italy)	Oct. 1991
Dr. R. Dronskowski	Cornel Univ., Baker Lab.	(USA)	Oct. 1991
Mr. J. Pescatore	Univ. of California	(USA)	Oct. 1991
Prof. H. Scher	BP Res. International	(USA)	Oct. 1991
Dr. M. Stolka	Xerox Corp., Webster Res. Center	(USA)	Oct. 1991
Prof. E. Canel	Rockefeller Univ.	(USA)	Oct. 1991
Dr. S. Etemad	Bellcore	(USA)	Oct. 1991
Mr. A.R. Brown	Cavendish Lab.	(UK)	Oct. 1991
Mr. O.M. Gelsen	Cavendish Lab.	(UK)	Oct. 1991
Dr. P. Di Marco	CNR - Frae - Consigll	(Italy)	Oct. 1991
Prof. J. Kalinowski	CNR	(Italy)	Oct. 1991
Dr. E.E. Havinga	Philips Res. Lab.	(The Netherlands)	Oct. 1991
Prof. P.E. Yianoulis	Univ. of Patras	(Greece)	Oct. 1991
Mr. T. Enderle	The Univ. of Basel	(Switzerland)	Oct. 1991
Dr. D. Kohler	The Univ. of Basel	(Switzerland)	Oct. 1991
Prof. U.P. Wild	Swiss Fed. Inst. of Tech. (ETH)	(Switzerland)	Oct. 1991
Prof. E.F. Sheka	Lumumba Friendship Univ.	(Russia)	Oct. 1991
Dr. I. Renge	Estonian Acad. of Sci.	(Estonia)	Oct. 1991
Dr. R. Baumann	Univ. of Bonn	(Germany)	Oct. 1991
Prof. J. Daub	Inst. fur Organische Chem., Univ. 31	(Germany)	Oct. 1991
Prof. D. Haarer	Univ. of Bayreuth	(Germany)	Oct. 1991
Dr. L. Kador	Univ. of Bayreuth	(Germany)	Oct. 1991
Dr. C. Kryschi	Heinrich - Heine- Univ.	(Germany)	Oct. 1991
Prof. P. Reineker	Univ. Ulm	(Germany)	Oct. 1991
Dr. R. Richert	Univ. of Marburg	(Germany)	Oct. 1991
Prof. M. Schwoerer	Univ. of Bayreuth	(Germany)	Oct. 1991
Dr. H. Wachtel	Univ. Stuttgart	(Germany)	Oct. 1991
Prof. C. Brauchle	Inst. fur Phys. Chem.	(Germany)	Oct. 1991
Prof. H.C. Wolf	Univ. Stuttgart	(Germany)	Oct. 1991
Prof. H.-P. Trommsdorff	Univ. I de Grenoble	(France)	Oct. 1991
Prof. T. Luty	Tech. Univ. of Wroclaw	(Poland)	Oct. 1991
Dr. P. Petelenz	Jagiellenian Univ.	(Poland)	Oct. 1991
Dr. A. Tamulis	Inst. of Theoretical Phys. & Astronomy	(Lithuania)	Oct. 1991
Prof. Jiabai Qui	Acad. Sinica	(China)	Oct. 1991
Prof. Cheng Ye	Acad. Sinica	(China)	Oct. 1991
Prof. Poh-Kun Tseng*[4]	Natl. Taiwan Univ.	(Taiwan)	Oct. 1991, Apr. 1992
Prof. Way-Faung Pong*[4]	Tamkang Univ.	(Taiwan)	Oct. - Nov. 1991
Ms. S.J. Rosenthal	Univ. of Chicago	(USA)	Oct. - Nov. 1991
Mr. Zongrong Xu*[2]	Chengdu Univ. of Sci.	(China)	Oct. 1991 - Jan. 1992
Dr. Sung-Hong Kim*[4]	Kyungpook Natl. Univ.	(Korea)	Oct. 1991 - Sep. 1992
Dr. V.F. Kamalov*[2]	Inst. Chem. Phys.	(Russia)	Oct. 1991 - May 1992
Dr. I. Stroganova	Inst. Fine Chem.	(Russia)	Oct. 1991 - May 1992
Prof. R.F. Borkman*[5]	Georgia Inst. Tech.	(USA)	Oct. 1991 - Jun. 1992
Dr. Shu-Qin Zhou*[4]	Inst. of Chem.	(China)	Oct. 1991 -
Dr. P.B. Bisht	Tata Inst. Fundamental Sci.	(India)	Oct. 1991 -
Dr. A. Yartsev*[2]	Inst. of Spectroscopy	(Russia)	Oct. 1991 -
Dr. Bongsoo Kim*[2]	Univ. of California, Berkeley	(USA)	Oct. 1991 -
Dr. A.J. Bell*[2]	Univ. of Southampton	(UK)	- Nov. 1991
Prof. P.C. Eklund*[2]	Univ. of Kentucky	(USA)	Nov. 1991
Prof. Chin-Yuan Yao*[2]	HESYRL, Univ. Sci. & Tech., China	(China)	Nov. 1991
Prof. Shou-Gen Yin*[2]	HESYRL, Univ. Sci. & Tech., China	(China)	Nov. 1991
Prof. Sheng-Shen Hu*[2]	HESYRL, Univ. Sci. & Tech., China	(China)	Nov. 1991
Prof. Wei-Min Xu*[2]	HESYRL, Univ. Sci. & Tech., China	(China)	Nov. 1991
Dr. Shou Ming Yu	HESYRL, Univ. Sci. & Tech., China	(China)	Nov. 1991
Dr. Liu Si Sheng	HESYRL, Univ. Sci. & Tech., China	(China)	Nov. 1991
Prof. Ren-Yuan Qian	Inst. of Chem. Acad. Sinica	(China)	Nov. 1991

Dr. R.H. Baughman	Allied Signal Corp.	(USA)	Nov. 1991
Prof. M. Schröder	Univ. of Edinburgh	(UK)	Nov. 1991
Prof. M. Aresta	Univ. of Bari	(Italy)	Nov. 1991
Prof. E. Negishi	Purdue Univ.	(USA)	Nov. 1991
Prof. S.J. Cyvin	Univ. of Trondheim	(Norway)	Nov. 1991
Dr. F.H. Mies*2	NIST	(USA)	Nov. - Dec. 1991
Dr. K.V. Kaznacheev	Kurchatov Inst. of Atom. Energy (Russia)	(KIAE)	Nov. - Dec. 1991
Dr. G. Gorecki*5	Polish Acad. Sci.	(Poland)	Nov. 1991 -
Prof. Kee Hag Lee*2	Won Kang Univ.	(Korea)	- Dec. 1991
Prof. Shie-Ming Peng	Natl. Taiwan Univ.	(Taiwan)	- Dec. 1991
Prof. D.S.F. Crothers		(UK)	Dec. 1991
Dr. A.V. Sharkov	Lebedev Phys. Inst.	(Russia)	Dec. 1991
Dr. A.V. Konyashechenko	Lebedev Phys. Inst.	(Russia)	Dec. 1991
Mr. E.V. Khoroshilov	Lebedev Phys. Inst.	(Russia)	Dec. 1991
Dr. S.R. Meech	Heriot-Watt Univ.	(UK)	Dec. 1991 - Jan. 1992
Prof. M.S. Gordon*2	North Dakota Sate Univ.	(USA)	Dec. 1991 - Feb. 1992
Mr. K. Nguyen*4	North Dakota State Univ.	(USA)	Dec. 1991 - Feb. 1992
Mr. N. Matsunaga*4	North Dakota State Univ.	(USA)	Dec. 1991 - Feb. 1992
Mr. Chul Hyun Kang*4	Inha Univ.	(Korea)	Dec. 1991 - Feb. 1992
Mr. Jeong-Min Kweon*4	Kyungpook Natl. Univ.	(Korea)	Dec. 1991 - Feb. 1992
Prof. A. Bandrauk*5	Univ. of Sherbrooke	(Canada)	Dec. 1991 - Aug. 1992
Prof. R. Gordon	Univ. of Illinois, Chicago	(USA)	Jan. 1992
Prof. R.M. Noyes*1	Univ. of Oregon	(USA)	Jan. 1992
Prof. Z. Herman*1	J. Heyrovsky Inst. Phys. Chem. & Electrochem.	(Czechoslovakia)	Jan. 1992
Prof. W.H. Miller*1	Univ. of California & Lawrence Berkeley Lab.	(USA)	Jan. 1992
Prof. C.T. Chang*1	Inst. of Atom. & Mol. Sci.	(Taiwan)	Jan. 1992
Prof. M.S. Jhon*1	Center for Mol. Sci., KAIST	(Korea)	Jan. 1992
Prof. M. Inokuti*1	Argonne Natl. Lab.	(USA)	Jan., Jul. 1992
Mr. Shaoren He*4	Beijing Normal Univ.	(China)	Jan. - Jun. 1992
Prof. V. Saile	CAMD, Lovtsiana Univ.	(USA)	Feb. 1992
Prof. Y.A. Berlin	Semenov Inst. of Chem. Phys.	(Russia)	Feb. 1992
Prof. J.M. Dyke*2	Univ. of Southampton	(UK)	Feb. - Apr. 1992
Dr. J.F. Riehl*2	Centre Univ. Paris-Sud	(France)	Feb. 1992 -
Dr. A. Douhal*2	Kadi Ayyad Univ.	(Morocco)	- Mar. 1992
Prof. W.E. Smith	Strathclyde Univ.	(UK)	Mar. 1992
Dr. G. Singh*2	Centre Advanced Tech., Indore	(India)	Mar. 1992
Dr. Yonglian Yan*2	BSRF, Inst. High. Energy Phys.	(China)	Mar. 1992
Dr. Yijuan Zhang*2	BSRF, Inst. High. Energy Phys.	(China)	Mar. 1992
Dr. D. Horn	BASF Aktiengesellschaft	(Germany)	Mar. 1992
Dr. F. Branclstetter	BASF Aktiengesellschaft	(Germany)	Mar. 1992
Dr. T. Muhlenbernd	BASF Aktiengesellschaft	(Gernamy)	Mar. 1992
Dr. A. Ticktin	BASF Aktiengesellschaft	(Germany)	Mar. 1992
Prof. K.H. Bowen*1	Johns Hopkins Univ.	(USA)	Mar. 1992
Prof. P.M. Johnson*1	State Univ. of New York at Stony Brook	(USA)	Mar. 1992
Prof. H.O. Lutz*1	Univ. Bielefeld	(Germany)	Mar. 1992
Dr. K. Muller-Dethlefs*1	Inst. of Phys. Chem., Tech. Univ. Munchen	(Germany)	Mar. 1992
Dr. M.G. White*1	Brookhaven Natl. Lab	(USA)	Mar. 1992
Dr. R.N. Compton*1	Oak Ridge Natl. Lab.	(USA)	Mar. 1992
Prof. J.M. Trour*2	South Carolina Univ.	(USA)	Mar. 1992
Prof. D. Mukherjee*2	Indian Inst. Cult. Sci.	(India)	Mar. - Apr. 1992
Prof. P. Day	Royal Inst.	(UK)	Mar. - Apr. 1992
Mr. Rimo Xi*4	Inner Mongolia Norm. Univ.	(China)	Mar. 1992 -
Dr. R. Whitehead*2	Univ. of Durham	(UK)	Mar. 1992 -
Prof. J.C. Polanyi	Univ. of Toronto	(Canada)	Apr. 1992
Prof. J.P. Simons	Univ. of Nottingham	(UK)	Apr. 1992
Prof. P. Brooks*2	Rice Univ.	(USA)	Apr. 1992
Prof. I. Hargittai*2	Tech. Univ. of Budapest	(Hungary)	Apr. 1992

Prof. P. Royo	Alcala de Henares Univ.	(Spain)	Apr. 1992
Dr. R.W. Dreyfus	IBM T.J. Watson Research Center	(USA)	Apr. 1992
Prof. C. Flytzanis	CNRS, Ecole Poytechnique	(France)	Apr. 1992
Prof. F. Franks	Univ. of Cambridge	(USA)	Apr. 1992
Dr. T.F. Heinz	IBM T. J. Watson Research Center	(USA)	Apr. 1992
Prof. Poh-kun Tseng*[4]	Natl. Taiwan Univ.	(Taiwan)	Apr. 1992
Prof. Way-Faung Pong*[4]	Tamkang Univ.	(Taiwan)	Apr. 1992
Prof. M.D. Zeidler	Reinische-Westfalischen Technischen Hochschule Aachen	(Germany)	Apr. - May 1992
Dr. B.N. Toleutaev	Moscow State Univ.	(Russia)	May 1992
Prof. J. Frederick	Univ. of Nevada, Reno	(USA)	May - Jul. 1992
Dr. V. Denisov*[4]	St. Petersburg State Univ.	(Russia)	May 1992 -
Prof. C.N.R. Rao	Indian Inst. of Sci.	(India)	Jun. 1992
Prof. S.K. Joshi	Council of Sci. & Industrial Res.	(India)	Jun. 1992
Prof. P.R. Rao	Dept. of Sci. & Tech.	(India)	Jun. 1992
Dr. R. Chidambaram	Bhabha Atom. Res. Centre	(India)	Jun. 1992
Prof. Changtao Qian	Shanghai Inst. of Organic Chem.	(China)	Jun. 1992
Prof. D.M. Schrader	Marquette Univ.	(USA)	Jun. 1992
Dr. S.C. Irick	ALS, Lawrence Berkeley Lab., Univ. of California	(USA)	Jun. 1992
Dr. J. Beijersbergen	FOM Inst. for Atom. & Mol. Phys.	(The Netherlands)	Jun. 1992
Prof. Hai-Lung Dai	Univ. of Pennsylvania	(USA)	Jun. 1992
Prof. E.C. Lim	The Univ. of Akron	(USA)	Jun. 1992
Prof. A. Plonka	Tech. Univ. of Lodz	(Poland)	Jun. 1992
Prof. D.E. Fenton	The Univ. of Sheffield	(UK)	Jun. 1992
Dr. D. Kondakov*[2]	St. Petersburg State Univ.	(Russia)	Jun. 1992 -
Prof. Sehun Kim*[2]	KAIST	(Korea)	Jun. 1992 -
Mr. Chul Huh*[4]	Inha Univ.	(Korea)	Jun. - Aug. 1992
Dr. D. Wales*[2]	Univ. of Cambridge	(UK)	Jun. 1992 -
Ms. D. Choueiri*[4]	Purdue Univ.	(Lebanon)	Jun. 1992 -
Dr. V. Lozovsky	Inst. of Chem. Phys., Acad. of Sci.	(Russia)	Jul. 1992
Prof. P.R. Ogilby	Univ. of New Mexico	(USA)	Jul. 1992
Mr. E.V. Khoroshilov	P.N. Lebdev Phys. Inst.	(Russia)	Jul. 1992
Dr. E. Forest*[2]	Lawrence Berkeley Lab., Univ. of California	(USA)	Jul. 1992
Prof. Hackjin Kim*[4]	Chungnam Natl. Univ.	(Korea)	Jul. 1992 -
Prof. Hong Lae Kim	Kangweon Natl. Univ.	(Korea)	Jul. 1992
Prof. T.K. Sham*[2]	Univ. Western-Ontario	(Canada)	Jul. 1992 -
Mr. R. Serra*[4]	Univ. Autonoma Barcelona	(Spain)	Jul. 1992 -
Prof. P.J. Taik*[2]	KAIST	(Korea)	Jul. 1992 -
Prof. R.L. Christensen	Bowdoin Coll.	(USA)	Jul. - Aug. 1992
Prof. K.A. Nelson*[2]	Massachusetts Inst. of Tech.	(USA)	Jul. - Aug. 1992
Prof. Y.S. Choi	Inha Univ.	(Korea)	Jul. - Aug. 1992
Dr. A.M. Mebel*[4]	Inst. of New Chem. Problems	(Russia)	Jul. 1992 -

AWARD

Professor Morokuma's Scientific Achievements

Prof. Keiji Morokuma of Department of Theoretical Studies received the Award of the Chemical Society of Japan in 1992 for his contributions to "Theoretical Studies on Molecular Interaction and Chemical Reactions."

1. Theoretical studies of molecular interaction. He has developed a theoretical method for decomposing the interaction energy into physically meaningful energy components. The application of the method to varieties of complexes, including hydrogen bond complexes, donor-acceptor complexes and transition metal complexes, has led to clarification of the origin of interaction in a unified scheme.
2. Theoretical studies of potential energy surface and dynamics of chemical reactions. He has pioneered and contributed significantly to the application of the energy gradient method to determination of the transition state structure and tracing the intrinsic reaction coordinate. Recently he has made active contributions to the theoretical study of so-called transition state spectroscopy.
3. Theoretical studied of structure and reactions of transition metal complexes. He has made important contributions to ab initio MO studies on transition metal complexes. He has determined transition state structures and energies of several elementary reactions of transition metal complexes, and succeeded in obtaining the potential energy profile of an entire homogenous catalytic cycle.

Professor Saito's Scientific Achievements

The 37th Nishina Memorial Prize (for 1991) was given to Prof. Shuji Saito (Department of Molecular Structure) for his spectroscopic studies of interstellar molecules. The Nishina Prize is given to scientists who have shown remarkable insights in the field of atomic physics and its application, and Prof. S. Saito is the third chemist among the winners of the Nishina Prize. Prof. Saito has developed a highly sensitive technique of microwave spectroscopy, detecting and assigning characteristic lines of the many short-lived molecules, such as free radicals and molecular ions, that are substantial in the interstellar space. On the basis of these laboratory data, he was able to assign many spectral peaks from astronomical data that had not yet been understood. A typical example of such a study is the identification of the 45,379 MHz Line of TMC-1 as showing the presence of CCS. Prof. Saito's achievements in this field have been rated very highly internationally, and we are very happy to celebrate his award.

Dr. Mori's Scientific Achievements

Dr. Takehiko Mori received a Chemical Society of Japan Award for Young Chemists in 1992 for his contribution to "Chemistry and Physical Studies of Organic Superconductors".

Dr. Mori's contributions in studies of organic superconductors are as follows.

1) Synthesis of novel organic superconductors.
   In the family of $(BEDT\text{-}TTF)_2X$ salts, Dr. Mori synthesized new type of organic superconductors, i.e. $(BEDT\text{-}TTF)_3Cl_2(H_2O)_2$, κ-$(BEDT\text{-}TTF)_2Ag(CN)_2H_2O$, and $(BEDT\text{-}TTF)_4Pt(CN)_4H_2O$. He has carried out a systematic study on the effect of anion size or other structural factors.
2) Energy band calculation of organic superconductors.
   Dr. Mori succeeded in the calculation of band structures of many important organic superconductors with using tight-binding approximation based on intermolecular overlaps of molecular orbitals. He clarified Fermi surface structures of these materials, and elucidated the physical properties based on these calculations.
3) Physics of mobile (conduction)-localized electrons in DCNQI systems.
   $(DCNQI)_2M$ forms a family of highly conductive radical anion salts, and shows very novel physical properties, especially temperature or pressure dependence of the resistivity. Dr. Mori found out 1.3+ mixed valence state of Cu in $(DCNQI)_2Cu$ salt, and the instability of its metallic state under pressure and/or at low temperatures.

Dr. Asano's Scientific Achievements

The Scientific Award of the Japanese Spectroscopic Society for Young Chemist in 1991 was given to Dr. Motoko Asano, who had been an IMS fellow in the Molecular Dynamics Laboratory (April, 1990 – October, 1991) and is now a research associate in the Tokyo Institute of Technology (after marriage, her name has changed to Asano-Someda). This award is given to a young scientist below 36 years old who published a distinguished paper in the Journal of the Spectroscopic Society of Japan. Dr. Asano was awarded this prize for her paper, "Relaxation Processes of Photoexcited Metalloporphyrin Complexes".

LIST OF PUBLICATIONS

N. KOGA and K. MOROKUMA, "Ab Initio MO Studies of Catalytic Elementary Reactions and Catalytic Cycles of Transition Metal Complexes", *Chem. Rev.* **91,** 823 (1991).

N. KOGA, K. YAMASHITA, and K. MOROKUMA, "On Incorrect Behavior of Single Annihilation Equations of Spin-projected UHF and UMP Energies", *Chem. Phys. Lett.* **184,** 359 (1991).

N. KOGA and K. MOROKUMA, "Carbonyl Insertion into Pd-H Bond of HPd(R)(CO)(PH_3)(R=CH_3, H) and Comparison with That into Pd-CH_3 Bond. Ab Initio MO Study", *New J. Chem.* **15,** 749 (1991).

K. YAMASHITA and K. MOROKUMA, "Ab Initio Molecular Orbital and Dynamics Study of Transition-state Spectroscopy", *Faraday Disc. Chem. Soc.* **91,** 47 (1991).

H. KATO, K. YAMASHITA, and K. MOROKUMA, "Ab Initio MO Study of Neutral and Cationic Boron Clusters", *Chem. Phys. Lett.* **190,** 361 (1992).

H. KAWAMURA-KURIBAYASHI, N. KOGA, and K. MOROKUMA, "An Ab Initio MO Study on Ethylene and Propylene Insertion into the Ti-CH_3 Bond in $CH_3TiCl_2^+$ as a Model of Homogeneous Olefin Polymerization", *J. Am. Chem. Soc.* **114,** 2359 (1992).

U. NAGASHIMA, H. TANAKA, and K. MOROKUMA, "An Ab Initio and Monte Carlo Study on Structure and Stability of $H_3^+(H_2)_n$(n=3–16)", *J. Phys. Chem.* **96,** 4294 (1992).

K. YAMASHITA and K. MOROKUMA, "New Ab Initio Potential Surfaces and Three-Dimensional Quantum Dynamics for Transition State Spectroscopy in Ozone Photodissociation", *Chem. Phys. Lett.* **191,** 515 (1992).

F. MASERAS and K. MOROKUMA, "Application of The Natural Population Analysis to Transition Metal Complexes. Should The Empty Metal p Orbitals be Included in The Valence Space?", *Chem. Phys. Lett.* **195,** 500 (1992).

N. KOGA and K. MOROKUMA, "Ab Initio MO Study of C_{60} Anion Radical: The Jahn-Teller Distortion and Electronic Structure", *Chem. Phys. Lett.* **196,** 191 (1992).

E. NAKAMURA, Y. MIYACHI, N. KOGA, and K. MOROKUMA, "Theoretical Studies of Heteroatom-Directed Carbometalation. Addition of MeCu, Me_2Cu^- and MeLi to Substituted Acetylenes", *J. Am Chem. Soc.* **114,** 6686 (1992).

M. SASAI, I. OHMINE, and R. RAMASWAMY, "Long Time Fluctuation of Liquid Water; $1/f$ Spectrum of Energy Fluctuation in Hydrogen Bond Network Rearrangement Dynamics" *J. Chem. Phys.* **96,** 3045 (1992).

I. Ohmine and H. TANAKA, "Dynamics of Liquid Water; Fluctuations and Collective Motions" 'Molecular Dynamics Simulation', Springer-Verlag, Solid State Sciences **103,** 130 (1992).

S. TAKADA, A. OHSAKI, and H. NAKAMURA, "Reaction Dynamics of D+H_2 → DH+H: Effects of Potential Energy Surface Topography and Usefulness of the Constant Centrifugal Potential Approximation", *J. Chem. Phys.* **96,** 339 (1992).

M. BAER and H. NAKAMURA, "Variational Principles for Reactive Collisions Based on the Generalized Lagrange Multiplier Method", *J. Chem. Phys.* **96,** 6565 (1992).

M. KIMURA, H. KATO, K. SOMEDA, and H. NAKAMURA, "Coupled Channel Treatment of Transitions between Na($^2P_{1/2}$,m_j) and Na($^2P_{3/2}$,$m_{j'}$) in Collision with Na($^2S_{1/2}$,$m_{j''}$)", *J. Chem. Phys.* **96,** 7423 (1992).

H. NAKAMURA, "Nonadiabatic Tunneling in One-dimensional Finite Periodic Potential System", *J. Chem. Phys.* **97,** 256 (1992).

C. ZHU, H. NAKAMURA, N. RE, and V. AQUILANTI, "The Two-state Linear Curve Crossing Problems Revisited. I. Analysis of Stokes Phenomenon and Expressions for Scattering Matrices", *J. Chem. Phys.* **97,** 1892 (1992).

C. ZHU and H. NAKAMURA, "Stokes Constants for a Certain Class of Second-Order Ordinary Differential Equations", *J. Math. Phys.* **33,** 2697 (1992).

K. IWANO and K. NASU, "Spectral Shape of Optical Absorption in Extended Peierls-Hubbard Model", *Synthetic Metals* **41–43,** 2781 (1991).

X. SUN, Z. SHUAI, K. NASU, D. LIN, and T. GEORGE, "Electron Interaction and Optical Gap of Conjugated Polymers", *Phys. Rev.* **B44,** 11042 (1991).

K. NASU, "Suppressed Metal-Insulator Transitions, Enhanced Superconductivity and Reduced Isotope Effect due to Quartic Anharmonicity of Phonons in a Peierls-Hubbard Model", *Phys. Rev.* **B44,** 7625 (1991).

K. NASU and M. SUZUKI, "New Aspect of Exciton Relaxation: Nonlinear Lattice Relaxation Process", *Buturi (in Japanese)* **47,** 462 (1992).

K. NASU, "Excessively Suppressed Metal-Insulator Transitions, Enhanced Superconductivity and Reduced Isotope Effect by Hard-core Type Anharmonicity of Phonons in Peierls-Hubbard Model", *Physica* **C185/189,** 1595 (1991).

X. SUN, K. NASU, and C.Q. WU, "Frequency Dependence of Third Harmonic Generation of Polyacetylene", *Applied Physics* **B54,** 170 (1992).

M. SUZUKI and K. NASU, "Nonlinear Lattice Relaxation Process of Exciton in Quasi One-Dimensional Halogen-Bridged Mixed-Valance Metal Complexes, Self-Trapping, Solitons and Polarons", *Phys. Rev.* **B45,** 1605 (1992).

H. ZHENG and K. NASU, "New Approach to Local Polaron Model in Fluctuating-Valence System", *Phys. Rev.* **B45,** 2148–2163 (1992).

K. IWANO and K. NASU, "Theory for Spectral Shape of Optical Absorption in Halogen-Bridged Mixed-Valent Metal Complexes", *J. Phys. Soc. Jpn.* **61,** 1380 (1992).

K. NASU, "Superconductivities, Metal-Insulator Transitions, and Strong Enhancement and Reduction of Isotope Effects in Anharmonic Peierls-Hubbard Model", *J. Phys. Condense. Matter* **4,** 3793 (1992).

M. KUMAKURA and N. MORITA, "Visible Observation of Metastable Helium Atoms Confined in an Infrared/Visible Double Resonance Trap", *Jpn. J. Appl. Phys.* **31,** L276 (1992).

A. FUJII and N. MORITA, "Rotational State Dependence of Decay Dynamics in the Superexcited *7f* Rydberg state (v=1) of NO", *J. Chem. Phys.* **97,** 327 (1992).

Y. MIZUTANI, S. TOKUTOMI, K. AOYAGI, K. HORITSU, and T. KITAGAWA, "Resonance Raman Study on Intact Pea Phytochrome and its Model Compounds; Evidence for Proton Migration during the Phototransformation.", *Biochemistry* **30,** 10693 (1991).

N. KITAJIMA, T. KODA, S. HASHIMOTO, T. KITAGAWA, and Y. MOROOKA, "Synthesis and Characterization of the Dinuclear Copper (II) Complexes $[Cu(HB(3,5\text{-}Me_2pz)_3)]_2X$ ($X=O^{2-}$, $(OH)_2^{2-}$, CO_3^{2-}, O_2^{2-})", *J. Am. Chem. Soc.* **113,** (1991).

S. TAKAHASHI, T. OGURA, K. ITOH-SHINZAWA, S. YOSHIKAWA, and T. KITAGAWA, "Observation of the Cu_A-ligand Stretching Resonance Raman Band for Cytochrome *c* Oxidase.", *J. Am. Chem. Soc.* **113,** 9400 (1991).

S. SATO, M. ASANO-SOMEDA, and T. KITAGAWA, "Time-resolved Resonance Raman Spectra of Free-base Octaethylporphyrin in the S_1 and T_1 States.", *Chem. Phys. Lett.* **189,** 443 (1992).

N. KITAJIMA, K. FUJIWARA, C. FUJIMOTO, Y. MORO-OKA, S. HASHIMOTO, T. KITAGAWA, K. TORIUMI, K. TATSUMI, and A. NAKAMURA, "A New Model for Dioxygen Binding in Hemocyanin. Synthesis, Characterization, and Molecular Structure of the μ-η^2:η^2 Peroxo Dinuclear Copper (II) Complexes, $[Cu(HB(3,5\text{-}R_2pz)_3)]_2(O_2)$ (R=iPr and Ph).", *J. Am. Chem. Soc.* **114,** 1277 (1992).

Y. HAYASHI, M. SUZUKI, A. UEHARA, Y. MIZUTANI, and T. KITAGAWA, "(μ-Alkoxo)diiron (II, II) Complexes of N,N,N',N'-tetrakis(2-(6-methylpyridyl)methyl)-1,3-diamino-propane-2-olate and the Reversible Formation of the O_2 Adducts.", *Chem. Lett.* 91 (1992).

S. KAMINAKA and T. KITAGAWA, "Time-resolved UV Resonance Raman Study on Bohr Effects of Hemoglobin.", *J. Am. Chem. Soc.* **114,** 3256 (1992).

K. ISHIMORI, K. IMAI, G. MIYAZAKI, T. KITAGAWA, Y. WADA, H. MORIMOTO, and I. MORISHIMA, "Site-directed Mutagenesis in Hemoglobin: Functional and Structural Role of Inter- and Intrasubunit Hydrogen Bonds as Studied with 37β and 145β Mutations.", *Biochemistry* **31,** 3256 (1992).

Y. SAKAN, T. OGURA, and T. KITAGAWA, "Detection of the Fe-CO Stretching Raman Band for Recombination Transient Species of Photodissociated Carbonmonoxy Myoglobin by Using Pump/probe Time-resolved Technique.", *Chem. Phys. Lett.* **196,** 150 (1992).

S. KAMINAKA, H. TAKIZAWA, T. HANDA, H. KIHARA, and T. KITAGAWA, "Resonance Raman Study on Active Site Structure of an Cooperative Hemerythrin.", *Biochemistry* **31,** 6997 (1992).

T. EGAWA, H. MIKI, T. OGURA, R. MAKINO, Y. ISHIMURA, and T. KITAGAWA, "Observation of the $Fe^{IV}O$ Stretching Raman Band for a Thiolateligated Heme Protein; Compound I of Chloroperoxidase.", *FEBS Lett.* **305,** 206 (1992).

H. OKAMOTO, H. HAYASHI, K. YOSHIHARA, and M. TASUMI, "Femtosecond Time-resolved Coherent Anti-Stokes Raman Scattering from Carotenoids in vivo and in vitro: Comparison of Vibrational Relaxation Times (T_2) of the In-phase C=C Stretching Bands", *Chem. Phys. Lett.* **182,** 96 (1991).

V. KUBECEK, S. KUMAZAKI, Y. TAKAGI, K. YOSHIHARA, and G.C. REALI, "Self-Defocusing of Mode-Locked Nd:YAG Laser Radiation in GaAs, CdSe and InP", *Jpn. J. Appl. Phys.* **30** 10B, 1805 (1991).

V. KUBECEK, S. KUMAZAKI, Y. TAKAGI, G.C. REALI, and K. YOSHIHARA, "Actively and Passively Mode-Locked Nd:YAP($YAlO_3$) Laser with Negative Feedback Using CdSe and GaAs", *Jpn. J. Appl. Phys.* **30** 11A, 1889 (1991).

H. KANDORI, K. YOSHIHARA, H. TOMIOKA, and H. SASABE, "Subpicosecond Transient Absorption Spectrum of the Excited State of a Retinal Protein, Halorhodopsin", *Chem. Phys. Lett.* **187,** 579 (1991).

R. HOWELL, H. PETEK, D. PHILIPS, and K. YOSHIHARA, "An Investigation of the Fluorescence Behaviour of 4-(N,N-Dimethylamino) Benzonitrile Cooled in a Supersonic Jet", *Chem. Phys. Lett.* **183,** 249 (1991).

R.B. PANSU and K. YOSHIHARA, "Diffusion of Excited Bianthryl in Microheterogeneous Media", *J. Phys. Chem.* **95,** 10123 (1991).

T. TANI, T. SUZUMOTO, K. KEMNITZ, and K. YOSHIHARA, "Picosecond Kinetics of Light-Induced Electron Transfer from J-aggregated Cyanine Dyes to AgBr Microcrystals: Effect of Aggregate Size", *J. Phys. Chem.* **96,** 2778 (1992).

H. PETEK, A.J. BELL, R.L. CHRISTENSEN , and K. YOSHIHARA, "Fluorescence Excitation Spectra of the S_1 States of Isolated Trienes", *J. Chem. Phys.* **96,** 2412 (1992).

S. KUMAZAKI, V. KUBECEK, Y. TAKAGI, G.C. REALI, and K. YOSHIHARA, "Feedback-Controlled Mode-Locking of Nd:Glass Laser Using GaAs", *Jpn. J. Appl. Phys.* **31,** 413 (1992).

Y. TAKAGI, T. KOBAYASHI, K. YOSHIHARA, and S. IMAMURA, "Multiple- and Single-shot Autocorrelator Based on Two-photon Conductivity in Semiconductors", *Opt. Lett.* **17,** 658 (1992).

M.V. ALFIMOV, V.F. KAMALOV, I.A. STURUGANOVA, and K. YOSHIHARA, "Excited State Relaxation of Crown Ether Styryl Dyes: Photoisomerization", *Chem. Phys. Lett.* **195,** 262 (1992).

H. KANDORI, K. YOSHIHARA, H. TOMIOKA, and H. SASABE, "Primary Photochemical Studies by Subpicosecond Time-Resolved Spectroscopy", *J. Phys. Chem.* **96,** 6066 (1992).

V. KUBECEK, Y. TAKAGI, and K. YOSHIHARA, "Lithium Triborate Picosecond Optical Parametric Oscillator", *Opt. Commun.* **91,** 93 (1992).

H. KANDORI, K. YOSHIHARA, H. TOMIOKA, and H. SASABE, "Primary Photochemical Events in Halorhodopsin Studied by Subpicosecond Time-Resolved Spectroscopy", *J. Phys. Chem.* **96,** 6066 (1992).

H. HAYASHI, Y. FUJIMURA, H. OKAMOTO, and K. YOSHIHARA, "Origin of Subpicosecond Decay Components Revealed in Time-profiles of Coherent Anti-Stokes Raman Scattering from Neat Benzene", *Chem. Phys. Lett.* **196,** 44 (1992).

H. KANDORI, K. KEMNITZ, and K. YOSHIHARA, "Subpicosecond Transient Absorption Study of Intermolecular Electron Transfer between Solute and Electron Donating Solvents", *J. Phys. Chem.* **96,** 8042 (1992).

K. SAWABE and Y. MATSUMOTO, "Structure of adsorbed N_2O on a Pt(111) Surface and Photodissociation at 193 nm: Effective Formation of Oxygen Adatoms", *Chem. Phys. Lett.* **194,** 45 (1992).

M. TAKAYANAGI and I. HANAZAKI, "SEP-LIF Study on Dynamics of Vibrationally Excited States of van der Waals Complexes: The Anisole · Ar Complex", *Chem. Phys. Lett.* **190,** 115 (1992).

P.K. SRIVASTAVA, Y. MORI, and I. HANAZAKI, "Photo-inhibition of Chemical Oscillation in the $Ru(bpy)_3^{2+}$-catalyzed Belousov- Zhabotinskii Reaction", *Chem. Phys. Lett.* **190,** 279 (1992).

I. HANAZAKI, "Cross Section of Light-induced Inhibition and Induction of Chemical Oscillations", *J. Phys. Chem.* **96,** 5652 (1992).

H.S.YOO, N.S LEE, and I. HANAZAKI, "Fourier Transform Surface-enhanced Raman Scattering of Flavins in Silver Colloid Using Nd:YAG 1064 Excitation", *J. Raman Spectropy.* **23,** 239 (1992).

M.K. PARK, H.S. YOO, Y.K. KANG, N.S. LEE, and I. HANAZAKI, "Conformational Analysis of Catecholamines — Raman, High Resolution NMR, and Conformational Energy Calculation Study", *Bull. Korean Chem. Soc.* **13,** 230 (1992).

M. YOSHIMOTO, K. YOSHIKAWA, Y. MORI, and I. HANAZAKI, "Asymmeyric Coupling Stabilizes the Out-of-phase Mode; Experimental Evidence in the Belousov-Zhabotinsky Reaction", *Chem. Phys. Lett.* **189,** 18 (1992).

K. KANDA, H. ITO, K. SUZUKI, T. KONDOW, and K. KUCHITSU, "Formation of $CN(A^2\Pi_i)$ Fragment from BrCN in an Argon Flowing Afterglow," *Chem. Phys. Lett.* **185,** 225 (1991).

K. KANDA, H. ITO, K. SUZUKI, T. KONDOW, and K. KUCHITSU, "Pressure-Dependent Intensity Anomalies in the $B^2\Sigma^+ \sim {}^4\Pi$ Perturbed Rotational Lines of the $CN(B^2\Sigma^+\text{-}X^2\Sigma^+)$ 14-14 Band," *Bull. Chem. Soc. Jpn.* **65,** 481 (1992).

H. ITO, Y. OZAKI, K. SUZUKI, T. KONDOW, and K. KUCHITSU, "Emission Spectrum of the $CN(B^2\Sigma^+\text{-}X^2\Sigma^+)$ Tail Band System. $B^2\Sigma^+ \sim {}^4\Pi$ Perturbations in the v_B=9, 12, and 17 Levels," *J. Chem. Phys.* **96,** 4195 (1992).

K. KANDA, H. ITO, K. SUZUKI, T. KONDOW, and K. KUCHITSU, "A Comment on the Vibrational Assignment of the $CN(^4\Pi)$ in 'Pressure-Dependent Intensity Anomalies in the $B^2\Sigma^+ \sim {}^4\Pi$ Perturbed Rotational Lines of the $CN(B^2\Sigma^+\text{-}X^2\Sigma^+)$ 14-14 Band'," *Bull. Chem. Soc. Jpn.* **65,** 1195 (1992).

T. IDA, K. YAKUSHI, H. KURODA, H. YAMOCHI, and G. SAITO, "Pressure Dependence of the Polarized Reflectance Spectrum of a Solid Charge-Transfer Complex, Perylene-Hexacyanobutadiene (HCBD)", *Chem. Phys.* **156,** 113 (1991).

A.A. ZAKHIDOV, K. IMAEDA, A. UGAWA, K. YAKUSHI, H. INOKUCHI, Z. IQBAL, R. H. BAUGHMAN, B. L. RAMAKRISHNA, and Y. ACHIBA, "Microwave Low-Field Absorption and ESR in $K_X(C_{60})_{1-y}(C70)_y$ and K_XC_{70}", *Physica C* **185—189,** 411 (1991).

A.A. ZAKHIDOV, A. UGAWA, K. YAKUSHI, K. IMADEA, H. INOKUCHI, I.I. KHAIRULLIN, and P.K. KHABIBULLAEV, "Low-Field Microwave Absorption in Organic Superconductor κ-$(ET)_2[Cu(NCS)_2]$", *Physica C* **185—189,** 2669 (1991).

K. OSHIMA, K. ARAKI, H. YAMAZAKI, K. KATO, Y. MARUYAMA, K. YAKUSHI, T. MORI, H. INOKUCHI, H. MORI, and S. TANAKA, "The Fermi Surfaces in the κ-Type BEDT-TTF based Organic Superconductors", *Physica C,* **185—189,** 2689 (1991).

M. TAMURA, H. TAJIMA, K. YAKUSHI, H. KURODA, A. KOBAYASHI, R. KATO, and H. KOBAYASHI, "Reflectance Spectra of κ-$(BEDT\text{-}TTF)_2I_3$: Electronic Structure of Dimeric BEDT-TTF Salts", *J. Phys. Soc. Jpn.* **60,** 3861 (1991).

M. TOKUMOTO, N. KINOSHITA, H. ANZAI, A.G. SWANSON, J.S. BROOKS, S.T. HANNAHS, C.C. AGOSTA, M. TAMURA, H. TAJIMA, H. KURODA, A. UGAWA, and K. YAKUSHI, "Fermi Surface Study of Two-Dimensional Organic Metals $(BEDT\text{-}TTF)_2X$" *Synthetic Metals* **41—43,** 2459 (1991).

I. IKEMOTO, K. KIKUCHI, K. SAITO, S. SUZUKI, Y. ACHIBA, A. UGAWA, and K. YAKUSHI, "Structure and Property of C_{60} Single Crystal", *Jpn. J. Appl. Phys.,* Series 7, *Mechanism of Superconductivity* 367 (1992).

A. UGAWA, H. ISHII, K. YAKUSHI, H. OKAMOTO, T. MITANI, M. WATANABE, K. SAKAI, K. SUZUI, and S. KATO, "Design of an Instrument for Far-Infrared Microspectroscopy using a Synchrotron Radiation (SR) Source" *Rev. Sci. Instrum.* **63,** 1551 (1992).

R. DANIELI, V.N. DENISOV, G. RUANI, R. ZAMBONI, C. TALIANI, A.A. ZAKHIDOV, A. UGAWA, K. IMAEDA, K. YAKUSHI, H. INOKUCHI, K. KIKUCHI, I. IKEMOTO, S. SUZUKI, and Y. ACHIBA, "Low Energy Electronic Excitations and Fano Resonance in K Doped C_{60} from Raman Scattering Excited at 1.16 eV", *Solid State Commun.* **81,** 257 (1992).

A.A. ZAKHIDOV, I. IMAEDA, D.M. PETTY, K. YAKUSHI, H. INOKUCHI, K. KIKUCHI, I. IKEMOTO, S. SUZUKI, and Y. ACHIBA, "Enhanced Isotope Effect in ^{13}C-rich Superconducting M_XC_{60} (M=K, Rb): Support for Vibronic Pairing", *Phys. Lett. A* **164,** 355 (1992).

K. TANAKA, A.A. ZAKHIDOV, K. YOSHIZAWA, K. OKAHARA, T. YAMABE, K. YAKUSHI, K. KIKUCHI, S. SUZUKI, I. IKEMOTO, and Y. ACHIBA, "Magnetic Properties of TDAE-C_{60} and TDAE-C_{70}. A Comparative Study.", *Phys. Lett. A* **164,** 221 (1992).

T. ISHIDA, K. KANODA, T. TAKAHASHI, and K. KOGA, "Origin of Spin Susceptibility in $Bi_2Sr_2Ca_{n-1}Cu_nO_{2n+4}$ (n=1, 2, 3)", *Physica C* **178,** 231 (1991).

T. ISHIDA, K. KOGA, K. KANODA, and T. TAKAHASHI, "Magnetism of $Bi_2Sr_2Ca_{n-1}Cu_nO_{2n+4+\delta}$", in "The Physics and Chemistry of Oxide Superconductors" Y. Iye and H. Yasuoka Ed., Springer-Verlag, p.377 (1991).

K. KANODA, K. SAKAO, T. TAKAHASHI, T. KOMATSU, and G. SAITO, "NMR Study of an Organic Superconductor, κ-(BEDT-TTF)$_2$Cu[N(CN)$_2$]Br, *Physica C* **185—189,** 2667 (1991).

T. TAKAHASHI, K. KANODA, and G. SAITO, "Novel Aspects of Organic Superconductors: NMR and Magnetic Susceptibility", *Physica C* **185—189,** 366 (1991).

T. ISHIDA, K. KOGA, K. KANODA, and T. TAKAHASHI, "ESR Detection of Cu^{2+} Spins in Oxide Superconductors", *Physica C* **185—189,** 1201 (1991).

T. NAKAMURA, G. SAITO, N. MIURA, T. OSADA, S. KAGOSHIMA, H. MORI, K. KANODA, and T. TAKAHASHI, "Fermi Surface Topology and Electronic Structures of Two-Dimensional Organic Conductors Based on BEDT-TTF and MDT-TTF", *Phosphorus, Sulfur, and Silicon* **67,** 377 (1992).

J.A. SCHLUETER, Y. ORIHASHI, M.G. KANATZIDIS, W. LIANG, T.J. MARKS, D.C. DEGROOTS, H.O. McCARCY, C.R. KANNEWURF, and T. INABE, "Charge Transport and Optical Properties of the First Highly Conductive One-Dimensional Molecular Metal Containing Fluoride Counterions: (TSeT)$F_{0.25}Cl_{0.50}$", *Chem. Mater.* **3,** 1013 (1991).

Y. MARUYAMA, T. INABE, H. OGATA, Y. ACHIBA, S. SUZUKI, K. KIKUCHI, and I. IKEMOTO, "Observation of Metallic Conductivity and Sharp Superconducting Transition at 19K in Potassium-Doped Fulleride, C_{60}, Crystal", *Chem, Lett.* **1991,** 1849.

Y. MARUYAMA, T. INABE, H. OGATA, H. HOSHI, N. NAKAMURA, Y. MORI, Y. ACHIBA, S. SUZUKI, K. KIKUCHI, and I. IKEMOTO, "Electronic Properties of C_{60} and Alkali metal Doped C_{60} Thin Films or Single Crystals", *Physica C* **185—189,** 413 (1991).

H. OGATA, T. INABE, H. HOSHI, Y. MARUYAMA, Y. ACHIBA, S. SUZUKI, K. KIKUCHI, and I. IKEMOTO, "Charge Transport and Superconducting Transitions in C_{60} Single Crystals and Thin Films Doped with Rubidium", *Jpn. J. Appl. Phys.* **31,** L166 (1992).

S. TAKEDA, H. CHIHARA, T. INABE, T. MITANI, and Y. MARUYAMA, "NMR Study of Proton Dynamics in the NHO Hydrogen Bonds in the Thermochromic Crystals of *N*-Salicylideneanilines", *Chem. Phys. Lett.* **189,** 13 (1992).

T. INABE, K. OKANIWA, H. OKAMOTO, T. MITANI, Y. MARUYAMA, and S. TAKEDA, "Proton Transfer in *N*-Salicylideneanilines — Effect of Charge-Transfer Interaction", *Mol. Cryst. Liq. Cryst.* **216,** 229 (1992).

Y. MARUYAMA, T. INABE, H. OGATA, H. HOSHI, N. NAKAMURA, Y. MORI, Y. ACHIBA, S. SUZUKI, K. KIKUCHI, and I. IKEMOTO, "Novel Molecular System C_{60}: Fullerites and Fullerides", *Mol. Cryst. Liq. Cryst.* **218,** 297 (1992).

K. AWAGA, T. INABE, U. NAGASHIMA, T. NAKAMURA, M. MATSUMOTO, Y. KAWABATA, and Y. MARUYAMA, "α-Nitronyl Nitroxide Cation Radicals", *Chem. Lett.* **1991,** 1777.

K. AWAGA, T. INABE, and Y. MARUYAMA, "Ferromagnetic Intermolecular Interaction and Crystal Structure of the *p*-Pyridyl Nitronyl Nitroxide Radical", *Chem. Phys. Lett.* **190,** 349 (1992).

K. AWAGA, T. INABE, Y. MARUYAMA, T. NAKAMURA, and M. MATSUMOTO, "Ferromagnetic and Antiferromagnetic Intermolecular Interactions in the Two-Dimensional Triangular Lattice of the *m*-*N*-Methylpyridinium Nitronyl Nitroxide Cation Radical", *Chem. Phys. Lett.* **195,** 21 (1992).

M. MORI, K. KAMIYA, S. MATSUO, T. ISHIMASA, H. NAKANO, H. FUJIMOTO, and H. INOKUCHI, "Resonant Photoemission Study of the AL-Cu-Fe Icosahedral Phase.", *J. Phys.: Condens. Matter* **4,** L157 (1992).

N. UENO, H. KUROSU, K. SEKI, G. SAITO, K. SUGITA, and H. INOKUCHI, "Anomalous Temperature Dependence of Low-energy-electron Transmission Spectra of Thin Films of Tetrakis(nonylthio)-tetrathiafulvalene (TTC$_9$-TTF).", *Mol. Cryst. Lig. Cryst.* **218,** 171 (1992).

N. UENO, K. KAMIYA, K. OGAWA, H. YONEHARA, M. TAKAHASHI, H. NAKAHARA, K. SEKI, K. SUGITA, K. FUKUDA, and H. INOKUCHI, "Angle-resolved Photoemission from Langmuir-Blodgett Films of Copper tetrakis(n-butoxycarbonyl)phthalocyanine with Synchrotron Radiation.", *Thin Solid Films* **210/211,** 678 (1992).

S. HINO, K. MATSUMOTO, S. HASEGAWA, K. KAMIYA, H. INOKUCHI, T. MORIKAWA, T. TAKAHASHI, K. SEKI, K. KIKUCHI, S. SUZUKI, I. IKEMOTO, and Y. ACHIBA, "Ultraviolet Photoelectron Spectra of C_{84} and K_xC_{84}.", *Chem. Phys. Lett.* **190,** 169 (1992).

T. TAKAHASHI, T. MORIKAWA, S. HASEGAWA, K. KAMIYA, H. FUJIMOTO, S. HINO, K. SEKI, H. KATAYAMA-YOSHIDA, H. INOKUCHI, K. KIKUCHI, S. SUZUKI, I. IKEMOTO, and Y. ACHIBA, "Comparative Photoemission Study of Rb_xC_{60}, Rb_xC_{70} and RbC_8. A Pseudo-gap at the Fermi Level in the Fulleride.", *Phisica C* **190,** 205 (1992).

T. TAKAHASHI, S. SUZUKI, T. MORIKAWA, H. KATAYAMA-YOSHIDA, S. HASEGAWA, H. INOKUCHI, K. SEKI, K. KIKUCHI, S. SUZUKI, I. IKEMOTO, and Y. ACHIBA, "Pseudo-Gap at the Fermi Level in K_3C_{60} Observed by Photoemission and Inverse Photoemission.", *Phys. Rev. Lett.* **68,** 1232 (1992).

C. NAKANO, P. WANG, T. MORI, Y. MARUYAMA, H. INOKUCHI, H. YAMOCHI, and G. SAITO, "Structural Study of the Two Phases of Tetrakis-(methylseleno) tetrathiafulvalene ($TSeC_1$-TTF)," *Bull. Chem. Soc. Jpn.* **64,** 3690 (1991).

C. NAKANO, P. WANG, K. IMAEDA, Y. MARUYAMA, H. INOKUCHI, H. YAMOCHI, and G. SAITO, "Crystal Structures of TXC_8-TTF (X=Se, Te)," *Bull. Chem. Soc. Jpn.* **65,** 1482 (1992).

C. NAKANO, T. MORI, K. IMAEDA, N. YASUOKA, Y. MARUYAMA, H. INOKUCHI, N. IWASAWA, and G. SAITO, "Crystal Structures and Molecular Packing of Tetrakis(alkylthio)tetrathiafulvalene (TTC_n-TTF); part I (n=3, 4, 6)," *Bull. Chem. Soc. Jpn.* **65,** 1878 (1992).

C. NAKANO, T. MORI, K. IMAEDA, N. YASUOKA, Y. MARUYAMA, H. INOKUCHI, N. IWASAWA, and G. SAITO, "Crystal Structures and Molecular Packing of Tetrakis(alkylthio)tetrathiafulvalene (TTC_n-TTF); part II (n=7, 9, 11)," *Bull. Chem. Soc. Jpn.* **65,** 2086 (1992).

K. IMAEDA, Y. YAMASHITA, Y. LI, T. MORI, H. INOKUCHI, and M. SANO, "Hall-Effect Observation in the New Organic Semiconductor Bis(1,2,5-thiadiazolo)-*p*-quinobis(1,3-dithiole) (BTQBT)" *J. Mater, Chem.* **2,** 115 (1992).

T. ENOKI, K. NAKAZAWA, K. SUZUKI, S. MIYAJIMA, T. CHIBA, Y. IYE, H. YAMAMOTO, and H. INOKUCHI, "Two-Dimensional Metallic Hydrogen Lattice in Potassium-Hydrogen-Graphite Ternary Systems," *J. Less-Common Metals* **172—174,** 20 (1991).

K. MASHIMA, H. NAKANO, T. MORI, H. TAKAYA, and A. NAKAMURA, "Rational Preparation and Characterization of Tandem Tetrametal Clusters. Crystal Structure of Tetrakis(6-diphenylphosphino-2-pyridonato) dimolybdenum", *Chem. Lett.* **1992,** 185.

H. MORI, I. HIRABAYASHI, S. TANAKA, T. MORI, Y. MARUYAMA, and H. INOKUCHI, "Superconductivity in $(BEDT\text{-}TTF)_4Pt(CN)_4H_2O$", *Solid State Commun.* **80,** 411 (1991).

T. MORI, K. KATO, Y. MARUYAMA, H. INOKUCHI, H. MORI, I. HIRABAYASHI, and S. TANAKA, "Structural and Physical Properties of a New Organic Superconductor, $(BEDT\text{-}TTF)_4Pd(CN)_4H_2O$", *Solid State Commun.* **82,** 177 (1992).

T. MORI and H. INOKUCHI, "Structural and Conducting Properties of (TTF)(DMeT-DCNQI)", *Bull. Chem. Soc. Jpn.* **65,** 1460 (1992).

H. YAMOCHI, T. NAKAMURA, T. KOMATSU, N. MATSUKAWA, T. INOUE, G. SAITO, T. MORI, M. KUSUNOKI, and K. SAKAGUCHI, "Crystal and Electronic Structures of the Organic Superconductors, κ-$(BEDT\text{-}TTF)_2Cu(CN)[N(CN)_2]$ and κ'-$(BEDT\text{-}TTF)_2Cu_2(CN)_3$", *Solid State Commun.* **82,** 101 (1992).

H. MORI, I. HIRABAYASHI, S. TANAKA, T. MORI, Y. MARUYAMA, and H. INOKUCHI, "New Organic Superconductor, $(BEDT\text{-}TTF)_4Pt(CN)_4H_2O$", in "*Advances in Superconductivity IV,*" ed by H. Hayakawa and N. Koshizuka, Springer, Berlin (1992) p.199.

M. YOSHIMURA, H. SHIGEKAWA, T. MORI, M. KAGASHIMA, H. KATO, Y. SAKISAKA, G. SAITO, and A. KAWAZU, "Electronic Structure of the Organic Superconductor κ-$(BEDT\text{-}TTF)_2Cu(NCS)_2$ Studied by Angle-Resolved Photoemission Spectroscopy", *Jpn. J. Appl. Phys.* **31,** 1341 (1992).

T. MORI and H. INOKUCHI, "Synthesis of Tetrathiafulvalene Derivatives by the Use of Organoaluminium Reagents", *Chem. Lett.* **1992,** 1873.

S. HIRAYAMA, H. YASUDA, M. OKAMOTO, and F. TANAKA, "Effect of Pressure on the Natural Radiative Lifetimes of Anthracene Derivatives in Solution", *J. Phys. Chem.* **95,** 2971 (1991).

A.D. SCULLYM, H. YASUDA, M. OKAMOTO, and S. HIRAYAMA, "The Effect of Pressure on the Dynamic Quenching by Oxygen of the Excited Singlet State of 9,10-Dimethylanthracene in Solution", *Chem. Phys.* **157,** 271 (1991).

A.D. SCULLYM, A. MATSUMOTO, and S. HIRAYAMA, "A Time-resolved Fluorescence Study of Electronic Excitation Energy Transport in Concentrated Dye Solutions", *Chem. Phys.* **157,** 253 (1991).

F. TANAKA, S. HIRAYAMA, and K. SHOBATAKE, "S_1-T_2 Level Inversion of 9,10-Dimethylanthracene caused by the Coordination of One Rare-gas Atom, *Chem. Phys. Lett.* **195,** 243 (1992).

K. NAKASUJI, K. SUGIURA, J. TOYODA, Y. MORITA, H. OKAMOTO, K. OKANIWA, and T. MITANI, "Cooperative Proton-Electron Transfer (PET) Systems as New Molecular Systems", *Mol. Cryst. Liq. Cryst.* **216,** 213 (1992).

K. YAMAGUCHI, M. OKUMURA, J. MAKI, T. NORO, H. NAMIMOTO, T. FUENO, and K. NAKASUJI, "MO Theoretical Studies of Magnetic Interactions in Clusters of Nitronyl Notroxide and Related Species", *Chem. Phys. Letters* **190,** 353 (1992).

K. YAMAGUCHI, M. OKUMURA, T. KAWAMURA, T. NORO, and K. NAKASUJI, "Theoretical Studies of CT Ferromagnets and Ferrimagnets: Metallocenium-TCNE Complexes" *Mol. Cryst. Liq. Cryst.* **218,** 229 (1992).

K. SUGIURA, J. TOYODA, H. OKAMOTO, K. OKANIWA, A. KAWAMOTO, J. TANAKA, and K. NAKASUJI, "Three-Dimensional Structure of an Unsymmetrical Proton-Electron Transfer System Containing a Disufide Bond: The Bis(4-hydroxyphenyl)-disufide-Benzoquinone Complex", *Angew. Chem. Int. Ed. Engl.* **31,** 852 (1992).

K. UMAKOSHI, K. MURATA, S. YAMASHITA, and K. ISOBE, "Reactivity of $[Cp^*RhPtCl_6](Cp^*=\eta^5\text{-}C_5Me_5)$. Synthesis and Structures of $[(Cp^*Rh)_2(\mu\text{-}Cl)_3[PtCl_5(CH_3CONH_2)]$ and $[(Cp^*Rh)_2(\mu\text{-}Cl)_3]_2[PtCl_6]$.", *Inor. Chim. Acta* **190,** 185 (1991).

H. AKASHI, K. ISOBE, Y. OZAWA, and A. YAGASAKI, "β-Methallylrhodium (III) Supported on a Vanadium Oxide Cluster: Synthesis, Structure, and Reaction.", *J. Cluster Sci.* **2,** 291 (1991).

M. EBIHARA, K. ISOBE, Y. SASAKI, and K. SAITO, "Synthesis, Structure, and Properties of Oxidized Hexamolybdenum Clusters $[Mo_6X_7Y)X'_6]^{2-}$ (X=X'=Cl, Br; Y=S, Se).", *Inorg. Chem.* **31,** 1644 (1992).

Y. OZAWA, A. VÁZQUEZ DE MIGUEL, and K. ISOBE, "μ-Methylene Rhodium Complexes with SH Ligand: Synthesis and Structures of $[Rh_2Cp^*_2(\mu\text{-}CH_2)_2(\mu\text{-}SH)]BPh_4$ and *trans*-$[Rh_2Cp^*_2(\mu\text{-}CH_2)_2(SH)_2](Cp^*=\eta^5\text{-}C_5Me_5)$.", *J. Organomet. Chem.* **433,** 183 (1992).

S. OKEYA, Y. FUJIWARA, S. KAWASHIMA, Y. HAYASHI, K. ISOBE, Y. NAKAMURA, H. SHIMOMURA, and Y. KUSHI, "Novel Bis(triphenylphosphine)platinum (II) Complexes Containing a Thiourea or a 1,3-Diethylthiourea Dianion as an N,S-Chelating Ligand.", *Chem. Lett.* 1823 (1992).

J. KATSUKI and J. INANAGA, "One-Pot Conversion of *O*-Acetylsugar Lactones into 2,3-Dideoxysugar Derivatives via Platinum-Catalyzed Hydrogenolysis", *Tetrahedron Lett.* **32,** 4963 (1991).

J. INANAGA, Y. YOKOYAMA, Y. BABA, and M. YAMAGUCHI, "Selective Reduction of Alkynes by the Reagent SmI_2-Transition Metal Catalyst-Proton Donors", *Tetrahedron Lett.* **32,** 5559 (1991).

J. INANAGA, Y. YOKOYAMA, Y. HANDA, and M. YAMAGUCHI, "Preparation of Medium- and Large-Sized Carbocycles by Means of SmI_2-Promoted Intramolecular Reformatsky Reaction", *Tetrahedron Lett.* **32,** 6371 (1991).

J. INANAGA, Y. HANDA, T. TABUCHI, K. OTSUBO, M. YAMAGUCHI, and T. HANAMOTO, "A Facile Reductive Dimerization of Conjugated Acid Derivatives with Samarium Diiodide", *Tetrahedron Lett.* **32,** 6557 (1991).

J. INANAGA, S. SAKAI, Y. HANDA, M. YAMAGUCHI, and Y. YOKOYAMA, "Selective Conjugate Reduction of α,β-Unsaturated Esters and Amides via SmI_2-Promoted Electron Transfer Process, *Chem. Lett.* 2117 (1991).

J. INANAGA, Y. SUGIMOTO, and T. HANAMOTO, "A Novel Method for the Generation of 2,3-Naphthoquinodimethanes Utilizing Samarium(II) Iodide-Promoted Allene Synthesis", *Tetrahedron Lett.* **33,** 7035 (1992).

H. TAKEMURA, T. SHINMYOZU, and T. INAZU, "Syntheses and Properties of Highly Symmetrical Cage Compounds: Pyridine Analogs of "Hexametaxylylenetetramine.", *J. Am. Chem. Soc.* **113,** 1323 (1991).

M. MISHIMA, T. ARIGA, Y. TSUNO, K. IKENAGA, and K. KIKUKAWA, "Gas Phase Basicities of α-Trimethylsilylstyrenes. Intrinsic Effect of α-Trimethylsilyl Group on the Stability of Carbenium Ions," *Chem. Lett.* 489 (1992).

M. MISHIMA, C.H. KANG, M. FUJIO, and Y. TSUNO, "Gas Phase Basicities of Acetophenones toward Trimethylsilyl Cation," *Chem. Lett.* 493 (1992).

M. MISHIMA, T. TERASAKI, M. FUJIO, Y. TSUNO, Y. TAKAI, and M. SAWADA, "Substituent Effect on the Gas Phase Basicity of Pyridine N-Oxide," *Chem. Lett.* 1081 (1992).

M. MISHIMA, T. ARIGA, M. FUJIO, Y. TSUNO, S. KOBAYASHI, and H. TANIGUCHI, "Gas Phase Substituent Effect on Basicity of Phenylacetylene. Intrinsic Resonance Demand of Phenylvinyl Cation," *Chem. Lett.* 1085 (1992).

K. NAKATA, H. NOMURA, M. MISHIMA, Y. SAEKI, K. NISHIMOTO, T. MATSUSHITA, M. FUJIO, and Y. TSUNO, "Substituent Effect on Gas Phase Stabilities of α-t-Butyl-α-methylbenzyl Cations," *Mem. Fac. Sci., Kyushu Univ., Ser. C,* **18(2),** 287 (1992).

M. TAKAHASHI, K. OKUYAMA, and K. KIMURA, "Two-Color Threshold Photoelectron Spectroscopy: Cation Vibrational Spectroscopy", *J. Mol. Struct.* **249,** 47 (1991).

A. HIRAYA, Y. ACHIBA, K. KIMURA, and E.C. LIM, "Multiphoton Ionization Photoelectron Spectroscopy of Molecular Excited States in Supersonic Jet: Low-Lying Electronic States of Isoquinoline", *Chem. Phys. Lett.* **185,** 303 (1991).

M.C.R. COCKETT, M. TAKAHASHI, K. OKUYAMA, and K. KIMURA, "REMPI Threshold Photoelectron Spectra of the *cis* and *trans* Rotational Isomers of Jet-Cooled m-Chlorophenol", *Chem. Phys. Lett.* **187,** 250 (1991).

H. OZEKI, M. TAKAHASHI, K. OKUYAMA, and K. KIMURA, "Absence of Photoelectron Spectroscopic Evidence for 'Proton Tunneling' in the Cation Ground State of Jet-Cooled Tropolone", *J. Chem. Phys.* **95,** 9401 (1991).

M. WATANABE, G. ISOYAMA, M. KAMADA and K. KIMURA, "Status of UVSOR Facility — 1991", *Rev. Sci. Instrum.* **63,** 1584 (1992).

M. TAKAHASHI, "Two-Color (2+1′) Multiphoton Ionization Threshold Photoelectron Study of the Ar-NO van der Waals Complexes: Observation of Intermolecular Vibrational Progressions of the Ar-NO^+ Cation", *J. Chem. Phys.* **96,** 2594 (1992).

M. TAKAHASHI, H. OZEKI, and K. KIMURA, "Vibrational Spectra of Aniline-Ar_n van der Waals Cations (n=1 and 2) observed by Two-Color Threshold Photoelectron [Zero Kinetic Energy (ZEKE)-Photoelectron] Spectroscopy", *J. Chem. Phys.* **96,** 6399 (1992).

K. FURUYA, K. KIMURA, and T. HIRAYAMA, "Energy Partitioning in the Dissociation Reaction $Ar_3^+ \rightarrow Ar_2^+ + Ar$", *J. Chem. Phys.* **97,** 1022 (1992).

K. OKUYAMA, M.C.R. COCKETT, and K. KIMURA, "Observation of Torsional Motion in the Ground-State Cation of Jet-Cooled Tolane by Two-Color Threshold Photoelectron Spectroscopy", *J. Chem. Phys.* **97,** 1649 (1992).

M.C.R. COCKETT, K. OKUYAMA, and K. KIMURA, "Laser Threshold Photoelectron Spectra of the *cis* and *trans* Rotational Isomers of *p*-Dimethoxybenzene-Ar_n (n=0, 1, 2): Observation of the Intermolecular Van der Waals Stretching and Bending Vibrational Modes in the Cation", *J. Chem. Phys.* **97,** 4679 (1992).

T. MATSUSHIMA, K. SHOBATAKE, K. NAGAI, Y. OHNO, and K. TABAYASHI, "Velocity Distribution of Desorbing Products in the Oxidation of Carbon Monoxide on Palladium (110) Surfaces", *Chem. Phys. Lett.* **187,** 277 (1991).

K. TABAYASHI and K. SHOBATAKE, "Photodissociation Dynamics of Ethylene Sulfide and Allene at 193 mm Studied by Time-of-flight Mass Spectroscopy", *J. SPIE-Internl. Soc. Optical Eng.* **1638,** 185 (1992).

Y. OHNO, T. MATSUSHIMA, K. SHOBATAKE, and H. NOZOE, "Reaction Diagram of Carbon Monoxide and Oxygen on Palladium (100) and Angular Distribution of Reactive Carbon Dioxide Desorption", *Surf. Sci.* **273,** 291 (1992).

T. MATSUSHIMA, K. SHOBATAKE, Y. OHNO, K. NAGAI, and K. TABAYASHI, "Anisotropic Velocity Distribution of Desorbing Product in Carbon Monoxide Oxidation on Palladium (110)", *J. Chem. Phys.* **97,** 2783 (1992).

M. KONDO, Y. KUBO, S. HIRAYAMA, and K. SHOBATAKE, "Radiative Lifetime and Electronic Relaxation of 9-Cyanoanthracene in Rare gas Clusters and in Rare gas Matrices", *Chem. Phys. Lett.* **198,** 214 (1992).

S. SUZUKI, K. MITSUKE, T. IMAMURA, and I. KOYANO, "Negative-Ion Mass Spectrometric Study of Ion-Pair Formation in the Vacuum Ultraviolet. VI. $CH_3X \rightarrow X^- + CH_3^+$ (X=F, Cl, Br)", *J. Chem. Phys.* **96,** 7500 (1992).

Y. SAITO, O. YAMAOKA, and A. YOSHIDA, "Plasmaless Etching of Silicon Using Chlorine Trifluoride", *J. Vac. Sci. Technol. B* **9,** 2503 (1991).

R. KUMAR, A. YOSHIDA, and R.M. MEHRA, "Physical Properties of Amorphous $Ge_{20}Sb_{25-x}Bi_xSe_{55}$ Thin Films", *J. Non-Cryst. Solids* **130,** 248 (1991).

K. YASUDA, M. TAKEDA, H. MASUDA, I. NAKAGAWA, H. MATSUI, and A. YOSHIDA, "Electron Irradiation Effects in a Bi-Pb-Sr-Ca-Cu Oxide Superconductor", *Phys. Stat. Sol.(a)* **125,** 279 (1991).

M. NISHIO, H. OGAWA, and A. YOSHIDA, "Effect of Ar Laser-illumination upon ZnTe Growth in Atmospheric-pressure MOVPE", *J. Cryst. Growth* **115,** 284 (1991).

T. YAMAGUCHI, Y. BABA, M. NISHIMURA, J. MATSUFUSA, and A. YOSHIDA, "Thermal Crystallization of Copper Indium Diselenide Films in Flowing or Pressurized Atmosphere", *Phys. Stat. Sol.(a)* **128,** 455 (1991).

Y. SAITO, M. HIRABARU, and A. YOSHIDA, "Anisotropic and Damageless Etching of Single-crystalline Silicon Using Chlorine Trifluoride Molecular Beam", *J. Vac. Sci. Technol. B* **10,** 175 (1992).

T. YAMAGUCHI, J. MATSUFUSA, and A. YOSHIDA, "Optical Transitions in RF Sputtered $CuIn_xGa_{1-x}Se_2$ Thin Films", *Jpn. J. Appl. Phys.* **31,** L703 (1992).

T. YAMAGUCHI, J. MATSUFUSA, and A. YOSHIDA, "Thin Films of $CuInSe_2$ Prepared by RF Sputtering from Various Compositional Powder Targets", *Solar Energy Mat.* **27,** 25 (1992).

Y. SAITO, M. HIRABARU, and A. YOSHIDA, "Plasmaless Dry Etching of Silicon Nitride Films with Chlorine Trifluoride Gas", *IEICE TRANS. ELECTRON.* **E75-C,** 834 (1992).

Y. SAITO and A. YOSHIDA, "Vacuum-ultraviolet-light-induced Defects in Hydrogenated Amorphous Silicon Films", *Philos. Mag. B* **66,** 219 (1992).

Q.X. GUO, O. KATO, and A. YOSHIDA, "Chemical Etching of Indium Nitride", *J. Electrochem. Soc.* **139,** 2008 (1992).

S. SATO and T. OHMORI, "IR Study on the Photochemistry and Adsorption States of Iron Carbonyls Adsorbed on Alumina.", *J. Phys. Chem.* **95,** 7778 (1991).

T. OHMORI and S. SATO, "Effects of Surface Basic Sites on the Photolysis of Iron Carbonyls Adsorbed on Silica.", *J. Photochem. Photobio. A:Chem.* **64,** 201 (1992).

Y. UKISU, S. SATO, and T. OHMORI, "Photochemistry of Iron Pentacarbonyl Adsorbed on Titanium Dioxide.", *Appl. Organomet. Chem.* **5,** 243 (1991).

Y. UKISU, S. SATO, G. MURAMATSU, and K. YOSHIDA, "Surface Isocyanate Intermediate Formed during the Catalytic Reduction of Nitrogen Oxide in the Presence of Oxygen and Propylene.", *Catal. Lett.* **11,** 177 (1991).

T. KAWAMOTO and Y. KUSHI, "Synthesis and Characterization of Trinuclear Metal Complex Showing Helical Chirality", *Chem. Lett.* 297 (1992).

T. KAWAMOTO and Y. KUSHI, "Carbon-Carbon Bond Formation in Helical Nickel (II) Complex, cis-Bis[2-N-(phenylmethylideneamine) benzenethiolato]nickel (II)", *Chem. Lett.* 893 (1992).

H. SHIMOMURA, S. KOMORITA, H. KUMA, and Y. KUSHI, "Rotamers of 1-Phenylethylamine Ligands in (R,S)- and (S,S)-trans-Bis(succinimidato)bis(1-phenylethylamine)palladium (II) Complexes", *Chem. Lett.* 913 (1992).

T. KAWAMOTO and Y. KUSHI, "Crystal and Molecular Structure of Tetra palladium Cluster with a C,N,S-Tridentate Ligand", *Chem. Lett.* 1057 (1992).

Y. SOHRIN, H. KOKUSEN, S. KIHARA, M. MATSUI, Y. KUSHI, and M. SHIRO, "X-ray Structure of $[Be[B(pz)_4]_2]$ and $[Be_3(OH)_3\{HB(pz)_3\}_3]$", *Chem. Lett.*, 1823 (1992).

T. KAWAMOTO and Y. KUSHI, "Helical Bis[2-N-(ferrocenylmethylenamino)benzenethiolato]M (II) Complexes (M=Ni, Zn and Pd), and a Related Merculy (II) Complex", *J. Chem. Soc. Dalton Trans.* 3137 (1992).

Y. MATSUURA, K. OKUDE, H. ICHIDA, T.K. MIYAMOTO, and Y. SASAKI, "[(1R,2R)-1,2-Diaminocyclohexane]bis(5-phenyldibenzo-[b,d]phophole)platinum (II) Dinitrate Dihydrate, *Acta Crystallogr., Sect. C* **48,** 357 (1992).

N. SATO and Y. FUKUDA, "Anion-Sensing Electrodes Based on Nickel (II) Mixed Ligand Complexes", *Chem. Lett.* 399 (1992).

F. KAWAIZUMI, S. KODA, M. KIMURA, and H. NOMURA, "Dissolved State of Ionene Polymers in Water-Acetone and Their Relation to Ionic Partial Molar Adiabatic Compressibility and Volume." *J. Solution Chem.* **20,** 1129 (1991).

S. KODA, T. HORI, H. NOMURA, and F. KAWAIZUMI, "Hydration of Methyl Cellulose.", *Polymer* **32,** 2806 (1991).

M. TANAKA, H. NOMURA, and F. KAWAIZUMI, "A Simple Method for the Evaluation of Enthalpy of Proton Dissociation in Water.", *Bull. Chem. Soc. Jpn.* **65,** 410 (1992).

M. OHBA, F. KAWAIZUMI, and H. NOMURA, "Effects of Molecular Conformation on the Packing Density in the Liquid State. 3. Partial Molar Volume Differences of Cis and Trans Conformers at Infinite Dilution.", *J. Phys. Chem.* **96,** 5129 (1992).

F. KAWAIZUMI, "Partial Molar Volumes of Halogeno Complexes of Platinum and Palladium in Aqueous Solutions and Differences in Volume between Tetra- and hexa-cordinated Forms.", *J. Chem. Soc., Faraday Trans.* **88,** 2351 (1992).

H. SATOH, Y. KIKUCHI, K. SATOH, T. SUZUKI, and K. SAWADA, "High Sensitive Spectrophotometer System Coupled with Solvent Extraction/Continuous Phase Separation, and Application for Simultaneous Determination of Iron (III), Copper (II) and Aluminum (III)." *Bunseki Kagaku* **40,** T119 (1991).

H. SATOH, Y. KIKUCHI, T. SUZUKI, and K. SAWADA, "Determination of Trace Amount of Copper by a Highly Sensitive Spectrophotometer System Based on Solvent Extraction/Continuous Phase Separation," *Bunseki Kagaku* **40,** T167 (1991).

K. SAWADA, M. KURIBAYASHI, T. SUZUKI, and H. MIYAMOTO, "Protonation Equilibria of Nitrilotris(methylenephosphonato)- and Ethylenediaminetetrakis(methylene-phosphonato)-Complexes of Scandium, Yttrium, and Lanthanoids," *J. Solution Chem.* **20,** 829 (1991).

Y. KIKUCHI, N. TAKAHASHI, T. SUZUKI, and K. SAWADA, "Liquid Extraction of Alkali Metal Ions with Non-ionic Surfactant Having Poly(oxyethylene) Chain," *Anal. Chim. Acta* **256,** 311 (1992).

Y. KIKUCHI, Y. NOJIMA, H. KITA, T. SUZUKI, and K. SAWADA, "The Solvent Extraction and Dissociation of Alkali Metal Complex of Monodisperse Poly(oxyethylene) Derivatives with Picrate Ion." *Bull. Chem. Soc. Jpn.* **65,** 1506 (1992).

Y. KIKUCHI, T. SUZUKI, and K. SAWADA, "Liquid-Liquid Extraction of Alkaline Earth Metal Ions with Nonionic Surfactant Having Poly(oxyethylene) Chain," *Anal. Chim. Acta* **264,** 65 (1992).

M. NONOYAMA and K. NONOYAMA, "Cyclometallation of N,N- Dimethyl-furan-2(and 3)-carboselenoamide with Palladium (II), Rhodium (III), and Ruthenium (II)", *Polyhedron* **10,** 2265 (1991).

K. WAIZUMI, H. MASUDA, H. OHTAKI, M.Y. SCRIPKIN, and K.A. BURKOV, "Crystallographic Investigations of $[Mg(H_2O)_6]XCl_3$ Double Salts (X^+=K^+, Rb^+, Cs^+, NH_4^+): Crystal Structure of $[Mg(H_2O)_6]CsCl_3$", *Amer. Mineralogist* **76,** 1884 (1991).

H. OHTAKI and N. FUKUSHIMA, "Nucleation Processes of NaCl and CsF Crystals from Aqueous Solutions Studied by Molecular Dynamics Simulations", *Pure & Appl. Chem.* **63,** 1743 (1991).

Y. TAMURA, H. OHTAKI, and I. OKADA, "An MD Simulation of Concentrated Aqueous Solutions of Caesium Iodide", *Z. Naturforsch.* **46a,** 1083 (1991).

H. OHTAKI and N. FUKUSHIMA, "A Structural Study of Saturated Aqueous Solutions of Some Alkali Halides by X-Ray Diffraction", *J. Solution Chem.* **21,** 23 (1992).

H. OHTAKI, "An Attempt to Parameterize the Structuredness of Solvents", *J. Solution Chem.* **21,** 39 (1992).

T. RADNAI, S. ISHIGURO, and H. OHTAKI, "X-Ray Diffraction Studies on the Structure of the Tri- and Tetrathiocyanatomanganate(II) Complexes and Solvated Lithium Ion in *N,N*-Dimethylformamide", *Bull. Chem. Soc. Jpn.* **65,** 1445 (1992).

K. WAIZUMI, H. MASUDA, and H. OHTAKI, "X-Ray Structural Studies of $FeBr_2 \cdot 4H_2O$, $CoBr_2 \cdot 4H_2O$, $NiCl_2 \cdot 4H_2O$, and $CuBr_2 \cdot 4H_2O$. *cis/trans* Selectivity in Transition Metal(II) Dihalide Tetrahydrate", *Inorg. Chim. Acta* **192,** 173 (1992).

K. OZUTSUMI, T. TAKAMUKU, S. ISHIGURO, and H. OHTAKI, "EXAFS and X-ray Diffraction Studies on the Structure of the Tetrathiocyanatocadmate(II) Complex in Dimethyl Sulfoxide", *Bull. Chem. Soc. Jpn.* **65,** 2104 (1992).

K. WAIZUMI, H. OHTAKI, H. MASUDA, N. FUKUSHIMA, and Y. WATANABE, "Density Functional Calculations on the Geometries and Dissolciation Energies of $[M(H_2O)_6]^{2+}$ Ion. M^{2+}=Cr^{2+}, Mn^{2+}, Fe^{2+}, Co^{2+}, Ni^{2+}, Cu^{2+}, and Zn^{2+}", *Chem. Lett.* 1489 (1992).

E. KIMURA, H. KUROSAKI, T. KOIKE, and K. TORIUMI, "X-ray Structural Study of Zinc (II) Inclusion Complex of a Phenolate-Pendant Cyclam", *J. Inclusion Phenomena* **12,** 377 (1992).

E. KIMURA, T. KOIKE, M. SHIONOYA, and M. SHIRO, "A Versatile Macrocyclic [12]aneN$_3$ for Interconversion of Tetrahedral and Trigonal Bipyramidal Zinc (II) Complexes. Relevance to Four- ⇄ Five-Coordinate Geometries of Zinc (II) in Carbonic Anhydrase", *Chem. Lett.* 787 (1992).

T. KOIKE, E. KIMURA, I. NAKAMURA, Y. HASHIMOTO, and M. SHIRO, "The First Anionic Sulfonamide-Binding Zinc (II) Complexes with a Macrocyclic Triamine: Chemical Verification of the Sulfonamide Inhibition of Carbonic Anhydrase", *J. Am. Chem. Soc.* **114,** 7338 (1992).

E. KIMURA, H. KUROSAKI, Y. KUROGI, M. SHIONOYA, and M. SHIRO, "pH-Dependent Coordination Mode of New Bleomycin Synthetic Analogues with Copper (II), Iron (II), and Zinc (II)", *Inorg. Chem.* **31,** 4314 (1992).

E. KIMURA, X. BU, M. SHIONOYA, S. WADA, and S. MARUYAMA, "A New Nickel (II) Cyclan Complex Covalently Attached to Ru(phen)$^{2+}$. A New Candidate for the Catalytic Photoreduction of Carbon Dioxide", *Inorg. Chem.* **31,** 4542 (1992).

E. KIMURA, M. SHIONOYA, A. HOSHINO, T. IKEDA, and Y. YAMADA, "A Model for Catalytically Active Zinc (II) Ion in Liver Alcohol Dehydrogenase: A Novel "Hydride Transfer" Reaction Catalyzed by Zinc (II)-Macrocyclic Polyamine Complexes", *J. Am. Chem. Soc.* **114,** 10134 (1992).

Y. KURODA, T. SERA, and H. OGOSHI, "Regioselectivities and Stereoselectivities of Singlet Oxygen Generated by Cyclodextrin Sandwiched Porphyrin Sensitization", *J. Am. Chem. Soc.* **113,** 2937 (1991).

Y. AOYAMA, M. ASAGAWA, Y. MATSUI, and H. OGOSHI, "Two-Point hydrogen-Bonding Strategy for the Construction of Face-to-face Porphyrin-Quinone Architectures: Molecular Recognition of Quinones", *J. Am. Chem. Soc.* **113,** 6233 (1991).

Y. AOYAMA, S. NONAKA, T. MOTOMURA, H. TOI, and H. OGOSHI, "Multi-Point Interaction of Phosphates with Protonated Porphyrins. Discrimination of Monoalkyl and Dialkyl Phosphates", *Chem. Lett.* 1241 (1991).

T. EMA, Y. KURODA, and H. OGOSHI, "Selective Syntheses of Unsymmetric Meso-Arylporphyrins", *Tetrahedron Lett.* **32**(35), 4259 (1991).

Y. KOBUKE, M. YAMANISHI, I. HAMACHI, H. KAGAWA, and H. OGOSHI, "A New Transmembrene Electron Channel Containing Flavin Units.", *J. Chem. Soc., Chem. Comm.* 895 (1991).

H. OGOSHI, Y. SUZUKI and Y. KURODA, "Olefin Oxidation Catalyzed by Electron Deficient Metalloporphyrin", *Chem. Lett.* 1574 (1991).

H. OGOSHI, H. HATAKEYAMA, J. KOTANI, A. KAWASHIMA, and Y. KURODA, "New Mode of Porphyrin Complexation with Nucleobase", *J. Am. Chem Soc.* **113,** 8181 (1991).

T. YOSHIMURA, H. TOI, S. INABA, and H. OGOSHI, "Iron (III) Porphyrin Substituted with Highly Electron Withdrawing CH_3 Groups: Electronic Absorption, MCD, and EPR Spectral Study", *Inorg. Chem.* 30, 23, 4315 (1991).

Y. KOBUKE, Y. SUMIDA, M. HAYASHI, and H. OGOSHI, "Metall-unterstutzte Organization statt Praorganisation beim Aufbau Makrocyclische Wirte", *Angew. Chem.* **103,** 1513 (1991).

A. SUZUKI, H. TOI, Y. AOYAMA, and H. OGOSHI, "Synthesis of 1-Fluoro-1-demethylmosoporphyrin-IX", *Heterocycles* **33,** 87, (1992).

T. YOSHIMURA, H. TOI, S. INABA, and H. OGOSHI, "Bis(1-methylimidazole)iron (II) Complexes of Porphyrins Substituted with Highly Electron-Withdrawing CF_3 Groups; Electronic Spectra with Split Q-Band and MCD Spectra with Unusal Features", *Bull. Chem. Soc. Jpn.* **65,** 1915 (1992).

M. ASAKAWA, H. TOI, Y. AOYAMA, and H. OGOSHI, "Remarkably Slow N-H Tautomerism in Meso-Monosubstituted Octaethylporphyrins as Studied by Variable-Temperature Dynamic ^{1}H NMR Line-Shape Analysis", *J. Org. Chem.* **57,** 5796 (1992).

D.K. MOON, T. MARUYAMA, K. OSAKADA, and T. YAMAMOTO, "Chemical Oxidation of Polyaniline by Radical Generating Reagents, O_2, H_2O_2-$FeCl_3$ Catalyst, and Dibenzoyl Peroxide", *Chem. Lett.* 1633 (1991).

T. YAMAMOTO, A. TANIGUCHI, S. DEV, E. KUBOTA, K. OSAKADA, and K. KUBOTA, "New Organosols of Nickel Sulfide, Palladium Sulfide, Manganese Sulfide, and Mixed Metal Sulfides and Their Use in Preparation of Semiconducting Polymer-metal Sulfide Composites", *Colloid Polym. Sci.* **269,** 969 (1991).

T. ITO, S. SUGIMOTO, T. OHKI, T. NAKANO, and K. OSAKADA, "Reaction of Bis(cyclopentadienyl)hydridophenyltungsten (IV) with Carboxylic Acids, Carbon Dioxide, and Related Compounds", *J. Organomet. Chem.* **428,** 69 (1992).

T. YAMAMOTO, S. WAKABAYASHI, and K. OSAKADA, "Mechanism of C-C Coupling Reaction of Aromatic Halide to Give Biaryl Promoted by Ni(cod)$_2$ in the Presence of 2,2′-Bipyridine and PPh_3", *J. Organomet. Chem.* **428,** 223 (1992).

F. OZAWA, T.I. SON, S. EBINA, K. OSAKADA, and A. YAMAMOTO, "Preparation and Properties of (π-Allyl)palladium and -platinum Carbonato Complexes", *Organometallics* **11,** 171 (1992).

K. OSAKADA, A. TANIGUCHI, E. KUBOTA, S. DEV, K. TANAKA, K. KUBOTA, and T. YAMAMOTO, "New Organosols of CuS, CdS, ZnS, HgS, NiS, and Mixed Metal Sulfides in N,N-dimethylformamide, and Dimethylsulfoxide. Preparation Characterization, and Physical Properties.", *Chem. Mater.* **4,** 562 (1992).

T. YAMAMOTO, A. TANIGUCHI, E. KUBOTA, S. DEV, K. TANAKA, K. OSAKADA, and M. SUMITA "Electrically Conducting Metal Sulfide-Polymer Composites Prepared by Using Organosols of Metal Sulfides", *Chem. Mater.* **4,** 570 (1992).

T. YAMAMOTO, M. SHIMURA, K. OSAKADA, and K. KUBOTA, "Random π-Conjugated Copolymers Constituted of Electron-donating Thiophene Units and Electron-accepting Pyridine Units", *Chem Lett.* 1003 (1992).

T. ITO, S. KURISHIMA, M. TANAKA, and K. OSAKADA "Oxidative Addition of N-Substituted Amides to Molybdenum (II) Involving N-H Bond Cleavage to Give (η^2-N-Acylamido-N,O)hydridomolybdenum (II) Complexes: X-ray Molecular Structure of the Seven-coordinate Complex $MoH\{N(COCH_3)(CH_3)\}\{(C_6H_5)_2PCH_2CH_2P(C_6H_5)_2\}_2]$", *Organometallics* **11,** 2333 (1992).

K. NAKAJIMA, N. TOKIDA*, M. KOJIMA, and J. FUJITA*** "Structure of Two Geometrical Isomers of Dioxo[(*S*)-*N*-salicylidene-3-aminopyrrolidine]vanadium (V)", *Bull. Chem. Soc. Jpn.* **65,** 1725 (1992).

T. TANAKA and K. TANAKA, "Chemical Simulation of the Nitrogen Cycle and the Carbon Dioxide Fixation in Microbial System.", *Trends in Inorganic Chemistry* **1,** 41 (1991).

N. KOMEDA, H. NAGAO, T. MATSUI, G. ADACHI, and K. TANAKA, "Electrochemical Carbon Dioxide Fixation to Thioesters Catalyzed by $[Mo_2Fe_6S_8(SEt)_9]^{3-}$.", *J. Am. Chem. Soc.* **114,** 3625 (1992).

H. TANAKA, H. NAGAO, S-M. PENG, and K. TANAKA, "Crystal Structure of *cis*-(Carbon monoxide)(η^1-carbon dioxide)bis(2,2′-bipyridyl)ruthenium, an Active Species in Catalytic CO_2 Reduction Affording CO and $HCOO^-$.", *Organometallics* **11,** 1450 (1992).

H. KAMBAYASHI, M. NAKAMOTO, S.M. PENG, and K. TANAKA, "Crystal Structure of $(Ph_4As)_2[Fe_4S_4(SAd)_4]$ and Stabilization of $[Fe_4S_4(SAd)_4]^-$ State in Aqueous Media.", *Chem. Lett.* 919 (1992).

H. TANAKA, H. NAGAO, and K. TANAKA, "Synthesis and Characterization of Bis(2,2′-bipyridyl)nitrocarbonylruthenium (II) Hexafluorophosphate." *Inorg. Chem.* **31,** 1971 (1992).

H. TANAKA, B.C. TZENG, H. NAGAO, S.M. PENG, and K. TANAKA, "Structure and Bonding of *cis*-$[Ru(bpy)_2(CO)(C(O)OCH_3)](B(C_6H_5)_4) \cdot CH_3CN$(bpy=2,2′-bipyridine).", *Organometallics* **11,** 3171 (1992).

T. TAKAHASHI, M. HASEGAWA, N. SUZUKI, M. SABURI, C.J. ROUSSET, and E. NEGISHI, "Zirconium-Catalyzed Highly Regioselective Hydrosilation Reaction of Alkenes and X-ray Structures for Silyl(hydrorido)zirconocene Derivatives", *J. Am. Chem. Soc.* **113,** 8564 (1991).

C.J. ROUSSET, E. NEGISHI, N. SUZUKI, and T. TAKAHASHI, "Novel Head-to-Tail Alkyl-Alkene Coupling via Zirconium Catalyzed Reactions of Alkylmagnesium Derivatives with Monosubstituted Alkenes", *Tetrahedron Lett.* **33,** 1965 (1992).

N. SUZUKI, Y. MIYAMA, T. TAKAHASHI, H. NOGUCHI, M. SABURI, and Y. UCHIDA, "Polymerization of Epoxides Catalyzed by Early Transition Metal Compounds. Role of the Ligands of Catalysts", *J. Polymer. Sci. Lett.* **30,** 2067 (1992).

T. TAKAHASHI, N. SUZUKI, M. HASEGAWA, Y. NITTO, K. AOYAGI, and M. SABURI, "Zirconium Mediated Regioselective Carbon-Carbon Bond Formation Reactions", *Chem. Lett.* 331 (1992).

T. TAKAHASHI, K. AOYAGI, R. HARA, and N. SUZUKI, "Monohalogenation of Zirconacyclopentane Complexes via Alkylalkoxyzirconocene", *Chem. Lett.* 1693 (1992).

M. SABURI, H. TAKEUCHI, M. OGASAWARA, T. TSUKAHARA, Y. ISHII, T. IKARIYA, T. TAKAHASHI, and Y. UCHIDA, "Asymmetric Hydrogenation of Prochiral Carboxylic Acids Catalyzed by the Five-Coordinate Ruthenium (II)-Hydride Complex $[RuH(binap)_2]PF_6$ (binap=(R)- or (s)-2,2′-bis(diphenylphosphino)-1,1′=binaphthyl), *J. Organometal. Chem.* **428,** 155 (1992).

E. NEGISHI, T. NGUYEN, J.P. MAYE, D. CHOUEIRI, D.R. SWANSON, N. SUZUKI, and T. TAKAHASHI, "Factors Affecting the Unusual Reactivity Order in the β-Hydrogen Abstraction of Dialkylzirconocenes", *Chem. Lett.* 2367 (1992).

K. NAKATA, A. NAGASAWA, N. SOYAMA, Y. SASAKI, and T. ITO, "Kinetic Studies on the Terminal-Ligand Substitution Reactions of Acetate-Bridged Trinuclear Molybdenum and Tungsten Cluster Complexes, $[Mo_3(\mu_3\text{-}CCH_3)(\mu_3\text{-}O)(\mu\text{-}CH_3COO)_6(L)_3]^+$ (L=H_2O or pyridine) and $[W_3(\mu_3\text{-}O)(\mu\text{-}CH_3COO)_6(H_2O)_3]^{2+}$" *Inorg. Chem.* **30,** 1575 (1991).

T. OCHI, Y. SASAKI, T. YAMAGUCHI, and T. ITO, "Rapid Unidentate-Chelate Equilibrium of Acetate Ligands on the Ruthenium-Analog of the Hemerythrin Active Center and the Crystal structure of $[Ru_2(\mu\text{-}O)(\mu\text{-}CH_3COO)_2(CH_3COO)_2(H_2O)(CH_3OH)(P(C_6H_5)_3)_2] \cdot H_2O$ Having Unidentate Acetates", *Chem. Lett.* 2019 (1991).

H. KATO, K. NAKATA, A. NAGASAWA, T. YAMAGUCHI, Y. SASAKI, and T. ITO, "Preparation and Properties of Oxo-Centered Trinuclear Chromium (III) Complexes with Bridging Optically Active Amino Acids, $[Cr_3(\mu_3\text{-}O)(\mu\text{-}O,O'\text{-aminoacid})_6(H_2O)_3]^{7+}$", *Bull. Chem. Soc. Jpn.* **64,** 3463 (1991).

Y. SASAKI, M. SUZUKI, A. NAGASAWA, A. TOKIWA, M. EBIHARA, T. YAMAGUCHI, C. KABUTO, T. OCHI, and T. ITO, "Preparation, Structure, and Properties of the Bis (μ-acetato)(μ-oxo) Ruthenium (III) Dimers $[Ru_2(\mu\text{-}CH_3COO)_2(\mu\text{-}O)(py)_6]^{2+}$ and $[Ru_2(\mu\text{-}CH_3COO)_2(\mu\text{-}O)(bpy)_2(py)_2]^{2+}$", *Inorg. Chem.*, **30,** 4903 (1991).

D. AKASHI, H. KIDO, Y. SASAKI, and T. ITO, "Preparation and Electrochemical Responce of Poly (4-vinyl-pyridine)-Coordinated Oxo-acetato Triruthenium Cluster Film", *Chem. Lett.* 143 (1992).

H. KOBAYASHI, N. URYU, A. TOKIWA, T. YAMAGUCHI, Y. SASAKI, and T. ITO, "Magnetic Properties of Oxygen Centered Trinuclear Ruthenium (III) and Rhodium (III) Complexes", *Bull. Chem. Soc. Jpn.* **65,** 198 (1992).

M. ABE, Y. SASAKI, A. NAGASAWA, and T. ITO, "Kinetic Studies on the Terminal Pyridine Exchange Reactions of Some Oxo-Acetate Bridged Trinuclear Ruthenium Complexes. Influence of the Metal Oxidation State and Non-leaving Terminal Ligand (CO)", *Bull. Chem. Soc. Jpn.* **65,** 1411 (1992).

M. ABE, Y. SASAKI, T. YAMAGUCHI, and T. ITO, "X-ray Structure, Ligand Substitution, and Other Properties of Trinuclear Ruthenium Complexes, $[Ru_3(\mu_3\text{-}O)(\mu\text{-}C_6H_5COO)_6(py)_3](PF_6)$ (py=pyridine), and X-ray Structure of Dinuclear Ruthenium Complexes, $[Ru_2(\mu\text{-}C_6H_5COO)_4Cl]$", *Bull. Chem. Soc. Jpn.* **65,** 1585 (1992).

K. NAKATA, T. YAMAGUCHI, Y. SASAKI, and T. ITO, "Synthesis of Trinuclear Molybdenum Cluster Complex with Novel Skeleton, $[Mo_3(\mu_3\text{-}CCH_3)(\mu_3\text{-}O)(\mu\text{-}C_6H_5COO)_6(CH_3OH)_3]Cl$ through Bridging Carboxylate Ligand Substitution", *Chem. Lett.* 983 (1992).

Y. IHARA, Y. SATAKE, Y. FUJIMOTO, H. SENDA, M. SUZUKI, and A. UEHARA, "X-Ray Crystal Structures of Octahedral Diaqua-bis(N,N-dialkylethylenediamine)nickel (II) Complexes Possessing Elongated Nickel (II)-Nitrogen Bonds along Axial Direction", *Bull. Chem. Soc. Jpn.* **64,** 2349 (1991).

Y. IHARA, Y. SATAKE, M. SUZUKI, and A. UEHARA, "Cis-Trans Isomerization among the Octahedral Daiquabis(N,N- or N,N'-dialkylethylenediamine)nickel (II) Complexes and Their Thermal Reaction Products", *Bull. Chem. Soc. Jpn.* **64,** 3647 (1991).

M. SUZUKI, Y. HAYASHI, K. MUNEZAWA, M. SUENAGA, H. SENDA, and A. UEHARA, "Synthesis and Characterization of a Novel Dimer of Di(μ-oxo)manganese Dimers with Two coordinated Water Molecules in (III, IV, III, IV) Oxidation State", *Chem. Lett.* 1929 (1991).

E. ITO, K. YAMAMOTO, M. FUNATO, M. SUZUKI, and A. UEHARA, "Preparation of Chromium (III) Complexes with a series of tetra-azacycloalkanes, [12]aneN$_4$ to [16]aneN$_4$, and Solid-State Thermal Isomerization of cis-$[CrCl_2([15]aneN_4$ or [16]aneN$_4)]^+$", *Thermochim. Acta* **195,** 51 (1992).

E. ITO, M. SUZUKI, and A. UEHARA, "Thermal Isomerization of cis$[CrCl_2([15]aneN_4)]SCN$ in Solid State", *Thermochim. Acta* **195,** 329 (1992).

Y. HAYASHI, M. SUZUKI, A. UEHARA, Y. MIZUTANI, and T. KITAGAWA, "(μ-Alkoxo)diiron (II, II) Complexes of N,N,N',N'-Tetrakis[2-(6-methyl-pyridyl)methyl]-1,3-diaminopropane-2-olate and the Reversible Formation of the O_2-Adducts", *Chem. Lett.* 91 (1992).

Y. YAMASHITA, T. SUZUKI, Y. KOBAYASHI, T. MUKAI, and T. MIYASHI, "Preparation and Properties of Tetracyanoquinodimethane radical-anion salts with azaazulenium and diazaazulenium ions", *Synthetic Metals* **45,** 213 (1991).

Y. YAMASHITA, S. TANAKA, and M. TOMURA, "Structure and Redox Reactions of Tricyclic Pyridinium N-Imines", *Heterocycles* **33,** 47 (1992).

Y. TSUBATA, T. SUZUKI, Y. YAMASHITA, T. MUKAI, and T. MIYASHI, "Tetracyanoquinodimethanes Fused with 1,2,5-Thiadiazole and Pyrazine Units", *Heterocycles* **33,** 337 (1992).

Y. YAMASHITA, S. TANAKA, K. IMAEDA, H. INOKUCHI, and M. SANO, "4,7-Bis(1,3-dithiol-2-ylidene)-4,7-dihydro-2,1,3-benzothiadiazoles. A Novel Type of Electron Donors Affording Organic Metals", *Chem. Lett.* 419 (1992).

Y. YAMASHITA, S. TANAKA, and M. TOMURA, "Tetrathio-Derivatives of *p*-Quinodimethanes Fused with Selenadiazole Units", *Phosphorous, Sulfur, and Silicon* **67,** 327 (1992).

T. SUZUKI, H. FUJII, Y. YAMASHITA, C. KABUTO, S. TANAKA, M. HARASAWA T. MUKAI, and T. MIYASHI, "Clathrate Formation and Molecular Recognition by Novel Chalcogen-Cyano Interactions in Tetracyanoquinodimethanes Fused with Thiadiazole and Selenadiazole Rings", *J. Am. Chem. Soc.* **114,** 3034 (1992).

T. SUZUKI, H. SHIOHARA, M. MONOBE, T. SAKIMURA, S. TANAKA, Y. YAMASHITA, and T. MIYASHI, "Tetrathienylethylenes, a New Class of Electron Donors-Dications Twisted by 90° Stabilized by Formation of Polymethine Units", *Angew. Chem. Int. Ed. Engl.* **31,** 455 (1992).

F. MISAIZU, K. TSUKAMOTO, M. SANEKATA, and K. FUKE, "Photoionization of Clusters of Cs Atoms Solvated with H_2O, NH_3, and CH_3CN", *Chem. Phys. Lett.* **188,** 241 (1992).

F. MISAIZU, M. SANEKATA, K. TSUKAMOTO, and K. FUKE, "Photodissociation of Size-Selected $Mg^+(H_2O)_n$ Ions for n=1 and 2", *J. Phys. Chem.* **96,** 8259 (1992).

H. UMEMOTO, T. OHNUMA, H. IKEDA, S. TSUNASHIMA, K. KUWAHARA, F. MISAIZU, and K. FUKE, "Intersystem Crossing and Intramultiplet Mixing of Excited Zn Atoms by Xe", *J. Chem. Phys.* **97,** 3282 (1992).

K. FUKE, F. MISAIZU, K. TSUKAMOTO, and M. SANEKATA, "Photoionization of Solvated Cs Atoms", in "Physics and Chemistry of Finite Systems: From Clusters to Crystals, Vol. II", ed. by P. Jena, S.N. Khanna, and B.K. Rao, Kluwer Academic, p.925 (1992).

A. IZUOKA, M. FUKADA, T. SUGAWARA, M. SAKAI, and S. BANDOW, "Magnetic Property of 1,3,5-Tris(4',4',5',5'-tetramethylimidazolin-2'-yl)benzene 3',3",3"'-Trioxide 1',1",1"'-Trioxyl in 1:1 Mixed Crystals with 1,3,5-Trinitrobenzene", *Chem. Lett.* 1627 (1992).

S. BANDOW, H. KITAGAWA, T. MITANI, H. INOKUCHI, Y. SAITO, H. YAMAGUCHI, N. HAYASHI, H. SATO, and H. SHINOHARA, "Anaerobic Sampling and Characterization of Lanthano-Fullerenes: Extraction of LaC_{76} and other LaC_{2n}", *J. Phys. Chem.* **96,** 9609 (1992).

K. AWAGA, T. INABE, U. NAGASHIMA, T. NANAMURA, M. MATSUMOTO, Y. KAWABATA, and Y. MARUYAMA, "α-Nitronyl Nitroxide Cation Radicals", *Chem. Lett.* 1777 (1991).

K. AWAGA, T. INABE, and Y. MARUYAMA, "Ferromagnetic Intermolecular Interaction and Crystal Structure of the *p*-Pyridyl Nitronyl Nitroxide Radical", *Chem. Phys. Lett.* **180,** 327 (1992).

K. AWAGA, T. INABE, T. NANAMURA, M. MATSUMOTO, and Y. MARUYAMA, "Ferromagnetic and Antiferromagnetic Intermolecular Interactions in the Two-Dimensional Triangular Lattice of an a-Nitronyl Nitroxide Cation Radical, 2-(3-N-Methylpyridinium)-4,4,5,5-tetrametyl-4,5-dihydro-1H-imidazol-1-oxyl 3-*N*-Oxide", *Chem. Phys. Lett.* **195,** 21 (1992).

H. OKAMOTO, T. MITANI, K. TORIUMI, and M. YAMASHITA, "Control of CDW State in Halogene-Bridged Metal Complexes.", *Material Science and Engineering* **B13,** L9 (1992).

H. OKAMOTO, K. TORIUMI, T. MITANI, and M. YAMASHITA, "Control of CT Instability in 1-D Mixed-Valence Systems.", *Mol. Cryst. Liq. Cryst.* **218,** 247 (1992).

H. KITAGAWA, N. KOJIMA, N. MATSUSHITA, T. BAN, and I. TSUJIKAWA, "Studies of Mixed-Valence States in Three-Dimensional Halogen-Bridged Gold Compounds, $Cs_2Au^{I}Au^{III}X_6$ (X=Cl, Br, I). Part 1. Synthesis, X-Ray Powder Diffraction, and Electron Spin Resonance Studies of $CsAu_{0.6}Br_{2.6}$.", *J. Chem. Soc., Dalton Trans.* 3115 (1991).

H. KITAGAWA, N. KOJIMA, and T. NAKAJIMA, "Studies of Mixed-Valence States in Three-Dimensional Halogen-Bridged Gold Compounds, $Cs_2Au^{I}Au^{III}X_6$ (X=Cl, Br, I). Part 2. X-Ray Photoelectron Spectroscopic Study.", *J. Chem. Soc., Dalton Trans.* 3121 (1991).

H. KITAGAWA, N. KOJIMA, and H. SAKAI, "Studies of Mixed-Valence States in Three-Dimensional Halogen-Bridged Gold Compounds, $Cs_2Au^{I}Au^{III}X_6$ (X=Cl, Br, I). Part 3. Gold-197 Mössbauer Spectroscopic Study.", *J. Chem. Soc., Dalton Trans.* 3211 (1991).

T. MITANI, H. KITAGAWA, H. OKAMOTO, J. TOYODA, K. NAKASUJI, and M. YAMASHITA, "A New Molecular System: Cooperation of Transition Metal Chain and CT Stack *via* Intermolecular H-Bonds.", *Mol. Cryst. Liq. Cryst.* **216,** 73 (1992).

K. OKANIWA, H. OKAMOTO, T. MITANI, T. INABE, J. TOYODA, Y. MORITA, K. NAKASUJI, H. YAMAMOTO, T. DENO, and S. HONMA, "Intra- and Inter-Molecular Charge Transfer Interactions in H-Bonded DTPP Crystals.", *Mol. Cryst. Liq. Cryst.* **216,** 241 (1992).

M. YAMASHITA, Y. WADA, K. TORIUMI, and T. MITANI, "Mott-Hubbard State in One-Dimensional Iodo-Bridged Binuclear Metal Dithioacetato Complexes, $M_2(dta)_4I$ (M=Pt and Ni).", *Mol. Cryst. Liq. Cryst.* **216,** 207 (1992).

N. HOSHINO, H. TAKAHASI, Y. MATSUNAGA, H. OKAMOTO, and T. MITANI, "Thermotropic Mesophases of Benzene Derivatives with Terminally Hydroxylated Groups.", *Mol. Cryst. Liq. Cryst.* **216,** 265 (1992).

T. INABE, I.G.G. LUNEAU, N. HOSHINO, K. OKANIWA, H. OKAMOTO, T. MITANI, U. NAGASHIMA, and Y. MARUYAMA, "Structure and Optical Properties of Thermochromic Shiff Base. Charge Transfer Interaction and Proton Transfer in the N-Tetrachlorosalicylideneaniline and N-Tetrachlorosalicylidene-1-Pyrenylamine Crystals", *Bull. Chem. Soc. Jpn.* **64,** 801 (1991).

S. TAKEDA, H. CHIHARA, T. INABE, T. MITANI, and M. MARUYAMA, "NMR Study of Proton Dynamics in the NHO Hydrogen Bonds in the Thermochromic Crystals of N-Salicylidenanilines.", *Chem. Phys.* **189,** 13 (1992).

T. INABE, K. OKANIWA, H. OKAMOTO, T. MITANI, Y. MARUYAMA, and S. TAKEDA, "Proton Transfer in the N-Salicylidenanilines-Effect of the Charge Transfer Interaction.", *Mol. Cryst. Liq. Cyst.* **216,** 229 (1992).

M. TOMURA, T. MITANI, and M. TOMURA, "Phase Transition of Excited State of a Pyren Single Cryatal.", *Mol. Cryst. Liq. Cryst.* **218,** 67, (1992).

Y. KANEMATSU, J.S. AHN, and T. KUSHIDA "Resonance Fluorescence Spectra of Dye-Doped Polymers.", *J. Lumin.* **53,** 235 (1992).

M. FUJITA, H. NAKAGAWA, K. FUKUI, H. MATSUMOTO, T. MIYANAGA, and M. WATANABE, "Polarized Reflection Spectra of Orthorhombic $PbCl_2$ and $PbBr_2$", *J. Phys. Soc. Jpn.* **60,** 4393 (1991).

E. ISHIGURO, K. YAMASHITA, H. OHASHI, M. SAKURAI, O. AITA, M. WATANABE, K. SANO, M. KOEDA, and T. NAGANO, "Fabrication and Characterization of Reactive Ion Beam Etched SiC Gratings", *Rev. Sci. Instr.* **63,** 1439 (1992).

M. WATANABE, G. ISOYAMA, M. KAMADA, and K. KIMURA, "Status of the UVSOR Facility – 1991", *Rev. Sci. Instr.* **63,** 1584 (1992).

T. MURATA, T. MATSUKAWA, S. NAOE, T. HORIGOME, O. MATSUDO, and M. WATANABE, "Soft X-Ray Beamline BL7A at the UVSOR", *Rev. Sci. Instr.* **63,** 1309 (1992).

K. YAMASHITA, S. TAKAHASHI, S. KITAMOTO, S. TAKAHAMA, T. TAMURA, I. HATSUKADE, M. SAKURAI, M. WATANABE, A. YAMAGUCHI, H. NAGATA, and M. OHTANI, "Characterization of Multilayer Reflectors and Position Sensitive Detectors in the 45-300 Å Region", *Rev. Sci. Instr.* **63,** 1513 (1992).

K. YAMASHITA, M. WATANABE, O. MATSUDO, J. YAMAZAKI, I. HATSUKADE, T. ISHIGAMI, S. TAKAHAMA, K. TAMURA, and M. OHTANI, "Characterization of Platinum-Carbon, Tungsten-Silicon, and Tungsten-B_4C Multilayers", *Rev. Sci. Instr.* **63,** 1217 (1992).

M. KAMADA, O. AITA, K. ICHIKAWA, M. OKUSAWA, and K. TSUTSUMI, "Photoelectron Spectroscopic Study of the Decay Process of Excited 4d States in Cesium Halides", *Phys. Rev.* **B45,** 12725 (1992).

H. OGASAWARA, A. KOTANI, B.T. THOLE, K. ICHIKAWA, O. AITA, and M. KAMADA, "La 5p Core Photoemission Spectra at the 4d-4f Resonance in LaF_3", *Solid State Commun.* **81,** 645 (1992).

K. ICHIKAWA, O. AITA, K. AOKI, M. KAMADA, and K. TSUTSUMI, "Nonradiative Decay Processes of 4d Hole States in CsF, BaF_2, and LaF_3", *Phys. Rev.* **B45,** 3221 (1992).

S. HIROSE and M. KAMADA, "Photo-Stimulated Desorption of Excited-State Alkali Atoms from Alkali-Halides Irradiated with Undulator Radiation", *J. Phys. Soc. Jpn.* **60,** 4374 (1991).

M. KAMADA and S. HIROSE, "Molecular Luminescence from Electron-Bombarded $YBa_2Cu_3O_{7-x}$", *Jpn. J. Appl. Phys.* **30,** 2802 (1991).

N. TAKAGI, N. MINAMI, S. TANAKA, and M. NISHIJIMA, "Promoted Oxidation of the K-Modified Si(100)(2X1) Surface: Electron Energy Loss Spectroscopy and Thermal Desorption Studies", *Phys. Rev.* **B44,** 12945 (1991).

A. HIRAYA, T. HORIGOME, N. OKADA, N. MIZUTANTI, K. SAKAI, O. MATSUDO, M. HASUMOTO, K. FUKUI, and M. WATANABE, "Construction of Focusing Soft X-Ray Beamline BL1A at the UVSOR", *Rev. Sci. Instr.* **63,** 1264 (1992).

T. IBUKI, A HIRAYA, and K. SHOBATAKE, "Vacuum Ultraviolet Absorption Spectra and Photodissociative Excitation of $CHBr_2Cl$ and $CHBrCl_2$", *J. Chem. Phys.* **96,** 8793 (1992).

G. ISOYAMA, "Present Status of the UVSOR Light Source", *Nucl. Instr. Meth. Phys. Res.* **A308,** 31 (1991).

A. LIN, H. HAMA, S. TAKANO, and G. ISOYAMA, "Measurement of the Bunch Length on the UVSOR Storage Ring", *Jpn. J. Appl. Phys.* **31,** 921 (1992).

Review Articles and Textbooks

H. NAKAMURA, "Semiclassical Approach to Charge Transfer Processes in Ion-Molecule Collisions", *Adv. Chem. Phys.* LXXXXII. p.243 (1992).

S. SAITO, "Laboratory and Astronomical Spectroscopy of New Interstellar Molecules.", in "*Atoms, Ions, and Molecules: New Results in Spectral Astrophysics.*", A.D. Haschick and P.T.P. Ho, Eds., Atron. Soc. Pacifi. Conf. Series Vol. **16,** pp.349–361 (1991).

S. SAITO, "Microwave Spectroscopy of Transient Molecules.", in "*Chemistry and Spectroscopy of Interstellar Molecules.*", D.K. Bohme, E. Herbst, N. Kaifu, and S. Saito, Eds., Univ. Tokyo Press, pp.103–109 (1992).

S. SAITO, "Interstellar Molecules and Chemistry of Dark Clouds.", in "*From Fields of Cosmic Studies.*", Vol. **1,** N. Kaifu Ed., Japan Soc. Prom. Sci., (in Japanese), pp.108–124 (1992).

T. KITAGAWA, T. EGAWA, T. OGURA, Y. IMAI, R. MAKINO, and Y. ISHIMURA, "Resonance Raman studies of cytochrome P-450: the O-O stretching for P-450_{cam} and the Fe-CO stretching for P-450 (ω-1) mutants.", in "*Cytochrome P-450: Biochemistry and Biophysics*", A.I. Archakov and G.I. Bachmanova, Eds., pp.83–88, INCO-TNC Joint Stock Corp., Moscow (1992).

T. KITAGAWA, Y. MIZUTANI, T. TOKUTOMI, and K. AOYAGI, "Resonance Raman spectra of pea intact phytochrome.", in "*Spectroscopy of Biological Molecules*", R.E. Hester and R.B. Girling, Eds., pp.423–426, Royal. Soc. Chem. (1991).

T. KITAGAWA, "Investigation of higher order structure of proteins by ultraviolet resonance Raman spectroscopy.", *Prog. Biophys. Mol. Biol.*, **58,** 1–18 (1992).

T. KITAGAWA, "Allosteric transition revealed by time-resolved resonance Raman spectroscopy.", *Biophysics,* (in Japanese) No.6, (1992).

K. YOSHIHARA and K. KEMNITZ, "Picosecond Dynamics of Dyes in Heterogeneous Environments", in "Photochemical Processes in Organized Molecular Systems", K. Honda, Ed., North-Holland, Amsterdam, p.117 (1991).

K. YOSHIHARA, "Introduction to Fluorescence Spectroscopy", Experimental Chemistry 4th Edition, Spectroscopy II K. Yoshihara, Ed. (in Japanese), p.339 (1991).

K. YOSHIHARA, I. YAMAZAKI, M. SUMINANI, and T. KOBAYASHI, Measurement of Fluorescence Decays, Experimental Chemistry 4th Edition, Spectroscopy II (in Japanese), K. Yoshihara, Ed., Maruzen, Tokyo p.364 (1991).

K. YOSHIHARA, "Ultrafast Molecular Dynamics", *Appl. Phys.* (in Japanese) **60,** 891 (1991).

T. KONDOW and K. SUZUKI, "Reactions Studied by Molecular Beams" (in Japanese), in "Advanced Modern Physical Chemistry", M. Seno, N. Hirota, M. Tasumi, Y. Iwasawa, Ed., Kodansha Scientific, pp.345–363 (1992).

S. HIRAYAMA, "Time-Resolved Fluorescence Microscopy", in Progress in Photo Chemistry and Photophysics Vol. 6, pp.1–42, ed. by J.F. Rabek

J. INANAGA, T. HANAMOTO, Y. YOKOYAMA, and Y. SUGIMOTO, "Samarium", in "Experimental Organometallic Chemistry for Synthetic Chemists" (in Japanese), F. Sato, K. Yamamoto, and T. Imamoto, Eds., Kodansha, Tokyo, Chapter III–2, pp.232–244 (1992).

S. KATSUMATA and K. KIMURA, "Excited Electronic States and Ionic States of Molecular Oxygen", *Appl. Spectrosc. Rev.*, **27,** 193 (1992).

M. UKAI, K. KAMETA, K. SHINSAKA, Y. HATANO, T. HIRAYAMA, S. NAGAOKA and K. KIMURA, "State Selective Ionization of O_2 in a Framework of Van der Waals Molecules", in "Synchrotron Radiation and Dynamic Phenomena", ed. by A. Beswick, American Institute of Physics, Proceedings No. 258, p.179 (1992).

M. TAKAHASHI and K. KIMURA, "Molecular Ion Vibrational Spectroscopy by a Time-Resolved REMPI Threshold Photoelectron Technique", in "Time-Resolved Vibrational Spectroscopy V", ed. by H. Takahashi, Springer-Verlag, p.327 (1992).

K. KIMURA and M. TAKAHASHI, "High-brightness cm^{-1}-resolution threshold photoelectron spectroscopic technique", in Optical Methods for Time- and State-Resolved Chemistry", ed., by C.-Y. Ng, SPIE - The International Society for Optical Engineering, Vol. 1638, p.216 (1992).

K. SHOBATAKE, "Chemical Reactions Involving Vibrational State- and Bond-Selected H_2O Molecule, *Kagaku (Chemistry) (in Japanese),* **47,** 150 (1992).

S. SATO, "Surface Photochemistry of Metal Carbonyls.", *Hyoumen Kagaku,* (in Japanese), **13,** 225 (1992).

K. SAWADA, "Analytical Chemistry" ed. by T. Kawashima, Hirokawa (in Japanese) (1992).

K. SAWADA, "Introduction to Chemical Kinetics," Bunseki (in Japanese) 2–10 (1991)

H. WAKITA and H. OHTAKI, "Molecular Structure and Physico-chemical Properties of Water", (in Japanese) *Sen-i Gakkaishi,* **48,** 44 (1992).

H. OHTAKI, "Properties of Water", (in Japanese) $\mu\alpha$, No. 6, 13 (1992).

K. OZUTSUMI and H. OHTAKI, "The Structure of Water" (pp.27–34), **H. YOKOYAMA and H. OHTAKI,** "Hydration Phenomena" (pp.47–58), **T. YAMAGUCHI and H. OHTAKI,** "Solution X-Ray Diffraction Method" (pp.126–133), in "New Science of Water and Technology for the Utilization of Water", (in Japanese) Eds. K. WATANUKI and M. KUBOTA, Science Forum, Tokyo (1992).

H. OHTAKI and H. YAMATERA, Eds., "Structure and Dynamics of Solutions", Elsevier, Amsterdam, The Netherlands (1992).

T. RADNAI, T. YAMAGUCHI, and H. OHTAKI, "Structure of Liquids and Solutions by X-Ray and Neutron Diffraction" (pp.15–24), **H. OHTAKI, N. FUKUSHIMA, and T. YAMAGUCHI,** "Structure of Solvated Ions and Metal Complexes in Solution Studied by the Diffraction Method" (pp.24–39), **H. OHTAKI and K. HEINZINGER,** "The Structures of Hydrated Ions in Aqueous Solutions as Studied by the Molecular Dynamics Simulations" (pp.105–115), **S. ISHIGURO and H. OHTAKI,** "Thermodynamic Aspects of Complex Formation Reactions in Nonaqueous Solutions" (pp.299–306), in "Structure and Dynamics of Solutions", Eds. H. OHTAKI and H. YAMATERA, Elsevier, Amsterdam, The Netherlands (1992).

E. KIMURA, "New Development in Macrocyclic Polyamine Chemistry", in Crown Ethers and Analogous Compounds", ed. by M. Hiraoka, Studies in Org. Chem., Elsevier Science Publishers, Amsterdam, **45,** 381 (1992).

K. OSAKADA and T. YAMAMOTO "Recent Development of Polymerization Using Transition Metal Complex as Catalyst", *Yukagaku,* (in Japanese) **41,** 2 (1992).

K. OSAKADA, "Spectroscopic Characterization of the Intermediate of C-H Bond Activation Promoted by Transition Metal Complexes", *Kagaku,* (in Japanese) **47,** 495 (1992).

K. TANAKA, "Simulation of Biological Carbon Dioxide Fixation." *Chemistry and Biology,* **30,** 530 (1992) (Japanese).

K. TANAKA, "Electrochemical Fixation of Carbon Dioxide.", *Chemical Industry,* **43,** 661 (1992) (Japanese).

E. NEGISHI and T. TAKAHASHI, "Zirconocene-Alkene Complexes; Their Formation, Structure and Reactions", *Reviews on Heteroatom Chem.,* **6,** 177 (1992).

T. MIYASHI, Y. YAMASHITA, and T. MUKAI, "Cage Molecules in Photochemistry" in "Carbocyclic Cage Compounds" E. Osawa and O. Yonemitsu, ed., VCH, pp.365–382 (1992).

K. FUKE, "Reactions of Small Clusters: A New Approach to Chemical Reaction Dynamics", *Shinku,* (in Japanese) **35,** 762 (1992).

K. FUKE, "Chemisorption Studies of Metal Clusters in Molecular Beam", *Shokubai (Catalyst),* (in Japanese) **34,** 13 (1992).

M. WATANABE and G. ISOYAMA, "Synchrotron Radiation and its Source" in Textbook of Experimental Chemistry, Spectroscopy II" ed. by H. Inokuchi, Maruzen (in Japanese), p.123 (1991).

E. ISHIGURO and M. WATANABE, "Vacuum Ultraviolet Monochromators and Optical Elements", in Textbook of Experimental Chemistry, Spectroscopy II" ed. by H. Inokuchi, Maruzen (in Japanese), p.200 (1991).

E. ISHIGURO, "Techniques for Vacuum Ultraviolet Spectroscopy on Gases", in Textbook of Experimental Chemistry, Spectroscopy II" ed. by H. Inokuchi, Maruzen (in Japanese), p.217 (1991).

J. YOSHINOBU, S. TANAKA and M. NISHIJIMA, "Elementary Chemical-Reaction Processes on Silicon Surfaces", *Oyo Buturi,* (in Japanese) **60,** p.1196 (1991).

AUTHOR INDEX-RESEARCH ACTIVITIES AND SPECIAL RESEARCH PROJECTS

Abe, Masaaki 124
Achiba, Yohji 33, 57, 58, 59, 64, 67, 68
Adachi, Gin-ya 121
Agosta, C.C. 59
Aita, Osamu
Akashi, Daisuke 125
Akune, Yasuhiro 146
Alfimov, Mikhail V. 36
Amatatsu, Yoshiaki 12, 13
Anchell, James L. 20
Anzai, Hiroyuki 59
Aoyagi, Katsuhiro 32
Aoyagi, Koichiro 123
Aoyama, Yasuhiro 119
Appelman, Evan 32
Aquilanti, Vincenzo 23
Asakawa, Masumi 119
Asano-Someda, Motoko 32
Awaga, Kunio 57, 138, 154

Baba, Yoshiyasu 81
Baer, Michael 22
Bandow, Shunji 136, 137, 141
Bell, Andrew J. 34, 35
Bisht, Prem B. 46, 151
Borkman, Raymond F. 40, 41
Brooks, J.S. 59
Brown, David A. 18
Bu, Xianhe 117
Burkov, Kim A. 114

Chernykh, Ludmila 114
Chiba, Takehiko 70
Chihara, Hideaki 63
Choi, Young S. 34, 35
Choueiri, Daniele 123
Christensen, Ronald L. 34, 35
Cockett, Martin C.R. 88, 90, 91, 92, 153

Danieli, R. 58
Denisov, Victor N. 58
Deno, Takashi 144
Do, Youngkyu 77
Doi, Takashi 62, 71
Dorigo, Andrea E. 15
Douhal, Abderrazzak 37, 40, 41
Dyke, John M. 91

Ebihara, Masahiro 80
Egawa, Tsuyoshi 30
Ema, Tadashi 118
Enoki, Toshiaki 70
Eu, Byung Chan 156

Fang, Shaoli 64
Fitzpatrick, Noel J. 18
Fleming, Robert J. 65
Fraunfelter, Frank A. 30
Fujii, Asuka 27, 150
Fujii, Hiroshi 130
Fujii, Toshiaki 12
Fujimoto, Hitoshi 65, 66, 67, 68
Fujimoto, Tetsuo 95, 152
Fujio, Mizue 86, 87
Fujita, Junnosuke 112, 120
Fuke, Kiyokazu 131, 132, 133, 134, 135, 136, 154
Fukuda, Kiyoshige 67
Fukuda, Yutaka 108, 109
Fukushima, Nobuhiro 113
Furuya, Kenji 93, 94

Gejo, Tatsuo 50, 51
George, Thomas F. 25
Gorecki, Jerzy 53, 54, 55, 156
Goto, Masahiro 26
Groarke, Peter J. 18
Guo, Qixin 103

Hama, Hiroyuki 144, 145
Hammerich, Audrey D. 12
Hanamoto, Takeshi 80, 81, 82, 152
Hanazaki, Ichiro 48, 49, 50, 51, 52, 53, 54, 55, 155, 156
Handa, Takashi 29
Hannahs, S.T. 59
Hara, Ryuichiro 123
Harasawa, Masako 130
Hasegawa, Maki 122, 123
Hasegawa, Shinji 59, 67, 68
Hashimoto, Fujiko 13
Hashimoto, Kenro 12, 14
Hashimoto, Shinji 31
Hashimoto, Yukie 116
Hatakeyama, Hitoshi 118
Hatanaka, Kunio 75, 155
Hattori, Hideo 99, 100, 101
Hayashi, Naoyuki 137
Hayashi, Yoshihito 31, 126, 127
Hayashida, Hiromi 117
He, Shaoren 14
Hilti, B. 60, 61
Hino, Shojun 59, 67, 68
Hirabaru, Masahiro 103
Hirabayashi, Izumi 70
Hiraya, Atsunari 96, 97, 146
Hirayama, Satoshi 72
Hirayama, Takato 93
Hirose, Sayumi 147
Hirota, Shun 32, 151

Honda, Chikako 110
Honda, Kazuhiko 128
Honda, Kazuhiro 50
Honma, Seiji 144
Horigome, Toshio 95
Hoshi, Hajime 64, 153
Hoshino, Ayumi 117
Hoshino, Naomi 153
Huh, Chul 86

Ibuki, Toshio 97
Ichida, Hikaru 108
Ichikawa, Kouichi
Ichimura, Kenji 69
Ida, Takashi 57, 59
Iitaka, Yoichi 115
Ikeda, Hiroyuki 136
Ikeda, Kumi 61
Ikeda, Takuya 117
Ikeda-Saito, Masao 30
Ikegami, Isamu 39
Ikemoto, Isao 57, 58, 59, 62, 64, 65, 67, 68
Imaeda, Kenichi 57, 58, 59, 69, 70, 129
Imamura, Takashi 99, 100
Inaba, Ryoji 42, 43, 151
Inaba, Shinji 118, 119
Inabe, Tamotsu 63, 64, 138, 144, 153
Inada, Yasuzi 24
Inanaga, Junji 80, 81, 82, 152
Inazu, Takahiko 83, 84, 85
Inokuchi, Hiroo 57, 58, 59, 65, 66, 67, 68, 69, 70, 71, 129, 137
Ishiguro, Eiji 146
Ishiguro, Shin-ichi 113
Ishii, Hideshi 60
Ishimasa, Tsutomu 66
Ishimura, Yuzuru 30
Ishiyama, Tomoe 110
Isobe, Kiyoshi 77, 78, 79, 80
Isoyama, Goro 144, 145
Ito, Kouji 95
Ito, Tasuku 124, 125
Itoh, Tetsuji 76, 155
Iwai, Masahiro 23
Iwano, Kaoru 25
Iwasaki, Kentaro 59, 60, 67, 153
Iwasawa, Naoko 69, 70
Iwasawa, Yasuhiro 20
Iwata, Suehiro 14, 132, 133
Iye, Yasuhiro 70

Kabuto, Chizuko 130
Kageyama, Motohiro
Kakuta, Noriyoshi 105

Kamada, Masao 147
Kamalov, Valey F. 36, 43
Kambayashi, Hide 121, 157
Kaminaka, Shoji 29, 30
Kamiya, Kohji 65, 66, 67, 68
Kamogawa, Keiji 32, 33
Kandori, Hideki 37, 39, 40
Kang, Chul Hyun 86
Kanoda, Kazushi 60, 61, 62
Kasai, Kayoko 108
Kasuga, Kuninobu 57
Katayama-Yoshida, Hiroshi 67
Kato, Hajime 22
Kato, Hiroshi 15
Kato, Kiyonori 60, 62, 70
Kato, Minako 60
Kato, Osamu 103
Kato, Reizo 62, 71
Kato, Shinji 60
Kato, Tatsuhisa 33, 92
Katsumata, Shunji 93
Kawabata, Yasujiro 138
Kawaizumi, Fumio 109, 110
Kawamoto, Atsushi 59, 60, 75
Kawamoto, Tatsuya 108, 154
Kawamura-Kuribayashi, Hiroshi 19
Kawasaki, Hisano 127
Kawase, Haruo 83
Kawashima, Ayato 118
Kawata, Satoshi 33
Kayatani, Takayuki 127
Kemnitz, Klaus 37, 38
Khabibullaev, Pulat K. 59
Khairullin, Ilias 59
Kido, Hiroaki 125
Kihara, Hiroshi 29
Kikuchi, Koichi 33, 57, 58, 59, 62, 64, 65, 67, 68
Kikuchi, Yoichi 111, 112
Kikumoto, Junko 84
Kim, Bongsoo 43, 44, 151
Kimura, Eiichi 115, 116, 117
Kimura, Katsumi 88, 89, 90, 91, 92, 93, 94, 153
Kimura, Keisaku 69
Kimura, Misako 22
Kinoshita, Nobumori 59
Kita, Masakazu 112
Kitagawa, Hiroshi 137, 141, 142, 143, 154
Kitagawa, Teizo 29, 30, 31, 32, 33, 127, 151
Kitajima, Nobumasa 31
Kitaura, Kazuo 14, 128
Kobayashi, Akiko 62, 71
Kobayashi, Hanako 124
Kobayashi, Hayao 62, 71
Kobayashi, Yoshiaki 60
Koda, Takayuki 31
Koeda, Masaru 146
Koga, Nobuaki 13, 14, 16, 17, 18, 19, 20
Kohama, Keiichi 64
Koike, Tohru 115, 116
Kojima, Masaaki 120
Kojima, Norimichi 142
Komatsuzaki, Tamiki 21
Komeda, Nobutoshi 121, 157
Komorita, Seiko 108
Kondow, Tamotsu 97
Kono, Mitsuhiko 72, 95, 96, 97
Kono, Takumi 49, 51
Koppel, Ilmar A. 86
Koshiba, Hisato 105
Kosloff, Ronnie 12
Kotani, Jun 118
Koyano, Inosuke 99, 100
Kozaki, Masatoshi 130
Kubecek, Vaclav 45, 151
Kubo, Yoshiharu 72
Kuma, Hiro 108
Kumakura, Mitsutaka 28, 150
Kumazaki, Shigeichi 45, 151
Kuribayashi, Misao 110
Kuroda, Haruo 59
Kuroda, Yasuhisa 118
Kurogi, Yasuhisa 115, 116
Kurosaki, Hiromasa 116
Kurosu, Hisao 67
Kushi, Yoshihiko 108, 154
Kusumoto, Shirou 83
Kuwahara, Kazuya 136

Le Quere, Frederic 13
Lee, Beck Sim 24
Lee, Sungyul 23
Leforestier, Claude 13
Li, Xue-Kui 17
Li, Yongfang 70
Lie-Ming, Li 25
Lin, Duo Liang 25

Maeda, Hironobu 71
Maezawa, Hideki 146
Makino, Ryu 30
Maruyama, Hiroshi 71
Maruyama, Shinobu 117
Maruyama, Yusei 57, 62, 63, 64, 65, 69, 70, 138, 141, 153, 154
Marzilli, Luigi G. 117
Mase, Kazuhiko 98, 99
Maseras, Feliu 14, 17
Masuda, Hideki 113, 114
Masuda, Yoshio 111
Masuda, Yuichi 108
Matsuda, Shotaro 74
Matsufusa, Jiro 103
Matsui, Tatsuji 121
Matsui, Yuichi 119
Matsukawa, Nozomu 61
Matsumoto, Kazuo 59, 67, 68
Matsumoto, Mutsuyoshi 138
Matsumoto, Yoshiyasu 47, 151
Matsunaga, Tomonori 85
Matsuo, Susumu 66
Matsushima, Tatsuo 98
Matsushita, Mayumi 83, 85
Matsushita, Michio 92
Matsushita, Toshio 87
Matsuura, Hiroatsu 33
Mattera, Rafael 30
Maye, John P. 123
Miki, Hideho 30
Misaizu, Fuminori 131, 132, 133, 134, 135, 136, 154
Mishima, Masaaki 86, 87
Mitani, Tadaoki 60, 63, 75, 76, 137, 141, 142, 143, 144, 153, 154
Mitsuke, Koichiro 99, 100, 101, 102
Miyachi, Yoshimitsu 16
Miyajima, Seiichi 70
Miyakawa, Sigeki 126
Miyakubo, Keisuke 143
Miyamoto, Hiroshi 110
Miyamoto, Ryo 121, 157
Miyashi, Tsutomu 60, 129, 130
Mizukawa, Tetsunori 120, 157
Mizuno, Hiroyuki 112
Mizutani, Nobuo 95, 141
Mizutani, Yasuhisa 31, 127
Moc, Jerzy 15
Mogi, Iwao 124
Monobe, Masayuki 130
Moon, Doo-Kyong 119
Mori, Hatsumi 61, 62, 70
Mori, Masahiro 66
Mori, Nobuo 142
Mori, Takehiko 60, 61, 69, 70, 71
Mori, Yoshihisa 64, 65
Mori, Yoshihito 51, 52, 53, 155, 156
Morikawa, Takashi 59, 67, 68
Morita, Norio 27, 28, 150
Morita, Yasushi 74, 75, 144, 155
Moro-oka, Yoshihiko 31
Morokuma, Keiji 12, 13, 14, 15, 16, 17, 18, 19, 20
Muguruma, Chizuru 14
Mukai, Toshio 129, 130
Muramatsu, Gyo 105
Musaev, Djamaladdin G. 16, 17, 19

Nagai, Kiyoshi
Nagakura, Saburo 55, 152
Nagano, Tetsuya 146
Nagao, Hirotaka 120, 121, 122, 157
Nagasawa, Yutaka 37, 44, 151
Nagashima, Umpei 15, 138
Nagata, Masaaki 141
Naito, Toshio 71
Nakahara, Hiroo 67

Nakahara, Yusuke 69
Nakajima, Kiyohiko 120
Nakamoto, Masami 121
Nakamura, Eiichi 16
Nakamura, Eiken 94
Nakamura, Hiroki 22, 23, 24
Nakamura, Ikushi 116
Nakamura, Naoki 64, 153
Nakamura, Takayoshi 138
Nakano, Chikako 69, 70
Nakano, Hiroshi 66
Nakao, Tadahiro 57
Nakasuji, Kazuhiro 74, 75, 76, 77, 144, 155
Nakata, Kazuhide 87
Nakazawa, Keisuke 70
Nasu, Keiichiro 24, 25
Negishi, Ei-ichi 122, 123
Nelson, Keith A. 151
Nguyen, Thinh 123
Nishimoto, Kichisuke 87, 128
Nishimura, Nozomu 124
Nishio, Mitsuhiro 103
Nishioka, Takanori 78
Nishiya, Teruhiko 49, 50, 51
Nitto, Yu 123, 157
Nomura, Hideyuki 87
Nomura, Hiroyasu 109
Nomura, Sachiyo 83
Nonaka, Hiroe 84
Nonoyama, Kiyoko 112
Nonoyama, Matsuo 112
Noro, Takeshi 75
Nozoye, Hisakazu 98

Ogata, Hironori 63, 64, 153
Ogawa, Hiroshi 103
Ogawa, Hisashi 105
Ogawa, Kimiya 67
Ogoshi, Hisanobu 118, 119
Ogura, Takashi 30, 31, 32, 151
Ohashi, Haruhiko 95, 98, 99, 152
Ohba, Masaharu 109
Ohmae, Takeshi 74
Ohmine, Iwao 20, 21
Ohmori, Tadayoshi 104
Ohno, Yuichi 98
Ohnuma, Toshiharu 136
Ohsaki, Akihiko 22
Ohsaku, Masaru 16
Ohtaki, Hitoshi 113, 114, 115, 157
Ohto, Akihiro 124
Okada, Norio
Okahara, K. 59
Okamoto, Hiromi 42
Okamoto, Hiroshi 60, 63, 75, 142, 143, 144, 153
Okaniwa, Kaoru 63, 75, 76, 144, 153
Okazaki, Noriaki 53
Okumura, Mitsutaka 75
Okuyama, Katsuhiko 88, 89, 90, 91, 92, 93, 94, 153
Osakada, Kohtaro 119
Oshima, Kokichi 60, 62, 71
Ozawa, Fumiyuki 119
Ozawa, Yoshiki 77, 78, 79
Ozeki, Hiroyuki 88, 89, 90, 91, 92, 153
Ozutsumi, Kazuhiko 113

Peng, Shie-Ming 121, 122
Petek, Hrvoje 34, 35, 46, 151
Petho, Gabor 117
Petty, David M. 58

Radnai, Tamas 113, 117, 157
Ramaswamy, Ramakrishna 20
Re, Nazzareno 23
Reali, Giancarlo C. 45
Riehl, Jean-Frédéric 17
Rimo, Xi 78, 79
Ronis, David 156
Rousset, Christophe J. 122, 123
Ruani, G. 58
Rudziński, Jerzy M. 83, 85

Saburi, Masahiko 122, 123, 157
Saeki, Yoshihiro 87
Saito, Gunzi 61, 67, 69, 70
Saito, Kazuo 80
Saito, Kazuya 57, 62
Saito, Shinji 20, 21
Saito, Shuji 26
Saito, Yahachi 137
Saito, Yoji 102, 103, 104
Sakai, Kusuo 60
Sakai, Yasuhiro 94
Sakamoto, Yoichi 83
Sakan, Yoshinao 30
Sakimura, Tomoo 130
Sako, Katsuya 83, 84
Sakurai, Makoto 146
Sanekata, Masaomi 131, 132, 133, 134, 135
Sano, Kazuo 146
Sano, Mizuka 70, 129
Sasabe, Hiroyuki 39
Sasai, Masaki 20
Sasaki, Yoichi 80, 124, 125
Sato, Hiroyasu 137
Sato, K. 57
Sato, Keiichi 108
Sato, Noriko 108
Sato, Shin-ichiro 32
Sato, Shinri 104, 105
Satoh, Hideji 112
Satoh, Keiichi 110, 112
Sawabe, Kyoichi 20, 47, 151
Sawada, Kiyoshi 110, 111, 112
Seki, Kazuhiko 59, 65, 67, 68
Sekiguchi, Tetsuo 52
Sekikawa, Taro 143
Shichida, Yoshinori 39
Shida, Norihiro 21
Shida, Tadamasa 92
Shimomura, Hiroshi 108
Shinmyozu, Teruo 83, 84, 85
Shinohara, Hisanori 137
Shinzawa-Itoh, Kyoko 31, 32
Shiohara, Hiroaki 130
Shionoya, Mitsuhiko 115, 116, 117
Shirakura, Yasuhiro 111
Shiro, Motoo 115, 116
Shiromaru, Haruo 33
Shobatake, Kosuke 72, 95, 96, 97, 98, 99, 152
Shuai, Z. 25
Sokolov, V. Yu 59
Someda, Kiyohiko 22
Son, Tae-il 119
Srivastava, Prem, Kumar 52
Stock, Leon, M. 86
Struganova, Irina A. 36
Suenaga, Masahiko 83, 84
Sugimoto, Hideki 126
Sugimoto, Yuichi 82, 152
Sugita, Kazuyuki 67
Sugiura, Kenichi 75, 76, 77, 155
Sumitani, Minoru 56, 152
Sun, Xin 25
Suzui, Mitsukazu 95
Suzuki, Kaoru 55, 97, 152
Suzuki, Kazuya 70
Suzuki, Keinosuke 112
Suzuki, Koichi 60
Suzuki, Masatatsu 31, 121, 126, 127
Suzuki, Noriyuki 122, 123, 157
Suzuki, Satoru 67
Suzuki, Shinzo 33, 57, 58, 59, 64, 65, 67, 68, 99, 100
Suzuki, Takanori 59, 60, 129, 130
Suzuki, Toshio 110, 111, 112
Suzuki, Yasuhiko 118
Suzumoto, Takeshi 38
Swanson, A.G. 59
Swanson, Douglas, R. 123

Tabayashi, Kiyohiko 95, 96, 97, 98, 99, 152
Tadokoro, Makoto 76, 155
Taft, Robert, W. 86
Tajima, Hiroyuki 59
Takada, Shoji 22
Takagi, Yoshihiro 45
Takahashi, Hiroki 142
Takahashi, Masahiko 88, 89, 90, 91, 92, 153
Takahashi, Masahiro 67
Takahashi, Satoshi 31, 32, 151

Takahashi, Takashi 59, 67, 68
Takahashi, Tamotsu 122, 123, 157
Takahashi, Toshihiro 60, 61, 62
Takamuku, Toshiyuki 113
Takamura, Motomu 33
Takano, Shiro 144, 145
Takasu, Yoshio 105
Takayanagi, Masao 48, 49, 50, 51
Takayanagi, Toshinobu 94
Takeda, Sadamu 63, 143, 153
Takemura, Hiroyuki 83, 84
Takizawa, Hideo 29
Taliani, Carlo 58
Tamura, Masafumi 59
Tamura, Yusuke 157
Tanaka, Fujio 72
Tanaka, Hideki 15
Tanaka, Hiroaki 120, 122, 157
Tanaka, Jiro 75
Tanaka, Kazuyoshi 59
Tanaka, Koji 120, 121, 122, 157
Tanaka, Motoharu 109
Tanaka, Naoki 137
Tanaka, Shin-ichiro 147
Tanaka, Shoji 62, 65, 68, 70, 129, 130, 154
Tani, Tadaaki 38
Tanino, Kichiya 146
Tasumi, Mitsuo 42
Terui, Toshifumi 65, 154
Toda, Fumio 74
Toi, Hiroo 118, 119
Tokida, Nobuko 120
Tokiwa, Ayako 124
Tokumoto, Madoka 59
Tokuoka, Youko 62
Tokutomi, Satoru 31, 40
Tominaga, Keisuke 151
Tomioka, Hiroaki 39
Tomura, Masaaki 129, 130, 154
Topsom, Ronald D. 86
Toriumi, Koshiro 78, 142
Toyoda, Jiro 74, 75, 76, 77, 144, 155
Tsubata, Yoshiaki 129
Tsubokura, Yuichi 61
Tsuda, Ken-ichiro 22
Tsuda, Mitsunori 128
Tsukahara, Aiichiro 95, 152
Tsukahara, Keiichi 124
Tsukamoto, Keizo 131, 132, 133, 134, 135
Tsunashima, Shigeru 136
Tsuno, Yuho 86, 87
Tsutsumi, Kenjiro
Tzeng, Biing-Chiau 122

Uchiyama, Koichi 140
Uehara, Akira 31, 121, 126, 127
Uehara, Katsuhiro 110
Ueno, Akifumi 105
Ueno, Nobuo 67, 68
Ugawa, Akito 57, 58, 59, 60, 153
Ukisu, Yuji 104, 105
Umemoto, Hironobu 136
Uozumi, Kounosuke 126
Urisu, Tsuneo 98, 99
Uryu, Norikiyo 124

Vazquez De Miguel, Amelio 79

Wada, Senji 117
Waizumi, Kenji 113, 114, 157
Wales, David 20
Wang, Bateer 78, 79
Watanabe, Makoto 60, 94, 146
Watanabe, Youichi 113
Wu, C 25

Yakushi, Kyuya 57, 58, 59, 60, 67, 153
Yamabe, Tokio 59
Yamada, Kasumi 109
Yamada, Yasuko 124
Yamada, Yuko 117
Yamaguchi, Hiroki 137
Yamaguchi, Kizashi 75
Yamaguchi, Tadashi 124
Yamaguchi, Toshiyuki 103
Yamakado, Hideo 57, 153
Yamamoto, Akio 119
Yamamoto, Hiromichi 70
Yamamoto, Hiroshi 144
Yamamoto, Takakazu 119
Yamaoka, Osamu 104
Yamashita, Koichi 13, 15
Yamashita, Masahiro 142, 143
Yamashita, Yoshiro 59, 60, 65, 68, 70, 129, 130, 154
Yamauchi, Kotaro 33
Yamazaki, Hitoshi 62, 71
Yanagihara, Mihiro 146
Yano, Shigenobu 124
Yartsev, Arkadiy 37, 44, 151
Yasumatsu, Hisato 97
Yasuoka, Noritake 69, 70
Yokoi, Michiko 84
Yokoyama, Yasuo 80 81, 82
Yonehara, Hisatomo 67
Yoshida, Akira 99, 102, 103, 104
Yoshida, Hiroaki 99, 100, 101
Yoshida, Hisashi 94, 95
Yoshida, Kiyohide 105
Yoshida, Shoji 112
Yoshida, Tohru 18
Yoshida, Yukihiro 124
Yoshihara, Keitaro 34, 35, 36, 37, 38, 39, 40, 41, 42, 43, 44, 45, 46, 151
Yoshikawa, Hiroshi 95, 152
Yoshikawa, Kenichi 156
Yoshikawa, Shinya 31, 32, 151
Yoshimoto, Minoru 156
Yoshimura, Tetsuhiko 118, 119
Yoshizawa, K. 59

Zakhidov, Anvar A. 58, 59
Zamboni, Roberto 58
Zambounis, J. 60, 61
Zhu, Chaoyuan 23, 24

Institute for Molecular Science, Myodaiji, Okazaki 444, Japan